1

Complex Plasma – Why It Is an Unusual State of Matter?

We start here with some declarations, and subsequent discussion in this book is entirely devoted to their clarification and experimental proof. Complex plasmas consist of electrons, ions, neutrals, and solid micro-particles (dust grains) interacting strongly with each other in such a way that the mutual influence of the components determines physical parameters of the system. There is nothing unusual with this mutual influence. When speaking of a state of matter we usually have in mind either solid, liquid, gaseous, or plasma states. The latter is an ionized state: partially ionized (with the presence of neutral particles) or fully ionized (an ideal case encountered in high-temperature "hot" plasmas such as those in the interior of stars). However, complex plasma is qualitatively different from those ordinary states of matter.

1.1 General Physical Differences Between Complex Plasma and Ordinary Matter

There exist *two main differences between a complex plasma and an ordinary state of matter*:

(1) The *grain charges are very high* causing new phenomena in grain plasma as well as grain–grain interactions.

(2) The *grains strongly absorb plasma components* (electrons and ions) and the sources replenishing them make the whole highly dissipative system to be thermodynamically open with high tendency to form various types of structures (often called "self-organized structures").

The huge charges (up to 10^6 of the elementary electron charges per grain) on the grain component in a complex plasma make interactions of grains with other plasma components as well as between them rather strong, even for relatively low grain density. But this is rather quantitative than qualitative difference. There are differences in qualitative characteristics. One of them is that the grain charge varies, depending on surrounding plasma particles

V. N. Tsytovich et al.: *Complex Plasma – Why It Is an Unusual State of Matter?*, Lect. Notes Phys. **731**, 1–45 (2008)
DOI 10.1007/978-3-540-29003-2_1

and on the presence of other grains. Such systems have no analogy to known systems of elementary particles with fixed charges. The possibility of an energy gain from self-energies of particles due to changes in their charges does not exist in any collection of elementary particles (or in ordinary matter), but it does exist in a complex plasma.

This is not a single qualitative difference. In ordinary matter there exist quantum exchange interactions which are in the foundation of the quantum particle binding, the formation of molecules, and therefore in physics and chemistry of free-boundary solid states. Natural solids without external confining forces are of quantum nature. Complex plasmas can provide an example of the formation of classical binding states, classical molecules of grains with the same sign of charge, and classical free-boundary crystals. This new binding of classical nature should be explained in physical terms and our aim is to provide such an explanation.

Along this line another surprising property of a complex plasma arises. An important point is that *particle interactions are collective*, i.e., *cannot be considered as a sum* of all pair interactions. The pair interactions depend on such collective parameters as average densities and average charges of the grain component of the system. This becomes obvious if one takes into account the aforementioned variability of grain charges and their dependence on the presence of other grains. In ordinary matter we deal with similar phenomenon where interactions are collective and the total energy of them for a particular component is not the sum of all pair interactions. However, in ordinary matter on a microscopic level the interaction energies are still considered to be the sum of individual pair interactions even for collective interactions. It is different in principle in a complex plasma since the charges can be changed externally and the grain self-energy depending on them (as well as on the interactions) is also changed.

Another qualitative feature of a complex plasma is a natural *appearance of self-organization properties* and easy formation of various structures. Complex plasma systems can be used for modeling some biological systems resembling their primitive aspects (note that more complex aspects such as possible memory can be also found in complex plasma structures). The tendency for self-organization is related with high rate of dissipative processes due to the presence of grains.

The last and not the least important qualitative property is the *flexibility of screening* of huge grain charges. The screening determines the characteristic length of interactions which appears to be depending strongly on the presence of other particles. This makes investigations of binary interactions of isolated grains of little importance for understanding of collective states such as liquids or solids of grains. This means that interactions in a system of large number of grains are *in principle collective*. This of course does not mean that interactions of two isolated grains, or small number of grains, are of no interest or reveal no new features as compared to those in ordinary matter. But physical effects involved in the case of large collections of grains differ from those for

small collections of grains, and both cases should be investigated separately. Moreover, the grain shielding is often non-linear due to the large charges. That is, the potential energy of plasma particles producing the screening is much larger than their kinetic energy in the vicinity of grains. This introduces new qualitative effects absent in usual matter.

Thus a system of interacting grains in a complex plasma cannot be considered as that of bare Coulomb-interacting particles and, as we show, always creates *long-range grain interactions of both repulsive and attractive types*. Finally, due to strong plasma absorption on grains and an ensuing necessity to support the plasma density by external sources of ionization, *the usual concept of free energy is not applicable to a complex plasma*. Complex plasmas actually represent a thermodynamically open system.

1.2 General Terminology in Complex Plasma and Ordinary Matter

The Encyclopedia Britannica [1] defines a plasma as "a collection of electrically charged particles about equal number or density that is produced when atoms or gas become ionized." While this definition is reasonable in some restricted sense, it is in general incomplete. It has to be remembered that in practice the term "plasma" is used for different states of matter.

First, neutrality is not a general property of plasmas, and deviation from the so-called quasi-neutrality can be rather large, especially if the plasma contains relativistic particles. There is a term "charged plasmas" for plasmas in relativistic rings and accelerators. Furthermore, the conditions that the charged particles must interact weakly and that their kinetic energy must be much larger than their average interaction energy also do not constitute criteria for plasma as a state of matter. Fully ionized gases which consist of weakly interacting electrons and one type of ions are often described as "ideal plasmas," while plasmas containing a neutral component are called as "partially ionized plasmas"; if there are different ion types they are referred to as "multi-component plasmas"; in the extreme case where only one component varies or exists, one uses even the term "one-component plasma" (OCP). Finally, plasmas containing impurities, e.g., small interacting solid particles (grains), are called "colloidal," "complex," or "dusty plasmas."

With exception of "ideal plasmas" and "non-neutral plasmas," the other types listed above are often collectively termed "non-ideal plasmas." Interactions between plasma components in non-ideal plasmas are usually weak or moderate, which separate this state of matter from solids and liquids where the interactions are strong. In "complex plasmas," interactions between grains are not weak and this also changes interactions of the grain component with other plasma components. Traditionally, liquids containing colloidal suspensions are referred to as "complex liquids." Interactions of components in complex liquids are also strong. The chemistry, if important, is complex both in complex

plasmas and in complex liquids since it includes chemical processes on dust surfaces. The latter can be important since chemical reaction rates on the grain surfaces are larger than volume chemical reaction rates (the so-called heterogenic chemistry) and because the total surface of grains in a complex plasma or complex liquid can be large. The liquid and crystal states formed by grains in complex plasmas are often called "plasma liquids" and "plasma crystals," respectively. The conversion to the plasma crystal or plasma liquid state is called as "plasma condensation" in a complex plasma [2, 3, 4, 5, 6, 7, 8].

It has become clear in the last few years that the "complex plasma" physics is very important for plasma processing, thin-film deposition, complex materials, combustion, and plasma fusion reactors as well as in environmental research. Like liquid colloids (or complex liquids), complex plasmas appear to be a key in, for instance, the fundamental research of phase transitions. The importance of complex plasma research is growing in surface and boundary physics and in paving the way toward certain areas of nanotechnology (e.g., the manufacture of mesoporous silicates). It is taking on growing importance in etching, technics, producing computer chips by plasma etching, where strongly interacting clouds of complex plasmas are observed levitating above the etched substrates, causing major contamination of the final product. We simply mention this here; the industrial and technological applications of complex plasmas are discussed in the next chapter.

Another important concept in a complex plasma is the term "particle," which is used to describe "grain" or "dust" particles without adding the word "dust" or "grain" before it [9]. In plasma physics or elementary-particle physics, the term "particle" is used for any particle including ions, electrons, or atoms, which are also the components of complex plasma systems. Historically, the term "particle" or "micro-particle" has been used only for dust grains, while for electrons, ions, and neutral atoms the term "particle" is often not used. One should always have in mind this usage when reading the literature in this field. In this book, we use this terminology as well, as it is widely accepted among physicists working in the field of complex plasmas.

1.3 History: Complex Plasmas in Space Physics

Historically, the main interest to the problems of plasmas containing dust was related not to industrial aspects of complex plasmas but to space physics [10]. The important role of dust in space physics was realized a century ago. The research was started in astrophysics as research on dusty plasmas [11, 12, 13, 14]. It should be mentioned that up to 5% of matter in dust-reach galaxies is in a state of dust, that dust determines most properties of interstellar media and plays an important role in the formation of stars and planets. Dust space clouds obscure almost completely some part of the sky.

Plasmas containing electrons and ions may be thought of as extremely hot gases when the thermal energy is sufficient to ionize the gas atoms. The

term "hot gases" for plasma is still used in astrophysics, although it is not relevant since even for a very low degree of ionization the main properties of this hot gas are determined by the charged component. Nevertheless, the term "hot gas" underlines the fact that the kinetic pressure is very high in plasmas and that plasmas should be confined (otherwise, their internal pressure will cause them to expand). Expanding plasmas are often found in nature in such violent phenomena as supernova explosions, solar wind, or interstellar media. Confinement in nature is either gravitational (most stars are gravitationally confined plasmas) or magnetic (for instance, the radiation belts in the earth's magnetosphere).

The term "dusty plasma" is most appropriate in the case where dust does not introduce new collective effects. Space research started out using an approach that dust grains can be considered as impurities in plasmas which do not change the plasma properties essentially, i.e., the effects used to explain phenomena in space plasmas containing dust component were considered to be the sum of the effects occurring for individual grains. At present it is obvious that such a consideration is not complete and needs to take into account the new effects related to the collective behavior of plasmas containing dust grains, i.e., to use more general aspects of complex plasmas. We nevertheless mention some of the first investigations of dusty plasmas in space. Dust exists in almost all plasma space environments including Earth's upper atmosphere and magnetosphere, in plasmas around other planets, and in cometary tails. As mentioned above, dust plays a major role in the formation of solar system, planets, and stars; it is the main source of material absorbed by black holes, etc. In space, dust grains strongly interact, and to neglect these interactions as was done in many previous investigations is not, strictly speaking, correct.

Dusty plasmas for a long time received considerable attention in astrophysics, e.g., in the physics (and chemistry) of interstellar clouds [15, 16], of the influence of dust on the dynamics of stellar wind, on the role of dust in nova and supernova explosions and in the formation of stars and planets [11, 15, 16, 17, 18]. Similarly, the importance of dusty plasmas in the solar system received a tremendous boost, over and above the established fields of cometary physics [19] and the investigation of the zodiacal light clouds [20], when Jupiter's ring was discovered and the active volcanism on Io [21, 22], with its ejection of fine "ash" into the Jovian magnetosphere, was first "seen" by the detector aboard the Voyager spacecraft [23] and inferred from the data [24]. This was followed by a wealth of new discoveries in Saturn's rings [16], in particular the "spokes" [25], the structure of the F-ring and the E-ring [26], and an unusual electromagnetic angular transport in the B-ring [27]. It is often assumed that inter-planetary dust can create instabilities [28]. In all these observations the dust particles were highly charged but assumed not to be strongly interacting, i.e., assumed to form dusty plasmas but not complex plasmas. Strictly speaking, the role of new effects in complex plasmas has not yet been analyzed for these natural dust plasmas. In some conditions of

rarified dust this approach can be appropriate, but there are many collective effects that have to be investigated in future astrophysical applications of complex plasmas; these are the new effects to which this book is devoted.

Here we only mention some of new problems that have not yet been resolved in the field of astrophysics, which historically showed the first interest in grain-containing plasmas. Complex plasmas with their recently found properties can play an important role in condensed dust clouds in space [12, 14, 29], in grain condensations behind supernova shocks [29, 30], and in planet and star formation [15]. We mention also the possible role of collective effects in natural complex magnetospheric plasmas [31] (in particular, interactions between magnetospheres of giant planets and planetary rings) [15, 17, 32, 33, 34] and the physical importance of complex plasmas in the formation of planets, new astrophysical objects like dust planets or dust stars, etc. The strong interaction can play a role in generation of atmospheric lightning [31]. Dust grains in the atmosphere are the seeds for growing clouds and global cloudiness and can determine the effect of global warming. The problems of ozone depletion are also deeply related to the physics of complex plasmas since the depletion occurs on the surfaces of contaminated ice-dust grains present in the upper partially ionized atmosphere.

1.4 Problems of Strong Coupling in Plasmas

1.4.1 Phase Space for Strong Coupling in Ordinary Plasmas

In the laboratory, various electric and magnetic configurations are used, e.g., storage rings, Paul traps, electrostatic potentials in Radio-Frequency (RF) or Direct Current (DC) discharges, or simply confinement by the walls of vacuum chambers [35]. It is these different production and confinement techniques that allow laboratory investigations of physical processes to determine our basic understanding of these complex, and in part extreme, states of matter, as well as the assessment of their usefulness for industrial applications (e.g., etching, deposition in manufacturing of semiconductor devices [9, 36, 37, 38] and their potential as energy sources (plasma nuclear fusion reactors [39], solar cells [40], etc.)).

In many laboratory conditions (as well as in space conditions) plasmas are not fully thermal. This is certainly the case when the degree of ionization is low and a large number of neutral atoms are present that contact walls and collide often with ions. The ion and neutral temperatures are then much lower than the electron temperature by two or more orders of magnitude. Also, ionization processes can create non-thermal electron distributions.

We start nevertheless with showing the phase space (or state space) for plasmas characterized by two parameters – density n and temperature T – assuming that the temperatures of all components (electrons, ions, and neutral atoms, where dust is absent) are equal. This phase space is extremely broad.

Plasma densities vary from the most tenuous inter-galactic values (less than one particle per cubic meter) and interstellar values (from less than 10^{-2} to 1 particle per cubic centimeter) to the most compact values in stellar interior (from $5 \times 10^{26}\text{cm}^{-3}$ at the center of our sun up to 10^{30}cm^{-3} in white dwarfs), in temperatures ranging from sub-micro degrees Kelvin in laser-cooled one component plasmas (OCPs) up to tens of millions of degrees Kelvin (1.5Kev in the center of our sun), maybe even billions of degrees in compact stellar objects that accrete matter from a companion (binary) star. Figure 1.1 presents a summary of selected plasmas and the phase space (density, n, and temperature, T) they occupy (adapted from the Naval Research Laboratory (NRL) Plasma Formulary [41]). Let us emphasize that in this figure dust grains are absent.

Two lines marking important plasma characteristics are drawn in this phase space regime. The dashed line indicates the (n, T) values at which a hydrogen plasma in local thermal equilibrium would be 50% ionized. To the left of this dashed line the ionization fraction is smaller, to the right the

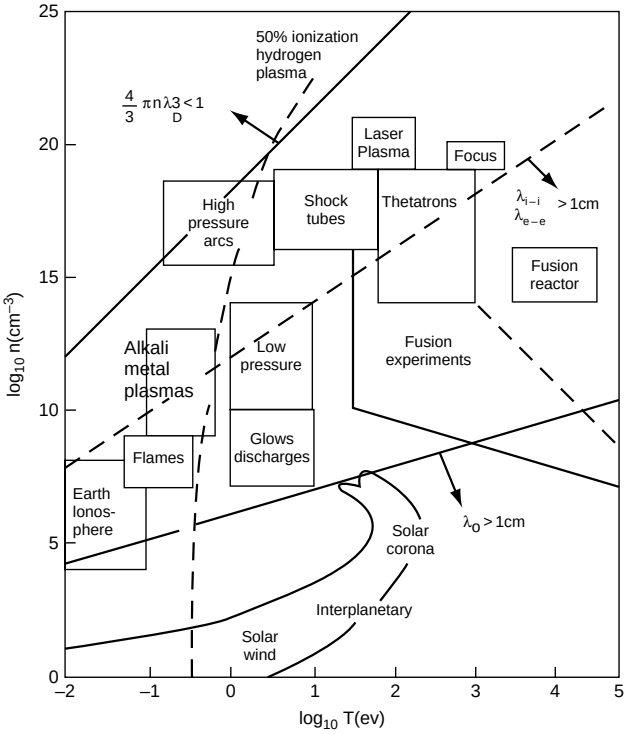

Fig. 1.1. Phase diagram showing different plasmas existing in space and laboratory. Here, n is the number of particles in cm^{-3}, λ_D is the Debye length, and T is the temperature [41]

plasma approaches the ideal fully ionized state. But even for the ionization degree much less than 50% the charged plasma component starts to play a dominant role in interactions. The continuous line denotes the approximate boundary between "strongly coupled" plasmas (the regime above the line) and the "weakly coupled" plasma regime. The strong coupling is here the one between the plasma particles; it is different from the case when grains are present, and the coupling between the grains can be strong as in complex dusty plasmas. The strong coupling is defined here by setting the thermal energy T (we use the energy units for the temperature where the Boltzmann's constant $k_B = 1$) equal to the mean Coulomb energy between neighboring particles, $Q^2 n^{1/3}$ (where Q is the particle charge equal to the value of the electron charge e for singly ionized ions). The dimensionless number defining the degree of coupling Γ is given by

$$\Gamma = \frac{Q^2(4\pi/3n)^{1/3}}{T} \tag{1.1}$$

and is called the "coupling constant." Note that in this estimate the particles are considered as not screened. In fact, in complex plasmas the screening is strong and is non-linear, and the real particle interaction which takes into account the screening should be different from bare particle Coulomb interaction which is assumed in (1.1). Nevertheless, (1.1) has a physical meaning as an expression estimating the average interaction energy as compared to the kinetic energy **for a fictitious case of unscreened particles**. Here we give some first-step consideration for bare particles just to demonstrate how strong can be the grain interactions if their field is not screened (later we discuss the role of screening in real complex plasmas).

In Fig. 1.1, it was assumed that the atoms are singly ionized, i.e., $Q = |e|$ (e is the electron charge), and the solid line gives $\Gamma = 1$. The density increases above this "strong coupling line," particles are closer together, and the effect of their mutual Coulomb interaction is to decrease their individual mobility – the plasma "freezes." Below the "strong coupling line" the opposite occurs – elastic Coulomb collisions between electrons and ions can thermalize the system, which behaves essentially like a hot gas with electrons and ions forming separate components. The further we are from the solid line, the slower is the thermalization process, and much phase space is left for developing plasma instabilities, which usually cause the particle distributions to deviate from the thermal distribution. Figure 1.1 has therefore a limited region of applicability keeping in mind that the ionization sources also cause the particle distributions to deviate from the thermal distributions. However, it serves as a good criterion for dividing strongly and weakly coupled plasmas. The parameter Γ increases with density and decreases with temperature. For example, in the center of the sun, where the density (close to $n \approx 5 \times 10^{26}\mathrm{cm}^{-3}$) and the temperature (close to 1.5Kev) are high, we have $\Gamma \approx 0.1$, i.e., it is still small.

It should be noted that the phase space region above the "strong coupling line" has thus far remained essentially unexploited experimentally. There are

two reasons for that. First, extremely high densities make this an experimentally very demanding area of research and, second, quantum effects (degeneracy) begin to play a role and new physical processes become involved. Exceptions are the very cold Magnesium_ions in OCP model stored in Paul traps and storage rings [42, 43], the 2D electron lattices (again OCP [44]) on super-cooled hetero-junctions, which are of interest for quantum Hall effect [45], and, at the other extreme, the short-lived high-power laser-induced shock vaporization studies [46]. The diagnostic of the latter is, of course, very difficult. The time scales are very rapid, the system is optically thick, and at present it is not feasible to either maintain or control the plasma. Hence investigations of strongly coupled plasmas are largely concentrated on theoretical investigations using various numerical techniques, such as particle codes and hybrid codes [47] and Monte-Carlo simulations [48, 49].

A breakthrough in this field appeared from an unexpected direction – from the study of "complex," "dusty," or "colloidal" plasmas. The breakthrough for the problems of strong coupling came from the realization that the grain particles in most observed cases in both space and laboratory plasmas have rather large charges. The connection to strongly coupled plasmas occurs as follows: the coupling constant $\Gamma = Q^2((4\pi/3)n)^{1/3}/T$ can be increased by raising the particle density n (e.g., in laser-induced shocks), by lowering the particle temperature (as in laser cooling techniques) whilst making sure that recombination is not possible (e.g., in OCPs), and, most importantly, because of its quadratic dependence on charge Q, **by raising the charges** on "ions" whose role in a complex plasma is played by **dust grains**. The difference between this strong coupling and that denoted by the solid line in Fig. 1.1 is that it can occur between grains only while other plasma particles can interact weakly. This state is called "complex dusty plasma."

1.4.2 Physics and Consequences of Large Grain Charges

The possibility of strong coupling in complex plasmas is directly related to the possibility of very large charges on the grains. This in fact is due to the relative large grain sizes as compared to sizes of other plasma particles (electrons, ions, and neutral atoms). For example, sizes of ions or neutral atoms are of the order of $(10^{-8}-10^{-7})$cm, while the grains (which can be of various sizes) have a the typical size of $10\mu\,\mathrm{m} = 10^{-3}$cm, which is four or five orders of magnitude larger than the atomic size.

Simple physical arguments show that the grain charge $Q_d = -eZ_d$ is proportional to its size a resulting for typical grain sizes if $Z_d \gg 1$. The usually considered charging process is extremely simple: the thermal electron mobility is much larger than the thermal ion mobility (note that the thermal electron velocity is much larger than the thermal ion velocity even for equal temperatures due to the much lower mass of the electrons). When embedded into a plasma, the grain is very soon charged negatively by the thermal

electron flux, and starts to repel electrons and attract ions until ion and electron fluxes become equal. The grain then has a floating potential equal to the electron temperature ($Z_d e^2/a \approx T_e$), and for a fixed electron temperature T_e the grain charge is proportional to its size ($Z_d \propto a$). In practical terms, grains that are of 10μ in size can have charges 10^4–10^5 larger than the electron charge e. This is confirmed by numerous laboratory experiments. The grain sizes in some laboratory experiments are even larger up to several hundred μm, and their charges can be larger by one or more orders of magnitude. It is useful to characterize the grain charge by the dimensional value z defined as

$$\mathrm{z} = \frac{Z_d e^2}{a T_e} \tag{1.2}$$

which ranges in most cases from 1 to 2–4, with the average value about 2.

The Coulomb interaction energy between the grains (and the parameter Γ) is proportional to Z_d^2 and consequently can be very large although the separation between the grains can be larger than that between the plasma particles. Thus the grain component can become strongly coupled for relatively low grain densities forming a complex plasma state. Elementary physical arguments show that strong coupling between grains can be a natural phenomenon in a complex plasma. We can compare the value of Γ_i for (singly ionized) ions with Γ_d for bare (unscreened) grains by using the parameter P:

$$P = \frac{n_d Z_d}{n_i} \,. \tag{1.3}$$

It is clear from the quasi-neutrality condition that

$$n_i = n_e + n_d Z_d, \tag{1.4}$$

and the grain component contributes substantially in the average electrostatic interaction if P is of the order of 1. In most existing experiments on complex plasmas, the parameter P is indeed of the order of 1 or less than 1. Then the aforementioned ratio can be written as

$$\frac{\Gamma_d}{\Gamma_i} = P^{1/3} Z_d^{5/3} \frac{T_i}{T_d} \,, \tag{1.5}$$

where T_i and T_d are the ion and grain temperatures, respectively. For Z_d from 10^4 to 10^5, (1.5) gives an increase in Γ from $4.6 \cdot 10^6$ to $2.2 \cdot 10^8$, which shows that it is possible to produce plasmas (albeit complex plasmas) with a considerably increased coupling constant. This is the suggestion made by Ikezi in 1986 [50]. But at present it is not clear whether large grain charges induce strong grain interactions. The interactions are strong indeed when the grains are close to each other, but this is the same for all particles in ordinary matter. It can happen that the grains do not spend much time at the distances where

their interaction is strong and form correlated states at distances where their interaction is relatively weak. This depends largely on the grain screening and on the collective nature of grain interactions. We will discuss this problem in detail later.

Experimental investigations took about 10 years before the first results were published – and, as sometimes happens in research, two groups (one located in Taiwan [3], the other in Germany [2]) submitted their results within a week of each other while a third group from Japan [5, 51], also working independently, published their results in a similar time frame. Priority should be given to [2] since the abstract of the report in which the main results of [2] were given was published first in the conference proceedings [52].

The experiments showed conclusively that a complex plasma can "condensate," i.e., it can exist in liquid as well as in solid, or crystalline, state. This certainly implies the presence of long-range interactions. One should not be confused by ordinary matter behavior, where the long-range correlations are present only for strong interactions. Because a complex plasma is an unusual state of matter, one should investigate the other possibility – that the long-range correlations are a specific property of complex plasmas and can appear even in the case where interactions are not strong.

1.4.3 Physics and Consequences of Dust Charge Screening

The Coulomb field is a long-range field and usually is screened in plasmas. The screening substantially changes the grain interactions. Assume, for example, that the Coulomb field of the grain is completely screened at (some sphere) the distance λ_{scr}. Then the strong interaction is absent outside this sphere and the grains "feel" each other only when the distance between them is equal to or less than the screening distance. Otherwise they behave as a kind of "hard spheres" not-interacting until they touch (contact) each other at the distance equal to the screening length.

Thus the criteria of complex plasma condensation should depend strongly on the effect of screening. We demonstrate here that large charges (of the values of interest for the plasma condensation) are screened differently than small charges (of the order of a single electron charge) in ordinary plasmas. For small charges the Boltzmann density distribution of the plasma polarization charges around them is approximated by the first terms of expansion of the potential $n_0 \exp(-e\phi/T_e) \approx n_0(1-e\phi/T_e)$ and $n_0 \exp(e\phi/T_i) \approx n_0(1+e\phi/T_i)$ for electrons and ions, respectively. The Poisson's equation for the dust charge screening is then reduced to a linear equation for the screening factor

$$\phi = \frac{-Z_d e}{r}\psi(r)\ ; \qquad \frac{\mathrm{d}^2\psi}{\mathrm{d}r^2} = \frac{\psi}{\lambda_D^2}\ ; \qquad \frac{1}{\lambda_D^2} = 4\pi n_0 e^2\left(\frac{1}{T_i}+\frac{1}{T_e}\right), \tag{1.6}$$

where λ_D is the Debye screening length. By assuming that both the distance from the grain r and the grain size a are given in units of the Debye screening

length (thus r corresponds to r/λ_D and a corresponds to a/λ_D), yielding the exponential screening factor (sometimes called "Yukawa screening")

$$\psi = \exp\left(-(r-a)\right) \approx \exp(-r); \qquad a \ll 1. \tag{1.7}$$

It is not correct to consider the exponential decrease of the potential as fast if we are interested in distances of the order of the screening distance. For example, at 4.6 screening distances the interaction decreases only by a factor of 100. Since the Coulomb interaction is huge and Γ can be of the order of 10^4, a decrease in the interaction by a factor of 100 still corresponds to strong coupling $\Gamma \gg 1$. Defining for the screened Coulomb interaction the dimensionless parameter

$$K \equiv \frac{1}{n_d^{1/3}\lambda_D}\ , \tag{1.8}$$

we find

$$\Gamma_{lin} = \frac{Q^2(4\pi n_d/3)^{1/3}}{T_d}\exp(-K)\ . \tag{1.9}$$

This exponential factor shows the importance of screening for strong coupling and plasma condensation. But first we should answer the question as to whether the screened Coulomb interaction is applicable to cases where large charges are used for plasma condensation to occur. The distribution of both electrons and ions close to the grain is always non-linear in the sense that the Boltzmann exponent for their density around the grain contains the potential of the interacting particles. The question is when this exponent can be expanded with respect to the potential, and only the first term of such an expansion (linear in the potential) can be used (as it was performed above). Indeed at the grain surface, using the estimated dust charge, we have the Boltzmann exponent equal to $\exp(-z)$ for electrons and $\exp(z/\tau)$ for ions, where

$$\tau = \frac{T_i}{T_e} \tag{1.10}$$

is the ratio of the ion to electron temperatures. In laboratory experiments the condensation was observed experimentally as $\tau \approx 10^{-2}$; in astrophysical conditions often $\tau \approx 1$. It is therefore certain that close to the grain surface, the exponents for electrons and ions cannot be expanded with respect to the potential, and the screening there is always non-linear. Moreover, for ions this exponent can be huge, $\exp(200)$ or even $\exp(400)$, and distribution of ions should differ substantially from the Boltzmann distribution. As we look at distances far from the grain, the potential decreases and at some point it can satisfy the requirement for the linear approximation; that allows us to make an estimate. The screened Coulomb (Yukawa) potential can be approximately correct at large distances if at a distance of the order of λ_D the linear approximation is appropriate. This condition is

$$Z_d \ll 4\pi n_i \lambda_{Di}^3 = 37\sqrt{\left(\frac{10^9\mathrm{cm}^{-3}}{n_i}\right)}\ . \tag{1.11}$$

For optimistic treatment of the sign "much less" as a factor 1/3 we obtain $Z_d < 100$ for the ion density of the order of $10^9 \mathrm{cm}^{-3}$. The density can vary for different experiments but it cannot be larger than that by an order of magnitude in either direction. Then the restriction obtained from (1.11) varies from $Z_d < 30$ to $Z_d < 300$. But it is certain that it is outside the domain where complex plasmas are investigated, $10^4 < Z_d < 10^6$. This means that the *screened Coulomb potential cannot describe strong interactions of grains in a complex plasma.*

To find a qualitative picture for the role played by non-linearity in screening, one can assume that the screening charge is reduced to being proportional to some power of the potential, and use an equation

$$\frac{\mathrm{d}^2\psi}{\mathrm{d}r^2} = \psi^\nu \,, \qquad \nu < 1 \,, \tag{1.12}$$

for the screening factor ψ [53, 54, 55] instead of linear equation (1.6). In (1.12) the distance is normalized in the screening length different from the Debye screening length. The solution of (1.12), with a corresponding adjustment in the definition of the screening length λ_{scr}, is given by

$$\psi = \left(1 - \frac{r}{\lambda_{scr}}\right)^{2/(1-\nu)} \,. \tag{1.13}$$

We use this simple illustration to show that at $r = \lambda_{scr}$ the screening factor becomes exactly zero (in contrast to the exponential screening).

Then the coupling factor is

$$\Gamma_{nonl} = \frac{Q^2(4\pi n_d/3)^{1/3}}{T_d}(1 - K_{nonl})^{2/(1-\nu)} \,, \tag{1.14}$$

where $K_{nonl} = 1/n_d^{1/3}\lambda_{scr} = K/s$ with $s = \lambda_{scr}/\lambda_D$. Usually, the characteristic length of non-linear screening $\lambda_{scr} \gg \lambda_D$ and depends on both $\tau = T_i/T_e$, the ratio of ion to electron temperatures, and a/λ_D, the ratio of the grain size to the Debye screening length. In comparing the non-linear screening with linear screening we should keep in mind that the parameter s varies from $10-30$ in laboratory plasmas down to $1-2$ in space plasmas. Figure 1.2, giving a ratio $\Gamma_{nonl}/\Gamma_{lin}$ as a function of K and s, illustrates the difference of the values of the coupling constant between the realistic model of screening and the linear screening.

Thus the interaction becomes very sensitive to the screening, and the "tail" of the grain potential at distances of the order of the screening distance is very important. The effects of plasma condensation are rather sensitive to the character of screening. All collective interactions are of long range and start to play an important role at distances of the order of (or larger than) the screening length. That is why they can be so important in the treatment of complex plasma states.

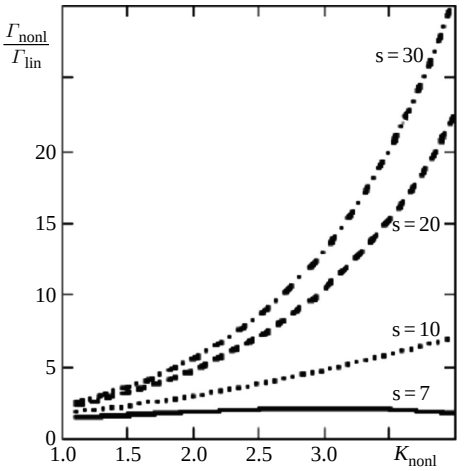

Fig. 1.2. Ratio of the coupling constant for the non-linear and linear screening. Here, $s = \lambda_{scr}/\lambda_D$ is the ratio of the non-linear screening length to the Debye length, the value of K_{nonl} corresponds to that given by expression (1.14)

1.4.4 Phase Space for Strong Coupling in Complex Plasmas

Plasmas generated by different techniques offer themselves for investigations of strong coupling in complex plasmas: Radio Frequency (RF) plasmas, Inductively Coupled Plasmas (ICP), Direct Current (DC) discharges, Ultraviolet (UV) plasmas, radioactive plasmas, and combustion plasmas [35]. Of these, RF discharges are currently the most widely used [2, 4, 5] (the first reported experiments also used RF discharge plasmas see below for a description of these first and many other experiments in RF discharge plasmas). The strongly coupled states were obtained in DC glow discharge plasmas [6, 56], in combustion plasmas [57], in UV-irradiated plasma [58, 59], and with ionization excited by radioactive nuclei [60, 61] (see also [62]).

To show the accessible range of the parameter space we re-draw Fig. 1.1 in slightly different way – see Fig. 1.3 [63]. The vertical axis is now $Z_d^6 n_d$, which is proportional to $\Gamma_d^3 T_d^3$. The different regions of the phase space that can be accessed using complex plasma are shown as the shaded columns. The lower limit is due to the electrostatic levitation against gravity; the upper limit is due to the electron depletion in plasma caused by absorption on dust particles. In space, where gravitational force is much smaller, the accessible phase space can be larger. It is immediately obvious that all stages of plasma condensation can in principle be examined experimentally over a vast range of parameter space. It may be possible to use other laboratory plasmas and extend the research limits even further, but such investigations are only just beginning.

We have indicated in Fig. 1.3 the range of phase space where the Debye screening can be important. The curve for non-linear screening can be also drawn but usually at the point where the Coulomb potential becomes almost

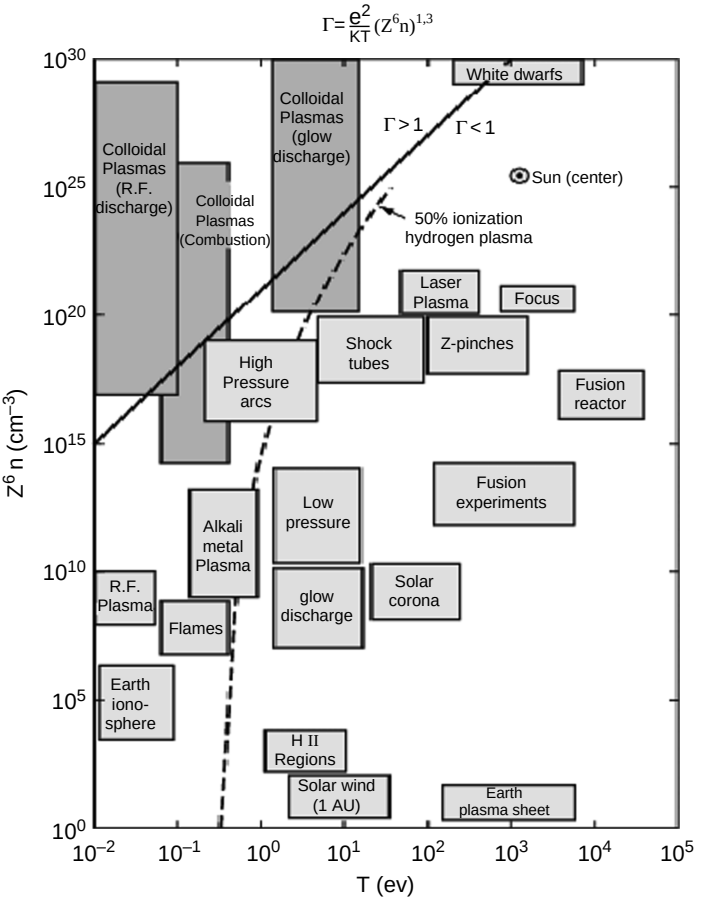

Fig. 1.3. Parameter ranges applicable to different laboratory and natural plasmas. "Colloidal plasmas" (complex dusty plasmas) allow for the experimental investigation of strongly coupled regimes including liquid and crystalline complex plasma states. The solid line shows $\Gamma \approx 1$ line, which marks the transition from strongly to weakly coupled states

entirely screened other type of collective interaction can be also important. Experimental determination of the correct value of the screening factor and the deviations of the potential from the screened Coulomb potential as well as the possible presence of dust attraction is a field of vigorous experimental and theoretical investigation at present. This renewed interest has, of course, been triggered by the discovery of plasma condensation, where not only the screening process itself (screening in the general sense of changing the potential including possible attraction) but also interactions of screened particles are of great importance.

1.5 Openness of Complex Plasma Systems and Long-range Collective Interactions

1.5.1 Variability of Grain Charges

Complex plasma at first glance consists of several components (dust, electrons, ions, and neutral atoms) and the question is whether the dust component can be considered as very heavy and highly charged ions. Complex plasmas behave quite differently from multi-component plasmas with fixed charges on ions. Multi-component plasmas were investigated both theoretically and experimentally many years ago ([64, 65]). The difference is in *variability of grain charges*. This variability is related to the dust charge determined by the local plasma parameters such as electron and ion densities and temperatures. This is obvious since the charging process depends on plasma currents and therefore on local plasma parameters. One can say that the dust charge is not fixed by any external condition but is determined by local properties of a complex plasma system. Moreover, it depends on the presence of other dust particles, their proximity to each other, and other conditions for dust.

Indeed, from the quasi-neutrality condition (1.4) one finds the electron to ion density ratio to be

$$\frac{n_e}{n_i} = 1 - P \,, \tag{1.15}$$

and the local value of it should obviously determine the dust charge since it appears as the balance of electron to ion currents on dust surfaces. Since $P = n_d Z_d / n_i$ depends on dust characteristics such as mean dust separation (dust density) and on the values of dust charges, it is also obvious that the charge of each dust particle depends on how close to it are other dust particles. By moving one particle from one place with a certain dust density to another place with another dust density, the dust charge should change. One can say that the dust charges are adapting to the charges of neighboring dust particles and to the local plasma parameters. This is quite different from multi-charged ions.

When forming strongly coupled state in complex plasma systems, the final position of "frozen" dust particles are determined not only by the interaction energy of the fixed dust charges. Indeed, due to the variation in dust charges in the formation of the strongly coupled state, the charges of dust particles and the forces between them are adjusted in this transition. Moreover, one can expect that interactions between dust particles and their charges depend on dust density. Thus we can expect that the strongly coupled state in complex plasma systems is qualitatively different from the ordinary strongly coupled state discussed previously. Presence of such a charge-adjusting process depends on how fast is the charging process as compared to the characteristic time of the dust kinetic process related to their possible movement. Due to the large dust masses the latter process is much slower than the charging process (the explicit estimate is given below) and the presence of the process of

charge adjustment and the change of inter-dust interactions can be foreseen from physical point of view.

We should emphasize that this charge variation should not be mixed with charge fluctuations which should, as usual, in the first approximation correspond to the law of random numbers $(\delta Z_d)^2 \approx Z_d$, where Z_d is the equilibrium charge determined by local complex plasma parameters and δZ_d is the fluctuation of the dust charge. The relative value of the charge fluctuations is small (could be less than 1%),

$$\frac{(\delta Z_d)^2}{Z_d^2} \approx \frac{1}{Z_d} \ll 1 \tag{1.16}$$

for $Z_d \gg 1$ (estimates for $Z_d \approx 10^4$ demonstrate that the relative charge fluctuations are less than 1%).

Regarding dust variations, we have in mind the *variation of the equilibrium charge itself.* Indeed the variation of the equilibrium charge $(Z_{d,1} \sim Z_{d,2})/Z_{d,1}$ (where $Z_{d,1}$ and $Z_{d,2}$ are two values of the equilibrium dust charge at different positions 1 and 2) can be much larger than the fluctuations (by an order of magnitude); this relative change should be estimated as a relative change in plasma particle densities or a relative change in the parameter P. Thus *the main difference between complex plasmas and multi-component plasmas is the charge variability and the collective effects related to changes in interactions due to the presence of many grain particles – collective effects of grain–grain interactions.* Generally in such physical situations, in fact, the grain charge must be considered as an independent new variable to describe the transition to the strongly coupled state. The variability of dust charges is an important source not only for the formation of strongly coupled states, but also in weakly coupled states of complex plasmas for processes slower than dust charging including many new collective complex plasma modes.

A major consequence of the charge variability is that *the electrostatic field force acting on grains* $-Z_d e\mathbf{E}$ *is not potential* since $\nabla Z_d \mathbf{E} = \mathbf{E} \cdot \nabla Z_d \neq 0$ and dusty plasmas are non-Hamiltonian systems. Therefore,

1)The energy of grains in an electrostatic field cannot be given by the common expression $-Z_d e\phi$ (with ϕ being the potential of the electrostatic field). It cannot be even defined without fixing external sources that can change the grain charges. *Free energy is, strictly speaking, impossible to define without fixing the free energy of the sources charging the grains.*

2) *Complex plasma systems are not Hamiltonian systems.*

3)The *grain vortex formation* is a rather general phenomenon in complex plasmas ($\nabla \times Z_d \mathbf{E} \neq 0$), which is determined by self-consistent gradients of grains charges.

4) In "multi-component plasmas," the charge of heavy ions is usually fixed. Therefore, *complex dusty plasmas are quite different from multi-component*

plasmas. Both of them are described by different physical processes. This means that the strongly coupled states in multi-component plasmas and in complex plasmas can be very different.

All these statements mean that such strongly correlated states in a complex plasma as liquid and crystalline states should have specific properties unlike those known previously for liquids and crystals in ordinary matter. An additional difference between strong coupling in a complex plasma and the usual strong coupling is that only one of the components of the system (namely the grain component) is strongly coupled. All the aforementioned effects lead to important qualitative differences between strongly coupled complex plasmas and the strongly coupled systems of ordinary matter.

1.5.2 Openness of Complex Plasma Systems

Another important difference between complex plasmas and ordinary matter is the much greater openness of complex plasma systems. Thermodynamically, we generally require that the system is an "open" system if energy has to be supplied in order to maintain its equilibrium. This equilibrium is practically established by some physical process such as particle collisions. The main question is whether these physical processes are fast enough as compared to the energy and plasma supply. If they are not fast enough, we deal with a real open system which is far from equilibrium. The presence of grain changes substantially influences the equilibrium not only because of the variability of the grain charges but also because the grain-charging processes are very effective and the rate of electron/ion absorption on grains is very high. The equilibrium grain charges needed for strong coupling require also a high rate of energy supply to the system to compensate the electron/ion losses on the grains due to their charging.

The presence of ionization is always necessary for complex plasmas to exist since due to the fast ion and electron absorption the absence of an ionization source results in fast plasma decay. One can argue that recombination would ultimately turn ionized plasma into a neutral gas, i.e., into a different state of matter, e.g., in space plasmas. But in laboratory plasmas the volume recombination is negligible as compared to that on dust grains absorbing electrons and ions or on the walls of experimental devices. Of course, the recombination time in some tenuous astrophysical systems may be even longer than the age of the universe. But the thermalization of complex plasma components can be also very long in laboratory plasmas as compared to the time-scale of experiments. In complex plasma systems, the process can establish full equilibrium only for very large time scales. Presence of grains changes considerably the recombination of plasma particles: for actual experiments plasma electrons and ions are recombining mainly on dust particles.

Let us make some simple estimates and show that recombination on grain particles is so fast in a complex plasma that it requires a strong ionization

source. In most experiments such a source always exists (examples are experiments in RF discharge or those using UV radiation). This source should work almost continuously to compensate the high rate of plasma recombination on grains. Thus the complex plasma system becomes *completely open since the source should rapidly supply the system with both energy and plasma particles.* The supply of new electrons and ions can be either a volume process operating inside the grain cloud or a surface process. In the latter case, electrons and ions are supplied by an external flux of plasma from the region where the grains are absent.

We have been speaking about the equilibrium grain charges that are reached when the flux of electrons on a single grain becomes equal to the flux of ions on the grain. When embedding a new grain into the plasma, its equilibrium charge is established in a short time, called the **charging time**. After the equilibrium charge is established, it is further maintained by these fluxes of electrons and ions, which do not change the grain charge since the electrons and ions bring equal charges but *the flux of electrons and ions on dust particles is continuously present after the equilibrium charge is reached.*

Thus, roughly speaking, there exists the plasma sink at the position of every grain. The whole stationary state with some average electron and ion densities can be established only if this sink is continuously compensated by the ionization source. For example, for relatively low dust density $n_d \approx 10^4 \mathrm{cm}^{-3}$ and room ion temperature, the time of the ion–electron recombination on grains in an argon plasma is a fraction of milliseconds (10^{-4}–10^{-5}sec). In such short times, the complex plasma completely disappears if not supported by an external ionization source. Thus dust grains having large charges are not only centers of the electrostatic fields which can be visualized as electrostatic outward field lines (as indicated by the outward lines in Fig. 1.4) existing up to the screening distances but also centers of plasma flux absorption and flux field which can be visualized as plasma flux inward lines (the inward lines in Fig. 1.4 starting at the characteristic size λ_{flux}, where the main flux is created; outside λ_{flux} the total flux is conserved, and the flux at distance $r > \lambda_{flux}$ per unit surface area is $\propto 1/r^2$).

One can easily understand how in principle to measure the electric field strength of a single grain (field lines shown in Fig. 1.4) or to measure the dust charge itself (which was performed in a number of experiments; the first measure of the dust charge in a strongly coupled state of a complex dusty plasma was done in [4]). The question is, could there exist direct or indirect experimental evidence of the presence of the plasma flux shown by the flux lines in Fig. 1.4? Dust particles used in experiments are not completely spherical even in those experiments where specially prepared almost spherical dust particles are used. The reason for that is the material deposition on the grains in plasma and dust agglomeration [9, 37, 38, 66]. Therefore, at least in a weakly correlated state the presence of plasma flux on dust particles can be manifested by a rotational motion of dust particles since the flux usually transfers an angular momentum that decreases with an increase in

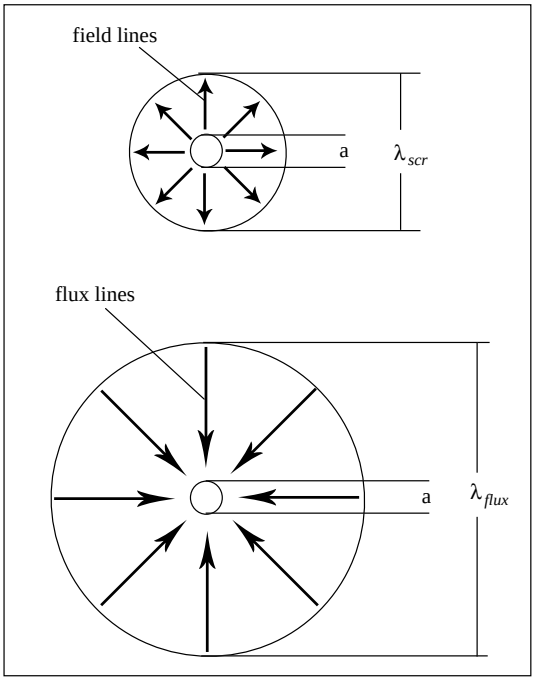

Fig. 1.4. Sketch of the effective screening length λ_{scr} of a dust grain and the effective length λ_{flux} where the flux in the grain is formed

the spherical symmetry of the dust particles. Such rotation for non-spherical grains has been seen in some experiments [2, 3, 4, 5]. An interesting question is, how this rotation can influence the plasma condensates in a strongly coupled state? We return to this problem later.

The electric field lines of individual grains should be screened at some charge-screening distance, say λ_{scr}, by the plasma polarization charges which are accumulated close to the dust particles. The flux lines also have some characteristic length, say λ_{flux}, at which the flux is formed, and this length is determined by the mean-free path of plasma particles to charge the grain and therefore depends on the dust density. Thus we should deal in complex plasmas with *two lengths instead of one screening length, as in ordinary plasmas.*

Note that the grains can be considered in some approximation as point particles only if the grain charge screening length is much smaller than the size of grains

$$a \ll \lambda_{scr} \tag{1.17}$$

since usually $\lambda_{flux} > \lambda_{scr}$. In existing experiments, this condition is often fulfilled and the grains are approximately point particles although in many aspects (such as the grain–grain interactions) the finite size of grains is very important and there exist forces important for the grain dynamics vanishing in the limit where the grain size becomes zero. In space plasmas, inequality (1.17) is usually also fulfilled since the screening length is very large.

In the approximation (1.17), the second "screening" length λ_{flux} is determined by the charging process and usually is much larger than the first one, λ_{scr} (as we demonstrate later, $\lambda_{flux} \approx \lambda_{scr}^2/aP \gg \lambda_{scr}$ for $a \ll \lambda_{scr}$ and $P \sim 1$). The expression for λ_{flux} can be estimated from the charging length (see below Sect. 3.3.1). The presence of flux changes completely the physics of grain interaction and screening of grain fields. The main physical reason for that is that the screening polarization charge density depends on the plasma flux, and the flux depends on the screening polarization charge. This mutual influence of flux and screening changes qualitatively both the screening and the grain interactions. We consider the important role of the screening lengths in grain interactions later in more detail.

It should be emphasized that the collective flux can be different from the sum of fluxes of individual grain particles because each of them is changing the flux directed to other particles. The collective flux can cause in a complex plasma a new phenomenon, namely the *confinement of finite size complex plasma systems like complex plasma bubbles by the self-generated flux*. This is especially important in the case where a complex plasma is surrounded by an ordinary plasma without grains, and the external flux to the bubble (cloud of grains) is related to the grain charging. The phenomenon of collective fluxes should be taken into account in all physics of complex plasmas and its condensation into liquid and crystalline states.

Let us clarify this point and consider a cloud of grains of a certain size surrounded by plasmas without grains. The individual flux on each grain creates the total collective flux on the surface of the cloud, which by its ram pressure can confine the complex plasma system of a certain size. One can expect that such a confinement can occur for sizes not larger than some critical size. Whether the latter is correct or not can be checked in experiments by trying to create a strongly coupled system of the maximum size. The problem of the maximum possible size of a strongly coupled system does not arise in ordinary matter where in principle crystals can be created of any size. But ordinary mono-crystals in ordinary matter are not larger than a certain size. In a complex plasma, the size of the plasma crystal can be determined by confinement via collective flux and otherwise a poly-crystal can be created. Thus the situation in a complex plasma is quite different from that in ordinary matter, where the size of a strongly coupled system is either unlimited or is determined by the molecular or surface forces. In a complex plasma, it is mainly an experimental question: how large can the mono-crystal structure grow?

Summarizing the above arguments, we should emphasize that from a physical point of view a *complex plasma in both the weakly and the strongly coupled states represents a state of matter quite different than that usually ordinarily met*. Experiments are available to investigate the unusual properties of complex plasmas.

1.5.3 Long-range Unscreened Grain Interactions

The flux on an individual grain is conserved and exists at distances much larger than the screening distance. This flux therefore exists at distances where other grains can be located and the fluxes from different grains can be superimposed creating a collective flux. This leads to collective dust interactions, depending on the average dust density or on the parameter P. All these long-range interactions depend on the dust size a or the dust surface πa^2 and therefore can be named the "shadow forces."

It has long been known that a single isolated grain the field, due to the presence of plasma absorption, is not completely screened [67, 68] and far behind the screening radius there exist an unscreened potential decreasing with the distance as $1/r^2$ (recall that the unscreened Coulomb potential decreases with distance as $1/r$). The appearance of the unscreened potential for an isolated grain is related to the non-collective flux on dust particles and is proportional to the dust size a. The factor ψ (in front of the Coulomb potential) for this unscreened potential is found to be [67, 68]

$$\psi = \frac{a}{2r} \, . \tag{1.18}$$

This kind of potential exists only for single grains or, in the case of many grains, if the mean-free path for ions absorbed by grains is much larger than the size of the system or the inter-grain distance.

The shadowing of grain fluxes for two isolated grains creates the potential of an attractive type (see the detailed description below Sect. 5.2 in this book):

$$\psi \approx \frac{a^2}{\lambda_{scr}^2} \, . \tag{1.19}$$

The attraction is substantially changed and increased by collective effects, and is determined by P. The unscreened attractive potentials are usually weak as compared to the Coulomb unscreened repulsion potential, but the latter can be screened sometimes almost completely. When the screened Coulomb potential is small, the attraction starts to play a role; this attraction is determined by parameters related to the openness of the system and the presence of collective or non-collective fluxes. Thus intuitively one can expect that due to the effects of flux and screening, the grain interaction is a classical analogue of molecular interactions: repulsive at small inter-particle distances and attractive at large inter-particle distances. This can be the basis for formation of a new type of molecules, of a new periodic system of grain clusters, and, finally, of grain crystals. The pressure from outside by using an external confining potential can also help to form crystal states. As was mentioned, the transition to the plasma crystal state is called "plasma condensation" in the physics of complex plasmas.

1.6 Plasma Condensation

1.6.1 First Observations of Plasma Condensation

Complex plasma condensation is quite unlike other known condensations such as gas–liquid, gas–crystal, or liquid–crystal condensations in ordinary matter. The usual transitions that occur when a hot ionized gas is cooled are characterized by recombination, possibly some gas phase chemistry, eventually liquefaction and then solidification. In plasma condensation, the plasma retains its identity, as indicated by the definition quoted at the beginning of the introduction, i.e., plasma particles still interact among themselves weakly and the average kinetic energy of electrons, ions, and even neutral atoms is still much larger than their interaction energy. The charged grain components interact strongly enough to generate macroscopic (on relevant plasma scale lengths) correlations – up to long-range ordering – as in crystals. These correlations exist in all other components induced by the grain component, although the relative change in density and other parameters of these components is not large since their kinetic energy is still large. But in the strongly coupled complex plasma state the grain interaction energy can be larger or much larger than the dust kinetic energy (we are speaking here only about unscreened grain interactions with a view to correct this picture by taking properly into account the grain screening). This leads to the typical complex plasma condensation, and the corresponding complex "**liquid plasmas**" as well as the complex "**plasma crystals**" are therefore new states of matter of a type not previously discovered.

The properties of these complex plasma states may be – and probably are – substantially different from other types of condensations occurring in nature. The last statement is not 100% certain since there are many places in space occupied by low-temperature plasma clouds containing a lot of grains, and such condensation probably can occur also in nature. We note that not only the plasma condensation states can have unknown new properties but also all states preceding the condensation in a complex plasma can have unusual properties. Thus the transition itself is from new type of states to new correlated states either with short-range correlations or with long-range correlations. New phenomena which could occur are, e.g., long-range correlations for different degrees of freedom (such as translational degrees and rotational degrees) that do not appear simultaneously.

Figure 1.5 shows the long-range ordered state observed in one of the first experiments [2]; this is one of the first observed images of the condensed plasma state. We see the crystalline state and one lattice plane. The bright dots are the individual particles (micro-spheres) injected into the plasma. The particles are illuminated with laser light and observed via reflected light. Next Fig. 1.6 shows the crystalline state first observed in DC glow discharges [6].

It is obvious that to use complex plasmas for the investigation of condensed plasma states and to observe the transitions to these states one should have in mind the existing restrictions:

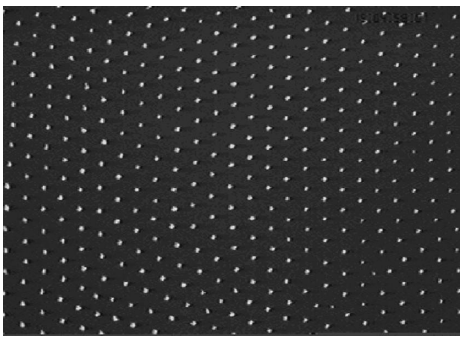

Fig. 1.5. CCD image of a horizontal lattice plane of a plasma crystal: (top view obtained in one of the first experiments on new complex plasma states [2]). Experiments were performed in the plasma sheath; the area shown is 6.2mm^2 and contains 392 grains of $\approx 7\mu\text{m}$ diameter

- The grain component should be sufficiently cold not only to meet the criterion of transition to the strongly coupled state but also not to be melted (these are injected micro-spheres in experiments [2]). Of course, the micro-spheres or other shaped particles in particular experiments could be made from special material. But in general the injection of grains of different types [69] or creation of grains in a plasma (possibly by chemical reactions as in [3]) is possible. The question is, whether the grains will grow or melt in plasma? This is the question for current experiments and the temperature ranges used. The question is one of balance of the different processes that can lead either to growth in the grain's size or to decrease in size and melting. It is certain that there exist numerous experiments, especially in etching industry and deposition techniques [9, 37, 38] where only or, more precisely, preferentially the grain growing is observed. The process of the grain charging described above means that ions and electrons which collide with the grain surfaces are attached to them. Such processes were confirmed experimentally. The presence of a continuous plasma flux on grains means a deposition of material at the grain surface and the growth in its size. This process indeed takes place in a certain electron temperature range of several eV up to 8–15eV, and the ion temperature

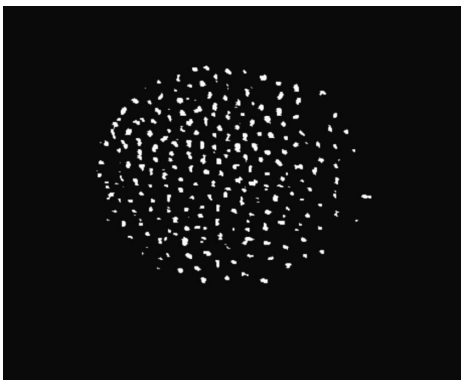

Fig. 1.6. Image of a dust plasma crystal obtained in one of the first experiments in DC glow discharge [6, 59] using Al_2O_3 dust grains for a gas pressure of 0.3 Torr

less or of the order of 0.03eV. Experimentally it was observed that dust can grow in low-temperature discharges up to a millimeter size. For higher temperatures new processes can be involved (secondary electron emission, etc.). The process of grain destruction by electrostatic forces related to their large charges operates only for small grain particles. Thus a rather broad range of temperatures where the micro-spheres or other grain particles can survive for very long time really exists and the grain particles in this range can grow in size; moreover in some conditions it is even difficult to avoid the processes leading to growth in grain size.

- For long-term investigation of transitions to strongly coupled state, one should always keep in mind that the plasma has to be replenished due to its fast recombination on dust particles. If this is provided by some external source, the plasma particle distributions can be fast replenished and can be determined by the source itself. It is certain that the absorption on grains due to the charging process makes the electron and ion distributions non-thermal. This process competes with (usually also non-thermal) production of electron–ion pairs by the source, while the binary plasma particle collisions and the collisions with walls both have a tendency to make the plasma particles to be thermal (if the walls are kept for certain thermal conditions). The requirement of compensation of continuous electron–ion recombination on grains can be usually fulfilled only by continuously operating ionization source.
- For long-term investigations one should avoid grain agglomeration, where two or more grain particles of relatively large sizes merge to one agglomerated large grain particle. This process was observed in etching technology [9, 37, 38] and occurs on rather large time scales (etching is carried out over several hours or several days). The physics of agglomeration is determined by forces between dust particles and we return to discussion of this problem in detail later.
- In laboratory experiments on Earth, one should take into account restrictions imposed by the Earth's gravity. The larger is the size of grains the larger is the possibility to obtain a strongly coupled state since the charge on the grain, as it was pointed before, is proportional to the grain size. But the larger is the size of the grain the larger is the gravitational force. On the Earth grains should be suspended electrostatically against gravity. The balance with gravity restricts the position of grains and in large part avoids the grain-charge adjustment in the formation of strongly coupled states. The crystalline state shown in Fig. 1.5 was obtained within the Earth's gravity field. Much more flexibility for complex plasma condensation appears for experiments carried out under micro-gravity conditions.

The listed restrictions are not very difficult to satisfy. With these restrictions, a number of plasmas generated by different techniques offer themselves for the investigations – RF plasmas, inductive plasmas, DC discharges, UV plasmas, radioactive plasmas, and combustion plasmas. Of these, RF

discharges are at present the most widely used (Fig. 1.5 was obtained by using RF plasmas). The strongly coupled states were also obtained in DC glow discharge plasmas [6, 56, 59] (an example is given by Fig. 1.6), as well as in other plasmas already mentioned.

1.6.2 Grain Interactions

An important aspect of the problem of complex plasma condensation is the investigation of the grain interactions in the state before the condensation happens as well as in the state after the condensation has already occurred. *The interaction does not appear to be of the types of screened Coulomb potential as in ordinary plasmas*. It could be different and includes other type of potentials or forces, such as *attraction forces*.

The main physical reason for the phase transitions to crystal states, e.g., in an ion crystal, is not only the presence of a molecular type of binary attraction between the atoms but also a rearrangement of particle distributions in such a way that an enlarged electron density occurs between equally charged particles, which can cause their additional attraction. The openness of the complex plasma system and the constant presence of plasma fluxes (needed to support the system) can change the grain–grain interactions. To explain this point in detail we should provide a description of the elementary processes in complex plasmas; such a description can also serve as an introduction to the physics of a complex plasma.

Without an understanding of simple physical processes in complex phenomena encountered, the process of condensation would be incomprehensible. Indeed, it is rather difficult to be oriented in complex phenomena met in the process of condensation. Without such an understanding, the description of plasma condensation is merely a phenomenology. *Understanding of the physics of strongly coupled states is the most important aspect of the problem*; it is also the most difficult one since the effects related with condensation are collective in nature and therefore we need to understand the processes taking place in the presence of many grains. The elementary processes described below do not provide such full treatment but at least their knowledge is important to make further steps to understanding the collective interactions. Some of these steps can be achieved by considering interactions of two test particles in the "sea" of homogeneously distributed grain particles. This kind of interaction referred to below as collective grain–grain interaction is described by a simple balance of forces for the "ground sea" grain particles and gives some elementary sense for what kind of interactions can happen in the process of condensation in complex plasma systems.

The most favorable interaction for the formation of long-range correlations can be an interaction that is repulsive at short distances (as the Coulomb interaction should be for lengths less than the charge screening length) and attractive at larger distances (say, larger than the screening length). Then the potential of interaction of two grain particles can look like an ordinary

molecular potential. This has consequences for the formation of long-range correlations similar to those in ordinary matter, with the exception that the size at which the attraction appears is not determined by quantum effects (as in usual matter) but by classical effects of collective nature. The nature of these effects is related to the presence of a collective plasma flux absorbed on each grain particle. As we demonstrate later, these effects indeed exist [70, 71, 72, 73, 74] (due to both the non-collective flux and the collective flux). We will discuss the accessibility of experimental detection of such an attraction later since it should be discussed both in the context of experiments already performed and in the context of a discussion of other possible attraction forces acting between grain particles. Several indirect experimental evidences that the attraction forces do indeed exist in a complex plasma were reported in experimental work [75].

1.7 Special Aspects of Complex Plasma Investigations

1.7.1 Kinetic Level for Dust Investigation in Experiments

An important aspect of experiments in complex plasmas is the possibility of obtaining a kinetic level of description of macroscopic properties. We use Figs. 1.7 and 1.8 to illustrate a general aspect in the complex plasma research – *the possibility of visualizing individual grains* [53, 76] – and follow their trajectories, dynamics, and evolution not only in the final condensed state but through all transition stages. We demonstrate in Figs. 1.7 and 1.8 the change in particle vibration energy during the transition from the plasma crystal state to a disordered gaseous state [53, 76]. The fluctuations can be easily measured and their dependence on the scale of fluctuations can be determined.

Figure 1.9 illustrates the possibility of investigating on the kinetic level of crystal melting and crystal formation. By decreasing the ionization power, one can melt the crystal and then, by restoring the power, investigate the process of recrystallization on the kinetic level. This process can start and propagate as a crystallization wave [77] with a thickness of several lattice separations.

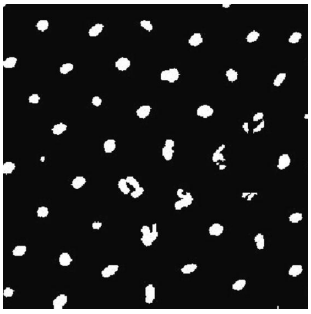

Fig. 1.7. The side view of the plasma crystal in the vibrational state before melting. This figure illustrates that the vibrations of the particles are essentially isotropic. The time of exposition is larger than the period of vibrations; therefore the size of the white spots gives the measure of the amplitude of oscillations. For short time interval one can follow the vibrational motion of an individual grain. Melting begins at the bottom of the crystal [63, 76]

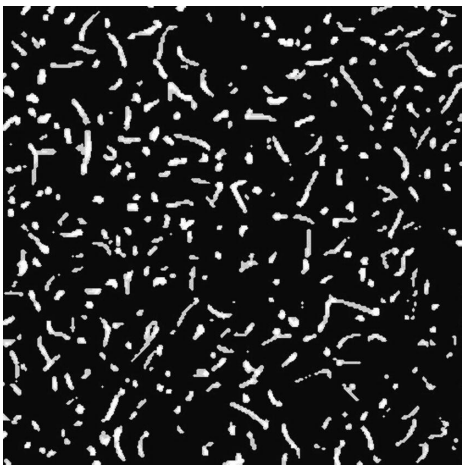

Fig. 1.8. Start of the disordered state. The original video image taken with an exposure time of 0.02s at the neutral gas pressure of 0.13 mbar. The area shown is $3.9 \times 4.1\,\mathrm{mm}^2$. The white lines represent the motions of individual grains during the exposure time [63]

The crystallization can start at different positions depending on the initial density compression conditions, and different crystal structures can propagate in different directions, creating a dislocation after crossing the crystallization fronts. When the initial conditions for the first crystallization and for the recrystallization are different, the crystal defects appear to be different [77]. One should mention that in these experiments the plasma crystals have 100 planes, while in the first experiments there were maximum number of 15–17 crystal planes. The scales in Figs. 1.10 and 1.11 are much smaller than those in Fig. 1.9. This was done in order to show the whole crystal including all its planes.

The main problem in ordinary matter crystals is whether they are mono-crystals or poly-crystals and whether for poly-crystals the crystal structure is the same (or it is different) in different parts of the crystal. In the first case we deal with crystals with the same crystal structure but with defects, while

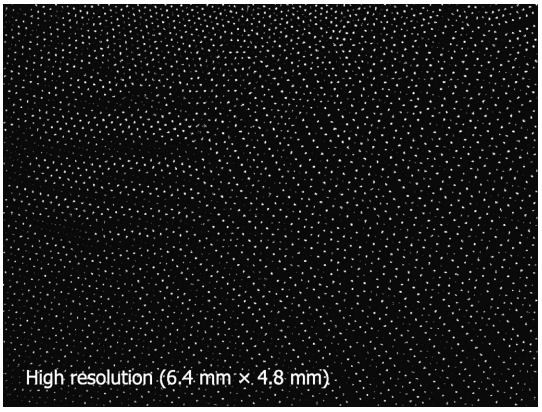

Fig. 1.9. The crystallization that started in the lower left corner propagates to the right upper corner, where the system is in the gaseous state. The horizontal and the vertical scales are given in units of 0.01mm

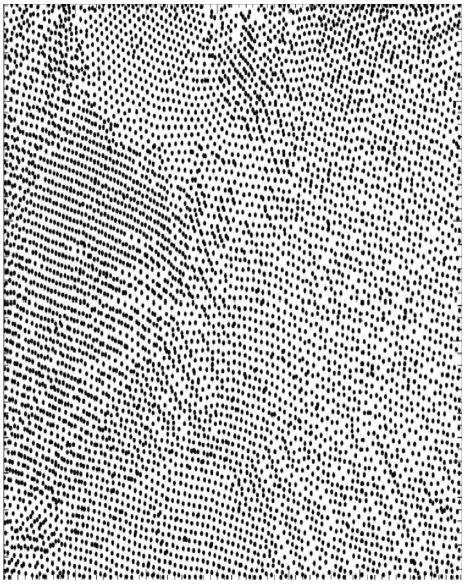

Fig. 1.10. The crystal structure before melting [72]

in the second case we are dealing with crystals formed by different crystal structures in their different parts. In fact, this problem can be considered as a problem of defects in the crystal lattices. Note that the problem of crystal defects is one of the major problems in crystal physics. Figure 1.10 shows

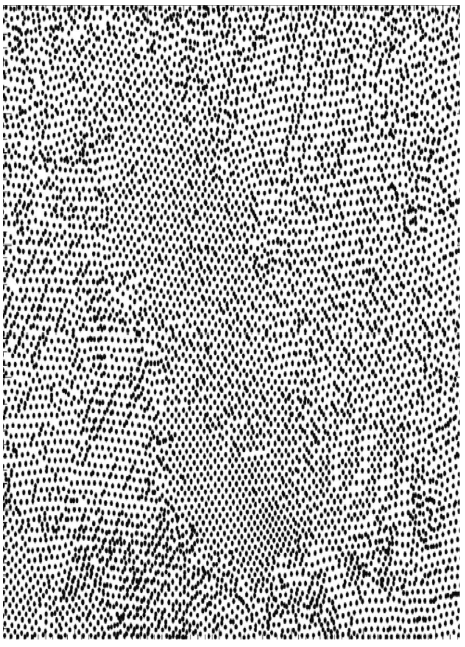

Fig. 1.11. The crystal structure restored after the perturbation causing the melting is removed [77]

the presence of a complex set of defects in the crystal before melting and subsequent recrystallization [77], and Fig. 1.11 illustrates the structure of the crystal when it is restored as soon as the perturbation causing the melting is removed. The structure of defects is substantially changed after recrystallization [77]. This result can be obtained on the kinetic level observing any particular defect in the crystal structure. It is therefore rather important in future complex plasma physics when using these crystals (on future industrial applications of complex plasmas see Chap. 2).

Many details of the process of crystallization from the gaseous state can be also measured and investigated. Such possibilities of investigation of the process of crystallization itself and fluctuations during the crystallization cannot be measured in ordinary matter. Therefore they are of fundamental interest in general physics of complex plasmas.

Thus condensation can be investigated experimentally on the kinetic level in a complex plasma. Of course the grains constitute only one component of the system but this component is the most important in a strong coupling situation. Such possibilities do not exist in transitions in ordinary matter; for phase transition one deals with average properties and the structure of fluctuations, i.e., with deviations from average properties, but one cannot follow the individual particles or investigate the transitions on the kinetic level.

Apart from the condensation phenomena in a complex plasma it becomes possible to investigate the kinetics of the gaseous phase and check some general assumptions previously used without experimental proof in the present kinetic approach to ordinary matter. Also by measuring the full distribution function of grains $f_d(\mathbf{r}, \mathbf{p}, t)$ we have an unprecedented tool for developing a plasma transport theory, at least in principle. The type of distribution function $f_d(\mathbf{r}, \mathbf{p}, t)$ can be used only for fast motions, while for slow motions the grain charges should be considered as a new independent variable Q. New kinetic description of a complex plasma should use the distribution function $f_d(\mathbf{r}, \mathbf{p}, Q, t)$, and such a kinetic approach can be referred to as the kinetics of new complex plasma states (some first theoretical steps have already been made in the theory in [78]). The problem of the experimental investigation of the kinetic of complex plasma can be stated and determined and is a task for future research. We return to the problems of new kinetics later.

1.7.2 Obstacles in Complex Plasmas

New research possibilities also opened in investigations of the kinetics of flows around obstacles [79]. Ordinary air and liquid flows of ordinary matter around obstacles are not fully understood even in the simplest hydrodynamic approach, although enormous efforts have been made in this direction due to the importance of the processes for such applications as airplane resistance to flows, hydraulic technology, air and liquid flows at the edges of material

bodies creating a shear flow, turbulence formation, etc. These are only a few examples of the extremely broad area of hydrodynamic research with far-reaching applications. The research in this field is still half phenomenological. The reason for this is not only that a complicated system of vortices, shear flows, etc., is excited by different hydrodynamical motion and not only that they strongly interact with each other, but also the necessity to describe the processes kinetically.

Most theoretical or numerical investigations are based on the hydrodynamics with different dissipation processes such as friction, viscosity diffusion, etc. These investigations show that the size of the shear flow, vortex creation, etc. is of the order of the collision mean-free path. But the hydrodynamics is applicable only to inhomogeneities that are much larger than the collision mean-free path. Thus the kinetic description is obviously necessary since the characteristic size is in between the hydrodynamic limit and the collisionless limit. Complex plasma research provides a visualization of the process related to the excitation of vortices, shear flows, and turbulence.

In Fig. 1.12, we present the results of first experiments of observation of a micro-particle flow around an obstacle [79]. The wake behind the body exhibits two eddy systems as reminiscent of a so-called Karman vortex street and is schematically shown in Fig. 1.13, while further along the grain flow a shear mixing layer can be seen which is related to formation of turbulence [79]. This region with a shear flow is magnified in Fig. 1.14. Both the Karman street and the shear flow could be investigated on the kinetic level following the dynamics of individual grains. The shear flow describes interaction of two different clouds of grains with different velocities far from the interaction

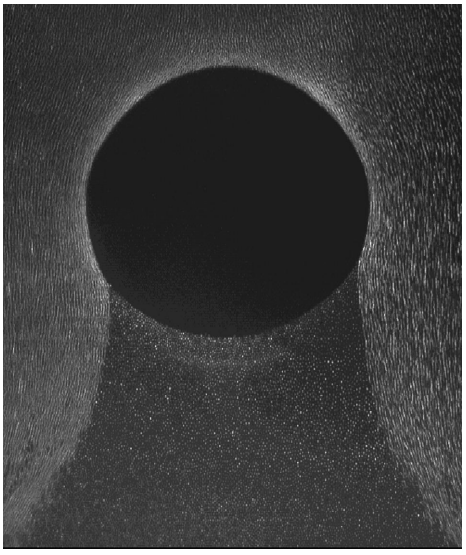

Fig. 1.12. The structure of the grain flow behind a spherical obstacle [79]

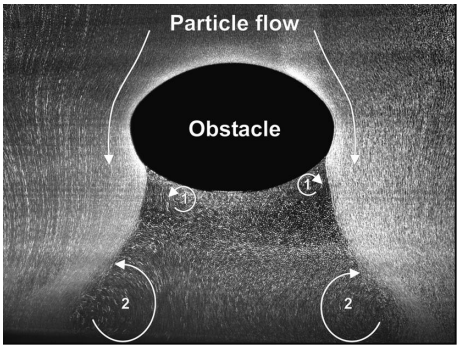

Fig. 1.13. The scheme of Karman vortex street excited behind an obstacle in a grain flow. 1. region behind the obstacle where small size vortices are created, 2. region behind the obstacle where large vortices are created [79]

shear region where the grain velocity continuously varies from one cloud (the moving cloud as in the example described above) to that of another cloud (the cloud at rest as in the example described above).

1.7.3 Interactions of Grain Clouds and Fast Grains with Plasma Crystals

There can exist other important interactions of grain clouds including a penetration of one cloud through another. These clouds can be in different states, either gaseous, liquid, or crystal. In the first case we expect the two-stream instability; in the second we expect the liquid mixing or Kelvin-Helmholtz instability; and in the third case quite a new phenomenon appears that for finite-size crystals can be called "walking through the wall" [80]. Indeed, this name is appropriate if one crystal can penetrate through another crystal and

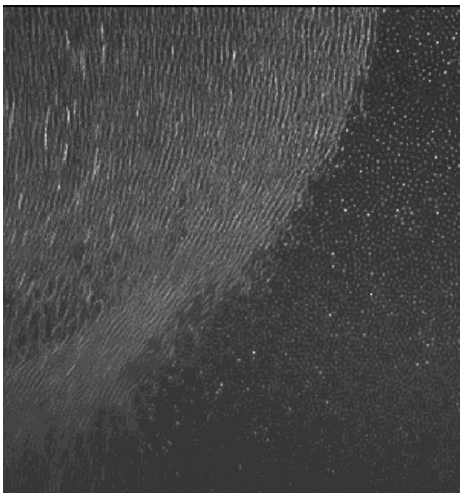

Fig. 1.14. The shear flow excited by an obstacle in the grain flow [79]. The shown region corresponds to the zoomed region in the lower left edge of Fig. 1.12

finally both of them are restored in the original form. This is a collective effect where many particles of one crystal collectively disturb the positions of particles of another crystal in such a way that they can, with smaller momentum, penetrate through the second crystal. Also, a single particle could move through a cloud of particles by decreasing the charges of particles on its path though the crystal. Thus the penetration of fast particles through crystals has no direct analogy with the channeling of particles though crystals in ordinary matter. The propagation of a cloud of particles through plasma crystals is even more complicated and is related to collective tunneling. The latter can be considered a kind of spatial instability that moves the particles of the crystal and changes their charges in such a way that the cloud can penetrate through the crystal.

First observations of these processes on the kinetic level were made in experiments under gravity in complex plasmas between the planar electrodes. Usually, close to electrodes there exists an ion flow toward the electrodes related to their negative charge. Close to the lower electrode the gravity and the ion-flow drag operate in the same direction and the electric field in the opposite direction; thus the grain can levitate forming either a gaseous, liquid, or solid state. At the upper electrode, the gravity and the drag force operate in opposite directions, however, the levitation is still possible for large drag, but the dust cloud observed is usually smaller. It can be also in different states – gaseous, liquid, or solid state. This experiment is performed using thermophoretic force to levitate the particles in the earth gravity. By changing the potential and the thermophoretic force between the electrodes one can create the conditions where the upper cloud becomes unstable. This starts with single dust grains falling to the lower cloud and develops to the falling of the whole upper cloud to the lower cloud. In this manner one can investigate on the kinetic level both the penetration of single grains through grain clouds and the interaction of two clouds. Figure 1.15 shows the first stage of instability of the upper cloud, where a single dust grain starts to fall to the lower cloud, and Fig. 1.16 shows the development of a two-stream instability of interacting clouds [80].

Propagation of a fast grain through a crystal should be accompanied by a local change in grain charges at the position of the propagating grain followed by excitation of different crystal modes. The dissipation of energy during the processes of crystallization is also related to the excitation of different modes in both the crystal and the gaseous states. The propagation of fast particles through a medium is a large branch of physics, but this process has never been investigated on the kinetic level.

A special case is when the grain velocity is larger than the phase velocity of the corresponding waves in the crystal. Then the fast particles excite the Mach cones. Often these cones are non-linear due to interactions of different excited modes. This process has also never been investigated on the kinetic level. In Fig. 1.17, we show the first experimental results of the excitation of a

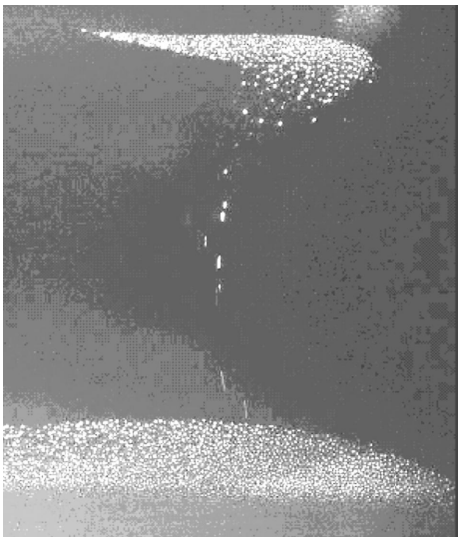

Fig. 1.15. Starting stage of the instability of the upper grain layer where a single dust grain starts to fall on lower grain layer [80]

Mach cone by a fast particle moving below a two-dimensional plasma crystal at distances less than the length of the excited wave.

Propagation of one cloud through another can be followed by the formation of streets of fast grains where they penetrate behind one another forming the so-called lanes. The lane formation is followed also by grain charge reduction along the lanes and excitation of waves in the direction perpendicular to the streaming velocity. The first observation of the lane formation is shown in Fig. 1.18. Another example of how the process can be observed on

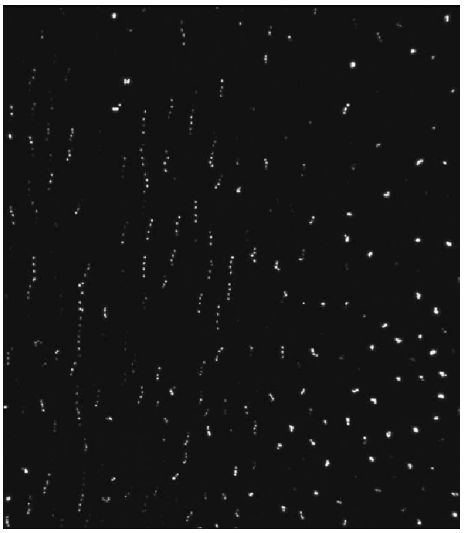

Fig. 1.16. Two-stream instability created by interaction of two dust clouds [80]

Fig. 1.17. Mach cone excited by a fast particle [81]

the kinetic level is the channeling of a single grain through a crystal. Usually the stopping power of fast particles is related to a decrease in the fast particle velocity component along its original velocity direction while the total velocity in elastic scattering is changed very little. Thus if every other scattering changes the direction of the fast particle velocity in the direction opposite to that of the previous scattering, the stopping power can be significantly decreased. This is exactly what happens in the process of the so-called channeling of particles through the crystals in ordinary matter, used widely in different physics experiments (especially in accelerator physics). With the

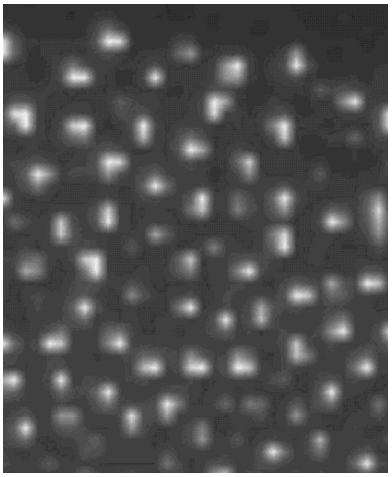

Fig. 1.18. First experimental observation of "penetration through the wall" in interaction of two grain clouds [80]

help of complex plasma physics one can investigate the process of fast particle channeling on the kinetic level [80].

These examples serve as first indications of the possibilities that have opened in the research of many processes on the kinetic level using complex plasmas. Certainly one can observe only the grain component, and this component is different than atoms or molecules – the components of ordinary matter. The difference has been in many respects already discussed. The problem of modeling the processes in ordinary matter on the kinetic level using complex plasmas consists in finding those effects that are common to ordinary matter and complex plasmas. Obviously complex plasmas are much more reach in physical processes than the ordinary matter. This investigation is for that reason even more interesting and holds the promise of many new discoveries.

1.8 Structures and Self-organization in Complex Plasmas

1.8.1 Observations of Structures in Complex Plasmas

An important and exceptional property of a complex plasma is the simultaneous presence of different structures. We mentioned already excitation of dust vortices, but complex plasmas are much richer allowing creation of many other structures. Usually, the slow motions of non-compressive liquids or gases are known to be described in terms of a system of only vortices and thus the structures created by slow motions are the vortices. We know, on the other hand, how complicated can be the motion of liquids and gases including creation of single or several vortices, creation of many interacting vortices, or formation of a vortex turbulence. Nevertheless, this motion is still a superposition of non-linearly interacting vortices.

Slow motions in complex plasmas can excite much larger types of structures. The richness of structures in complex plasmas is related to their unusual properties as a state of matter. In all motions the charge variation and presence of flux absorbed on grains is very important. A collective ion flux can drag grains from one region to another forming a concentration of dust in some regions of space and dust rarefication in other regions. In the presence of ionization, an increase in the ion density can be accompanied by an increase in the electron density to which the ionization rate is proportional. Additional ionization can increase the collective flux and increase the effect of the separation in space regions with larger grain densities from the regions with lower dust densities [82]. This can result in the complete separation of complex plasmas in grain clumps (bubbles) and grain voids. Dust voids are defined as regions with a complete absence of dust. Such structures have indeed been observed. The formation of dust voids was first observed in laboratory experiments on Earth [83] by using gas discharges with high ionization rate and

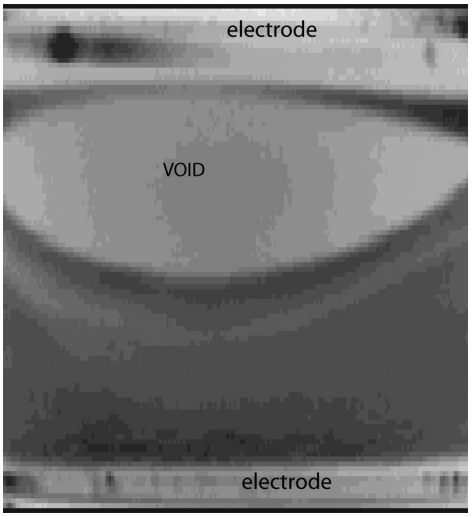

Fig. 1.19. First laboratory observations of dust voids in a complex plasmas between two plane electrodes [83]

small grains (the latter for decreasing the gravity forces). Figure 1.19 shows the first observation of dust voids in a complex plasma.

More grain voids were observed in numerous experiments under micro-gravity conditions including those on parabolic flights and on board the International Space Station. Figure 1.20 shows a quadrant of the space between two ring plane electrodes obtained in first micro-gravity experiments on parabolic plane flights [84]. The void region is the empty region while in the other region the grain rotation is observed. This rotation corresponds to a grain vortex. Thus the void is surrounded by vortices (regarding the mechanism of vortices excitation see [85]). Grain clumps (layers) surrounded by two voids can also

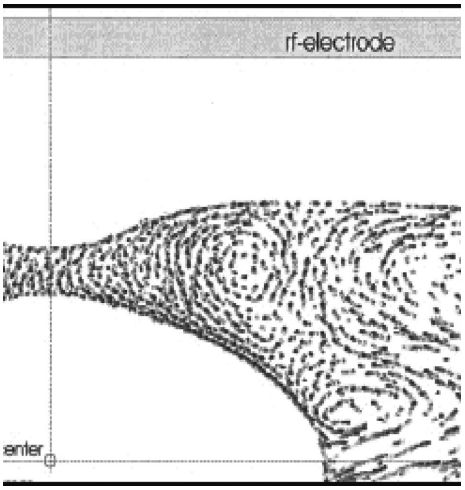

Fig. 1.20. First micro-gravity observations of a dust void surrounded by vortices. The actual dust distribution is axially symmetric about the chamber axis. The figure shows a quarter of the planar cross-section of the distribution in the chamber

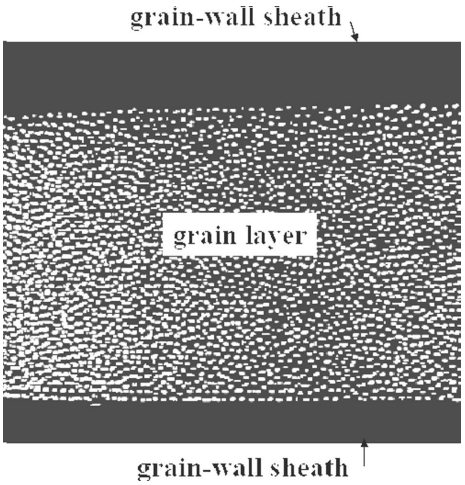

Fig. 1.21. First observations in micro-gravity conditions of a self-confined grain layer between two plane electrodes. The grain layer is separated from electrodes by the grain-wall sheath, where the grains are absent

be created [86] (see Fig. 1.21). In this case, the grain sheath is self-confined by the ram pressure of the collective flux created by the grains. The first-observed spherical grain structure of this kind is shown in Fig. 1.22. This flux is also created by a charge of the total clump that can be considered as a "super-grain." The super-grains can be collected in much larger clumps.

Most impressive is the system of a big void (like an "eye") surrounded by many vortices which was recently obtained in experiments on the International Space Station [87], (Fig. 1.23). With grains of two sizes, the system of vortices surrounding the "eye" (the grain void) becomes more complicated, with different size grains separated in space by a thin interface layer [87], (Fig. 1.24).

Different forms and types of grain structures can be formed in complex plasmas including spherical and cylindrical structures. All of them have a self-confining and self-generated drop of electrostatic potential. The spherical

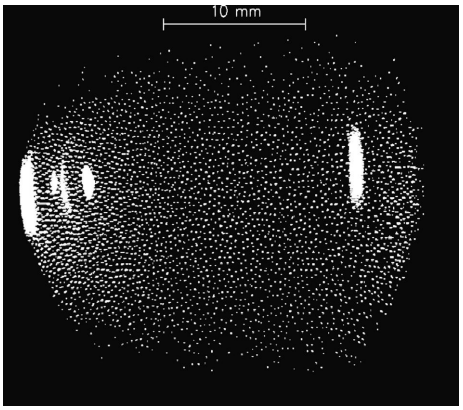

Fig. 1.22. First observation in micro-gravity conditions of a self-confined grain spherical structure. The ram pressure of the collective flux confines the structure. The bright regions are due to the light reflection by the cameras

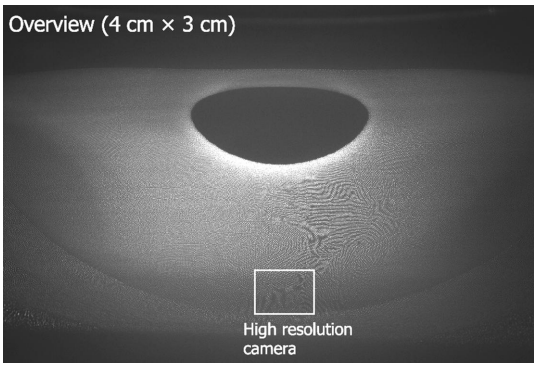

Fig. 1.23. Observation in micro-gravity conditions of a big void (an "eye") surrounded by moving grains that form vortices or grain layers including the crystalline structure (in the region of high resolution)

structure can be regarded as a kind of "anti-star" with an influx of plasma into the structure, opposite to that of ordinary stars with an out-flux of plasmas. The cylindrical structures may have intriguing properties to confine the larger size grains, which can form a spiral structure [54, 55]. The latter can be single, double (like in DNA), etc. The spiral structures can have bifurcations in the grain rotation angle, which can serve as an element of "memory."

1.8.2 Self-organization in Complex Plasmas

The concepts of self-organization is often used in modern physics [88], although at present there still does not exist an understanding and agreement about the mathematical description of the process of self-organization, which requires a high rate of dissipation leading to the processes of decay (disorganization) of many degrees of freedom of the system except those that became more organized. As a result, the entropy of the system as a whole increases while the entropy of some of degrees of freedom decreased. Hasegawa [88] has formulated a variational principle that can be used to calculate the organized degree of a system but this principle has yet to be validated, although in many cases

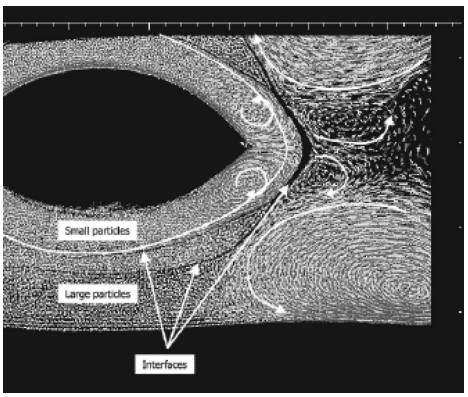

Fig. 1.24. Recent observation of a complex plasma system of grain structures with two sizes of grains. The void is surrounded immediately by smaller grains, and further out by larger grains. Many vortices can be seen around them

the theoretical results obtained using the principle are in agreement with observations. Several important points are clear:

1) Self-organization ultimately leads to some structure as the most probable one.

2)The presence of dissipation is a necessary element of self-organized structures.

3) In the presence of dissipation, the structures can survive for a long time only in an open system, i.e., they require the presence of a continuous supply of energy and material.

4)The structures should be separated in space to have boundaries where the dissipation and supply of energy are high.

5) **Self-organized structures are determined by only few parameters** (those that belong to the non-dissipated degrees of freedom).

This means that many other characteristics of self-organized structures are determined through the basic parameters of several organized degrees of freedom. It is amazing that very often such self-organized structures are encountered in nature. The living objects are among them and have additionally a memory by which they are able to transfer information about their self-organization. Complex plasma structures have all the elements of self-organized structures: the high rate of dissipation is provided by the absorption of plasma fluxes on dust grains; the boundaries between the structures can be very sharp, which is supported by many observations; the plasma flux can serve as "food" for these structures; and the system of structures is obviously an open system. Therefore the structures in complex plasmas can be used for more profound investigation of self-organization processes in nature to find a mathematical description of self-organization processes and general laws that govern these processes in nature.

From an experimental point of view, self-organization is rather important since in self-organized structures the distributions of all components are deeply related to each other and are determined by only a few parameters that can be regulated experimentally such as power applied, pressure, and the geometry of the installation. If one of the components, the dust, is measured much more easily than other components (distributions of grains can be measured in almost all cases, but not the distributions of electrons and ions), then for self-organized structures one can determine distributions of other components by knowing the distribution of the measured component. It is also important that the kinetics of dust self-organized structures is different than the kinetics of structures in ordinary matter, thus the advantage that exists in dusty plasmas for direct observation of structures on the kinetic level cannot always be extrapolated to the kinetics of structures in ordinary matter. The physical

processes that drive grains can be different than those in ordinary matter. For example, the vortices in complex or dusty plasmas can be driven by gradients of grain charges, while in ordinary gas they are driven by gradients of temperature. But some general phenomena of vortex creation can be similar, and the analogy with complex plasmas can be used to understand the physics of turbulence and structures and phase transitions on the kinetic level in ordinary matter.

In space the plasma state exists everywhere together with grains. Then the question of a different type of "life" formed by self-organized complex plasma structures arises naturally. Some aspects of "memory" in complex plasma helical structures are indeed possible. The competition and evolution processes of complex plasma's self-organized structures is a possible topic for future investigations. A search of these structures in space has not yet been undertaken and could promise some interesting results in the future. The dust in space is detected by infrared radiation, which is the result of heating of cosmic dust by different sources of energy. The modulation of the infrared emission can be one of the indications that such structures have been formed. It is not excluded that such structures can be present in nature. To find any indications of them would be an interesting task for future research; the new infrared telescope "Spitzer" could be exploited for this purpose.

1.9 Outlook of the Subsequent Presentation

Although this book is not devoted to applications of complex plasmas, in the next chapter we give a short list of such applications because the real progress made so far in these applications has often been related to a deeper understanding of complex plasmas as a new state of matter, and in all likelihood future progress in applications also will be due to such an understanding. Therefore the reader should have in mind the most important possible applications while encountering the new physics of complex plasmas. Further, we describe the elementary processes related to the plasma flux absorption by grains and to the shielding of grain fields. Without describing these elementary processes we will not be able to introduce the new physics related to the presence of grains in a system. The next and simplest issue is how the structures in complex plasmas develop from weak disturbances and weak perturbations of the basic state of a complex plasma.

We demonstrate that the homogeneous state of a complex plasma is universally unstable with respect to formation of structures among which can be different structures including those with long-range correlations (such as plasma crystals and liquids) and short-range correlations. All these processes are related to the effects of plasma fluxes. Even the basic state of a system, as we demonstrate, depends on the plasma flux creation. Thus all linear modes also depend on the fluxes and their perturbations. One might think that the presence of flux absorbtion would create only an additional damping

of collective modes. This appears to be incorrect – not only new modes do appear and not only the flux absorption strongly limits the range of their existence, but outside the mode interval the linear mode shows an instability that is similar to a gravitational self-contraction. This is considered to be the reason for the appearance of structures in complex plasmas and, in particular, for the formation of the plasma condensation.

To describe the physics and current understanding of plasma crystal formation we consider in more detail the influence of plasma fluxes on grain–grain interactions. This allows us to give the most probable physical explanation for the formation of plasma crystals and for the role of collective flux phenomena in this formation. The main emphasis is on the fluctuations of collective plasma fluxes that create a collective grain attraction when the grains are at a significant distance from one another. The aim is to provide a rough explanation of three major puzzles of observation: the large coupling constant, the low temperature value of phase transitions, and the large grain separation. Formation of other structures in the gaseous state or in an external confining potential is discussed in the last chapter, where the concept of an average flux is used. Thus we provide the reader not only with observational data but also with a rough physical understanding and possible interpretation of observations. Of course, after having read our presentation of all the fundamental relations and possible physical understanding of existing observations, the reader is free to come up with their own estimates and to devote themselves to this new, fast-developing, and fascinating field of research.

References

1. *The New Encyclopedia Britannica* (1983), Encyclopedia Britannica Inc., The Chicago University, Chicago, **14**, 505.
2. H. Thomas, D. Morfill, V. Demmel and J. Goree (1994). *Phys.Rev.Lett.* **73**, 652.
3. J.U. Chu and I. Lin (1994). *Physica* **A 205**, 183.
4. A. Melzer, T. Trottenberg, and A. Piel (1994). *Phys.lett.* **A 191**, 301.
5. Y. Hayashi and K. Tachibana (1994). *Jpn. Appl. Phys.* **33**, L804.
6. V. Fortov, A. Nefedov O. Petrov, A. Samarin and A. Chernychev (1996) *Phys. Let.*, **A 219**, 89.
7. S. Nonomura, N. Ohno, and S. Takamura (1997). *Jpn. J.Appl.Phys.2 Lett.* **36**, L949.
8. S. Nonomura, N. Ohno, and S. Takamura (1998). *Physics of Plasmas*, **15**, 3517.
9. A. Gasgarden *et al.* (1994) *Plasma Sources Sci Technol.* **3**, 329.
10. L. Spitzer, (1978). *Physical Processes in the Interstellar Medium*, John Wiley and Sons, New York.
11. S. Kaplan and S. Pikel'ner (1970). *The Interstellar Medium*. Harvard University press, London.
12. W. Watson and E. Salpeter (1972) *Ap.J.* **174**, 321.
13. S. Weidenschilling and J. Cuzzi (1993). "Formation of Planetesimals in the solar nebula" In: E. Levy and J. I. Lunine eds., *Protostars and Planets III*, p. 1031, University of Arizona Press Tucson.

14. M.Horanyi, H. Houpis and D. Mendis (1988), *Astrophys. Space Sci.* **144**, 212.
15. S. Kaplan and S. Pikel'ner (1974), *Ann. Rev. of Astronomy and Astrophys.* **12**, 113.
16. S. Kaplan (1966). *Interstellar Gas Dynamics*. Pergamon Press.
17. G. Morfill and M. Scholer eds. (1992) *Physical Processes in Interstellar Clouds*. Reidel Publ. Comp.
18. J. Winters, J. Keady, A. Gauger, and P. Sada (2000). *Astron. Astrophys.* **359**, 651.
19. K. Koshevaya, S.V. Tecpoyotl-T., M. Gutierrez-D., E.A. Burlak and G.N. Kotsarenko(2000). *Rev. Mex. Astron. Astrofis. Ser. Conf. Mexico* **9** , 112.
20. G. Morfill and S. Grun S (1979). *J.Geophys.Res.* **256**, 27.
21. B. Mauk, E. Keath, and S. Krimigis (1990). *J. Appl. Tech. Phis.* **11**, 63–71.
22. A. Galeev and I. Khabibrachmanov (1985). *Pisma v Astron. Zh. Rus.* **11**, 292.
23. W. Kurth, D. Gurnett, F. Scarf, R. Poynter and J. Sullivan (1981). J. *Geophys. Res.*, **86**, 8402.
24. K.-H. Glassmeier, N. Ness, M., Acuna, F., Neubauer (1989). J. Geophys. Res., **94**, 15063.
25. F. Verheest (1999). Plasma Phys. Control. Fusion **41 , suppl.3A**, A445.
26. E. Marouf, G., Tyler, P., Rosen (1986). Icarus **68**, 120.
27. M. Tagger, R., Henriksen, J., Sygnet, R., Pellat (1990). Astrophys. J., **353**, 654.
28. F. Verheest (1996). Space Sci. Rev., **77**, 267.
29. R. Bingham and V. Tsytovich (2001), Astron. Astrophys.Lett **376**, L43.
30. R. Chevalier, (1992) Nature **355**, 691.
31. P. Meaking (1991), *Rev. Geophys. Res.* **29**, 317.
32. R. Greeberg and A. Brahic eds. (1984). *Planetary Rings*. The University of Arizona Press, Tucson Arizona.
33. D. Kempf, S. Pfalzner, and T. Henning (1999). *Icarces* **141**, 388.
34. T. Eidhammer and O. Havnes (2001). *J. Geoph. Res.* **106**, 24831.
35. S.V. Vladimirov, K. Ostrikov, and A.A. Samarian (2005). *Physics and Applications of Complex Plasmas* (Imperial College, London).
36. G. Selwyn, J. Heidenrich, and K. Haller (1990). *Appl.Phys. Lett.* **57**, 1867.
37. A. Boushoule *et al.*(1991) *J.Appl.Phys.* **70**, 1991.
38. L. Boufendi and A. Boushoule A. (1994). *Plasma Sources Sci. Technol.* **3**, 262.
39. V.Tsytovich and J. Winter J. (1998). *Physics Uspekchi* **41**, 815.
40. P. Shewee and B. Steain (2002). *Physics News Update AIP* Numver 682, Aprill 13 (2004), *J.Mat.Sci.*
41. *NRL Plasma Formulary*, p. 41. Washington Naval Research Laboratory 1990.
42. J. Bollinger, D. Wineland, and D. Dubin (1994). *Phys. of Plasmas* **1.1**, 1403.
43. K-J. Bessonov and K-J. Kim (1996). *Phys. Rev. Let.* **76**, 431.
44. J. P. Shiffer (1996). *AIP Conf.Proc.* **31**, 191.
45. Intern.Worksh. on electronic Crystals-99, (1999). *J. Phys. IV, Proc.France* **9**, No 10.
46. S. Fliezer, Z. Henis, and Y. Paiss (1994). *AIP Conf. Proc.* **318**, 362.
47. S. Swift, (1996). *J. Comput. Phys.* **126**, 109.
48. S. Ogata, S. Ichimaru (1990). *Phys. Rev. A* **42**, 4867.
49. Proceedings of the Yamada Conference XXI, S. Ichimaru and S. Ogata eds. *Strongly Coupled Plasma Physics*. 1990.
50. H. Ikezi (1986). *Phys. Fluids* **29**, 1764.

51. H. Iizuka and N. Sato (1994) *J. Mater. Sci.* **29**, 894.
52. G. Morfill, A. Ivlev *et al.* (2004). *Contr. Plasma Physics* **44**, 450.
53. V. Tsytovich (2003). Facing New Problems in Complex Plasmas, *Workshop Complex plasmas*, Shlossringer, Germany.
54. V. Tsytovich, N. Gusein-zade, and G. Morfill (2004). IEEE *Trans.Sci.* special issue Dusty plasmas, April.
55. V. Tsytovich, N. Gusein-Zade, and G. Morfill. Dust Helical Structures in Laboratories and Space. Proceedings EPS-2003 International Conference on Plasma Phyisics and Controlled Fusion, St. Petersburg, 2003.
56. A. Lipaev, V. Molotkov, A. Nefedov, O. Petrov, V. Torchinskii, V. Fortov, A. Khrapak, and S. Khrapak (1997). *Zh. Eksp. Teor. Fiz.* (Russia), **112**, 2030.
57. V. Fortov, A.Nefedov, O.Petrov, A. Samarian, and A.Chernyschev (1996). *Phys. Rev. E* **54**, R2236.
58. A. Nefedov, O. Petrov, Ya. Khodataev, and S. Khrapak (1999) *Zh. Eksp. Teor. Fiz.* (Russia), **115**, 837.
59. V. Fortov, V. Molotkov, A. Nefedov, and O. Petrov (1999). *Phys. Plasmas* **6**, 1759–68.
60. V. Fortov, A. Nefedov, V. Vladimirov, L. Deputatova, V. Molotkov, V. Rykov, and A. Khudyakov (1999). *Phys. Lett. A* **258**, 305.
61. O. Vaulina, A. Nefedov, O. Petrov, and V. Fortov (2000). *Zh. Eksp. Teor. Fiz.* (Russia), **118**, 351.
62. A. Nefedov, O. Petrov, and V. Fortov, (1997). *Usp. Fiz. Nauk* (Russia), **167**, 1215.
63. G. Morfill, H. Thomas, U. Konopka, and M. Zusic (1999). *Phys. Plasmas* **6**, 1769.
64. A. Mikhailovskii (1974). *Instabilities in Inhomogeneous Plasma*. Consultants Bureau 1974.
65. A. Akhiezer A.I. *et al.* (1975). *Plasma Electrodynamics*. Pergamon Press.
66. S.V. Vladimirov and K. Ostrikov (2004). *Phys. Rep.* **393**, 175.
67. I. Bernstein and I. Rabinovich (1959). *Phys. Fluids* **2**, 112.
68. L. Pitaevsky (1966). *JETP* (Rus.ed.), **43**, 27.
69. E. Tomme, B. Annaratone, and J. Allen (2000). *Plasma Sources Sci. Technol.* **9**, 87.
70. V.Tsytovich, Ya., Khodataev and R. Bingham (1996). *Comments on Plasma Physics and Controlled Fusion* **17**, 249.
71. A. Ignatov (1995), Comments P.N.*Lebedev Inst.A* **58**, 1.
72. Ya. Khodataev, G. Morfill, and V. Tsytovich (2001). *J. Plasma Phys.* **65**, 257.
73. V. Tsystovich and U.de Angelis (2001). *Phys.Plasmas* **8**, 1141.
74. V. Tsytovich and G. Morfill (2002). *Plasma Phys.Rep.* **28**, 195.
75. W. Steel, D. Law, B. Annaratone, and J. Allen (1997) *P*roceedings XXIII International Conference on Phenomena in Ionized Gases. Contributed Papers **1**, 194.
76. H. Thomas and G. Morfill (1996). *Nature* **379**, 806.
77. M. Rubun-Zuzic, G.E.Morfill, A.V. Ivlev *et al.* (2006). *Nature Physics* **21**, 181.
78. V. Tsytovich and O. Havnes (1993). Comments on Plasma Physics and Controlled Fusion **18**, 267.
79. G.Morfill, M.Rubin-Zuzic, and H. Rothermel *et al.* (2004).*P*hys.Rev.Lett. **92**, 175004.
80. Morfill G.E., Konopka U., Kretschmer M. *et al.* (2006). *New Jour. Phys.*, **8**, 7.

81. D. Samsonov, J. Goree, Z. Ma, A. Bhattacharjee, H. Thomas, H., and G. Morfill, (1999). *Phys. Rev. Lett.* **83**, 3649.
82. V. Tsytovich and G. Morfill (2000). *Plasma Physics Reports* **26**, 682.
83. D. Samsonov and J. Goree (1999). *Phys. Rev. E* **59**, 1047.
84. G. Morfill H. Thomas, U. Konopka, H. Rothermel, M., Zuzic, A. Ivlev, and J. Goree (1999). *Phys.Rev.Lett.* **83**, 1598.
85. A. Bouchoule, G. Morfill, and V. Tsytovich, V. (2000). Comments in Modern Physics, Part C. *Comments in Plasma Physics an Controlled Fusion* **1**, 131.
86. V. Tsytovich, G.Morfil, U. Konopka, and H. Thomas (2003). *New Journal of Physics* **5**, 1.
87. A. Nefedov, G.Morfill, V. Fortov *et al.* (2003). *New Journal of Physics* **5**, 33.
88. A. Hasegawa (1985). *Adv.Phys.* **34**, 1.

2

Why Complex Plasmas Have Many Applications in Future Technology?

The material given in the previous chapter shows that recently discovered complex plasmas present a new kind of matter not previously encountered and that investigation of this new field of physics is only in its first stage. Many new discoveries can be expected in the very near future. The field is very rapidly developing and is of major importance to fundamental science. Usually, most new discoveries in fundamental science have many future applications. It is very difficult to predict such discoveries, and new discoveries usually require some time to be incorporated into everyday life. But the situation with complex plasmas is different because the recent boom in the field not only stems from scientific discoveries but was simultaneously dictated by several problems of industry.

2.1 Main Discoveries in Applications of Complex Plasmas

The story of complex plasmas started in late 1980s with problems related to the production of computer micro-electronics and was deeply connected to computer technology [1]. This stimulated scientific investigations in the field. It appears that surface physics, surface covering with thin films, and deposition of material on surfaces also require a knowledge of complex plasma properties. Solutions of these problems cannot be found completely phenomenological by the approach used up to the present time. On the other hand, it was recently (in mid-1990s) realized that the future energy production is also a field where knowledge of complex plasmas is required. And, finally, environmental problems have been found to be related to complex plasmas.

In technological aspects, the use of complex plasmas has only begun, but these first steps give us the possibility to extrapolate the existing tendencies and to give some basis for predicting trends in industrial applications of complex plasmas. Also, experiments in complex plasmas will certainly take place

V. N. Tsytovich et al.: *Why Complex Plasmas Have Many Applications in Future Technology?*, Lect. Notes Phys. **731**, 47–66 (2008)
DOI 10.1007/978-3-540-29003-2_2

in the near future, and one can easily speculate about future industrial applications that would make these experiments possible. Thus the situation with complex plasmas is not like predicting the impossible, i.e., future discoveries. This allows us to discuss possible future applications of complex plasmas.

The four main possible industrial applications of complex plasmas are as follows: a) *plasma-processing computer technology*; b) *production of new surfaces covered with complex plasma components*; c) *new mechanisms of energy production*; and d) *new solutions for environmental problems*. It is worthwhile to mention that these four problems will play a crucial role in future advances in complex plasmas.

2.2 Computer Technology

2.2.1 Simple Principles Used in Computer Technology

The industrial production of electronic micro-chips in the early 1990s was based on simple principles of RF gas discharges producing low-temperature plasmas [1, 2, 3, 4]. The RF chambers are used where low-pressure gas is weakly ionized by RF radiation; the ionization corresponds to a continuous production of electrons and ions from neutral gas atoms and molecules. The density of electrons and ions is many orders of magnitude less than the density of the neutral gas. Ionization automatically leads to a charging of the wall by electrons that have larger mobility than ions.

In experiments, a plasma sheath appears close to the wall in which the ions are accelerated toward the wall. As the walls are floating, they have the potential of the order of the electron temperature which could have been around several electron volts. A drop in the electrostatic potential in the plasma sheath is about the electron temperature, which is natural since the walls are charged by the electrons. The energy of ions reaching the wall is thus close to the temperature of the electrons. This is much greater than the initial ion energy, which should have been close to the temperature of neutral gas (around room temperature).

The accelerated ions close to the wall form an ion beam that bombards the wall; the energy of the ions of the beam is around the temperature of the electrons. If the wall has a mask made by a material that could not be melted by the ion beam, but the material of the sample at the wall can be melted by the ion beam, then only that part of the sample which is opened by the mask is melted.

First, the sample needed for etching was placed on the wall, this sample was then covered by the mask and the process of etching was allowed to take place by switching on the RF power. In this way, micro-schemes for computers were produced. The etching took several hours or even about a day. The etching chamber was completely closed so that no impurities or dust could

interfere with the etching process. Also, all rooms where the process of etching was performed had to be specially cleaned so that there was no dust; the staff can enter these rooms only wearing special clothing. This continued up to early 1990s when the discovery was made that in the chamber the etching process itself produces grain particles that contaminate the etching samples. This discovery was made by making windows in the chambers and using them by examining the interior by laser-light scattering [5, 6]. A complicated grain structure such as a grain cloud was found to levitate above the etching sample [7].

Thus all efforts to exclude the sample contamination by external dust were illusive since it was found that the etching process produces its own grains in the chamber, which is the main source of the sample contamination. The main cost for computer production was related to separation of the uncontaminated from the contaminated samples. Figure 2.1 shows the complicated dust cloud found to be levitating above the etching sample in the first experiments [5] by using the laser scattering on dust in the etching chamber. Thus it became obvious that the appearance of dust clouds during etching process and the dust falling from them on the etching samples was one of the greatest problems in the computer chip technology.

2.2.2 Investigation of Dust Clouds in Etching Devices

An important discovery regarding the properties of grain clouds was that the grain size was continuously growing during the etching process. The physics of grain formation and grain growth in the first stages of etching is now investigated in many publications (the details can be found in [4, 8, 9]). The grains either start to grow by chemical processes or are emitted directly from the walls as a result of the etching process. Chemical processes are involved

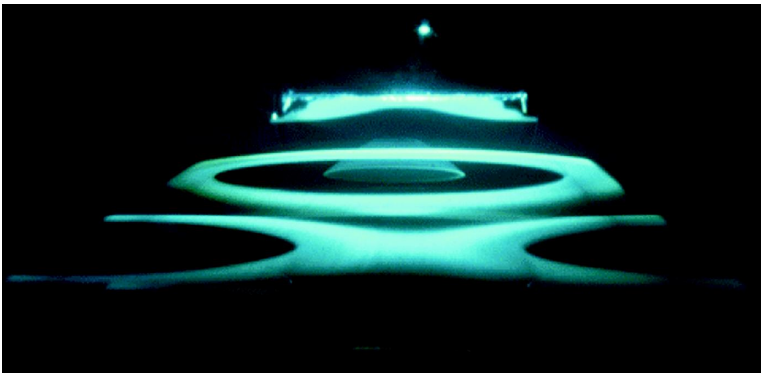

Fig. 2.1. Dust clouds found by laser scattering above an etching sample in the first experiments [5]

in the formation of atomic complexes whose size increased over time. The grains vary widely in sizes from an atomic-sized molecular complex (less than a fraction of a nanometer) up to tens of nanometers.

Particles are considered as grains starting from a few nanometers in size; the threshold for the grain detection by laser scattering is around 10nm or larger but grain-detection methods show a maximum grain density of 10^7–10^9 grain particles per cubic centimeter, which corresponds to about 3nm [3]. At that stage, the initially slow process of grain growing becomes a faster process of dust agglomeration [8, 9]. These agglomerates are not big and the agglomeration process is subsequently stopped by an increasing Coulomb repulsion due to increasing grain size. Recall that grain charges are proportional to the grain size and in the case of 3 μm charges they are around 10^3 electron charges, and thus for 3 nm grains the charges should be around several electron charges, and the Coulomb repulsion can start to take effect and is the most probable process for stopping fast agglomerations.

But the grain growth does not stop after this stage of agglomeration; they grains continue growing (although more slowly) due to the deposition of material in the plasma flux to the grains. This stage is completed at the next stage of agglomeration, where rather large agglomerates of grains appear. This second stage of agglomeration [1] occurs for large size grain charges and is probably due to collective complex plasma phenomena. To these grains, a part of the etching material is added that is due to the processes of re-ejection as grains start to levitate above the etching sample in the plasma volume. The growing grains reach the stage where the electric field of the plasma sheath can marginally support them against the gravity while larger grains fall on the sample and contaminate it.

But even in the first stages of investigation it was found that the contamination can occur not only because of the fall of individual grains but also due to collective effects. It was observed that for some reason the process of sample contaminations can be related to an instability in the levitating grain cloud when the whole cloud could potentially fall on the sample [10]. The plasma volume becomes free of grains, forming the grain void structure already discussed. Later on, the sequence of events is repeated. After the etching is finished, some grains are big enough to be observed with the naked eye. The structure of the large grains (before the instability starts) depends largely on the material used for etching. For some materials (e.g., SiO_2, which is often used in plasma etching), the agglomerated grains in their latest stage look like "cauliflower." Figure 2.2 shows such a "cauliflower"-shaped grain found in etching experiments [1].

Some special experiments can be conducted without masks. They are known as sputtering discharges and are accompanied by the creation of grain clouds levitating above the sputtered surface and can use different sputtering materials at the surface to determine the grain types appearing in the sputtering discharges. Surface processing and sputtering is another branch of industry [11, 12, 13, 14, 15]. It was found that the timing of grain cloud formation and

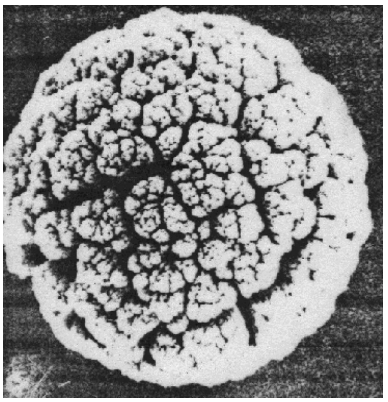

Fig. 2.2. "Cauliflower"-shaped dust grain observed in the etching experiments [1]

the appearance of the largest grain before the onset of instability depends largely on the material of the walls. An important point is that the grain cloud levitating above the sample or above the sputtered surface *is a liquid cloud where grain interactions are sufficiently strong but somewhat below the value necessary to create a plasma crystal state*. In other words, it is a complex plasma cloud. Figure 2.3 shows the filament-shaped grain agglomerates [10].

In computer technology, it is desirable to avoid both contaminations, i.e., that due to large individual grains falling on a sample (due to their large masses which cannot be supported against gravity by near wall electric fields) as well as the contamination due to collective instability arising from the fall of the whole grain cloud on the sample. Some projects of mid-1990s – such as using the vacuum cleaner technique by pushing grains in the levitating grain cloud by flux of neutral gas; or getting rid of grains by evaporating them with lasers – were shown not to operate properly. Success came only in the late 1990s from the use of specific properties of complex plasmas.

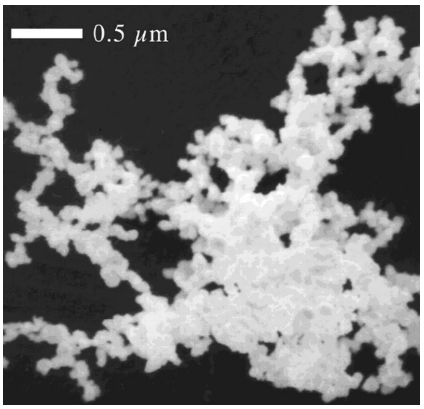

Fig. 2.3. Filament-shaped grain agglomerates observed in surface sputtering experiments [10]

2.3 First Steps to Using Complex Plasma Properties in Computer Industry

Thus far only the first steps have been taken toward using the special properties of complex plasmas to resolve problems appearing in technology. We give here a short description of two such techniques:

1) Using the properties of a complex plasma when it is converted to the liquid state to evacuate grains from the etching chamber.

2) Using the special properties of vortex formation in a complex plasma for evacuating grains from the discharge chamber.

The first method uses directly the properties of the liquid complex plasma state where the grains interact strongly. Let us illustrate this method by a simple example from everyday life. Take a plate filled with water and tip it – the water spills onto the floor. This is due to interactions of the particles constituting the water that require them to follow each other. The effect is produced by gravity. The same method can be used for complex liquid clouds in an etching device. By tipping the device we can get rid of grains. Such cleaning procedure uses such complex plasma property where the grains interact strongly but not the other plasma components. Thus only the grains are removed; they are not accompanied by the flow of gas and plasma (neutral atoms, electrons, and ions). The main problem is to find the moment at which the grains start to interact strongly but still do not fall onto the sample because of the instability that can be caused by collective interactions [16]. The exact timing of this process is absolutely crucial for every device used. The other method was invented by N. Sato [17]. As we mentioned above, different structures can be excited in complex plasmas including vortices. One of the simplest vortex systems consists of two vortices rotating in the opposite directions. In the center of the vortices, the grains flow in the same direction. The vortices can be excited by external probes, which makes the drag and electric forces non-collinear and creates the grain cloud rotation. Assume that a negative external probe was introduced in the central part of the two vortices where grains are rotating in the same direction and that this negatively charged probe is hollow. Then the flux of grains will penetrate inside the hollow part of the probe and can be removed. The main question is whether such a negatively charged probe will indeed excite this set of two grain vortices rotating in opposite direction. The probe invented by Sato [15, 17] does this and serves as a very effective grain removal device.

At the first glance, one can expect that in order to collect negative grains one should introduce into a complex plasma a positive probe to attract the grains. In reality, one should do quite the opposite – the negative probe should have enough electrostatic potential to repel the grains and excite the vortices in the way that forces the grains to rotate such that they are transferred to

the central hollow region of the probe. Note that these vortices are special properties of a complex plasma (and this technique cannot operate and the vortices cannot be excited if the grain charge is fixed). Only grains are significantly affected in these vortices while the electron, ion, and neutral atom number densities are changed only slightly. Thus, like the previous method, only the grain component is removed from the discharge region.

In Fig. 2.4, we show the sketch of the principle behind the Sato's cleaning device; one panel shows a system of two complex plasma vortices without a hollow probe and another shows a system of two vortices with the cleaning probe. Note that the vortices in this device are excited by the probe itself due to its negative potential and due to the electric field created close to the probe as a consequence of non-collinearity of the ion flux lines (and the ion drag force acting on grains) and the electric field lines.

2.3.1 New Laboratory Experiments in Complex Plasmas Inspired by Computer Technology Problems

It is clear that some laboratory experiments on complex plasmas can enable application of complex plasma physics to computer technology.

1. The physics of dust vortices is currently not fully understood. Dust vortices differ substantially from vortices in ordinary matter, e.g., in their gaseous and liquid states. The physics of dust vortices includes the dust-charging process as a necessary element. Therefore the vortices are regulated by the charging process, as well as by dust drag processes and distributions of the electric field potential. These vortices can be changed by external electric field inhomogeneities, the dust attachment coefficient, and neutral gas pressure. The latter can determine the threshold of the

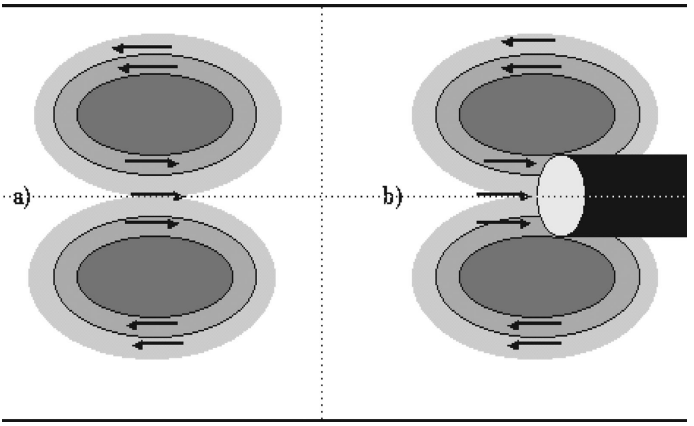

Fig. 2.4. The principle of the Sato's cleaning probe: **a**) the system of two dust vortices without a probe; **b**) the system of vortices with the probe [15, 17]

vortex excitation. The first serious investigations of the nature of dust vortices has just started.
2. Excitation of dust vortices can help not only in the processes of dust removal but in the etching process itself by mixing different components of the material ejected from the samples.
3. The physics of dust agglomeration is not understood completely and the different proposed mechanisms of the agglomeration have not been verified experimentally, especially at their second stage, where the "cauliflower," or fractal dendric, types of grains are created. In the future, experiments will be needed to investigate different mechanisms of dust agglomeration and dependence of the agglomeration on dust charges and the presence of charging process (plasma fluxes on dust surfaces).

2.4 New Surfaces, New Materials

2.4.1 New Surfaces

Monolayer complex plasma crystals can be created with quite different structures and with grains with quite different physical and chemical properties [12, 13]. In many industries, it is desirable to change surface properties of materials. These monolayer crystals can be created in complex plasma levitating in the electric field close to the wall of the materials. The levitation is due to the electric field, which operates against the gravity of the grains and is switched off as soon as the ionization source is switched off. Then the monolayer crystal falls onto the surface of the material and becomes attached to and deposited on it, which changes the material's surface properties. In technology, materials with rather different surface properties are needed, including very rough surfaces or surfaces with different chemical activity properties including catalyzers of chemical reactions. Thus complex plasmas can be used for industrial *production of materials with given surface properties* including those that can be used as catalyzers.

Another possibility for using the phenomenon discovered in the etching industry is opened up by the existence of continuous growth of dust grains in etching devices or surface sputtering technology devices. As mentioned after the first stage of agglomeration (stopped by the onset of grains charges) and before the second stage of agglomeration (when other attractive forces start to compete with repulsion forces of large grain charges), the grains grow slowly but continuously by deposition of the material due to the charging process. The most important observation is that *the grains at this stage of the growth process become almost completely spherically symmetric*. Figure 2.5 shows the formation of spherical grains in surface sputtering experiments [10].

From physical point of view, formation of spherical grains in deposition processes is not surprising since plasma flux collected by the grains is originated quite far from the grains at the charging surface [1, 12, 13], (see Fig. 1.4).

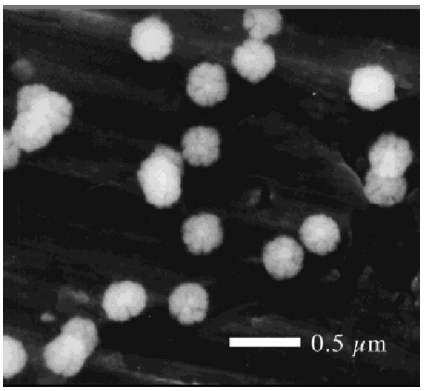

Fig. 2.5. Formation of spherical grains in surface sputtering experiments [10]

From this distance any grain is approximately a point grain, i.e., its size is much less than the size of the collection radius and therefore the flux operating in the deposition process is almost completely spherical. It was observed that if one injects into the gas discharge non-spherical grains corresponding in size to those that appear in the etching or sputtering discharges, they grow slowly and eventually become spherical over time, with surfaces deposited from the volume material. In this way one can produce spherical grain powders for industry applications [11].

On this basis, the industry of production of almost completely spherical powder grains is starting to develop. Moreover, grain surfaces can be coated with different materials including the chemicals that serve as catalyzers. The catalytic effect is known to depend on the total surface with which the chemicals are in contact. The whole surface increases substantially if it is distributed among many small grains. In this way the catalytic effects can be magnified. But the powder technique has also started to be used to cover the grains with a perfume material, and the technique starts to be used widely in perfumeries. There exist also many other applications including powders with artificially changed dust surfaces.

2.4.2 New Materials

The procedure of deposition of a mono-layer complex plasma crystal on the surface of a material can be continued by depositing one surface layer after another, and each of the subsequent mono-layers can either have a different crystal structure or be composed of different types of grains. This is the way to produce a **new composite material**. This possibility of using complex plasma mono-layer crystals to create materials with different surface properties as well as the possibility of producing new composite materials have been discussed in literature, but no serious effort has been made so far to proceed in this direction.

There are restrictions in such a use of complex plasmas for creating new materials related to the size of the grains, which should be sufficiently large to have strong interactions, since for small grains the monolayer crystals will not be certainly formed due to a decrease in inter-grain interactions with the decrease in grain sizes. As of now, the mono-layer crystal can be created with a minimum separation of several hundred nanometers. In future one can produce perhaps mono-layer plasma crystals with the inter-grain separation of about 100 nm. This is somewhat larger than nano-size composite materials. Advances in this field can be made by using nano-tubes as rod grains. The rods are grains where one of the longitudinal directions is much larger than the other directions. The latter can even be of a few nano-meters in sizes. First experiments with rod grains [18] show that they can be oriented in the discharge either vertically or horizontally. On the other hand, it is known that the grain-charging effect can operate in such a way as to transfer not only the material to the grains but also the momentum and the angular momentum. For specially prepared nano-tubes with an attachment coefficient different in their upper and lower parts, their charging is accompanied by their rotation due to the transfer of the angular momentum at different rates to the upper and lower parts of the rod (nano-tube). In this way, the nano-tubes can be oriented along the ion flow which always exists in gas discharges close to the walls. In future, we can expect that from such oriented nano-tubes one will be able to create complex plasma mono-layer crystals and deposit them on the surface of a material. Subsequent deposition of systems of nano-tubes will create a forest or nano-tube constructions. In principle, they can be used in nano-hydraulics or other nano-technology. So far, little has been done in this direction.

In this context, one should notice the success of implanting in nano-tubes the fullerene molecules which can serve as valves in possible future nano-hydraulic technology. All this is only provisional, and attempts have been made to initiate experiments on complex plasmas with nano-tubes or experiments for the creation of nano-hydraulics. We describe here these possibilities only to give an example of numerous opportunities opening up in novel technologies by using complex plasma properties.

2.4.3 New Magnetic Materials

Experiments on complex plasmas with magnetic particles have only started. Ferromagnetic particles are shown to be supported against gravity by inhomogeneous external magnetic fields, which can be an essential achievement for experiments in the Earth's gravity since the electric field (for support of grains against gravity) can be excluded [19]. On the other hand, the magnetic field forces can cause rotation of not only the whole complex plasma cloud but individual particles as well. The properties of complex plasma crystals in a strong magnetic field have not yet been investigated and new discoveries are naturally expected. Figure 2.6 [20] illustrates a complex liquid cloud rotating

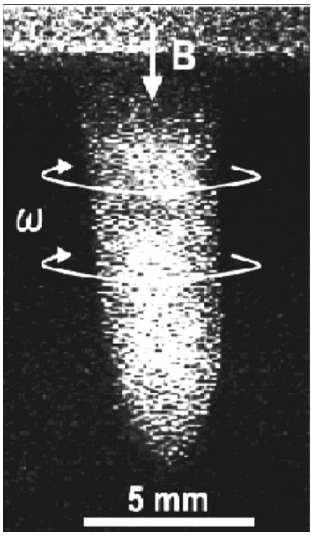

Fig. 2.6. Observation of liquid dust cloud rotating in an external magnetic field [20]

in a magnetic field. Mono-layer magnetic crystals also await laboratory discovery and detailed investigations. Covering materials with magnetic monolayer crystals can be of major importance for new technologies. Another possibility is related to the creation of a magnetic field by complex plasma crystals. This possibility is due to the aforementioned alignment of asymmetric dust grains to the ion flow [21, 22]. If the grains are ferromagnetic and their size is one magnetic domain, the magnetic field created on their surface can be rather large, and if these grains are aligned (with no external field present), they can create a strong magnetic field. If a film deposited on the surface in such a plasma is in the liquid state, the possibility of manipulating the direction of the magnetic field in the film can also open new technological opportunities.

All these examples represent only a superficial outlook of the present stage of understanding the complex plasma systems in the important field related to new composed materials. Obviously, future investigations of complex plasmas in external magnetic fields will open up other possibilities for using magnetic complex plasma structures in new technologies.

2.5 New Energy Production

2.5.1 Necessity of New Energy Sources

Exiting sources of energy such as coal, oil, gas, and nuclear materials are limited and even will last for some centuries but not for hundreds of centuries. Natural directions are to use unlimited sources of energy such as the following: a) controlled nuclear fusion, and b) direct or indirect solar radiation. Both directions face problems related to dust.

Energy production by controlled nuclear fusion started to be investigated half a century ago; one of the goals is to reach such plasma temperatures and densities that would allow us for the onset of controlled fusion reactions. In this direction significant advances were made using plasmas in toroidal magnetic traps such as tokamaks, where an average temperature of one order of magnitude larger than needed was achieved and a necessary high density level was also reached. The high temperatures and high densities were obtained not simultaneously in the same set of experiments, but at least the latest experiments indicate that in future fusion reactors the threshold for the controlled thermonuclear reaction can be reached. Further problems are related to the question how this energy can be harnessed from these devices [23, 24], because after the start of the reaction the wall of the installation soon becomes radioactive and the installation can no longer be used [25]. This is the so-called problem of interaction of the energy flux with the first wall. In these problems, the effects of complex plasma start to play an important role [26].

Another energy source is the direct conversion of solar energy into electricity by using solar cells. The effectiveness of such cells depends largely on the coating of their surfaces, and thus once again the complex plasma phenomenon is encountered.

A third possibility exists in the irradiation of complex plasma crystals and liquids with very intense laser radiation. We discuss here all three of these possibilities.

2.5.2 Controlled Fusion Devices

The wall conditions in fusion devices differ from those of etching plasmas, but still the temperature close to the walls can be sufficiently low for long-term dust survival. The thermal flux on the walls is rather high, which can lead not only to evaporation of the thin film coating the walls but can destroy them and cause wall flaking. The temperature of the walls can be even lower than in other low-temperature industrial devices due to the radiation cooling of plasmas. It especially occurs in so-called detached regions, where the thermal flux to the wall is almost converted to a radiation flux. In these regions close to the walls of fusion devices, the temperature can be as low as 0.5 eV. One should expect in these conditions not only the survival of dust produced by the walls but also its levitation in the electric field of the sheath close to the wall [23, 24].

The difference between fusion devices and other devices with low-temperature plasmas such as those used for etching or surface treatment is probably that the electron and ion temperatures are almost equal in fusion plasmas (while in the other plasmas the ion temperature is much lower than the electron temperature). Also, the plasma density close to the walls is by two orders of magnitude larger. Another important property of fusion devices is that their operation usually requires that the walls are already covered by

thin films (this is the so-called wall boronization or wall carbonization). It is described in detail in [24] (see also [23]).

Thus the questions are, whether in fusion devices the dust grains are really produced in the walls, how long they survive and what their characteristics are? Dust particles were for the first time collected after many discharges [26] and it was found that they are really present in all fusion machines. They range between a few nanometers and a few tenths of a millimeter. For several hundred discharges their total mass is estimated at about 100g [26]. Recent investigations show that dust is created in all fusion discharges and especially in large numbers in the so-called disruptions, where the plasma flux on the walls is rather high – at about the same level as the flux expected in future fusion devices such as ITER [25]. The dust grains collected after many discharges vary in size, and one often finds dust agglomerations, (see Figs. 2.7 and 2.8). It is difficult for these agglomerates to be formed in a single discharge since the estimated time of formation of the agglomerates is much larger than the period of one discharge (the discharges last for a maximum of several tenths of a second, while the formation of agglomerates of the size observed needs at least several hours). This indicates that dust grains can grow from discharge to discharge while attached to the wall between the discharges and lifted after the next discharge to levitate close to the walls. Levitating in the sheath region at the wall during the discharge time, the grains apparently are growing continuously from one discharge to another.

In existing fusion devices, dust does not play a major role in confinement, although it can influence the discharge onset and control the rate of impurities injected into the discharge. Dust can play a more important role close to the limiters and in the detached regions. In future fusion devices such as ITER dust will be a major problem due to the much larger heat flux on the walls, the much longer operation time, and the radioactivity of dust grains [25]. Wall erosion is a well-established phenomenon and is directly related to dust formation. The presence of radioactivity in future reactors means that

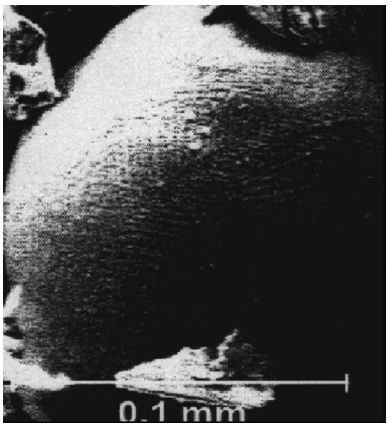

Fig. 2.7. Example of a large grain collected after many discharges in a fusion device [23, 24, 26]

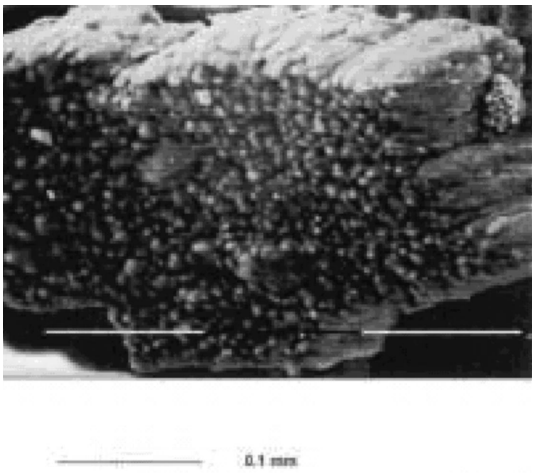

Fig. 2.8. Agglomerates of grains collected after many discharges in a fusion device [23, 24, 26]

radioactive dust grains can be formed if any leak appears in the device, which can be dangerous. The uni-polar arcs at the surface are also well known in fusion devices and can produce in principle dusts with complex shapes such as carbon nano-tubes (the standard method in nano-tube production is to use arc discharges). Thus it is not surprising that close to the wall of nuclear fusion devices one finds nano-tubes levitating in the surface electric field. It has been claimed that such nano-tubes were observed in tokamaks [27]. Observations [27] are indirect, and since the nano-tubes were not collected after discharges, they should have been destroyed somehow in the following discharge. Observations show that many grains collected after discharges are off have strong magnetic properties, although no magnetic materials were used for surface coating or treatment. This means that magnetic dust is created during discharges. On the other hand, high power loading during disruptions or in edge-localized modes leads to the evaporation of wall films, which was observed, and dust grains are known to grow effectively from over-saturated vapors. Coagulation of the grains can be due to collective or non-collective attraction. The average size of the grain agglomerates seen in fusion devices after dust coagulation is about $0.1\,\mu$m. The mechanism of dust growth in the case of high-power loading can be checked by exposing the carbon material to electron gun flux repeatedly using high-power electron beam [27]. The average power to which the carbon material was exposed in these experiments was about $1\mathrm{GWm}^{-2}$ and the evidence of formation of fullerene-like materials, as well as formation of dust agglomerates, was established. It is known that fullerenes can be produced at the periphery and carbon nano-tubes can be produced at the center in the same arc discharge. Therefore this observation serves as independent argument for possible presence of nano-tube dust structures close to the walls of fusion devices [27]. Formation of magnetic dust close to the wall is of special interest both from the general physical point of view

and from the point of view of applications for the onset of fusion discharges when the magnetic dust collected in the minimum B region can act as a source of impurity raising the emission rates. In future fusion devices, the main concern will be the dust radioactivity [26]. This raises many safety issues. A new technique for dust removal during discharges should probably be used [15, 25]. At present, researchers investigating interactions between high energy fluxes and walls that are expected to take place in the next generation of controlled fusion devices agree that the thin films covering the walls will be removed from the walls before any discharges occur as dust and as evaporated gas, but they still will rely on recycling of the wall covering by thin films needed for subsequent discharges. According to the present observations this recycling of the wall properties is not possible.

The last but not the least important problem associated with dust formation in future fusion devices is the radioactivity of dust excited by nuclear reactions. If this radioactive dust is to be removed somehow, the volume of radioactive waste would be tens of tons per year. This means that such reactors will not necessarily be radioactively clean, as it was thought before for controlled nuclear fusion. Thus one should remove dust from reactors before the reactions begin. The main technological problems in future controlled fusion energy production are related to wall-plasma interactions, in addition to complex plasma behavior.

2.5.3 Table Size Fusion and Neutron Sources

This is also known as dust cluster fusion. The first stage is to form a sort of cold collection of dust grains that can be either in suspension or in a complex plasma state. The second step is to irradiate them with short-pulse intense laser radiation [28, 29, 30]. The same can be done for single-layer plasma crystals or dust clusters confined externally in a parabolic potential well. No attempts have been made to perform the latter experiments. It is important that many grains are simultaneously subjected to an intense laser pulse. Each grain then explodes, evaporates, and forms an expanding cloud. Plasma electrons are heated up to 0.5 MeV and act on ions by ambipolar forces increasing their energy above the nuclear reaction threshold. Each expanding cloud that is initially packed close to other clouds will have a large nuclear density to produce nuclear reactions. The laser absorption rate is larger for materials formed by clusters or plasma crystals than in ordinary dense matter.

This is considered as a possible method for future fast neutron sources and new fusion table size energy devices. At present, investigations in this field are very intense, but the only foreseeable application so far is the creation of an intense neutron source because the efficiency of energy production is at present very low. Experiments with complex plasma crystals have not yet been performed and the role of strong grain interactions in both energy production and neutron output has not been investigated.

2.5.4 Solar Cells

The main problem with energy production by direct conversion of solar energy into electricity is that of effective solar cell production. Using composite materials made from complex plasma monolayer depositions is one possible way of making a progress in this field, but much research will have to be conducted first. The possibility that a method of efficient energy production will eventually be found still cannot be excluded [31].

2.6 Environmental Problems

2.6.1 Dust is Found Everywhere

It is amazing that dust is everywhere. There are four sources of dust in atmosphere: a) disintegration of meteorites upon reaching the atmosphere; b) volcanoes; c) human activity; and d) dust agglomerates produced by cosmic rays. The relative role of the first three sources of dust remains unknown; the cosmic ray source may be responsible for global warming of the atmosphere, and we discuss it later.

Since the rate of ionization is rather low in the lower atmosphere, we cannot speak about the role of complex plasma effects. Some sporadic ionization is always present starting at an altitude of 50 km, and at about 100 km stationary ionization takes place and the first E-layer of the ionosphere is located. At that altitude, the degree of ionization is almost the same as in present low-temperature laboratory plasma experiments. More dust can be found at even larger altitudes.

The magnetosphere is full of dust, and interplanetary media have a lot of dust that is transferred in both directions, i.e., from Earth to other planets and from other planets to Earth (in different regions of space). Planetary rings are formed from dust and have unusual properties that can probably be explained only by collective effects, namely some rings are extremely thin (about several meters) and extremely wide in the plane of the ring. The rings of Saturn are well-known (many of them are not visible but the well-known ones made of large grains and stones are visible). The Earth also has a dust ring just like all the other planets. The planets themselves and the Sun are formed from a dust cloud by gravitational condensation and it is difficult to exclude the possibility that at this stage the collective effects do not play any role. At present, star formation near dust clouds is observable and the role of ionization in this formation seems to be important. Some young stars are usually surrounded by dust clouds (the so-called cocoons), and some of them emit dust grains from their surface and this dust is quickly agglomerated while expanding in the star's wind. The dust is clearly visible behind the shocks felt after supernova explosions, the process of dust agglomeration is visible, and the interstellar region is full of dust. Some galaxies are rather

rich in dust (about 10–20% of their mass), etc. Finally, it is worthwhile to mention that archeology would be impossible if dust on the surface of the earth has not covered previously existing culture layers of past societies. The amount of dust falling on the earth's surface per year is about 100 million tons [32, 33, 34, 35, 36, 37, 38].

Thus we are living in a world where dust plays an important role. We mention these effects only to indicate the proper role of complex plasma not only in fundamental physics but also in our understanding of our place in the world.

2.6.2 Global Warming

There are two explanations for to the observed global warming effect. The first is related to the influence of human activities; the second involves natural phenomenons. We discuss here only the second possibility.

It is rather not clear from the first glance that global warming can be related to the influence of cosmic rays, i.e., very fast particles approaching the Earth's atmosphere from space. The maximum of the energy spectrum of these particles is about 1 GeV. Solar wind, if sufficiently strong, can whisk these particles away, not allowing them to penetrate into the Earth's atmosphere. When the solar wind is not so strong, the cosmic rays of energies of about 1 GeV (and even lower) can penetrate the upper atmosphere. It is known that cosmic rays can set a chain of chemical reactions that create radicals in the atmosphere. The sequence of subsequent events is very similar to that in etching. The radicals form ever-larger clusters until they are of the size of small grains. The small grains serve as seeds for the formation of water droplets and, thus, clouds. The total cloudiness determines the average temperatures.

If this is the correct sequence of events, the cloudiness and warming depend largely on the strength of the solar wind, which in turn depends on the solar activity. This dependence of cloudiness on solar activity can be checked with good accuracy against centuries-old records with very good agreement between the cloudiness and the solar activity. According to this point of view, the global warming is a natural effect related to the variation of either the solar activity or the intensity of galactic cosmic rays. To check the possibility of grain formation by cosmic rays, laboratory experiments are planned to be performed by using fast protons from the existing accelerators [39].

As is well known, other weather phenomena such as thunderstorms and tornadoes are related to the presence of dust as well.

2.6.3 Noctilucent Clouds

Noctilucent clouds and usual clouds are formed at the altitudes where the atmospheric temperature is minimum. The second minimum (about $100°\mathrm{K} \approx -170°\mathrm{C}$) exists at a height of 90 km [33, 40]. At this altitude one can see the so-called noctilucent clouds. It was discovered in 1989 [42] that noctilucent [33]

clouds scatter radar radiation anomalously. They must be dust clouds since the width of the reflected signal indicates that the velocities of the particles that create them are in millimeter range, and even at low temperatures there can be no electrons, ions, or neutral air particles. Subsequent rocket experiments confirmed that indeed noctilucent clouds consist of dust; more exactly, ice grains that include many impurities. It is interesting to note that noctilucent clouds had not been observed before the Industrial Revolution, but at that time no proper observations could be made. At present, accurate observations were made by rocket [37] experiments in which dust is collected from noctilucent clouds. These observations demonstrate that the amount of dust in these clouds is increasing with time, which can mean that it is due to human activity. According to observations, noctilucent clouds are extremely thin and they are perhaps in the state of complex plasma liquid.

2.6.4 The Ozone Layer

It was once believed that the ozone layer is located at 30 km above the Earth's surface. This is not fully correct since the "layer" has a broad distribution at altitudes from 25 km up to 90 km, with a maximum intensity at about 30 km. This means that ionization can be important there. On the other hand, ozone of the "layer" is not in the molecular state in the volume; it exists in impurities embedded in ice grains. Thus complex plasma physics can be related to the ozone problems. It is also deeply related to motions of middle and upper atmosphere, its convection, and exchanges existing between the upper and the lower atmosphere as well as in the atmosphere between poles and equator [41].

2.6.5 Industrial Emissions and Car Exhausts

There exists a large body of literature devoted to possible methods of decreasing the dust component in industrial emissions and car exhausts. However, most of them propose the creation of a gas discharge to charge grains and take them away via some electric field. The literature gives an impression that it is almost the same as in etching problems. The difference is in the gas pressure, which is much larger, and in the equality of electron and ion temperatures. We have already discussed that the direct use of electric fields is completely ineffective in etching. The same can be expected in issues of industrial emission reductions. Success is likely to be achieved only through the use of equipment discovered for cleaning etching devices or at least through the use of the special properties of complex plasmas.

Finally, we note that this book's focus is neither astrophysical nor industrial applications of complex plasmas. We introduced these topics so that the reader may have a complete picture of the amount of problems with which the complex plasma physics is concerned.

References

1. A. Gasgarden A. *et al.* (1994). *Plasma Sources Sci. Technol.* **3**, 329.
2. A. Boushoule *et al.* (1991). *J.Appl.Phys.* **70**, 1991.
3. L. Boufendi and A. Boushoule A. (1994). *Plasma Sources Sci. Technol.* **3**, 262.
4. A. Bouchoule, (1999). *Technological Impacts of Dusty Plasmas*in: *Dusty Plasmas: Physics, Chemistry and Technological Impacts in Plasma Processing*. John Wiley and Sons.
5. G. Selwyn, J. Heidenrich, and K. Haller (1990). *Appl.Phys. Lett.* **57**, 1867.
6. G. Selwyn, J. McKillop, K. Haller, and J. Wu (1990). *J.Vac.Sci.Technol.* **18**, 1726.
7. G. Selwyn, *Optical Characterization of Particle Traps*. Proceedings of NATO Advanced Research Workshop on Formation, Transport and Consequences of Particles in Plasmas, Chateau de Bonas, Castera-Verduzan, France (1994). Plasma Sources, *Science and Technology* **3**, 340.
8. S.V. Vladimirov, K. Ostrikov, and A.A. Samarian (2005). *Physics and Applications of Complex Plasmas*, Imperial College, London.
9. S.V. Vladimirov and K. Ostrikov (2004). *Phys. Rep.* **393**, 175.
10. D. Samsonov, J. Goree (1999) *J.Vac Technol.A* **17**, 2836.
11. K. Horiuchi, S. Iizuka, S., and N. Sato (2000). *Surf. Coat. Technol.* (Switzerland), **131**, 243.
12. E. Stoffels, W. Stoffels, H. Kersten, G. Swinkels, and G. Kroesen (2001). *Phys. Scr.* **T89**, 168.
13. H. Kersten, E. Stoffels, W. Stoffels, M. Otte, C. Csambal, C. Deutsch, and H. Hippler (2000). *J. Appl. Phys.* **87**, 3637.
14. S. Veprek, S. Reiprich, and L. Shizi, L. (1995). *Appl.Phys.Lett.* **66**, 2640.
15. T. Oku, T. Hirata, N. Motegi, R. Hatakeyama, N. Sato, T. Mieno, N.Y., Sato, H. Mase, M. Niwano, and N. Miyamoto (2000). *J. Mater. Res.* **15**, 2182.
16. Report on 3d European Conference on Dusty Plasmas, 1999.
17. N. Sato (2002). *J.Phys. Society Japan*.
18. B. Annaratone, A. Khrapak, A. Ivlev *et al.* (2001) *Phys.Rev.E* **63**, 036406.
19. U. Konopka, D. Samsonov, A. Ivlev, J. Goree, V. Steinberg, V., and G. Morfill, G. (2000). *Phys. Rev. E* **61**, 1890.
20. N. Sato, G. Uchida, Y. Kaneko, S. Dhimizu, and S. Iizuka (2001). *Phys. Plasmas* **8**, 1786.
21. V. Tsytovich and S. Vladimirov (2004). *IEEE Trans. Plasma Sci.* **32**, 659.
22. V. Tsytovich, S. Sato, and G. Morfill (2003). *New Journal of Physics* **4**, 43.
23. J. Winter (1996). *Plasma Phys. Control Fusion* **38**, 1503.
24. J. Winter (1998) *Plasma Phys. Control Fusion* **40**, 201.
25. J. Winter, A. Nefedov, and V. Fortov (2001). *J. Nucl. Materials* **290–293**, 509.
26. V. Tsytovich and J. Winter (1998). *Phys. Uspekchi* **41**, 815.
27. A. Kukushkin and A. Rantzev-Kartinov. *Long Lived Filaments in Fusion Plasmas: Review of Observations and status of Hypothesys of micro-product assembled skeletons* (Preprint INNN RFS "Kurchatov Institute").
28. T. Ditmire, T. Donnelly, R. Falcone, and M. Peny, M. (1995). *Phys. Rev. Lett.* **17**, 3122.
29. T. Ditmire, T. Donnelly, A. Rubenchik, R. Falcone, and M.Perry (1996). *Phys. Rev. A* **53**, 3379.
30. T. Ditmire, J. Zweiback, V. Yanovsky, T. Cowan, G. Hays and K. Wharton (1999). *Nature* **398**, 489–92.

31. P. Shewee, B. Steain (2002). *Physics News Update AIP* Numver 682, April 13 (2004), *J.Mat.Sci.*
32. M. Horanyi, H. Houpis, and D. Mendis (1988). *Astrophys. Space Sci.* **144**, 212.
33. W. Ecklund and B. Basley (1981) *J.Gephys.Res.* **86**, 7775.
34. S. Kaplan and S. Pikel'ner (1974), *Ann. Rev. Astronomy and Astrophys.* **12**, 113.
35. G. Morfill and M. Scholer eds. (1992). *Physical Processes in Interstellar Clouds.* Reidel Publ. Comp.
36. R. Chevalier (1992). *Nature* **355**, 691.
37. O. Havnes, T. Aslaksen, and A. Brattu (2001). *Physica Scripta* **T89**, 133.
38. V. Tsytovich, O. Havnes Proceedings ICPDP-2002, Contributed papers (2002).
39. *Ion -aerosol-cloud interactions*, **007**,Proceedings CERN workshop. Ed.J.Kirkby (2001).
40. T. Backnouse (1985). *Meterol. Mag.* **20**, 133.
41. M. Christie (2001). *The Ozone Layer* A Philosophy of Science Perspective, Cambridge University Press, N.Y., London.
42. O. Havnes (1989). Abstracts of Proceedings of the First Workshop on Duty Plasmas, Capri 1989, Napoly University, Italy.

3

Elementary Processes in Complex Plasmas

In this chapter, we give the basic description of the main physical processes which create large sinks of plasma by dust grains. We consider first an individual grain embedded in a plasma to study screening, scattering, and absorption of plasma particles. Then we estimate the effect of many grains on other plasma components; in particular, the rate of damping and the scattering introduced by the presence of grains. These are the elementary processes of the creation of plasma fluxes in complex plasmas. These fluxes also inevitably change the ground state of the dust-plasma system, the mode propagation and the grain interactions, which are the subjects of consideration in subsequent chapters.

3.1 Screening of Grain Field in a Plasma

3.1.1 Elementary Estimates

First of all, we remind that any object embedded in a plasma becomes charged (usually, this is a negative charge). This is due to the larger mobility of plasma electrons. Usually the grains acquire the so-called floating potential. This occurs if other possible sources of grain charging such as the ultraviolet radiation, the secondary electron emission, etc. are not effective. This is the simplest case to understand the processes of grain screening and the presence of large charges on dust grains in plasmas.

The charge on the grain can be estimated by equalizing the potential on the surface of the grain $\phi_s \approx Z_d e^2/a$ (here, a is the grain size and Z_d is the grain charge in units of the electron charge e) to the electron temperature T_e. Indeed, when the grain is inserted in a plasma, the electrons reach the grain first, moving on average with the electron thermal velocity which is much higher than the plasma ion velocities. The negative grain charge therefore increases until it is sufficiently high to reflect the main part of the plasma electrons (with velocities of the order of the average electron velocity). Thus

V. N. Tsytovich et al.: *Elementary Processes in Complex Plasmas*, Lect. Notes Phys. **731**, 67–140 (2008)
DOI 10.1007/978-3-540-29003-2_3

only fast electrons with velocities larger than the electron thermal velocity are able to reach the grain but their flux to the grain is much smaller than that of the main part of plasma electrons and can be equalized by the plasma ion flux.

Starting from this stage where the electron and ion currents are equal, the charge of the grain becomes stationary and the total net current on the grain surface is equal to zero. The potential of the grain surface is then somewhat larger than the electron temperature and therefore the dimensionless grain charge can be estimated as $z = Z_d e^2/aT_e \approx 2 - 4$, as has been stated before. This estimate is valid only in the case where the electron distribution is thermal and can be determined by the electron temperature T_e. The energy of the ions which are attracted by the grain will increase when reaching the grain up to $(2 - 4)T_e$, which is usually much larger than the ion average energy in a low-temperature plasma, where $\tau = T_i/T_e \ll 1$ (the typical value for most experiments on complex plasmas is $\tau \approx 0.01$).

Therefore one can expect that the ions penetrate quite deep in the grain surface and are attached to the grain material. Similarly, the electrons which are able to reach the grain also have large energies and penetrate deep inside the grain. The sticking coefficient of both electrons and ions can be expected to be close to 1. The charging of the grain is accompanied by continuous deposition of material on the grain (deposition of both electrons and ions which in a sense recombine on the grain; naturally, the main mass deposition is due to plasma ions). The growth of the grain mass because of this process is quite slow at least for most of the present experiments. Finally, when electrons and ions inside the grain "meet" each other and recombine, the time of diffusion to the surface where they can form neutral atoms that can leave the grain is also very large. These processes should be taken into account only for small grains with small grain charges and for long-time grain evolution which can be met mostly in astrophysics or specially for small aerosols with several electron charges on their surface. We deal here only with the physics of highly charged grains of large size (say larger than μm) and with experiments with relative short timescales (say, minutes or hours) where these processes of the grain growth in size can be neglected.

The described simple picture of the grain charging is confirmed by most of existing low-temperature plasma experiments. According to this charging process, each grain becomes a sink of plasmas in short timescales (estimated to be of the order of microseconds for typical experimental conditions). The charging time is the shortest time in the problems of the grain motions since the change of the grain charge when the grain moves from one point to another is almost instantaneous.

Although simple in principle, the appearance of large grain charges poses many problems not resolved yet. It is complicated due to various processes including the effects of non-linearities and the presence of large number of neutral atoms in the low-temperature plasmas that makes the ion and electron collisions with them important. The charge can depend on the polarization

around the grain, i.e., on the screening of the grain field, and the latter can in turn depend on the grain charge.

The condition that the screening is linear requires that the potential energy of particles which take part in the screening of a large grain charge, namely the electron energy $|e|\phi$ and the ion energy $Z_i e\phi$, is much less than their kinetic energy T_e and T_i, respectively. This requirement is more restrictive for plasma ions since their kinetic energy is usually two orders of magnitude smaller than that of electrons.

3.1.2 Linear Debye Screening

We first remind the commonly used concept of linear screening where the nonlinearity is not taken into account. The classical way to derive the screening of a charged body inside a plasma is to use the Poisson's equation

$$\nabla^2\phi = -4\pi(Z_i e n_i(r) - e n_e(r)) \,, \tag{3.1}$$

where Z_i is the charge state of ions (usually in a low-temperature plasma, $Z_i = 1$) and $n_i(r)$ and $n_e(r)$ are the r-dependent ion and electron densities, respectively. In the case of Boltzmann distributions for the densities (which is actually questionable for large charges – see Sect. 3.1.3), we have $n_i(r) = n_i \exp(-Z_i e\phi/T_i)$ and $n_e(r) = n_e \exp(e\phi/T_e)$. As was mentioned, the shielding of a grain is nonlinear. Only in the case of $e\phi \ll T_{e,i}$, we can expand the exponential to get

$$\frac{1}{r^2}\frac{\partial}{\partial r}\left(r^2\frac{\partial\phi}{\partial r}\right) = \frac{1}{\lambda_D^2}\phi \,, \tag{3.2}$$

where λ_D is the total plasma Debye length and

$$\frac{1}{\lambda_D^2} = \frac{1}{\lambda_{D,e}^2} + \frac{1}{\lambda_{D,i}^2} = \frac{4\pi n_e e^2}{T_e} + \frac{4\pi n_i e^2 Z_i^2}{T_i} \,. \tag{3.3}$$

For $\tau \ll 1$, the linear screening is determined by the ion Debye length

$$\frac{1}{\lambda_D^2} = \frac{1}{\lambda_{D,i}^2}(1 + \tau(1 - P)) \,. \tag{3.4}$$

The best way to consider the screening is to introduce the screening factor $\psi(r/\lambda_{Di})$,

$$\phi = -\frac{Z_d e}{r}\psi \,, \tag{3.5}$$

and consider this factor as a function of the ratio of the distance to the ion Debye length (recall that for $\tau \ll 1$ the plasma Debye length is approximately the ion Debye length). The equation for the linear screening factor ψ is the simple linear equation

$$\frac{d^2\psi}{dr^2} = (1 + \tau(1 - P))\psi \approx \psi \ , \tag{3.6}$$

where the last approximate expression is written for $\tau \ll 1$ often met in current experiments. The solution for this linear screened potential is an exponent and the potential is often called the "Debye potential" (we use the subscript D for it)

$$\psi_D = \exp(-(r - a)) \ , \tag{3.7}$$

where a is the grain size in units of Debye screening length. Sometimes the term "Yukawa potential" is used if the screening has the form of the Debye screening but both the charge and the screening length do not correspond to the Debye screening

$$\psi_{\rm Y} = q_Y \exp(-(r - a)/R_Y) \ . \tag{3.8}$$

where q_Y is the ratio of effective charge to the grain charge and R_Y is the ratio of effective screening length to the Debye length. Although no physical reasons exist for using Yukawa potential, this term is rather spread in the literature. The reason is that when trying to approximate the real screening potential by Debye screening potential, one usually finds discrepancy: an approximate fit can be reached only with (3.8) in restricted range of distances with $q_Y \neq 1$ and $R_Y \neq 1$. The Yukawa potential should be considered only as a mathematical fit for real potential and can be cited only as that without giving any physical interpretation for the existing discrepancy of the real screening factor and the Debye screening factor. Our aim will be to explain the physics of such discrepancy and to describe more adequate fits of really found screening factors. The main reason for the discrepancy is that the linear approximation is not a good one for dust particles, especially if their charges are large (as should be in complex plasmas to observe the dust-plasma condensation). Not only at the surface of the grain where for ions the factor in the Boltzmann exponent is usually huge of the order of $z/\tau \approx 400$ and the expansion of the exponent can never be used, but also far from the grain this factor survives to be rather large. *The Debye potential based on the linear expansion of the Boltzmann distribution is usually not valid for dust charge values of present experiments.* The screening is non-linear and cannot be described in the form of Debye or Yukawa potential. One could be more flexible in the statements saying that perhaps the linear approximation is not valid close to the grain surface but it starts to be valid far from the grain surface as Yukawa potential with some $q_Y \neq 1$ and $R_Y \neq 1$. The problem is that in order to use the Yukawa potential with some effective dust charge and effective screening length, one needs at least the linear approximation valid at the distances of the order of the ion Debye length and this is not the case for the values of dust charges in most existing experiments. Thus for small distances the screening cannot have the form of Yukava screening. At large distances where one can hope that the screening could be linear the Yukawa screening also cannot be used. The reason is that for real conditions at the distances

where one hopes that the screening is linear the other grains are sufficiently close to the considered probe grain and influence its screening, which starts to be collective (see next chapters). Thus the screening of grains in complex plasmas cannot be described by Yukawa form.

3.1.3 Non-linear Screening

Conditions for the Screening to be Non-linear. Let us estimate the ion potential at the surface of the grain and far from the grain surface. Linear expansion of the Boltzmann factor $\exp(e\phi/T_i)$ close to the grain being $\approx \exp(200) - \exp(400)$ is impossible and the screening at short distances is always non-linear. To estimate the applicability of the linear screening at larger distances we can assume in some rough approximation the decrease of the grain potential as $\propto 1/r$ as if the screening is still small and the potential of the grain is simply the Coulomb potential. Then we obtain that even for sufficiently large distances from the grain surface, $r \approx az/\tau \gg a$; the non-linearity is still large. For the Boltzmann distribution of the electron polarization charge close to the grains, $\phi \propto \exp(z)$, is also non-linear but for some not-very-large distances from the grain, $r \gg za \approx (2-4)a$, it can be already linearly approximated. For standard values used in current experiments for the ion density of the order of $n_i \approx 10^9 \mathrm{cm}^{-3}$ and for the room ion temperature, one has the estimate $\lambda_{Di} \approx 37\,\mu\mathrm{m}$, while for $a \approx 5\,\mu\mathrm{m}$ the distance where the screening is still non-linear is $az/\tau \approx 3000\,\mu\mathrm{m} \gg 37\,\mu\mathrm{m}$.

The non-linearity in screening has the consequence that the electrons and ions before being absorbed by the grain move on trajectories different than that in the Coulomb potential or even Yukawa potential. Therefore there could be some particles which do not reach the grains and do not contribute to the current at the grain surface although the conservation laws of the energy and momenta allow them to reach the grain in principle. This effect could be most important for ions and known as the problem of the potential barriers. In the presence of the barriers some of low-energy ions are not able to reach the grain thus making its negative charge larger than that in the absence of the barriers [1, 2].

The non-linearity in screening also has more serious consequences. Indeed, assume that we inserted a grain into a plasma and its charge starts to grow continuously until it reaches its equilibrium value. Then in the stage where the ions start to behave non-linearly one should divide their distribution into two parts – the trapped ions and the un-trapped "free" ions. At some point r outside the grain the ion energy can be larger than the potential $e\phi(r)$ and at another point it could be less than $e\phi(r)$. In the second case the ions are either trapped or absorbed by the grain. This will depend on the angle of the velocity of these ions relative to the direction to the grain – in some cone around this direction the ion trajectories will touch the grain and the ions will be absorbed by the grain (obviously this angle can be rewritten trough the value of the angular momentum). In case an isotropization mechanism acts

on ions with energies less than $e\phi(r)$, all of them are finally absorbed by the grain and then no ions with energies $< e\phi(r)$ are present around the grain.

The isotropization mechanism could be weak, but one should have in mind that we are interested in the equilibrium state of the grain, and the timescale of the isotropization will only then determine the timescale of reaching the equilibrium grain charge. The absence of ions with energies less than $e\phi(r)$ changes the polarization charge around the grain and therefore the trajectories of ions that either reach the grain surface or cannot reach the grain surface. This changes the ion absorption and the charge of the grain. Since at the surface of the grain $e\phi(s) \gg T_i$, we conclude that for any complex non-linear distribution of the polarization charge around the grain there should exist a broad region where the ion energies are less than $e\phi(r)$. In partially ionized plasmas, there are many neutral atoms and the ion-neutral collisions can provide an effective mechanism of isotropization. The charge exchange collisions can produce a new trapped ion from the untrapped ions when the fast ion gives its energy to the fast neutral, and the left slow ion can be trapped. We therefore should discuss the problem of trapped ions in the grain screening.

The charging process also creates an additional space charge close to the grain since the grain is absorbing both electrons and ions, and in the vicinity of the grain the ions and electrons are moving mainly toward the grain but not from it. For a single isolated grain in a plasma, this space charge creates a long-range non-screened potential which is modified significantly in the presence of many grains (see below).

One of the most important parameters determining the non-linearity in screening is the degree of non-linearity at the distance of the linear Debye length

$$\beta = \frac{za}{\lambda_{Di}\tau} \ . \tag{3.9}$$

For $\beta \ll 1$ the non-linearity is small and for $\beta \gg 1$ it is large. The plasma condensation is observed for $\beta \approx 35-50 \gg 1$. For $\beta \gg 1$, the ion scattering by the grain field occurs for impact parameters much larger than the ion absorption [80] and therefore the screening potential can be found independently of the plasma absorption by the grains. Influence of absorption on the screening can be then shown to be small and the problem of the potential barriers can be resolved explicitly by using analytic expressions for the non-linear screening in the absence of absorption [2].

Using the non-screened potential at a distance of order ion Debye length and requiring that at this distance $e\phi/T_i \ll 1$, one then obtains the inequality $Z_d \ll 3N_{D,i}$, where $N_{D,i}$ is the total number of ions in the ion Debye sphere. This inequality is indeed valid for the case of a single ion in plasma where Z_d should be replaced by 1 and where usually $N_{D,i} \gg 1$ (by the definition of a weakly coupled plasma). In complex dusty plasmas the dust charge range is $Z_d \approx 10^3$–10^5, while $N_{D,i}$ is of the order of 10 and the mentioned inequality is not satisfied. The condition of applicability of the Yukawa screening can be

written as

$$Z_d \ll 52 \left(\frac{10^9 \mathrm{cm}^{-3}}{n_i} \right) . \tag{3.10}$$

Thus for most complex plasma experiments where the plasma condensation was observed *the screening was non-linear and* $\beta \gg 1$.

The Physics of the Non-linear Screening. For the case of large charges in the absence of trapped ions, the solution is known as the Gurevich screening [3, 4]. However, it is not often used in the description of the grain screening. More often used is the Yukawa screening, which is not applicable to the values of grain charges in most of the present experiments in complex plasmas. The reason is perhaps that although the physical argument used in [3, 4] are very simple, their final expressions are complicated and it is rather difficult to imagine the real difference between linear and non-linear screening without numerical computation. The latter were in fact not fully performed for the most interesting case $\tau \ll 1$. Thus we proceed here with the analysis aiming to reach a simple expression for the non-linear screening and to demonstrate the qualitative differences between linear and non-linear screening. The simplified expressions we are giving here are also useful for other physical and numerical studies of the screening effect in complex plasmas.

The arguments to introduce the non-linear screening are as follows [3, 4]: in the case where there is no trapped ions, the screening occurs due to ions which can penetrate into the vicinity of a grain from distances far from the grain. Since the potential of the grain at the surface and at any point surrounding the grain is negative and the potential at "infinity" is zero, we should take into account only those ions which have a positive kinetic energy at the "infinity", i.e. use the inequality $m_i v^2/2 > -e\phi$ (here, e is the absolute value of electron charge) for integration of the ion distribution with respect to velocity to obtain the ion number density in the Poisson's equation. It is assumed that this distribution is still Maxwellian. The electrons are repelled by the grain and for them it is possible to use the simple Boltzmann distribution. The integration of the ion distribution taking into account the mentioned restriction is straightforward, leading to an expression containing error functions [4]:

$$\frac{d^2\psi(r)}{dr^2} = R(\psi(r), r) , \tag{3.11}$$

with

$$R(\psi, r) = \frac{r}{a}\frac{\tau}{z} \left(I(x_i) - \exp(-\tau x_i) \right) \tag{3.12}$$

and

$$I(x) = \exp(x)(1 - erf(\sqrt{x})) + \frac{2}{\sqrt{\pi}}\sqrt{x}; \quad x_i = \frac{za\psi}{r\tau} . \tag{3.13}$$

The last term in the brackets of (3.12) represents the electron contribution, it is of order unity. For $\sqrt{x_i} \ll 1$ we obtain the Yukawa (Debye) approximation. As mentioned above, at the dust grain surface $x_i = z/\tau \approx 400-200$. Figure 3.1

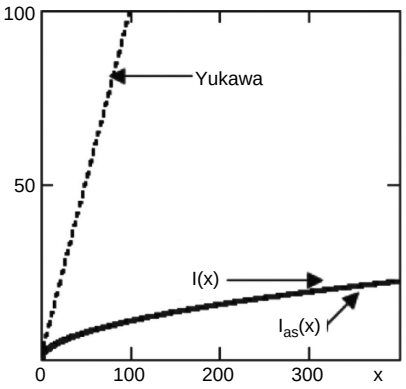

Fig. 3.1. $I(x)$, the *solid line*, and $I_{as}(x)$, the *dotted line*, almost coincide with each other within a broad range of x; note that the Yukawa approximation deviates substantially from both of them. The difference between the lines $I(x)$ and $I_{as}(x)$ (between the *solid line* and the *dotted line*) is actually difficult to see; this coincidence is used to develop the simplified model of non-linear screening

shows the Yukawa approximation where $I(x_i) \approx 1 + x_i$ and the function $I(x)$ in the range of x from 0.1 to 400 as well as its asymptotic expression $I_{as}(x) = 2\sqrt{x}/\sqrt{\pi}$. It is clear that within a broad range of x the exact function $I(x)$ can be approximated by $I_{as}(x)$.

The Gurevich Polarization Charge. This model was proposed in [5]; we describe the main feature of this approach. Taking into account only the asymptotic expression, (3.11) describing the non-linear shielding can be rewritten into a simpler form by using renormalization of the distance r (including the constants in the normalization of the distances). We give later the final results for the effective screening length; here, since at this point the normalization of the distances is not important, we pay attention mainly to the form of equation for screening. We find the equation in the form (where r the ratio of the distance to the Debye length times a constant factor [5])

$$\frac{d^2\psi(r)}{dr^2} = \sqrt{\psi r}\,. \tag{3.14}$$

Numerical investigation of this equation shows that its solutions are quite different from the Yukawa solution: the function ψ is larger than the Yukawa screening factor at small distances (corresponding to smaller screening) and is smaller at large distances (corresponding to larger screening), but then it becomes zero at a finite distance, say r_0. This is an important feature since the Yukawa exponent is usually not so small and if the screening factor tends to zero at the finite distance then all relatively small effects related to different processes including the dust attraction become dominant (roughly speaking, they "should be compared" with zero, not with the small exponent). It is possible to use (3.14) only for the conditions opposite to the case of the linear expansion where the Yukawa screening is operating. Thus at some large distances we need to match the solution of (3.14) with the Yukawa solution. This is the case when we consider only a single isolated grain. In reality the inter-grain distance is not so large as compared with

the non-linear screening distance and therefore at the distances where the non-linear screening starts to be small one should take into account the influence of the fields of other grains. Then the non-linear screening when it becomes weak should be matched not with the Yukawa screening of much smaller amplitude but with more complicated expressions which take into account the presence of other particles (we describe this effect of the collective screening later).

Here, we first try to show that in the range where the screening is highly non-linear the characteristic screening length is much larger than the linear Debye screening length. We give an estimate of the distance where the non-linear screening becomes weak and the assumption of the strong non-linearity in the screening starts to be violated, and after that we proceed with further simplification of the description of the non-linear screening.

The solution of (3.14) depends on the boundary conditions which can be chosen at the surface of the grain, $r = a$. One of them is trivial, $\psi(a) = 1$, and another is the value of the derivative of ψ with respect to r at the surface. The value of this derivative depends on the screening. We choose it as a negative one and adjust its value in a way that the solution after decreasing with r does not further increase and does not cross the line $\psi = 0$, i.e., does not become negative. Then the only solution is reaching at some point the value close to zero. The value of the derivative of the screening factor is determined by the screening itself and in the described way can be found with the precision of 5 digits after the point. As soon as ψ becomes close to zero, the solution of (3.14) is not valid anymore and should be matched with the linearized solution. The main point is that this junction appears at a finite distance where the dust charge is already almost (about 90%) screened and the left non-screened charge is much smaller than the value of the original grain charge. Then for an isolated grain where the non-linear screening should be joint with the Yukawa screening the "tail Yukawa screening" (although existing) is usually much smaller than the other effects. This certainly is true especially when many grains are considered and the dust–dust interactions are included. Therefore (as we will estimate further on) the Yukawa tail has no particular interest in complex plasma problems and we can approximately put, when interested in the non-linear screening, the screened potential to be zero at the point $r = r_0$, where the solution of (3.14) reaches $\psi = 0$.

Simple Explicit Expression for the Gurevich Polarization Potential. We can simplify the model of interaction by substituting $r = r_0$ in the right-hand side of (3.14). Then, after a new re-normalization of the distances, we obtain the equation

$$\frac{d^2\psi(r)}{dr^2} = \sqrt{\psi} \tag{3.15}$$

which has an analytical solution with qualitatively the same features as that of (3.14). Using the corresponding conditions for the decrease of the potential with distance and the relation $\psi(a) = 1$, we find the following solution of (3.15)

$$\psi = \left(1 - \frac{r-a}{\sqrt{12}}\right)^4 . \tag{3.16}$$

Here, we can give an exact expression for the normalized distances: the distances are normalized with respect to

$$\lambda_{Di}\left(\frac{\pi}{4}\frac{a}{\lambda_{Di}}\frac{z}{\tau}\right)^{1/5} . \tag{3.17}$$

We then use the following procedure to approximate the screening factor by the solution of the type

$$\psi = \left(1 - \frac{(r-a)}{\lambda_{scr}}\right)^4 . \tag{3.18}$$

The approximation done is that the size of the grain is much less than the screening length.

Equation (3.18) is adjusted with an exact solution of (3.14) (see Fig. 3.2); this allows us to find the numerical factor in λ_{scr}:

$$\lambda_{scr} = 3.4\lambda_{Di}\left(\frac{\pi}{4}\beta\right)^{1/5}; \quad \beta = \frac{a}{\lambda_{Di}}\frac{z}{\tau} . \tag{3.19}$$

For $r > \lambda_{scr}$ there appears the complete screening ($\psi = 0$) (of course in the approximate model that we use here). This model can then be named as the "hard sphere model" of the non-linear screening. The estimate of λ_{scr} for the existing experiments gives $\lambda_{scr} \sim (5{-}8)\lambda_{Di}$. It is amazing that this value is close to the dust separation in the dust-plasma crystals. The collective effects for 3D crystals can alter the interactions, but probably also giving attraction at distances larger than λ_{scr}.

One observation should be mentioned here: in no experiment performed so far the grain separation of the order of λ_{Di} was observed. The observed separations are significantly larger (about one order of magnitude) than λ_{Di}. One can argue that many experiments were performed in the plasma sheath conditions close to the walls where one can expect a large super-thermal ion

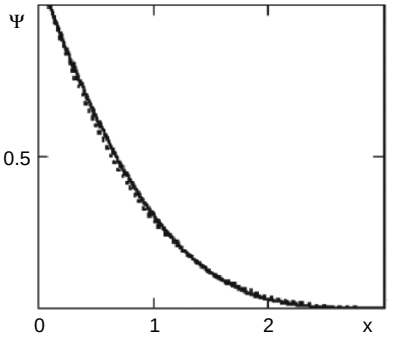

Fig. 3.2. The function ψ, *solid line*, is the solution of (3.14) for $a = 0.1$; the *dotted line* represents the solution $(1 - (r-a)/3.4)^4$

flow to the wall. In the case where the the ion drift velocity substantially exceeds the ion thermal velocity in the linear theory at least the contribution to the ion screening disappears, the screening is determined by electrons, and the electron Debye length is one order of magnitude (or more) larger than the ion Debye length. This seems to be of the order of the grain separation observed. However, these arguments do not take into account many important features of observations as well as the non-linearity in screening. Indeed, many dust structures were observed not in the sheath but in the pre-sheath, where the ion drift velocities are much smaller than those in the sheath. Moreover, the observation of structures with several hundred or more layers will completely exclude the effect of the ion drift. One should also take into account the friction of ions in the neutral gas which substantially decreases the ion drift velocity if the size of the structure is significantly larger than the ion-neutral mean-free path (which is the case of the present experiments). Thus it is doubtful that the ion flow can decrease the screening even in the linear approximation of screening. Further complications appear due to non-linearity of screening – the estimates show that the non-linearities are much less sensitive to the ion flow than the linear responses. Thus the observation raises a puzzle, why even after being compressed the grains are not decreasing their separation. The only reasonable answer is that they still repel each other and this can be the case if their Coulomb field is still not screened. The non-linear screening length (3.19) is indeed one order of magnitude larger than the ion Debye screening length and can provide a possible explanation of the observations.

General Non-linear Polarization Charge and Non-linear Screened Potential. Recently [6], the non-linear screening was considered (for arbitrary non-linearity) for the polarization potential proportional to $|\phi|^\nu$, $0 < \nu < 1$. It was shown that the general properties of the non-linear screening are very similar to that of Gurevich–Parker screening, namely (1) the finite size of the screening, (2) dependence of the screening on the parameter β, and (3) the non-linear screening length being substantially larger than the linear screening length λ_{Di}. The screening can be well given by the simple expressions

$$\psi_{nl}(r) = \left(1 - \frac{r}{R(\beta,\nu)}\right)^{2/(1-\nu)} \quad , \quad R_{nl}(\beta,\nu) = \lambda_{scr,nl} = d(\nu)\beta^{(1-\nu)/(3-\nu)} \ , \tag{3.20}$$

where the function $d(\nu)$ is determined by fitting the exact solution of the Poisson's equation with the ion polarization charge $\rho_i \approx |e\phi/T_i|^\nu$. The fitting should be performed in the same manner as for the Gurevich polarization charge and gives the function $d(\nu)$ shown in Fig. 3.3. The expression shown in Fig. 3.3 can be approximated by the analytical expression

$$d(\nu) \approx (2.1 + 12\nu^3) \ . \tag{3.21}$$

The dependence of the non-linear screening radius $R(\beta,\nu)$ on the non-linear parameters β and ν is demonstrated in Fig. 3.4.

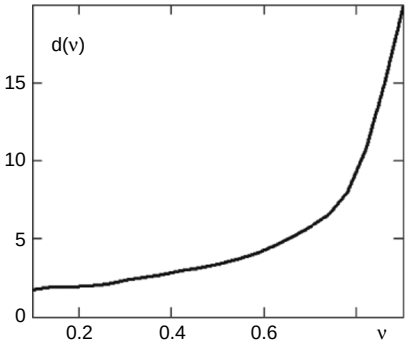

Fig. 3.3. The coefficient of the non-linear screening $d(\nu)$ as a function of the degree of non-linearity in the polarization charge ν found by numerical fitting of the exact solution of the Poisson's equation with the non-linear polarization charge $\rho_i = |e\phi/T_i|^\nu$ with the analytical solution (3.20)

It can be seen that for ν close to 1 (such as $\nu = 0.9$) the non-linear screening radius increases substantially. This effect is related with the fact that the screening character approaches that of the Yukawa screening (which is valid only for $\nu = 1$) since $(1 - r(1-\nu)/2R_Y)^{2/(1-\nu)} \to \exp(-r/R_Y)$ when $\nu \to 1$. Therefore it is worthwhile to demonstrate $R_Y = R(1-\nu)/2$ by the value which has the physical meaning only for $\nu \to 1$ (where the screening approaches the Yukawa screening) (see Fig. 3.5).

We can see that the screening for $\nu = 0.9$ is indeed close to the Yukawa screening although the factor in the exponent R_Y is not exactly equal to 1 (varying with β from 0.96 to 1.2), and obviously the Yukawa exponent operates only for $r \ll R_{nl}$. The last figure only illustrates that the screening tends to the Yukawa screening for $\nu \to 1$ while the screening radius is given by R_{nl} but not R_Y. Thus the general non-linear description of the polarization charge is useful to demonstrate the continuous change of the screening character with the change of the degree of non-linearity (ν) reaching the limit of the Yukawa screening which is not relevant for complex plasmas. But since some computations were done using the Yukawa screening, it is useful to have a more general analytic expression for the screening that generalizes the Yukawa

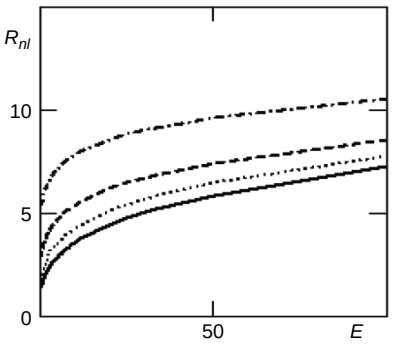

Fig. 3.4. The non-linear screening radius R_{nl} as a function of two non-linear parameters β and ν; the *thick solid line* corresponds to $\nu = 0.1$, the *dotted line* corresponds to $\nu = 0.3$, the *dashed line* corresponds to $\nu = 0.5$ (the Gurevich potential), and the *dash-dotted line* corresponds to $\nu = 0.7$. The line $\nu = 0.9$ is not shown; its value is increasing with β up to the value close to $20 = 2/(1-\nu)$

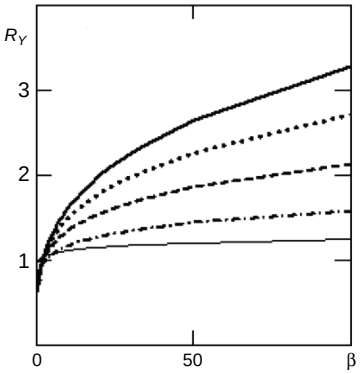

Fig. 3.5. The non-linear screening radius $R_Y = R(\nu)/2$ as a function of two non-linear parameters β and ν. The *thick solid line* corresponds to $\nu = 0.1$, the *dotted line* to $\nu = 0.3$, the *dashed line* to $\nu = 0.5$ (the Gurevich potential), and the *dash-dotted line* to $\nu = 0.7$. The line corresponding to $\nu = 0.9$ is not shown; its value is increasing with β from 0.96 up to 1.2, being close to 1 corresponding to the Yukawa potential

screening and approaches the latter in the corresponding limit (where the non-linearity becomes small).

The non-linear screening derived here is valid only in the limit of strong non-linearity. In the case where the non-linearity becomes weak, it should be usually matched with the linear screening (for a single grain) or the collective screening (for a system of grains, see below the details). For $\beta \gg 1$, the screened grain charge for the matching distance appears to be often of the order of 90% of the non-screened charge, i.e., the non-linear screening can almost totally screen the grain charge. But the tail of the screening also appears to be very important, especially in the presence of many grains where the linear screening becomes collective.

Thus for a single grain the "tail Yukawa screening," although it generally exists, is usually much smaller than other effects. In the case of many grains, the collective effects start to be especially important on the "tail" of the screened potential. As we demonstrate later, they can determine the grain–grain interactions. Therefore the Yukawa tail has no particular importance in complex plasma problems both in the case of the single grain screening and in the case where the collective effects are important. Thus by neglecting the "tail" potential we can (in the first approximation) put the screened Coulomb potential as zero after the point $r = R = \lambda_{scr}$, where the solution of (3.18) or (3.20) reaches $\psi = 0$.

We demonstrated already that the condition for condensation in a complex plasma strongly depends on the character of screening. Here, we can conclude that for most interesting applications this screening should always be the *non-linear screening.*

3.1.4 Problems to Solve in Grain Screening

There are several unsolved problems in the grain charge screening. Here, we list them together with brief description of approaches that can be used for deriving their solution.

- *How the grain charging influences the screening?*
  The charging process affects the screening in two ways: 1) it changes the charge density distribution close to the grain, and 2) it creates additional non-screened tail of the grain potential. Both these effects we consider in detail in the next section.
- *How the loss-cone instability influences the dynamics of screening?* We already mentioned that if an uncharged grain is inserted in a plasma, the charge on the grain starts to grow gradually until it reaches its equilibrium stationary value. On the other hand, it was demonstrated that in the final stage there exists a difference in the shielding by ions which locally satisfy the condition $|e\phi(r)| < m_i v^2/2$ and ions with $|e\phi(r)| > m_i v^2/2$. The latter cannot be transferred to the distances far from the grains, the "infinity." Some of them at the distance r have velocities directed within the angular interval corresponding to their trajectories eventually crossing the grain surface; these ions are absorbed by the grain on a short timescale (of the order of the transit time from the point r to the grain surface). The ions with other angular intervals are turned around the grain and can be considered as trapped particles. The concept of the trapped particles can be introduced only for the case where only a few ions are trapped; otherwise the ions produce a collective field which influences their motion so the concept of individual ions becomes meaningless.

  In the process of charging, when the charge of a dust grain increases, there can appear either a few trapped ions or even a sufficiently large number of them; this is where their collective field becomes important. The second case can appear even when the ion density of trapped ions is not so high to change the screening character. In this case, the ion distribution is a loss-cone distribution which is well known in plasma physics to be extremely unstable. An estimate of the growth rate of this instability (see, e.g., [7]) gives that it is of the order of the ion plasma frequency multiplied by the degree of anisotropy. This timescale is very fast and is in fact the fastest in the processes considered here. One should have in mind that usually the ion density significantly increases at the distances close to the grain. But even neglecting this increase, the growth rate of the instability is very high. We note that no efforts have been made so far to investigate this instability taking into account the spacial inhomogeneity of the loss-cone which is increasing while approaching the grain. Thus a definite conclusion can be made only after such investigation is performed. However, we can foresee the consequences of this instability if it develops fast indeed. The field excited by this instability reacts on the ion distribution in a way to close the cone in it, i.e., to convert the ions to that domain in the phase space where they are rapidly absorbed by the grains. The same final result can be produced by any process of ion scattering by collisions. The foreseen result is that the domain $|e\phi(r)| > m_i v^2/2$ and so the "trapped" ions will not appear during the dynamics of charging [3, 4]. Note that similar

problems appear for the cone created in the charging process, namely, can it be closed by the loss-cone instability?

- *How ion-neutral collisions, including charge exchange collisions, influence the screening?*
  This problem was first addressed in [8] and [9] estimating the role of the ion-neutral charge exchange collisions on the screening. In [9], an analytic theory was developed based on some physical assumptions that need to be investigated more in detail. One of these assumptions, that the trapped ions are collisionless with the Maxwell–Boltzmann distribution and with energy restrictions, is the same as that we have used while assuming for the non-trapped ions that the kinetic energy is positive at infinity and that the angular interval where the ions can reach the grain is determined by the energy and angular momentum conservation laws. The final conclusion of [8, 9] is that the number of trapped ions is independent on the ion-neutral charge-exchange collisions. Their physical arguments in favor of such an independence are that both rates of trapping and de-trapping are proportional to the frequency of these collisions. This statement survives even for the case $\lambda_{in} \gg \lambda_{scr}$, where the collisions should play no role. In fact, this result creates a puzzle. A possible resolution of the puzzle can be found in detailed solution of the kinetic equation including the ion-neutral collisions. First of all, these collisions can be treated as small perturbations, especially in the case where $\lambda_{in} \gg \lambda_{scr}$. A simple consideration with the collision term proportional both to the collision frequency and to the distribution function definitely shows that the perturbed distribution depends not only on the particle velocity and distance (as in the absence of collisions) but also on the angle between the velocity and the radius-vector. An equation for the perturbations becomes the partial differential equation in the distance, velocities, and angles. Its solution for the non-linearly screened potential is not a simple problem.

  Here, we can only outline a probable physical picture of the processes which seem to be important in such consideration. The presence of the angular dependence certainly raises the question of possible mechanisms of the particle isotropization. There can operate at least two of them: one due to the collisions and another due to collective fields created by the instability excited in the formation of the anisotropic ion distribution (the already discussed loss-cone instability). First of all consider the charge exchange collisions. It is known that their cross-section is almost independent on the velocity within a broad range of the ion energies up to 10–50 eV. Ions approaching the grain indeed increase their energy but still up to the highest energy at the grain surface the cross-section is almost constant and thus the collision frequency is proportional to the ion velocity. Thus the highest collision rate includes the ions which are already close to the grain surface and have the energies substantially larger than both the thermal ion energy and the thermal neutral energy. As a result of the charge exchange collision of the fast ion with a thermal-neutral atom, the latter gets

the high energy of the ion and takes it away while the ion becomes almost isotropically distributed with the energy of the order of the neutral atom temperature. The low-energy ions, created in the charge exchange collisions and located close to the grain, satisfy the relation $m_i v_i^2 < e\phi$. Those ions which are within the angular interval for their trajectories crossing the grain surface will fall on the grain and this angular interval in their velocity space will become empty on the timescale they reach the grain, r/v. Other ions which are outside this cone will be "trapped" by the grain. Thus any mechanism that scatters ions from one angular interval where they are trapped to the angular interval where they can reach the grain can serve as a mechanism of losses of trapped ions. One of the possible mechanisms of the ion isotropization is provided by collisions of low-energy trapped ions with low-energy neutrals. These collisions have a rate lower than the charge exchange collisions and were ignored in [9]. The loss-cone distribution instabilities are well investigated in plasma physics and provide another mechanism of the ion isotropization which is much faster than the collisions with low-energy neutrals [7]. Then the rate of creation of trapped ion is proportional to the neutral density and the rate of the trapped ion losses is independent of the neutral density. Thus the number of trapped ions decreases to zero when the neutral density tends to zero. We believe that solution of the puzzle of trapped ions can be found using the above arguments.

- *How the presence of an ion flow can change the screening?* For many plasma-dust grain systems, in the presence of the ion-neutral collisions, influence of the ion drift on the screening is small. On the other hand, there are experiments with one or a few mono-layer grain systems located in the plasma sheath close to the wall where the ion drift velocity can reach the ion-sound velocity. For those conditions, influence of the ion drift on the grain screening is significant. It was shown that the polarization cloud in the supersonic case (i.e., when the ion flow is supersonic) forms a supersonic electrostatic wake behind the grain which in the reference frame of stationary ions correspond to that of the ion-sound wave emitted by the grain [10, 11, 12]. Physically, the effect is analogous to the case of a grain moving with respect to an isotropic plasma with the velocity equal and opposite to that of the ion drift. The recent interest to this process in the complex plasma research is related to the effect of the wake forming the regions of negative polarization charge which can serve as a potential well for other grains [10, 11, 12]. As a result, the pairing effect takes place which could have some analogy to pairing [13] of electrons in superconductors. The anisotropy related to the wakes created by grains can be responsible for the observed alignment of grains observed in the crystal states in the sheath [14, 15, 16], in specifically designed dedicated experiments [17], experiments on and modeling of pairing of two dust particles [18, 19, 20, 21], and experiments and simulations [22, 23, 24].

The linear supersonic case where the charge emits electromagnetic waves via the Cherenkov process is well known [25]; it can be described in other terms as the formation of the electromagnetic wake field (similar to that the left behind an object moving on the water surface with the velocity larger than the surface wave velocity).[1] The case considered in [10, 11, 12] deals also with the linear approach but for the emission of electrostatic waves, namely ion-acoustic and dust-acoustic waves for stationary dust particles (as well as those for moving dust particles [26]); this case has some specific features which show the difference with the emission of electromagnetic waves. It was found that the linear electrostatic wake has a form of an oscillating potential with positive and negative potential values behind the grain (later, the theory of the ion wake was developed in a number of studies [27, 28, 29, 30, 31, 32, 33]; note that one of the simplest models of the wake formation [30] considers it as just an excessive positive charge located downstream the dust particle). The first potential minimum appears at approximately $\pi\lambda_{De}M$, i.e., is at distances even larger than the electron screening length. The grain is screened by the electrostatic fields and these fields form the stationary Mach cone of ion-acoustic waves if the ion flow moves with velocity larger than the ion-sound velocity. However, the wake survives even for the Mach number less than 1 [27]. On the other hand, it is known from the linear theory of screening that the Debye screening is valid only if a charge moves in a plasma with the sub-thermal velocity [34]. The velocity of the ion drift corresponding to the Mach number of order unity is $1/\sqrt{\tau}$, which is larger than the ion thermal velocity. Within the range where the drift velocity is larger than the ion thermal velocity and less than the sound velocity, the screening produced by ions gradually decreases and the wake gradually increases until it is erupted as an emitted sound wave. Generally, for charges moving with velocities much larger than the ion thermal velocity but much less than the electron thermal velocity the linear ion screening disappears while the electron screening survives (note that in an isotropic plasma for $\tau \ll 1$ only the ion screening is important). The Debye screening length is then determined by the electron Debye length, not the ion Debye length, and is anisotropic. For the applications to the real case of grains embedded in the plasma sheath, one should note that the drift velocity of ions in the sheath is only of the order of the sound velocity and usually not substantially larger than that.

Other complications come from the presence of the temperature anisotropy of the ion distribution in the sheath which was obtained experimentally [41], showing that the parallel ion distribution (along the ion

[1] The wake field formation was also the subject of investigations for the so-called collective "wake accelerators" [35]; first consideration of the non-linear wake accelerator was proposed in [36, 37, 38], and for later developments in the wake accelerator studies see [39, 40].

flow) has a much larger temperature than the perpendicular ion distribution (perpendicular to the ion flow). This can substantially affect the screening in the presence of such an anisotropic ion flow distribution [27]. Generally, there exist numerous unsolved problems of the physics of formation of such anisotropic ion distributions including instabilities excited by the flow and by the inhomogeneous electric field in the sheath. Indeed, even a simple homogeneous ion flow is known to be unstable, and the influence of the fluctuating field excited by this instability on the distribution of ions close to the grain is not yet considered. Moreover, we note that the linear theory can hardly be applicable for screening of large grain charges in the presence of the ion drift – as is the case in the absence of the ion drift. However, some characteristics appearing in the linear theory are always necessary to have in mind as well as the range of their applicability. Since for many applications in complex plasmas the non-linear screening is important, theory of the wake formation should be complemented by taking into account the non-linearity in the presence of the ion flow. Note that the non-linear screening is also anisotropic [42]. This problem can be investigated only numerically since any solutions for particle distributions close to the grain require the knowledge of the angular particle distributions, and the solutions of the Poisson's equation also depend on the angles between the direction of the flow and the direction toward the grain center. Both equation are partial differential equations which are difficult to solve. Several approaches to the anisotropic screening were applied to this problem using numerical computations. Among them, direct integration of the equations of motions of the plasma particles represents a numerical experiment with significant approaching experiments in the laboratory. The particle-in-cell (PIC) simulations [43] clearly demonstrated formation of the wake potential with the potential wells attracting the grains underneath. The *ab initio* three-dimensional molecular dynamics (MD) studies [44, 45, 46, 47] also show the region of the strong ion focusing behind the grain for the case of a single grain as well as two grains aligned parallel and perpendicular to the ion flow. In simpler cases, the asymmetry has been modeled by adding a dipole component to the Debye-Hückel potential [48] (see also [30, 49, 50]). Clearly, solution of the anisotropic charging problem is formidable, and important are the consequences for determination of the interaction of two grains. We will return to this problem later in the section devoted to grain–grain interactions. We also mention numerical results [51] that give the potential distribution around a grain embedded in a plasma streaming at the relative velocity of $0.8v_{Ti}$, just below the ion thermal speed. The measurements of the grain wake field were performed in [52, 53]. Generally, both the numerical simulations and the experiments show that the wake as a collection of excessive positive space charges appear behind a single grain particle embedded in plasma, i.e., downstream the ion flow and that this wake space charge appears not only for Mach numbers larger than 1, which is natural for Cherenkov effect, but also for

Mach numbers somewhat less than 1. These disturbances are strongly influenced by non-linear effects. The ion focusing is found in this case in the "wake" field (which is not the real wave-wake since the velocity of the drift is sub-thermal) and creates an over-dense region of positive charges so that the localized "particle-plasma system" resembles a Debye-Hückel potential with added dipole component. However, this analogy cannot be simply extended to the case of the super-thermal drift and cannot be extended to find the grain interactions in the plasma sheath. In the case where the plasma flow is supersonic, an asymmetry occurs in the information transfer downstream and back upstream – the emission of waves is obviously not a reversible process. But irreversibility can occur only in the sub-sonic flow due to Landau damping [27]. These special effects can be investigated experimentally [52, 53]. It was also shown [54] that the ion-neutral collisions do not destroy much the wake created by a dust grain in the ion flow. Finally, we note that the anisotropic screening problem is too far to be fully investigated either numerically, analytically, or experimentally.

- *How the collective effects change the screening?* The grain shielding and charging in the presence of many grains can be and is indeed different from that of a single grain (the details see below Sects. 5.3 and 5.4). One cannot directly apply the information about an isolated grain for interpretation of effects of strong coupling which is a collective effect occurring in the presence of many grains. In particular, the collective effects change the shielding in the absence of an ion flow and create maximum and minimum of the potential (this can create grain pairing in the absence of an ion flow). The single-grain effects such as creation of the wakes can be used only in the case of a small number of almost isolated grains and also can serve as rough intuitive pictures for understanding more complex collective phenomena of many grains. They can operate in conditions where the collective effects can be estimated to be small, such as a single layer of grains levitating in the sheath. The collective effects can also change the wake fields. The presence in the wake potential of the collection of positive space charges can be important for interaction of grains but it does not mean that the wake type of attraction is not substantially modified in the presence of many grains and that the interaction between them will not be changed qualitatively and quantitatively. In fact the wake is strongly modified by collective effects. Moreover, the qualitative difference of collective interactions of grains is in particular (as we will demonstrate) in the possibility of *attraction* of similarly charged grains even in the absence of an anisotropy or in the absence of an ion flow; this seems to be an important effect for the problems of strongly coupled states. All these changes occur for dust density exceeding some critical values. For the grain number density less than the critical value (or for isolated grains and even for a single layer of grains) the results of screening and charging are approximately the same as for a single grain, as discussed in this section. The main physical problem is to estimate the critical grain densities

where the interaction and screening becomes collective. It is a challenge for both theory and experiments. Here, we will be able to give estimates only in order to demonstrate that the collective regime is really achievable in experiments (and apparently is already achieved in the most existing experiments). These reservations are necessary to state at this point to put the research of the screening, charging, and interactions of small number of grains in its real place among all processes which are of interest for strongly coupled systems (see next chapter).

3.2 Charging of Grains in Partially Ionized Plasma

3.2.1 Introductory Remarks

We restrict ourselves here to some simplest models of charging. Any approximation is based on small parameters. All possible small parameters of the problem are as follows:

1. The ratio of the grain size to the screening length, a/λ_{scr}.
2. The ratio of the grain size to the ion-neutral mean-free path, a/λ_{in}.
3. Either the ratio of the screening length to the ion-neutral mean-free path (the "collisionless" case), $\lambda_{scr}/\lambda_{in}$, or the inverse ratio of the ion-neutral mean-free path to the screening length, $\lambda_{in}/\lambda_{scr}$ (the "collision-dominated" case) – we have marked these cases by quotes because other type of collisions which determine the charging process are always taken into account, such as the ion-dust and electron-dust collisions.
4. The ion to electron temperature ratio, $\tau = T_i/T_e$.
5. The ratio $1/\beta = \lambda_{Di}z/a\tau$ of the linear screening length λ_{Di} to the length where the non-linearity is dominant, az/τ.

We demonstrate that the combination of the first and the fourth parameters can divide the applicability limit of the Orbit Motion Limited Model (OML) and the Radial Drift Model(RDM) for the collisionless limit while in the collision-dominated limit one can deal with the Diffusion Limited Model (DLM). In our simple treatment we assume that the presence of potential barriers is not important. The OML model is based on conservation laws and can be valid for both linear and non-linear screening. But the non-linearity creates the potential barriers which can influence the charging. We intend to discuss this problem after describing different models for charging.

3.2.2 Equation for Micro-particle Charging

Equation describing change in time of the grain charge Q is determined by the balance of currents:

$$\frac{1}{e}\frac{\mathrm{d}Q}{\mathrm{d}t} = \frac{\mathrm{d}Z_d}{\mathrm{d}t} = -I_e + Z_i^+ I_i^+ - Z_i^- I_i^- + I_s + I_{ph} \tag{3.22}$$

where the charging current I (per absolute value of the electron charge $e > 0$) can be due to electrons (subscript e), positive and negative ions (subscript i), secondary electrons (subscript s), and photoelectrons (subscript ph). In fact, the right-hand side represents the flux of different charged particles the presence of which is an important feature of complex plasmas (as discussed before). With all the considerations we use dimensionless variables. This is desirable by several reasons:

1. The dimensionless variables are rather often the values of the order of 1 (sometimes being 2–4 as for the dimensionless charge introduced above). Therefore, by writing the variables in the dimensionless form we can get an immediate estimate of their actual value for certain experimental conditions.
2. In most of numerical problems only the dimensionless form can be used.

We introduce a dimensionless expression as soon as it appears in due course. Here, we list the dimensionless variables used for the charging process: the dust charge z, the temperature ratio τ, the ion to electron mass ratio m, the ion drift velocity u, and the Mach number for the ion drift M.

$$z \equiv \frac{Z_d e^2}{aT_e}; \qquad \tau \equiv \frac{T_i}{T_e}; \qquad m \equiv \frac{m_i}{m_e}\ ;$$
$$u \equiv \frac{u_i}{\sqrt{2}v_{Ti}} = \frac{u_i}{\sqrt{2T_i/m_i}}; \qquad M \equiv \sqrt{2\tau}u\ . \tag{3.23}$$

The total dimensionless current on the grain surface is $I(z, u...)$. Usually the charging time is one of the fastest in the system (in this case we are interested in grain motion which is very slow due to the large mass). The equilibrium charge should be then found from

$$I(z_{eq}, u...) = 0\ . \tag{3.24}$$

Equation for charges close to the equilibrium charge is easily obtained from (3.1) by linear expansion

$$\frac{\mathrm{d}\delta z}{\mathrm{d}t} = -\delta z; \qquad \delta z = z - z_{eq}; \qquad t \to -t\frac{\mathrm{d}I(z_{eq})}{\mathrm{d}z_{eq}}\frac{e^2}{aT_e}\ , \tag{3.25}$$

where t is a dimensionless time, measured in time units, needed for the grain charging $aT_e e^2(dI/dz)^{-1}$. Each model of charging predict somewhat different charging times but all models give their values much less than the timescale for the grain motions. In experiments, the charging time is million or more times shorter than the typical experimental timescale. In this sense it is the shortest timescale for the grain particle processes. Then in the first approximation the charging can be regarded as instantaneous. But of course there could exist faster processes related to wave propagation with periods shorter than the charging time – in this case the time delay in charging is important. We estimate the charging time for every model that we consider for grain charging.

3.2.3 Orbital Motion Limited Model

The assumptions used in the OML model seem to be quite general, but in fact the OML approach requires several restrictions listed below [1]:

- For those ion and electron orbits touching the grain surface, the angular momentum conservation is used:

$$v_s^{e,i} a = v_\infty^{e,i} p_{max} \ , \tag{3.26}$$

  where p_{max} is the impact parameter, v_s is the particle velocity at the surface of the grain, and v_∞ is the particle velocity far from the grain.
- To determine the electron and ion surface velocity, the energy conservation is used

$$\frac{m_{e,i}(v_s^{e,i})^2}{2} + e_{e,i}\phi_s = \frac{m_{e,i}(v_\infty^{e,i})^2}{2} + e_{e,i}\phi_\infty \ . \tag{3.27}$$

An important point is that these assumptions can be used for any interaction potential (since the conservation laws are valid for any potential) and therefore the results as well as the OML approach itself seem to be very general. However, strictly speaking, this conclusion is not correct due to more assumptions made in OML to obtain the cross-sections. The impact parameter p in (3.26) is assumed to be the maximum impact parameter in the OML theory. All impact parameters larger than p correspond to trajectories which do not touch the grain and they are not counted in the OML approach. All trajectories with impact parameters less than p approach the grain and these particles are absorbed by the grain (the potential barriers are therefore assumed to be absent). Only in this case we can use the expression for the capture cross-section in the form

$$\sigma_c = \pi p_{max}^2 \ . \tag{3.28}$$

Correctness of the latter statements could depend both on the form of the interaction potential as well as on all effects of the non-linear screening and the ion capture. In other words, if we imagine a plane far from the grain which is perpendicular to the direction of the grain, draw a circle of the radius p in this plane and consider the projectile particles moving through this circle to the grain, it is possible that some of them will not reach the grain being reflected, while some particles outside this circle can reach the grain being scattered (e,g., by collisions with neutrals). This case is usually referred due to the presence of the potential barriers. Thus all restrictions of the applicability of the OML approach and dependence on the near-grain charge polarization potential distribution came only from the assumption that expression (3.28) is correct with p determined by the Orbit Limited trajectory – when the plasma particle just touches the grain surface at the periphery of the grain.

Relations (3.26)–(3.28) give the cross-sections for electron and ion capture, assuming $\phi_s \gg \phi_\infty$ [55]:

$$\sigma_c^e = \pi a^2 \left(1 + \frac{2e\phi_s}{m_e v^2}\right) \ , \tag{3.29}$$

$$\sigma_c^i = \pi a^2 \left(1 - \frac{2e\phi_s}{m_e v^2}\right) . \tag{3.30}$$

In case the grain is charged negatively, $\phi_s \approx -Z_d e/a < 0$, which means that the grain is capturing only the fast electrons with $v > v_{cr}$:

$$(v_{cr})^2 = z\frac{2T_e}{m_e} . \tag{3.31}$$

Asymptotically, for $v \gg v_{cr}$ the cross-section of the electron capture reaches the value of the geometrical cross-section πa^2. Electrons with velocities less than v_{cr} are reflected by the grain. We can find the cross-section averaged with respect to the electron thermal distribution:

$$\langle \sigma^e \rangle = e^{-z}\pi a^2 . \tag{3.32}$$

For negatively charged grains, the (positive) ions are always attracted and therefore their trajectories contract toward the grain. This is why the capture cross-section for ions is always larger than the geometrical cross-section. For $\tau \ll 1$ one can find the ion capture cross-section averaged with respect to the ion thermal distribution given by

$$\langle \sigma_c^i \rangle \approx \frac{z}{\tau}\pi a^2 \gg \pi a^2 . \tag{3.33}$$

This cross-section can be two orders of magnitude larger than the electron collection cross-section. Figure 3.6 illustrates dependence of the cross-sections, normalized with respect to the geometrical cross-section πa^2, $s_{e,i} = \sigma_{e,i}/\pi a^2$, on the ratio of the particle energy to the thermal energy $\epsilon_{e,i} = mv_{e,i}^2/2T_{e,i}$.

Using the above cross-section, we can easily find the electron and ion fluxes (currents per unit charge):

$$I_e = n_e 2\sqrt{\frac{2\pi m_e}{T_e}} a^2 e^{e\phi_s/T_e} = n_e 2\sqrt{\frac{2\pi m_e}{T_e}} a^2 e^{-z} , \tag{3.34}$$

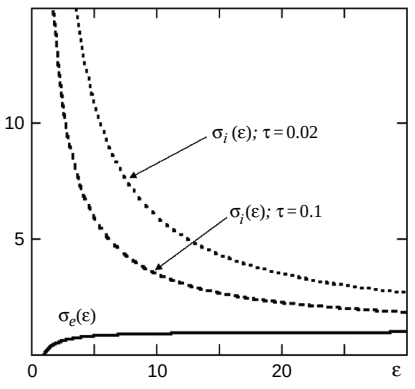

Fig. 3.6. Dependence of the OML capturing cross-section of ions and electrons on the ratio of the particle energy ϵ to the particle thermal energy $T_{i,e}$

$$I_i = n_e 2\sqrt{\frac{2\pi m_i}{T_i}} a^2 \left(1 + \frac{z}{\tau}\right) . \tag{3.35}$$

In case we neglect the secondary electron and the photoelectron emissions as well as the negative ion contribution, we obtain equation for the stationary grain charge

$$\exp(-z_{eq}) = \frac{1}{\sqrt{m\tau}} \frac{Z_i n_i}{n_e} (z_{eq} + \tau) . \tag{3.36}$$

If we neglect the presence of other dust particles, we can use the quasi-neutrality condition in the form $Z_i n_i = n_e$ and then (3.36) does not contain electron and ion densities and in the limit $\tau \ll 1$ it contains only a single parameter

$$\mu = \sqrt{m\tau} , \tag{3.37}$$

i.e., the product of the temperature ratio and the mass ratio:

$$\exp(-z_{eq}) = \frac{1}{\mu} (z_{eq} + \tau) . \tag{3.38}$$

Figure 3.7 gives the solution of such equation for the parameter μ varying from 5 to 50. For a given temperature ratio (e.g., for $\tau = 0.02$, typical for existing experiments) the charge on grains depends on the ion mass ($z = 1.4$ for hydrogen, 2.63 for argon, and 2.75 for krypton), while for $\tau = 1$ the corresponding value of charges are 2.5, 3.95, and 4.3.

An important question is, what are the *applicability conditions of the OML approach?* Values of grain charge estimated from the OML approach are often in agreement with experimentally measured grain charges [56, 57]. Naturally, the agreement exists if the applicability conditions of the OML approach are fulfilled. Apart from the effects of the non-linear screening and the potential barriers mentioned above (which can limit the trajectories of electrons in a way that some of them will not reach the grain surface in the range of impact parameters less than the maximum impact parameter p, or

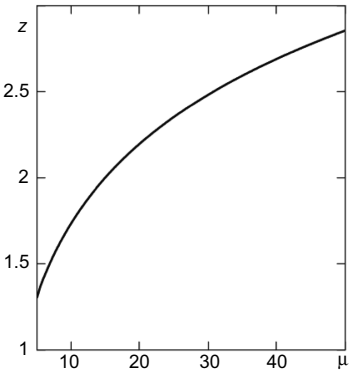

Fig. 3.7. The charge z given by the OML approach as a function of the parameter μ

will reach the grain for impact parameters larger than p) there exist trivial conditions:

1. The screening length λ_{scr} should be less than both the ion-neutral mean-free path λ_{in} and the electron-neutral mean-free path λ_{en} (the collisionless limit); otherwise there are collisions on the path of the ion or electron to the grain and the conservation laws cannot be used (in other words, the collisions can scatter the trajectories of the electrons and ions in a way that when having initially one value of the impact parameter they can get another value of the impact parameter);
2. The grain size a should be less than the screening length λ_{scr}; otherwise "there is no space" to move from "infinity" to the grain surface which was used for calculations of the cross-sections.

The case where the size of the grain is larger than the screening length rather describes probes in plasmas (see [1, 58]). The question whether the mentioned two points are sufficient for the relative contribution of the trajectories not satisfying the OML assumptions to be small is still not completely clear at the moment. However, for the non-linear screening the problem of the potential barriers is intensively discussed in [2] and explicit expressions for the charging in the presence of barriers were found.

Assumptions used for calculations shown in Fig. 3.7 are as follows: the velocity distributions of electrons and ions "at infinity" (far from the grain surface) are thermal, the sticking coefficients of electrons and ions equal unity, there is no secondary emission as well as photo emission. The general experimental and theoretical trend is to prove that for applicability of the OML approach one should have $a \ll \lambda_{scr}$ (see below and [59, 60]). The assumption of the thermal distribution of electrons and ions can be easily changed and the results can be obtained for any non-thermal distributions as well as for any value of the sticking coefficient.

The *dynamics of grain charging* can be described by an equation which for the OML approach acquires a simple form

$$\frac{\mathrm{d}z}{\mathrm{d}t} = -\frac{1}{\sqrt{2\pi}} \frac{v_{Ti} a}{\lambda_{Di}^2} \left(z + \tau - \mu \exp(-z)\right) \ . \tag{3.39}$$

Linear approximation in the charging equation can be used only if the grain charge reaches the values close to the equilibrium value. Since the charging process is slowing in time, the linear approximation describes the slowest rate corresponding to the latest phase of charging. When expanding for small deviations $\delta z = z - z_{eq}$ we use (3.25), which is written here for the dimensional t:

$$\frac{\mathrm{d}\delta z}{\mathrm{d}t} = -\frac{1}{\tau_{ch}} \delta z = -\nu_{ch} \delta z \ , \tag{3.40}$$

where τ_{ch} is the *characteristic charging time* and ν_{ch} is the *charging frequency*:

$$\nu_{ch} = \frac{1}{\sqrt{2\pi}} \frac{v_{Ti} a}{\lambda_{Di}^2} (1 + z_{eq} + \tau) \ . \tag{3.41}$$

In the last expression, z is the equilibrium charge value and in obtaining (3.41) we used equation for the equilibrium charge. The charging frequency is proportional to the grain size, which means that the charging is faster for larger grains. When the charging process starts with charges far from the equilibrium, we can distinguish two stages of charging – the first (faster) stage is determined by the electron capture by the grain and is simply related with the time needed for an electron to reach the grain ($\nu_{ch} \approx v_{Te}a/\sqrt{2\pi}\lambda_{Di}^2$), while the second (longer time) stage is determined by the ion capture and by the time needed to reach the equilibrium charge value (it is of the order of $t_{ch} = 1/\nu_{ch}$). This can be seen from numerical solution of the charging non-linear equation. It is easy to demonstrate the change of the grain charge during the charging process by using the normalized equation where the time is normalized by the charging time $(v_{Ti}a/\sqrt{2\pi}\lambda_{Di}^2(1+z_{eq}+\tau))^{-1}, t_N = tv_{Ti}a/\sqrt{2\pi}\lambda_{Di}^2(1+z_{eq}+\tau))$ and z is normalized by $z_{eq}, \zeta = z/z_{eq}$:

$$\frac{\mathrm{d}\zeta}{\mathrm{d}t_N} = \frac{1}{z_{eq}+\tau+1}\left[\zeta + \frac{\tau}{z_{eq}} - \left(1+\frac{\tau}{z_{eq}}\right)e^{-z_{eq}(\zeta-1)}\right] \tag{3.42}$$

Figure 3.8 gives solutions of (3.23) for $\tau = 0.02$ and different values of z_{eq}.

Estimates of the charging frequency for typical experiments show that the corresponding time is very short, i.e., the charging is extremely fast. For example, for $T_i \approx 300\mathrm{K}, n_i \approx 10^9\mathrm{cm}^{-3}, a = 10\mu\mathrm{m}, z = 3$ we have $\nu_{ch} \approx 1\mathrm{MHz}$. The consequence of the charging process is very drastic – all modes with frequencies less than the charging frequency are changed by the grain charging (for more details see below Chap. 4). On the other hand, the timescale of dust charging is usually much less than the characteristic timescales of dust motion as well as the timescales of duration of experiments on plasma condensation which indicates that for these experiments the dust charging is almost an instantaneous process.

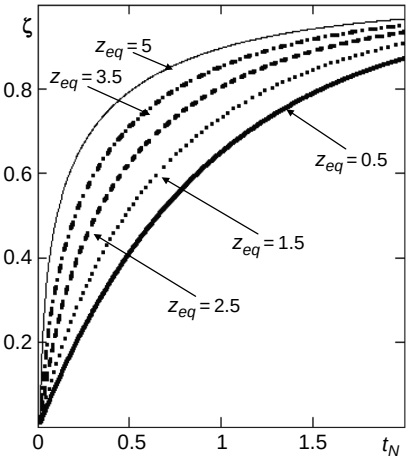

Fig. 3.8. Time dependence of the normalized grain charge $\zeta = z/z_{eq}$ as a function of the normalized time t_N for different values of z_{eq} and $\tau = 0.02$ given by the OML approach

An important value is also the charging length λ_{ch}, which is defined as the distance traveled by thermal ion during the charging time:

$$\lambda_{ch} = \frac{v_{Ti}}{\nu_{ch}} \approx \frac{\lambda_{Di}^2}{a} \,. \tag{3.43}$$

It is always larger than the ion Debye screening length for $a \ll \lambda_{Di}$ (which is the case in most experiments).

3.2.4 Extensions of OML Approach

Charge Reduction due to "Contamination of Plasma" by Dust Grains. Until now we were dealing with a single grain in a plasma neglecting influence of other grains. When many grains are present, the charging flux becomes collective. However, some simple estimates can be made starting with the simple OML approach.

There exist at least two mechanisms of reduction of grain charges due to the presence of other dust grains: 1) the depletion of the electron density, and 2) the change of the electron and ion distributions due to the charging processes on many grains. In case the quasi-neutrality condition is not fulfilled, the ratio of the electron to ion density can be included in the parameter μ. Figure 3.7 indicates how the dust charge decreases with the decrease of the electron density. In particular, the electron density in "contaminated plasma" when the ratio of the dust density to the electron or the ion density increases. Using the quasi-neutrality condition in the presence of other dust grains we have

$$\mu \cdot \rightarrow \mu \cdot (1 - P), \tag{3.44}$$

where the parameter P is defined by (3.22). The critical dust density when the depletion of individual dust charges occurs is then defined by $P_{cr} = 1$ or

$$\frac{n_{d,cr}}{n_i} = z\frac{aT_e}{e^2} \,. \tag{3.45}$$

For the typical values of interest in low power RF plasma ($n_i = 10^9\text{cm}^{-3}, T_e = 2\text{eV}, a = 1\mu\text{m}, z = 2.63$ for argon plasma), we obtain $n_{d,cr} = 6.2 \cdot 10^4\text{cm}^{-3}$ for the typical grain separation of 100μm. This grain charge reduction (relative to the charge on an isolated grain) was investigated in [61], using the so-called "Havnes parameter" P_H was

$$P_H = \frac{P}{z} = \frac{n_d}{n_i}\frac{aT_e}{e^2} \,. \tag{3.46}$$

In some cases it is more convenient to use the parameter P_H which does not depend explicitly on the value of the grain charge Z_d. However, the dust charge is itself the function of dust size and vice-versa and this independence of P_H on the grain charge is somewhat illusive. One should also distinguish between

the case where the dust contamination changes the charges but still leaves the parameter z of the order of unity and the case where the dust contaminations makes $z \ll 1$. For the latter the parameter P should be close to 1, namely $1 - P \ll 1/\mu$ when almost all electrons are attached to the grain surface due to the charging process.

The other effect that can deplete the charges on individual grains is the change of the plasma particle distribution function. This effect for a single grain is not important since new electrons and ions are reaching the grain during the charging. But in the case of many grains the change of the distribution function occurs everywhere. Numerical solutions of equations for grain charging solved self-consistently with equations for the electron and ion distributions (with the change of the particle distributions due to the charging processes) show [62, 63] that as soon as the parameter P becomes larger than 0.1 the part of fast electrons in the electron distribution is strongly depleted, and there lesser number of electrons take part in the charging process although the total electron density is depleted not as much as the part corresponding to fast electrons. Also, substantial change in the ion distribution can take place [63].

The charge reduction on micro-spheres begins noticeable experimentally [1, 64] (in the percentage range) for $P \leq 0.1$ and becomes significant when $P \leq 1$. For the electron temperature of 1eV, the unperturbed ion density of about 10^9cm^{-3}, and for micro-spheres with radius 5μm, this corresponds to the grain density $n_d > 3 \times 10^5\text{cm}^{-3}$ or the mean grain separation of $\Delta \geq 150\mu\text{m}$. For the unperturbed plasma density this implies that the number of ions in the "sphere of influence", Δ^3, of one grain is $N_i = n_i\Delta^3 = 3.5 \times 10^3$. This is approximately the number of electrons captured by grains – as expected. This effect of charge depletion is peculiar to complex plasmas. It plays a significant role in a variety of physical processes ranging from the equation of state to wave propagation, elasticity in strongly coupled states, etc.

Adiabatic Charge Variation. Due to the very fast charging, the grain charge is quickly adjusted locally to parameters of surrounding plasma if these parameters are changed. As an example, we can find relation for the change δz of the dust charge occurring when dust is displaced with the change of the electron density δn_e and the ion density δn_i by differentiating the charging equation

$$\frac{\delta z}{z} = \frac{1}{1+z}\left(\frac{\delta n_e}{n_e} - \frac{\delta n_i}{n_i}\right) , \tag{3.47}$$

which mathematically expresses the variability of dust charges discussed above. In the presence of the ion drift the dust charges vary also with dust drift, and variations due to presence of other dust particles can be found through the electron and ion variations.

Secondary Electron, Photo, and Thermionic Emission Currents. In the case where secondary emission is taken into account the charging equation is changed by the secondary emitted currents. This equation can have (in the

parameter domain where the secondary emission is important) simultaneously two solutions, with positive and negative charges. This was considered as one of the possibilities to interpret the observed grain agglomeration [65, 66]. There exist also a more probable mechanism of agglomeration related with attractions of like-charged grains [67], which we discuss below.

The photo-emission current is usually produced in the presence of an external source of radiation acting on the surface of the grain. In the case where the photo-emission dominates, the ion current is usually negligible and the current balance in the grain charging occurs between the photoelectron emission current and the plasma electron current. With an increase of the photoelectron current the charge of the grain, being initially negative, decreases in absolute value and with large photoelectron current the grain charge becomes positive. In case the grain is sufficiently hot it can operate as a thermal source of electrons emitting the so-called thermionic current which also is changing the charge balance in the charging equation and for large grain temperatures makes the charge of the grain positive [68].

Role of Ion Drift. Let us first explain why and when in existing experiments the grains can be located in the regions of plasma having substantial drift velocity of the ion components. Some of the experiments are done under gravity conditions where the electric field force (of the sheath close to the wall) acting on the grain is balanced by the gravitational force. In the sheaths the ion drift is present inevitably. There exist different types of experiments in the sheath: the grains at the positions where the ion drift velocity is large as well as where the ion drift velocity is small. For the first case the grains are located in the so-called wall plasma-sheath, while in the other case they are located outside the wall plasma-sheath in the so-called wall pre-sheath. At the region separating the sheath and the pre-sheath the ion drift velocity is approximately equal to the sound velocity which is $1/\sqrt{2\tau}$ larger than the ion thermal velocity. The Mach number M (the ratio of the ion drift velocity to the sound velocity) is there $M = 1$ – this is the so-called Bohm criterion of the wall sheath. The pre-sheaths can be collision-dominated or collisionless. The division between them is determined by the ion-neutral collisions (the same definition as that used for the charging processes), i.e., by the size of the pre-sheath as compared to the ion-neutral mean-free path λ_{in}.

The ion drift velocities in the pre-sheath decrease as soon as the distance from the wall increases; they are usually subsonic and in the collision-dominated pre-sheath the decrease of the ion drift velocity with the distance from the wall occurs faster than for the collisionless pre-sheath. At the end of the pre-sheath the drift velocity becomes even sub-thermal and therefore the influence of the ion flow on the grain charging is negligible there.

When there exist many layers of dust levitating one above each other close to the wall (as is in the case of the experiments shown above on plasma condensation in RF-exited plasmas), the physical question is, starting from which layer the influence of ion drift on the charging becomes small? The answer depends on the distance between the layers and on the gas pressure determining

the ion-neutral mean-free path λ_{in}. For the above-mentioned experiments on plasma condensation in RF discharges, λ_{in} is of the order of 200μ, the distance between the layers is about 100μ, and therefore the presence of the ion drift will affect only a few layers, say 4–7, while for other layers the influence of the ion drift is small. In the latest experiment where the condensation was observed for several hundreds layers in the bulk plasma, the ion drift is negligible for most of the grains. In case of a single layer the influence of ion drift can be large. To this case we pay special attention further in the book describing the corresponding experiments and calling such condensations as grain clusters.

Under micro-gravity conditions, it is desirable to produce the plasma condensation far from the wall where the ion drift is very small. Note that it was thought in first investigations of plasma condensation that the presence of the ion drift is crucial for the condensation. At present it is clear that this is not the case and experimentally the plasma condensation can be obtained in the bulk plasmas in the absence of the ion flow. Still the problem of the grain charging in the presence of the ion flow is one of important ones for the existing experiments and modeling [45].

One important point should be also mentioned here. It is generally expected that close to the wall the average ion flow velocity is large as compared to the ion thermal velocity. However, the real velocity distributions were measured only in a few experiments and rather far from the wall surface. Thus one cannot be sure that the drifting Maxwellian distribution describes the actual existing ion distribution in the wall sheath. At least assuming that the ion distribution is the shifted Maxwellian distribution one can calculate the OML current and find how the charging equation will be altered by the ion flow in the limit $\beta \ll 1$ assuming no barriers to be present.

The calculations are straightforward, and therefore we give here only the equation in the limit $u \equiv u_i/\sqrt{2}v_{Ti} \gg 1$ (u_i being the ion drift velocity) assuming that the Mach number of the ion flow, $M = \sqrt{2\tau}u$, is arbitrary. The latter is possible to be valid for $\tau \ll 1$ ($\tau = 0.01 - 0.02$ is the typical value for present experiments).

$$\exp(-z) = \sqrt{\frac{\pi}{4m}} \left(\frac{z}{M} + \frac{M}{2} \right) \frac{Z_i n}{n_e} \,. \tag{3.48}$$

(Note that in the absence of other grains we can as before take into account the quasi-neutrality condition $Z_i n/n_e = 1$.)

Solution of the charging equation depends on the sort of gas (the ion to electron mass ratio m) and the value of the Mach number. Figure 3.9 presents results of numerical computations of (3.48) for argon gas within the range of Mach numbers $0.1 < M < 10$ and for $\tau = 0.01$. Figure 3.10 illustrates dependence of the grain charge on the Mach number and on the parameter $\mu = \sqrt{m\tau}$. According to Figs. 3.9 and 3.10, with an increase of the Mach number the charge first increases and then decreases. This result qualitatively agrees with experimental observations.

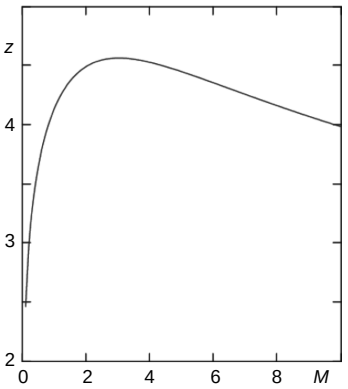

Fig. 3.9. Dependence of the grain charge on the Mach number M of the ion flow for argon gas and $\tau = 0.02$. Calculations use the OML approach with the drifting Maxwellian ion distribution

In application of relation (3.48) to real experiments for charging of grains in the plasma sheath, the problem is that the real ion distribution is not well known in this region. Recent experiments [41] show that the distribution is of a type of drifting distribution, but the ion temperature along the drift velocity is much larger than the ion temperature perpendicular to the drift velocity: along the drift the ion temperature becomes close to (but less than) the electron temperature, while perpendicular to the drift the ion temperature is almost the same as that far from the sheath. This ion heating along the drift is probably due to collective phenomena in interaction of ions with strong electric fields of the sheath. The charging for such anisotropic ion distribution was considered in [27], the ion current is larger and the dust charges are lower than in the absence of the temperature anisotropy.

In the presence of super-thermal ion drift the charging frequency can be expressed through the Mach number, and for $\tau \ll 1$ it is given by

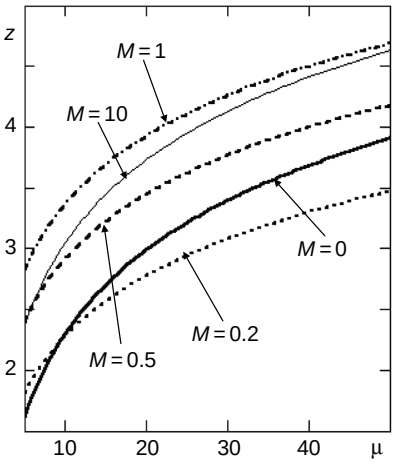

Fig. 3.10. Dependence of the grain charge on the Mach number M and the parameter μ for $\tau = 0.01$. Calculations use the OML approach with the drifting Maxwellian ion distribution

$$\nu_{ch} = \frac{a v_{Ti}\sqrt{\tau}}{4\sqrt{2}\lambda_{Di}^2}(z+1)\left(\frac{z}{M}+\frac{M}{2}\right) . \tag{3.49}$$

For $\tau \ll 1$ and $M \sim 1$ (as it is the case in the plasma sheath) the charging time is $\sqrt{\tau}$ less than that for sub-thermal drifts.

Role of Super-thermal Electrons. It is well known that plasmas are often turbulent and create super-thermal tails of electrons which have power-law distributions. To describe that a distribution is often used where the usual Maxwellian exponent is substituted by $1/(1 + mv^2/2T_e)^\nu$ (note that T_e has now meaning different from that in the usual Maxwellian distribution). Since the tail electron play a significant role in the grain charging, the change of the tail distribution can create different or even much larger grain charges [69]. In Fig. 3.11, we give examples of solutions of the charging equation for distributions of electrons approaching the power-law distributions at $mv^2/2T_e \gg 1$ for $\nu = 2.5, 3, 3.5, 4$. This figure illustrates that the charges of the grains are significantly affected by electron distributions of this kind.

Role of Strong Magnetic Field. As soon as magnetic field exceeds the critical field (for which the electron gyro-radius is equal to the collection radius of electrons by dust grains), those electrons taking part in the charging process can be considered as moving straight to the grains, but the low-energy electrons are reflected backwards (not deflected as usual in the absence of magnetic field). The negative charge of the grain particle creates the reflected electron flow in the opposite direction (along the magnetic lines) and only electrons which are fast enough are able to reach the grain and charge it. The cross-section for the magnetized electrons is changed, namely for $\omega_{Be} = eB_0/m_e c \gg ve/a$ it becomes equal to πa^2. By using the energy conservation law for electrons moving along the magnetic field we find that

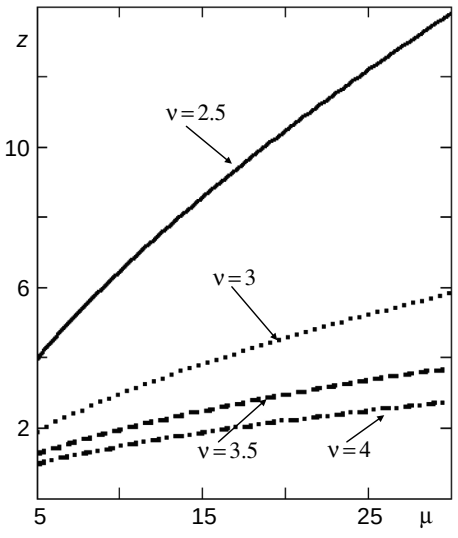

Fig. 3.11. Grain charging for the tail electrons with power-law distributions

the absorbed electrons should have the velocity larger than a critical velocity, namely $v_e^2/2v_{Te}^2 > z$ and that the electron current on the grain is determined by them. A simple calculation of this current for the thermal distribution $\propto \exp(-v_z^2/2v_{Te}^2 - v_\perp^2/2v_{Te}^2)$ shows that the electron current is reduced by the factor 4 as compared to the electron current in the absence of a magnetic field. On the other hand, if the magnetic field is not so strong and the ion gyro-radius is still much larger than the ion–grain absorption length $\approx a\sqrt{z/\tau}$, the ions are attracted to the grain approximately at the same rate as in the absence of the magnetic field and their effective cross-section is much larger than the geometrical cross-section πa^2 (approximately equal to that in the absence of the magnetic field). The ion current on the grain is changed not substantially.

The reduction of the electron current means a decrease of the grain charge. The charging equation then takes the form

$$\exp(-z) = \frac{4z}{\mu}; \qquad \mu = \sqrt{\frac{m_e}{m_i\tau}}\,. \tag{3.50}$$

In deriving the relation (3.50), we assumed that for electrons the cross-section coincides with the geometrical cross-section and the electrons (neglecting their rotation around magnetic field lines) move straight along the magnetic field. The charges on dust particles become somewhat smaller (see Fig. 3.12). A simple estimate for condition necessary to neglect the $\mathbf{E}\times\mathbf{B}$ drift of electrons in the vicinity of the grain (caused by the electric field of the grain) gives that the ratio of the grain size to the electron gyro-radius should be larger than z. The values of z are approximately 1–4 as found from (3.50) and thus the criterion of electrons to be magnetized is not changed by the $\mathbf{E}\times\mathbf{B}$ drift in the vicinity of the grain.

For much stronger magnetic fields where the ion gyro-radius becomes smaller than the dust size, both the ion and the electron currents are modified and the equation for the dust charge can be written as

$$\exp(-z) = \tau\sqrt{\frac{m_e}{m_i\tau}}\,. \tag{3.51}$$

In addition to μ, (3.51) contains another parameter τ. Therefore we show in Fig. 3.12 the dependence of the grain charge on the parameter μ for the solutions of (3.50) and we show three values of $\tau = 1, 0.01, 0.0005$ for the solution of (3.51). As can be seen from Fig. 3.12, the value of the dust charge in the strong magnetic field can be substantially larger (up to 12 times) than in the absence of magnetic field. In the latter case the criterion for neglecting the ion $\mathbf{E}\times\mathbf{B}$ drift in the vicinity of the grain is more restrictive.

The inequality requiring that the size of the grain particle is larger than the electron gyro-radius can be written in the practical units as follows:

$$B_{cr}^e(kG)a(\mu m) > 41.37\sqrt{\frac{T_e(\mathrm{eV})}{3\mathrm{eV}}}\,. \tag{3.52}$$

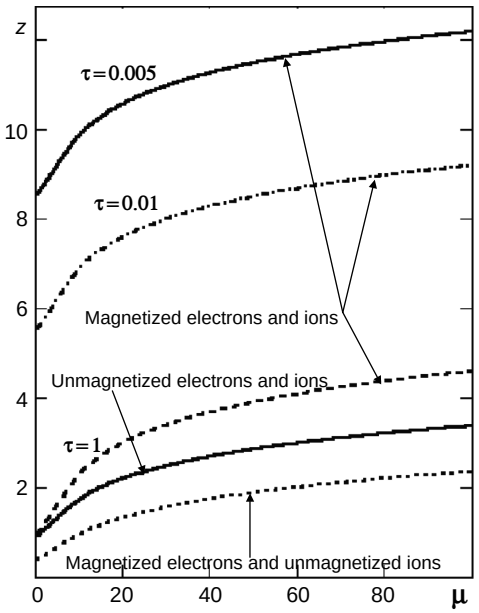

Fig. 3.12. Grain charging in the strong magnetic field

For $a \approx 10\mu$m the critical field B_{cr} is about 4kG. The corresponding critical field where the size of a dust grain is larger than the ion gyro-radius is μ times larger. As can be seen from Fig. 3.12, for fields larger than that given by the expression (3.52) the grain charge z is reduced but not very substantially (not more that by a factor of 1.5). Much more substantial change of the grain charge occurs for $B > B^i_{cr}$.

Effect on Grain Screening. Long-Range Potential Created by Grain Charging. The long-range potential of grains is created by the processes of charging and plasma absorption by grains. This is related to the presence of plasma fluxes on grain surfaces. For a few (low number density of) grains, the fluxes on individual grains do not overlap and we can find an additional grain potential due to the plasma flux by considering each grain individually and neglecting the presence of other grains.

Consider the simplest case of the linear screening for $\beta \ll 1$. The conservation of flux shows that it should exist independently of whether the distance from the grain is less or larger than the screening distance. The flux on a single isolated grain creates an additional charge density and a non-screened part of the potential [3, 70, 71, 72, 73] which survives outside the region where the main part of the field is screened. The first notice of existence of the non-screened potential was done many years ago [70]. Absorbtion of ions by a grain is the most important process in creating the non-screened potential if $\tau \ll 1$. Indeed, at some distance from the grain within some angular interval around the direction toward the grain center there is no ions (as well as no electrons). This angular interval decreases rapidly with the distance from the grain. To

find this angular interval we can use (as before in the OML approach) the conservation laws for the energy and momentum of plasma particles to relate their values at the grain surface with those at the distance r. Taking into account that this distance is far enough from the grain, we neglect the potential $\phi(r)$ as compared to the potential at the surface of the grain ϕ_s. Thus for the critical angle θ_{cr} in which the ions are absent due to absorption by the grain we obtain

$$\sin^2(\theta) \approx \theta^2 = \frac{a^2}{r^2}\left(1 - \frac{2eZ_i\phi_s}{m_i v_i^2}\right) . \tag{3.53}$$

The additional charge related to the absence of ions within this angular interval is $eZ_i n_{0,i}(1-\cos(\theta))/2 \approx eZ_i n_{0,i}\theta^2/4$. As mentioned above, the screening close to the grain is non-linear and at some large distances it becomes linear. For the case where the non-linearity in screening is small $\beta = za/\tau\lambda_{Di} \ll 1$, we have for $\tau \ll 1$ the linear polarization charge produced mainly by ions: $n_{eff,i}Z_i(1-eZ_i\phi/T_i)$. From requirement of quasi-neutrality at these distances and after averaging with respect to the ion thermal distribution, we find [74] the long-range potential created by the charging process

$$\frac{\phi}{\phi_s} = \frac{Z_i a^2}{2r^2} . \tag{3.54}$$

The most important feature of this potential is that it is not screened and therefore the long-range potential created by the charging process dominates for distances much larger than the screening distance. Let us illustrate in more detail how the charging process changes the charge density distribution close to the grain. We use here the OML approach to calculate the change in the charge density. We consider a distance r from the grain and write the energy and momentum conservation relations to relate the corresponding values at the distance r with those at the grain surface:

$$av_s = rv\sin(\theta); \frac{m_{e,i}v_{e,i}^2}{2} + e_{e,i}\phi = \frac{m_{e,i}v_{e,i}^2}{2} + e_{e,i}\phi_s . \tag{3.55}$$

Since particles touching the grain are assumed to be absorbed (attached to the grain) there are no particles moving from the grain within certain angular interval, when θ is less than that determined by (3.55). Therefore, in finding the charge densities of electrons and ions close to the grain we should exclude the empty angular interval $\sin(\theta) < \sin(\theta_{cr})$ from integration over the solid angle Ω [75]:

$$\frac{1}{4\pi}\int d\Omega = \frac{1}{2}(1-\cos(\theta_{cr})) , \tag{3.56}$$

where the critical angle θ_{cr} is determined by

$$\sin^2(\theta_{cr,e}) = \frac{a^2}{r^2}\left(1 - \frac{z}{y_e}\left(1-\psi\frac{a}{r}\right)\right); \sin^2(\theta_{cr,i}) = \frac{a^2}{r^2}\left(1 + \frac{z}{\tau y_i}\left(1-\psi\frac{a}{r}\right)\right) . \tag{3.57}$$

Here, the grain size a and the distance r are in units of the ion Debye length ,$y_{e,i} = v_{e,i}^2/2v_{Te,i}^2$. In (3.56) the positive expression for $\cos(\theta_{cr})$ found from (3.57) should be used (i.e., directions corresponding to the particles moving from the grain). The ion and electron number densities, $n_{e,i}(r)$, should have the term excluding these particles, i.e., from the already used expressions we should subtract ones with the factor (3.56) under the integral with integration with respect to the velocity where $\sin^2(\theta_{cr,e,i}) < 1$. It is easy to find that the latter does not restrict integration over the velocity of electrons while for ions the previous restriction for the energy to be positive at "infinity" competes with the restriction $\sin^2(\theta_{cr,i}) < 1$. We then obtain the modified Poisson equation [75] that takes into account the change of the grain shielding by the charging process. Details of the numerical solution are described in [75]; the results are that for a single grain and for $z/\tau \gg 1$ the appreciable change of the grain screening due to the plasma absorption occurs only either for distances rather close to the grain surface where r is of the order of a or at distances of the order of the screening length or larger $r \geq \lambda_{scr}$, where the approximate expression for ψ tends to zero and the linear approximation can be used. In the latter region the unscreened long-range potential appears, the same as described above and $\psi \approx a/2r$.

The reason for the substantial changing of the screening potential for large distances is that the corrections due to the charging conserve the flux of particles absorbed by dust grains and are never screened, while the other parts which do not take the absorption into account are completely screened at some distances. The non-screened part related with the grain charging therefore dominates eventually at large distances where other contributions are already screened. The difference of the non-linear and linear screening is only in the distance at which the non-screened potential, $\psi = a/2r$, is starting. For the linear screening this distance is of the order of λ_{Di}, the linear shielding length, while for the non-linear screening this distance corresponds to λ_{scr}. However, the anisotropic distribution of ions due to the charging process can be related with possible instabilities created by it. This problem has not been investigated yet. The possibility exists that if the instability is developed then the excited electric field can fill the empty cone created by the charging process. This problem stays unsolved both for the linear and for the non-linear screening. For many grains in the system, a single grain consideration is not valid since the plasma flux becomes collective (about the new physics involved in the collective screening and its consequences for the complex plasma condensation see Chap. 6).

3.2.5 Role of Potential Barriers in Non-linear Screening for Grain Charging

The polarization charge around the negatively charged grain is positive and can reflect some ions not allowing them to contribute to the ion current to the grain. This problem is known as the problem of potential barriers. For

the non-linear screening described in the previous section this problem has a complete solution [2]. Indeed, the radial motion of any ion close to the grain is determined by the screened potential of the grain and the centrifugal energy determined by the angular momentum of the incident ion (by its impact parameter). In this analysis it is useful to measure all lengths, namely the impact parameter ρ and the distance from the grain r in units of the non-linear screening radius R_{nl} introduced in the previous section ($\rho \to \rho/R_{nl}; r \to r/R_{nl}$). Defining also the effective energy V_{eff}, which takes into account both the potential energy and the centrifugal energy in units of the energy of incident ion with the velocity $v_i (V_{eff} \to V_{eff} 2/m_i v_i^2)$, we can write

$$V_{eff}(r, \rho, y) = \frac{\rho^2}{r^2} - 2\gamma(y)\frac{\psi(r)}{r} \,, \tag{3.58}$$

with

$$\gamma(y) = \frac{\beta \lambda_{Di}}{2y^2 R} \,, \tag{3.59}$$

and

$$y = \frac{v_i}{\sqrt{2} v_{Ti}}; \qquad v_{Ti} = \sqrt{\frac{T_i}{m_i}} \,, \tag{3.60}$$

where v_{Ti} is the ion thermal velocity. The potential barrier is determined by the condition that the effective energy is larger than or equal to the energy of incident ion. This gives the dependence of the ion energy (the dimensionless y which determines it) as a function of r_b (position of the barrier) and ρ_b (the corresponding impact parameter where the ion reaches the barrier). For the "top" of the barrier, y is determined by

$$V_{eff}(r_b, \rho_b, y) = 1 \,. \tag{3.61}$$

Other two conditions for the barriers are as follows: the first derivative of V_{eff} with respect to r is zero, and the second derivative of V_{eff} with respect to r is negative. This gives three relations:

$$r_b + 2\gamma(y) \left[\psi(r_b) + r_b \psi'(r_b)\right] = 0 \,, \tag{3.62}$$

$$\frac{\rho_b^2}{r_b^2} = \frac{2\gamma(y)}{r_b} \left[\psi(r_b) - r_b \psi'(r_b)\right] \,, \tag{3.63}$$

and

$$\psi'' > \frac{1}{r_b^2} \left[\psi(r_b) - r_b \psi'(r_b)\right] \,, \tag{3.64}$$

where prime stands for derivative with respect to r. To calculate the cross-section of the absorption and the absorbed ion flux in the presence of barriers, one should distinguish two ranges for the barrier impact parameter, namely $\rho_b < \rho_{\mathrm{OML}}$ and $\rho_b > \rho_{\mathrm{OML}}$, where ρ_{OML} is the absorbtion impact parameter in the OML approach given by (for $\tau \ll 1$)

$$\rho_{\rm OML} = a\sqrt{\frac{z}{\tau y^2}} = \beta\lambda_{Di}\sqrt{\frac{a}{\lambda_{Di}y^2}} \tag{3.65}$$

(here, ρ and a are in units of R_{nl}). Both ρ_b and $\rho_{\rm OML}$ depend on the normalized velocity y and, hence, the two ranges of ρ_b can be distinguished in terms of y. For $\rho_b > \rho_{\rm OML}$ the absorbtion cross-section is $\sigma_{abs}(y) = \pi\rho_{\rm OML}^2$, while for $\rho_b < \rho_{\rm OML}$ the cross-section is $\sigma_{abs}(y) \simeq \pi\rho_b^2$. This determines the ranges of integration with respect to y. From conditions (3.62)–(3.64) we find the barrier position (in units of R_{nl})

$$r_b > r_{b,cr}; \qquad r_{b,cr} = \frac{(1-\nu)(\nu+\sqrt{3+2\nu})}{(1+\nu)(3-\nu)} \,. \tag{3.66}$$

For Yukawa screening $R_{nl}(1-\nu)/2 \to 1$ or in dimensional units it is λ_{Di} and $r_{cr} = \lambda_{Di}(1+\sqrt{5})/2$. The actual position of the barrier depends on the ion velocity and is determined by transcendental equation

$$\gamma(y) \equiv \frac{\beta\lambda_{Di}}{2y^2R_{nl}} = \frac{r_b}{\left(\frac{3-\nu}{1-\nu}r_b - 1\right)(1-r_b)^{\frac{1+\nu}{1-\nu}}} \tag{3.67}$$

(here, λ_{Di} and R_{nl} are in usual units).

The right-hand side of (3.67) is an increasing function of r_b and the increase of r_b occurs either due to the increase of β or the decrease of the ion velocity y. For the minimum critical barrier value we find the minimum possible value, $\gamma_{cr}(\nu)$, by substituting $r_b = r_{cr}(\nu)$ in the right-hand side of (3.67). We have

$$\gamma_{cr}(\nu) = \frac{(1-\nu)(\nu+\sqrt{3+2\nu})}{(3-\nu)(\sqrt{3+2\nu}-1)\left(\frac{3+\nu-(1-\nu)\sqrt{3+2\nu}}{(1+\nu)(3-\nu)}\right)^{\frac{1+\nu}{1-\nu}}} \,. \tag{3.68}$$

Since $\gamma_{cr}(\nu)$ is of order 1, we can conclude from definition of γ by using (3.67) that for the thermal ions ($y \approx 1/\sqrt{2}$) the barriers influence the charging only for $\beta > R_{nl}/\lambda_{Di} > 7$–10, i.e., only for large values of the non-linear parameter β. For $\beta \ll 1$ and $a \ll \lambda_{Di}$, the role of potential barriers is very small and we can use the OML approach without any improvement due to possible presence of the potential barriers. Thus for $\gamma > \gamma_{cr}$ we can assume $\beta \gg 1$. Only ions with $\rho < \rho_b$ can reach the grain surface, where

$$\rho_b^2 = r_b^2\frac{1-\nu+(1+\nu)r_b}{(3-\nu)r_b+\nu-1} \,. \tag{3.69}$$

We find the critical value of the impact parameter ρ_{cr} by substituting into ρ_b the value of the critical barrier radius r_{cr}:

$$\rho_{cr}^2 = \frac{(1-\nu)^2(\nu+\sqrt{3+2\nu})^2(3+\sqrt{3+2\nu})}{(3-\nu)^3(1+\nu)(\sqrt{3+2\nu}-1)} \,. \tag{3.70}$$

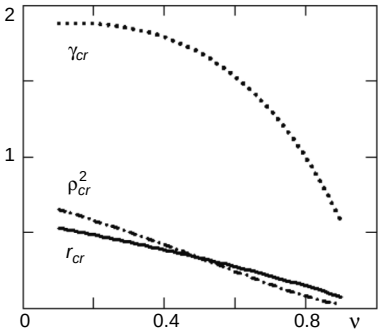

Fig. 3.13. Critical values for potential barriers as functions of the parameter ν within the range $0.1 < \nu < 0.9$

Figure 3.13 shows dependence of these three critical barrier parameters r_{cr}, γ_{cr}, and ρ_{cr}^2 on the parameter ν.

The barriers do not prevent ions from penetrating into the grain surfaces if $\gamma(y) < \gamma_{cr}$. We are interested here in large values of β where the asymptotic values for the barriers can be used. For small $\beta \ll 1$ the barriers cannot prevent the absorption by grains. The absorption drag coefficient corresponds to the known OML cross-section $\sigma_{\rm OML} = \pi a^2 z/\tau$ (for $z/\tau \gg 1$). For $\beta \gg 1$, there are ions with high velocities which can penetrate into the grain surfaces and their cross-section is the same as in the absence of barriers and there are ions for which the cross-section is determined by the difference of $\pi(r_b^2 - a^2 z/\tau)$. The division of ions (in the velocity range) into those able and not able to penetrate the barrier is determined by the critical value of $y = v/\sqrt{2}v_{Ti}$ denoted as $\tilde{y}$ and given by

$$\tilde{y}^2 = \frac{\beta a \lambda_{Di}}{R^2} \ . \tag{3.71}$$

The charging equation in the presence of potential barriers can be found by calculating the ion flux on the grain in the presence of barriers. We write this equation in the form containing the dimensionless charge $z = Z_d e^2/aT_e$ (in the absence of barriers), the dimensionless charge z_b (in the presence of barriers), and the modified dust charge $Z_{d,b}$: $z_b = Z_{d,b}e^2/aT_e$ (note that β is calculated for z, i.e., in the absence of barriers). Then we find the charging equation assuming as usual that the thermal ion distribution is not changed by barriers

$$e^{-(z_b - z)} = \frac{z_b}{z} \Gamma_{ch}\left(\tilde{y}^2 \frac{z_b}{z}\right) \ , \tag{3.72}$$

where y_{cr} is defined by expression (3.71) and

$$\Gamma_{ch}(x^2) = 2\left[\int_0^x t\exp(-t^2)\left(1 - \frac{t^2}{x^2}\right)dt + \int_x^\infty \exp(-t^2)tdt\right]$$
$$= 1 - \frac{1}{x^2} + \exp(-x^2)\left(1 + \frac{1}{x^2}\right) \ . \tag{3.73}$$

The parameter Γ_{ch} as a function of $\tilde{y}^2 z_b/z$ is shown in Fig. 3.14. The decrease of Γ_{ch} does not cause a large increase in the grain charges since it enters as usual under the sign of logarithm and the decrease of Γ_{ch} is no more than 40% as can be seen from Fig. 3.14. Nevertheless, Γ_{ch} returns to its value corresponding to $x^2 \ll 1$ only for $x^2 \approx 100$.

3.2.6 Radial Drift Limited Model

The radial drift model was proposed in order to have better agreement with probe measurements [76]. It was found [76] that if it is assumed that ions move radially in the charging process and use simple conservation laws, one gets better agreement with probe observations in low-temperature collision-dominated plasmas. The collisions indeed can form a radial ion flow toward the grain. Nevertheless, here we still deal with the collisionless limit when the screening length is mush less than the ion-neutral mean-free path. The probe theory is a very old and broad subject of investigation but it deals with the opposite case where the size of the probe is much larger than the screening length. Here we discuss whether the hypotheses of the radial ion drift is acceptable in the physics of the grain charging.

The radial drift hypothesis is based on the physical argument that in the OML approach the individual ion velocity at the grain surface is much larger than the ion thermal velocity, and the energy of ions approaching the grain is close to the electron temperature, i.e., individual ions are accelerated toward the grain. However, ions approaching the grain are randomly distributed in the velocity directions. To use the Radial Drift Limited (RDL) model for the grain charging, one assumes that the ions have both the random velocities and the directed radial drift velocity toward the grain and that the ion current to the grain related to the ion drift is larger than that related to the ion thermal motion [76]. Thus the radial regular drift is assumed to be large, while in the previous OML approach only the random thermal flux on the grain was taken into account.

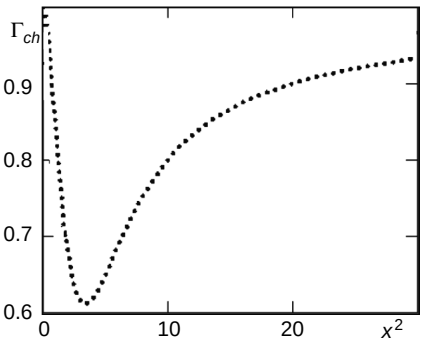

Fig. 3.14. The parameter Γ_{ch} entering charging equation in the presence of potential barriers as a function of $x^2 = \tilde{y}^2 z_b/z$

The ion-neutral collisions in the collision-dominated case can indeed create the ion radial drift motion since in the hydrodynamic description (appropriate to the collision-dominated case) the ion friction force is proportional to the ion drift velocity and, being balanced by the radial electric field, creates the radial ion drift. Note that in the case of the spherical symmetry there is no other direction for the hydrodynamic velocity of ions and therefore in the collision-dominated case the radial drift hypothesis seems to be natural. In the collisionless case there exist at least two possibilities for adapting this assumption:

- The mechanism which is responsible for formation of the radial ion drift is a collective stochastic process which creates an effective friction proportional to the ion drift velocity [76]. At present this problem was not attacked from the point of view of modern concepts of dynamical chaos although many processes at the so-called absorption radius [1, 76] could be similar to those already treated in the dynamical chaos approach [77].
- Although in the collisionless limit the mean-free path for the ion-neutral collisions is much larger than the screening length ($\lambda_{in} \gg \lambda_{scr}$), the ion-neutral collisions can create the radial flux outside the screening length for $r \gg \lambda_{scr}$. The radial drift velocity there could be small but due to continuity of the ion flux the radial drift is present also in the collisionless region up to the grain surface.

It is possible to find some estimates. One can obtain the value of the radial ion drift velocity created by the long-range potential outside the screening length and compare it with the thermal velocity. The gain of the ion energy as compared to the thermal energy is determined by the energy conservation law. We can use expression

$$\epsilon_i \equiv \frac{m_i v^2}{T_i} \approx \frac{z}{\tau} \frac{a^2}{\lambda_{scr}^2} \, , \tag{3.74}$$

where we put the screening length to be approximately equal to the ion Debye length. Expression (3.74) shows that (due to the large factor z/τ) the ion drift velocity approaching the screening radius can start to be super-thermal if the radius of the grain is in the range

$$1 \gg \frac{a}{\lambda_{scr}} > \sqrt{\frac{\tau}{z}} \, . \tag{3.75}$$

This means that the RDL model with super-thermal ion drift is applicable inside the screening length only for sufficiently large grains.

For electrons their drift velocity is small as compared to the electron thermal velocity and we can use their thermal distribution to obtain the electron flux, while for the ion flux we find (the ion current is obtained by multiplying by $Z_i e$)

$$I_i = 4\pi a^2 n_s v_s \, , \tag{3.76}$$

where n_s and v_s are the ion density and the ion drift velocity at the dust surface. This expression is valid only in the case where the ion flux related to the ion drift significantly exceeds the ion thermal flux considered previously. To compare these fluxes we need to estimate the ion density at the surface. We use the continuity equation in condition of the spherical symmetry

$$\frac{1}{r^2}\frac{\partial n v r^2}{\partial r} = 0 \; . \tag{3.77}$$

The ion density reaches the unperturbed value n_0 at the distance of the order of the screening length and then the expression for the linear density approximation where $e\phi \ll T_i$ can be used. Using (3.76), this gives approximately

$$I_i = 4\pi n_s v_s a^2 = 4\pi s^2 n_0 v_{Ti}\sqrt{\epsilon_i}\lambda_{scr}^2 \; , \tag{3.78}$$

where ϵ_i is given by (3.75). Comparing, then, expression (3.78) with that for the ion thermal flux, we again obtain inequality (3.75).

Equalizing the electron and ion currents, we have equation for the dust charge

$$\exp(-z) = \frac{z}{\sqrt{m\tau}}\left(\sqrt{\frac{\pi}{2}}\frac{\lambda_{scr}}{a}\sqrt{\frac{\tau}{z}}\right); m = \frac{m_i}{m_e} \; . \tag{3.79}$$

We wrote this equation in the form similar to that in the OML case (except for the numerical factor on the right-hand side of the charging equation which is always small according to relation (3.75)). Thus the expression (3.41) can be easily used to compare the OML and RDL models. Due to condition (3.75), the RDL model gives always lower values of dust charges than the OML model since the effective parameter μ is smaller. The difference between the RDL model and the OML model is that the charge in the RDL model becomes independent on τ but dependent on the dust size a. One should have also in mind that the RDL model is valid in the limited range of large sizes, $\sqrt{z/\tau}\lambda_{Di} \ll a \ll \lambda_{Di}$. Analytically, the charging equation in the RDL case differs from that in the OML case by having on the right-hand side $\sqrt{z}$ instead of z as in the following expression:

$$\exp(-z) = \frac{1}{\nu_{RM}}\sqrt{z}; \nu_{RM} \approx \sqrt{m}\frac{a\sqrt{2}}{\lambda_{Di}\sqrt{\pi}} \; . \tag{3.80}$$

Figure 3.15 shows numerical solution of this equation for ν_{RM} varying from 5 to 50 compared with the OML case, where the parameter μ was varying in the same range (have in mind the difference of μ and ν_{RM}).

There exist a long-standing debate over the merits of the OML and RDL approaches [1, 76] including screening in the RDL approach. It is also not possible to develop directly (without numerical calculations) the theory of potential barriers for the RDL model since the previous achievements in the barrier theory were based on the energy conservation law which is not valid

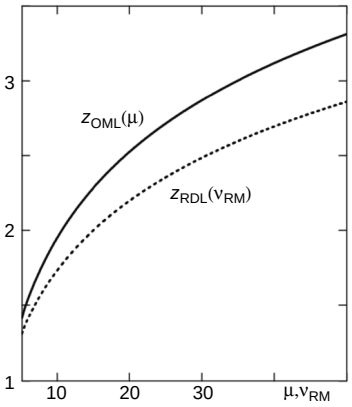

Fig. 3.15. Comparison of results for the grain charging for the OML and RDL models. The actual ratio of the coefficients μ and ν_{RM} depends on the dust size

in the presence of collisions. Nevertheless, in some approximation the theory of barriers can be used if the distance r_{cr} for the barriers is much less than the mean-free path for the collisions. This aspect still waits for future investigations.

3.2.7 Diffusion Limited Model

The Diffusion Limited Model (DLM) of the grain charging is even less developed than the RDL model. The main argument to develop such a model is the high rate of the ion-neutral collisions which in some circumstances can make the ion-neutral mean-free path even smaller than the screening distance. Here, we discuss only some aspects of the influence of the neutral background gas on the ion transport to the grain surface and the grain charging in the partially ionized plasma. We discuss the regime $a \ll \lambda_{in} \ll \lambda_{scr}$, where the ion-neutral collision mean-free path (as usual) can be written as $\lambda_{in} = 1/n_n\sigma_{in}$, with the typical ion-neutral collision cross-section $\sigma_{in} \approx 5 \times 10^{-15}\text{cm}^{-3}$ and n_n is the neutral gas density. For a plasma with $T_e \approx 1eV$ and ionization fraction $n_e/n_n = 10^{-8}$ this implies the gas density $n_n > 7.2 \times 10^{14}$ or the pressure at room temperature (300K of $P > 0.03$ m Bar), quite a common situation in low power RF discharges. Then $\lambda_{in} \approx 0.14\text{cm} = 1400\,\mu\text{m}$. For larger pressures the mean-free path could be close to a few tenths of μm and comparable or less than the Debye length.

In the presence of collisions, ions do not move freely to the grain surface but rather diffuse to it. The ion current is then determined by the radial diffusion equation which takes into account the ion diffusion in the neutral gas

$$\frac{1}{r^2}\frac{\partial}{\partial r}(r^2 v_i n_i) - \frac{1}{r^2}\frac{\partial}{\partial r}\left(r^2\kappa\frac{\partial n_i}{\partial r}\right) = 0\ , \tag{3.81}$$

with absorbing boundary at the dust surface $r = a$, and κ being the diffusion coefficient, $\kappa \approx \frac{1}{3}\lambda_{in}v_{Ti}$. Equation (3.81) can be written through the total flux Φ which includes both the convection flux nv_i and the diffusion flux:

$$\frac{1}{r^2}\frac{\partial(r^2\Phi)}{\partial r} = 0; \Phi = n_i v_i - \kappa\frac{\partial n_i}{\partial r} \ . \tag{3.82}$$

This equation leads to

$$\Phi = \Phi_0 \frac{a^2}{r^2} \ , \tag{3.83}$$

where Φ_0 is the total flux on the unit surface area of the grain. The total flux on the whole surface is $I_i = 4\pi a^2 \Phi_0$:

$$\kappa\frac{1}{n_i}\frac{\partial n_i}{\partial r} = v_i - \Phi_0 \frac{a^2}{n_i r^2} \ . \tag{3.84}$$

The similar ion density logarithmical derivative enters in the equation for ions in which we balance the ion pressure force by the electric force and the friction force of ions in collisions with neutral gas particles. This equation includes the electric field and one needs to find its distribution close to the grain, i.e., to solve the non-linear screening problem. Here, we do not proceed in detailed description of the electron and ion changes in the sphere where the flux is altered by non-quasi-neutrality of the diffusion region which needs a full consideration of the processes of non-linear screening. In the last stage where the distance to the grain is of the order of the ion-neutral mean-free path, the diffusion solution has no meaning and should be matched with the collisionless solution, then the flux reaching the grain becomes entirely convective.

Such detailed consideration is one of the problems for future research and we return to it after discussing the processes of the ion-neutral collisions and ion trapping due to the ion-neutral collisions, the problem which is deeply related with the charging process as well as with the non-linear screening of the grain. We therefore give here only some rough results obtained in [75] for the form of the charging equation to have at least some feeling as to what kind of changes one can expect to have for large ion-neutral collision rate:

$$I_i = 4\pi a^2 n_0 v_{Ti} \sqrt{\frac{z}{3\tau}\frac{\lambda_{in}}{a}} \ , \tag{3.85}$$

and the charging equation in the form

$$\exp -z = \frac{1}{\nu_{DL}}\sqrt{z}; \nu_{DL} = \sqrt{2\pi m}\frac{a}{\lambda_{in}}(1-P); m = \frac{m_i}{m_e} \ . \tag{3.86}$$

The form of this equation is the same as in the RDL collisionless model, but the parameter ν_{DLM} is determined by the ratio a/λ_{in} instead of a/λ_{Di}. This is natural since we assumed that $\lambda_{in} \ll \lambda_{Di}$.

3.2.8 Problems for Modeling of Grain Charging

We described here several processes of the grain charging in order to illustrate that even these elementary processes for a single isolated grain are not simple.

Numerous investigations are needed to be done and more precise theoretical models to be developed. Of big importance is also experimental verification of the models. From the description we presented here one can see the trends of investigations in this field. Different models give different values of the ion current on the grain while the electron current to the grain is almost the same in all cases. The ion currents were already written in the form which allows a simple comparison of different models. In the RDL and DLM cases the ion currents have always large factors as compared to the OML case. Thus the ion current is the smallest for the OML case and therefore the grain charges are lower in the DLM and RDL cases than those in the OML case. The RDL model and the DLM model in the limit of small grain sizes do not depend on the temperature ratio τ. The RDL model has some unsolved problems for proving the assumption of the radial flux, but when these assumptions are accepted one can show that this model is applicable only for large grain sizes. The limitations of the OML model and RDL model have been reviewed by [1]. Still in these simplest models there are many unsolved problems, in particular:

- *How the screening can alter the charging?* Within the frame of the OML approach it is not clear whether for all impact parameters in the range $0 < p < p_{max}$ the trajectories of ions touch the grain surface. The deviations from the trajectories can be caused by the space polarization cloud around the grain. As an example let us consider a simplest model assuming for the moment that the screening is so non-linear that at certain finite distance the field of the grain is completely screened. This means that the field of the grain is completely confined between two spheres, the first one is the grain surface sphere with the radius a, and the second one is the screening length sphere with the radius λ_{scr}. We can call this screening as the "hard sphere screening" because there is no field of the grain for the distances from the grain center larger than λ_{scr}. We assume $\lambda_{scr} \gg a$. Let us then consider the projectile ion moving toward the grain with the velocity v and the impact parameter p is the distance between the straight line trajectory far from the grain along the ion velocity and the line in the same direction crossing the center of the grain. Let us compare two examples of the non-screened Coulomb potential and the "hard sphere screening" potential. Consider $p < p_{max} = a\sqrt{z/\tau}$. For the Coulomb potential the ion is accelerated toward the grain, and its trajectory due to attraction is contracted to the grain surface. This process is starting from large distances from the grain center and the ion always hits the grain surface if $p < p_{max}$, so it is absorbed by the grain and contributes to the ion current to the grain. For the "hard grain screening," an ion hits the grain only if $p < \lambda_{scr}$, otherwise the ion passes the grain on a straight trajectory not feeling the grain field and not contributing to the ion current on the grain. Thus for $\lambda_{scr} < p_{max}$ for the "hard sphere screening" there exists a range of the ion trajectories, $\lambda_{scr} < p < p_{max}$, which do not contribute to the ion current, while in the OML approach these ions are all counted to contribute to the ion current.

Of course, the "hard sphere model" is a very simplified model of screening and the real screening is more complicated, but this model still illustrates the problem one should consider in detail in future, namely the non-linear screening can modify ion trajectories in a way that either more or less ions contribute to the ion current. As a rule, the non-linear screening radius is substantially larger than the linear ion Debye screening radius. In this case the non-linearity operates in the way that the grain charges are less influenced by the screening.

- *How the potential barriers change the grain charges?* There could appear potential barriers for the ion penetration into the grain. The effectiveness of the barriers depends on the ion energy. Any barrier reduces the ion current and therefore increases the grain charge (which is negative) by enlarging its absolute value. The theory of potential barriers needs to be developed in future in the presence of collisions.
- *How the ion-neutral collisions can affect the charging?* One should have in mind that the number density of the neutral component in low-temperature plasmas is rather high (at least 5–6 orders of magnitude higher than the number density of ions) and although the corresponding cross-sections are not big, the mean-free path of the ion-neutral collisions could be of the order of other characteristic lengths of the system such as λ_{scr}, etc.[8, 9, 78] For fast ions appearing close to the grain in the charging process (the energy of ions is increased about $1/\tau$ times) the charge-exchange collisions with ions can be of importance. For future, there exist at least three effects to be investigated in detail: (a) the change of the ion trajectories in the ion-neutral collisions which result in changes in the ion trajectories in such a way that those ions which are absorbed by the grain in the absence of collisions will not be absorbed in the presence of collisions, and vice versa; (b) the collisions which convert the non-trapped ion trajectories to the trapped ones, and vice versa – In this case the ions which were trapped by any reason previously are starting to contribute to the ion current; (c) if the trapped ion population becomes important in the grain shielding, the main problem is the stability of the trapped ion distribution.
- *How the secondary electron emission from the grain and the thermionic emission currents from the grain can affect the charging?* The first investigations of the role of secondary electron emission [56, 65, 66] show that in some range of the parameters the effects of the secondary emission lead to such equation of charging which has simultaneously the solutions for dust charges with different signs (negative and positive). More detailed investigation in this field should take into account effects of the non-linear screening which always exist for large charges in real experiments. Such consideration has not yet been performed although it is expected to be important in applications.
- *How non-Maxwellian distributions of electrons and ions affect the charging process?* The main problem is that in the presence of many grains the

electron distribution is depleted in the range of high electron energies since the high energy electrons are effectively absorbed by the grains and the ion distribution is depleted in the range of low-energy ions since the low-energy ions are mainly absorbed by the grain. These depletions increase with increasing dust density (although these depletions can obviously also be restored by ionization sources). The depletions lead to decreased currents on the grain surface. Thus the whole problem stays as an unsolved problem strongly depending on the ionization sources.

The most important feature is that *a separation of charging and shielding is generally not possible* since shielding depends on charging and charging depends on shielding. It is clear that this field, being started many years ago, has recently become very active due to new features related with the large grain charges, the large neutral gas densities, and the low ion-to-electron temperature ratio, with further investigation strongly motivated by recent studies of complex plasmas. New numerical and theoretical simulation studies become important. What seems to be needed most is a precise experimental input to test the theoretical approaches over a wide range of plasma conditions.

How the charging influences the screening? Let us illustrate how the charging process changes the charge density distribution close to the grain. We use here the OML approach to calculate the change in the charge density. We consider a distance r from the grain and write the energy and momentum conservation relations which connect values at the distance r with those at the grain surface:

$$av_s = rv\sin(\theta); \frac{m_{e,i}v_{e,i}^2}{2} + e_{e,i}\phi = \frac{m_{e,i}v_{e,i}^2}{2} + e_{e,i}\phi_s \ . \tag{3.87}$$

Since the particles hitting the grain are assumed to be absorbed (attached) by the grain there are no particles moving from the grain in certain angular interval. Therefore, in finding the charge densities of electrons and ions close to the grain we should exclude from the solid angle Ω integration the empty angular interval $\sin(\theta) < \sin(\theta_{cr})$ [75]:

$$\frac{1}{4\pi}\int d\Omega = \frac{1}{2}(1 - \cos(\theta_{cr})) \ , \tag{3.88}$$

where the critical angle θ_{cr} is determined by

$$\sin^2(\theta_{cr,e}) = \frac{a^2}{r^2}\left(1 - \frac{z}{y_e}\left(1 - \psi\frac{a}{r}\right)\right); \sin^2(\theta_{cr,i}) = \frac{a^2}{r^2}\left(1 + \frac{z}{\tau y_i}\left(1 - \psi\frac{a}{r}\right)\right) \ . \tag{3.89}$$

Here, the size of the grain a and the distance r are in units of the ion Debye length, $y_{e,i} = v_{e,i}^2/2v_{Te,i}^2$, and the positive expression for $\cos(\theta_{cr})$ found for directions corresponding to the particles moving from the grain should be used. The ion and electron density numbers, $n_{e,i}(r)$, should have the term excluding these particles, i.e., from the expressions already used one should

subtract ones with a factor under the integral with an integration with respect to velocity where $\sin^2(\theta_{cr,e,i}) < 1$. It is easy to find that the latter does not restrict the velocity integration of electrons while for ions the previous restriction for energy to be positive at "infinity" competes with the restriction for $\sin^2(\theta_{cr,i}) < 1$. We find then the modified Poisson equation (see [75]) which takes into account the change of shielding by the charging process. The details of its numerical solution are described in [75]. The results are that for a single grain and for $z/\tau \gg 1$ the appreciable change of screening due to absorption occurs only either for distances rather close to the grain surface where r is of the order of a or at distances of the order of the screening length or larger $r \geq \lambda_{scr}$ where the approximate expression for ψ tends to zero and the linear approximation can be used. In the latter region the unscreened long-range potential appears, the same as described above and $\psi \approx a/2r$.

The reason for the substantial change of the screening potential at large distances is that corrections due to the grain charging conserve the flux of particles absorbed by dust grains and are never screened, while the other parts which do not take the absorption are completely screened at some distances. The non-screened part related with charging therefore eventually dominates at some large distances where other contributions are already screened. The difference in the non-linear and linear screening is only in the distance at which the non-screened potential $\psi = a/2r$ starts. For the linear screening this distance is of the order of λ_{Di}, the linear shielding length, while for the non-linear screening this distance corresponds to λ_{scr}. The problems of this effect of anisotropic distribution of ions due to the charging process are related with possible instabilities which can be created by this anisotropic distribution of ions. This problem is not yet investigated. The possibility exists that if the instability is developed then the electric field excited by this instability can fill the empty cone created by the charging process. This problem stays unsolved for both linear and non-linear screening. Finally, note that the single grain consideration is not valid for many grains since the flux becomes collective.

3.3 Forces Acting on Ions

3.3.1 Absorption of Ions on Grains. The Charging Coefficient

We introduce *two coefficients* which play an important role in complex plasmas, namely *the charging coefficient* α_{ch} and *the drag coefficient* α_{dr}. The charging coefficient can be introduced by considering the friction force acting on ions due to their absorption on the grains in the charging process. We assume homogeneous grain distribution and introduce n_d as an average grain density.

Consider the simplest case where the absorption of ions on each grain occurs independently of the presence of other grains and the total absorption is a sum of absorptions on individual grains. Since any ion on its path through

dust-containing region reaches subsequently different grains and has a probability to be absorbed by one of them, the density of ions penetrating through complex plasma decreases. To find the correspondent dissipation term in the ion continuity equation, we sum the absorptions on individual grains. The flux of ions on an individual grain is determined by I_i (remember that we introduced I_i as a current on individual grain per unit charge and therefore I_i coincides with the ion flux on each grain). It is useful to introduce the charging coefficient α_{ch} written as

$$I_i = 4\pi\sqrt{2}v_{Ti}n_i\frac{z}{\tau}\alpha_{ch} \ . \tag{3.90}$$

In the limit of small ion drift velocity $u \ll 1$; $\mathbf{u} \equiv \frac{\mathbf{v}_i}{\sqrt{2}v_{Ti}}$; $v_{Ti} = \sqrt{\frac{T_i}{m_i}}$, we have for the OML model

$$\alpha_{ch} \approx \frac{1}{2\sqrt{\pi}}\left(1 + \frac{\tau}{z}\right) \ . \tag{3.91}$$

It is easy to write the charging coefficient for other models that we discussed above such as RDL or DLM, or include the ion drift, etc. The only restriction for using (3.90) is that the ion distribution is assumed to be thermal, otherwise we cannot introduce the thermal velocity in the definition (3.90). It is also useful (for writing both the charging equation and the friction force) to extract from the definition of the ion flux the numerical coefficient and the factor z/τ. The charging equation has then the form

$$exp(-z) = 2\sqrt{\pi}z\frac{1}{\mu} \ . \tag{3.92}$$

With expression (3.90), we are able to find absorption of ions by grains for any charging model. The continuity equation for ions which takes into account the effect of ion absorption on grains is given by

$$\frac{\partial n_i}{\partial t_{ac}} + \frac{\partial n_i \mathbf{v}_i}{\partial \mathbf{r}_{ac}} = -n_d I_i \ . \tag{3.93}$$

This equation has much simpler form if we use normalized expressions; in (3.93) we have used the subscript ac (which stays for actual) for time and variable to distinguish them from the normalized values for which we use no subscript. Equation (3.93) has a very simple form if we write it in dimensionless units, using, e.g., the characteristic charging length for normalization of distances and the characteristic charging time for normalization of time. However, such normalization is not very useful since these characteristic space and time units are in fact space-and time-dependent. For normalization, we should use here parameters which can be considered as time-or space-independent. Thus for normalization of distances we simply use $L = \lambda_{Di}^2/a = T_i/4\pi n_0 e^2 a$ instead of $\lambda_{ch} = \lambda_{Di}^2\sqrt{2\pi}/a(1 + \tau + z)$, and for the normalization of time we use the expression L/v_{Ti}. Here, n_0 is the constant density which can be naturally the plasma density outside the dust containing region or even any

other value relevant to the problem of consideration. This value should be constant thus excluding time-or space-dependent values from normalization. By the same reason we excluded the factor $1 + z + \tau$ since the grain charge could vary in space and time.

Thus we accept

$$\mathbf{r} \equiv \frac{\mathbf{r}_{ac}}{L}; t \equiv \frac{t_{ac} v_{Ti}}{L} \ . \tag{3.94}$$

For the ion density and drift velocity we use the natural normalization

$$n \equiv \frac{n_i}{n_0}; \mathbf{u} \equiv \frac{\mathbf{v}_i}{\sqrt{2} v_{Ti}} \ . \tag{3.95}$$

Multiplying (3.93) by $\lambda_{Di}^2 / a n_0 \sqrt{2} v_{Ti}$, we convert it into a very simple dimensionless form

$$\frac{\partial n}{\partial t} + \frac{\partial n \mathbf{u}}{\partial \mathbf{r}} = Q_i - P n \alpha_{ch} \ , \tag{3.96}$$

where $P = n_d Z_d / n_0$ is the parameter characterizing the relative grain charge density (here, we normalize the grain charge density by a constant value of the ion charge density), the dimensionless distance is $\mathbf{r} = \mathbf{r}^{ac} a / \lambda_{Di}^2$, and Q_i stays in (3.96) for the ionization source.

Equation (3.96) has *no small parameters* and a very simple form with all factors equal to 1. Note that for $P \sim 1$, in the case where there is no source supporting the ion density, the complex plasma disappears on the timescale of the charging process. In existing experiments, such an ionization source always exists, and it is often the volume ionization source. A reasonable model for this source is the one where the number of ions created is proportional to the electron density. We can describe it by putting an additional term Q_i on the right-hand side of equation (3.96):

$$Q_i = n_e / \tau_i = \alpha_i n_e \ , \tag{3.97}$$

where $n_e = n_{e,ac} / n_0$ is the normalized electron density and τ_i is the characteristic time of creation of an ion by ionization measured in L / v_{Ti}. Equation (3.96) with additional term (3.97) has a stationary solution when the ionization is compensated by absorption on dust particles.

With regard to the electron dissipation we note that the electron flux should be almost equal to the ion flux and the sink term as well as the source term in the electron continuity equation are the same as in the ion continuity equation since electrons and ions are created by ionization source in pairs (for usual laboratory weakly ionized plasma) and are absorbed on grains in pairs. On the other hand, behavior of electrons and ions is usually different since in most cases of interest the electron drift velocity is small as compared to the electron thermal velocity and often does not enter in the description of the electron component. Therefore one really does not need to consider the electron continuity equation to find the electron drift velocity. The electron density can be determined from the distribution of the electrostatic potential since electrons behave almost adiabatically in most cases of interest.

3.3.2 Friction of Ions in Gas of Grains. The Drag Coefficient

General Definition of the Drag Coefficient. The ions are not only absorbed by grains but, being absorbed, also transfer their momentum to the grains. The momentum transfer is zero if the distribution of ions is isotropic. If the ion distribution is not isotropic, e.g., it has non-zero flow velocity, the net effect of the ion momentum transfer in the absorption process is not zero and is proportional to the ion drift velocity (in the case the latter is much less than the ion thermal velocity). This is nothing else but the friction force acting on ions in a gas of grains.

There exist two types of interaction of ions with grains, both being caused by the screened grain field. The first one, already described, corresponds to ion trajectories which cross the grain surface and are absorbed by the grains. Another one corresponds to trajectories which do not cross the grain surface and the ions are scattered by the grain field. In the second process the ion momentum is also changed and transferred to the grain. The second mechanism conserves the number of ions and does not contribute to the continuity equation. For the conditions of $z/\tau \gg 1$ and small ion drift velocities, the second mechanism is much larger than the first one. For super-thermal drift velocities and the Mach number of the order of 1, both mechanisms are comparable and none of them is negligible.

As discussed before in this section, we consider here only the non-collective effects summing the momentum transfer in ion interactions with individual grains. The friction of ions in interaction with grains is proportional to the ion drift velocity only in the limit of small drift velocities. A rough estimate of the capturing friction force $\mathbf{F}_c$ and the capturing friction frequency ν_c related with the ion absorption (capture) for small drift velocities is very simple and can be done as

$$\mathbf{F}_c^{ac} = -\nu_c m_i \mathbf{v}_i; \nu_c \approx n_d v_{Ti} \sigma_i \approx n_d v_{Ti} \sqrt{2\pi} a^2 \frac{z}{\tau} \,. \tag{3.98}$$

Here, $\mathbf{F}_c^{ac}$ is the actual friction force acting on ions and v_i is the actual ion drift velocity. The last approximate expression in (3.98) is found from the OML approach in the limit $z/\tau \gg 1$. We introduce the normalized value for the ion drift velocity as $\mathbf{u}/\sqrt{2}v_{Ti}$. The normalization of the friction force is possible to do in two forms: (1) the first one (denoted simply as $\mathbf{F}$) uses as an unit force the value which decreases the energy of ions on T_e at the distance $L = \lambda_{Di}^2/a$, i.e., at the distance of the order of the charging length λ_{ch}; and (2) the second one (denoted as $\mathbf{F}_n$) uses as an unit the value which decreases the energy of ions on T_i at the length λ_{Di}. We have

$$\mathbf{F}_{dr} = -Pz\alpha_{dr}\mathbf{u}; \qquad \mathbf{F}_{dr,n} = -P\beta\alpha_{dr}\mathbf{u} = Pf_{dr}\mathbf{u} \,. \tag{3.99}$$

The last expression containing f_{dr} is useful for demonstrating the dependence of the drag force on the important parameter β (in the first form in $\mathbf{F}$ the normalizing factor contains β, while in $\mathbf{F}_n$ the factor β is excluded from the normalization).

The capture part of the drag coefficient that we have is given by $\alpha^c_{dr} = \frac{\tau}{2\sqrt{\pi z}}$. This expression has a nice and elegant form. α^c_{dr} is introduced as a part of the total *drag coefficient* related with capturing of ions by grains. The general expression is

$$\alpha_{dr} = \alpha^c_{dr} + \alpha^{sc}_{dr} + \alpha^{coll}_{dr} \ , \tag{3.100}$$

where α^{sc} is related to the ion scattering by the grains and is quite different for $\beta \ll 1$, and for $\beta \gg 1$, while the $\alpha_{dr}(c)$ is almost the same in both limits if (as we see in more detail later) the large-angle scattering for $\beta \gg 1$ does not contribute much in α^c_{dr}. In both cases, for $\tau \ll 1$ we obtain that α^c_{dr} is small as compared to the α^{sc}_{dr}. This can be already seen from simple hand-waving arguments for $\beta \ll 1$ but it is also true for $\beta \gg 1$. The coefficient α^{coll}_{dr} is the collective drag due to collective fields outside the non-linear screening radius. Collective effects are important but not for the case where the scattering drag coefficient is estimated usually of the order of the scattering part (see details below).

The reason why this coefficientα_{dr} (being a friction coefficient for ions) is called the *drag coefficient* is that the forces acting on grains from the ion flow can be found from the momentum conservation arguments having in mind that the grain velocity is in most cases much less than the ion drift velocity and therefore the ions act on the grains with the force proportional to the ion drift velocity and in a way to drag the ions. Expression (3.99) gives the estimate of the capturing force: for P of the order of 1 and for the ion drift velocity of the order of the ion thermal velocity this force decreases the ion momentum on the value of the thermal ion momentum and since this force is completely inelastic, it decreases the directed ion energy on the value of the ion thermal energy. The scattering friction force F_{sc} (part of the force related with scattering) acting on ions and determining the scattering coefficient α^{sc} strongly depends on the shielding of the grain field which, as we emphasized, is in most cases of interest non-linear.

Linear Drag Coefficient

The scattering in a non-linear potential is not as simple to calculate as in the standard non-screened Coulomb potential. We first give an estimate for the non-screened Coulomb field where we can use the standard way to obtain the cross-section by assuming that the effective radius of scattering corresponds to the potential of the grain equal to the kinetic thermal energy of ions

$$\mathbf{F}^{ac}_{sc} = -\nu_{sc} m_i \mathbf{v}_i ; \nu_{sc} \approx n_d v_{Ti} \sigma_{sc} \approx n_d v_{Ti} \pi r^2_{eff} \approx n_d v_{Ti} \frac{Z^2_d e^4}{T^2_i} \ . \tag{3.101}$$

Drag Coefficient in the Limit $\beta \ll 1$. The last estimate in (3.101) is valid only for $\beta \ll 1$ and is found in a standard way

$$\frac{Z_d e^2}{r_{eff}} \approx T_i \qquad r_{eff} \approx a \frac{z}{\tau} \ . \tag{3.102}$$

A simple algebra can be used to also express the scattering force (3.101) by extracting the factor T_e/L and writing the normalized force $\mathbf{F}_{sc}$ in the same way as for the absorption force

$$\mathbf{F}_{sc} = -\frac{z}{\tau}\frac{T_i a}{2\sqrt{2}\lambda_{Di}^2} P\mathbf{u} = -\alpha_{dr}^{sc} z P\mathbf{u}\,. \tag{3.103}$$

According to this estimate of r_{eff} we find that α_{dr}^{sc} is of the order of 1, which indicates that the scattering force could be z/τ larger than the capture force.

The estimates for the pure unscreened grain Coulomb field can serve only as a reference expression. In the Coulomb field, the most important is the scattering on small angles and the result is determined by the so-called Coulomb logarithm $\Lambda = \int_{p_{min}}^{p_{max}} dp/p$, where p is the impact parameter in the collisions. The Coulomb approximation and the Yukawa screened approximation can be used only for small charges (as we estimated $Z_d < 30$ in the existing experiments). Nevertheless we can give here an exact expression for the coefficient α_{dr} for the screened Yukawa interaction ($\beta \ll 1$) assuming that the dust grain is of a finite size a:

$$\alpha_{dr}^{sc,Y} = \frac{2}{3\sqrt{\pi}}\int_0^\infty \frac{sin^2(k)}{\left(k^2 + \frac{a^2}{\lambda_{Di}^2}\right)^2} kdk \approx \frac{1.8}{3\sqrt{\pi}} \ln\left(\frac{\lambda_{Di}}{a}\right)\,. \tag{3.104}$$

Since $\ln(\lambda_{Di}/a)$ in current experiments is about 2 we find, according to (3.104), $\alpha_{dr} \approx 0.677$. But the screening in complex plasmas is usual non-linear and use of the non-screened Coulomb or the screened Yukawa potentials of the grain is not appropriate for most of the experimental conditions. However, the result (3.104) can serve as a reference point.

Non-linear Drag Coefficient for Gurevich Potential. Remember that the non-linear screening looks more as a hard-sphere screening confining all grain field inside the sphere with the radius $\lambda_{scr} \approx 3.24(za/\tau\lambda_{Di})^{1/5}\lambda_{Di}$ (as compared with previous expression containing the factor 3.4, we use here $3.4(\pi/4)^{1/5} \approx 3.24$). Such a screening results in the presence of fields at distances larger than λ_{Di}. The collection radius (the maximum impact parameter where the ions touch the grain and are absorbed by the grain) is $a\sqrt{z/\tau}$ and for most experiments is less than λ_{scr}, just allowing the charging process to operate freely (as well as the friction force related to the capture of ions). If the screening is of Yukawa type, the latter statement is not quite obvious since the ions that should be captured should first move through that part of the grain field where screening cannot be neglected (charging does not depend much on the screening of potential but scattering does).

The estimated r_{eff} for the ion scattering is much larger than the collection radius; it is about az/τ and in current experiments it can be comparable or even larger than the screening length. On the other hand, an estimate of r_{eff} is based on the assumption that the change of the ion trajectory in its collisions with the grain is not large, which means that in the case where az/τ

is substantially larger than λ_{scr}, most of the trajectories inside the screening length correspond to the large scattering angle, or roughly after scattering the ions change the sign of their velocity and return to the direction of entering the grain's hard-sphere screening field. The range of lengths at which the scattering is strong can be estimated only approximately as being somewhat less that λ_{scr}. The cross-section of those scattering is $\pi\lambda_{sc}^2$. In a sense, the ions are reflected by the hard sphere in this scattering but in a backward direction, not undergoing the mirror reflection. In such scattering collisions, if the initial ion momentum is $m_i v_i$ then after the collision the ion momentum is $-m_i v_i$ and the total change of the momentum is $2m_i v_i$. This case is therefore easy to handle and the estimates are as follows:

$$\mathbf{F}_{dr}^{nsc} \approx \pi\lambda_{scr}^2 8\frac{1}{\sqrt{\pi}} T_i \mathbf{u} n_d \ . \tag{3.105}$$

Thus the radius of the cross-section of scattering is the screening length and the change of the momentum in scattering is $2m_i v_i$.

Those models where most of ions in the screening obey large-angle scattering is the limiting case which can be treated easily. The result is

$$\alpha_{dr}^{nsc} = (3.24)^2 \frac{2}{\sqrt{\pi}} z \left(\frac{az}{\lambda_{Di}\tau}\right)^{-8/5} \ . \tag{3.106}$$

For $a/\lambda_{Di} \approx 1/10$, $z = 4$, and $z/\tau \approx 100$, we find $\alpha_{dr} \approx 1.2$, not much different but about two times larger than the expression obtained from the Coulomb scattering (3.101). But the physical picture of scattering is changed completely and the dependencies from the plasma and dust parameters are quite different. Numerical computations of ion trajectories in the non-linear screening potential support the statement that for $a\sqrt{z/\tau} < \lambda_{scr} < az/\tau$ most ions do not reach the grain and are scattered. This means that the drag coefficient due to the ion scattering is substantially larger than that for the ion absorption. For the data of real experiments az/τ is often of the order of λ_{scr} and not all ions undergo large-angle scattering since some ions scatter at an angle of the order of one but not at an angle close to 2π. The contribution of these ions to the drag force is an important issue for future research in this field.

The role of large-angle scattering for the Yukawa potential for distances larger than the screening distance is discussed in [79]. The real problem is more complicated than that discussed by [79], since as we demonstrated, the non-linear screening potential deviates substantially from the Yukawa potential and the Yukawa potential cannot be used for the large grain charges of interest in current experiments. We present here a simple model where scattering is backwards (the large-angle scattering) and the small-angle scattering is neglected. Full investigation of the relative role of large-angle scattering into small-angle scattering for different ratios of complex plasma parameters is done in [80].

Of special interest is investigation of the dependence of the drag coefficient on the ion drift velocity. The expression given above can be used only for $u \ll 1$. In the literature, one can find expressions for the Coulomb scattering for $u \gg 1$, where α_{dr}^{sc} decreases naturally as $1/u^2$ (as it should decrease for the Coulomb interactions). However, currently there is no investigation performed for large drift velocities and for the non-linear screening. This is of interest for the special case of grains in the plasma sheath. For bulk plasmas, the ion drift velocity is not large because of ion stopping by friction due to collisions with grains as well as with neutral atoms. Different models for the ion momentum losses predict different ion-stopping powers when entering complex plasmas. The models can be checked by experiments injecting ions in a complex plasma and measuring related depletion of the ion density (some experiments of this kind already exist).

Non-linear Drag Coefficient for General Non-linearity. For $\beta \gg 1$ and the general form of non-linearity $\psi = (1 - r/R_{nl})^{2/(1-\nu)}$, the scattering transport cross-section $\sigma(\beta)$ corresponds to the large-angle scattering since the corresponding radius substantially exceeds the linear screening length λ_{Di}. The drag coefficient can be expressed through the total transport cross-section averaged on the ion distribution assumed to be thermal [80]:

$$\alpha_{dr} = \frac{1}{2\sqrt{2}\beta^2} \frac{\sigma(\beta)}{\pi\lambda_{Di}^2} \tag{3.107}$$

with

$$\frac{\sigma(\beta)}{\pi\lambda_{Di}^2} = \frac{8\sqrt{2}}{3\sqrt{\pi}} \int_0^\infty \sigma(y) y^5 \exp(-y^2) dy \,, \tag{3.108}$$

where

$$\frac{\sigma(\beta)}{\pi\lambda_{Di}^2} = \frac{8\sqrt{2}}{3\sqrt{\pi}} \int_0^\infty \sigma(y) y^5 \exp(-y^2) dy \tag{3.109}$$

and $\sigma(y)$ is the transport cross-section for the ion velocity determined by $y = v_i/\sqrt{2}v_{Ti}$. This cross-section is determined by the condition that the scattering occurs at a large angle since for $\beta \ll 1$ (contrary to $\beta \ll 1$) the small-angle scattering is negligible. The value of $R_{cs} = R_{nl}(1 - \Delta)$ should be found from expression for the non-linear screening potential and the condition that the scattering is occurring at a large angle:

$$\sigma_{nl}(\nu, \beta, y) = \eta\pi \left(R_{nl}(\nu, \beta)\right)^2 \left(1 - \Delta(\nu, \beta, y)\right)^2 \,, \tag{3.110}$$

where η is the fitting numerical coefficient found in [80] to be 2.5 and Δ satisfies the transcendent equation

$$\frac{\left(\Delta(\nu, \beta, y)\right)^{\frac{2}{1-\nu}}}{1 - \Delta(\nu, \beta, y)} = y^2 d(\nu) \beta^{-\frac{2}{3-\nu}} \,. \tag{3.111}$$

The latter can be solved numerically to calculate the drag coefficient according to (3.107) and the friction force coefficient $f_{dr} = \alpha_{dr}\beta$ entering in the

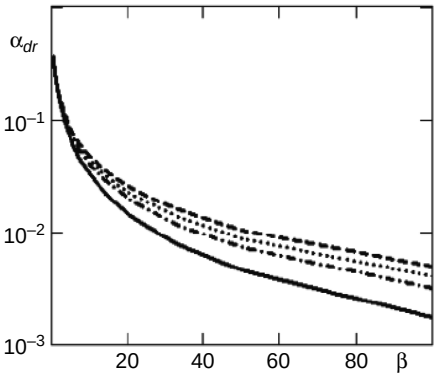

Fig. 3.16. The non-linear drag coefficient α_{dr} as a function of β for different values of ν. *Solid line* corresponds to $\nu = 0.9$, *dash-dotted line* corresponds to $\nu = 0.5$, *dotted line* corresponds to $\nu = 0.3$, and *dashed line* corresponds to $\nu = 0.1$

definition of the drag force $\mathbf{F}_{dr,n}$ in (3.99). The dependence of drag coefficient as a function of β and ν is demonstrated in Fig. 3.16.

As can be seen, for a typical value of $\beta \approx 35$ the non-linear drag coefficient is approximately two orders of magnitude less than that extrapolated from the linear Yukawa expression (constant value for $\beta \to 0$ in Fig. 3.16. The force coefficient for β is excluded from normalization f_{dr}. We can see an increase of f_{dr} but not so fast as for the linear case(where $f_{dr} \propto \beta$) (see Fig. 3.17). For large non-linearity, the drag coefficient at typical value $\beta = 35$ is much larger than that for the Yukawa screening but still less than that extrapolated for the linear screening $\propto \beta$.

3.3.3 Other Forces Acting on Ions

Here, we restrict ourselves to the simplest possible description of forces acting on ions and use the hydrodynamical approach. The first one is the simple ion pressure force $\mathbf{F}_{i,pr}$, which in the dimensionless units introduced above for the forces is given by

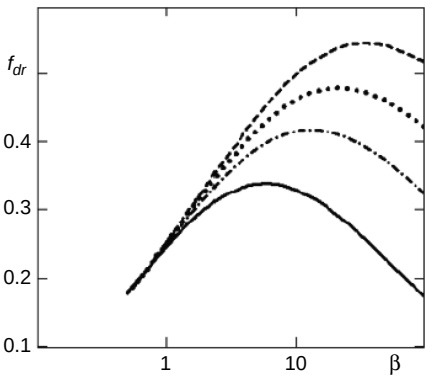

Fig. 3.17. The non-linear drag force f_{dr} as a function of β for different values of ν. *Solid line* corresponds to $\nu = 0.9$, *dash-dotted line* corresponds to $\nu = 0.5$, *dotted line* corresponds to $\nu = 0.3$, and *dashed line* corresponds to $\nu = 0.1$

$$\mathbf{F}_{i,pr} = -\tau \frac{1}{n} \frac{\partial n}{\partial \mathbf{r}} \,, \tag{3.112}$$

where we introduce the dimensionless distance $\mathbf{r}$ by

$$\mathbf{r} = \mathbf{r}^{ac} \frac{a}{\lambda_{Di}^2} \,. \tag{3.113}$$

Expression (3.112) shows that the pressure term contains a small parameter τ. The pressure force can still be important if the ion density gradients become large. Another natural force is the ion inertia force $\mathbf{F}_{i,inertia}$ written as

$$F_{i,inertia} = -\tau \mathbf{u} \cdot \nabla \mathbf{u} \,. \tag{3.114}$$

For small τ and small drift velocities $\mathbf{u}$, this force is small. Finally, the electric field force $\mathbf{F}_E$ in the dimensionless units is given by

$$\mathbf{F}_E = \mathbf{E}; \qquad \mathbf{E} = \frac{\mathbf{E}^{ac} e \lambda_{Di}^2}{a T_e} \,. \tag{3.115}$$

In the presence of a neutral gas there appears two effects related to the ion-neutral collisions, namely the ion diffusion in the neutral gas and the ion friction in the neutral gas. In the simplest approximation we can divide the total ion flux Φ on the convective flux and diffusion flux $\Phi = nu + \Phi_{diff}$. Expression for Φ_{diff} is more convenient to write using another normalization. The normalization used above (with respect to the ion-dust mean-free path) is useful for the case where the ion-neutral collisions are not important. In case they play an significant role it is better to normalize all expressions on the value containing the mean-free path for the ion-neutral collisions. It is important that we can find the form of the new normalization which *keeps all expressions for forces in the same form as above*. We introduce the conversion factor R given by

$$R = \frac{\tau \lambda_{Di}^2}{a \lambda_{in}} \,. \tag{3.116}$$

Then the re-normalization is

$$n, n_e, P, F, r \to (n/R, n_e/R, P/R, F/R, rR) \,. \tag{3.117}$$

All the above-written equations survive in the same form after such a change of normalization. This is convenient for the case where the ion-neutral collisions are added.

In the new units, the ion continuity equation can be written as

$$\frac{\partial n}{\partial t} + \frac{\partial \mathbf{\Phi}}{\partial \mathbf{r}} = \alpha_i n_e - P n \alpha_{ch} \,, \tag{3.118}$$

where $\mathbf{\Phi}$ is the total ion flux including the convection flux $n\mathbf{u}$ and the diffusion flux. The total flux is then written in a very simple form:

$$\mathbf{\Phi} = n\mathbf{u} - \tau \frac{1}{3\sqrt{2}} \frac{dn}{d\mathbf{r}} \,. \tag{3.119}$$

The second term can be written only in the collision-dominated case where the mean-free path for the ion-neutral collisions is much less than the mean-free path for the ion-dust collisions and the size of the density inhomogeneity is much larger than the ion-neutral mean-free path. Except for the large gradients of the ion density, the diffusion flux is usually small containing the small parameter τ. Obviously, the coefficients α_i in (3.96), (3.97), and (3.118) are different and have a different physical meaning: in (3.97) α_i describes the number of the electron–ion pairs created by the ionization source on the ion–grain mean-free path, while in (3.118) it describes that, correspondingly, on the ion-neutral mean-free path divided by τ. This makes it easy to use both equations (3.96) and (3.97) in the "collisionless" case where the collisions of plasma ions with neutral gas atoms can be neglected, and to use (3.118) in the "collision-dominated" case where the ion-neutral collisions are important.

This re-normalization allows us to easily introduce the friction force $\mathbf{F}_{in}$ of ions in the gas of neutrals

$$\mathbf{F}_{in} = -\mathbf{u} \,. \tag{3.120}$$

This expression is extremely simple and is valid for small ion drift velocities $u \ll 1$. Sometimes it is desirable to write a phenomenological expression for the friction force valid also for $u > 1$. It is known from ion mobility measurements; it can be also justified from the expression for the ion-neutral cross-section . We have

$$\mathbf{F}_{in} = -\mathbf{u}(1 + \alpha_N |\mathbf{u}|) \,, \tag{3.121}$$

where α_N is a phenomenological coefficient. The existing experiments show that $1 < \alpha_N < 4$, thus it is of order unity. Finally, equation for ions for $u \ll 1$ has the form

$$\tau \frac{\partial \mathbf{u}}{\partial t} + \tau \mathbf{u} \cdot \nabla \mathbf{u} = E - P\mathbf{u}n - \mathbf{u} - \tau \frac{1}{n} \frac{dn}{d\mathbf{r}} \tag{3.122}$$

which takes into account the above forces.

3.4 Forces Acting on Grains

Important forces acting on dust particles are the drag force created by the flux of ions, the electric field force, the dust pressure force, the thermophoretic force, the friction force in a neutral not-moving gas or the neutral drug force in a moving neutral gas, and, finally, the gravity and the dust inertia forces. Here, we describe all these forces and estimate their values for current experimental conditions.

3.4.1 Ion Drag and Electric Field Forces

The drag force has been first addressed in [81, 82]. The drag by an ion flux exists for small ion drift velocities, much less than the ion thermal velocity, as well as for large ion drift velocities, much larger than the ion thermal velocity. In current experiments, the ion drift velocities are usually of the order or somewhat larger than the ion thermal velocity, and in some experiments (e.g., for single-layer grains in the plasma sheath) of the order of ion-sound velocity (when the Mach number $M = u/\sqrt{2\tau}$ is about 1, $u = u_i/v_{Ti} \approx 1/\sqrt{2\tau} \approx 5$). Complex plasma experiments are often performed in the collision-dominated case (where the ion-dust mean-free pass is larger than the ion-neutral mean-free path) and the ion drift velocity is much less than the ion thermal velocity (and of course it is always much less than the electron thermal velocity).

Physically, the process of dust drag by the ion flux is the same as the loss of the ion momenta in interaction with dust particles discussed in detail above, and its presence is a direct consequence of the momentum conservation. We can make the same estimate as for the momentum transfer in the capturing process by using the sub-thermal ion flux with the corresponding change of the collision frequency determined now by the ion number density but not by the dust number density as previously. The same change should be done in estimating the drag due to non-linear scattering. Certainly, the force is determined by the difference of the ion drift and the dust drift velocities, but we neglect the dust velocity as compared to the ion velocity since almost in all cases of interest it is much smaller. Instead of parameter P as in previous calculations we get $Z_d n_i/n_0$. In general case of arbitrary ion drift velocity we find the same coefficient α_{dr} but multiplied by $Z_d n$ instead of P. If we use the same normalization as above we have for the normalized drag force a simple expression

$$F_{dr} = Z_d z n \alpha_{dr} \mathbf{u} \, . \tag{3.123}$$

The presence of the large factor Z_d in this expression is also a consequence of the momentum conservation law. Indeed (3.123) is written for a single dust particle. To find the momentum transferred in a unit volume we should multiply (3.123) by n_d and get the additional factor Pn_0. On the other hand, to find the momentum lost by ions in the unit volume we should multiply (3.105) by $n_i = n_0$ and then the sum of these expressions of the change of the total momentum in the unit volume is exactly zero.

The presence of the large factor Z_d in front of expression for the drag force is rather important since all other dimensionless parameters are usually of the order of 1 and the presence of such a large factor in (3.123) shows that the drag force is usually large. But due to large Z_d in the electric field force $\mathbf{F}_{el}$ acting on the grain particle, the electric force is also large. Normalizing the electric field in the same manner as previously for ions, we have

$$\mathbf{F}_{el} = -eZ_d \mathbf{E} \, . \tag{3.124}$$

For the sum of the electric field force and the ion drag force we obtain

$$\mathbf{F}_{el} + \mathbf{F}_{dr} = -Z_d(e\mathbf{E} - nz\alpha_{dr}\mathbf{u}) \,, \tag{3.125}$$

such that the factor Z_d appears as a common factor in the expression for the total force. Thus if we intend to find the force balance of these two forces by putting the left-hand side of equation (3.125) to zero, the appearing balance is not determined by the common factor Z_d [83, 84, 85]. This does not mean that the presence of Z_d in the expressions for the electric field force and for the drag field force has no physical consequences. In fact it has a very important consequence when other forces not having this large factor are added in the total force balance; these other forces can then be neglected. For instance, the dust pressure force $\mathbf{F}_{pr,ac} = -(T_d/n_d)(\partial n_d/\partial \mathbf{r_{ac}})$ in the normalized form is given by

$$\mathbf{F}_{pr} = \frac{\mathbf{F}_{pr,ac}}{F_0} = -\frac{T_d}{T_e}\frac{z}{P}\frac{\partial}{\partial \mathbf{r}}\left(\frac{P}{z}\right) = -Z_d\tau_d\frac{z}{P}\frac{\partial}{\partial \mathbf{r}}\left(\frac{P}{z}\right) \,, \tag{3.126}$$

where τ_d is the effective dimensionless dust temperature

$$\tau_d = \frac{T_d}{T_e Z_d} \,. \tag{3.127}$$

Due to the absence of Z_d in this force (or, in other words, the presence of large factor Z_d in the denominator of τ_d when Z_d is added in both the numerator and the denominator of this force to compare it with other forces) shows definitely that this force is small. The factor τ_d for any existing experiment is very small, $\tau_d \ll 1$.

The total force $\mathbf{F}_{tot}$ including the electric field force, the drag force, and the pressure force can be written as

$$\mathbf{F}_{tot} = -\frac{Z_d}{P}\left(\tau_d z\frac{\partial}{\partial \mathbf{r}}\left(\frac{P}{z}\right) + e\mathbf{E} - \alpha_{dr}nz\mathbf{u}\right) \,. \tag{3.128}$$

If we then write the force balance equation (not neglecting the dust pressure force) we obtain

$$\tau_d z\frac{\partial}{\partial \mathbf{r}}\left(\frac{P}{z}\right) = P(e\mathbf{E} - \alpha_{dr}nz\mathbf{u}) \,. \tag{3.129}$$

If we neglect the term with very small τ_d, we find

$$P(e\mathbf{E} - \alpha_{dr}nz\mathbf{u}) = 0 \,. \tag{3.130}$$

Thus we obtain two solutions of this equation, i.e., either the electric field force balances the ion drag force or $P = 0$. In the the region where the balance of the electric field force and the drag force exists, usually P is not zero. This means that there could and should exist boundaries with a jump of the parameter P and since z is a continuous parameter on these boundaries,

the dust density should have a jump on those boundaries. The term with dust pressure in the force balance equation can describe the fine structure of this "jump" as a continuous but still steep change of the dust density, with possible small oscillations at the spatial scales in which τ_d is smaller than other spatial scales of the problem.

Thus we can conclude that due to the presence of the large factor Z_d in the electric field force and in the drag force (which results in the smallness of τ_d and the possibility to neglect the dust pressure force), new type of boundaries can be created with all plasma parameters continuing with them except the dust density. Note that this is not only the theoretical possibility. In many different configurations the *sharp dust density gradients* were observed in experiments [86, 87, 88], and a large dust-void structure was observed in micro-gravity experiments on board the International Space Station [89]. For the theory see [83, 84, 90, 91, 92, 93], and for explanation of the observations of sharp boundaries in the micro-gravity experiments see [85, 94]. In [86] the boundary observed was very sharp and outside the dust cloud the dust was 100% absent. Several interesting structures with sharp separation of regions with dust particles of different size (the a size and the double size $2a$ particles were injected simultaneously) were observed in [87, 88]. This field is obviously the subject of future detailed investigations. Also, convection of dust was observed in Refs. [87, 88] and in experiments on the International Space Station [89].

We illustrated here all these relations using the case where the ion–dust collisions are the most important. All expressions survive formally the same in the case where the ion-neutral collision dominate (when the normalization should only be changed according to the expressions given in the previous section).

3.4.2 Temperature Gradients and Thermophoretic Force

In the case where ion–neutral collisions dominate over ion–dust collisions, the thermophoretic force, proportional to the temperature gradient in the neutral gas, can become comparable to other forces and therefore important. Physics of this force is that in the presence of the temperature gradient the neutral gas pressure acting on one side of the grain is larger/smaller than that on the other side of the grain. It was considered for dust grains far from the walls in neutral gas in [95] and for grains close to the walls in [96]. The ratio to the corresponding friction forces depends on the gas pressure; in current experiments this ratio is often of the order of 1.

The thermophoretic force $\mathbf{F_{tp,ac}}$ is determined by the neutral gas density n_n and by the gradient of the neutral gas temperature T_n [95]:

$$\mathbf{F}_{tp,ac} = 2.4 n_v \pi a^2 \lambda_{n,n} \frac{\partial T_n}{\partial \mathbf{r}_{ac}} \,. \tag{3.131}$$

The main physical problem in this regard is which processes in the neutral gas determine the temperature gradient. That can be an external source of heat or a temperature difference between the electrodes in an experimental device. If externally created temperature gradients are known then equation (3.131) determines the force completely. In general, the temperature gradient is determined by the heat conductivity which (in the condition determined by collisions with neutrals) is described as a diffusion equation with various heat sources. Then the question we need to answer is what kind of the temperature gradient in the neutral gas can be supported by dust. Thus we consider only the sources related with the presence of dust and the stationary heat transfer.

First, consider the heat balance at the surface of a dust particle. The flux of electrons and ions related to the charging process continuously supply the surface with the energy which is the energy of captured ions and electrons. This energy flux to the surface can be easily calculated using the OML cross-sections. Each ion is accelerated by the dust field almost to the energy corresponding to electron temperature. Therefore contributions of the electrons and ions to the heat flux onto the dust surface are almost equal (the direct calculations show that the difference is only in a factor $z/2$). This energy deposited on the dust surface cannot stay there since for a low ionization the neutral density is much larger than the ion density (in typical experiments by 6 orders of magnitude: $n_n/n_i \approx 10^6$) and the rate of dust collisions with neutral gas atoms $(n_n/n_i)(\tau/z)$ is $\approx 10^4$ times larger (the ion and neutral thermal energy in this estimate assumed as almost equal). The factor τ/z is the ratio of the cross-section on the neutral-dust collisions (which is the geometrical cross-section πa^2) to the cross-section of the ion–dust collisions $(z/\tau)\pi a^2$.

In the neutral-dust collisions, the neutral atoms are attached to the dust surface for a rather short time (called the "resident time") which is sufficient to equalize the dust the thermal energy of the attached neutral atoms with the dust surface temperature. Then the neutral atom takes the excess of energy which was deposited by ions and is re-emitted from the dust particle. As a result of this process, the dust surface temperature becomes almost equal to the neutral gas temperature. In the numerical example given here, the dust surface temperature can differ from the neutral gas only by a small value of the relative order of 10^{-4}[85]:

$$\frac{T_s - T_n}{T_n} \approx \frac{n_i}{n_n}\frac{\tau}{z} \,. \tag{3.132}$$

The heat transfer from the dust surface to the neutral atoms is very fast and although the surface temperature of dust is larger than the temperature of the neutral gas (this determines the direction of the heat transfer), this difference is very small.

Thus the energy deposited to dust in the charging process is finally a source of heating of local neutral atoms (the heating source q_d) that creates the temperature gradient. Thus the self-consistent thermophoretic force can be

unrelated with an external heating process. Of course, in reality the external source creates the ion flux which also deposits the energy in the neutral gas (heating source q_i) via the ion-neutral collisions and the ion-neutral friction.

The best way to write the heat conductivity equation with these heating sources on the right-hand side is to use the dimensionless distance already used above in the case where the collisions with neutral dominate, namely to normalize the distance on $\lambda_{nn}/\tau \approx \lambda_{in}\tau$ and the thermophoretic force on T_n/λ_{nn} (as above where the force was normalized by T_i/λ_{in}). We have

$$Z_d \mathbf{F}_{tp} = \frac{\mathbf{F}_{tp,ac}\lambda_{nn}}{T_n} \ , \tag{3.133}$$

where $\mathbf{F}_{tp}$ stands for the normalized thermophoretic force divided by Z_d in order to extract the factor Z_d as the common factor for all forces acting on dust particles (this makes the comparison of different forces quite simple). Then, according to expression for the thermophoretic force (3.131) containing the first derivative with the respect to the neutral temperature, we obtain the heat conductivity equation in the neutral gas in the form containing only the first derivative of the thermophoretic force with respect to the dimensionless distance. For simplicity we write this equation in the one-dimensional form expecting that the temperature depends only one coordinate x [85]:

$$\alpha_{tp}\frac{z\partial F_{tp}}{\partial x} = \tau(q_d + q_i) \ , \tag{3.134}$$

where α_{tp} is a numerical coefficient of order unity (in the region where the ion-neutral collisions dominate it is 2.4/3). The OML approach gives

$$q_d = \frac{1}{2\sqrt{\pi}} Pn(z++2)\alpha_{ch} \ . \tag{3.135}$$

Then a simple calculation with the friction force determined by the ion-neutral collisions gives for $u \ll 1$ (where the friction is proportional to u and the ion mobility is proportional to the electric field)

$$q_i = \frac{nu^2}{4\sqrt{2\pi}} \ . \tag{3.136}$$

For $u \gg 1$ (when the ion-neutral friction force is proportional to the square of the drift velocity and the ion mobility is correspondingly proportional to the squared electric field) we have an estimate of q_i which differs from (3.136) by the additional factor u.

Appearance of the small factor τ in (3.134) for the thermophoretic force is very important. In the case where all dimensionless values are of the order of 1, the presence of τ on the right-hand side of (3.134) allows us to conclude that in most cases of interest the thermophoretic self-consistent force is rather small and can be neglected. The only exclusion is the case of large ion drift

velocities where (3.136) can be large. This can occur only if the ion drift velocity exceeds the ion thermal velocity substantially, namely if τu^3 is of the order of 1 or if $M > \tau^{1/6}$, which means that for current experiments (where $\tau \approx 0.02$) $M > 0.5$. Thus the thermophoretic force can perhaps be important in the sheath region where $M \sim 1$. But this also requires high pressures for the ion-neutral (or neutral–neutral) collisions to dominate when the above-used expression for the thermophoretic force is valid. In existing experiments where the ion-neutral collisions dominate, the ion drift velocity $u \sim 1$, and $M \ll \tau^{1/6}$. The thermophoretic force in these conditions is small. Possible presence of sharp dust boundaries does not change this conclusion since (3.135) contains only P but not its derivatives with respect to the distance. In other conditions where the forces are determined by the non-linear balance which is not directly related to the neutral gas collision mean-free path, the thermophoretic force can be rather important. In particular it is important in interaction of two dust particles in the condition where the distance between them is larger than the collision mean-free path (we return to this problem later in detail). The thermophoretic force can be probably used for dust removal from the system by externally applying a temperature gradient.

3.4.3 Neutral Gas Drag force, Gravity force, and Dust Inertia

The neutral drug or neutral friction force appears in the case where a dust particle moves with some drift velocity $\mathbf{v}_d$ through the neutral gas. If the neutral gas moves itself, this force can lead to dust motion created by the neutral gas drag. The dust movement can appear also in the case where the gas is not moving but the balance of other forces acting on dust particle needs the neutral gas drag force to be included. For example, in the case where the ion drag force and the electric field force are not acting in the same direction they can be compensated in one direction without the neutral drag force but cannot be compensated in the other direction without the neutral drug force. Then these electric and ion drag forces support the dust motion in the direction in which the force balance cannot be established without the neutral drag force. This leads to the dust convection observed in many present experiments [97]. The physical explanation of the role of neutral gas drag force in the creation of dust convection is given in [6, 89, 98, 99]. The neutral gas drag force in the presence of gravity can compensate the gravity force and lead to the fall (with a constant velocity) of dust particles injected into the gas discharge.

The neutral drag force is also known as the Epstein drag force [100]; from the physical point of view, it appears because the impact rate of neutral atoms on the front surface of a dust grain is larger than the impact rate on the trailing surface. The difference in the collision rates between the front and the rear parts of the grain multiplied by the average momentum transferred by the impact of the gas atom equals the momentum transferred to the particle per unit time. This determines the rate of the neutral drag force. The neutral drag

force is given by the expression

$$F_{nd,ac} = -\frac{4}{3} n_n T_n \pi a^2 \frac{\mathbf{v}_{d,ac}}{v_{Tn}} = -m_d \nu_{nd,Ep} \mathbf{v}_{d,ac} \ , \tag{3.137}$$

where, as before, the index ac indicates that the corresponding value is the actual value, and $\nu_{nd,Ep}$ is the Epstein collision frequency of the momentum exchange of the dust particles with the neutral gas atoms.

We also introduce the normalized drag force. The neutral drag is important both in the case where the ion–dust collisions dominate (the normalization is then related with the ion–dust collisions) and in the case where the ion-neutral collisions dominate (the normalization is then related with the ion-neutral collisions).In the first case we have

$$\mathbf{F}_{nd} = \frac{\mathbf{F}_{nd,ac} \lambda_{Di}^2}{T_e a} = Z_d \frac{\mathbf{v}_d^i}{z} \ , \tag{3.138}$$

where we intentionally extracted the factor Z_d, common for all forces acting on dust particles. The normalized dust velocity $\mathbf{v}_{d,i}$ in the case where the ion–dust collisions dominate is equal to

$$\mathbf{v}_d^i = \frac{\mathbf{v}_{nd,ac}}{v_{d,*}} \ , \tag{3.139}$$

with

$$v_{d,*} = v_{Tn} \frac{3T_i}{T_n \tau^2} \frac{n_i}{n_n} \ . \tag{3.140}$$

This expression can be used to estimate the characteristic dust velocities which can appear in the disbalance of other forces acting on dust particles. For $T_n = T_i$ and $\tau = T_i/T_e \approx 0.02, n_n/n_i \approx 10^6$, we find $v_{d,*} = 7.510^{-3}, v_{Tn} \approx 120\text{cm/s}$ for krypton gas. Notice that this characteristic velocity does not depend on the dust size.

If the ion-neutral collisions dominate, we apply another normalization

$$\mathbf{F}_{nd} = \frac{\mathbf{F}_{nd,ac} \lambda_{in}^2}{T_i} = Z_d \frac{\mathbf{v}_d^n}{z} \ . \tag{3.141}$$

where

$$\mathbf{v}_d^i = \frac{\mathbf{v}_{nd,ac}}{v_{d,**}} \tag{3.142}$$

and

$$v_{d,**} = v_{Tn} \frac{3 Z_d T_i}{T_n} \frac{\sigma_{in}}{4\pi a^2} \ . \tag{3.143}$$

This velocity strongly depends on the dust size a ($\propto 1/a$ since $Z_d \propto a$) and for $Z_d \approx 10^4, T_n \approx T_i, \sigma_{in} \approx 510^{-15}\text{cm}^{-3}, a \approx 3\mu\text{m}$ we find $v_{d,**} \approx 1.310^{-4}, v_{Tn} = 2\text{cm/s}$ for krypton gas.

In the case where the neutral drag force is taken into account in the force balance equation, we have (neglecting the dust pressure force)

$$-e\mathbf{E} + \alpha_{dr} z n \mathbf{u} - \frac{\mathbf{v}_d}{z} = 0 \ . \tag{3.144}$$

This equation has the same form in both cases (i.e., where the ion–dust collisions dominate or the ion-neutral collisions dominate), the difference is in the corresponding normalization of n, $\mathbf{E}$, and $\mathbf{v}_d$. The dust inertia is neglected in (3.144), which is possible in stationary conditions when the drag friction force exceeds the inertia force $m_d(\partial v_{d,ac}^2)/2\partial x_{ac}$ or for the case where the ion–dust collisions dominate for

$$m_d v_{d,i} \ll m_{d,*} \,, \tag{3.145}$$

where

$$m_{d,*} = m_n \frac{Z_d T_n}{9 z T_i} \tau^3 \frac{n_n^2}{n_i^2} \,. \tag{3.146}$$

For $v_{d,i} \to 0$ the dust inertia can be neglected according to (3.145), but for $v_{d,i} \approx 1$ the dust inertia can be neglected only for small (light) dust particles $m_d \ll m_{d,*}$. For $n_n/n_i \approx 10^6$, $Z_d \approx 10^4$, $tau \approx 0.02$, $T_n \approx T_i$, $z \approx 3$, we find $m_{d,*}/m_n \approx 310^9$. This large value appears again because all other forces except the inertia force are proportional to Z_d and therefore Z_d appears in the expression for the critical mass. In the case where the ion-neutral collisions dominate we obtain the condition (to neglect the dust inertia) similar to (3.145), with substitutions of $v_{d,n}$ for $v_{d,i}$, and $m_{d,**}$ for $m_{d,*}$. For $v_{d,n}$ of the order of 1, we find

$$m_d \ll m_n \frac{T_n}{Z_d 9 T_i} \left(\frac{4\pi a^2}{\sigma_{in}} \right)^2 \,. \tag{3.147}$$

This expression, in contrast to the previous relation, contains Z_d in the denominator. For $T_n \approx T_i$, $\sigma_{in} \approx 510^{-15}$, $a \approx 3\mu$m, we find $m_d/m_n \ll 10^{18}$. This relation is usually fulfilled in current experiments. Note that this condition does not depend on the dust size if $m_d \propto a^3$, $Z_d \propto a$, which is valid if the dust particles are not hollow inside.

In case there exists a potential well for dust particles, a grain can reach the bottom of the well with velocity equal to zero and then the neutral drag force vanishes. In the presence of gravity, the balance equation should include the gravity force $F_{g,ac} = g m_d$, where g is the gravitational acceleration. The neutral drag force, being balanced by the gravity force $F_g = g m_d \propto a^3$, leads to a constant dust drift velocity through the neutral gas which is $\propto a$.

3.5 Forces Acting on Electrons: Characteristic Electric Fields

3.5.1 Electron Friction in Absorbing Collisions with Grains and Electron Inertia

Friction of electrons with grains is considered similarly to that of ions, and it appears to be rather small. We can derive the electron momentum balance and write it in the dimensionless form. It was mentioned already that

the electron drift velocity is of the order of the ion drift velocity and therefore the electron drift is reasonable to normalize in the same way as the ion drift, namely by $\sqrt{2}v_{Ti}$; we denote the normalized electron drift velocity as u_e. Taking into account the electron inertia, the electric force, the electron pressure force, and the friction force due to the presence of dust, we obtain the dimensionless equation for electrons valid in both the collisionless and the collision-dominated cases:

$$\tau\frac{m_e}{m_i}\left(\frac{\partial \mathbf{u}_e}{\partial t}+\frac{1}{2}\mathbf{u}_e\cdot\frac{\partial \mathbf{u}_e}{\partial \mathbf{r}}\right)=-e\mathbf{E}-\frac{1}{n_e}\frac{\partial}{\partial \mathbf{r}}-Pn_e z\alpha_{dr,e}\mathbf{u}_e\ . \tag{3.148}$$

Remember that for the collisionless case all lengths are normalized to λ_{Di}^2/a, and for the collision-dominated case they are normalized to λ_{in}/τ; the densities are normalized in the collisionless case to n_0, and in the collision-dominated case to $n_0\lambda_{Di}^2\tau/\lambda_{in}a$; and the electric field is normalized to $T_e a/\lambda_{Di}^2$, while in the collision-dominated case to T_i/λ_{in}.

In equation (3.123), the drag force is obtained by the same procedure as for the ion drag. We introduced the new electron drag coefficient $\alpha_{dr,e}$ and it should be calculated using the cross-sections of the electron dust charging, $\alpha_{dr,ch,e}$, and expressions for the elastic scattering collisions of electrons with dust particles $\alpha_{dr,nsc,e}$. We have

$$\alpha_{dr,e}=\alpha_{dr,ch,e}+\alpha_{dr,nsc,e}\ . \tag{3.149}$$

The electron charging cross-section in the OML approach is $\sigma_e=\pi a^2(1-2Z_d e^2/m_e v_e^2)$, and calculations give

$$\alpha_{dr,ch,e}=\frac{2}{3\sqrt{\pi}}\frac{\tau^2}{z^2}\sqrt{\frac{m_e}{m_i\tau}}exp(-z)(2+z)\ . \tag{3.150}$$

Using the OML charging equation we obtain

$$\alpha_{dr,ch,e}=\frac{2n_e(2+z)}{3\sqrt{\pi}nz}\left(\frac{m_e\tau}{m_i}\right)\left[\frac{\tau}{z}+\int_0^1\left(1+\frac{u^2\tau}{z}(y-1)^2\right)\right]\ . \tag{3.151}$$

The drag coefficient due to scattering can be somewhat larger but still very small. The calculations similar to those done above for ions give for electrons

$$\alpha_{dr,nsc,e}=\frac{2}{3}\tau\sqrt{\frac{m_e\tau}{m_i}}\ . \tag{3.152}$$

It should be mentioned that both the inertia term and the drag term have small factors $m_e\tau/m_i$. Thus the criterion for electrons to be adiabatic (when both the friction on ions and the electron inertia can be neglected) for the collisionless case is given by

$$\tau\ll\left(\frac{m_i}{m_e}\right)^{1/3}\ . \tag{3.153}$$

This is a very weak condition which is usually fulfilled in all current plasma experiments.

In the collision-dominated case one should take into account the electron diffusion on neutral atoms. Introducing the total electron flux Φ_e (similar to (3.119)) in the electron continuity equation, we write

$$\frac{\partial n_e}{\partial t} + \frac{\partial \mathbf{\Phi_e}}{\partial \mathbf{r}} = \alpha_i n_e - Pn\alpha_{ch} \; . \tag{3.154}$$

Normalization of Φ_e is again with respect to $2v_{Ti}^2\lambda_{in}/\tau$. The right-hand side of this equation is the same as that of (3.118) since electrons and ions are created in pairs in processes of plasma ionization, and are absorbed in pairs by grains. We find the following expression for the electron flux similar to that of the ion flux:

$$\Phi_e = n_e u_e - \frac{\sigma_{en} m_i}{3\sqrt{2}\sigma_{in} m_e} \frac{\partial n_e}{\partial \mathbf{r}} \; . \tag{3.155}$$

The electron diffusion should be taken into account only in the collision-dominated case where the scale of the density gradients is much larger than the electron-neutral mean-free path.

Under condition where the electron flux is equal to the ion flux (used often for consideration of the ambipolar diffusion) one should take into account that even in the quasi-neutral case the electron and ion densities are not equal (due to the presence of dust grains). Thus one finds the electron drift velocity

$$u_e = u\frac{n_e}{n} - \tau \frac{1}{n_e}\frac{\partial n_e}{\partial \mathbf{r}} + \frac{m_i \sigma_{en}}{3\sqrt{2} m_e \sigma_{in}} \frac{1}{n_e}\frac{\partial n_e}{\partial \mathbf{r}} \; . \tag{3.156}$$

If this expression is substituted on the left-hand side of equation (3.123) one finds that the first term is small with the factor $\tau m_e/m_i$ if the ion and electron densities are of the same order (which is the case in most experiments); the second term as compared with the electron pressure term is small with the factor $\tau\sigma_{en}/3\sqrt{(2)}\sigma_{in}$ (note that σ_{en} is usually smaller than $sigma_{in}$ by the factor 1/3 or 1/10 and τ is a small factor in most experiments); and the last term has a small factor τ as compared to the electron pressure. Due to this estimate, the electron diffusion on neutral atoms should be neglected and the only remaining forces are the electric field force and the electron pressure force.

3.5.2 Balance of Forces for Electrons

The electric field force in its normalized form is given by

$$\mathbf{F}_{E,el} = -e\mathbf{E} \; . \tag{3.157}$$

The electron pressure force can be written as

$$F_{el,pr} = -\frac{1}{n_e}\frac{\partial n_e}{\partial \mathbf{r}} \; . \tag{3.158}$$

Thus the balance equation for the electron forces is

$$e\mathbf{E} = -\frac{1}{n_e}\frac{\partial n_e}{\partial \mathbf{r}} \, . \tag{3.159}$$

The electrons therefore usually adiabatically follow the electric field. The concept of the ambipolar field often does not operate in complex plasmas since, first, the dust grains create fields much larger than those corresponding to the ambipolar electric fields and, second, because of the smallness of the parameter τ (which is the ratio of the ion to electron temperature) in most complex plasma experiments.

3.5.3 Electric Fields and Condition for Quasi-neutrality

High dissipation rates in a complex plasma can create rather a large field even in the quasi-neutral region. It is simple to estimate these fields in the limiting cases where the ion-neutral collisions are negligible and where they are dominant. In the first case we can equalize the friction force acting on ions by the electric field force. We should distinguish the case where the friction is determined by the ion–dust collisions as treated in the previous sections and the case where the friction of ions is determined by the ion-neutral collisions. In the case where the friction is due to the dust–ion collisions the balance of the friction and electric field forces gives the estimate of the equivalent electric field which we denote as $E_{0,id}$. We have

$$E_{0,id} \approx \frac{T_e a}{e\lambda_{Di}^2} \tag{3.160}$$

if the drift velocity is of the order of the thermal velocity and P is of the order of 1. For typical ion densities of the order of $n_i \approx 10^9 \mathrm{cm}^{-3}$, as well as $a \approx 30\mu\mathrm{m}$, $T_e \approx 2eV$, we can estimate $E \approx 10^3 V/cm$. In the case where the ion friction is determined by the ion-neutral collisions, we should use the mean-free path for the ion-neutral collisions λ_{in} instead of the charging length λ_{Di}^2/a in the previous estimate. The estimate of the electric field in this case also gives large values of the fields.

In the case where the characteristic length is determined by the charging length, the standard estimate of the quasi-neutrality condition is changed. We now use the dimensionless length normalized by $L = \lambda_{Di}^2/a$ and the dimensionless field normalized as

$$E \equiv \frac{E_{ac}}{E_{0,id}} \, . \tag{3.161}$$

The Poisson's equation then takes the form

$$\frac{\partial \mathbf{E}}{\partial \mathbf{r}} = \tau \frac{\lambda_{Di}^2}{a^2}(n - n_e - P) \, . \tag{3.162}$$

The condition of quasi-neutrality appears when we can set to zero the right-hand side of (3.137) and neglect the left-hand side. In the case where the

dimensionless electric field is of the order of 1 and the gradient of it (or the characteristic dimensionless length) is also of the same order of 1, this condition is determined by the relation

$$a \ll \lambda_{Di}\sqrt{\tau}\ . \tag{3.163}$$

This relation is the consequence of the large influence of dust on electrostatic phenomena in complex dusty plasmas. It is unusual only at first glance and was derived from the Poisson equation which in other conditions shows that the condition of quasi-neutrality is the condition in which the characteristic length of the inhomogeneity of the potential should be larger than the Debye length. There is no contradiction between these two statements since the last one is usually obtained from linearized Poisson equation while the condition where the length has to be the charging mean-free path (or the mean-free path for the ion–dust collisions) is related with the self-consistent non-linear behavior of the total complex system. Numerical solutions of self-consistent non-linear balance equations for dust-containing regions confirm that in these complex conditions relation (3.163) is really the condition for quasi-neutrality [101]. In other more simple conditions such as those where the dust does not play the crucial role, the condition of quasi-neutrality takes the usual form. The only important restriction to apply the relation is that the ion-neutral friction force should be negligible as compared to the friction on dust particles. In the condition where the ion-neutral collisions dominate we find the estimate of the characteristic electric field $E_{0,in}$:

$$E_{0,in} \approx \frac{T_i}{e\lambda_{in}} \approx E_{0,id}\tau\frac{\lambda_{ch}}{\lambda_{in}} = E_{0,id}R\ , \tag{3.164}$$

where

$$R = \tau\frac{\lambda_{ch}}{\lambda_{in}}\ . \tag{3.165}$$

The estimate (3.164) is obtained by a simple comparison of the ion-neutral collision friction force with the electric field force. The characteristic length differs from that introduced above by the same factor R, i.e, is not the ion-neutral mean-free path but the ion-neutral mean-free path divided by τ. The dimensionless ion and electron densities and the parameter P should be defined in this case by dividing not on n_0 as above but on n_0R (which in fact does not depend on n_0 since $\lambda_{Di}^2 \propto 1/n_0$. This result can be obtained from normalization of the whole set of the balance equations and is confirmed by many numerical results. The latter introduces the characteristic bulk density which usually is of the order of that observed in existing experiments. And, finally, the condition of quasi-neutrality (also confirmed in numerical investigation) in the conditions where the ion-neutral collisions dominate in friction is changed from (3.163) to the following one:

$$a \ll \lambda_{in}\ . \tag{3.166}$$

This change seems to be natural; it is also confirmed by numerical solutions for self-consistent dust structures [6, 85]. Remember that (3.166) is correct only if the characteristic length is forced to be λ_{in}/τ by non-linear self-consistent behavior of the complex plasma system.

References

1. J. Allen (1995). *Plasma Sources Sci. Technol.* **4**, 234.
2. V. Tsytovich, U. de Angelis, A. Ivlev, and S. Khrapak (2005). *Phys. Plasmas* **12**, 333.
3. Y. Al'pert, A. Gurevich, and L. Pitaevsky (1965). *Space Physics with Artificial Satellites*, p. 186 (Consultant Bureaut), London, NY.
4. J. Laframboise and L. Parker (1973). *Phys. Fluids* **16**, 629–636.
5. V. Tsytovich, N. Gusein-Zade, and G. Morfill (2004). *IEEE Trans. Sci.* Special issue, *Dusty Plasmas*, April 2004.
6. V. Tsytovich, G. Morfil, U. Konopka, and H. Thomas (2003). *New Journal of Physics* **5**, 1.
7. V. Tsytovich (1977). *Theory of Turbulent Plasmas*, Consultants Bureau, Plenum Publ. Corpor., New York.
8. J. Goree (1992). *Phys. Rev. Lett.* **69**, 277.
9. M. Lampe, V. Gavrishchaka, G. Ganguli, and G. Joyce (2001). *Phys. Rev. Lett.* **86**, 5278.
10. S.V. Vladimirov and M. Nambu (1995). *Phys. Rev. E* **52**, R2172.
11. S.V. Vladimirov and O. Ishihara (1996). *Phys. Plasmas* **3**, 444.
12. O. Ishihara and S.V. Vladimirov (1997). *Phys. Plasmas* **4**, 69.
13. P.G. de Gennes (1966). *Superconductivity of Metals and Alloys*, Benjamin, New York.
14. A. Melzer, V. Schweigert, I. Schweigert, A. Homann, S. Peters, and A. Piel (1996). *Phys. Rev. E* **54**, R46.
15. V. Schweigert, I. Schweigert, A. Melzer, A. Homann, and A. Piel (1996). *Phys. Rev. E* **54**, 4155.
16. S. Homann, A. Melzer, and A. Piel (1996). *Phys. Lett. A* **223**, 389.
17. K. Takahashi, T. Oishi, K. Shimomai *et al.* (1998). *Phys. Rev. E* **58**, 7805.
18. A. Melzer, V. A. Schweigert, and A. Piel (1999). *Phys. Rev. Lett.* **83**, 3194.
19. V. Steinberg, R. Sütterlin, A. V. Ivlev, and G. Morfill (2001) *Phys. Rev. Lett.* **86**, 4540.
20. S.V. Vladimirov and A.A. Samarian (2002). *Phys. Rev. E* **65**, 046416.
21. A.A. Samarian, S.V. Vladimirov, and B.W. James (2005). *JETP Lett.* **82**, 858.
22. G.A. Hebner, M.E. Riley, and B.M. Marder (2003). *Phys. Rev. E* **68**, 016403.
23. G.A. Hebner and M.E. Riley (2003). *Phys. Rev. E* **68**, 046401.
24. G.A. Hebner and M.E. Riley (2004). *Phys. Rev. E* **69**, 026405.
25. B. Bolotovskii (1957). Uspekhi, **62**, 201.
26. M. Nambu, S.V. Vladimirov, and P.K. Shukla (1995). *Phys. Lett. A* **203**, 40.
27. S. Benkadda, V. Tsytovich, and S.V. Vladimirov (1999). *Phys. Rev. E* **60**, 4708.
28. F. Melanso and J. Goree (1995). *Phys. Pev. E* **52**, 5312.
29. F. Melanso and J. Goree (1996). *Vac.Sci Techol. A* **14**, 511.
30. V. Shveigert (1995). *Pis'ma Zh. Tekh. Fiz.* (Russia), **21**, 69.

31. D.S. Lemons, M.S. Murillo, W. Daughton, and D. Winske (2000). *Phys. Plasmas* **7**, 2306.
32. M. Lampe, G. Joyce, G. Ganguli, and V. Gavrishchaka (2000). *Phys. Plasmas* **7**, 3851.
33. A.M. Ignatov (2003). *Plasma Phys. Rep.* **29**, 296.
34. V. Tsytovich (1995). Lectures on nonlinear Plasma Kinetics (Springer Verlag, Berlin).
35. T. Tajima and J. Dawson (1979). *Phys.Rev.Lett.* **43**, 267.
36. V. Tsytovich (1973). Publication of Int.Inst For Nuc.Res. Dubna Relativisyic solitons as particle accelerators.
37. S. Rubin and V. Tsytovich (1964). *Zhurn. Tech. Fiz.* (Russia), **34**, 3.
38. M. Rabinivich and V. Tsytovich (1977). Proc. P.N.Lebedev Inst **66**, 143.
39. L. Gorbunov and V. Kirsanov (1989). *Zh.Exp. Teor. Fiz.* **93** 509.
40. R. Bingham (1997). Fifth European Particle Accelerator Conference **1**, 120 ; (1998) *Phys. Scr.* **T75**, 125.
41. G. Bachet, L. Cherigier, and F. Doveil (1995). *Phys.Plasmas* **2**, 1.
42. Brodin, G. (2001). *Physics Scripta*, **T89**, 72.
43. D. Winske, W. Daughton, D.S. Lemons, and M.S. Murillo (2000). *Phys. Plasmas* **7**, 2320 (2000).
44. S.A. Maiorov, S.V. Vladimirov, and N.F. Cramer (2001). Plasma kinetics around a dust grain in an ion flow, *Phys. Rev. E* **63**, 017401/1–4.
45. S. V. Vladimirov, S. A. Maiorov, and N. F. Cramer (2001). *Phys. Rev. E* **63**, 045401.
46. S.V. Vladimirov, S.A. Maiorov, and N.F. Cramer (2003). *Phys. Rev. E* **67**, 016407.
47. S.V. Vladimirov, S.A. Maiorov, and O. Ishihara (2003). *Phys. Plasmas* **10**, 3867.
48. G. Lapenta (1995). *Phys. Rev. Lett.* **75**, 4409.
49. G. Lapenta (2000). *Phys. Rev. E* **62**, 1175.
50. G. Lapenta and G. Brackbill (1998). *Phys. Scr.* **T75** 264.
51. M. Lampe, M. Joyce, and G. Ganguli (2001). *Phys. Scr.* **T89**, 106.
52. V. Schweigert, M. Melzer, and A. Piel (2000). *J. Phys. IV*, Proc. (France), **10**, 421.
53. A. Melzer, V. Schweigert, and A. Piel (1996). *Phys. Scr.* **61**, 494.
54. D. Winske, W. Daughton, D. Lemons, M. Murillo, and W. Shanachan (2000). *Proc. Int.Conf.Phys.Dusty Pl. ICPDP-1999* (Elsevier Amsterdam), 513.
55. S.V. Vladimirov (1994). *Phys. Plasmas* **1**, 2762.
56. K. Watanabe (2000). Proceeding ICPDP-1999 Conference, p. 58.
57. A. Melzer, T. Trottenberg, and A. Piel (1994). *Phys.Lett.* **A 191**, 301.
58. J. Allen, B. Annaratone, U. de Angelis (2000). *J. Plasma Phys.* **63**, 299.
59. G. Lapenta (1999). *Phys.Plasmas* **6**, 1442.
60. J. Daugherty, R. Porteous, M. Kilgore, and D. Graves (1992). *J.Appl.Phys.* **4**, 219.
61. O. Havnes, C. Goertz, G. Morfill, and E. Grun (1987). *J. Geophys. Res.* **92**, 2281.
62. V. Tsytovich and U. de Angelis (2000). *Phys. Plasmas* **7**, 554.
63. P. Ricci, G. Lapenta, U. de Angelis, and V. Tsytovich (2001). *Phys. Plasmas* **8**, 769.
64. A. Boushoule *et al.* (1991). *J.Appl.Phys.* **70** 1991.

65. B. Walch, M. Horanyi, and S. Robertson (1994). *IEEE Trans. Plasma Sci.* **22**, 97.
66. M. Horanyi and R. Robertson (2000). Proc. Int.Conf.Phys.Dusty Pl. ICPDP-1999 (Elsevier Amsterdam), p. 313.
67. R. Bingham and V. Tsytovich (2001). *IEEE Trans. Plasma Sci.* **29**, 158-63.
68. S.V. Vladimirov, K. Ostrikov, and A.A. Samarian (2005). *Physics and Applications of Complex Plasmas*, Imperial College, London.
69. A.A. Samarian and S.V. Vladimirov (2003). *Phys. Rev. E* **67**, 066404.
70. I. Bernstein and I. Rabinovich (1959). *Phys. Fluids* **2**, 112.
71. L. Pitaevsky (1966). *JETP* (Rus.ed.), **43**, 27.
72. W. Steel, D. Law, B. Annaratone, and J. Allen (1997). XXIII International Conference on Phenomena in Ionized Gases, ICPIG Proceedings. Contributed Papers, **1**, 194.
73. V. Tsytovich, U. de Angelis, and R. Bingham (1989). *J.Plasma Phys.* **42**, 429.
74. Ya. Khodataev, R. Bingham, V. Tarakanov, and V. Tsytovich (1996). *Fiz. Plazmy* (Russia), **22**, 1028.
75. V. Tsytovich, G. Morfill, and H. Thomas (2002). *Plasma Phys.Rep.* **28**, 623.
76. C. Nairn, B. Annaratones, and J. Allen. (1998). *Plasma Sources Sci. Technol.* **7**, 478.
77. R. Sagdeev, D. Usikov, and G. Zaslavsky *Nonlinear Physics: From the Pendulum to Turbulence and Chaos*, Harwood Academic Publishers, New York.
78. J. Goree (1994). *Sci. Technol.* **3**, 400.
79. S. Khrapak, A. Ivlev, and G. Morfill (2003). Europhysical Conference Abstracts **27A**, O-1.1B.
80. V. Tsytovich, U. de Angelis, A. Ivlev, and S. Khrapak (2005). *Phys. Plasmas*, **12**, 469.
81. M. Barnes, J. Keller, J. Forster, J. O'Neal, and J. Coulytas (1992). *Phys.Rev.Lett.* **68**, 313.
82. N. Kilgore, J. Daugherty, R. Porteous, and D. Graves (1993). *J.Appl.Phys.* **73**, 7195.
83. V.N. Tsytovich, S.V. Vladimirov, G.E. Morfill, and J. Goree (2001). *Phys. Rev. E* **63**, 056609.
84. V. Tsytovich (2001). *Phys. Scr. Vol.* **T89**, 89.
85. G. Morfill, G. and V. Tsytovich *Phys. Plasmas* **7**, 235.
86. D. Samsonov, and J. Goree (1999). *Phys. Rev. E* **59**, 1047.
87. G. Morfill, H. Thomas, U. Konopka, and M. Zusic (1999). *Phys. Plasmas* **6**, 1769.
88. H. Thomas, D. Goldbeck, T. Hagl, A. Ivlev, U. Konopka, G. Morfill, H. Rothermel, R. Sutterlin, and M. Zuzic (2001). *Phys. Scr. Vol.* **T89** 16–19.
89. A. Nefedov, G. Morfill, V. Fortov *et al.* (2003). *New Journal of Physics* **5**, 33.
90. J. Goree, G. Morfill, V.N. Tsytovich, and S.V. Vladimirov (1999). *Phys. Rev. E* **59**, 7055.
91. V.N. Tsytovich, S.V. Vladimirov, and G.E. Morfill (2004). *Phys. Rev. E* **70**, 066408.
92. S.V. Vladimirov, V.N. Tsytovich, and G.E. Morfill (2005). *Phys. Plasmas* **12**, 052117.
93. V.N. Tsytovich, S.V. Vladimirov, and G.E. Morfill (2006). *JETP*, **102**, 334.
94. G. Morfill, H. Thomas, U. Konopka, and M. Zusic (1999). *Phys. Plasmas* , **6**, 1769.

95. R. Talbot R. Cheng., D. Schefer, and A. Willis (1980). *Fluid Mech.* **101**, 737.
96. O. Havnes, T. Nitter V. Tsytovich, G. Morfill, and G. Hartquist (1994). *Plasma Sources Sci. Technol.* **3**, 448.
97. D. Law, W. Steel, B. Annaratone, J. Allen (1999). XXIII International Conference on Phenomena in Ionized Gases, ICPIG Proceedings , Contributed Papers, **1**, 192.
98. V.N. Tsytovich, S.V. Vladimirov, O.S. Vaulina, O.F. Petrov, and V.E. Fortov (2006). Phys. Plasmas, **13**, 032305.
99. V.N. Tsytovich, S.V. Vladimirov, O.S. Vaulina, O.F. Petrov, and V.E. Fortov (2006). *Phys. Plasmas* **13**, 032306.
100. L. Landau and E. Lifshitz (1977). *Statistical Physics*, Pergamon Press, Oxford, NewYork.
101. V. Tsytovich (2000). *Plasma Physics Reports* **26**, 712.

4

Collective Effects in Complex Plasmas

The aim of this chapter is to demonstrate that a complex plasma requires formulation of a new ground state with the balance of fluxes as an inevitable feature. The flux variation has a strong effect on the propagation of collective modes leading not only to the mode damping but also to an instability which leads to formation of structures in complex plasmas.

4.1 Collective Linear Modes

4.1.1 Dispersion Relations for Low Frequency Modes

As a new state of matter, a complex plasma reveals new responses and new waves and instabilities due to the openness of the system, the large rate of plasma dissipation on grains, and the presence of external sources playing very important role. In the simplest model, these external sources are the homogeneous ionization sources described by the first term on the right-hand sides of the continuity equations. In the first approximation, waves and instabilities can be described by linear complex plasma responses, i.e., by linear dispersion relations for the waves and instabilities. The non-linearities can be treated by using non-linear responses which in complex plasmas are different as compared to usual plasmas. For proper formulation of the linear and non-linear responses, it is necessary to fix an external sources since the responses are different for different sources. Linear and non-linear waves in complex plasmas can be (and have already started to be) an important subject for experimental investigations.

We begin with the simplest disordered gaseous state of a complex plasma where it is simpler to formulate qualitatively how the presence of the microparticle component changes the modes and when these changes are important. From physical point of view one can estimate the range of wave numbers and frequencies where a complex plasma changes its linear modes and this estimate is the same for all kinds of external sources although the dispersion relation

V. N. Tsytovich et al.: *Collective Effects in Complex Plasmas*, Lect. Notes Phys. **731**, 141–195 (2008)
DOI 10.1007/978-3-540-29003-2_4

depends on the sources. Indeed, the frequency range where the changes are significant should be in the domain where the frequencies are either less than the charging frequency $\nu_{ch} \approx v_{Ti}a/\lambda_{Di}^2$ or equal to the friction frequency of plasma particles in their collisions with the dust particles $\nu_{ch}P_0$ (see previous Chapters). The latter is of the same order of magnitude as the charging frequency if P_0 is of the order of 1.

The wave number domain where the changes occur should correspond to the wave numbers less than ν_{ch}/v_{Ti} or $\nu_{ch}/v_{Ti}P_0$. This is a very broad range in the ω, k plane, where usually all low-frequency responses are located. This is because the charging frequency is only a/λ_{Di} less than the ion plasma frequency, which for present experiments is very large. The ratio a/λ_{Di} is of the order of 0.15–0.01 and the ion plasma frequency is of the order $\omega_{pi} \approx 10^7 s^{-1}/\sqrt{Z_i}$, where Z_i is the ion charge in the units of e (e being the electron charge). For argon and xenon gases, often used in current experiments, it is about 2MHz and MHz respectively. These are very high frequencies for the usual observation duration of several seconds.

All classical plasma physics written in textbooks (e.g., the classic "encyclopedia" by Mikhailovskii [1] on waves and instabilities in an ordinary plasma) should be changed in this range of the wave numbers and frequencies. The whole work for renewing this "table" of the waves and instabilities is not yet performed but it is clear, in general, that all so-called "negative energy waves" – among them are all beam modes and drift waves – will be much more unstable in a complex plasma than in an ordinary plasma. The reason is that for the negative energy waves it is necessary to have a dissipation of plasma disturbances for their growth, and a complex plasma provides very effective mechanisms of the dissipation via charging and friction on grains. We do not go into the details of such studies mentioning investigations of drift waves (e.g., [2, 3, 4]) which demonstrate that in a complex plasma the instability threshold of drift waves is less than that in the absence of dust while the growth rate is larger than that in absence of dust. The same is true for all beam instabilities, i.e., instabilities related with the propagation of electron and ion beams in complex plasmas.

The most important feature of a complex plasma is not only the changes of the known waves and instabilities but the appearance of *new modes and new instabilities*. In the liquid and the gaseous states of complex plasmas we have an example of the "Dust Acoustic Waves" (DAW). Their first investigations were started with simple rewriting of results well known [1] for multi-component plasmas including dust as one of the plasma component (namely a very heavy component) [5, 6, 7, 8, 9]. This is not appropriate as can be seen from previous discussions of the elementary processes in complex plasmas as well as it is clear from the conditions we wrote above in this section (see also detailed discussions [10, 11, 12]). Discussions of experiments and other references are given later in the context, with the corresponding description of DAW including all specific complex plasma processes as well as the description of other branches, namely "Dust Ion Sound Waves"

(DISW) [13], which are the low frequency part of the usual ion-sound waves well known in ordinary plasmas [14], the "Electrostatic Gravitation Like Instabilities"(EGLI) [15] related with dust non-collective dust attraction and Electrostatic Collective Gravitation Like Instabilities related with collective dust attraction (both similar to gravitational instabilities in usual gravitating systems), and "Structurization Instability" (SI) [16] related to the collective dust fluxes and describing the complex plasma clumping into structures, containing dust and dust-free regions (dust voids). Furthermore, presence of a magnetic field changes the wave propagation, and we can discuss this as well. At present these are examples of the most important new waves and instabilities in the disordered state investigated so far.

In plasma crystal states, new wave phenomena include "Dust Lattice Waves" (DLW), which can be of acoustic-type modes [17] and optic-type bending modes [18, 19, 20], and "Dust Shear Waves" (DSW) [21]. These are peculiar to the crystalline systems, and are not found in liquid or gaseous states. These waves may be excited in 1D "string" systems, in 2D plane lattices, and in 3D crystals. Their solid analogues are the crystal sound and shear waves. Under Earth gravity conditions we have to bear in mind that there is a fundamental asymmetry for particles located in the plasma sheath for 2D planar lattices, caused by the ion flow and that the non-linear screening (not the Debye screening as in [17, 21]) is important which changes numerical coefficients in the expressions for DLW and DSW. We consider these waves later, after we discuss problems of the dust-plasma crystals. In this chapter, we deal with collective modes only in the gaseous state of complex plasmas.

First, we simplify the consideration by finding linear relations from the forces acting on electrons, ions, and grains (as above), adding to the force balance equations the natural time-dependent terms $\partial/\partial t$, and then linearizing the equations for perturbations. The applicability of such approach is related with the requirement that we consider the low frequency and low wave number range (estimated above) and that the electron and ion distributions are assumed to be thermal. The latter is not a good assumption but the full kinetic treatment of the new mode is still waiting to be performed and with this assumption we are able to at least illustrate the main features of the new modes considering the temperatures $T_{e,i,d}$ as some averaged particle energies.

Another simplification we make is to assume for certain cases the quasi-neutrality of perturbations which makes then not necessary the consideration of the Poisson's equation for perturbations and which is valid for long size disturbances where the quasi-neutrality conditions can be fulfilled. DISW have phase velocities larger than both the dust and the ion thermal velocity and less than the electron thermal velocity; DAW have the phase velocities less than both the electron and the ion thermal velocity but larger than the dust thermal velocity. Both of them are approximately described by the linear dispersion laws $\omega_{disw} = kv_{disw}$ and $\omega_{daw} = kv_{daw}$, where v_{disw} is DISW speed (estimated often as $\sqrt{T_e/m_i}$) and v_{daw} is DAW speed (estimated often as $\sqrt{T_i Z_d P/m_d}$), where T_e, T_i are the electron and ion temperatures, m_i, m_d are the ion and

dust masses, and n_i, n_d are the ion and the dust number densities, respectively. Below, we give more exact expressions for these phase velocities and show that the multi-component approach is not appropriate by notifying the difference between its results and the proper complex plasma approach. Indeed, the main difference of a dusty plasma from the multi-component plasma is that the charge on dust particles is not fixed and its perturbations are different for different wave numbers. This is usually called as "charge variations"; several investigations were devoted to the influence of charge variations on DISW and DAW [10, 13, 21, 22, 23]. But there exist more important effects related with the dust charging and plasma dissipation on grains which should be taken into account. In most investigations of the influence of the dust charge variations it was not taken into account but the same process which is responsible for the change of grain charges is also responsible for the change of distributions of electrons and ions taking part in the charging process (first steps to take into account this effect were done in [2, 15, 23, 24, 25, 26]. Thus to treat the problem self-consistently one need to take into account self-consistently both the changes in the dust charges and the variations of the electron and ion distributions related with these changes. Here we use use such a self-consistent treatment [12].

4.1.2 Basic State of Complex Plasmas

An important difference of complex plasmas from usual (multi-component) plasmas is the ground state on which the disturbances appear and develop. This state (in which disturbances propagate as, e.g., DISW or DIAW) for complex plasmas is different from that for multi-component plasmas. Usually in multi-component plasmas this state is defined by the quasi-neutrality condition; in application to complex (dusty) plasmas the latter is changed to $n_i = n_e + n_d Z_d$. This expression was extensively used in many papers devoted to the treatment of DISW and DAW in a way similar to that in the multi-component plasma approach [5, 6, 7, 8, 9]. For the problems of wave propagation and instabilities we also use this quasi-neutrality condition for the basic state, assuming that the parameters in the quasi-neutral ground state are homogeneous. However, in dusty plasmas this quasi-neutrality relation is *not sufficient* for definition of the ground state. Plasma electrons and ions are both absorbed on dust grains in the charging process. Therefore, for a steady-state condition there should exist a source of electrons and ions to compensate this absorption and to keep the electron and ion densities constant [16, 23, 27]. This source can be called the "ionization source". Experiments indeed show that plasma just disappears in a very short timescale being absorbed on dust if its electron and ion densities are not supported by some source. In experiments performed in HF low-temperature plasmas [28, 29, 30, 31, 32] the plasma is absorbed in a timescale of a few micro-seconds if the HF source is switched off.

The necessity of the presence of an external source was emphasized and taken into account in the formulation of the kinetic theory of a dusty plasma [24, 26, 33, 34, 35, 36, 37]. Without the source it is not possible even to define the ground state of a dusty plasma and to introduce its perturbations. This difference of a complex plasma from a multi-component plasma leads to expressions for DISW and DAW different from that for a multi-component plasma. The condition for the balance of the parameters in the ground state fixes other parameters of the system.

The first treatment of DISW and DAW with a source, the strength of which is independent of plasma parameters, was done in [10, 11, 13, 23, 27], but in some of these papers not all processes influencing the waves were taken into account. Namely, although the absorption of electrons and ions on dust particles was treated self-consistently, the elastic scattering of electrons and ions on dust particles was not taken into account. It is indeed not important for $\tau = T_i/T_e \gg 1$. The present laboratory experiments are usually performed for the opposite condition, $\tau \ll 1$, where the elastic collisions dominate. Thus the result of [23] are correct for $\tau \gg 1$ and at least can give qualitatively correct expressions for $\tau \approx 1$, which we often meet astrophysical dusty plasmas. Here we deal mainly with the case $\tau \ll 1$ having in mind the laboratory applications. DISW and DAW were considered in detail in [11] by the kinetic approach including the case $\tau \ll 1$ but again as in [23] there it was assumed that the external source is independent of the plasma parameters. A substantial difference between expressions for DISW and DAW found in [11] and those of the multi-component plasma approach was clearly demonstrated in [11].

Here we consider the model which is much closer to the experimental situation assuming that intensity of the ionization source is proportional to the electron density. This case is of interest for many experiments performed for measurements of the dispersion and damping of DISW and DAW. The correct expressions are needed for comparison of the theoretical predictions with the results of these experiments. By investigating the dispersion relation in the self-consistent treatment of the dust charge variation and changes of the plasma particle distributions in the presence of an ionization source which is proportional to the electron density, it appears that for a certain wave numbers less or of the order of the critical wave number DISW and DAW branches are universally unstable and that for the wave numbers larger than another critical wave number (usually larger than the first critical wave number) there exists an appreciable damping of both types of waves, which was previously not recognized. The reason for appearance of both the instability and the enhanced dissipation is the deviations in the balance of the dissipation on dust and ionization caused by the wave perturbation of the ground state. Without the condition for the balance of ionization and losses on grains in the ground state these processes and the ground state itself cannot be defined. Therefore one cannot properly consider the perturbations and cannot treat both DISW and DAW without treating such a balance in the ground state.

We use dimensionless notations the same as before, introducing also the dimensionless dust size, the dimensionless frequency, the dimensionless wave numbers, and the dimensionless ratio of ion to dust mass by the relations

$$a \to \frac{a}{\lambda_{Di}}; \qquad \mathbf{k} \to \mathbf{k}\frac{\lambda_{Di}^2}{a}; \qquad \omega \to \frac{\omega\lambda_{Di}^2}{a\sqrt{2}v_{Ti}}; \qquad \mu = \frac{Z_d m_i}{2m_d} . \quad (4.1)$$

We consider only the case applicable to existing dusty plasma experiments and assume $\tau \ll 1$. For the ground state, we use the subscript 0.

The ionization rate we assume to be proportional to the electron density as it is already written in the continuity equations for plasma electrons and ions and consider first the collisionless limit where the ion–dust mean-free path is much less than the ion-neutral mean-free path.

The two equations for the basic state are the charge neutrality equation and the balance of absorption and ionization powers. Since in the basic state $n_i = n_0$ and $n \equiv n_i/n_0$, we have

$$n_{e0} = 1 - P_0 \quad (4.2)$$

and

$$\frac{1}{\tau_i} = \frac{P_0\alpha_{ch}}{n_{e0}} . \quad (4.3)$$

Using (4.2), we can calculate the dust charge z_0 in the basic state from the OML charging equation:

$$\exp(-z_0) = \sqrt{\frac{m_e}{m_i\tau}}\frac{z_0}{1-P_0} . \quad (4.4)$$

We can use P_0 as a single parameter determining the basic state, with all other parameters n_{e0}, α_i, and z_0 expressed through it. In this approach, n_0 remains as a parameter of the initial state but it enters only in the normalization of all other variables. It is thus the advantage of the used normalization allowing us to describe the basic state by a single parameter P_0.

4.1.3 Dispersion Relation for DISW

Consider linear perturbations of the ground state. First restrict the wave phase velocities to those in the range of DISW, defined earlier. For plasma electrons we use the balance of the electron pressure and the electric field, since other forces such as electron friction on dust and electron inertia are negligible. This gives for linear perturbations (all perturbations are denoted by the symbol δ except those which are zero in the ground state)

$$\delta n_e = (1 - P_0)\frac{ie(\mathbf{k}\cdot\mathbf{E})}{k^2} \quad (4.5)$$

.

For the ion density perturbations, we have two equations: the balance of forces where we take into account the ion inertia, the ion pressure, the electric field force, and the ion friction on dust; and the continuity equation for the ion density with perturbations of Q_{abs} and Q_{ion}. The first equation describes the change of the ion momenta due to the dust drag by the ion flux which appears in the perturbations of the ground state. This term is very important since it is one of the elements of the self-consistent treatment describing reaction of the ion distribution on interactions with dust particles and gives the necessary feedback effect which drives the instability. We have

$$e(\mathbf{E}\cdot\mathbf{k}) = \alpha_{dr,0}P_0 z_0(\mathbf{k}\cdot\mathbf{u}) + \tau i k^2\delta n - i2\tau\omega(\mathbf{k}\cdot\mathbf{u})\ . \tag{4.6}$$

Here, the left-hand side is the electric field force; on the right-hand side, first is the important term of the momentum transfer to ions in the dust drag creating the friction of ions proportional to both the dust density and the charge, the second term describes the ion pressure, and the last term describes the ion inertia.

Different models can be used for the drag coefficient α_{dr}. The non-linear drag depends also on the parameter β but since the ion drift velocity describes already a linear perturbation of the ground state, perturbation of α_{dr} should not be taken into account for the linear approximation. Thus $\alpha_{dr,0}$ in (4.6) for the non-linear drag contains $\beta_0 = z_0 a/\tau\lambda_{Di,0}$. Our description is valid for the linear as well as the non-linear drag.

The second equation is the continuity equation for ions:

$$i(\mathbf{k}\cdot\mathbf{u}-\omega)\delta n = \frac{\delta n_e}{1-P_0}\alpha_{ch}P_0 - \alpha_{ch}P_0\delta n - P_0\alpha_{ch}\frac{\delta z}{z_0}\ . \tag{4.7}$$

We assumed here that dust is not moving (and is not perturbed) in the DISW, and therefore

$$\frac{\delta P}{P_0} = \frac{\delta z}{z_0}\ . \tag{4.8}$$

Equation (4.7) takes into account the dust charge variations (the last term on the right-hand side) and the self-consistent change of the ion density due to the change of plasma ionization in the perturbations (the first term on the right-hand side) as well as the change of the ion absorption in the perturbations (the second term on the right-hand side). Thus it takes into account the change in the ion distribution due to the ion absorption on dust particles. This term describes the feedback of the ion distribution related with the charging process. It should be taken into account in any self-consistent treatment. The change in plasma ionization is also important since in different regions of the perturbations the electron–ion pairs are created differently, which means an increase or decrease of other forces acting on ions.

We use the OML charging equation corresponding to

$$\frac{\partial z}{\partial t} = \alpha_{ch}\left(\sqrt{\frac{m_i\tau}{m_e}}e^{-z}n_e - zn\right)\ , \tag{4.9}$$

with substitution of $n_0 + \delta n$ and $n_{e,0} + \delta n_e$ for n and n_e, respectively, and find

$$\frac{\delta z}{z_0} = \frac{\alpha_{ch}}{(1+z_0)\alpha_{ch} - i\omega} \left(\frac{\delta n_e}{n_{e0}} - \delta n \right) . \tag{4.10}$$

This converts (4.7) to

$$i(\mathbf{k}\cdot\mathbf{u} - \omega)\delta n = \frac{\alpha_{ch}^2 P_0 z_0}{(1+z_0)\alpha_{ch} - i\omega} \left(\frac{\delta n_e}{n_{e0}} - \delta n \right) . \tag{4.11}$$

Note that in the part of the DISW dispersion where the frequency is much less than the charging frequency, the $i\omega$ term in (4.11) is small and can be neglected assuming an almost instant charging.

Thus we obtain the ion density perturbation given by

$$\delta n = -\frac{ie(\mathbf{k}\cdot\mathbf{E})}{k^2} \frac{\left[1 - \frac{\alpha_{ch}^2 P_0 z_0 (\alpha_{dr} P_0 z_0 - 2i\tau\omega)}{((1+z_0)\alpha_{ch} - i\omega)k^2}\right]}{\left[\tau + \left(\frac{P_0 z_0 \alpha_{ch}^2}{(1+z_0)\alpha_{ch} - i\omega} - i\omega\right) \frac{(\alpha_{dr} P_0 z_0 - 2i\tau\omega)}{k^2}\right]} . \tag{4.12}$$

Finally, the general case of non-quasi-neutral perturbations is treated on the basis of the Poisson's equation in its dimensionless form. We have

$$ie(\mathbf{E}\cdot\mathbf{k}) = \frac{\tau}{a^2}(\delta n - \delta n_e - \delta P) = \frac{\tau}{a^2}$$

$$\times \left[\delta n \left(1 + \frac{\alpha_{ch} P_0}{(1+z_0)\alpha_{ch} - i\omega} \right) - \frac{\delta n_e}{n_{e0}} \left(1 - P_0 + \frac{\alpha_{ch} P_0}{(1+z_0)\alpha_{ch} - i\omega} \right) \right] . \tag{4.13}$$

Utilizing the above expressions, we find the dielectric permittivity

$$\epsilon_{\mathbf{k},\omega} = 1 + \frac{\tau}{k^2 a^2} \left\{ \left(1 - P_0 + \frac{\alpha_{ch} P_0}{(1+z_0)\alpha_{ch} - i\omega} \right) \right.$$

$$\left. + \left(1 + \frac{\alpha_{ch} P_0}{(1+z_0)\alpha_{ch} - i\omega} \right) \frac{\left[1 - \frac{\alpha_{ch}^2 P_0 z_0 (\alpha_{dr} P_0 z_0 - 2i\tau\omega)}{((1+z_0)\alpha_{ch} - i\omega)k^2}\right]}{\left[\tau + \frac{1}{k^2}\left(\frac{P_0 z_0 \alpha_{ch}^2}{(1+z_0)\alpha_{ch} - i\omega} - i\omega\right)(\alpha_{dr} P_0 z_0 - 2i\tau\omega)\right]} \right\} . \tag{4.14}$$

Mentioned that in actual (dimensional) values $1/k^2a^2$ is $1/k^2\lambda_{Di}^2$ and under the conditions of quasi-neutral disturbances $k^2\lambda_{Di}^2 \ll 1$, one can neglect the first term, 1, in (4.14).

Dispersion relation for electrostatic perturbations takes the form

$$\epsilon_{\mathbf{k},\omega} = 0 . \tag{4.15}$$

This equation for DISW for quasi-neutral disturbances becomes independent on the dust size in the dimensionless units. This is another advantage for using these units. In the absence of dust, $P_0 = 0$, we get the standard expression for the ion-sound waves for $k^2\lambda_{Di}^2 \ll 1$ in the dimensionless units in the case

when the phase velocity is much larger than the ion thermal velocity (which in the dimensionless units is just $\omega \gg k$):

$$\omega_{is}^2 = k^2 v_{is}^2 = k^2 \frac{1}{2\tau} , \tag{4.16}$$

where $v_{is} = 1/\sqrt{2\tau}$ is the dimensionless ion-sound speed. The influence of dust is determined by the parameter P_0, which is both in the first term and in the second term. In the first one, $1 - P_0$ describes the charge neutrality condition while the other term, proportional to α_{ch}, and the similar term in the first bracket of the second term describe the charge variation (these effects are usually taken into account in description of DISW), while all terms in the square brackets of the second term are related with the perturbation of the absorption and ionization balance of the ground state and are often neglected.

Certainly, the changes in the ground state are the most important as compared to the changes due to variations obtained from the quasi-neutrality condition and those due to simple charge variations. Indeed, if we neglect the latter contributions, we obtain an expression for DISW, where only the quasi-neutrality change and the charge variations are taken into account

$$\omega_{disw}^2 = k^2 v_{disw}^2 = k^2 \frac{1 + \frac{\alpha_{ch} P_0}{(1+z_0)\alpha_{ch} - i\omega}}{2\tau \left(1 - P_0 + \frac{\alpha_{ch} P_0}{(1+z_0)\alpha_{ch} - i\omega}\right)} \approx \frac{k^2}{2\tau(1 - P_0)} . \tag{4.17}$$

This equation differs from (4.16) by the factor $(1 - P_0)$ in the denominator appearing from the contribution of dust in the charge quasi-neutrality condition of the ground state. We wrote the first relation (4.17) to show that these terms which are due to the charge variations are small since the condition of validity of (4.17) is more rigid than $\omega \gg \alpha_{ch}(1 + z_0)$. The latter means that relation (4.17) is valid only for frequencies much larger than the charging frequency. Indeed, contributions of other terms missed in (4.17) can be neglected only if

$$\omega \gg \frac{\alpha_{dr} P_0 z_0}{2\tau}, \alpha_{ch}(1 + z_0); k \gg \alpha_{ch}\sqrt{P_0 z_0 \tau}; \omega \gg \alpha_{ch}(1 + z_0) . \tag{4.18}$$

For the coefficients α_{ch} and α_{dr} of the order of 1 (which is the case if $\beta \ll 1$) and for $\tau \ll 1$, $z_0 \sim 1$ and $P_0 \gg \tau$, fulfillment of the first inequality leads to fulfillment of other two. Therefore we write down the first inequality in the dimensional units:

$$k\lambda_{Di} \gg \sqrt{\frac{2}{\pi}} \ln \Lambda P_0 z_0 \sqrt{(1 - P_0)} \frac{a}{\lambda_{Di}\sqrt{\tau}} . \tag{4.19}$$

In most existing experiments (except those with very small dust particles) $a/\lambda_{Di} \approx 1/7, 1/10$ and $\tau \approx 0.02 - 0.01$, and the parameter P_0, although it should be always less than 1, is close to or of the order of 1. Thus the right-hand side of (4.19) is of the order of (or even larger than) 1, not leaving any

appreciable range in wave numbers to DISW to exist in their conventional form (4.16). Of course the condition (4.19) can be fulfilled for very small $P_0 \ll 1$ to create a certain interval of wave numbers where DISW can exist but those waves do not actually differ from usual ion-sound waves. All these arguments should be taken into account in comparing experiments with the theory. If in experiments the value of the parameter P_0 is not very small and dust can influence the spectrum of DISW then to satisfy the relation (4.19) one should use rather small dust sizes.

Even in the limit where the approximate expression for DISW coincides with the conventional one, the exact dispersion relation gives additional real and imaginary contributions to the frequency of the DISW. The most important is the imaginary parts creating a rather large damping. We write its expression in the conventional dimensional units:

$$\gamma_{disw} = Im(\omega)_{disw} = -\frac{P_0}{2\sqrt{2}}\omega_{pi}\frac{a}{\lambda_{Di}}\left[\frac{\alpha_{dr}z_0}{\tau} + 2P_0\alpha_{ch}^2 + 4\frac{\alpha_{ch}^3\tau(1+z_0)}{k^2\lambda_{Di}^2}\frac{a^2}{\lambda_{Di}^2}\right]. \tag{4.20}$$

The second and third terms of (4.20) are negligibly small as compared to the first one and we write them here only to demonstrate that the damping due to the charging process (both the charge variations, described by the second term, and the change in the ground state due the charging process, described by the third term) being related with the coefficient α_{ch} can be neglected. The damping described by the first term of (4.20) can easily exceed the collisionless Landau damping (taken often into account in the kinetic description of DISW) and becomes of the order of the frequency of DISW when the wave number k reaches its limit determined by the right-hand side of (4.19). This damping is collective (proportional to P_0); it increases with the dust charge proportionally to the square of the dust charge and it is large due to the presence of small factor τ in the denominator of (4.20). For DISW the ion inertia is important only in the range of frequencies close to the ion plasma frequency ω_{pi}, which is larger than the charging frequency $\approx \omega_{pi}a/\lambda_{Di}$. In this range also the kinetic electron Landau damping can be of importance but it is in most existing experiments (where P_0 is about 0.5–0.01) much less than that described by (4.20) [11].

In the limit opposite to that given by the inequality (4.18) DISW do not exist. As shown below in Sect. 4.2, in this region an instability appears operating for a homogeneous initial distribution of all complex plasma parameters and (in the kinetic approach) for completely isotropic velocity distributions of plasma particles.

4.1.4 Dispersion Relation for DAW

The frequency of DAW is much less than the charging frequency as well as the frequency of the ion–dust collisions. The phase velocity of DAW is much less than the ion and electron thermal velocity but is much larger than the

dust thermal velocity. The speed of these waves (due to the large dust charges $Z_d \gg 1$) is always larger than $\sqrt{T_i/m_d}$, which is close to the dust thermal velocity if the ion temperature is close to the dust temperature (as it is often the case in the gaseous state). The only expression we need to describe for DAW is the response of the dust. The dust response is then determined by the dust inertia, the dust pressure, and the Epstein drag force on the neutral atoms. For DAW, one can neglect the ion inertia but should take into account the dust inertia and the change of the dust density. The variation of the dust density appears both in the Poisson's equation (often taken into account), in the disturbance of the ion absorption, and in the ion continuity equation describing the deviations of the power balance (this effect is very important). Both effects in the dimensionless equation depend only on the perturbation of the parameter P. Here, we use

$$\frac{\delta P}{P_0} = \frac{\delta z}{z_0} + \frac{\delta n_d}{n_d} \tag{4.21}$$

instead of (4.9). The ion continuity equation therefore contains an additional term depending on $\delta n_d/n_d$ and describing the change in the ion absorption in DAW. Since the frequency of DAW is much less than the charging frequency, we use

$$\frac{\delta z}{z_0} = \frac{1}{1+z_0}\left(\frac{\delta n_e}{n_{e0}} - \delta n\right) \tag{4.22}$$

instead of (4.11).

Additional equations are the dust continuity equation and the dust force balance equation. In the latter, we take into account the dust pressure forc, the dust inertia force, and the ion drag force. We find for the dimensionless values

$$ie(\mathbf{E}\cdot\mathbf{k}) = \left(\tau_d k^2 - \omega^2\frac{\tau}{\mu}\right)\frac{\delta n_d}{n_d} + i\alpha_{dr} z_0(\mathbf{k}\cdot\mathbf{u})\,. \tag{4.23}$$

Using (4.23), the ion continuity equation, with (4.8) and (4.9), we obtain $\delta n_d/n_d$ and δn. Then, using the Poisson's equation, we find the dielectric permittivity for the low frequency range corresponding to DAW:

$$\epsilon_{\mathbf{k},\omega} = 1 + \frac{\tau}{a^2k^2}\frac{1}{\left(\tau + \frac{\alpha_{dr}\alpha_{ch}P_0^2 z_0^2}{k^2(1+z_0)}\right)}\left\{1 + \frac{P_0}{1+z_0} + \tau\left(1 - \frac{P_0 z_0}{1+z_0}\right)\right.$$

$$\left. - \frac{\alpha_{ch}\alpha_{dr}P_0^3 z_0^2}{k^2(1+z_0)}\frac{P_0k^2\left(\tau + \frac{\alpha_{ch}\alpha_{dr}z_0^2P_0(P_0-\tau)}{k^2(1+z_0)}\right)\left(\tau + \frac{\alpha_{dr}\alpha_{ch}P_0z_0(1+P_0)}{k^2}\right)}{\left[\left(\tau_d k^2 - \omega^2\frac{\tau}{\mu}\right)\left(\tau + \frac{\alpha_{dr}\alpha_{ch}P_0^2z_0^2}{k^2(1+z_0)}\right) - P_0z_0\alpha_{ch}\alpha_{dr}\tau\right]}\right\}. \tag{4.24}$$

This expression contains only the product of α_{ch} and α_{dr} and therefore all changes related with perturbations of the background are important only if both the drag and the charging processes are included. Also, the friction of ions described by α_{dr} can be related with the ion-neutral collisions if their

rate exceeds the drag force (the drag coefficient can describe the ion friction on dust as well as the dust drag). In conditions where the ion-neutral collisions dominate in the equation for the ion motion, the ion friction on dust should be used for the drag coefficient. The dust-neutral collisions change the dielectric permittivity in a way that one should substitute $\omega(\omega + i\nu_{dn})$ for ω^2 in expression (4.24).

In case we neglect all effects related with the perturbations of the balance of the ground state and neglect the charge variations we find the standard expression for DAW:

$$\omega_{daw}^2 = k^2 \mu P_0 \frac{1}{1+\tau(1-P_0)} + k^2 \frac{\tau_d}{\tau}\mu \approx k^2 v_{daw}^2; v_{daw}^2 = \mu P_0 \ , \tag{4.25}$$

where the second term describing the dust change of pressure can be usually neglected. In the conventional dimensional units (4.25) has the standard form

$$\omega^2 = k^2 \frac{P_0 Z_d T_i}{m_d(1+\tau(1-P_0))} + k^2 \frac{T_d}{m_d} \approx k^2 \frac{P_0 Z_d T_i}{m_d} \ . \tag{4.26}$$

In the case one does not neglect the charge variations but still neglects the changes in the ground state and the dust temperature (dust pressure) effects, we obtain for $\tau \ll 1$

$$\omega_{daw}^2 = k^2 \mu P_0 \frac{1+z_0}{1+z_0+P_0+\tau(1+z_0-P_0 z_0)} \approx k^2 P_0 \mu \frac{1+z_0}{1+z_0+P_0} \ . \tag{4.27}$$

The latter approximate expression is written for $\tau \ll 1$. The linear dispersion (the frequency proportional to the wave number) is valid for the wave numbers less than the ion Debye length, which in the dimensionless units corresponds to $k^2 \ll 1/a^2$; for $k^2 \approx 1/a^2$, (4.26) and (4.27) give $\omega^2 \approx \omega_{pd}^2 = \mu P_0/a^2$. The dust-plasma frequency ω_{pd} is here in the dimensionless units and in the conventional dimensional units it is written in the form

$$\omega_{pd}^2 = 4\pi e^2 n_d Z_d^2/m_d \ . \tag{4.28}$$

The linear wave dispersion exists only if the rigid restriction described by relation (4.6) is satisfied, which requires $a^2 \ll \tau$ or in the dimensional units

$$\frac{a^2}{\lambda_{Di}^2} \ll \tau \ . \tag{4.29}$$

In the conditions where (4.5) is still valid, the additional terms neglected in derivation of (4.27) give that the spectra of the waves differs from the linear law (where the frequency of the wave is proportional to the wave number). These corrections compete with those related with deviations from the quasi-neutrality:

$$\omega^2 \approx \omega_{daw}^2 \left(1 + \frac{\alpha_{dr}\alpha_{ch} P_0 z_0 (1+P_0)}{k^2 \tau} - k^2 a^2\right) \ . \tag{4.30}$$

The curvature of the dispersion curve introduced by the first correction of (4.30) is the opposite to the curvature of the curve introduced by the second correction. In current experiments, one can easily distinguish the two deviations from the linear law and the observation described in the next chapter corresponds to the first type of corrections. This is an indication that the effect described here is already observed and can be investigated experimentally in more detail. The condition that the dispersion corrections due to the perturbations of the basic state dominate is given by

$$\frac{1}{a^2} \gg k^2 \gg \frac{1}{a\sqrt{\tau}} \,. \tag{4.31}$$

which is consistent with inequality (4.29). For the opposite inequality, DAW do not exist. This domain corresponds to unstable perturbations.

4.2 Universal Instability of a Complex Plasma

4.2.1 Instability in the Range of DISW

First, consider the range of frequencies and wave numbers corresponding to those of DISW (the phase velocity larger than the ion thermal velocity but less than the electron thermal velocity). Here, we study disturbances in the case where DISW do not exist, i.e., in the limit opposite to the last inequality (4.29):

$$\omega \ll \frac{\alpha_{dr} P_0 z_0}{2\tau} \,. \tag{4.32}$$

We solve the dispersion equation relation and obtain

$$\omega = i \frac{1}{\alpha_{dr} P_0 z_0} \frac{\left(\alpha_{dr}\alpha_{ch}^2 P_0^3 z_0^2 - k^2((1+z_0)\alpha_{ch} + P_0\alpha_{ch} - i\omega)\right)}{((1-P_0)(1+z_0)\alpha_{ch} + P_0\alpha_{ch} - i(1-P_0)\omega)} \,. \tag{4.33}$$

The most important result here is that the damping is changed to *the instability* which can be seen by simple solution of the quadratic equation. This gives the critical value of the wave number

$$k_{cr,disw}^2 = \frac{\alpha_{dr} P_0^3}{1 + z_0 + P_0} \,, \tag{4.34}$$

which can also be found directly from (4.31). The critical wave number is determined only by the drag coefficient and is lower than the upper limit (4.32), i.e., it is inside the range (4.32).

The range (4.32) covers the most important values of wave numbers in existing experiments and the instability found here can be detected experimentally. Thus in the range of DISW (the wave phase velocities much larger than the ion thermal velocity) for the wave numbers less than the critical

value (4.39) the waves do not propagate and perturbations are *universally unstable*. This instability can play an important role in creating short-scale dust structures. Similar to the gravitational instability (GI), the growth rate of this instability reaches a constant value at $k = 0$ but one should have in mind that very low wave numbers are strictly speaking excluded by the condition that the effective phase velocity ($Im\omega/k$) in the DISW domain should be less than the electron thermal velocity. The reason for the instability to develop is the possibility of an ion collective flux which creates in turn the charge accumulations enhancing the ion flux.

Since for large dust sizes the allowed range of wave numbers for DISW is rather narrow, to match them experimentally is rather difficult. In particulate it is necessary to produce shock waves on the non-linear stage. The best way to produce them is to use small-size grains.

4.2.2 Instability in the Range of DAW

For the conditions opposite to (4.29), where DAW do not exist, i.e., for $k^2 \ll 1/\tau$ and $\tau \ll 1$, we find (the delay in dust charging is neglected)

$$\omega^2 = \frac{\mu}{\tau} \frac{\alpha_{ch}\alpha_{dr} z_0 P_0^2 (1+P_0)(1+z_0)}{\left[1+P_0+z_0-\frac{\alpha_{ch}\alpha_{dr}P_0^3 z_0^2}{k^2}\right]} \,. \tag{4.35}$$

The instability appears for all $k < k_{cr,daw}$ but the maximum growth rate corresponds to the wave numbers close to $k < k_{cr,daw}$:

$$k_{cr,daw}^2 \approx \frac{\alpha_{ch}\alpha_{dr} P_0^3 z_0^2}{1+z_0+P_0} \,, \tag{4.36}$$

which depends both on the charging and on the drag coefficients, and also is proportional to the square of the dust charge. For $\alpha_{ch} = 1/2\sqrt{\pi}$ and $z_0 \approx 2$, the critical wave numbers for DISW and DAW are of the same order of magnitude and do not differ much. For $k \gg k_{cr,daw}$, we find a new mode

$$\omega^2 = \frac{\mu}{\tau} \frac{\alpha_{ch}\alpha_{dr} z_0 P_0^2 (1+P_0)(1+z_0)}{[1+P_0+z_0]} \,. \tag{4.37}$$

The charging damping of this mode can be easily found by substituting $1 + z_0 - i\omega/\alpha_{ch}$ for $1 + z_0$. The damping rate is given by

$$\gamma = -\frac{\mu}{\tau} \frac{\alpha_{dr} z_0 P_0^3 (1+P_0)}{2(1+z_0)(1+z_0+P_0)} \,. \tag{4.38}$$

This damping rate is approximately $\sqrt{\mu/\tau}$ less than the frequency. The instability starts at the wave numbers less than $k_{cr,daw}$ but its maximum is close the critical wave number with the maximum growth rate being large as compared to that at $k \ll k_{cr,daw}$, where the growth rate γ is described by

$$\gamma = k\sqrt{\frac{\mu(1+P_0)(1+z_0)}{\tau}P_0 z_0}\,. \tag{4.39}$$

This growth rate increases with k proportional to k, and for $k \sim k_{cr,daw}$ (but not too close to $k_{cr,daw}$) it is of the order of

$$\gamma = \sqrt{\mu\alpha_{ch}\alpha_{dr}}\tau P_0\sqrt{((1+P_0)(1+z_0)(1+P_0+z_0)}\,. \tag{4.40}$$

The effective phase velocities γ/k are much larger than the dust thermal velocity for

$$T_d \ll T_e\frac{(1+P_0)(1+z_0)}{P_0 z_0}\,. \tag{4.41}$$

This inequality is usually satisfied in most existing experiments.

The infinity in (4.35) at $k = k_{cr,daw}$ is not reached if one takes into account the imaginary part related with the delay of the dust-charging process. We find then the shift in the wave numbers from the critical value and the value of the maximum growth rate:

$$\gamma_{max} = \frac{\sqrt{3}}{2}\left(\frac{\mu}{\tau}\alpha_{ch}\alpha_{dr}P_0^2(1+P_0)(1+z_0)\right)^{1/3}\,. \tag{4.42}$$

The instability threshold corresponds to wave numbers somewhat less that $k_{cr,daw}$, namely at $k = k_{cr,daw} - \Delta k_{thr}$. From (4.36) we find

$$\frac{\Delta k_{thr}}{k_{cr,daw}} \approx \gamma_{max}\frac{k_{cr}^2}{2\alpha_{ch}\alpha_{dr}P_0^3 z_0^2}$$

$$= \frac{\sqrt{3}}{4}\frac{\alpha_{ch}\alpha_{dr}P_0^3 z_0^2}{(1+z_0+P_0)^2}\left(\alpha_{ch}\alpha_{dr}P_0^2(1+P_0)(1+z_0)\right)^{1/3}\left(\frac{\mu}{\tau}\right)^{1/3}\,. \tag{4.43}$$

This consideration illustrates that large growth rates occur at a very narrow wave number range and that the system mainly excites only one mode, the most unstable mode, especially if the system has a finite size. This mode can create structures among which could be the modes turning the system to a crystal state. But depending on the distribution of initial perturbations a broad spectra can also be excited if the largest perturbations are not at $k_{cr,daw}$.

4.2.3 Instability Stabilization in the Range of DAW

Stabilization of the instability in the DAW range can be due to the dust pressure effect which is treated by including the dust pressure terms $k^2\tau_d$ in the dispersion equation. The criterium for the stabilization should include the maximum growth rate γ_{max}. We find

$$\tau_d > \frac{2(1+z_0+P_0)}{\sqrt{3}\alpha_{ch}\alpha_{dr}P_0^3 z_0^2}\left(\alpha_{ch}\alpha_{dr}P_0^2(1+P_0)(1+z_0)\right)^{2/3}\left(\frac{\mu}{\tau}\right)^{2/3}\,. \tag{4.44}$$

By assuming that the charging and the drag coefficients as well as z_0 are of the order of 1, we obtain the dependence of the critical temperature on the parameters of the system:

$$T_d > T_{d,cr} \ , \tag{4.45}$$

where

$$T_{d,cr} \approx T_i \frac{Z_d^{4/3}}{\tau^{4/3} P_0^{5/3}} \left(\frac{m_i}{m_d} \right)^{2/3} . \tag{4.46}$$

Using the data of current experiments $\tau = 0.02$, $Z_d = 10^3$, $P_0 \approx 1$, $m_d/m_i \approx 10^{10}$, we obtain $T_d > (1.5) \times T_i$. One should have in mind that a factor of the order of 1 is missed in the estimate (4.46). The obtained criterium is close to that observed in experiments for phase transition to the plasma dust crystal state. Therefore one can hope that the instability considered here can be relevant or can be the most probable candidate for the beginning of the plasma dust condensation and formation of the plasma dust crystal structures. For more exact treatment, of course, the non-linear approach is necessary. The linear consideration can give some orientations in the problem. However, the instability for wave numbers much less than the $k_{cr,daw}$ is not stabilized by the delay in dust charging and presents the universal instability of a complex plasma which can lead to separation of the plasma into dust clumps and dust voids.

4.2.4 Physics of the Instability

In usual plasmas, instabilities appear in the presence of non-equilibrium distributions such as anisotropy of particle distributions, inhomogeneity of the systems, etc. Complex plasmas are different in the sense that an instability can develop even in the absence of such non-equilibrium distributions. The source of the instability is the energy and the particle supply in the ground state. In this sense this is the Universal Instability (UI) for the complex plasma state. The physical reason for appearance of the instability is the possibility of effective attraction of equally charged dust particles in a complex plasma caused by the collective flux (see the next chapter). Only plasma ions are included in this instability in case the growth rate is fast enough and the dust particles are not able to follow the instability development because of their large mass. The dust particles are included in case the growth rate is sufficiently slow so that the dust particles can follow the development of the instability (plasma electrons are always adiabatic).

The physics of the instability can be described by hand waving as related with the charging and the friction (the ion friction is described here by the drag coefficient – this is the collisionless limit; in the collision-dominated limit the friction of ions is due to collisions with neutrals). The plasma disturbances are almost quasi-neutral. Assume for example that in some region of space due to the fluctuations the ion density becomes larger than in other regions. Then the electron density also increases in this region and the ionization rate

becomes larger, so that more ion–electron pairs are produced in the region and the ion density is further increased. The effect which does not allow the ions to leave the region with enhanced ion density is the friction of the ion flux on the dust particles (or in collisions with neutrals in the collision-dominated case). This friction only allows the ions to leave the region of the enhanced ion density with a finite velocity determined by the friction. Thus for large-enough size of the ion number density enhancement the ions have no time to leave the enhancement region before the new ions are produced by the ionization.

To estimate the critical length or the critical wave number where the instability starts to develop we note that in any dissipative system the resistance of the ion flux by dust or neutrals creates the electric field. This field in the dimensionless units is of the order of $E \approx -\alpha_{dr} P_0 u z_0$. On the other hand, the presence of the electric field creates an electron density gradient (due to the adiabatic behavior of plasma electrons $dE/dx \approx -E \approx \alpha_{dr} P_0 u z_0$). The ion flux is proportional to the electron density $du/dx \approx \alpha_{ch} P_0 n_e$. The coefficient in front of n_e is taken from the condition of the balance of the ionization and the absorption on dust grains in the ground state and we neglect for a moment the absorption of the ion flux on dust particles). Since the dimensionless length is in the units of the charging length L_{cr}, we find by these simple estimates the characteristic length L_{cr} to be $(\lambda_{ch}/L_{cr})^2 \approx \alpha_{dr}\alpha_{ch} P_0^2 z_0$ for the size of disturbances which start to be unstable (remember that $\lambda_{ch} \approx \lambda_{Di}^2/a$). This estimate shows that, indeed, the effect is determined by the product of the charging and the drag coefficients. This estimate is rough since it neglects the absorption of the flux on the dust grain, assuming that it is just of the same order of magnitude as the change of the ionization. In fact this cannot be true for $P_0 \to 0$ when the compensation of these effects could be strong.

Direct calculations using the corresponding dielectric function gives

$$k_{cr}^2 \lambda_{ch}^2 = \alpha_{dr}\alpha_{ch} P_0^2 \frac{z_0^2}{1 + z_0 + P_0} \,. \tag{4.47}$$

This expression demonstrates that the instability has a property similar to the GI since the collective ion attraction (see the next chapter) creates the ion enhancement and the force of the collective attraction is proportional to $\alpha_{dr}\alpha_{ch}$, which is nothing else but the values determining the threshold of the instability. For $P_0 \to 0$, the critical wave number decreases with P_0 as P_0^3, i.e., much faster than in the case of the previous rough estimate since in the estimate we neglected one term in the balance relation which for small P_0 almost compensates the one we took into account. The instability depends on whether the time is sufficient (or not sufficient) for the dust particles to react. In case it is fast enough, the correspondent growth rate has a maximum at $k = 0$, i.e., at the largest possible size in the system, similar to the GI.

4.2.5 Instability Rates

Investigating the UI of a complex plasma, it is possible to use a general dispersion relation not being restricted by the conditions for either the range of DISW or the range of DAW. The growth rate γ for the UI was first found by using this procedure in [16]; all dissipative and other effects described above and additionally the finite grain velocities and the grain friction in the neutral gas were included. It was found that a complex plasma is always unstable for $k = 0$ as it is the case for usual GI. For $P \ll 1$ and $k = 0$, the growth rate is universal and is described by the simple expression

$$\Gamma = \frac{\gamma}{v_{Ti}\sqrt{2}a/\lambda_{Di}^2} = \alpha_{ch} P_0^2 \frac{z_0}{2\sqrt{\pi}(1+z_0)(1-P_0)+P_0}\,, \tag{4.48}$$

where γ if the growth rate in the usual dimensional units. Remember that expression in the denominator on the right-hand side of (4.44) is of the order of the charging frequency and that $\alpha_{ch} =\approx 1/2\sqrt{\pi}$.

All instabilities considered here can lead to structure formation in a complex plasma and therefore altogether they can be called the "Structurisation Instability (SI)". We conclude then that complex plasmas are universally unstable with respect to structure formation. This is one of the main properties of complex plasmas as was mentioned earlier. In certain cases this instability is not directly stabilized by the ion pressure or the dust pressure effects and leads to formation of dust structures in the gaseous state of complex plasmas. Indeed, the instability appearing as continuation at low wave numbers of the DISW branch and created by the drag friction (by adding the ion friction on neutrals the growth rate of the instability even increases) and the ion pressure effect corresponds to SI, and at $k = 0$ the growth rate is maximal. The analysis of its dispersion relation supports this statements.

In [16], the general dispersion relation was obtained using the basic state and the perturbations of the basic state due to the force disturbances, as described above. These forces were the electric, the drag, and the friction of neutral forces, and dust inertia for dust particles; the ion pressure, the ion friction on dust and on neutrals, and the ion inertia for plasma ions; and the electron pressure and the electric force for plasma electrons. In the ion continuity equation, the ionization proportional to the electron density and absorption on dust were taken into account – exactly the same processes as described above but without any restrictions on the range of phase velocities. As a free parameter of the basic state, not P_0 was chosen but (directly related to this parameter) the ionization rate α_i. All equations were written for the normalization used above for the collisionless case, but all ion-neutral collisions were fully taken into account. The work [16] was the first which defines and introduces the basic state of complex plasmas.

Explanations given here are needed for showing the results obtained in [16] – the consideration is the same as above but using the parameter α_i to illustrate the dependence of UI on the ionization rate. The ion-neutral friction

force for this normalization can be written as $\nu\tau\mathbf{u}$, where the dimensionless ν is directly determined by the ratio of the ion-neutral mean-free path to the ion–dust mean-free path and is characterized the ion friction in the neutral gas while $\nu^* = \tau^2(n_n/2n_0)\sqrt{T_n/2T_i}$. The dust inertia is taken into account by the dimensionless parameter m_d being the mass of a dust grain in the units $m_i\tau n_n Z_d/3n_0$, where n_n is the number density of neutrals. For $m_d \ll 1$, the dust inertia is small and both ν and ν^* are for existing experiments of the same order of magnitude close to 1. Additionally, the condition of quasi-neutrality of perturbations, $\delta n = \delta n_e + \delta P$, was used. The reader easily can obtain such a dispersion equation from the forces written above and we only illustrate the result of its numerical solution in the limit $\tau \ll 1$: the general qualitative feature is that at $k = 0$ the growth rate is equal to (4.48), where all mentioned effects are taken into account, and that with the increase of k the growth rate starts to increase, having maximum at the wave number of the order of ion–dust mean-free path, and then decreases to zero.

Behavior of UI reminds in many aspects the gravitational instability, taking into account only the gravitational attraction and the gas pressure, which in dimensional units is described by

$$-\omega_{gr}^2 = \gamma_{gr}^2 = Gnm - k^2 v_s^2 \; . \tag{4.49}$$

Here, v_s is the sound speed and G is the gravitational constant. The value $2\pi/k$ corresponding to $\gamma = 0$ is the Jeans length L_J. The same happens for UI at certain value of k analogous to the Jeans length; that can be named as the Jeans Universal Instability Length (JUIL), L_{JUIL}. The difference between GI and UI is that between $k = 0$ and $2\pi/L_{CPJL}$ the growth rate of UI has a maximum. This kind of behavior was found within a broad range of frequencies of dissipation ν, ν^* and dust inertia m_d, which is illustrated by examples given in Figs. 4.1, 4.2, 4.3, and 4.4 while γ_{gr} is illustrated by Fig.4.5.

A comparison of curves for GI and UI suggests that attraction forces can operate between dust grains. These forces indeed exist and are due to the collective flux Φ acting in the systems with sizes larger than the dust–ion mean-free path, which is the case of UI. We describe them in detail in the next chapter and here we emphasize the *analogy between UI and GI.*

How to Measure the Critical Wave Numbers? For UI or SI, the critical wave number(s) crucially depend on P_0. Note that in several experiments the parameter P_0 was already specially made close to 1, and there exists no big

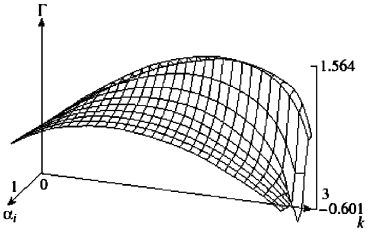

Fig. 4.1. Dependence of the instability growth rate γ on the wave number k and the rate of ionization α_i for argon plasma within the parameter ranges $0 < k < 3$ and $0.1 < \alpha_i < 1$ for $a = 0.1$, $\tau = 0.1$, $\nu = 1$, $\nu^* = 1$, and $m_d = 0.5$

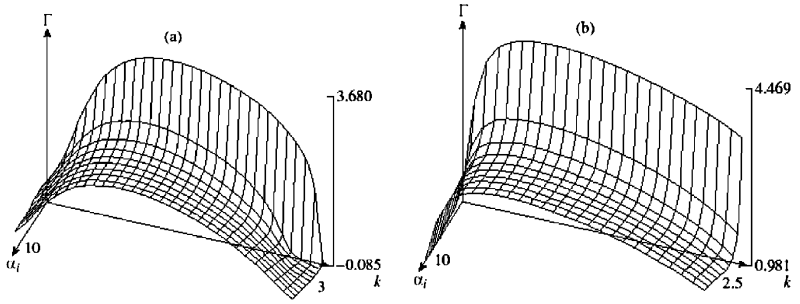

Fig. 4.2. Same as in Fig. 4.1 but (**a**) for $\nu = 0.01$; and (**b**) for $\nu = 10$

difficulty to obtain P_0 close to 1 in future experiments. The growth rate of UI is then rather large and the main question is about the critical wavelength determined. In the existing experiments on DISW and DAW this critical wave number was not reached. But there is no difficulty to reach it for other dust sizes and other Debye lengths. Indeed, for the parameters of a standard plasma crystal experiment, where $a/\lambda_{Di} \approx 1/10$, and for $P_0 = 0.6$, $z_0 = 3$, $\ln \Lambda = 3$, we have $k_{cr,disw}\lambda_{Di} = 0.037$, and for $\lambda_{Di} = 36\mu$m we find $k_{cr,disw} \approx 9\,\mathrm{cm}^{-1}$, which is within the range usually measured in current experiments. Thus UI can be measured at these and the lower wave numbers. For the wave numbers larger than the critical one (and for usual conditions where $\tau \ll 1$) there exist a range of wave numbers lower than the critical one. This range can be also covered in future experiments. Thus both UI and new dust modes can be a subject of future investigation. These modes can be thought to be excluded either choosing the size of the system L to be less than that determined by the critical wave number or by some non-linear stabilization if it occurs at a low level of the disturbances. The critical wave numbers can be larger than the mean-free path if

$$L \ll 1/k_{cr,disw} \approx \frac{\lambda_{Di}^2(\sqrt{(}1 + P_0 + z_0)}{aP_0^{3/2} z_0 \sqrt{\alpha_{ch}\alpha_{dr}}} \,. \tag{4.50}$$

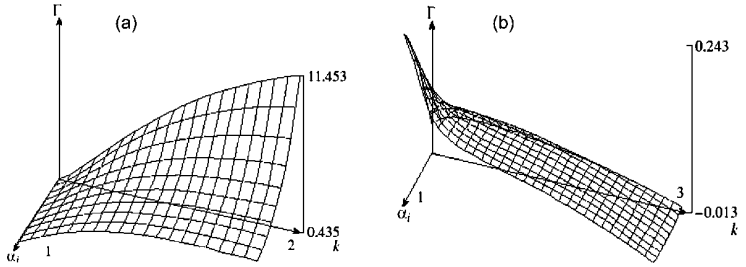

Fig. 4.3. Same as in Fig. 4.1 but (**a**) for $\nu^* = 0.1$; and (**b**) for $\nu^* = 10$

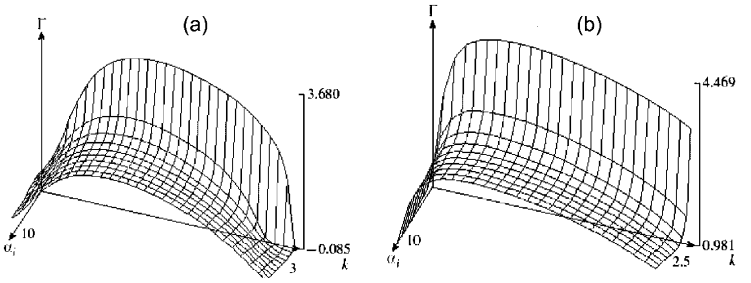

Fig. 4.4. Same as in Fig. 4.1 but (**a**) for $m_d = 5$; and (**b**) for $m_d = 50$

4.2.6 Effects of Finite Size

One of the necessary condition for the consideration [5, 6, 7, 8, 9] to describe DISW and DAW is the possibility to neglect processes of the ion/electron scattering and absorption of dust grain. The other one is to take properly into account the balance condition between the ionization and the ion/electron absorption on dust grains. Both of these conditions require that the size of the system L should be larger than the mean-free path for the ion/electron collisions on the grains, and both conditions contain the factor $1/P_0$. One can think that the results [5, 6, 7, 8, 9] can be qualitatively valid also for the system size L less than the mentioned mean-free paths. But, strictly speaking, the use of k and ω to describe the waves is possible only in an infinite system and it is known that it is much more complicated to describe the finite size system (see [1]) when changes of dispersion relation and new modes appear (the most known are the plasma drift modes). Also, if the system size is regulated by external fields it is necessary to include perturbations of these fields into consideration.

Thus results [5, 6, 7, 8, 9] need further clarification, and one can use only those results which in some limits coincide with the expressions obtained above for infinite systems. The question of the finite size effects is even more serious in the presence of UI making automatically the complex

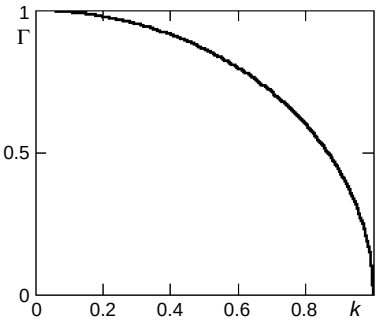

Fig. 4.5. Growth rate of the GI $\Gamma = \gamma/k_J v_s$, $K = k/k_J$

plasma inhomogeneous if it develops in the non-linear stage in a system of voids and dust clumps, as observed in many experiments. When they become stationary, the dust clumps (dust structures) have sharp boundary, an inhomogeneous distribution of all parameters, and can be theoretically described by self-consistently regulated stationary balance equations. Existing experiments also indicate that distributions of plasma and dust parameters inside the structures are inhomogeneous. This is one of the general fundamental properties of complex plasmas.

The theory and experiments show that the size of these structure is of the order or larger than the ion–dust (or dust-neutral) mean-free path while the approach used in [5, 6, 7, 8, 9] (also neglecting the change in the electron/ion distributions due to the ion/electron–dust collisions) is actually valid in the opposite limit. Thus it is difficult to imagine that this approach can be used at all to describe the reality. One can of course restrict the size of dust region externally by walls but investigations show that for the dust not to fall on the wall there should exist a dust–wall void separating dust in the structures from the wall and that the latter is possible to be created only in the case where the distance between the walls and the size of the dust structure inside them are larger than the mean-free path. Thus the only possibility left is to reduce the size by an external potential. Such experiments exist and the structures created are called "dust clusters" – their size is much less than the mean-free path for the dust-electro/ion collisions.

Waves in structures in the opposite limit are strongly influenced by the inhomogeneity of the structure, and their wavelengths change drastically as they propagate from the center to the periphery of the structures. Thus the problem arises for experimental checking of the critical wave numbers described above when converting to the size of the system as, e.g., in the simplest known equilibrium spherical structures, sun and stars, where the balance exists only between two forces, the pressure and the gravity. For sun, these modes were observed and detected experimentally and are subject of a large area of research known as solar seismology. In dust structures, the equilibrium is more complicated and is created by balance of all forces listed above. The critical wave numbers can be larger than the mean-free path if

$$L \ll 1/k_{cr,disw} \approx \frac{\lambda_{Di}^2(\sqrt{(}1 + P_0 + z_0)}{aP_0^{3/2} z_0 \sqrt{\alpha_{ch}\alpha_{dr}}} \,. \tag{4.51}$$

The presence of small parameters in the denominator of (4.51) can allow the experimental checking of these waves (see next chapter).

4.2.7 Electrostatic Gravitational-like Instability and Modes in Plasma Clusters

Systems with sizes less than the ion–dust mean-free path have usually the inter-grain distances also less than this mean-free path. The number of grains

is not large for these systems; they are usually called "dust clusters." The particle confinement in 2D dust clusters is usually produced experimentally by the parabolic external potential. The distribution of grains in these clusters is highly inhomogeneous. For small number of grains the clusters have a shell structure and are often called as "atomic-like structures." Their experimental investigation is described later, in the chapter devoted to experiments in complex plasmas. These clusters can be self-confined if attraction forces operate between the grains.

A general theory of two-dimensional (2D) clusters for arbitrary grain interactions was developed in [38]. Three-dimensional (or 3D) clusters were also the subject of both experimental and theoretical investigation. We mention here that these system could be the only ones where the modes can correspond to those considered in [5, 6, 7, 8, 9] since the size of clusters is less than the ion–grain mean-free path. However, dust grains in clusters, when distributed initially random, soon become very instable with respect to a new Electrostatic Gravitation-like Instability (EGLI) [15] appearing in this limit of the system sizes; the finite state of EGLI is inhomogeneous as in the case of UI. EGLI differs from UI since the flux on each grain is non-collective. It operates for systems in which the size is much less than the ion–dust mean-free path. It is also similar to the known GI and is described by

$$-\omega_{EGLI}^2 = \gamma_{gr}^{GLEI} = G^{eff} n_d m_d - k^2 v_{dav}^2 \ , \tag{4.52}$$

with

$$G_{non-coll}^{eff} m_d = \nu_{attr} Z_d^2 e^2 a^2 / (m_d \lambda_{Di}^2) \ . \tag{4.53}$$

This has a form similar to the equation for GI and differs from (4.49) by substitution of v_{dav} for v_s, G^{eff} for G and $m_d n_d$ for nm [15]. The corresponding Jeans Electrostatic Gravitation–like Instability length L_{JEGIL} is of the order of the mean-free path for the grain charging and differs from L_{JUIL} by the factor P which is always less than 1. In case $P \ll 1$ we have $L_{JEGIL} \ll L_{JUIL}$. One can see that EGLI is also related to a grain attraction but of a non-collective origin. In [39] it was demonstrated that for DAW at low wave numbers the instability has the same form as usual GI with effective gravitation constant determined by collective grain attraction, Electrostatic Collective Gravitation like Instability (ECGLI). In [39] the limit $\tau \ll 1$ was investigated and we give here the result in this limit:

$$G_{coll}^{eff} m_d = \frac{\alpha_{dr}(\beta)\alpha_{ch}(\beta)\beta Z_d^2 e^2 a}{m_d \lambda_{Di} \left(1 + \frac{P_0}{1+z_0}\right)}) \ . \tag{4.54}$$

The difference between (4.53) and (4.54) is that (4.53) contains the non-collective attraction coefficient (see next chapter) while (4.54) contains the collective attraction coefficient(see next chapter). It is also natural that the range of applicability of non-collective EGLI ($1/L_{JEGLIL} = k_{non-coll} \approx$

$\sqrt{G^{eff}_{non-coll} n_d m_d}/v_{dav} \gg 1/L_{eff}$) is different from the range of applicability of ECGLI ($1/L_{JECGLIL} = k_{coll} \approx \sqrt{G^{eff}_{coll} n_d m_d}/v_{dav} \ll 1/L_{eff}$)(see the next chapter for non-collective and collective dust–dust attraction and for criterion dividing the ranges their existence). Thus the collective mode reflects the effects of dust–dust interactions Which can be detected by measurement of the DAW dispersion. In the next chapter, we show that such an attraction of like-charged dust grains (both non-collective and the collective one) indeed exist and for non-collective case is known as the shadow attraction or Lesage attraction. The self-contraction of small dust clouds (dust clusters) due to development of EGLI can be examined numerically for a cloud containing a finite number of grains satisfying the condition that the size of the cloud and the inter-grain distances are less than the mean-free path for the grain charging. In this case, plasma fluxes on individual particles do not interfere and are non-collective [40]. The mean-free path for the grain charging is P times less that the mean-free path for the ion absorbtion on grains (remember that we always have $P < 1$). It was confirmed by numerical modeling [40] that the final stage observed (with the damping of grain motions due to the neutral-grain friction) is a boundary-free plasma cluster, which suggests that the cluster formation can occur due to the non-collective attraction operating between the grains. By starting from random grain distribution, the contraction of grain clusters observed in numerical computations was on the timescale of the EGLI inverse growth rate. The final cluster was of a size less than the mean-free path for the grain charging but was inhomogeneous with the inter-grain separation increasing to the periphery of the cluster (the latter was still of the order of the mean-free path for dust charging).

It is important that the final stable stage for a grain cluster is strongly inhomogeneous and therefore the actual results for the cluster modes are different from those of [5, 6, 7, 8, 9] since although the latter correspond to the conditions where the clusters can exist they do not take into account the inhomogeneity of grain distributions.

The ECGLI and UI are describing the first stages of formation of plasma crystals and other large-size dust structures (see Chap. 6)

4.2.8 Complex Plasma Structurization

The analogy between UI and/or EGLI/ECGLI and GI is suggesting that a complex plasma is always structurized. For GI, there are various well-observed scales of structures – stars, galaxies, clusters, and super-clusters of galaxies. This hierarchy of gravitational structures appearing as a result of GI is examined in detail in astrophysics. One can expect that depending on parameters of complex plasma systems (such as the grain temperature T_d, the parameter P, and the degree of ionization), the complex plasma either forms a plasma condensate (as for the case of UI in the range of DAW) or forms a system

of grain structures with the distribution of structure sizes as a hierarchy of scales similar to those observed for GI.

In a complex plasma, each grain structure should obey the condition of the non-linear force balance that includes all forces described above; it appears as a more complicated inhomogeneous structure than a simple gravitational structure where only two type of forces are important, the gravitational force and the pressure force. The formation of different structures in complex plasmas in the condition where the complex plasma condensation to the plasma crystal state does not occur was indeed seen in the majority of laboratory experiments performed so far and is expected to be the most important complex plasma property. Complex plasma structures can be of different form depending in experiments on the existing boundary conditions including the presence of walls, but formation of boundary-free structures and boundary-free clusters is also possible as suggested by the analogy with GI. In astrophysical conditions, the most probable complex plasma structures are the boundary-free structures. Detection of such structures is the problem of future astrophysical observations in the infrared range of cosmic spectra since dust in space is manifested by the infrared emission. An individual dust structure should be very inhomogeneous as are the observed gravitational structures. It is an open question whether dust structures similar to the star structures can exist in space. If they exist, they have properties opposite to the stars since they absorb the plasma flux and do not create it as the star wind. Investigations of non-linear balance equations for possible complex structures suggest that such structures can exist and this is the subject of detailed discussion later in this book.

4.3 Collective Modes Excited by Fast Particles

Mach cones are mainly observed within the crystal state as well as for particles moving close to the crystal. In this section, we consider the simplest effect where the Mach cones are excited by a particle moving inside a complex plasma in its non-correlated state. This is the problem to be addressed first before going on to more complicated consideration of the Mach cones excited in the crystal state (or by a particle moving close to the crystal). We postpone the discussion on Mach cones in the crystal states and also the data observed until we describe the data on the crystal state itself.

4.3.1 Mach Cones: General Remarks and the Cone Angle

It is well known that Mach cones can be excited in any material by objects moving faster than the phase velocity of waves propagating in the material. For charged particles in usual matter they correspond to the Cherenkov emission of waves by the particles [41]. It was first proposed in [42, 43] to use Mach cones for diagnostics of dusty plasma parameters: e.g., to determine

parameters of Saturn rings by observations of the Mach cones created by a big boulder (stone) moving in the ring. Recently [44] it was proposed that Mach cones developing in time could be a good diagnostic method in industry for the deposition technic and for film-covering of materials. The Mach cone measurements can serve as a good method of diagnostics of dusty plasmas parameters in technological applications [45, 46, 47, 48].

A Mach cone can be considered as a composition of linear waves if the source is not strong; it can be considered as a non-linear wave or even a shock wave if the source is strong enough. If a large grain moves through a uniform complex plasma in a gaseous state, the excited waves are of DAW type. A simple kinematics gives then the known relation for the cone angle

$$\cos^2(\theta) = \sin^2(\mu) = \frac{v_{daw}^2}{v^2} \ , \tag{4.55}$$

where $\mathbf{v}$ is the particle velocity, θ is the angle between $\mathbf{v}$ and the wave vector $\mathbf{k}$ of the emitted wave and μ is the angle between the Mach cone front and the particle velocity. Of course, the particle speed should be fast enough to exceed the DAW phase velocity and satisfy relation (4.55). The Mach cone simply describes the kinematics of the wave emission but the intensity of the emission depends on the interaction of the fast particle with a complex plasma. There are several complications in the Mach cone effect for complex plasmas as compared to the standard Cherenkov emission of waves, which creates Mach cones in the usual matter.

4.3.2 Wave Intensity and Distribution of Wavelengths

The first complication is related with the intensity of emitted waves. As we already emphasized, the field close to the grain is non-linear (and for large grains this is even more important). The linear picture of excitation of DAW can be approximately valid only if at the distance of the order of the emitted wavelength the non-linear excitation is small as compared to the linear one. A general consideration of this kind should be made first for the case of weak non-linearities, which requires the knowledge of the first–order non-linear responses and stays as a problem for future. At least one hopes that it can give a criterion showing where the results for the linear excitation can be used. Nevertheless, some information can still be obtained using the standard linear approach in derivation of the distribution of the intensity of the emitted waves with respect to the wave numbers or wavelengths.

The power I emitted per second for a charge $Z_d e$ moving in an infinite plasma (with a size much larger than the wavelength emitted) with the dielectric permittivity (4.24) can be found in calculation of the work produced by the field $\mathbf{E}$ excited by the particle on the current $\mathbf{j}$ of the particle. The field $\mathbf{E}$ in the linear approximation for a fixed value of the dust charge can be expressed through the charge density of the particle using the Poisson's equation, and the current $\mathbf{j}$ can be also expressed through the charge density. Such

calculations are well known (see [14]) and the expression of the power emitted can be written as

$$I = \frac{Z_d^2 e^2 v_{DAW}^2}{v} \int_{k_{cr}} F(k) k dk \left(1 - \frac{k_{cr}^2}{k^2}\right)^2 , \tag{4.56}$$

where

$$F(k) = \frac{1 + \frac{a^2}{\tau k^2 \lambda_{Di}^4} \alpha_{dr} \alpha_{ch} z_0 P_0 (1 + P_0)}{1 + \frac{P_0 (k_{drch}(0))^2 a^2}{\tau k^2 \lambda_{Di}^4}} \left[\frac{1 + z_0}{1 + P_0 + z_0}\right] . \tag{4.57}$$

Expression (4.57) does not take into account several important features of the complex plasmas: (1) the charge variations; and (2) the non-linear screening (for the validity of (4.57), it is necessary to assume $\beta \ll 1$). However, it takes into account the correct expression for the linear dispersion relation of DAW and in this sense it is of interest since it can give us some information about the distribution of the intensity of the emitted waves in the wave numbers.

In (4.57), $k_{drch}(0)$ is the expression for k_{drch} given above for the frequency $\omega = 0$. In expressions (4.56) and (4.57), we neglected the dust-neutral friction and considered $k \ll 1/\lambda_{Di}$, i.e., $\omega \ll \omega_{pd}$; k_{cr} is given by (4.47). Note that according to (4.57) the waves with $k < k_{cr}$ do not exist as it was pointed out before and they are not emitted; the largest intensity emitted corresponds to the largest k (the shortest wavelength), which is of the order of λ_{Di}. The results (4.56) and (4.57) serve only as an illustration, since for short wavelengths the non-linearities certainly play a role.

The wave dispersion can be important for the Mach cone broadening, since different wavelengths are emitted at different angles. For example, from (4.29) we obtain expression (4.57) only for $k^2 \gg k_{drch}^2 P_0/\tau$, while in the opposite limit and for $k \gg k_{cr}$ we find

$$\cos^2(\theta) = \frac{v_{daw}^2}{v^2} \frac{\alpha_{dr} \alpha_{ch} P_0 (1 + P_0) a^2}{k^2 \lambda_{Di}^4 \tau} . \tag{4.58}$$

A strong dispersion of the Mach cone directions should be recognized for this case.

4.3.3 Wave Excitation by Outside Particles Moving near Boundary

It is known that Mach cones are excited in a medium if the source (here the fast grain) moves in the channel of the size less than the emitted wavelength [41]. The fast grains make the channel themselves, but can collect other grains when moving through the system, just increasing its size and charge [44]. The Mach cones are the Dynamic Mach Cones (DMC) in this case; they can also be used for diagnostic purposes. Notice that if the size of the channel is less than the emitted wavelength, the Mach cone is in fact the same as in the

absence of the channel [41] (and for the grain size less than the ion Debye length, which is the minimal wavelength emitted).

It is also well known that Mach cones can be excited not only by the source moving inside the medium but also by the source moving close to the surface of the medium if the distance between the source and the surface is less than the wavelength of the excited waves [41]. As soon as the distance between the fast grain and the surface increases, the waves in the cone will have only the waves with the wavelengths larger than this distance. This can serve also as a powerful diagnostic method for measurements of spectra of the emitted waves since usually in the plasma sheath the distance of the fast grain from the surface is determined by its mass (the heavier grains move below the surface of a dust cloud at larger distances from the surface due to the balance of the gravity and electric forces). The Mach cone measurements in complex plasmas can also serve as an effective mechanism for the diagnostic of the plasma crystal state and its transitions. Excitation of the Mach cone can be produced by a fast grain moving with the velocity larger than the phase velocity of DAW, DLW, or DSW moving below the crystals.

Another important point is the possibility to excite the Mach cone close to the surface of the void. The presence of voids with sharp boundaries was demonstrated experimentally and the size of the grains in this case is not limited by the conditions to have a large grain charge as it is in the case of the grains in the plasma condensation (remember that the charge of the grain is approximately proportional to the grain size).

4.4 Observations of Collective Modes

4.4.1 Introductory Remarks

As we already demonstrated, collective waves such as DISW and DAW can exist only within limited ranges of frequencies and wave numbers. The best way to measure them is in a complex plasma in the gaseous state. The range of UI is the one where the unstable modes can be also observed experimentally but it is a more difficult problem for the experiment which should be done on the timescales of the order of (or much less than) the growth rate of the instability. Dispersion laws for DISW and DAW should be measured on timescales much larger than the wave period, and these are more simple experiments.

On the other hand, the unstable modes can soon saturate and then one is able to investigate the modes in the final non-linear stage. But then there exist two possibilities, namely either the system is converting to the crystal state (i.e., the plasma condensation occurs) or the system becomes a collection of strongly non-linear ensemble of dust clumps and void. In both cases the linear

modes are strongly modified in the non-linear stationary state of the development of UI. For crystal state, the modes are DLW and DSW (as pointed out above), and for clusters and voids the modes are strongly inhomogeneous in space.

Although development of stable and/or unstable perturbations can be a special area of research, such studies have not been started yet. Modes in the structures developing in the case where UI leads to voids and dust clumps are investigated only partially in the theory, and experiments of this kind are very rare not identifying the modes excited. Therefore we are able to discuss only the experiments on collective modes in almost stationary states and we start with the experiments performed in the gaseous state of a complex plasma.

Experiments on such collective modes in plasma crystals as DLW and DSW are discussed in the chapter devoted to observations of dust crystals and the dust condensation. The modes in isolated dust structures, being not in the crystal state, such as the dust convection and dust vortices formation are discussed in the chapter devoted to dust structures. Certainly, special conditions are necessary to extract one dust clump (dust structure) from a set of them which can be created by UI. But experiments show that a single isolated dust structure can be indeed observed. The most complicated problem is related to the modes in a system of structures with the wavelengths of the order of or larger than the separation between the structures. Theoretically such problem can be formulated but no experiments are expected to be done in the nearest future to check such an approach. In this section, we concentrate on problems of experimental verifications of the concepts of the collective mode propagation in the gaseous state of complex plasmas. Naturally, we are restricted to those ranges of sizes of the perturbations where such modes can exist.

4.4.2 Experimental Observations of DISW

For many experimental conditions where conversion to the plasma crystal states was observed and $a/\lambda_{Di} \approx 1/10\tau = 0.02$, $\ln \Lambda \approx 3$, the right-hand side of (4.19) is larger than 1. On the other hand, the linear relation between the wave frequency and the wave number is valid only for $k\lambda_{De} \ll 1$ and thus the range where DISW exist is absent. This is important since the non-linear steepening of the waves and formation of a shock wave is possible only for an approximate linear relation between the wave frequency and the wave number. The question is, whether the linear relation can survive with only the change of the velocity of DISW for the relation opposite to (4.19). The answer was found in [12] and it is that the wave does not survive – the dispersion relation describes a purely damped disturbance in this case, with the damping rate close to the frequency of the ion–dust collisions, ν_{id}. The result obtained in [12] for the damping rate is given by

$$Im\omega = -P_0 z_0 \ln \Lambda v_{Ti} \frac{a}{3\sqrt{2\pi}\lambda_{Di}^2 \tau} \ . \tag{4.59}$$

Thus the linear dispersion occurs only for small a/λ_{Di} or small P_0. Special experiments are needed to be performed to satisfy the condition (4.19). There are a few experiments in which DISW shock waves and DISW linear waves were observed [49, 50]. In [51], it is shown that the ratio $a/\lambda_{Di} \approx 10^{-2}$–$3\times10^{-3}$ and the effect of damping described by (4.59) is not large, but in [51] the ion Debye length λ_{Di} is shown to vary from 30μ up to 1cm, while the dust size varies from μm up to 10μm and the ratio a/λ could be of the order of 0.3. No investigations have been done yet on the dependence of the damping on the dust size which is predicted by (4.59). Let us discuss this point in more detail for the experimental data of [51]. In [51], the Q-machine Dusty Plasma Device was used with almost equal electron and ion temperatures, $T_e \approx T_i \approx 0.2eV$, and plasma densities within the range from 10^5cm^{-3} to 10^{10}cm^{-3}. The dust particles were falling with velocities about 30cm^{-3}, of which is small as compared to the estimated DISW velocity and therefore the dust motion is not unimportant. For equal temperatures, the Landau damping should be large but an important point here is that the DISW speed can be larger than the ion thermal velocity due to the factor $1-P_0$ in the denominator of (4.17). Thus the presence of dust can reduce substantially the Landau damping if P_0 approaches 1. The experiments in [51] represent the dependence of the phase velocity of the DISW as a function of the parameter $1-P_0$ (denoted in [51] as η). In Fig. 4.6 we represent the experimental results of [51] for the dependence of the phase velocity and spatial damping on the parameter $\eta = 1-P_0$.

The authors of [51] suggest that the main mechanism of damping is the Landau damping, which crucially depends on the phase velocity of the waves. In condition where the ion and electron temperatures are equal, the

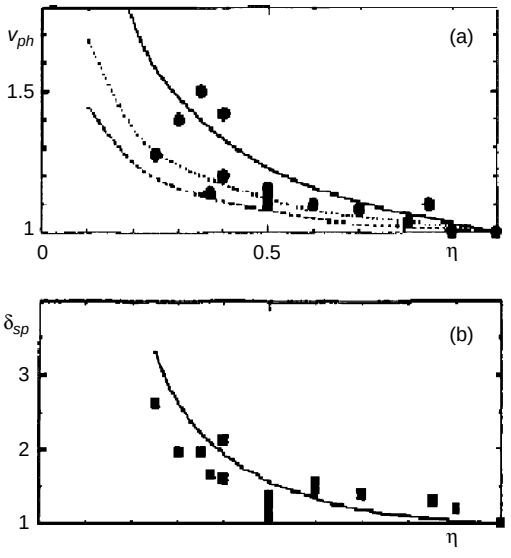

Fig. 4.6. Variations of (**a**) normalized DISW (named in the original figure [51] as "DIA waves") velocity v_{ph} (circles) and (**b**) normalized spatial damping parameter δ_{sp} (squares) on the parameter η. The curves in (**a**) are from the fluid theory, taking into account the drift along the magnetic field. The curve in (**b**) is obtained by taking into account the Landau damping only

DISW dispersion should take into account the ion pressure term and, instead of an increase of the phase velocity due to the presence of dust by the factor $1/\sqrt{1-P_0}$ as in the last approximate expression of (4.17), the factor which describes the change of the speed of ion sound waves by dust is $F = \sqrt{(1+(1-P_0))/2} = \sqrt{(1-P_0/2)/(1-P_0)}$. Thus the relative change of the spatial damping assumed to be the Landau damping is described by the additional factor iF.

$$F = \sqrt{\frac{1-P_0/2}{1-P_0}}; \quad iF = \exp\left(\frac{P_0}{1-P_0}\right)\left(\frac{1-P_0}{1-P_0/2}\right)^{3/2}. \tag{4.60}$$

These functions are shown in Fig. 4.7. Qualitatively they correspond to the experimental data shown in Fig. 4.7. More detailed correspondence can be obtained only if the damping due to the ion–dust collisions given by (4.59) is taken into account and detailed dependence on the dust sizes is investigated. The damping (4.59) does not allow the wave to propagate if its frequency is less than that determined by inequality (4.29). This effect strongly depends on the ratio a/λ_{Di} and the wavelength. In the experimental conditions [51], the range of parameters where this can be achieved is within that used in [51], but no information or investigation of the cutoff or the absence of waves with the wave numbers less than those determined by the inequality opposite to (4.29) is presented. In future studies, not only the threshold of the DISW existence but also the damping caused by the ion–dust collisions within the range of parameters where DISW exist should be examined experimentally. For this purpose it is obvious that more suitable is to use a complex plasma with $\tau \ll 1$ – the latter condition is the one more often found in experiments. For future experiments we give corrections for both the real part (the phase velocity) and the imaginary part (the spatial damping) of DISW (in the range where these waves exist and are damped weakly). Mention that the Landau damping of DISW is usually small if $\tau \ll 1$.

The exception are the experiments in Q-machines [52], where the Landau damping on ions is of importance due to low phase velocity of the waves for

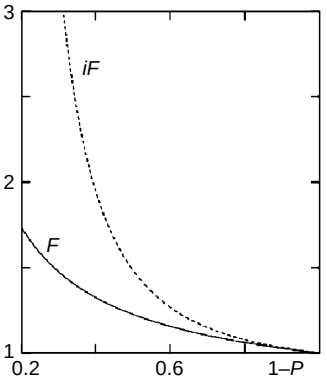

Fig. 4.7. Theoretical curves calculated according to (4.60)

equal ion and electron temperatures. The Landau damping on electrons is usually small due to the large mass ratio m_i/m_e for gases with heavy ions (often used in low-temperature experiments). In these conditions, where the damping is small, the effects of the ion–dust collisions, dust charging, and Landau damping can be simply added. Corrections to the phase velocity due to the charging and ion–dust collisions in the range of weakly damped DISW obtained [12] for the limit $\tau \ll 1$ are given by (4.20). These dispersion corrections are small – the first term because of condition (4.19) for the existence of DISW, and the second term because the wavelength should be less than the electron Debye length for quasi-neutrality deviations to be small. But the first term, being inversely proportional to k^2, can compete with the second term proportional to k^2 and this can be checked experimentally. The charging effect introduces some small change of damping ((4.20) [12]).

When a dusty plasma is perturbed by a large disturbance and the dispersion of DISW is linear (the frequency is proportional to the wave number), the steepening of the profile of the perturbation and formation of a shock wave is usually expected. To form the shock, the damping should not be large – for Q-machine device used in [49, 51] with equal electron and ion temperatures as in the experiments for linear DISW discussed above this can be reached only for a large value of the parameter P_0.

Experiments carried on in the double-plasma device [52] (see Fig. 4.8), which is similar to that of [51], demonstrated the steepening of a disturbance for $P_0 > 0.75$ created by launching a large square voltage pulse to the plasma grid. The plasma density was lower than $10^7 \mathrm{cm}^{-3}$ and the plasma Debye length was 0.3 cm, therefore a/λ_D was rather small, of the order of 10^{-3}; thus the wavelength at which the dust–ion collisions are important is about 10m – larger than the device size, while the steepening was observed at the distance of 30–40 cm. Figure 4.9 illustrates that without dust the applied pulses spread

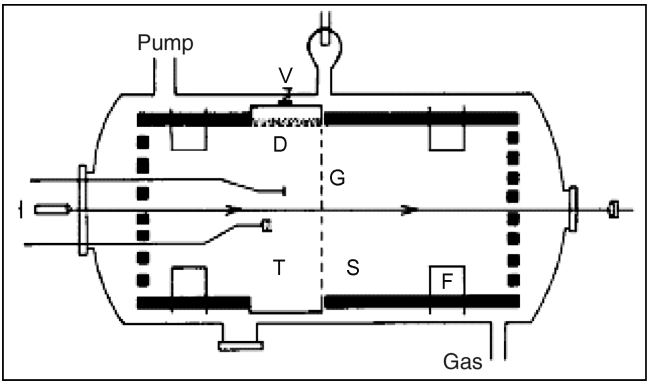

Fig. 4.8. Sketch of double-plasma device used in [52] for investigations of dust–ion sound shocks. V – applied voltage, G – grid dividing the space T from space S; F – hot filaments emitting electrons which ionize the gas; D – dust injector

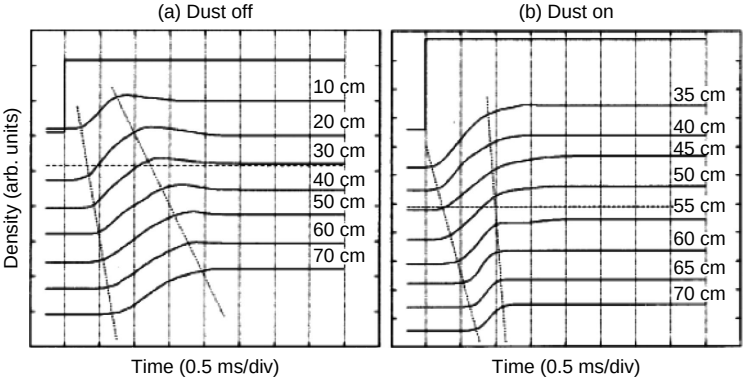

Fig. 4.9. Density versus different axial positions from the grid [52]. (**a**) No dust case, (**b**) Dust with $P_0 \approx 0.75$. In both (**a**) and (**b**) the horizontal lines are the zero levels corresponding to the uppermost n-versus z-trace. The top square wave is the pulse applied to the grid. The set of the dashed lines mark the advancement of the leading and the trailing edges of the pulses. In (**a**) the dashed lines diverge, indicating the spreading out of the pulses, while in (**b**) the lines converge indicating the steepening of the pulses

with an increase of the distance from the grid, while in the presence of dust for $P_0 > 0.75$ the steepening of the pulse and the shock formation were observed. Development of the shock wave is shown in Fig. 4.10. The thickness of the shock shown in Fig. 4.10 is about 40 cm. That cannot be explained either by the dissipation due to the dust charging or by the ion–dust scattering (it should be, according to the list of elementary processes in a complex plasma

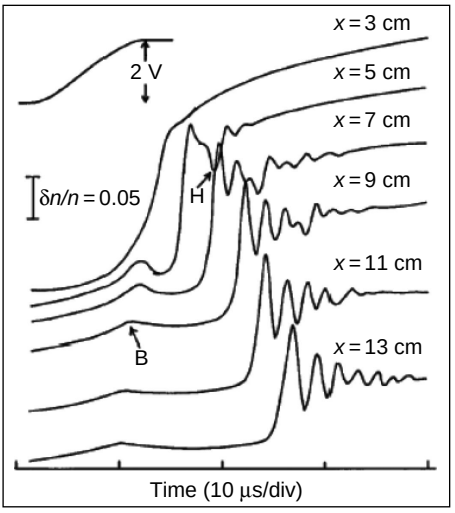

Fig. 4.10. Observation of the appearance of the oscillatory structure after steepening of the wave profile [52]. $n_d \approx 5 \times 10^4$ cm^{-3}, $\omega_{pi} \approx 3 \times 10^5$ rad/s

given earlier, of the order of $\lambda_d^2/a \approx 5$ m) and can be explained only by the Landau damping of the ion sound perturbations on ions. The dust increases the phase velocity of the waves to permit them to exist and to steepen their profile, but the dust still cannot cause the main dissipation in the shock.

We give more details on the experimental conditions before discussing possible mechanisms of phenomena observed in the experiments [50, 52, 53], namely the linear DISW, DISW solitons, and shocks. The low-temperature plasma was in [50, 52, 53] under conditions somewhat closer to those for the plasma crystal formation, but still not at the very low values of τ met in the plasma crystal experiments. We should therefore separate the discussed observations from their theoretical interpretation given in [50, 52, 53] and hence first present in detail the experimental conditions together with some estimates using the above-mentioned elementary processes in a complex plasma and then discuss how the theory can explain them.

The electron temperature was about $(1 - 1.5)$ eV and the ion temperature about 0.1 eV, thus $\tau \approx 0.1$ and the densities are in the range 10^8 cm^{-3} $< n_e <$ 10^9 cm^{-3}, the ion Debye length is in the range 90μm $<$ 230μm, while the dust size is $\approx 9\,\mu$m. For argon gas used in [50, 52, 53] we find $z_0 \approx 3.2$. The parameter P_0 varies in the experiments from 0.3 to 0.4. Then the inequality showing the range of existence of DISW means $k\lambda_{De} \equiv k/k_e > 0.1$ (where $k_e = 1/\lambda_{De}$). In this range of wave numbers, the results can be only those observed in [50, 52, 53]. This is not surprising since DISW cannot exist in other ranges. The gas pressure was about 10^{-4}Torr, and the mean-free path for collisions with neutral atoms was about 300 cm and it is larger than the size of the tube in the experiments. Thus the only important collisions are the ion–dust collisions. The experiments are able, in principle, to check the theoretical values of the frequency of the ion–dust collisions. The mean-free path for the ion–dust collisions, λ_{id}, can be estimated as $v_{Ti}/2Im\omega \approx \lambda_{Di}^2 3\tau\sqrt{\pi}/\sqrt{2}aP_0 z_0 \ln\lambda \approx (2500 - 500)$μm for $P_0 = 0.1$–0.4, which is 20 times less than that claimed by these experiments (see [52]). This estimate is important since the hydrodynamic concepts for the ion–dust collisions such as the ion viscosity can be used only for $\lambda \gg \lambda_{id}$. The wavelength varies in the experiments from the value close to $0.6\lambda_{Di}\sqrt{(1 - P_0)/\tau} \approx (420$–$227)\,\mu$m ($n_i \approx 10^8$cm^{-3} and in these experiments $0.1 < P_0 < 0.4$) up to the value 5 times larger ((2100–1135)μm), and all these estimates should be divided by 3.3 for densities $n_i \approx 10^9$cm^{-3}.

Using both the theoretical and the experimental estimates of the mean-free path for the ion–dust collisions we find that it is much larger than the wavelength and the concept of the viscosity should not be used in analyzing the observations (although it was employed in [52]). The estimate of the mean-free path 1.2 cm was obtained by fitting the results and adding the viscosity term. In the conditions where the wavelength is much less than the mean-free path, the viscosity should be considered to be zero. The results of the linear dispersion obtained in [52] should be compared with the linear dispersion

curves in which the viscosity is neglected. It gives dependencies qualitatively similar to those obtained experimentally.

For the non-linear case, DISW convert to shock waves [52] and solitons [56]. To compare the experimental results with theoretical predictions, we should use the proper non-linear description. The complete derivation of the KdV equation in the range of existing DISW takes into account the ion–dust absorption and the dust charge variations [54]. Comparisons for future observations should be done with this more appropriate theoretical model. Here we mention the main qualitative results of the observations [53] and their qualitative understanding:

1. With an increase of the dust density the Mach number M as a function of the soliton's height becomes lower. This can be understood theoretically [54]: for usual KdV soliton the soliton's height is proportional to $(M-1)v_s$ and since in the presence of dust $v_s \propto 1/\sqrt{1-P_0}$ the Mach number M should be proportional to the height times $\sqrt{1-P_0}$ and thus decreases with an increase of P_0.
2. The width of the soliton is increased when the dust density increases. This can be understood from the known general dependence of the width of the KdV soliton and the soliton's height [54], where it is inversely proportional to the square root of the height and since the height is decreasing with the dust density the width should be increasing.
3. The damping of the soliton is approximately proportional to the dust density. This can be understood since the damping is produced by the ion–dust collisions which are proportional to P_0.

Thus the experimental results are understood qualitatively while the detailed comparison with the theory appropriate for the open complex plasmas is still the subject for future investigations. Similar statement can be given for the shock wave structures observed [52].

Here, general remarks should be given in connection with these observations:

- First, it is obvious that the use of device with a larger (as compared to the plasma crystal experiments) ion temperature up to $\tau \approx 0.1$ was an important feature of the experiments on DISW waves and shocks, and these larger values of the ion temperature are related with the lower pressure of neutral atoms which cannot equalize their temperature with plasma ions. The large ion temperature leads to the existence of a range of wave numbers where DISW are not heavily damped. Thus these experiments are not dealing with usual low-temperature plasmas where the plasma condensation is observed (where the pressure is 3–4 orders of magnitude higher and $\tau \approx 0.01$–0.02). For the latter conditions one can hope to observe DISW only for rather small dust sizes, $a/\lambda_{Di} \approx 10^{-3}$ or even lower where the dust grain charges are not so large and the plasma condensation does not occur.
- Second, these experiments open possibility for direct measurements of the ion–dust collision frequency, but again in the conditions close to plasma

condensation the rate of these collisions could differ from that of the low density limit.

- Third, although linear DISW cannot exist if the corresponding condition is violated, strong non-linear perturbations can exist and can propagate even in this case. These non-linear structures, when excited and supported externally, can exist also if the ion–dust collisions are strong. Then the structures formed are strongly dissipative and they can be experimentally investigated separately. From the theoretical point of view, the non-linear set of equations for these structure can be easily formulated with exact non-linearities taken into account (not weak non-linearities as for the KdV approach). For this purpose one can assume that the non-linear wave moves with a constant velocity determined by the Mach number M. Then the equations are converted to 1D equations which can be solved numerically. The equations are the equations of ion motion and ion-continuity including the dust charge variation but assuming the dust to be at rest. These equations were written when we discussed the elementary processes in complex plasmas where no assumptions on weakness of the non-linearities were done. An example of a strong dissipative structure obtained by the numerical solution of these equations is given in [55].

Figure 4.11 shows the strongly non-linear dissipative structure demonstrating the absence of DISW shock waves without an external support by the electric field pump [55]. The curves were obtained by numerical solutions of the hydrodynamic balance equations for a structure with a profile moving with the constant velocity u_0 in the absence of an external electric field. As we can see from Fig. 4.11, distributions of the parameters in the structure (shown in the frame of the wave) are quite unusual. The structure is propagating from right to left with the Mach number $M = -u_0\sqrt{2T_i/T_e} = 3$, at the far left from the front the complex plasma is assumed to be not disturbed and the usual balance of power for the ground state is valid. The ion density is much enhanced in the structure, the ion–dust collision frequency is somewhat decreased in the structure

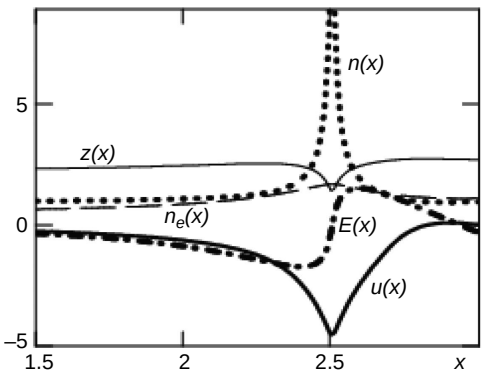

Fig. 4.11. Strongly non-linear dissipative structure: dependencies of the normalized ion drift velocity $u = u_i/\sqrt{2}v_{Ti}$, ion density $n = n_i/n_0$, electron density $n_e = n_e/n_0$, self-generated electric field $E = eE\lambda_{Di}^2/aT_e$, and dust charge $z = Z_d e^2/aT_e$, where n_0 is the ion density in the absence of the wave

because the charge of dust grains is decreased but the density of dissipation (per unit length) is highly increased because of the ion density enhancement in the structure.

- In general, the shock ion-sound waves as non–linear step-like structures with different values of the ion drift velocity on both sides of the shock front cannot exist in a complex plasma. Indeed, for the case of not-moving dust (which is true for the ion-sound disturbances) the ion motion is stopped by the ion-dust collisions and the ion drift velocity cannot be constant behind the shock even in the case where it is zero in front of the shock. This means that such structures, if observed, either should be supported externally (for example, by some external electric field behind the shock) or should not be stationary. Experimental observation of damping of an ion beam penetrating into dusty plasmas [27] is in a good agreement with the theoretical estimates obtained by using the ion friction given in the chapter devoted to the elementary processes in complex plasmas [27]. This supports the statement of the absence of stationary shocks in complex plasmas.
- Other various theoretical approaches used for DISW (except those of [12, 54]) do not take into account the power balance in the ground state as described above. Accounting for the power balance is the only way to determine the state on which the linear and non-linear perturbations develop.

4.4.3 Experimental Observations of DAW

We stressed many times that all waves in a complex plasma are completely changed in the low frequency and low wave number ranges. The first complete kinetic description of DAW [12] where the external source supporting the complex plasma was considered to be independent of plasma parameters has demonstrated that both the real frequency and the damping of DAW are quite different in a complex plasma as compared to the usual multi-component plasma [1, 6]. The full hydrodynamic description with a source proportional to the electron density was formulated in [12]. The frequency of the DAW kV_{DAW} (with v_{DAW} being the speed of DAW) obtained in [11, 12] is strongly dependent on the parameter P_0 and can approximately coincide with the expression given in multi-component approach only at high wave numbers and in the limit $P_0 \to 0$, i.e., in the case of effective absence of dust. It was also found in the kinetic consideration that the damping of DAW [11] is mainly determined by the charging frequency times P_0, and in the low frequency range $\omega \ll \nu_{ch} P_0$ the damping has an estimate, $k^2 V_{DAW}^2 / \nu_{ch} P_0$, very similar to the damping of usual acoustic waves in a neutral gas, $k^2 V_{AW}^2 / \nu$. The latter seems to be a natural result.

We do not intend to describe the kinetic description of DAW [11] here since such a description needs also a generalization for the case of the source depending on the plasma parameters and inclusion of the dust-drag effects,

which was included in [12]. We use here the definition of the ground state given above with a source proportional to the electron density. We also assume the power balance in the ground state which is necessary in any formulation of the linear theory. In some cases in this power balance the walls can be important where the ionized plasma component can recombine. This can happen only if the size of the system is less than the mean-free path for plasma absorption on dust grain, which can be estimated as λ_{Di}^2/aP_0. Since the opposite is valid for most experiments in complex plasmas, we assume the presence of the power balance in the ground state between ionization and absorption on dust. The DAW dispersion obtained [10, 21] by assuming the presence of the power balance that the losses are due to the plasma recombination on the walls (by simple expression for the frequency of losses $\nu_{loss} = v/L$, where L is the distance to the walls) differs from that found in [12] since the loss term of [10, 21] is independent of perturbations, while in [12] it depends on the electron perturbations and therefore on all other perturbations including the ion density, dust density, and dust charge perturbations. Since in most experiments the size of a plasma device is larger than the ion–dust mean-free path and the ionization source is proportional to the electron density, we use in comparison of the theory with experiments the results of [12] given in full theoretical description of DAW.

In a complex plasma, one cannot avoid variations of dust charges with disturbances of DAW being different in different parts of the wave profile. Also, the dispersion of DAW is also related with the imbalance of the ground state by DAW disturbances. The latter affects DAW in a way that the linear dispersion (where the frequency of the wave is proportional to the wave number) is valid only for large wave numbers approximately satisfying the inequality

$$k^2\lambda_{Di}^2 \gg P_0^2\alpha_{dr}\alpha_{ch}\frac{a^2}{\lambda_{Di}^2\tau}\,, \tag{4.61}$$

which together with the condition $\omega_{daw} \ll \omega_{pd}$ leads to the strong restriction (4.29). It is important to note that criterion (4.61) depends on the product of the charging and drag coefficients and therefore the simultaneous presence of both processes of the charging and drag is crucial for the changes in complex plasma responses. We remind here that in the case where (4.61) is valid, the DAW dispersion is described by

$$\omega_{daw} = kv_{daw}\,, \tag{4.62}$$

with

$$v_{daw}^2 = \frac{P_0 Z_d T_i}{m_d}\frac{1+z_0}{1+z_0+P_0+\tau(1+z_0-P_0z_0)}\,. \tag{4.63}$$

Thus linear relation (4.62) for DAW can exist only for small dust size particles (see relation (4.29)), i.e., when $a^2/\lambda_{Di}^2 \ll \tau$.

Deviations from the linear dependence (where the DAW frequency is proportional to the wave number) occurs both due to deviations from the quasi-neutrality and due to disturbances in the ground state, related with

the corrections in the small parameter existing due to inequality (4.59). The corrections are of the opposite sign and the opposite dependence on the wave number($\propto k^2$ and $\propto 1/k^2$) and are given by expression (4.30).

Let us briefly discuss the possible damping of DAW. Above we gave the damping rates for a given wave number k. Note that for externally driven systems (at frequency ω) the wave frequency is real and the wave number $k = k_r + ik_i$ is complex. The wavelength is related to k_r, and the damping or growth to k_i. The dispersion equation can be solved for k^2 as a function of ω^2. The wave damping, if small, is characterized by $k_i/k_r \approx \gamma/\omega$, the latter relation is written for the case where the wave frequency is found for a fixed k. Usually in experiments k_i and the ratio k_i/k_r are measured.

Apart from the damping mechanisms considered above in the hydrodynamic approach there can exist a kinetic mechanism of damping such as the Landau damping. First, the presence of the large factor $Z_d \gg 1$ in the expression for the DAW speed makes the speed not very small but still much larger than the dust thermal velocity $v_{Td} = \sqrt{T_d/m_d}$. Thus the Landau damping on dust grains being proportional to $\exp(-v_{daw}^2/2v_{Td}^2) \approx \exp(-P_0^2 Z_d^2 T_i/2T_d)$ is extremely small. Thus the Landau damping on dust grains is usually negligible. Second, the Landau damping on ions (which is much larger than that on electrons) is of the relative order $\omega_{daw}/kv_{Ti} \approx v_{daw}/v_{Ti} = \sqrt{Z_d P_0 m_i/m_d}$ and is also very small due to the large dust-to-ion mass ratio. As an example we can estimate the DAW speed for a typical current experiment with $a \approx 3\mu\text{m}\tau \approx 0.02$ to be $v_{daw} \approx (1-2)$cm/s, while the ion thermal speed for the room temperature is 3×10^4cm/s, which is four orders of magnitude larger.

Two effects related to the charging processes contribute to the damping: the first one directly related to the dust charging but modified by the change of the dispersion of the ground state and the second one related to the dissipation due to the imbalance of the ground state. The first effect has a relative order of $\omega_{daw}/\nu_{ch} \ll \omega_{pd}/\nu_{ch} \ll 1$ and the second effect is due to the mutual influence of drag and charging process and is proportional to the product of the charging and the drag coefficients. An important point is that the latter within the range of existence of DAW is determined by only a dispersion effect described by the first term of (4.30), which is always small (as soon as the range of existence of the linear relation for DAW is considered) and is also proportional to the small factor of the order of ω_{daw}/ν_{ch}, which is less than $\omega_{pd}/\nu_{ch} \approx \sqrt{m_i Z_d P_0/m_d}(\lambda_{Di}/a \ll 1)$. The difference between these two damping mechanisms is that the first one is proportional only to the charging coefficient while the second one is proportional to both charging and drag coefficients. They become of the same order of magnitude at the lower possible frequency of existence of DAW given above.

Finally, the damping of DAW can be related to the collisions with neutral atoms. The latter seems to be the most important in experiments. The corresponding ratio $k_i/k_r \approx \nu_{nd}/2\omega_{DAW}$ is nevertheless also small if $k \ll k_n = \nu_{dn}/V_{DAW}$. For a typical experiment with the pressure of a few tenths of mbar

that would correspond to the wave length $\lambda = 2\pi/k_n \approx (6-1)\cdot 10^2$cm while the actual wavelength is usually equal to a few fractions of cm. We therefore concentrate our attention on the general expression for the real part of the DAW frequency which takes also into account the dust charge variation and the presence of deviations of the DAW dispersion from the linear law.

For experimental measurements of DAW there exist two other limiting wavelengths: the first one is related to the system size L, and the second one is related to the mean micro-particle separation. The second one marks the transition from waves propagating in the "system" to the situation where the "system" has to be regarded as a local perturbation of a much larger field (another example is ocean waves, where a patch seaweed simply follows the wave wells but does not influence the waves significantly whereas a large oil slick has a profound effect on the waves). The latter marks the limit of the wave propagation due to the lack of information transport, which microscopically is due to discrete particle interaction (this is equivalent to the Debye frequency in crystals, which limits the acoustic wave propagation and is discussed in somewhat more detail in the context of the dust-lattice waves in Chap. 7.

First observations of DAW in laboratory dusty plasmas were reported shortly after the discovery of plasma crystals [56, 57]. These waves were self-excited in a dusty plasma, and further observations have been reported since then in many different experiments [58, 59, 60]. Clearly one of the important tasks for future studies is investigation of the instabilities leading to and associated with the wave production. Figure 4.12 shows schematically the glow discharge device used in experiments [56, 57, 58, 59, 60], and Fig. 4.13 shows the picture of the measurements of compressional DAW in the DC discharge plasma. The density peaks and rarefications of the micro-particle population are easily recognized.

The ion densities were $n_i \approx (4\text{–}8)\times 10^8\text{cm}^{-3}$ with the ion temperature (0.03–0.1)eV and the electron temperature 2.5eV, which correspond to $\tau \approx 0.04\text{–}0.013$, $\lambda_{Di} \approx (640\text{–}360)\mu$m, and since the dust size used was 0.7μm, the ratio of the dust size to the Debye length was $a/\lambda_{Di} \approx (2\text{–}1)\times 10^{-3}$. The condition necessary for the existence of DAW can be written as $(4\times 10^{-6} \ll 10^{-2})$ in this case. The measured wave numbers were in the range

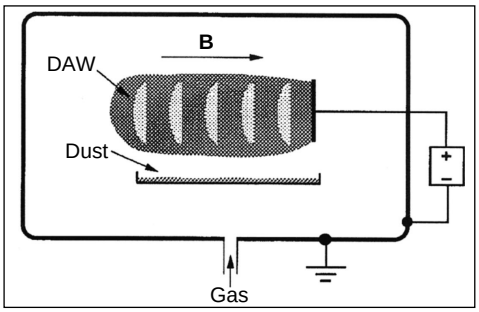

Fig. 4.12. Schematic diagram of the glow discharge device used to trap the negatively charged dust and observe DAW [56]

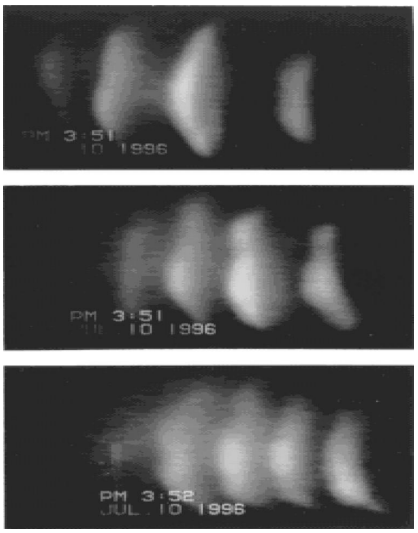

Fig. 4.13. Compressional DAW in DC discharge plasma. Several dust acoustic fronts are shown [56]

(5–15)cm^{-1} and thus $k\lambda_{Di} \approx 0.1$–$0.3$ when the contribution of the second term in the dispersion relation (4.30) is 0.01–0.1. The gas used was nitrogen and the charging equation gives $z_0 \approx 2$, $Z_d \approx 2 \times 10^3$, with $n_d \approx 10^5$cm^{-3}, which means that $P_0 \approx (0.5$–$0.3)$. For these parameters, contribution of the first dispersion term in (4.30) is approximately 0.1 for the lowest measured $k \approx 5$cm^{-1}, while the contribution of the second dispersion term is 0.01. Thus the dispersion should be related with this effect.

This can be seen from the experimentally measured dispersion relation shown in Fig. 4.14. The open circles in Fig. 4.14 correspond to the experimentally measured values, while the line is drawn corresponding to the multi-component approach. It can be seen from this figure that the DAW phase velocity should have a lower value than that predicted by the multi-component approach and the straight line for the theoretical prediction should go higher, for $z_0 = 2$, $P_0 \approx 0.5$, the decrease of the phase velocity is only 8%, but it better fits the observations and suggest directly that the dispersion is the one

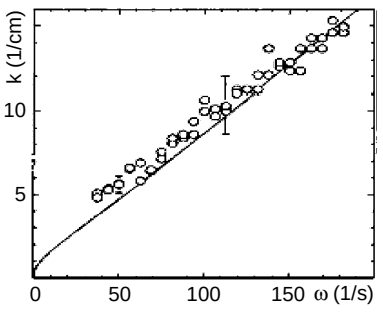

Fig. 4.14. Measured dispersion relation for DAW [56]

determined by the first term of (4.30), i.e., opposite to the usual dispersion for sound wave in a plasma. More precise measurements are of course desirable to perform in future to check all new features of DAW.

Controlled experiments, where the waves were excited externally, either by sinusoidally varying potential on a wire located in the plasma chamber or by chopped laser light pressure, were first reported in [56] and initiated a highly successful and growing research technology employing "active manipulation experiments". We do not describe these experiments here, but refer to them in the following chapters in the context of the dust-lattice waves and dust shear waves.

Now let us stress the most important points:

- Investigations of the DAW dispersion can serve as an effective method to determine parameters of complex plasmas. Generally, it includes investigation of the wave damping. The above consideration of elementary processes in a complex plasma allowed us to find directly (in the most simplest way) the dielectric response functions which include all the dispersion and damping effects by taking into account changes of the ground state (see expression (4.24)).
- The imaginary part in the first two terms in the wavy brackets of (4.24) describes the charging damping (sometimes named as "Tromso damping" [56]) but generalizes it by taking into account the dispersion produced by the ground state. The expression given here corresponds to the general description of such damping for the ground state defined by the mentioned balance conditions. The dispersion effect (dependence of the wave velocity on the wave number) vanishes in the case where the drag is not taken into account. The dispersion is important for any complex plasma system with a size larger than the charging length.
- In (4.24) and (4.30), the damping related with both the charging and the drag effect enters only in the dispersion terms $\propto 1/k^2$ and this damping is determined by the product of charging and drag coefficient (this means that in the absence of one of these effects both the dispersion and the damping related with the background change disappear). The damping described by these terms can be named as a "creation damping" (term used in [56]), having in mind that the plasma particles are continuously absorbed by dust grain and are replaced by "new" ions injected in the space. The exact formulation of this effect can be made only if one initially starts with a formulation of the basic state by using the power and particle balance equations as we have done here.
- The most important effect introduced by the basic state variations and the "creation damping" is that DAW do not exist (or are strongly damped) for small wave numbers approximately determined by relation (4.61). Expression (4.30) can be used to find the exact value of the critical wave number. This effect of the absence of low-frequency DAW is one of the most interesting to check in future experiments.

Finally, experimental observation of the dust-lattice waves and dust shear waves are discussed in sections devoted to experiments on dust crystals and dust clusters.

4.5 Problems to be Solved for Collective Modes

4.5.1 Structurization Instability and the Finite System Effects

The main problem of describing the modes in a complex plasma is that it has a natural tendency for structurization, dividing itself into (non-linearly equilibrium) stationary non-homogeneous structures. The inhomogeneity of these structures complicates the mode investigation since their wavelength is changing substantially in space. This problem should be solved individually for each type of the structure which can also depend on the boundary conditions related to the presence of walls. The boundary-free structures have also complicated distributions of complex plasma parameters since they are surrounded by finite-size voids (see Chap. 8). The propagation of waves through the dust-void surfaces creates the problems of the collective wave reflection from the surface of the dust voids and the wave propagation through the dust-void surface. The collective modes at one side of the dust void can be different from the collective modes at the other side of the void. This rises the problem of the collective mode transformation during the processes of wave reflection and transmission through the dust-void surface. The wave emission by sources like probes in the dust inhomogeneous structures and in dust voids is another problem arising in connection with the inhomogeneities of the dust structures. The new instabilities can also be driven by these inhomogeneities (similar to the drift instabilities in ordinary plasmas). All these problems are waiting to be solved.

4.5.2 Surface Waves

The appearance of a sharp boundary at the void surface creates a new problem of surface waves which can propagate close to the surface. The dust-void surface itself is also a complicated self-organized structure with strong inhomogeneity of structure parameters on its both sides. There does not exist so far any detailed investigation of the surface collective waves in a complex plasma. The most interesting problem is to solve them for the non–linear self-consistent treatment of the surface boundaries.

4.5.3 Induced Processes for Collective Modes

In ordinary plasmas, the wave-induced processes are well described by the so-called quasi-linear approach, which allows to self-consistently consider both the excitation of modes and their effect on the particle distributions. No

real effort has been taken so far for the generalization of this approach for a complex plasma although one can foresee many applications and use of such approach for future physics of complex plasmas. This should include also a self-consistent treatment of the dust charging including the change in the electron and ion distributions due to the charging process. The first steps in this direction were done in [35] using the new collision integrals for complex plasmas [26, 33, 36].

4.5.4 Collective Modes in the External Magnetic Field

The role of magnetic fields on the mode propagation in ordinary plasmas is a very large research topic [1]. Currently there is no such a detailed investigation of magnetic modes in complex plasmas. The existing papers on this subject do not contain the important starting point by not considering the basic state taking into account both the quasi-neutrality and the balance of power. The changes that can happen due to the magnetic field's influence on the UI have not been investigated so far.

4.5.5 Instabilities in Complex Plasmas

Consideration of instabilities of the beam-type distributions taking into account the balances in the basic state has not been done yet. This is also true for other types of instabilities such as the ring instability, or the instability due to the temperature anisotropy, or the loss-cone instability. All these topics are waiting to be investigated. In the presence of non-equilibrium distributions we should include other parameters which support the non-equilibrium ground states. For example, for the beam instability there should exist a source in the basic states which supports the velocity of the beam.

4.5.6 Non-linear Responses

In ordinary plasmas, non-linear responses are investigated in detail both theoretically and experimentally. No such attempts were made in complex plasmas. Without an answer to the problem of possible saturation of complex plasma instabilities by non-linear effects, it is difficult to draw a finite conclusion of the role of various instabilities. In principle, non-equilibrium distributions can be stabilized by non-linearities.

4.5.7 Strong Non-linearities and Modulational Interactions

The analogue of the set of Zakharov equations was written [61] but no further development of the problem of modulational instabilities and modulational interactions has been seen so far. This topic is very important for the problem of strong laser interactions with a complex plasma. The subject can be developed using the analogy with ordinary plasmas [62]. The parametric instabilities in complex plasmas is one of the topics to be solved in this context.

4.5.8 Kinetic Description of Collective Modes

Such a description should be based on the kinetic equations for complex plasmas taking into account the charge variability and the collision integrals. Only few steps have been taken in this direction [11, 26, 33, 34, 35, 36, 37]. Thus there exists a large field open for research.

4.6 Fluctuations, Collective Pair Interactions, and Pair Correlation Functions

This section serves as a bridge to the subsequent two chapters. On the one hand, all linear responses relate different quantities and in the case one finds correlations between some of them one can in first approximation find correlations between others. In the simplest kinetic approach [14] linear fluctuations determined by the linear dielectric function describe pair collisions which take into account all collective effects. We remind this result in the present section. In a complex plasma, a similar (although more complicated) procedure can take into account both the existence of a new basic state and the linear responses accounting for the collective effects [33]. In principle, if the kinetic responses are known, one is able to calculate directly all collective pair-grain interactions. In reality, this can be done only for the case of linear responses which we discussed above. We gave only a simple hydrodynamic average description of them but they take into account all new effects related with the presence of fluxes in a complex plasma system. It is a long and complicated way to generalize all linear responses for the kinetic description and this has not been fully performed yet. This way can lead to an exact and sophisticated description of the pair-grain interactions. But this is applicable only in the limit $\beta \ll 1$, whereas we are interested in both limits including specially the limit $\beta \gg 1$. To avoid the complicated treatment we can deal with the "test particle approach", which is much more simple and can give us the main new physical results of the collective grain interaction. Namely, it is shown (at least in the present plasma theory) that the particle interaction in the system is finally described in the same manner as any "test particle" embedded in plasma. Therefore we use the test particle interactions to describe the background ("sea") of many grains. This gives us information of real collective grain interactions in both limits $\beta \ll 1$ and $\beta \gg 1$.

4.6.1 Relations between Various Fluctuations

Fluctuations in a complex plasma can be of different types. First, there are fluctuations in the absence of collective fields which we call the "zero fluctuations"; second, there are fluctuations due to collective fields of waves (in the range where the collective waves can exist); and third, there are fluctuations of fields in the unstable ranges leading either to plasma condensation or to the

formation of a system of inhomogeneous dust clusters and dust voids. Up to this moment we discussed properties of average complex plasma parameters such as the number densities of all components n, n_e, n_d, the dust charges Z_d, etc., i.e., values averaged on the statistical ensemble. We denote such an average by angle brackets $\langle \ldots \rangle$. We denote the deviations from the average values by adding δ in front of the corresponding value. By definition for fluctuating parts of the corresponding complex plasma parameters we have

$$\langle \delta n \rangle = \langle \delta n_e \rangle = \langle \delta n_d \rangle = \langle \delta Z_d \rangle = 0 \, . \tag{4.64}$$

In the kinetic description, plasma particles are described by the particle distributions f in the particle velocities $\boldsymbol{v}$ or particle momenta $\boldsymbol{p}$. These distributions also have fluctuations δf (integration with respect to the velocities or with respect to the momenta leads to fluctuations of the densities). If the fluctuations are small (which is often the case for large systems in the first approximation), they can be considered as linear. The linearizations done above when describing deviations from the ground state of a complex plasma to describe the complex plasma waves and instabilities can also be used for fluctuations. Thus different fluctuations of the linear approximation are related to each other.

Due to relation (4.64) only the expressions containing the squares of fluctuations are not zero when averaged. Thus one can speak about fluctuations of densities describing them by $\langle (\delta n)^2 \rangle$ or about fluctuations of grain charges describing them by $\langle (\delta Z_d)^2 \rangle$. Due to the approximate linear relation between all fluctuations it is possible to express one type of fluctuations through another type of fluctuations by the linear relations given above in the previous sections. Thus the fluctuations of densities $\langle (\delta n)^2 \rangle$ can be simply expressed through the fluctuations of dust charges $\langle (\delta Z_d)^2 \rangle$. Also, the averages of combinations of different fluctuations, for example $\langle \delta n \delta Z_d \rangle$, can be expressed through the $\langle (\delta Z_d)^2 \rangle$. Such relations between fluctuations exist only as approximate relations since they are valid only in the linear approximation. The non-linearity can cause deviations from these relations. These non-linearities become especially important for all unstable modes. But in the case where the fluctuations are weak, the use of the linear expressions for expressing one type of fluctuations through another one is a reasonable approximation. The presence of relations between different fluctuations is an example of collective effects.

It is well known that phase transitions are accompanied by large fluctuations of all parameters which should be present and measured in the process of plasma condensation in a complex dusty plasma. These fluctuations are linear only in the initial stage of the transitions. The obvious new effect existing in a complex plasma is the variability of dust charges which leads to fluctuations of the charges. These fluctuations obviously should be taken into account in any approach for phase transitions in a complex plasma. Also it is probable that these fluctuations can play a dominant role in phase transitions for certain range of parameters. The theory of the phase transition to the strongly correlated state in a complex plasma is not developed yet. But

this comment should be taken into account in its future development. The particle interaction, as was already mentioned, is related to fluctuations. As we demonstrate, the fluctuations of the plasma fluxes and fluctuations of the grain charges introduce new type of the grain interactions.

We should distinguish the spontaneous fluctuations (often called as the "zero fluctuations") and the fluctuations created by random fields of waves and instabilities, i.e., the induced fluctuations. For phase transitions, the induced fluctuations play a dominant role. In all regions of the UI, the fluctuations are growing causing the transition either to the structurized state of the complex plasma or to plasma condensation. The dust charge fluctuations are also growing in these ranges together with other fluctuations of the complex plasma system.

It is important that even the zero fluctuations are deeply related to the pair particle interactions, which become collective in the sense that the interaction of each pair of probe particles in the system depends on other parameters of the system such as the average densities, etc. In particular, the pair-grain interaction depends on the average value of the parameter P_0, which is determined by the average grain density and the average grain charge. This effect can be foreseen for all previously known results of plasma physics. In the present plasma physics, collisions of two particles, scattering of waves on particles, and other effects are known to be collective [14]. Fluctuations of the grain charges as well as the pair-grain interactions should be collective as well, i.e., depending on other averaged complex plasma parameters.

4.6.2 Correlation Functions

Fluctuations at different positions in space can be related with each other, which is clear when, e.g., they are caused by propagation of random waves in the system. Fluctuations at different moments of time can be related to each other by the same reason or due to development of an instability (an instability can cause the wave randomization via non-linear interaction of different modes). Thus it is useful to investigate the so-called correlation functions. For example, in the case we are interested in the relations between densities at different positions in space we should investigate the pair correlation function $\langle \delta n(\mathbf{r}) \delta n(\mathbf{r}') \rangle$ and when we are interested in correlations in time at the same position in space we investigate the value $\langle \delta n(t) \delta n(t') \rangle$. In general, the full correlation function is $\langle \delta n(\mathbf{r}, t) \delta n(\mathbf{r}', t') \rangle$. Often (when the system is homogeneous) the correlation functions depend only on $\mathbf{r} - \mathbf{r}'$ since the displacement of both $\mathbf{r}$ and $\mathbf{r}'$ should not change the correlations of fluctuations. In the case the system already reaches a stationary state the time correlations depend only on $t - t'$. All these correlation functions are the subject of experimental investigation during developments of instabilities as well as for the stationary states, e.g., the plasma condensation. In the latter condition, often investigated is the correlation function integrated with respect to the time difference and therefore depending on the space separations $\mathbf{r} - \mathbf{r}'$ only. In the case of an

isotropic state these pair correlation functions depend only on $|\mathbf{R}| = |\mathbf{r} - \mathbf{r}'|$. Experimental investigations of these correlation functions are often used to determine the long-range order in the system and to prove that the system is converted to a crystal or liquid state. As we mentioned, there can exist fluctuations without instabilities – the zero fluctuations or the non-collective spontaneous fluctuations. They also play an important role. Due to development of UI, there always exist the grain charge fluctuations excited by the UI fields. But the ranges and the frequencies of these induced fluctuations are usually different from those of the zero fluctuations.

The pair correlation functions are important characteristics of a complex plasma in the phase transitions and in the final correlated states. An important point is that the correlation functions are determined by the collective pair interactions and by other collective phenomena in a complex plasma. Therefore their investigation is related to experimental methods of measurements of complex plasma collective effects.

4.6.3 Zero Fluctuations and Collective Pair Interactions of Grains

Already in an ordinary plasma in the absence of dust an important result was obtained showing that the pair correlations of particles are deeply related with their pair interactions. The simplest and the oldest result is the investigation of changes of the average particle distributions due to the spontaneous zero fluctuations. By the term 'zero fluctuations' we mean such fluctuations in a large system which occur when the particles do not interact at all. It is known from any course of statistical physics [63] that in this case the fluctuation of the total number of particles N (denoted as δN in the system volume V) satisfies the relation $\langle(\delta N)\rangle^2 = \langle N\rangle$. This relation can be written for the correlation function for fluctuations of the particle distribution function f as $\langle \delta f(\mathbf{r}, t)\delta f(\mathbf{f}(\mathbf{r}', t')\rangle$.

Via the Poisson's equation, the zero particle fluctuations excite the zero fluctuations of the electric field and the latter change the distribution of the average distribution function $\langle f\rangle$. An additional term in the equation for $\langle f\rangle$ is obtained by averaging the zero fluctuations of the expression $\langle \delta\mathbf{E}\delta f\rangle$ on the right-hand side of the equation for $\langle f\rangle$; it is called the Landau–Balescu collision integral and its simplest derivation in two lines is given, e.g., in [14]. This integral can be written through the probability of the pair collisions $w_{\mathbf{p},\mathbf{p}'}(\mathbf{k})$, where $\mathbf{p} = m\mathbf{v}$ and $\mathbf{p}' = m'\mathbf{v}'$ are the momenta of two colliding particles and $\mathbf{k}$ is the momentum transferred during the collisions from one particle to another. We have

$$\frac{d\langle f\rangle}{dt} = \frac{\partial}{\partial p_i}\int w_{\mathbf{p},\mathbf{p}'}(\mathbf{k})k_i k_j \left(\langle f'\rangle\frac{\partial\langle f\rangle}{\partial p_j} - \langle f\rangle\frac{\partial\langle f'\rangle}{\partial p'_j}\right) d\mathbf{k}d\mathbf{p}' \,, \tag{4.65}$$

where

$$w_{\mathbf{p},\mathbf{p}'}(\mathbf{k}) = 2e^2(e')^2\frac{1}{k^4|\epsilon_{\mathbf{k},\mathbf{k}\cdot\mathbf{v}}|^2} \,. \tag{4.66}$$

We present here this equation well known from the textbook [14] in order to demonstrate that in the usual plasma physics (where dust is absent) the probability of the pair collisions of two particles with the charges e and e' depends on the dielectric function $\epsilon_{\mathbf{k},\omega}$ which in turn obviously depends on the distributions of all other plasma particles. The pair interactions in plasmas are not the bare Coulomb interactions but are interactions of dynamically screened particles where the screening is produced by all other particles. Therefore the collisions are collective and the pair interactions and pair correlations depend on other particle distributions in the screening process. The pure Coulomb collisions correspond to the probability without the factor $1/|\epsilon|^2$. Therefore the full expression for the collisional cross section depends on the distributions of all other particles in the system, i.e., the pair interactions of particles in a plasma are collective.

In a complex plasma, there are more plasma components but the conclusion that the pair interactions are collective holds in general, and in particular, that the pair interactions of grains are collective depending on the grain density (or in general on the grain velocity distributions). This conclusion is very important and in the next chapter we describe these interaction in details. It also means that the pair correlation function of grains can be determined by the collective dust interactions which in turn means that the phenomenon of the complex plasma condensation can be determined by the collective grain interactions. From these arguments, we find the criteria for plasma condensation and demonstrate that in current experiments where the complex plasma condensation was observed the most probable condensation mechanism is the collective dust interaction, which appears to be the collective attraction at certain distances; the latter can be foreseen due to the analogy between UI and GI.

4.6.4 Dust Non-collective Charge Fluctuations

Consider here the zero fluctuations of the dust charges. Other fluctuations induced by the wave fields and instabilities can be treated similarly by substituting the correlation functions of these fields for the correlation function of zero fields. Note that although this kind of investigation of the induced fluctuations has no principle difficulties and predictions can be experimentally checked there does not exist any full investigation of the induced fluctuations so far.

Since all zero non-collective fluctuations of various parameters of a complex plasma are related one-to-one with the dust non-collective charge fluctuations, we illustrate here their derivation from a simple model. The dust charge fluctuations can be treated as a result of discreteness of the charging process. Due to the fact that the change of the dust charge is discrete – it is either equal to the electron charge $-e$ for dust absorption of a single electron or to $+e$ for dust absorption of a singly ionized ion. In plasma physics, discreteness is usually treated as a fluctuation of the electron and ion distribution function.

These fluctuations should lead to fluctuations of plasma currents on dust particles and therefore should lead to fluctuations of dust charges. The important question is, are these two possible treatments of the dust charge fluctuations identical? The answer is that the treatment of the dust fluctuations as due to the fluctuations of plasma currents on a dust particle is more general including in certain limit the effect due to discreteness of the charging process (the zero fluctuations of the electron and ion distributions).

In existing literature, the effect of discreteness of the charging process was first considered in [64, 65] (see also [66]) and the fluctuations of plasma currents on dust particles were first treated in [67]. It can be shown that the result [66] coincides with that obtained from the fluctuation of the electron and ion particle distributions due to their discreteness only in the limit where the electron and ion fluctuations can be considered as independent particle fluctuations, i.e., as parts of non-collective fluctuations. These types of fluctuations are known in the physics of plasmas as free particle fluctuations; other important plasma particle fluctuations are known as induced fluctuations [14].

The role of fluctuations induced by dust is the most important for the problem of complex plasma condensation [33]. The importance of this process is obvious since the electron and ion fluctuations in the dust charging (and therefore the dust charges) can be induced by the dust particles which absorb electrons and ions and therefore depend on dust fluctuations. Thus the corresponding treatment [33] relates the dust fluctuations with the long-range correlations in strongly correlated states.

Here, we consider the problem of the electron and ion fluctuations as fluctuations of independent particles neglecting the induced fluctuations related with electrons and ions as well as with dust. Mention that this problem was considered before [33, 66], and the results coincide with each other. Therefore we describe here the method [66] which is less general but more transparent. The distribution of fluctuations considered in [66] is a Gaussian one with the width equal to the charging frequency. The charge of each dust particle (when the collective effects are neglected) is considered to fluctuate independently and these fluctuations are not related with the collective processes in complex plasmas. The dust density could enter in these fluctuations from the quasi-neutrality condition as a kind of electron "contamination" by dust. We start with the non-collective fluctuations of the dust charges. First, we consider the approach treating fluctuations due to discreteness of the charging process. Then we consider the effect related with the discreteness of the electron and ion distributions leading to the current fluctuations due to independent electron and ion fluctuations.

Dust particles embedded in a plasma are generally multiply charged with $Z_d \gg 1$. Due to normal statistical fluctuations associated with the discrete impact of individual electrons and ions, the charge Q (and in turn the surface potential ϕ_s) of the dust particle fluctuates.

The Fokker–Planck description of the particle charging due to the discreteness of the charging process considers the charge fluctuations as resembling the Markov process: the charge varies in steps of $\pm e$, with the probability per unit time for the positive change given by I_i and for the negative change given by I_e (remember that by definition I_i and I_e are respectively the ion and electron currents on the total dust surface per absolute value of the electron charge $e > 0$). The probability $f(Q)$ for the particle to have the charge Q at the time moment t is then given by [66]:

$$\frac{\partial f_Q}{\partial t} = I_i f|_{Q-e} - I_e f|_{Q+e} - (I_i - I_e) f|_Q \ . \tag{4.67}$$

Equation (4.67) assumes that both the charging currents and the probability depend on the instantaneous charge $(Q-e, Q, Q+e)$ but not on the previous history. This is reasonable, provided the "history" in, e.g., plasma fluctuations occurs on sufficiently longer timescales and can be regarded as secular.

Treating Q as a continuous variable with the probability $f(q)$, normalized as

$$\int f_Q dQ = 1 \ , \tag{4.68}$$

we linearize the charging current around the steady state $\langle I_e \rangle + \langle I_i \rangle = 0$. We have

$$I_e + I_i = \delta Q(\langle I'_e \rangle + \langle I'_i \rangle) + \delta I_i + \delta I_i \ . \tag{4.69}$$

Then we neglect the fluctuating currents δI_e and δI_i; this yields the diffusion–convection type of equation

$$\frac{\partial f_Q}{\partial \tau} = \frac{\partial}{\partial Q}(\delta Q f_Q) + \langle (\delta Q)^2 \rangle \frac{\partial^2 f_Q}{\partial Q^2} \ , \tag{4.70}$$

where $\delta Q = Q - \langle Q \rangle$, and

$$\tau = \frac{t}{\tau_{ch}} = -te(\langle I'_e \rangle + \langle I'_i \rangle) \ , \tag{4.71}$$

with the steady state charging time tau_{ch}. For the OML model we find

$$\langle (\delta Q)^2 \rangle = \frac{e}{2} \frac{\langle I_e \rangle - \langle I_i \rangle}{\langle I'_e \rangle + \langle I'_i \rangle} \ , \tag{4.72}$$

which is the averaged square of dust charge fluctuation. This can be seen from the stationary solution of equation (4.70):

$$f(\delta Q) = \frac{1}{\sqrt{2\pi}\langle (\delta Q)^2 \rangle} \exp\left(-\frac{(\delta Q)^2}{2\langle (\delta Q)^2 \rangle} \right) \ . \tag{4.73}$$

For the considered OML model, a simple substitution of currents in the last expression yields

$$\frac{\delta Z_d^2}{Z_d} = \frac{\tau + z}{z(1+\tau+z)} \approx \frac{1}{1+z} \,, \tag{4.74}$$

where Z_d is, as before, the equilibrium dust charge in the units of the electron charge, and the last approximate expression is written in the limit $\tau \ll 1$.

As expected, the square root of the average square fluctuation of the dust charge is of the order of the equilibrium dust charge (although lower than it). This is the main result for the non-collective fluctuations of the dust charge. In reality the fluctuations of the grain charge are much larger in the UI range. These fluctuations are not spontaneous but are the fluctuations induced by the fields of the developing instability.

Temporal evolution of the dust particle charge can be written also as the Langevin equation

$$\frac{\partial Q}{\partial t} = -eI_e + eI_i + g(t) \,, \tag{4.75}$$

where $eI_i - eI_e = -(Q - \langle Q \rangle)/\tau_{ch} + \ldots$ ("..." stands for higher-order terms) is the linearized net current on the dust particle, and $g(t)$ is the stochastic forcing function with the zero mean. For non-correlated fluctuations, as assumed in equation (4.67), the forcing function has to satisfy

$$\langle g(t)g(t+t') \rangle = 2\tau_{ch} \langle (\delta Q)^2 \rangle \delta(t - t') \,, \tag{4.76}$$

where $\delta(t)$ is the Dirac delta function. Using this framework, it is possible to quantify the "lifetime" of a given charge fluctuation $|\delta Q|$ (i.e., the growth and dissipation times) as well as the charge auto-correlation function, power spectrum, etc. For instance, the auto-correlation function of the charge fluctuations is given by

$$\langle Q(t)Q(t+t') \rangle \propto \exp\left(-\frac{t'}{\tau_{ch}}\right) \,, \tag{4.77}$$

and the power spectrum is the Lorentzian one with the characteristic frequency $1/\tau_{ch}$.

The time of the charge fluctuations to grow from $\langle Q \rangle$ to $\langle Q \rangle + |\delta Q|$ is given by

$$t_{grow}(\delta Q) = \tau_{ch} \sqrt{\frac{\pi}{2}} \int_0^{|\delta Q|/\sqrt{\langle (\delta Q)^2 \rangle}} \exp(x^2/2) erf\left(\frac{x}{\sqrt{2}}\right) dx \tag{4.78}$$

and, correspondingly, the time required for the charge fluctuations to dissipate back to the equilibrium value from $\langle Q \rangle + |\delta Q|$ to $\langle Q \rangle$ is

$$t_{diss}(\delta Q) = \tau_{ch} \sqrt{\frac{\pi}{2}} \int_0^{|\delta Q|/\sqrt{\langle (\delta Q)^2 \rangle}} \exp(x^2/2) \left(1 - erf\left(\frac{x}{\sqrt{2}}\right)\right) dx \,. \tag{4.79}$$

This kind of theoretical derivation can be compared with Monte Carlo simulations and OML results (4.74) for the Maxwellian (non-fluctuating) distributions of electrons and ions. The result of such comparison shows a good

agreement between the Monte Carlo calculations and the theoretical fits based on the Fokker–Plank model. The numerical values were obtained for argon with T_e =1eV, $T_i = 500K$, $n_i = n_e = 10^9\text{cm}^{-3}$. Note that both the theory and the simulations take into account only the discreteness of the charging process. As mentioned, the result of [33] obtained from the zero fluctuations of the electron and ion distributions coincides with that of [66]. The new result of [33] which cannot be seen so clearly from the approach [66] is that the contributions of plasma electrons and ions in the fluctuations of the dust charge are equal.

4.6.5 Charge Fluctuations Induced by Dust Fluctuations

Important is the possibility of generalization of the current fluctuations used in [33] by taking into account induced fluctuations through the plasma and dust responses. The dust fluctuations induce additionally the electron and ion fluctuations, which results in the grain charge fluctuations. The result [33] is given by

$$\frac{\langle \delta Z_d \rangle^2}{Z_d^2} \approx n_d a \lambda_{Di} \frac{z^2}{\tau^2 (1+z)^2} \ . \tag{4.80}$$

For typical data of current experiments $a = 3\mu\text{m}$, $d_i = 30\mu\text{m}$, $n_d = 3 \times 10^3\text{cm}^{-3}$, and $\tau/z = 10^2$, we find that for the collective fluctuations $\langle (\delta Z_d)^2 \rangle / Z_d^2 \approx 4{\times}10^{-3}$, while for the non-collective fluctuations $\langle (\delta Z_d)^2 \rangle / Z_d^2 = 1/Z_d(1+z) = 3 \times 10^{-5}$. That is, the latter is two orders of magnitude lower, which means that in laboratory conditions the dust charge collective fluctuations can be much larger than those (expected earlier) non-collective fluctuations. This is an important point for further developments related with the role of the dust charge fluctuations in the plasma condensation to the strongly correlated states.

References

1. A. Mikhailovskii (1974). *Instabilities in Inhomogeneous Plasma*. Consultants Bureau.
2. S. Benkadda P. Gabai, V. Tsytovich, and A. Verga (1996). *Phys.Rev. E* **53**, 2717.
3. S.V. Vladimirov and V.N. Tsytovich (1998). *Phys. Rev. E* **58**, 2415.
4. S.Benkadda and V.Tsytovich. (2002), *Plasma Phys.Rep.* **28**, 432–435.
5. N. Rao, P. Shukla, and M. Yu (1990). *Planet. Space Sci.* **38**, 543.
6. P. Shukla and V. Silin (1992). *Phys. Scr.* **45**, 508.
7. M. Rosenberg (1993). *Planet. Space Sci.* **41**, 229.
8. M. Rosenberg (1996). *J.Vac.Sci.Technol.A* **14**, 631.
9. M. Rosenberg and V. Chow (1998). *Planet.Space Sci.* **46**, 103.
10. K.N. Ostrikov, S.V. Vladimirov, M.Y. Yu, and G.E. Morfill (2000). *Phys. Plasmas* **7** 461.

11. V. Tsytovich, U. de Angelis, and R. Bingham (2001). *Phys. Rev. Lett.* **87**, 185003.
12. V. Tsytovich and K. Watanabe. (2003) *Contr. Plasma Phys.* (Germany), **43**, 51–61, preprint NIFS-720 (2002).
13. S.V. Vladimirov, K.N. Ostrikov, and M.Y. Yu (1999). *Phys. Rev. E* **60**, 3257.
14. V. Tsytovich (1995). *Lectures on Nonlinear Plasma Kinetics*, Springer Verlag, Berlin.
15. V. Tsytovich, U. de Angelis, R. Bingham, and D. Resendes (1997). *Phys.Plasmas* **4**, 3882.
16. G. Morfill and V. Tsytovich (2000). *Plasma Phys.Rep* **26**, 727–736.
17. F. Melanso (1996). *Phys. Plasmas* **3**, 3890.
18. S.V. Vladimirov, P.V. Shevchenko, and N.F Cramer (1997). *Phys. Rev. E* **56**, R74.
19. S.V. Vladimirov, P.V. Shevchenko, and N.F Cramer (1998). *Phys. Plasmas* **5**, 4.
20. S.V. Vladimirov, V.V. Yaroshenko, and G.E. Morfill (2006). *Phys. Plasmas* **13** 030703.
21. A. Ivlev and G.Morfill (2000). *Phys.Plasmas* **7**, 1094.
22. F. Melandso, T. Aslaksen, and O. Havnes (1993). *J.Geophys.Res.* **98**, 13315.
23. V. Tsytovich and O. Havnes (1993). *Comments Plasma Phys.Contr. Fusion* **18**, 267.
24. S.V. Vladimirov (1994). *Phys. Plasmas* **1**, 2762.
25. V. Tsytovich and D. Resendes (1998). *Fiz.Plasmy* (Russia), **24**, 71.
26. V. Tsystovich and U. de Angelis (1999). *Phys.Plasmas* **6**, 1093.
27. Y. Nakamura, V. Tsytovich (2002). AIP Conf. Proc. (USA) **649**, 369–72.
28. H. Thomas, D. Morfill, V. Demmel, and J. Goree (1994). *Phys.Rev.Lett.* **73**, 652.
29. J.U. Chu and I. Lin (1994). *Physica* **A 205**, 183.
30. A. Melzer, T. Trottenberg, and A. Piel (1994). *Phys.Lett.* **A 191**, 301.
31. Y. Hayashi and K. Tachibana (1994). *Jpn. Appl. Phys.* **33**, L804.
32. V. Fortov, A. Nefedov, O. Petrov, A. Samarin, and A. Chernychev (1996). *Phys. Let.* **A 219**, 89.
33. V. Tsystovich and U. de Angelis (2001). *Phys.Plasmas* **8**, 1141.
34. V. Tsytovich, U. de Angelis (2000). *Phys. Plasmas* **7**, 554.
35. P. Ricci, G. Lapenta, U. de Angelis, V. Tsytovich (2001). *Phys. Plasmas* **8**, 769.
36. V. Tsytovich U. de Angelis (2002). *Phys. Plasmas* (USA), **9**, 2497–506.
37. V. Tsytovich and U. de Angelis (2004). *Phys. Plasmas* (USA), **11**, 496–506.
38. Sh. Amiranashvili N. Dusein-zade, and V.Tsytovich (1999). *Phys,Rev.A* **8**, 3110.
39. V. Tystovich (2006). *Phys. Scr.* **74**,CB1–CB2 (2006).
40. Ya. Khodataev, R. Bingham, V. Tarakanov and V. Tsytovich (1996), *Fiz. Plazmy* (Russia), **22**, 1028.
41. V. Ginzburg and V. Tsytovich (1992). *Transition Radiation and Transition Scattering* Adam Hilrger, Bristol, New York.
42. O. Havnes, T. Aslaksen, T. Hartquiat, F. Meklanso, G. Morfill, and G. Nitter (1995). *J.Geoph.Res.* **100**, 1731.
43. G. Morfill, O. Havnes, and C. Goertz (1993). *J.Geophys.Res.* **98**, 11, 285.
44. O. Havnes, F. Li, T. Hartquist, T. Aslaksen, and A. Brattli, A. (2001). *Planet. Space Sci.* (UK), **49**, 223.
45. D. Samsonov, J. Goree, Z. Ma, A. Bhattacharjee, H. Thomas, H., and G. Morfill (1999). *Phys. Rev. Lett.* **83**, 3649.

46. D. Samsonov, J. Goree, H. Thomas, G. Morfill (2000). *Phys. Rev. E* **61**, 5557–72.
47. A. Melzer, S. Nunomura, D. Samsonov, Z. Ma, and J. Goree (2000). *Phys. Rev. E* **2**, 4162–76.
48. O. Havness, T. Hatrquist, A. Bratti, G. Kroesen, and G. Morfill (2002). *The Dynamic Mach Cone as iagnostic method in reactive dusty plasma experiments* Phys Rev.Lett. submitted.
49. Q. Luo, N. D'Angelo, and R. Merlino (1999). *Phys. Plasmas* **6**, 3455.
50. Y. Nakamura and H.Bailung (2001). Proc. of the Workshop on the Physics of Dusty Plasmas, University of Iowa, Iowa.
51. R. Merlino, A. Barcan, C. Thompson, and N. D'Angelo (1977). *Plasma Phys. Contr.Fusion* **39**, A421.
52. Y. Nakamura, H. Bailung, and P. Shukla (1999). *Phys.Rev.Let.* **83**, 1602.
53. Y. Nakamura and A. Sarma (2001). *Phys. Plasmas* **8**, 3921.
54. R. Kompaneetz, V. Tsytovich, G. Morfill . (2004), *IEEE. Trans. Sci.* special issue "Dusty Plasma", "Weak Dust ion-acoustic and Dust-acoustic solitons with absorption of ions, ionisation and ion drag" (April 2004).
55. V. Tsytovich and G. Morfill (2002). Proceedings ICPDP3, South Africa 2002, AIP , "Dusty plasmas in Next Millenium", Elsevier, Amsterdam, NY, **326**, 321.
56. N. D'Angelo (1994), *Planet. Space Sci* **42**, 507.
57. A. Barkan, R. Merlino, and N. D'Angelo (1995). *Phys. Plasmas* **2**, 3563–5.
58. R. Merlino, A. Barkan, C. Thompson, and A. D'Angelo (1998). *Phys. Plasmas* **5**, 1607–14.
59. C. Thompson, A. Barkan, N. D'Angelo, and R. Merlino (1997). *Phys. Plasmas* **4**, 2331–5.
60. R. Merlino, A. Barkan, C. Thompson, and N. D'Angelo (1997). *Plasma Phys. Control. Fusion* **39**, 421–9.
61. V. Tsytovich and S. Benkadda (1997). *Phys Rev. Lett.* **124**, 57.
62. S.V. Vladimirov, V.N. Tsytovich, S.I. Popel, and F. Khakimov (1995). *Modulational Interactions and strong Turbulence*, Kluwer Academic, Dorderecht-Boston-London.
63. L. Landau and E. Lifshitz (1957). *Statistical Physics*, Pergamon Press, London, NY, Part I.
64. C. Chunshi and J. Goree (1994). *IEEE Trans. Plasma Sci.* **22**, 151.
65. J. Goree (1994). *Sci. Technol.* **3**, 400.
66. T. Matsoukas and M. Russel (1995). *J. Appl. Phys.* **77**, 4285.
67. A. Sitenko, A. Zagorodny and V. Tsytovich, (1995), AIP Conf. Proc. **345**, 311.

5

Micro-particle Collective and Non-collective Pair Interactions

5.1 General Properties of Micro-particle Pair Interactions

Although a general description of the pair grain interaction can be directly obtained from fluctuations of grain distributions and grain pair correlation function, we prefer here to give a simple description of the collective interaction using the model of a "test" grain in a "sea" of all other grains. In the limit of linear fluctuations this can lead to a direct description of the grain interaction in the presence of many grains (with collective effects included) for $\beta \ll 1$. But using this approach we will also be able to demonstrate how the non-linearity changes the collective interaction for $\beta \gg 1$.

5.1.1 Grain Pair Interactions in Crystals and Clusters

It was already mentioned that in general the grain pair interaction is collective, i.e., it depends on average parameters of a complex plasma including the average grain density. This statement can be given for large systems (or strictly speaking for infinite systems). This follows directly from the fluctuation pair correlation function in a large system of grains where many grains are present. The pair correlation function of grains is depending on the relative grain positions only in a homogeneous system (which is then obviously a large system). In the inhomogeneous systems the statement that the grain pair interactions are collective is not always correct. The latter is the case of, for example, a few isolated grains where no other grains are present in the system. Their interaction is not collective. Thus by increasing the number of grains in the system we can enhance the role of collective interactions.

For some existing experiments the number of grains is not very big, and for the number of grains less than certain critical value the non-collective description should be valid. The transition from the non-collective interaction to the collective interaction is still a subject of investigation and at present

V. N. Tsytovich et al.: *Micro-particle Collective and Non-collective Pair Interactions*, Lect. Notes Phys. **731**, 197–245 (2008)
DOI 10.1007/978-3-540-29003-2_5

only the limiting cases were considered: the limit of isolated grains and the limit of large number of grains where the system is almost homogeneous can be treated well. Note that even a simple thermodynamics of a system with small number of particles is not so much developed [1] and in general its further development is needed. Thus we consider here only the limit of the interaction of pair isolated grains (calling their interactions as non-collective) and the limit of pair interactions in the presence of large number of grains (and call such interactions as collective). In the case of collective pair interactions, the two grains considered can be any probe grains from other grains in the system, but could also be two grains with other parameters (size or charge) embedded in a homogeneous "sea" of grains.

One should have in mind the fundamental results of usual plasmas where any particle movement can be considered as superposition of regular motion and random motion, with a substantial change of the regular motion (and the regular fields) due to fields created in the random motion. Namely, any screening of the particle field is caused by the random motion of all other particles creating the Debye screening for any particle in a plasma system. This screening is obviously collective since it depends on the average density of particles and in this sense the screened Coulomb interaction in usual plasmas is collective. Thus it is not unexpected that the pair grain interaction in a complex plasma should depend on the grain density if the system is large, i.e., to be collective. But the way this dependence appears somewhat different from that in usual plasmas. In complex plasmas, it is mainly due to the openness of the system and due to the necessity to compensate the plasma losses on dust grains by ionization sources. Since in a large system the plasma losses depend on the grain density, the ionization which compensates them also depends on the dust density. In this sense the openness of the complex plasma systems creates a new channel of dependence of the pair grain interaction on the ionization and therefore on the grain density.

Let us remind that in usual plasmas the collective effects caused by the particle random motion can be very strong for some processes, but can be relatively weak for other processes. For example, the role of collective effects is different for different cross-sections of interaction of particles with each other and for cross-sections of interaction of particle with waves in usual plasmas [2]. In the first case, the collective effects can change only some factors under the logarithm sign, while in the second case the cross-sections are changed by several orders of magnitude. New effect of the openness of the complex plasma system is appropriate only for those systems where it can operate quite well and is able to create qualitatively different collective effects in the cross-sections. Thus the main problem in a complex plasma is to determine the conditions where the collective effects change substantially the cross-sections of interactions.

In this chapter, we consider only the grain pair interaction and demonstrate that both the non-collective and the collective pair interactions are changed in a complex plasma substantially. For sufficiently large distances

between the grains, the pair interaction becomes attractive although the grain charges are of the same sign (and they should repel each other if the new phenomena of absorption of plasma flux is not taken into account). This point is important to understand the physics of plasma condensation and the physics of formation of different structures in complex plasmas.

We can give the criterion for the system of grains to be either large or small. This criterion is found by investigation of the grain pair interactions. The grains have an important property of absorbing plasma fluxes when they are charged. They also scatter the plasma particles. It is natural that in the case where the fluxes for different grains do not interfere each other, the grain interactions can be considered as non-collective. As soon as these fluxes interfere, the flux becomes collective, and the collective effects start to be an important feature of the pair interactions. Thus large systems can be defined as those where the size of the system is much larger than the mean-free path for the dust–plasma particle absorption. Once the main role is played by the grain–ion interactions, one should refer to the ion–grain mean-free path. This criterion is easy to write using the above given estimates of elementary processes. The criterion for the collective interaction to operate for $\tau \ll 1$ is given by

$$L \gg L_{cr} = \frac{\lambda_{Di}^2}{aP} \,. \tag{5.1}$$

The plasma condensation and the formation of plasma crystals are observed for large systems satisfying condition (5.1). We demonstrate this explicitly while discussing experiments on the plasma crystal formation. Note that in existing observations [3, 4, 5, 6, 7] of the plasma condensation, L is of the order of $(1-10)$cm while λ_{Di} is about $30-50\mu$m, a is about $(5-10)\mu$m and P_0 is about $0.3-0.5$. Then L_{cr} is about $0.1-0.05$ cm which means that the physics of the pair interactions should be based on the collective interaction of grains. The latter is usually important for large distances (while it was already demonstrated that the screening is non-linear at short distances). Here, we state that the plasma condensation apparently corresponds to the collective pair interaction. The collective interactions can be important also for other structures in the gaseous or liquid states observed in complex plasmas.

There are experiments with small number of grains as well. It is also possible that a complex plasma system is much larger in one direction and is smaller in another direction than the corresponding mean-free path. This is the case of mono-layer 2D plasma crystals. In the case where interactions in the plane of the layer are important for formation of such systems (where the size of the layer is much larger than the mean-free path), the pair interactions can be considered as collective interactions. But the 2D mono-layer plasma crystals can have a more complex behavior since the pair interactions should be non-collective in the direction perpendicular to the plane. In some experiments, the grains are confined by an external parabolic potential, and the size of the confining potential is much less than the ion–grain mean-free path. In this case the pair interactions between the grains are non-collective in most

cases and one is able to find the total energy of the interactions as a sum of the pair interactions of grains. In this case we call the system not a plasma crystal but a plasma cluster. This term is often used in current literature. Here, we employ this definition and distinguish the crystalline structures (i.e., plasma crystals and plasma clusters) on physical grounds. The plasma clusters investigated experimentally are more close to classical atoms (with an external confinement), while the crystals represent the collective state of a complex plasma as a new state of matter. The plasma clusters can have a structure similar to that of the crystal state but are determined by other interactions between the grains. We describe here the pair interactions of grains for both non-collective and collective cases.

Finally, the system of small or large number of grains can be in the disordered gaseous state. For disordered systems larger than the ion–grain mean-free path, the universal instability (UI) converts them into dust clumps and dust voids, as we discussed and already demonstrated above by giving examples of experiments showing the structurization of a complex plasma. These systems we call the self-organized gaseous grain structures. These definitions are important for future description of different experimentally observed structures in complex plasmas.

5.1.2 Two Grains: Electrostatic Energy and Interaction Forces

Very unusual feature of a complex plasma is the presence of the variable large self-energy of grains depending on the grain charge Z_d and therefore serving as large reservoir of energy (supported by external sources of plasma ionization) which can be converted into other form of energy. In usual matter, the self-energy of particle is fixed and is included in their mass (so called mass renormalization in the modern field theory concepts) and no energy can be taken from the particle self-energy. The opposite is in a complex plasma. We demonstrate this phenomenon by using a simple model of the change of electrostatic energy of two grains when they approach each other.

It should also be mentioned that usual matter is dominated by quantum effects, and it is well known that the electron finally falls on the nucleus in the classical model of an atom. All chemical bonding and molecular types of interactions (with repulsion at small distances and attraction at large distances) are of quantum nature related to the exchange interactions when the size of the attraction well is determined by the overlapping of the wave functions of electrons of different nuclei. Complex plasmas are completely classical systems. But they have specific properties, related to the openness of the system and to the presence of the large reservoir of self-energy. This energy reservoir must be supported by a continuous process of energy supply, which maintains the charge on the grains, Z_d. For this self-energy in the unit volume of a complex plasma, we have an estimate

$$U_{self} = n_d \frac{Z_d^2 e^2}{a} \,. \tag{5.2}$$

This energy is much larger than the average Coulomb energy V_{Coul}, which we already discussed in connection with strong interactions in a complex plasma and the effect of plasma condensation (see Chap. 1). The Coulomb energy V_{Coul} can be obtained from (5.2) by substituting the expression for the average distance between the grains $(4\pi n_d/3)^{1/3}$ for $1/a$. Since the average distance between the grains is always larger than the grain size we conclude that

$$U_{self} \gg V_{Coul} \ . \tag{5.3}$$

For usual plasmas, the self-energy of particles is a constant value and is not altered by any effects. Contrary to that, expression (5.2) for a complex plasma depends on the grain charge Z_d, which varies in time and space, and therefore the energy (5.2) can be changed in the grain interactions. Note that even small changes of (5.2) are important due to inequality (5.3).

Let us consider as an example two dust charges of equal size embedded in a complex plasma with the fixed electron temperature T_e. The dust charge is then a function of the distance between dust particles $r_{1,2}$. Assume any distance when the field of each particle is non-linearly screened and include the non-screened long-range field and the total potential described by $Z_d eV(r_{1,2})/r_{1,2}$, where $r_{1,2} = |\mathbf{r}_1 - \mathbf{r}_2|$ and $V(a) = 1$. Qualitatively, the dust charge dependence on the distance between two dust particles follows from the total potential on each dust particle (the particles are of equal size) to be approximately equal to the electron temperature $(Z_d e^2/a) + (Z_d e^2 V(r_{1,2})/r_{1,2}) \approx T_e$ or [8]

$$Z_d = \frac{Z_{d,\infty}}{\left(1 + \frac{aV(r_{1,2})}{r_{1,2}}\right)} \ , \tag{5.4}$$

where $Z_{d,\infty}$ is the value of the dust charge when the separation of charges is infinite. Thus the dust charge on each dust particle decreases as their inter-particle distance decreases. The screened Coulomb interaction energy then increases. But the total electrostatic energy decreases since it is determined by the sum of the screened Coulomb energy V_{Coul} and the self-energy of two dust particles:

$$U_{self} \approx 2 \times Z_d^2 e^2/2a \approx (Z_{d,\infty}^2 e^2/a)(1 - 2aV/r) \ . \tag{5.5}$$

The total change of the electrostatic energy when the particles are displaced from ∞ to $r_{1,2}$ is not $Z_d^2 e^2 V/r_{1,2}$ (as would be for the case where the dust charges do not change with the distance) but is $-Z_d^2 e^2 V/r_{1,2}$ as if the dust particles attract each other [8]. This paradox is well known in electrostatics: the sign of the electrostatic energy of two conducting charged spheres changes if the potential of the spheres is kept constant. The potential can be kept constant by external sources which in the equilibrium condition produce a work on the charges in a way that the change in the self-energy of the grains is compensated by the work produced by the external forces changing their

charges. Then the total force should be calculated as the derivative of the total electrostatic energy with an opposite sign [9, 10], and this gives the repulsion of equal sign charges. But the solution of this paradox in the conditions of the thermodynamic equilibrium gives no answer for a complex plasma which is a thermodynamically open system.

5.1.3 Role of Openness of Complex Plasma Systems

In general, compensation of the self-energy change by the work of external sources is not valid for open systems, and complex plasmas usually are open systems. But this effect depends on the way the energy is supplied to the system. Obviously, in the case where the electron temperature is kept constant the question is about the region where the electrons get most of their energy. In the majority of RF gas discharges, electrons are created by the ionization homogeneously in the whole plasma volume but acquire the most energy at the edges of plasma in the so-called plasma sheaths, where the strong sheath electric field heats the electrons. In this case the time needed for electrons to propagate from the edge of the plasma to the interacting grain particles is of the order of L/v_{Te}, where v_{Te} is the electron thermal velocity. If this time and the charging time ($\approx \lambda_{Di}/a\omega_{pi}$) are much less than the characteristic time of dust motion ($\approx 1/\omega_{pd}$), the temperature close to the grains is T_e and the work produced by an external source is not delayed to the dust charge changes. In this case the self-energy changes are compensated by the work of the external sources. But in the presence of many grains there could exist a delay for "receiving the information" about the work of external sources by two interacting charges. Indeed, plasma electrons and ions can be absorbed by the grains and have to transfer this energy to the neutral gas which then can act to produce the thermophoretic force acting differently on two interacting grains. Also the electron energy losses in their collisions with neutrals can play some role if the system is much larger than the electron-neutral collision mean-free path. Both effects are collective.

The openness of the system assumes the presence of not only two dust particles but many other dust particles (the collective effect). These dust particles create a constant sink of energy, a homogeneous one if they are distributed horrendously and create a decrease of the electron energy (or the electron temperature when the distributions are approximated as thermal) which should be compensated by external sources. Thus the attraction in an open system could be of collective nature: many dust particles are needed as a sink of energy to produce the attraction between the two probe dust particles. Also, the electrons and ions do not have time to be thermalized since the ion–grain collision rate is larger than the binary collision rates for the ion–ion and electron–electron collisions for $Z_d P \gg 1$, and the charging process in the presence of many grains creates always a non-thermal electron distributions (as the volume ionization process does). Thus the above arguments using the electron thermal distributions are not correct and give only an indication for

more detailed consideration to be done. In what follows, we show that indeed a gain of energy can exist from the work of external sources which do not completely compensate the change in the self-energy causing an attraction between the grains at distances $r_{1,2} \gg a$.

5.1.4 Pair Interaction and Non-linearity in Screening

The dust charge screening in a complex plasma is often non-linear. For large grain charges used in experiments on plasma condensation $\lambda_{scr} = R_{nl} \gg \lambda_{Di}$ one can, roughly speaking, expect that approximately non-screened Coulomb field exists on the distances larger than those for small charges for $\beta \gg 1$. Nevertheless, it does not mean that the collective effect could be absent for $\beta \ll 1$ for small charges where the screening without collective effects taken into account is of the simple screened Coulomb (Debye) type. It is easier to illustrate the physics of the collective interaction for the case $\beta \ll 1$ since all calculations can be done completely analytical using the linear approach in this case. This illustration allows us to show in a simple manner that even for small charge the collective effects can drastically change the screening converting the grain repulsion to grain attraction at some (large) distances between the grains. The physics of this attraction can be illustrated in the simplest way for small grain charges since even for them the Debye-type interactions are not correct if the collective effects are important.

The collective effects are naturally not important for small grain densities or small value of the parameter P since only this parameter enters in the definition of the ground state and only this parameter determines the plasma responses to the probe charge. As we have shown, all balance equations can be written in a way that the dust density enters only through the parameter P. Thus one should expect the existence of a critical value $P = P_{cr}$ such that for $P > P_{cr}$ the collective interactions are dominant at some distance between the grains. After the linear case $\beta \ll 1$, we consider also effects appearing in a complex plasma for $\beta \gg 1$ where the screening is non-linear.

Some indication of the possible role of collective effects can be found by considering forces acting on a third grain caused by perturbations of the field of two linearly screened grains with the same charge sign (other grains are absent so the "background" of grains creating the collective interactions is absent, too). One can demonstrate that for small grains for which the non-linearity is weak there exist small perturbations in their screening caused by the third grain that creates a concentration of polarization charges of the sign opposite to the signs of both (equally charged) grains. This effect can be considered as an attraction well for another (third) grain. Due to non-linearity, the screening of two dust particles cannot be superimposed on each other. The simplest case to treat this non-linearity is to consider large distances between the dust grains where the non-linearity is weak. Note that non-linearity can be important even in the case where the fields of each individual dust particles are screened exponentially (as it should be approximately true for a

weak non-linearity). Two dust grains with equal negative charges can create a non-screened potential in the direction perpendicular to the line connecting their centers, i.e., to $\mathbf{r}_{1,2}$. This means that in this perpendicular direction the non-linearity of the fields of two dust particles can create a bunch of positive polarization charges which can serve as a potential well for another dust grain.

We start with the equation neglecting the electron screening and the electron non-linearities

$$\Delta\phi = -4\pi e n_i \left(e^{-\frac{e\phi}{T_i}} - 1\right) + 4\pi Z_{d,1}\delta(\mathbf{r} - \mathbf{r}_1) + 4\pi Z_{d,2}\delta(\mathbf{r} - \mathbf{r}_2) \,. \tag{5.6}$$

The last two terms describe the charge densities of two point charges at the positions $\mathbf{r}_1$ and $\mathbf{r}_2$. The linear potential of each of them is given by

$$\phi_{1,2} = \frac{1}{2\pi^2\lambda_{Di}} e Z_{d,1,2} \int \exp\left(i\mathbf{k}\cdot\left(\frac{\mathbf{r} - \mathbf{r}_{1,2}}{\lambda_{Di}}\right)\right) \frac{d\mathbf{k}}{k^2 + 1} \,, \tag{5.7}$$

which leads to the screened Coulomb interaction

$$V_{1,2} = \frac{Z_{d,1}Z_{d,2}e^2}{r_{1,2}} \exp\left(-\frac{r_{1,2}}{\lambda_{Di}}\right) \,. \tag{5.8}$$

The non-linearity on the right-hand side of (5.6) can be found by expanding the exponent and taking into account the term with the product of potentials (5.7) of each grain $\propto \phi_1\phi_2$. The terms $\propto \phi_1^2$ and $\propto \phi_2^2$ describe small corrections to the screening and were already discussed when considering the non-linear screening of a single dust particle; they describe the small correction to (5.8).

Consider the line connecting two dust particles, the distances $r_{1,2}$ counted from the center of this line or from any other point on this line. The latter makes no difference since we assume that $r \gg r_{1,2} = |\mathbf{r}_1 - \mathbf{r}_2|$. Then simple calculations lead to an additional potential ϕ_{nonl} created by two dust particles and to an additional energy for the third dust particle which appears to be negative in contrast to (5.8):

$$V_3 = eZ_{d,3}\phi_{nonl} = -\frac{e^4 Z_{d,1}Z_{d,2}Z_{d,3}}{2\pi T_i r \lambda_{di}} \exp\left(-\frac{r_{1,2}}{\lambda_{Di}}\right) \,. \tag{5.9}$$

This energy does not contain the factor $\exp(-r/\lambda_{Di})$, and as a function of r it is inversely proportional to r. Therefore the interaction is not screened. Of course any use of the linear approximation assumes that the distances are large and presumably larger than λ_{Di}. Thus the exponent with $r_{i,2}$ in (5.9) is acting, but the only restriction is the applicability of the linear approximation in the potential and the non-linearity to be weak. Also, we assumed $r \gg r_{1,2}$. One can therefore expect that this attraction, which increases with the decrease of r, is maximum at $r \approx r_{1,2}$. One can estimate that at these distances the ratio of the attraction V_3, $V_{1,3}$, or $V_{2,3}$ is of the order of

$$\frac{z_3}{2\pi}\frac{a}{\lambda_{Di}}; z_3 = \frac{Z_{d,3}e^2}{aT_e}\ , \tag{5.10}$$

which can obviously be larger than 1. This result seems to be important for the attraction of grains in the plane perpendicular to the line between two other grains. It is valid only for grains with small charges. This example illustrates the possibility of creation of the attraction even for the presence of three grains. The collective attraction deals with the effects related to the presence of many grains. Thus for the non-linear screening of two negatively screened grains it is not unusual that one finds an "over-screening" of the polarization charge and creation of the regions with positive polarization charge. The effect of attraction is also related with the presence of the ion flux, its creation and absorption, and with ions concentrated between two equal-sign grains forming the attraction potential well.

5.2 Shadow Non-collective Attraction Forces

We start with the case of non-collective interactions showing that the presence of a flux absorbed by grains can cause attraction in the limit where the distance between the grains and the size of the system is much less than the mean-free path for the plasma absorption by grains.

5.2.1 Shadow Attraction Created by Ion Flux

We consider here the non-collective shadow effect [11, 12, 13, 14, 15], which takes place for two isolated dust particles in the absence of other dust particles ($P = 0$). In the case of the non-collective pair grain interaction the charging process creates a new phenomenon associated with the presence of non-screened attraction forces. During the charging both electrons and ions are absorbed by the grain. The momentum of ions is much larger than that of electrons due to their larger mass. For a single spherical dust grain, the total transferred momentum is zero since the momentum transferred from an ion approaching the grain from one direction is compensated by the momentum of the ion approaching from another direction. In the presence of a second grain this symmetry is lost and there appears the shadow force (see Fig. 5.1).

For simplicity we assume that the distance between two dust particles can be of the order of (or larger than) the screening length. The order of the magnitude of the length which is effective for the non-collective attraction is the charging length about λ_{Di}^2/a; we assume that the latter is much less than the ion-neutral mean-free path λ_{in}. In these conditions one can neglect the ion-neutral collisions. The non-linear screening length (3.64) $\lambda_{scr} = 3.6\lambda_{Di}(az/\lambda_{Di}\tau)^{1/5}$ is for current experiments of the order of λ_{Di}^2/a and since the non-linear law for the screening factor $\psi = (1 - (r/\lambda_{scr}))^4$ describes the flattening of the screening curve at $r \sim \lambda_{scr}$ the effective length

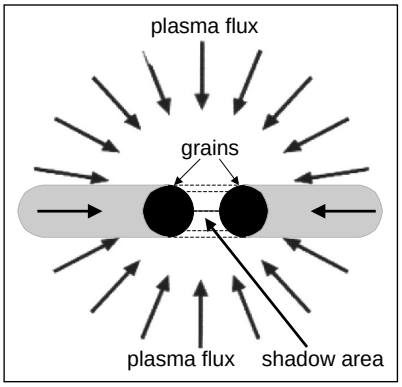

Fig. 5.1. Schematic drawing of shadowing the plasma flux on one grain by another grain

λ_{Di}^2/a is often reached at the distance where the Coulomb field is almost screened. The important point here is that the additional shadow screening force should be added to the screened Coulomb force and does not depend on whether screening is a simple exponential screening or the (strongly) nonlinear screening. It has a different nature, namely the bombardment of the surface of the grain by ions of the flux approaching the grain. This bombardment force is not the electric field force, and both these forces can be simply added.

The physics of the shadow attraction is very simple: the flux going to one particle is shadowed by another dust particle and therefore the ram pressure of the ion bombardment from the outer sides of two dust particles is larger than that from the inner side. Mostly the ion bombardment is of importance; this is due to the larger ion mass as compared to the electron mass. It is simple to perform an estimate for the case where the distance between the grains $r_{1,2}$ is larger than the size of the grains a. The area of the ion collection by the single grain for $z/\tau \gg 1$ is $\pi a^2 z/\tau$. The mentioned solid angle to shadow the flux is small if $a^2/r_{1,2}^2 \ll \tau/z$. We consider the case where the latter inequality is valid. The force due to the ion shadow $\mathbf{F}_{sh,i}$ is determined by the product of this shadow solid angle and the transfer of the ion momentum $m_i v_{Ti} I_i$ through the middle of the plane between two dust particles (we use here the momentum conservation in the grain interaction [14]),i.e., it is approximately $n_i T_i 4\pi a^2 z/\tau$ (an additional factor 4 appears due to arguments of [14]). The force is along the line connecting the two dust particle, i.e., is proportional to $\mathbf{r}_{1,2}/r_{1,2}$. This gives

$$\mathbf{F}_{sh,i} \approx a^2 \frac{\mathbf{r}_{1,2}}{r_{1,2}^3} n_i T_i 4\pi a^2 \left(\frac{z}{\tau}\right)^2 . \tag{5.11}$$

The last expression of (5.11) corresponds to $z/\tau \gg 1$. This calculation oversimplifies the problem since it does not take into account that not only the flux which is captured is shadowed but also the flux related with the ion scattering by the dust particle is also shadowed. The latter in the absence of

the second dust particle is symmetric, the flux is scattered from all sides of the dust surface and in this conditions the net momentum transferred to the dust particle is zero. In the presence of another particle this is violated. Thus the shadow effect has two parts, one part is related with the flux captured by the grain and another part is related with the flux scattered by the grain field (which can include the effect of the non-linear screening and the long-range non-screened field). Below we discuss these processes quantitatively. We also refer to the simplest expression as the standard one and find additional coefficients which mathematically describe the mentioned effects.

Expression (5.11) has some general features which should be listed:

- The force is attractive and has the same dependence on the inter-particle distance as the non-screened Coulomb force $\propto 1/r_{1,2}^2$;
- Contrary to the Coulomb force, this force is not screened and should dominate for distances larger than the Coulomb field screening length;
- It is smaller than the Coulomb force at the distances where the Coulomb field is not screened ($r_{1,2} \ll \lambda_{scr}$). Indeed substituting one of a^2 by $Z_d^2 e^4/z^2 T_e^2$ we have

$$F_{sh,i} \approx -\frac{Z_d^2 e^2}{r_{1,2}^2} \frac{a^2}{\lambda_{Di}^2}. \tag{5.12}$$

  Expression (5.12) is useful for comparison of the shadow force with the bare Coulomb force. The first factor in this expression coincides with the non-screened Coulomb field (with the opposite sign), and the estimate of the second factor should be improved by taking into account the shadow effect for the scattering. The most important is the last factor, $a^2/\lambda_{Di}^2 \ll 1$, which shows that indeed the absolute value of the attraction force is much less than the absolute value of the non-screened Coulomb force since for most cases of interest in complex plasmas $a \ll \lambda_{Di}$. Thus it can dominate only for distances where the Coulomb field is screened (at least partially);
- The shadow attraction is proportional to a^4 and rather sharply increases with an increase in the grain size. The size of dust particles is growing slowly but continuously in many existing experiments (e.g., on plasma etching) and the role of the shadow force in these conditions increases with time;
- The shadow force appears only for finite size particles and is zero for point charges. For strong coupling in a complex plasma the size of dust particles should be sufficiently large; usually it is about $\lambda_{Di}/7$ in length and the coefficient a^2/λ_{Di}^2 is about 0.02, which means that not very large screening of the Coulomb field is required for the shadow force to dominate.

These general features are common to all attraction forces except for the attraction force caused by the neutral particle shadowing. The latter can even exceed the bare Coulomb force (see below) and is caused by the presence of the large factor $n_n/n_i \gg 1$ proportional to the neutral density n_n. Using the

given hand-waving estimate we write a general expression for the shadow force in the form [11]

$$\mathbf{F}_{sh} = -\frac{\partial U_{sh}(r_{1,2})}{\partial \mathbf{r}_{1,2}}; \qquad U_{ch}(r_{1,2}) = -\eta_{sh}\frac{Z_d^2 e^2}{r}\frac{a^2}{\lambda_{di}^2}\,, \tag{5.13}$$

where general expression for the shadow coefficient η_{sh} contains a sum of the effects due to the ion capture $\eta_{sh,ic}$, the ion scattering $\eta_{sh,si}$, and the neutral particle flux if the neutrals can be partially attached to the grain $\eta_{sh,n}$ (this is discussed in the next subsection)

$$\eta_{sh} = \eta_{sh,ic} + \eta_{sh,si} + \eta_{sf,n}\,. \tag{5.14}$$

Consider first in more detail the shadow effect due to the ion capture. To find the force, it is possible to invert the problem and calculate the capture force for the case where the ions are present only within the shadow angle cone, since due to the net value of the momentum transfer (in the absence of the shadow) the effect is equal to the value we are interested in. We integrate the expression for the momentum transferred to a single ion with respect to distribution in angles and velocities assuming that the ion distribution far from the grain is thermal. The shadow flux far from the grain is almost flat and the cross-section should be πa^2. We have

$$\eta_{sh,ic} = \frac{1}{\sqrt{\pi}}\frac{\tau^2}{z^2}\int_{y_{min}}^{\infty}\left(y+\frac{z}{\tau}\right)^2\exp(-y)dy; \qquad y_{min} = \frac{a^2}{r_{1,2}^2}\frac{z}{\tau}\,. \tag{5.15}$$

For $z/\tau \gg 1, r_{1,2} \gg a\sqrt{z/\tau}$ we obtain

$$\eta_{sh,ic} \approx \frac{1}{\sqrt{\pi}} \approx 0.56\,. \tag{5.16}$$

Now, estimate the shadow effect in the scattering. Note that the advantage of the OML approach for evaluating the shadow capturing force is that it uses simple conservation law without particular potential distribution close to the grain (the only requirement is that the potential far from the grain is much less than at the grain surface). For the shadowing of scattering we need to know the particular potential. The potential is strongly non-linear for $z/\tau \gg 1$ and the Coulomb potential can be used approximately only for z/τ of the order of 1. The calculations performed for the latter case with the Coulomb potential [16] showed that $\eta_{sh,sc}$ is approximately of the order of $\ln(\lambda_{Di}/a)$. But this result can be used only for small grain charges. For existing experiments, the case $\tau/z \gg 1$ is more appropriate. Due to the strong screening in this case it is possible to expect that $\eta_{sn,sc}$ is quite different from that obtained for the case of pure Coulomb field.

As for the drag coefficient, we can estimate the role of scattering in the shadow effect by considering the model of back-scattering from the sphere somewhat less than the non-linear screening length (omitting the numerical

factor 3.24 in the expression for the backscattering radius). The calculations are the same as those for obtaining expression (5.11). Substituting $\lambda_{scr}/3.24$ for $a\sqrt{z/\tau}$ we find an estimate of the scattering shadow coefficient for a strong non-linear screening:

$$\eta_{sh,is} \approx \left(\frac{\tau\lambda_{Di}}{za}\right)^{6/5} . \tag{5.17}$$

An exact expression for $\eta_{sh,is}$ in case $z/\tau \gg 1$ can be obtained only numerically using an explicit form of the non-linear screening potential. This is still to be performed. For existing plasma experiments $a/\lambda_{Di} \sim 0.2$ and $\tau/z \approx 0.03$, we have $\eta_{sh,ic} \approx 0.02$, $\eta_{sh,is} \approx 0.065$, i.e., the scattering shadow coefficient is of the same order (and about twice smaller) as the shadow-charging coefficient. According to (5.17) for larger values of τ and smaller grain sizes a the scattering attraction can be rather big and comparable with Coulomb repulsion at shorter distances, but the back reflection model used to obtain (5.17) is valid only for a large-enough ratio z/τ.

We remind that the shadow attraction potential is a long-range unscreened potential operating even at distances much larger than the screening distance where the non-collective non-screened long-range repulsion potential also operates. Remember that the potential energy related to the latter is approximately $(Z_d^2e^2/r_{1,2})(a/2r_{1,2})$, while the potential energy related to the shadow attraction due to the charging process is of the order of $-\eta_{sh}(Z_d^2e^2/r_{1,2})(a^2/\lambda_{Di}^2)$. This comparison shows that in the long-range domain (distances larger than the screening distance) the attraction due to the shadow effect becomes comparable with the repulsion at distances

$$r_{1,2} > \frac{1}{\eta_{sh}}\frac{\lambda_{Di}^2}{a} . \tag{5.18}$$

In the case where only the shadow effect due to the charging process is taken into account, the right-hand side of relation (5.18) is of the order of the charging length λ_{Di}^2/a. From the physical point of view the ion-capturing attraction is directly related with the charging process and this estimate is very natural. The estimate (5.18) for dominating the shadow force is valid only for $r_{1,2} \gg \lambda_{scr}$ where the long-range repulsion is operating.

It should be mentioned that the attraction due to the neutral flux depends much on the neutral density n_n and for high neutral densities it can be larger; the distances where it can dominate can be shorter. In the conditions where the non-collective attraction is taken into account, the whole potential curve for the interaction potential of two dust particles is similar to the usual molecular potential curve: at short distances the screened Coulomb repulsion dominates and at larger distances a potential well appears, with the minimum value V_{at} given by

$$V_{at} = -(\eta_{sh})^2 Z_d^2 e^2 \frac{a^3}{2\lambda_{Di}^4} . \tag{5.19}$$

For typical experimental conditions $Z_d \approx 10^4$, $T_i \approx 0.02\,\mathrm{eV}$,$T_e \approx 3\,\mathrm{eV}$ $a \approx 10\mu m$, and $\eta_{sh} \approx 0.2$ we find $V_{at} \approx 16\,\mathrm{eV}$, which corresponds to the approachable binding energy (since the average ion temperature almost coincides with neutral temperature) of about 0.02eV. Thus two dust particles with equal sizes can form a dust molecule, and several dust particles can form dust clusters. The 2D dust clusters (clusters where the grains are located on 1D plane) were investigated in several experiments by using an external confining potential (see the detailed description in Chap. 7). The role of the shadow attraction in the formation of these clusters could be large. The prediction from the shadow-force theory is that the clusters could exist even without any external confining potential and this can be checked experimentally. Experiments can also be performed in the presence of an external confining potential to measure the value of η_{sh} and to check the shadow force physics. A general theory of modes, oscillation frequencies, and stability of 2D clusters was recently developed in [17] and can be used for the experimental detection of non-collective shadow attraction forces.

5.2.2 Shadow Attraction Created by Neutral Flux

In low-temperature plasmas, the flux of neutral atoms on the surface of a dust particle substantially exceeds the ion flux. This flux is not related to the dust charging and is mainly returned back from the dust surface. The neutral atoms are nevertheless absorbed by the surface, are kept by it for a rather small resident time, and then are re-injected into the plasma. The resident time is still sufficient to exchange the energy and almost equalize it with the surface temperature. Thus in the presence of a small difference in the temperature of the neutral gas and the temperature of the dust surface there could exist a net energy and momentum transfer and therefore there could exist the shadow force. One can rigorously prove that when collisions of neutral atoms with the dust surface are completely elastic the net force due to the neutral atom flux is exactly zero.

If all neutral atoms are absorbed by the surface it is easy to obtain the shadow force for the distances between the grains less than the mean-free path of ions in the neutral gas λ_g, which is of the order of λ_{in} [12, 18]. In this case one needs to calculate the momentum transferred to the dust surface by taking into account the straight trajectories of neutral atoms reaching the grain. Then the attraction force is given by [18]:

$$\mathbf{F}_{sh,dn} = -\frac{\mathbf{r}_{1,2}}{r_{1,2}^3}\frac{3}{4}\pi a^4 n_n T_n \,. \tag{5.20}$$

This expression corresponds to the qualitative estimate given above, but since in existing experiments $n_n/n_i \approx 10^6$ the force (5.20) is many orders of magnitude larger than that related with the ion flux. In reality, the attachment coefficient κ_{at} taken in (5.20) to be equal to 1 while the detachment coefficient

κ_{det} taken to be zero is not correct and the difference between them is very small, $\delta\kappa = \kappa_{at} - \kappa_{det} \ll \kappa_{at}$. Also, the temperature of the dust surface T_s is not equal to the neutral dust temperature T_n. Taking into account these differences we find instead of (5.20)

$$\mathbf{F}_{sh,dn} = -\frac{\mathbf{r}_{1,2}}{r_{1,2}^3}\frac{3}{4}\pi a^4 n_n T_n \left(\kappa_{at} - \kappa_{det}\sqrt{\frac{T_s}{T_n}}\right) . \tag{5.21}$$

As we already noticed, the dust surface temperature is often larger than the neutral temperature, and in case they differ substantially the force (5.21) describes repulsion. There are conditions where the dust is cooling fast (this happens in astrophysical conditions where the radiative cooling is very effective).

In typical laboratory conditions both the difference of the temperatures and the difference between the attachment and the detachment coefficients are very small. Thus the sign of the force is determined by the interplay of two small parameters $\delta\kappa/\kappa$ and $\delta T/T$. The latter, as we discussed already, is of the order of 10^{-3}. The difference between the attachment and the detachment coefficients [19, 20] can be larger than that value, especially for rough dust surfaces and for fractal dust. Then the attraction can exist and dominate up to the distances where the two grains touch each other. This strongly depends on the structure of the dust surfaces and other delicate problems of the surface physics. Notice that in principle the value of the attraction force can be at least 3 orders of magnitude larger than that estimated from (5.21). Since (5.21) is larger than the ion-capturing shadow force by the large factor n_n/n_i, the neutral shadow force can exceed the ion shadow force by several orders of magnitude. We have an estimate [13]

$$\eta_{sh,nd} \approx \frac{3}{16}\frac{\tau^2}{z^2}\frac{n_n}{n_i}\delta\kappa , \tag{5.22}$$

where we neglect the difference of the temperatures.

For the conditions where the distance between the grains is larger than the mean-free path of atoms in the gas, the physics is changed and the main role is played by the thermal flux q equal to the difference between the thermal fluxes to and from the dust surface. The thermal flux created by one dust particle at the position of another dust particle is

$$\mathbf{q} = -\frac{\mathbf{r}_{1,2}}{r_{1,2}^3} n_n a^2 \sqrt{\frac{2}{\pi}} v_{Tn}(\kappa_{at} T_n - \kappa_{det} T_s) . \tag{5.23}$$

This leads to the temperature gradient at the position of the other dust particle:

$$\frac{\partial T_n}{\partial \mathbf{r}_{1,2}} = \frac{\mathbf{q}}{\kappa_T} , \tag{5.24}$$

where κ_T is the coefficient of the thermal conductivity of the gas. A dust grain placed in this temperature gradient experiences a thermophoretic force which can be expressed through the thermal conductivity coefficient:

$$\mathbf{F}_{tp} = -\frac{16}{15}\sqrt{\frac{\pi}{2}} v_{Tn} a^2 \kappa_T \frac{\partial T_n}{\partial \mathbf{r}_{1,2}} \,. \tag{5.25}$$

Thus the thermal conductivity coefficient gets canceled and we find for the shadow force due to the neutral flux again the expression (5.21) with the additional numerical coefficient $64/45\pi \approx 0.45$ [13].

5.2.3 Agglomeration of Grains

The forces discussed above act between charged grains. In case the grains are not charged, only the Van der Waals and chemical forces operate between the grains and cause their attraction, first forming aggregates of small grains. Sometimes this stage is called as the first stage of the grain agglomeration or grain coagulation. At this stage the grains are growing by the atoms sticking and attaching themselves to the grain surface [21, 22]. This process was investigated first for astrophysical conditions [23] where the grains and the surrounding gas are cooled to a low temperature, the ionization is assumed to be absent and the agglomeration is a very slow process related with the atom attachment to the grain due to their collisions and weak Van der Waals forces acting at small distances from the grain. It is caused by the Brownian motion-driven grain motion, and the rate of the grain growth was considered in detail both theoretically and numerically [24, 25, 26] in applications for the formation of dust molecular clouds in space and the proto-planetary planetesimals preceding the planet formation and confirmed recently by the micro-gravity experiments [27].

For laboratory plasmas this first stage was also investigated in detail [21, 22, 28, 29, 30]. These processes are mainly related with the dipole–dipole interactions (induced dipole interaction or Van der Waals force). In the presence of ionization the first important effect is the appearance of dust charges which can change substantially this stage of the grain agglomeration by the charge–dipole interaction. It was shown that the runaway cluster growth exists in the presence of the charge–dipole interactions. This process of the runaway growth of clusters of grains is named as the "grain gelation". The gelation process can be substantially enhanced by the charge–dipole interactions. As soon as the grains acquire large charges, their Coulomb repulsion usually stop further agglomeration [28], but the charged grains continue to grow by accretion of the ion flux [31] until their size is sufficient for the grain shadow attraction to dominate (the shadow attraction is proportional to the fourth power of the grain size).

For large gas pressures and for large dust sizes, the neutral shadow attraction can obviously be larger than the Coulomb repulsion at all distances

between the grains (even in the domain of the bare Coulomb field) up to the distances where the grains touch each other. The grains are continuously growing in gas discharges due to the deposition of the material onto grain surfaces and they should eventually reach the stage where they have only the attraction forces and therefore can go to the second stage of agglomeration forming large agglomerates of grains.

The phenomenon of formation of large dust agglomerates is common in most etching devices operating for a long time being sufficient for the dust particles to grow to large sizes [21, 22, 28, 31, 32]. The observations show that the dust particles grow up to sizes of the order of few parts of mm [31] and that many of them finally have the form of cauliflower agglomerates. Theoretically the criterion of the dust agglomeration due to the neutral shadow attraction was first considered in [19, 20, 33] and can be obtained by comparison of the neutral attraction force (5.21) with the bare Coulomb force. The agglomerates of dust particle were observed also in tokamak plasmas [34], and the problem of dust in future fusion devices mainly dealing with large plasma fluxes on the walls is a big issue in future fusion technology [22, 34, 35, 36]. It can also be applied to interpret the new observations in space on fast dust creation in H-stars and behind the supernova shocks [29]. Generally, it is expected that further development of the physics of shadow forces can provide a natural explanation for the observed phenomenon of dust agglomeration in both space and laboratory plasmas.

5.2.4 Problems of Non-collective Grain Attraction

Ion Scattering on Small Angles. The non-linear screening of the grain field forms a sphere which has a thin layer at its surface where the fields are weak and the scattering occurs at small angles. The angle of the ion scattering is eventually growing up to almost total reflection by the main part of the screening sphere. The exact value of the shadow-scattering coefficient should take into account both the effects of the large-angle scattering and the small-angle scattering. With a decrease of the grain size (and, consequently, with a decrease of the grain charge) the role of the scattering at small angles increases until it becomes a simple a Coulomb scattering for rather small grain sizes, with the scattering rate determined by the Coulomb logarithm. The problem to be solved in this context is to find the continuous change of the scattering shadow coefficient with the decrease of the grain size and the decrease of the grain charge. It is to be mentioned that the coefficient (5.17) increases rather rapidly with the decrease of the grain size but the outstanding problem is to find the critical size where the scattering at small angles starts to dominate and where this relation starts to be incorrect. This value of the grain size determines the maximum possible shadow attraction force.

Mutual Influence of Two Interacting Grains. The grain non-linear screening is produced by the polarization cloud around the grain. We have demonstrated in the previous section that the mutual influence of grains on the

polarization cloud can affect the shielding of each of the interacting grains. Since the shadow effect is depending on the scattering process, the problem is to determine the change in the mutual screening when the two grains come closer to each other. It is clear that when the two interacting grains are almost at the same position (being close to each other) their polarization cloud is common and it is not possible to separate it into two polarization clouds. There are no attraction forces due to the shadow in the scattering of the ion flux. However, the shadow attraction occurs at large distances between the grains where the separation of the polarization clouds is possible. The problem is to find the critical distance between the grains where the separation of the ion-scattering shadow effect is still possible. The same problems (but even more serious one) appear for the wake non-collective interactions of grains in case these two grains are embedded in the ion flow (which is usually present in the plasma sheath) [21]. It was shown in [37, 38, 39] by self-consistent MD numerical simulations of the wakes of two grains that the wakes merge with each other for the case where the distance between the grains becomes small.

Thus for the two large charge grains, the positive charge between them can appear only if the distance between the grains is large enough. If this polarization charge can be in some approximation considered as a point charge between the two large grains it is obvious that its value should be larger than half of the charges of each large grain (assuming that the charges of large grains are equal). This is just one of the conditions for the attraction to the polarization charge to be larger than the repulsion from the other grain charge. Obviously, the polarization charge between large grains is somehow elongated in the direction between the grains and is not a point charge and thus its value should be somewhat larger than half of the the interacting charges.

In the case where the positions of the two interacting charges coincide the polarization charge between them is absent. Increasing the distance between the charges first increases the polarization charge between them and then decreases it. Having in mind the non-linear nature of the polarization it is not quite clear that the polarization charge between the grains can reach the value of half of the grain charge. Thus it is not clear at which distance the attraction (if exists) has its maximum value. The lowering of the polarization charge can only lower the attraction potential well or move it to larger distances. Obviously the attraction related with the ion absorption on the grains is affected much less since the impact parameter for the ion absorption is usually less than the non-linear screening length. The neutral flux shadow attraction is not influenced at all by the effects of non-linear screening.

Attraction in the Plasma Sheath.

The plasma sheath existing close to the wall is also produced by the non-linear screening. The size of the sheath is of the order of several-electron Debye length. In case the grains levitate in the sheath at the distance determined by the balance of the gravity and the sheath electric field forces (and they

are of the same charge and the same weight), their distance from the wall is the same and their interaction depends on their spatial separation along the sheath.

The question is whether their non-linear screened potential and the forces between dust particles depend on the sheath potential? The answer obviously depends on the distance of the grains from the wall. Generally, such a dependence exists if the non-linear screening length is of the order of the sheath thickness. Note that the electric field at the grain surface is much larger than the sheath electric field (the potential is approximately a/λ_{De} times less), and one probably can foresee that at small distances the non-linear shielding is not changed much by the sheath. But λ_{De} is of the order of the non-linear screening length λ_{scr}, and for the distance between the grains (in the direction perpendicular to the sheath plane) of the order of λ_{scr} the grain potential becomes of the order of the sheath potential.

For even larger distances where $r \gg \lambda_{scr}$, the potential of the sheath dominates (and it is non-linear). The latter means that the space charge of the sheath $\rho(\phi)$ is a non-linear function of the total potential $\phi = \phi_{sh} + \phi = \phi_Q$, where $\phi = \phi_{sh}$ is the potential of the sheath and $\phi = \phi_Q$ is the potential of the grain. This means that even in the range of the linear description of the shielding there exists a polarization charge, $d\rho/d\phi \times \phi_{sh}$, which contributes to the linear grain shielding. This argument shows that even the linear grain shielding in the plasma sheath close to the wall can be different from that in the plasma bulk.

The usual expectation for the linear shielding in the bulk plasma in the presence of an ion flow with the Mach number of the order of 1 is that the ion shielding is absent and the shielding is determined be the electron Debye length. The above-given arguments show that the real situation in the sheath is more complicated and that even within the range of the linear approximation for the shielding the latter can be changed by the sheath. An important point is that at present there does not exist an excepted model for the sheath potential distribution in the absence of grains. The grains being close to the wall at the distances less than the non-linear screening distance can also change the distribution of the sheath potential. The whole problem of interactions and shielding of grains in the plasma sheath is one of the important experimental and theoretical problems. The interest in this completely non-linear problem is also related to numerous applications, e.g., in plasma technology.

5.3 Collective Attraction for Linear Screening

5.3.1 Collective Attraction in the Limit $\beta \ll 1$

The mechanism of collective attraction of dust particles was first discussed in [40]. In was considered for systems containing large number of grains where the plasma fluxes on dust grains are not separable. This is opposite to the case

of the shadow mechanism of attraction when applied to a collection of grains (grain clusters where the fluxes on dust grains should be separable). For the number of grains exceeding a critical value in the system, the fluxes become collective and therefore the attraction is called collective attraction. The collective attraction was obtained in [40] by proving that the static dielectric permittivity changes its sign for small wave numbers (sufficiently large distances), and the physical processes leading to this attraction were analyzed later [41].

We consider the basic state with a "sea" of grains described, as above, by the parameter P_0. In this state one can look for an influence of an additional charged grain which can be considered as a probe grain. This additional grain can have any charge including either the case of a small charge or the case of a large charge. By the term "small charge" we mean that for the perturbations introduced by it the linear approximation can be considered. The large charge is the one where the linear treatment is not possible and the screening is strongly non-linear. The case of the small charge is useful for explanation of the main physical processes appearing when the probe charge is embedded in a complex plasma ground state. This case called here as the linear collective attraction, $\beta \ll 1$, is simply treated mathematically by using linear perturbations of the ground state. For a point charge its static field can be found from the Poisson equation using the static dielectric permittivity $\epsilon_{\mathbf{k}} = \epsilon_{\mathbf{k},0}$ (the last argument of ϵ which is written as 0 is the frequency of the perturbation ω). We have

$$\phi(\mathbf{r_{1,2}}) = -Z_d e \int \frac{d\mathbf{k}}{2\pi^2 \epsilon_{\mathbf{k}}} exp(i\mathbf{k} \cdot \mathbf{r}_{1,2}) \,, \tag{5.26}$$

where ϕ is the potential of the static grain field.

The case of a large grain is called as the non-linear collective attraction. This case can be treated only numerically. For the linear collective attraction, expression for the static linear dielectric function in a complex plasma can be easily obtained as a linear perturbation of the basic state. In the basic state, both the charge balance and the balance of ionization and absorption on dust grains are taken into account. We write here in the usual dimensional units the dielectric function as

$$\epsilon_{\mathbf{k}} = 1 + \frac{1}{k^2 \lambda_{Di}^2} \left(1 + \tau(1 - P_0) - (1 + \tau) \frac{k_0^2}{k^2 + k_0^2} \right) \,, \tag{5.27}$$

where

$$k_0^2 = \frac{P_0^2 \alpha_{dr} \alpha_{ch} z_0^2}{(1 + z_0)} \frac{a^2}{\tau \lambda_{Di}^4} \,. \tag{5.28}$$

First two terms in the large brackets of (5.27) correspond to the Debye screening (the first term, 1, describes contribution by plasma ions, while the second term $\tau(1 - P_0)$ describes contribution by plasma electrons. It is easy to see that for $k \ll k_0$ the expression in the brackets in (5.27) changes its sign and becomes $-P_0\tau$. The wave number k_0 is small containing the small parameter a/λ_{Di} and this can be regarded as an indication for the grain repulsion to

change to attraction at large distances $r_{1,2} \gg 1/k_0$. The presence of zeros of the static dielectric function does not contradict any general theorem since the system is open being always supported by the ionization source. On the other hand, it is an indication of a possible instability. As we already demonstrated, UI is indeed developing. Still it has some time for being developed and it is reasonable to ask the question on what are the forces between the grains before this instability grows substantially. This question can be turned around in a way that the presence of attraction forces causes an instability similar to the attractive gravitational forces causing the gravitational instability.

The zero of the dielectric function (which changes the repulsion to attraction) for wave numbers on the real axis leads to the problem of determining the rule for the pole treatment in the calculation of the interaction potential. In the problem of the attraction this rule is as fundamental as the rule for poles leading to the Landau damping of plasma modes [2]. The mathematical treatment of the poles of the static dielectric function when considering the collective screening of the field of a test grain in the limit of $a/\lambda_{Di} \ll 1$ was given in [41]. In the paper [40], the integrals were calculated by taking half-residues of the poles on the real axis. This rule should be proved to be correct and if so the ranges of parameters where it is correct should be found. Such problem cannot be solved without more deep consideration of the physical conditions which lead to the collective attraction.

We show that the problem of the poles can be solved by taking into account the finite sizes of grains. Note that the change of sign of the static dielectric function is determined by k_0, which is proportional to the grain size. Thus the finite grain size effects are very important (as well as for the non-collective shadow attraction discussed earlier). Effects of both the collective and the non-collective attraction are determined by a^2, i.e., they are proportional to the surface area of the grains. Thus one can expect that the two types of the grain attraction are complimentary: the non-collective attraction operate for system sizes mush less than the mean-free path for the ion–grain interaction while the collective attraction takes place in the opposite limit. It is easy to estimate that having a finite number of grains in the system, the fluxes on individual grains do not intersect much with each other for the system's size is less than the mean-free path for the ion–grain collisions. In this case the total energy of the grain interaction (including the non-collective attraction) can be easily found by the sum of the pair interactions of each grain with another as, for example, in Coulomb systems in the usual matter. Although the finite size effects are important for the collective attraction, expression (5.27) for the point charge gives the correct result of [40] in the limit $a \ll \lambda_{Di}$, as shown in [41].

5.3.2 Physics of Collective Attraction

A simple physical explanation for the appearance of regions where the collective attraction is present is that disturbances of the basic state due to an external grain embedded in a dusty plasma create the polarization charge

around the grain, with the sign of the charge density opposite to the sign of charges corresponding to the shielding polarization charge densities. The main point is that the disturbances of the basic state made by the embedded charge inevitably create ion fluxes, transferring plasma ions from regions where the ionization exceeds the absorption to the regions where the absorption exceeds the ionization. The ion fluxes create the regions of the positive charge accumulation which are interchanged with the regions of the negative charge accumulation. The accumulation of positive charges is stabilized when excessive positive charges build up.

The presence of such stationary ion fluxes is a new phenomenon which leads to the new effect of dust attraction and dust pairing, similar in certain respect to the Cooper's pairing [21]. Thus a dusty plasma starting from grain temperatures below a certain critical grain temperature can convert to the system of dust molecules. It should be mentioned that plasma electrons created by the ionization source are repelled from the region of two negatively charged grains so they leave the region between the grains rather fast (in fact, they do so even for another sign of the grains) and start to be distributed adiabatically according to the potential profile between the grains. Contrarily, plasma ions are attracted to the region between the negative grains and cannot freely leave this region due to the friction which is in the collisionless case due to the ion–grain scattering (and in the collision-dominated case it can be the friction of ions in the neutral gas). One can expect that in the further development, the grains rapidly decrease their temperature (or the average dust kinetic energy) thus creating complexes of dust grains and, finally, the dust–plasma crystals. In usual plasmas, such processes do not operate and any charge embedded in a plasma is screened in the way that only space charges of the opposite sign are created around it, such that a positive charge is screened by the excess of electrons and depletion of ions and the negative charge is screened by the excess of ions and depletion of electrons.

5.3.3 Attraction of Finite Size Grains

We consider here only a grain with a finite size a. We employ the balance equations describing the fields and fluxes outside the grain and use the boundary conditions on the grain surface to determine amplitudes of the disturbanced introduce by the probe grain in the ground state of a complex plasma.

For the case where all quantities depend only on the absolute value of the distance from the embedded probe grain, the ion continuity equation can be written in the following dimensionless form:

$$\frac{1}{r^2}\frac{d}{dr}r^2 nu = a\alpha_{ch}P_0\left(\frac{n_e}{1-P_0} - n\frac{P}{P_0}\right) . \tag{5.29}$$

Here, r and a are in the units of λ_{Di}, and n, n_e, and P_0 are, as usual, in the units of n_0, and the ion drift velocity u is, as usual, in the units of $\sqrt{2T_i/m_i}$.

In the basic state, the right-hand side of (5.29) is zero due to the balance of absorption, the last term on the right-hand side of (5.29), and ionization (the first term on the right-hand side), such that no ion fluxes exist in the ground state $nu = 0$.

However, the probe grain inevitably creates plasma fluxes in its surrounding by disturbing this balance. We can introduce the factor ψ describing the screening of the grain field by the relation

$$e\phi = -Z_{d,1}e^2\psi/r; \qquad V_{1,2} = \frac{Z_{d,1}Z_{d,2}e^2}{r_{1,2}}\psi(r_{1,2}) \; . \tag{5.30}$$

The disturbance of the ion density can be written as $\delta n = N/r$. Due to adiabatic character of the electron density perturbations, we have $\delta n_e/n_{e,0} = \delta n_e/1 - P_0 = -z_1 a\psi(r)/r$, where $z_1 = Z_{d,1}e^2/aT_e$ is the dimensionless value of the charge of the grain 1. Denote then $G(r)$ by

$$G(r) = \psi(r) - \tau N(r)/z_1 a \; . \tag{5.31}$$

The force balance equation for plasma ions then have a simple form

$$\frac{d}{dr}\left(\frac{G}{r}\right) = \frac{z_0}{z_1}\alpha_{dr}P_0 u \; . \tag{5.32}$$

This equation includes the balance of the electrostatic force, the ion pressure force, and the force related with the ion friction on dust grains.

Disturbances appear not only for plasma electrons and ions (which excite the ion fluxes) but also in dust charges of the basic state

$$\delta P/P_0 = \delta z/z_0 = 1/(z_0 + 1)(\delta n_e/n_{e,0} - \delta n) \; .$$

In general, this process should be taken into account but it does not change much the final effect qualitatively leading to the additional numerical factor $z_0/1 + z_0$ in the expression determining the collective attraction. The success in further calculations obtained for spherically symmetric case is due to an observation that the combination of (5.29) and (5.32) together with the Poisson equation can be transferred to a system of two linear equations containing the derivatives with respect to the radius from the center of the embedded charge. We have

$$\frac{d^2G(r)}{dr^2} = k_0^2(G(r) - (1+\tau)\psi(r)) \; , \tag{5.33}$$

$$\frac{d^2\psi(r)}{dr^2} = \left(1 + \frac{P_0}{1+z_0} + \tau\left(1 - \frac{P_0 z_0}{1+z_0}\right)\right)\psi(r) - \left(1 + \frac{P_0}{1+z_0}\right)G(r) \; , \tag{5.34}$$

and

$$k_0^2 = \frac{\alpha_{dr}\alpha_{ch}z_0 a^2 P_0^2}{\tau}\left(\frac{z_0}{1+z_0}\right) \; . \tag{5.35}$$

Here, k_0 is in the units of $1/\lambda_{Di}$, and a and r are in the units of λ_{Di}. In case one does not take into account the grain charge variations of the background state, the Debye screening factor in the first term on the right-hand side of (5.34) takes the standard form $1+\tau(1-P_0)$, and the last factor $z_0/(1+z_0)$ in expression (5.35) for the coupling constant k_0^2 should be omitted. Solution of this set of equations, taking into account that the coefficients in front k^2 are real and excluding the solutions which increase indefinitely with an increase of the distance r, has the form

$$\psi(r) = \psi_e \exp(-k_e r) + \psi_c \cos(k_c r) \ , \tag{5.36}$$

$$k_e = \sqrt{\frac{R+S}{2}}; k_c = \sqrt{\frac{R-S}{2}}; R = \sqrt{S^2 + 4k_0^2 P_0 \tau} \ , \tag{5.37}$$

and

$$S = k_0^2 + 1 + \frac{P_0}{1+z_0} + \tau\left(1 - \frac{P_0 z_0}{1+z_0}\right) \ . \tag{5.38}$$

The second term of (5.35), with the changeable sign, describes the set of potential wells decreasing with distance. The potential energy of another embedded grain with the charge Z_d is found by multiplying (5.36) by $Z_d z a T_e/r$. Contrary to usual plasmas, the potential (5.35) contains always an exponential term and an cos-type term. Thus the effect of attraction appears for any boundary condition which leads to the non-zero value of ψ_c. Thus the phenomenon of the grain collective attraction is a general one and exists for any sort of grains. The amplitude of this attraction can depend on the surface grain properties and the rate at which the grain can absorb the flux.

Equations (5.33) and (5.34) describe the coupling between the electrostatic field potential and the flux field potential with the coupling constant k_0^2 proportional to some power of the collective parameter P_0. Thus for $P_0 = 0$ the coupling of these fields is absent and the collective effects disappear. The presence of coupling of these two fields in a complex plasma is a natural effect since the flux influences the polarization charge around the grain and the polarization charge influences the flux. The appearance of collective effects is therefore simple in the physical interpretation and should be inevitable in any complex plasma system.

5.3.4 Natural Boundary Conditions

The first natural requirement is that the total charge of the embedded grain is equal (with the opposite sign) to the total polarization charge. A simple investigation gives this requirement:

$$\psi(a) - a\frac{d\psi(r)}{dr}\bigg|_{r=a} = 1 \ . \tag{5.39}$$

The second requirement is that the change of the total power in the disturbed region outside the embedded grain is equal to the power absorbed by the embedded grain

$$a\frac{dG(r)}{dr}\bigg|_{r=a} - G(a) = w; \quad w = \alpha_{dr} P_0 a(4\pi a^2 nu\big|_{r=a}) \,. \tag{5.40}$$

This flux is changing the value of the embedded charge. In the approach used here this change is small although it can be taken into account for the absorbing embedded charge. We give here the result for using the boundary conditions for the simplest case $w = 0$

$$\psi_e = \frac{\exp(k_e a)}{(1 + k_e a)} \left[\frac{k_e^2 - k_0^2}{k_e^2 + k_c^2}\right] \tag{5.41}$$

and

$$\psi_c = \frac{1}{\cos(k_c a) + k_c a \sin(k_c a)} \left[\frac{k_c^2 + k_0^2}{k_e^2 + k_c^2}\right] \,. \tag{5.42}$$

These expressions can be used to obtain conditions where the results of [40] are valid and the range of applicability of the corresponding expressions. For the term with the cos function, leading to the collective attraction, the condition where the field of the charge can be approximated as a field of a point charge is found for $k_0\lambda_{Di} \ll 1$ to be $a^2 \ll \lambda_{Di}^2$, i.e., the size of the embedded grain is much smaller than the ion Debye radius. This restriction seems to be natural and expectable since the attraction in this limit coincides with that found in [40]. For $k_0\lambda_{Di} \gg 1$, the applicability range of results [40] for the collective attraction is much enlarged, $a/\lambda_{Di} \ll 1/\sqrt{P_0\tau}$ (note that the right-hand side of this inequality is usually larger than 1).

The fulfillment of conditions (5.39) and (5.40) is checked by the obtained solutions and by the condition of the adiabatic exclusion of interactions at infinite distances: to be able to integrate with respect to the distances of the terms with cos means inclusion of damping (e.g., on neutral atoms) with subsequent application of the limit where this damping tends to zero. Thus this point is not trivial and needs a physical approach to regularize the calculations. The last statement was checked by calculations where the friction of ions in a neutral atom gas was taken into account.

For better comparison with the non-collective attraction, we can introduce the collective coefficient $\eta_{coll} = k_0$ and the screening factor f_{scr} which shows the difference of the screening in the limit $\eta_{coll} \ll 1$ from the Debye screening. We have

$$f_{scr} = \sqrt{1 + \frac{P_0}{1 + z_0} + \tau\left(1 - \frac{z_0 P_0}{1 + z_0}\right)} \,. \tag{5.43}$$

The physical meaning of the difference introduced by f_{scr} not equal to 1 ($f_{scr} = 1$ corresponds to the ion Debye screening) is that both the electron grain charge variations in the ion screening (the second term under the square

root sign) and the electron screening together with the changes due to the grain charge variations (the third term under the square root sign) are taken into account.

5.3.5 Limiting Expressions for Collective Attraction

Only in the limit $\eta_{coll} \ll 1$ the collective attraction term plays a role of small correction to the Debye screening when

$$V_{1,2} = \frac{Z_d^2 e^2}{r_{1,2}} \left[\exp\left(-f_{scr} \frac{r_{1,2} - a}{\lambda_{Di}} \right) + \frac{\eta_{coll}^2}{f_{scr}^2} \cos\left(\frac{\eta_{coll} r_{1,2} \sqrt{P_0 \tau}}{f_{scr} \lambda_{Di}} \right) \right] . \quad (5.44)$$

In the opposite limit $\eta_{coll} \gg 1$ we have

$$V_{1,2} = \frac{Z_d^2 e^2}{r_{1,2}} \left[\frac{P_0 \exp\left(-\eta_{coll}(r_{1,2} - a)/\lambda_{Di}\right)}{(1 + z_0)\eta_{coll}^2 \left(1 + \eta_{coll} a/\lambda_{Di}\right)} + \cos\left(\sqrt{P_0 \tau} \frac{r_{1,2}}{\lambda_{Di}} \right) \right] . \quad (5.45)$$

Note that expression (5.45) is derived for $\beta \ll 1$. Since k_0^2 can be written in the form $k_0^2 = \beta z_0 P_0^2 \alpha_{dr} \alpha_{ch} a/(1 + z_0)$ and $a \to a/\lambda_{Di}$ is small, the product $\alpha_{dr}\alpha_{ch} < 1$ for $\beta \ll 1$ and the condition of validity of (5.45) is usually violated. Still an important observation is that with an increase of η_{coll} the role of the collective cos term rapidly increases and has a tendency to be dominant in the screening, with the exponential term being small. The latter limit is not reached since for $\beta \gg 1$ the drag coefficient decreases more rapidly than $1/\beta$. Nevertheless for $\eta_{coll} \ll 1$ the second cos term becomes important when the first exponential term is small, and it can change the sign thus describing the effect of the collective attraction.

In (5.44), the collective attraction is similar to the non-collective attraction due to the ion flux and at small distances the Coulomb screened part of the interaction dominates while the attraction starts to dominate at large distances where the Coulomb repulsion is screened. A difference of course is that the collective attraction coefficient is proportional to P_0 and is absent if $P_0 \to 0$. But in real experiments P_0 is often of the order of 1. The other factor a^2/λ_{Di}^2 is the same as in the non-collective ion flux attraction. The coefficient η_{coll} depends also on the product of the drag and the charging coefficients as well as on z_0; this dependence is also important, but in the absence of the ion drift these coefficients for $\beta \ll 1$ are of the order of 1 (in the case of the presence of the ion drift the expressions given above are not valid since additional terms proportional to the ion drift velocity and derivatives of the drag coefficient appear).

An important feature of the collective attraction term is the appearance of a small parameter τ in the denominator in front of the cos term, which is absent for the non-collective attraction. This makes the amplitude of the collective attraction larger than that of the non-collective attraction at least by one or two orders of magnitude (if of course P_0 is of the order of 1 and τ is of the order of 10^{-2} as usual in current experiments). Still due to the condition

$\eta_{col} \ll 1$ the coefficient in front of the collective term in (5.44) is small and the attraction operates only at distances where the Coulomb potential is screened, similar to the case of the non-collective attraction. Thus we see that in general in the limit $\eta_{coll} \ll 1$ the collective attraction has some similarities with the non-collective attraction.

Similar type of attraction forces can be obtained in the case where the distance between two dust particles is larger than the ion–neutral mean-free path when the ion-neutral friction should be substituted for the ion–dust friction and the effect of ion diffusion on neutral atoms should be taken into account in the continuity equation. It appears that for $\tau \ll 1$ the diffusion can be neglected (its contribution is τ times less than the ion pressure) but the balance of the plasma sink and ionization is determined by the charging process in the way it was described before. Then the only change occurs in the value of the collective parameter η_{coll}, which now depends on the ion-neutral mean-free path λ_{in}. We denote the new parameter as $\eta_{col,in}$. Simple calculations yield

$$\eta_{col,in} = \frac{P_0 \alpha_{ch} z_0}{1 + z_0} \frac{a}{\lambda_{in}} \,. \tag{5.46}$$

Since $a \ll \lambda_{in}$, the coefficient $\eta_{col,in}$ is always less than 1. It means that for the case where the ion-neutral collisions dominate the collective effects are described by expression (5.44) with substitution of $\eta_{coll,in}$ for η_{coll} and the attraction occurs at the distances where the Debye screened part of the potential is small. Since $\eta_{col,in}$ does not depend on τ the attraction can dominate for $\exp(-r_{1,2}/\lambda_{Di}) \ll aP_0/\lambda_{in}$ although the distance of the first minimum $\approx \lambda_{Di}\lambda_{in}/aP_0\tau$ depends strongly on τ. Figure 5.2 illustrates the dependence of the screening factor $V_{1,2}/(Z_d^2 e^2/r_{1,2})$ as a function of the ratio of distance to the ion Debye length $r = r_{1,2}/\lambda_{Di}$ for $\tau = 0.2$, $P_0 = 0.5$, and $\eta_{coll} = 1/3$.

In existing experiments, the presence of the ion drift is usually important. In case the experiments are performed not in the plasma sheath but, e.g., in striations of a glow discharge [7] the electric field is still present and also creates the ion drifts. A simple generalization of the consideration described

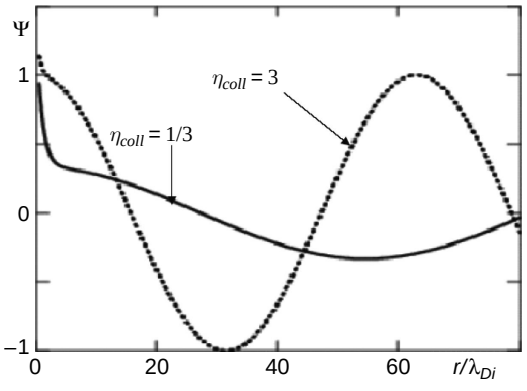

Fig. 5.2. The "screening" factor ψ for the collective interactions of two grains $\psi = V_{1,2} r_{1,2}/(Z_d^2 e^2)$ as a function of distance r in the units of the ion Debye length λ_{Di}. The solid line corresponds to the relatively small value of the collective parameter $\eta_{coll} = 1/3$ and the dotted line corresponds to the relatively large value $\eta_{coll} = 3$

here can be performed with more general expressions for the dielectric constant including effects of the ion drift, the ion-neutral collisions, and the dust pressure.

5.3.6 Attraction in an Ion Flow for $\beta \ll 1$

In the presence of an ion drift (e.g., in the plasma sheath) the distribution of all parameters is inhomogeneous and the definition of the basic state is much more complicated. We consider here a homogeneous state with the ion drift in a model approach. The presence of friction of ions on dust can create a homogeneous ion drift in case this friction is balanced by another external force. The external force supporting the ion drift does not appear in the responses in case this external force does not depend on plasma parameters. Of course this model can serve only to qualitatively illustrate of the problem. We thus assume that such a force exists and supports the constant ion drift.

Then we obtain the static dielectric permittivity (in a way similar to that in the previous section) by taking into account small perturbations from the initial ground state [42]. There is no reason to call this effect the collective wake effect since (as in the case of the absence of an ion flow) the attraction appears in all directions, not only in the direction of the ion flow. Specifically, attraction appears also in the plane perpendicular to the ion flow. We do not give here an expression for the linear complex plasma response because it is rather cumbersome. We only mention that the basic state, in addition to the quasi-neutrality condition and the condition of the balance of plasma absorption and ionization, is determined by the (third) condition which is the maintenance of the ion flux by the external force.

We illustrate the results of numerical computation [42] for the interaction perpendicular to the ion flow for the normalized potential energy $U = V_{1,2}\lambda_{Di}/Z_d^2 e^2$ just including the $1/r$ dependence showing a decrease of the potential minima with increased separation between the grains (see Figs. 5.3 and 5.4). Figure 5.3 demonstrates that the depth of the potential

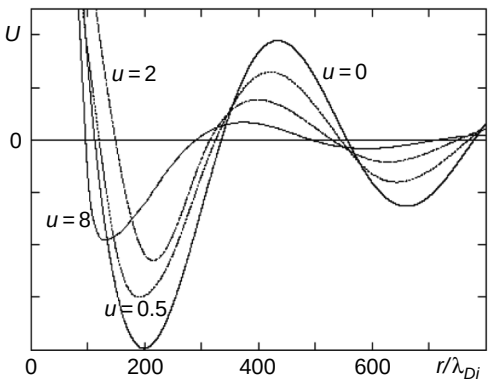

Fig. 5.3. The collective interaction U in the presence of an ion flow for the direction perpendicular to the flow for different values of the drift velocity $u = u_{flow}/v_{Ti}$ and $P_0 = 0.6$, $\tau = 0.02$, $z = 2$, and $a/\lambda_{Di} = 0.02$ as a function of the (large) separation r of the grains. The units for U are arbitrary; the depth of the potential wells can be compared with the shown curve for $u = 0$

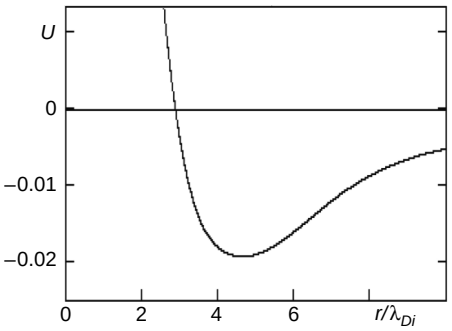

Fig. 5.4. The same as in Fig. 5.3 but for small separations between the grains for $u = 2$, only the first potential well is shown. Such a potential well at short grain separation does not exist for $u = 0$, therefore on the vertical axis the values of U are shown

wells decreases with increasing ion drift velocity and decreases with increasing separation between the grains. The depth of the first potential well also decreases with an increase of the ion flux velocity. The presence of an attraction well at short distances in the presence of an ion flow is a new phenomenon which should be investigated more in future.

5.3.7 Attraction in a Magnetic Field for $\beta \ll 1$

Recent experiments using magnetic fields in complex dusty plasmas show interesting structures, rotations, and modification of the dust motion [43, 44]. Here, we discuss the influence of magnetic fields on the collective grain–grain interaction [45], assuming that the ground state is the same as in the absence of a magnetic field and the absence of any ion drift excited externally.

Since in most current experiments the magnetic field is not so strong to change the dust charging and drag coefficients we consider only the influence of the magnetic field on the ion disturbances of the ground state. The latter are due to the embedded probe grain. All other disturbances of the ground state are changed by the magnetic field $\mathbf{B}$ only due to their dependence upon the ion disturbances which are changed by the appearance of the $[\mathbf{E} \times \mathbf{B}]$ ion drift caused by the grain field $\mathbf{E}$.

In the presence of such magnetic fields, the equilibrium conditions of the power balance and plasma quasi-neutrality are the same as in the absence of the magnetic field since the Lorentz force is zero for the zero ion drift velocity in the ground state. The calculation of the static dielectric permittivity is straightforward and similar to that performed above. The only additional term is the Lorentz force acting on ions. For electrons, the magnetic field changes their motion when they are magnetized but does not change their contribution to the static dielectric function (as in the absence of the magnetic field it gives the Debye screening contribution).

We introduce the dimensionless magnetic field in a way similar to that for the electric field:

$$\mathbf{B} \to \frac{\mathbf{B}^{ac}\sqrt{2}v_{Ti}\lambda_{Di}^2}{acT_e} \,. \tag{5.47}$$

The dimensionless Lorentz force $\mathbf{F}_L$ is then given by

$$\mathbf{F}_L = e\mathbf{u} \times \mathbf{B} \,, \tag{5.48}$$

where the superscript ac is used (as before) for the actual field strength. Straightforward calculations give us the value of the static dielectric permittivity in the form

$$\epsilon_{\mathbf{k}} = 1 + \frac{\tau}{\lambda_{Di}^2 k^2} \left[1 - \frac{P_0 z_0}{1+z_0} + \left(1 + \frac{P_0}{1+z_0} \right) \frac{R_B - \frac{P_0^2 z_0^2 \alpha_{ch} \alpha_{dr}}{k^2 (1+z_0)}}{\tau R_B + \frac{P_0^2 z_0^2 \alpha_{ch} \alpha_{dr}}{k^2 (1+z_0)}} \right] \,, \tag{5.49}$$

where

$$R_B = \frac{k_z^2}{k^2} + \frac{k_\perp^2}{k^2} \frac{P_0^2 z_0^2 \alpha_{dr}^2}{P_0^2 z_0^2 \alpha_{dr}^2 + B^2} \,. \tag{5.50}$$

For $B \to 0$, we obtain the previous result. Therefore the critical strength of magnetic fields which starts to influence the dust–dust interaction corresponds to the value where the Lorentz force is equal to the ion friction on dust (due to dust drag) and is completely determined only by the drag coefficient. Because both forces are proportional to the ion drift velocity, the latter does not enter in the expression for the critical magnetic field. In our dimensional units, we have

$$\frac{B_{cr}^2}{2\pi n_0 m_i c^2} = \frac{a^2}{\lambda_{Di}^2 \tau^2} P_0^2 z_0^2 \alpha_{dr}^2 \,. \tag{5.51}$$

For practical applications we can write the critical field in the number of Gauss:

$$B(Gauss) = 9.4 \times 10^4 \left(\frac{0.02}{\tau} \right) \sqrt{\left(\frac{n_0}{10^9 \mathrm{cm}^{-3}} \right)} P_0 z_0 \frac{a}{\lambda_{Di}} \ln \Lambda \,, \tag{5.52}$$

where $\ln \Lambda$ is the Coulomb logarithm (remember that we consider small charge probe grain where the drag coefficient is determined by the Coulomb scattering). Note that this criterion strongly depends on the dust size a. Expression (5.51) shows that the magnetic field introduces an anisotropy in the attraction; with an increase of the magnetic field, the attraction is suppressed in the direction perpendicular to the magnetic field and enhanced in the direction along the magnetic field.

Numerical calculations show that a stronger magnetic field also introduces an anisotropy in the attraction. In this case, the increasing magnetic field leads to the attraction larger both in the perpendicular and in the parallel direction but the distance between the particles corresponding to the minimum of the attraction potential well is decreasing in the perpendicular direction and increasing in the longitudinal direction. Figure 5.5 illustrates the collective attraction along the magnetic field and Fig. 5.6 shows the collective attraction perpendicular to the magnetic field. We see that relatively high magnetic fields make the potential well deeper with a shorter extension in the direction perpendicular to the field [45].

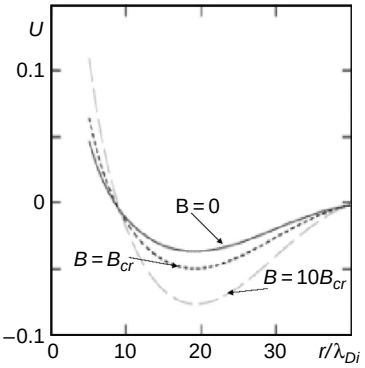

Fig. 5.5. Potential of the collective dust–dust interaction U (in the units of $Z_d^2 e^2/r$) along the magnetic field. The solid curve corresponds to $B = 0$, the dotted curve corresponds to $B = B_{cr}$, and the dash curve corresponds to $B = 10B_{cr}$

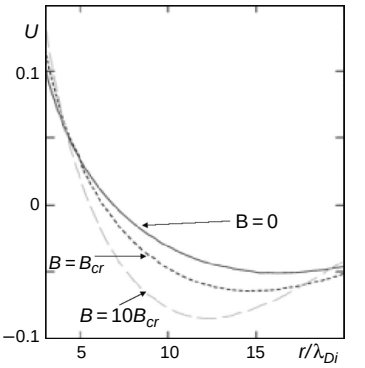

Fig. 5.6. Potential of the collective dust–dust interaction U (in the units of $Z_d^2 e^2/r$) perpendicular to the magnetic field. The solid curve corresponds to $B = 0$, the dotted curve corresponds to $B = B_{cr}$, and the dash curve corresponds to $B = 10B_{cr}$

5.4 Collective Interactions for Non-linear Screening

5.4.1 Collision-dominated Case $\beta \gg 1$

As we pointed out earlier, the non-linear screening is most appropriate for experiments in complex plasmas. To treat the collective effects for non-linear screening we note that the non-linear screening is usually strong and at distances where it operates the non-linearity suppresses the collective effects. On the other hand, all collective lengths obtained so far are larger than the non-linear screening length. Approximate non-linear screening fields were found above in the limit where the linear "tail" part was neglected. In the absence of many grains (when the collective effects are absent) this non-linear part should be matched with the linear screened Coulomb "tail" (as mentioned before).

In the presence of many grains where the collective effects are important the non-linear screening expressions should be matched with the linear one which takes into account the collective effects. Generally, the collective effects and the non-linear screening should be considered together. But to illustrate the main physical consequence of the non-linear screening on collective interactions it is sufficient to use a simpler approach. This approach neglects the collective effects in the non-linear part of the grain screening and, at distances

where the non-linearity becomes small, matches this screening with the linear expressions which take into account the collective effects. The physical difference between the linear and the non-linear screening then appears to be very substantial and can be demonstrated in this simple approach.

In any case, in the absence of collective effects one can also find separately the non-linear screening solution and the screened Coulomb solution and join them at the distances where the non-linearity becomes weak. This procedure gives almost the same result as an exact solution without separating the parts with the strong and weak screening. The collective effects add additional terms in the linear solutions and the coefficients of two terms (the exponential and the cos-type terms) can be found from the boundary condition at the edge of the non-linear screening.

The previous consideration for $\beta \ll 1$ was performed with boundary conditions at the grain surface. This is the only difference in formally obtaining the collective effects for the linear and non-linear screening. But there is also a different physics included and this is related with the previously mentioned qualitative difference between the linear and the non-linear screening. Namely, in the case of non-linear screening the screening factor is vanishing at a finite distance which means formally that substantially larger derivatives of the screening factor ψ takes place and therefore the attraction appears just after the linear approximation starts to be valid, i.e., not due to the change of the sign of the oscillating cos-type term but due to the negative value of the coefficient in front of it. In this aspect the non-linear collective attraction becomes even more similar to the non-collective one where the corresponding screening term is always negative.

Another important point for the non-linear collective effects is the rapid decrease of the drag coefficient with increasing β, which means that the main effect retarding the ion between two interacting grains is the ion friction on neutrals (collision-dominated case). We restrict ourselves here only to the latter case [46, 47].

5.4.2 Ionization Proportional to Electron Density

The case of ionization source proportional to the electron density is the most interesting for existing experiments. In this case, the linear solution for ψ contains an exponent and the oscillating cos-type term; their amplitudes can be found by matching with the non-linear solution for $\psi = (1-r/R_{nl})^{2/(1-\nu)}$. The non-linear function ψ depends on two non-linear parameters β and ν (the degree of non-linearity in screening, $0 < \nu < 1$) via $R_{nl} = R_{nl}(\beta, \nu)$. We consider the range $0.5 < \beta < 100$. We write the collective solution in the form

$$\psi_{coll} = A(\beta,\nu)\exp(-\lambda_1(r-R_{nl}(\beta,\nu)(1-\Delta(\beta,\nu)))+B(\beta,\nu)\cos(\lambda_2 r)\ , \quad (5.53)$$

where all distances and the grain size are in the units of λ_{Di}. For the collision-dominated case we have

$$\lambda_1 = \sqrt{k_0^2 + 1 + \frac{2\sqrt{\pi}\alpha_{ion}}{(1+2\sqrt{\pi}\alpha_{ion})(1+z)}}, \quad \lambda_2 = \frac{k_0}{\lambda_1}\sqrt{\frac{2\tau\sqrt{\pi}\alpha_{ion}}{1+\alpha_{ion}2\sqrt{\pi}}}\,, \quad (5.54)$$

and

$$k_0^2 = \alpha_{ion}\frac{z}{1+z}\frac{a}{\lambda_{in}}, \quad P_0 = \frac{2\sqrt{\pi}\alpha_{ion}}{1+2\sqrt{\pi}\alpha_{ion}}\,. \quad (5.55)$$

Here, $R_{nl}(\beta,\nu)(1-\Delta(\beta,\nu))$ is the distance between the grains where the non-linear screening is matched with the linear collective screening. The function $\Delta(\beta,\nu)$ is found by a numerical solution of the transcendent equation

$$\frac{(\Delta(\beta,\nu))^{2/(1-\nu)}}{1-\Delta(\beta,\nu)} = d(\nu)\beta^{-2/(3-\nu)}\,. \quad (5.56)$$

The result is presented in Fig. 5.7 [47]. The two "screening" factors in the units of $R_{nl}(1-\Delta(\beta,nu))$ are given by Fig. 5.8.

Then the continuity conditions give us the following coefficients:

$$A(\beta,\nu) = \Delta^{(1+\nu)/(1-\nu)} \times \frac{(2/(1-\nu))\cos(\lambda_2 R(1-\Delta)) - \lambda_2 R\Delta\sin(\lambda_2 R(1-\Delta))}{\lambda_1 R\cos(\lambda_2 R(1-\Delta)) - \lambda_2 R\sin(\lambda_2 R(1-\Delta))} \quad (5.57)$$

and

$$B(\beta,\nu) = \Delta^{(1+\nu)/(1-\nu)} \times \frac{\lambda_1 R\Delta - 2/(1-\nu)}{\lambda_1 R\cos(\lambda_2 R(1-\Delta)) - \lambda_2 R\sin(\lambda_2 R(1-\Delta))}\,. \quad (5.58)$$

These (calculated numerically) coefficients are shown in Fig. 5.9 for $\tau = 0.1$, $a/\lambda_{in} = 0.5$, and for the relatively large ionization rate $\alpha_{ion} = 2.5$. Figure 5.9 demonstrates that the effective charge left for the collective screening is rapidly

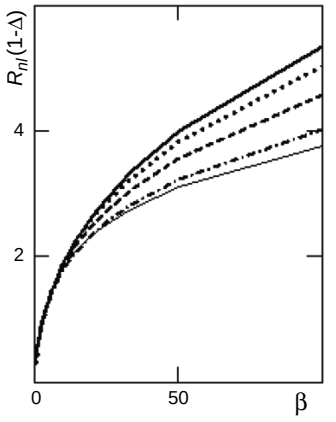

Fig. 5.7. The radius $R_{nl}(\beta,\nu)(1-\Delta(\beta,\nu))$, where the non-linear screened electrostatic potential of the grain field ψ_{nl} should be matched with the collective potential ψ_{col}. The thick solid line corresponds to $\nu = 0.1$, the dotted line corresponds to $\nu = 0.3$, the dashed line corresponds to $\nu = 0.5$, the dash-dotted line corresponds to $\nu - 0.7$, and the thin solid line corresponds to $\nu = 0.9$

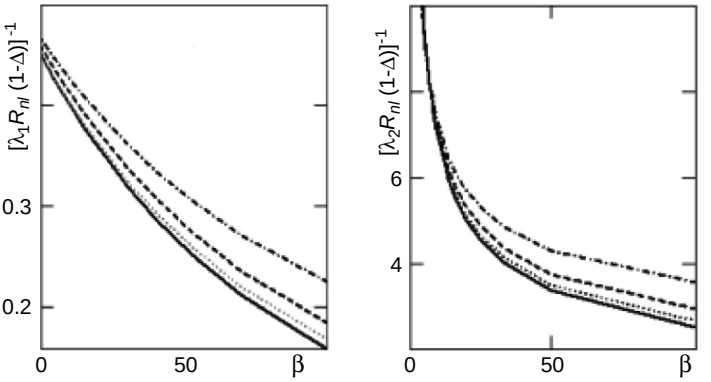

Fig. 5.8. The collective radii $1/\lambda_1 R_{nl}(\beta,\nu)(1-\Delta(\beta,\nu))$ and $1/\lambda_2 R_{nl}(\beta,\nu)(1-\Delta(\beta,\nu))$ of the collective exponential screening in the units of $R_{nl}(\beta,\nu)(1-\Delta(\beta,\nu))$, where the non-linear screened electrostatic potential of the grain field ψ_{nl} is joint with collective potential. The thick solid line corresponds to $\nu = 0.1$, the dotted line corresponds to $\nu = 0.3$, the dashed line corresponds to $\nu = 0.5$, and the dash-dotted line corresponds to $\nu = 0.9$

decreasing with β. But the important effect is that the non-linear screening produces a negative value of the coefficient B for $\beta \gg 1$. This indicates the presence of grain attraction just outside the non-linear screening radius, i.e., at much shorter distances than those for the linear case $\beta \ll 1$. The difference between the non-linear screening ($\beta \gg 1$) and the linear screening

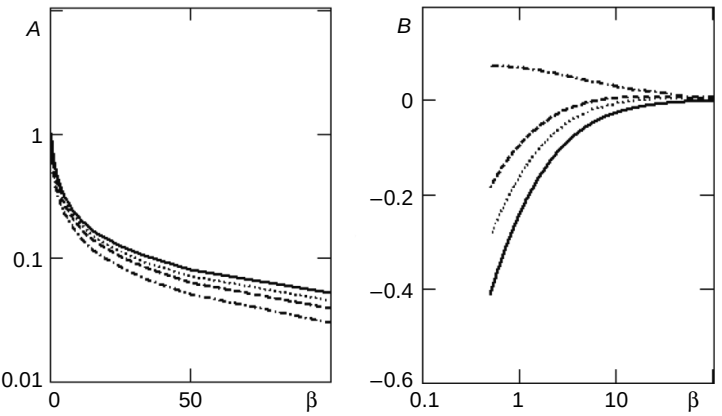

Fig. 5.9. The coefficients $A(\beta,\nu)$ and $B(\beta,\nu)$. The thick solid line corresponds to $\nu = 0.1$, the dotted line corresponds to $\nu = 0.3$, the dashed line corresponds to $\nu = 0.5$, and the dash-dotted line corresponds to $\nu = 0.9$. The value of the coefficient B is negative for most cases causing grain attraction with the exception of $\nu = 0.9$ close to the screened Coulomb potential, where this coefficient is positive

($\beta \ll$)1 is in the larger value of the potential at the "joining" distance (found from the continuity of the potential) determining not only the effective charge left for the collective screening but also the flux to the surface of the grain which is found by the continuity of the electric field at the joining distance.

Due to the negative value of the coefficient B, the first attraction well can be located close to the non-linear radius R. With an increase of β, the absolute value of B decreases and the location of the first potential well can be shifted to distances where $\cos(\lambda_2 r)$ becomes negative. This is illustrated by Fig. 5.10. The energy at the bottom of the first potential well corresponds to the energy of the grain trapping. This energy becomes smaller as soon as the potential well starts to be located at the distance determined by the change of sign of $\cos(\lambda_2 r)$. Therefore we have shown the obtained results in two scales in Fig.5.11. We can see that the trapping energy is quite large in the case where the potential well is located close to R_{nl} and is related with the plasma flux (negative B). The trapping energy for large β is much smaller than that for smaller β. The presence of two possible locations of the potential well can be related with observations of different crystal structures in different parts of a complex plasma.

Thus the non-linearity in grain screening makes the collective attraction much larger. This is important for applications since experimental conditions for the plasma condensation correspond to the case of non-linear screening, $\beta \gg 1$.

5.4.3 General Properties of Non-linear Collective Attraction

Constant Ionization Source. Dependence of the collective attraction on the character of the ionization source is one of general problems to be solved. The simplest case is to treat a constant source of ionization independent of

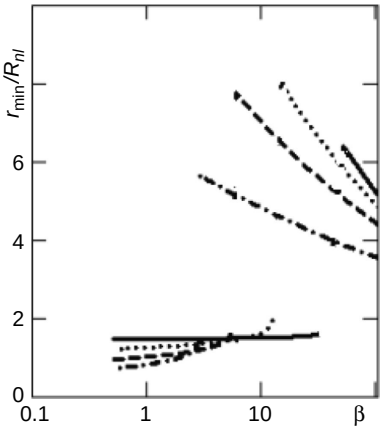

Fig. 5.10. Location of the first attraction minimum; the distances are in the units of the non-linear screening radius R_{n1}. The sudden change of the minimum's position is related with the disappearing potential well at small distances due the negative value of B and the appearing well due to the change of sign of $\cos(\lambda_2 r)$. The solid line corresponds to $\nu = 0.1$, the dotted line corresponds to $\nu = 0.3$, the dashed line corresponds to $\nu = 0.5$, and the dash-dotted line corresponds to $\nu = 0.7$

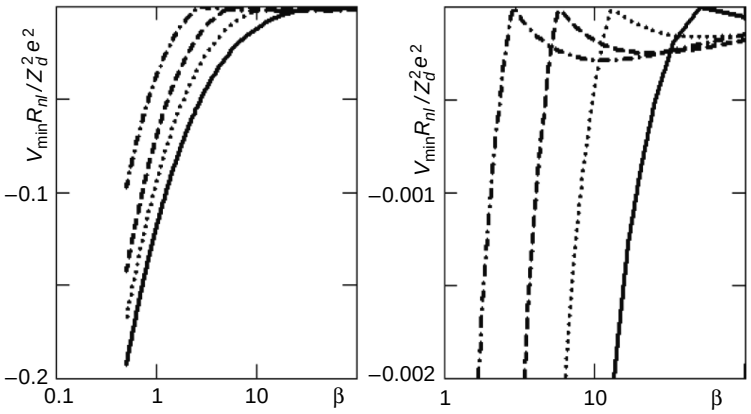

Fig. 5.11. The confining energy in the units of $Z_d^2e^2/R$ at the location of the first attraction minimum in the region of small and large β. The solid line corresponds to $\nu = 0.1$, the dotted line corresponds to $\nu = 0.3$, the dashed line corresponds to $\nu = 0.5$, and the dash-dotted line corresponds to $\nu = 0.7$

the electron density. Investigation of the case $\beta \ll 1$ [48] shows that there exist two exponents in the screening factor ψ with always positive expressions under the exponential functions. The second exponent (similar to the case of an ionization source proportional to the electron density) is decaying on much larger distances than the first exponent decaying on the distances of the order of the Debye length. The coefficient in front of the second exponent can be negative only for a special case of low z_0 or $\tau \approx 1$. For $\tau \ll 1$ the coefficient in front of the second exponent is always positive and no attraction takes place. Investigation of strongly non-linear screening [49] shows the opposite: the coefficient in front of the second exponent is always negative and the related attraction is always present. The position of the first attraction well does not jump as in the case where the ionization source is proportional to the electron density but just disappears (the cos-type change of sign of ψ is not present).

General Ionization Source. The previous investigation shows us that in the presence of coupling of the flux field and the electrostatic field there always appear two exponents in the screening factor ψ. For the case where the source is proportional to the electron density, one of the λs in the exponents is positive and the other is purely imaginary, while for the constant ionization source both $\lambda_{1,2}$ in the exponents are positive. In the case where these are two types of the ionization source the factors $\lambda_{1,2}$ are always complex and

$$\psi = Re\{A\exp(-\lambda_1 r) + B\exp(-\lambda_2 r)\}\ . \tag{5.59}$$

Only solutions decaying with the distance are of physical meaning. This shows that the collective attraction is a general phenomenon appearing for any ionization source. Its physics is related with the coupling of the plasma flux with

the plasma polarization giving two exponents, with one decaying with the Debye length and the other decaying with the mean-free path for the plasma absorption on grains. Certainly, the coupling itself changes the factors of the decaying exponent but the presence of two exponents (the screening field potential and the flux potential) is very natural. The collective effects related with the flux have a very simple physical reason to exist. They are inevitable in a complex plasma, i.e., a plasma with a large influence of plasma fluxes on the behavior of the system.

Collective Drag Effect. Since additional fields related to the collective effects are present around the grains, the natural question is about their role in the ion scattering to produce an additional drag force which should be called the "collective drag force". This problem was treated in [50] and the result is that this additional drag force is of the order of the usual drag force. It can change the corresponding coefficient in the total drag force by not more than a factor of 2. This force is important for moderate values of β about 2–20 and it decreases with an increase of β.

Interference of Non-linear Screening and Collective Effects. To solve this problem mathematically, one need to take into account simultaneously the non-linear effects and the collective effects. This was performed by generalizing the Gurevich non-linear screening potential [51, 52] for collective effects using the hydrodynamic type of description for average densities [53]. In this treatment the collective effects are also modified by non-linearities. The equations found [53] are non-linear both for ψ and for G. They were solved numerically for a particular set of parameters; it was shown that the depth of the attraction well increases when the problem is treated as completely non-linear. This indicates a new possibility of investigation of the collective attraction but needs a large amount of numerical work to scan all possible solutions and to decide whether this enhancement is an often-occurring or rare phenomenon. We restricted ourselves here to a simpler approach which leads to explicit final results although in the case where the non-linear screening length appears to be of the order of the collective scale length, the approach used can give only estimates by the order of magnitude.

Interaction in a Strong Magnetic Field. At present, even the simpler problem of the linear collective grain attraction in the presence of a strong magnetic field for different directions to the magnetic field is not analyzed yet. This problem is not complicated and in principal can be solved by numerical computations but requires efforts to be taken. The non-linear problem of the grain attraction and the drag coefficient in the presence of a strong magnetic field has not even started so far. However, it is important for future experiment where a complex plasma is placed in a strong magnetic field.

Interaction in the Plasma Sheath and in the Presence of an Ion Flow. The general scheme for theoretical investigation of this problem is clear but a lot of efforts should be taken to solve it.

5.5 Measurements of Screened Potential in Grain–grain Collisions

Problems related to measurements of the grain screening, field non-linearities, and the grain–grain interactions are very important and constitute a broad area of (mainly future) research. We therefore discuss here the first pioneering work in this field (dealing with specific experimental conditions available at that time) which gives the grain interaction and screening for these conditions. We also discuss the possibility to transfer these results to other conditions and the question as to what could be done to obtain more general experimental information on the grain–grain interactions and screening in a complex plasma.

The first pioneering measurements of grain–grain interactions were performed in the laboratory conditions on Earth when the gravity force is significant [54, 55, 56]. To balance the Earth's gravity by the electric field, these experiments were done in the plasma sheath. All complications coming from the the sheath structure, due to the presence of the wall and the ion flow to the wall are important in this case. These experiments describe the grain collisions in the sheath and, in the absence of an appropriate model of the plasma sheath, it is difficult to extrapolate them to the grain interactions in the plasma bulk. For the latter, no experiment exists at present, and only future experiments can answer the main questions on the physics of such interactions.

These experiments in the sheath are the direct scattering experiments. There exist several indirect methods to measure the grain–grain interactions which we discuss below. The collision scattering experiments are in principle similar to those already used many years ago to determine nuclear potentials by deriving the force field from the measured trajectories of interacting particles. The difference is that for two dust particles in the sheath to collide, each of them should have the same distance from the wall which requires that the charges and the masses of the particles be equal. The experiments performed to determine the nuclear potentials are usually done with probe particles with masses much less than the mass of the nuclei (and the charge different from the charge of the nuclei). In future, one can use hollow grains in the collision experiments in a way that the charge-to-mass ratio is the same for grains of different size; this has not been performed yet.

5.5.1 Experimental Technique

The scattering experiments conducted so far use the RF discharge plasmas. The plasma chamber is basically a GEC (Gaseous Electronics Conference) reference cell [54, 55, 56] modified so that it is possible to view the interior from the side and from the top through the upper (grounded) electrode (Fig.5.12). The gases in the chamber are either helium, argon, or krypton, depending on the research requirements. The gas is "ignited" using a 13.56MHz

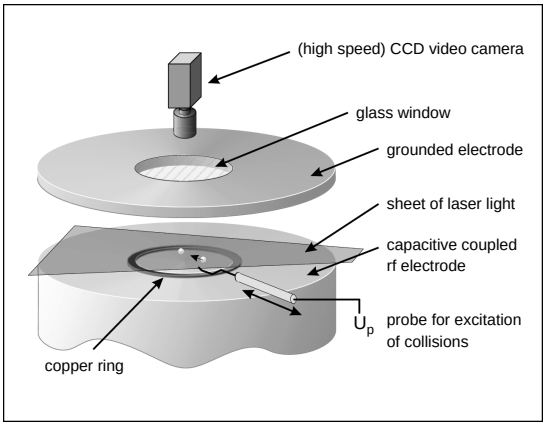

Fig. 5.12. Sketch of experimental setup for measuring the grain–grain interaction potential in the grain collision experiments

signal applied to the lower (powered) electrode. This experimental technique was used to experiments in complex plasmas other than that of measurements of the screened potential. The requirement for study of complex plasmas in the strong coupling limit, especially for investigation of phase transitions to the liquid and crystalline states, implies the use of low RF power and hence a low ionization fraction (typically 10^{-6}–10^{-7}). This ensures that both ions and neutral atoms are in the collisional equilibrium at room temperature.

Let us briefly review that requirement. In order to ignite the plasma with a 13.56MHz signal, the electron neutral $(e-n)$ collision time should be longer than the time needed to accelerate the electron from zero to the first ionization potential of the gas used (typically about 10eV). In practice, it is sufficient that "some" electrons in the distribution reach the ionization potential. The conditions for this are easily calculated. Assume that the RF potential varies as $V(t) = V_0 sin\omega t$, where $f = \omega/2\pi$ is the 13.56MHz signal frequency used. Assume further that the instantaneous electron energy $E_e(t) = eV(t)$ and that we only need to consider the initial (linear) phase of the cycle,i.e., $E_e(t) \approx eV_0\omega t$. This assumes $\omega t \ll 1$, but in any case the calculation can easily be repeated for the $\sin(\omega t)$-dependence. Writing $E_e(t) = (m_e/2)(dx/dt)^2$ and integrating

$$\int_0^{\lambda_{en}} dx = \int_0^{t_{coll,en}} \left(\frac{2eV_0\omega t}{m_e}\right)^{1/2} dt \,, \tag{5.60}$$

we obtain for the electron-neutral collision time

$$t_{coll} = \left(\frac{3m_e}{4eV_0\omega n_n^2\sigma_{en}^2}\right)^{1/3} \,. \tag{5.61}$$

Here, the collision electron-neutral mean-free path is $\lambda_{en} = 1/n_n\sigma_{en}$, with n_n being the neutral gas density and σ_{en} the electron-neutral collision cross-section. Hence the condition $E_e(t_{coll,en}) > \bar{E}_e$ yields after some algebra

$$\frac{eV_0}{\bar{E}_e} > \left(\frac{4\bar{E}_e n_n^2 \sigma_{en}^2}{3m_e\omega^2} \right)^{1/2} . \tag{5.62}$$

Substituting typical values for the gas density (10^{16}cm^{-3}) and cross-section (10^{-15}cm^2), we have

$$eV_0 > 36.7\bar{E}_e . \tag{5.63}$$

Thus a typical peak voltage of the order of 100 V is sufficient to initiate the discharge. This implies also that low-power RF devices can be used, where the gas (as well as the ion) temperature is essentially the environment (room) temperature, as desired for many applications.

5.5.2 Collision Experiments

The advantage of using micro-spheres for collision experiments is the possibility to visualize their trajectories by fast microscopy. However, the disadvantage is that not all regions of the plasma are accessible for such experiments because the micro-sphere particles have to be electrically suspended against gravity. For instance, the electrostatic field required to support a (typical) micro-sphere of the mass 10^{-10}g carrying the surface charge $Q = eZ_d \approx 10^4 e$ is about 10V/cm, as can be calculated from the force balance:

$$QE = mg . \tag{5.64}$$

This implies that only the sheath regions of a plasma [57] or striations in a DC discharge [3] (corresponding to significantly inhomogeneous plasma regimes) can be investigated in this way. Fortunately, the plasma sheaths are of interest to physicists in their own right because they mark the transition from the subsonic ion flow to the supersonic one; from the applications point of view, the sheaths are important because they are regions for plasma technological processes such as deposition and etching.

Typically, the collision experiment proceeds in two stages:

- First, a single particle is released. Its trajectory is determined by the forces, which are mainly the gravity, electrostatic, neutral drag, and ion drag forces. For the low pressure and low power conditions, other forces such as thermophoretic, photophoretic, pressure gradients, neutral convection, etc. are negligible. The neutral gas is at rest and provides the damping of the particle's motion. From the particle trajectory it is possible to derive the form of the electrostatic trapping potential $\phi_T(\mathbf{R})$ as a function of the distance R from the axis of the axially symmetric plasma chamber.
- Second, a binary collision experiment is performed. From the trajectories of two colliding particles, both of which move in the known confined potential $\phi_W(R)$, it is then possible to derive their interaction potential $\phi_I(r)$ (the total potential is $\phi_T = \phi_W + \phi_I$). Since the particle motion only takes place in the horizontal plane (to the first order), the vertical force balance

is assumed to act at all times instantaneously (observation of the particles taken from the side confirms this assumption). The equation of motion is then given by

$$m\frac{d\mathbf{v}_d}{dt} = -Q\nabla\phi_T - \mathbf{F}_D \ , \tag{5.65}$$

where the neutral drag force $\mathbf{F}_D$ is given by the standard Epstein drag law (the applicability of this description requires the neutral–neutral collision mean-free path to be much larger than the particle size). The force $\mathbf{F}_D$ is linearly proportional to the grain particle velocity $\mathbf{v}_d$. It is also implicitly assumed that the charge of the micro-sphere does not vary either systematically or stochastically. The variations can be independent of each charge on the grain trajectories when they collide as well as dependent on the inter-grain distance. The absence of the first type of variations implies homogeneous plasma conditions on the trajectory of each charge. The absence of the second type of variations implies that at least the distance between the colliding particles is larger than their size. From our previous discussion on the charge fluctuations we can conclude that a constant charge is a good assumption for micron-sized particles. Also, because of the rapid charging rate, it is reasonable to assume that the equilibrium charge is attained instantaneously compared with the dynamic scales involved. This implies that the experiments are conducted with particles moving with substantially sub-thermal velocities in a plasma.

When experiments are performed with equal size particles, both of them can experience non-linear screening which in general does not obey the law of linear superposition. It is not clear whether in the collisions the grains interact only with their "tail" screening which is linear (and the principle of superposition is valid). It is possible that the non-linearities are important at the closest distance of collisions or at other distances as well. This does not make the results less interesting because they give then the effect of collisions of equal non-linear screened grains. Therefore most probably these experiments deal with a new phenomenon not much investigated theoretically. Those experiments where one of the micro-spheres serves as a test particle with the linear screening needs this particle to be small such that the problem of detection of its trajectory by methods other than the fast microscopy arises.

For the first stage of experiment, it is observed that particles released without an initial angular momentum oscillate radially through the center (which is the point of the axial symmetry of the system). This simplifies the calculations considerably, because in this case the one-dimensional form of the equation of motion can be used. We have

$$m_d\frac{d^2x}{dt^2} = -Q\frac{\partial\phi_T}{\partial x} - \eta\frac{dx}{dt} \ . \tag{5.66}$$

Expanding the confining potential in powers series and fitting the theoretical particle trajectory to the measured one allows us to determine ϕ_T and

the friction constant η. It turns out that in almost all applications a simple parabolic potential of the type

$$\phi_T = \phi_0 + b(x - x_0)^2 \ ,$$

where x_0 locates the center and b and ϕ_0 are constants, is a sufficiently accurate description.

The next, second, stage of the collision experiments between two particles shows the following. Without angular momentum and by selecting central collisions, both particles move purely radially again. As with a single particle, the one-dimensional form of the equation can be used in this case, too. It is given by

$$m_j \frac{d^2 x_j}{dt^2} = -Q_j \frac{\partial \phi_I}{\partial x}|_{x_j - x_i} - Q_j \frac{\partial \phi_W}{\partial x}|_{x_j} - \eta \frac{dx_j}{dt} \tag{5.67}$$

for particle j interacting with the particle i, with a similar equation for the particle i interacting with the particle j. Using two identical particles ($m_i = m_j = m$ and $Q_i = Q_j = Q$), we write the difference equation by subtracting the i-equation from the j-equation. We obtain

$$m \frac{d^2 x_r}{dt^2} + \eta \frac{dx_r}{dt} + 2bx_r + 2Q \frac{\partial \phi_I}{\partial x}|_{x_r} = 0 \ , \tag{5.68}$$

where $x_r = x_i - x_j$. The sum of the i and j equations leads to the differential equation for the center of mass, $x_c = x_i + x_j$, given by

$$m \frac{d^2 x_c}{dt^2} + \eta \frac{dx_c}{dt} + 2b(x_c - x_0) = 0 \ . \tag{5.69}$$

Measuring the trajectories of both particles yields b and η from the last equation; this can be compared with the corresponding result for a single particle. From that, it is possible to obtain the interaction potential between the two particles as a function of separation distance x_r. Figure 5.13 shows the center of mass trajectories of two colliding micro-spheres. The solid line is the calculated trajectory for a parabolic potential and the friction damping due to collisions with the neutral gas. The fitted values are in agreement with the Epstein drag law as calculated from the known gas pressure and temperature. Figure 5.14 gives the derived interaction potential between the particles. The solid line is calculated on the basis of the particle motion in a parabolic potential and the Debye interaction potential. Note from Fig. 5.13 that the particles come to rest at the equilibrium separation $\langle x_r \rangle = 2.2\lambda_D$, where λ_D is the screening length fitted to the measurements. We return to this result later. Figure 5.15 shows that the screening length λ_D does not depend much on the pressure of the neutral gas (neutral particle density). The measured λ_D is much larger than the ion Debye length and is close to the electron Debye length. The smallest distance where the exponential screened potential is measured is $0.5\lambda_D$.

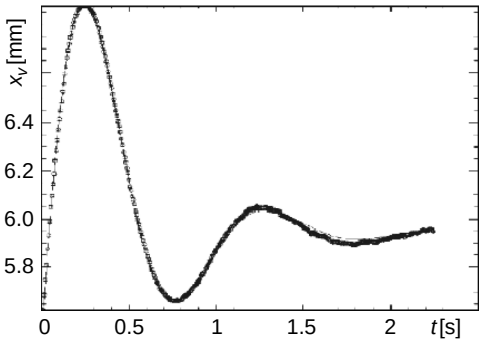

Fig. 5.13. Trajectories of the center of mass coordinate x_v for two colliding dust grains in the RF plasma sheath of argon discharge at the pressure of 2.1Pa and the weak voltage 145V. The solid line is the fitted harmonic oscillator with the damping constant $R = 2.5 \times 10^{-12}$kg/cm and the constant $b = 1.1 \times 10^{-11}$kg/s^2

Let us discuss whether the non-linear screening can be detected in these experiments. A general feature of the non-linear screening is that it operates from the radius of the grain a up to a value somewhat less than $\lambda_{srt} = 3.6\lambda_{Di}/\mu^{1/5}$, where $\mu = \tau\lambda_{Di}/za$. For the pressure of a few Pa the ion density is in the range (3–30) $\times 10^7$cm^{-3} and $\lambda_{Di} \sim (67-210)$μm, $z/\tau \approx 300$, and $a \approx 10$μm resulting in the estimate $0.022 < \mu < 0.07$, $0.466 < \mu^{1/5} < 0.588$, and $6.22\lambda_{Di} \approx 1.59\text{mm} < \lambda_{sc} < 7.725\lambda_{Di} \approx 0.64\text{mm}$.

The linear screening starts at distances less than the non-linear screening length λ_{scr}, namely $\lambda_{nonl,max} = \lambda_{scr}(1 - \Delta)$, where Δ satisfies $\Delta^4 = 3.6\mu^{4/5}$ and $\Delta = 0643.0.81$ for the lowest and largest possible values of μ. Thus we have $0.236\text{mm} < \lambda_{nonl,nax} < 0.302\text{mm}$. Assuming that the observed λ_D is of the order of λDe, we have the estimate of the lowest distances where the screening was measured, $1.3\text{mm} < 0.5\lambda_{Di} < 0.4\text{mm}$. Comparing that value with the maximum possible value where the non-linear screening operates, we can conclude that in these experiments the range of distances (where the screening was measured) is larger than that where the screening is non-linear and thus the effect of the non-linear screening apparently could not be detected. The main property of the non-linear screening is that the potential drops down faster than that for the linear screening, and at certain finite

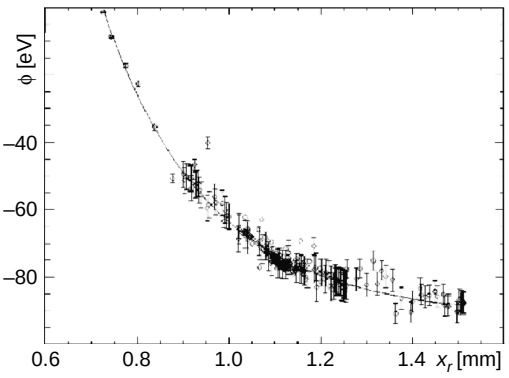

Fig. 5.14. The interaction potential between two charged dust grains in the plasma sheath. The solid line shows the fit with the exponentially screened Coulomb potential

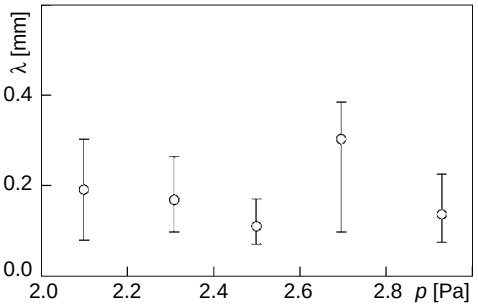

Fig. 5.15. Dependence of the screening length λ_D on the neutral gas pressure

length the linear screening starts to operate. The range of distances from 10μ up to 300μm = 0.3mm is not small, but it is smaller than that measured in experiments. The charge left for the linear screening is $Z_{d.eff} = Z_d 3.4\mu^{4/5}$ and ranges as $0.17Z_d < Z_{eff} < 0.429Z_d$ for the ranges of the parameter μ given above.

A direct application of these results to the interaction in plasma crystals seems to be difficult since in these experiments the pressure is much higher and the parameter μ is much smaller while the inter-grain distance is of the order of the non-linear screening length. On the other hand, these estimates were based on expressions for the non-linear screening in the absence of an ion flow, while in experiments in the sheath region the ion flow is present. The non-linearity is more complicated then since the non-linear effects in the sheath itself are spread up to the distances of a few λ_{De} and they can interfere with the non-linearities of the grain screening. Another important point is the role of the ion-neutral collisions in the grain screening which is yet in the early stage of investigations.

There exists a problem related to the role of the sheath potential which in turn can be estimated only qualitatively. In the linear approach, the ion drift caused by the sheath electric field should diminish the ion contribution to the screening and, roughly speaking, the screening should be determined by electrons, i.e., to be of the order of the electron Debye length which approximately corresponds to the experimental results. However, the possibility to use the linear approach for the grain screening when the charges are large is questionable. More detailed analysis of the role of the sheath field which is of the order of the particle screened field (especially when this field drops due to the screening) has not been done yet and therefore more studies are needed.

Another problem is related with the accuracy of experimental results, especially for the largest distances measured in the experiments. Although it is often difficult to see directly from experimental data, one should note that experimental errors increase with distances. Also, at distances where the grain potential becomes small (of the order of the sheath potential which is approximately $3T_e/\lambda_{De}$), the sheath potential can influence the charge potential even

at distances less than the electron Debye shielding length (in other words, almost within the whole range of the screening measured).

All these questions are listed here not with the aim to undermine the role of these collision experiments but to underline the complexity of the system and the necessity of additional theoretical work to be done to understand the experimental results. The discussed experiments deal with screening of individual grains, and correspond to non-collective grain interactions in the sheath. While measurements of the screening of the grain potentials in the plasma sheath are completely relevant for describing grain interactions in the sheath, the problem of the grain screening in the plasma bulk is still an open field of research demanding future investigations.

Summarizing the experimental results of determination of the grain screening potential ϕ_I, we conclude the following:

- The experiments performed so far have probed the range $0.5\lambda_D < r < 3\lambda_D$. The potential is represented very well by the Debye type of potential, but the value of λ_D is close to the electron screening length or probably to the non-linear screening length (which is of the same order of magnitude or less) but not the ion Debye screening length.
- The experiments were performed for equal-size particles, where the non-linear screening of both particles is not separable and theoretical investigations are required for quantitative comparison of the screening length with the experimental results. The real difficulty of the theoretical interpretation is that the influence of the sheath field on the screening is difficult to estimate and there does not exist any reliable theoretical model for the potential distribution in the sheath.
- The ratio λ_D/a was large in these experiments, of the order of 100, where the long-range attraction interaction is too small. The shadow attraction potential is of the relative order of $a^2/\lambda_{Di}^2 \approx 10^{-3}$. This implies that the long-range shadow attraction effects are very weak and the associated attractive forces related with the ion flux is hard to detect. On the other hand, detection of these forces needs at least $r > 5\lambda_D$, which was not the case. The shadow forces due to the neutral flux can be appreciably large for larger gas pressures.
- Thus experiments with bigger particles, larger distances, and higher gas pressure are required to detect effects of the non-linear screening and the attraction forces.
- The inter-grain distance for the closest collisions was still much larger than the grain size. In these conditions there is no much hope to detect charge changes in the grain collisions. Experiments with bigger particles and/or smaller distances between colliding particles are required in this respect.
- The experiments were performed in the plasma sheath. Plasma ions accelerate vertically in the sheath electric field and reach super-thermal drift velocities. This implies that the shielding is quite different than that in the absence of the ion drift: in the linear approach it is determined by

the electron (not the ion) Debye length. The non-linear case is not much investigated numerically or analytically; also, the drift changes the shadow attraction as discussed above in previous sections. Experiments with vertically interacting particles could be designed to investigate the wake field and the flow shadowing effects. Other experiments using the micro-gravity conditions are probably needed in future.

- Estimates of the particle charge have not been compared with the charging theories so far. Such comparison is not simple due to the mutual influence of the charging and screening and because the main grain charge is already screened non-linearly at distances shorter than the minimum distances of the colliding particles in these experiments. This should be a future task, in particular when different conditions and different (e.g., electro-negative or photo-emission) plasmas are probed.

5.5.3 Problems for Future Experiments

Collisions of Particles with Different Sizes. The binary collision technique is a novel tool to investigate the basic physics of dust-plasma interactions in the sheath. The technique can be extended to include grains of different sizes either by using the thermophoretic force or by using the hollow grains. The technique can be extended to answer outstanding questions, including the role of the non-linear interference of two interacting particles in collisions of particles with equal sizes. It is important that in principle the projectile particle can be made small and energetic in a way it does not change the screening field of the larger grain. Such experiments will be of fundamental importance if it is possible to increase the size of the projectile particle and look continuously how the non-linear interference of the shielding of the two colliding particles changes their interactions. This demands experiments on collisions of particles of substantially different sizes and continuous change of the sizes up to the sizes of both colliding particles being equal. This allows us to detect the effect of the non-linear shielding of grains in the presence of the sheath field, and the interference of the shielding field with the sheath field. It gives us also information on the role of the presence and absence of the shielding asymmetry in the presence of an anisotropic ion flow as a function of the particle distance from the wall and as a function of the gas pressure. The latter can modify the sheath field both for the collisionless sheath field and for the collision-dominated sheath field.

Detecting Interactions in Plasma Bulk. The present technique allows us to suspend grains in the plasma bulk by means of the thermophoretic force. An experiment of this kind has difficulties similar to those for experiments in the sheath since the suspended grains of different sizes have different positions in the bulk plasma. To collide the grains with different charges one needs a special technique for having the particle positions at the same hight (e.g., one can use hollow particles). An obvious advantage of such an experiment is that the influence of the poorly known field and ion flux distributions in the

sheath are excluded. In this way it is desirable to investigate the short-range non-linear screening, the long-range part of the grain interaction (including the shadow attraction), and the ion drag effect. As for the case of the grain in the sheath, one obviously should distinguish the effect of the grain screening and the effect of the grain interaction especially for the case where the mutual change of the shielding field can occur in the interaction of colliding grains. The search of long-range and attractive potentials, as suggested by the theory, is one of important tasks for future experiments.

Detecting Collective Attraction. It is important to investigate experimentally the two-particle interaction in the presence of many other particles in a complex plasma. Particles determining the basic complex plasma state (the "sea") should be chosen as the particles of a different size (perhaps much smaller than the size of the particles used to investigate their interactions). This seems to be the way to investigate the collective interactions in a complex plasma, which can be one of the most important for creation of strongly correlated states. Such investigation can be made both in the plasma sheath and in the plasma bulk.

Indirect Methods. Several indirect methods of investigation of the collective grain interactions can be proposed. A simplest example is the case where one considers interaction of large grains injected in a gaseous disordered structure of small grains creating a self-consistent distribution of the densities, Havnes parameter P_0, and other parameters of the structure. The size of the structure is much larger than the mean-free path for the ion–grain interaction with the "sea" particles. An external parabolic confining potential can also be used. Several large grains injected in this system can form grain clusters. These grains are few and for them the mean-free path for the ion–grain collisions is much larger than the size of the system (size of the structure of the smaller-size grains). The large grains interact with each other via pair interactions, which is the subject to detection. The spatial distribution of the large grains in the external confining potential and their modes of oscillation around equilibrium positions can give more information on the pair interaction of the large grains, including the long-range collective attraction forces.

References

1. D. Gross (2001). *Micro-canonical Thermodynamics, Phase Transitions in "Small" Systems*, World Scientific Lecture Notes in Physics **66**.
2. V. Tsytovich (1995). *Lectures on Nonlinear Plasma Kinetics* Springer Verlag, Berlin.
3. H. Thomas, D. Morfill, V. Demmel, and J. Goree (1994). *Phys.Rev.Lett.* **73**, 652.
4. J.U. Chu and I. Lin (1994). *Physica* **A 205**, 183.
5. A. Melzer, T. Trottenberg, and A. Piel (1994). *Phys.Lett.* **A 191**, 301.
6. Y. Hayashi, K. Tachibana (1994). *Jpn. Appl. Phys.* **33**, L804.

7. V. Fortov, A. Nefedov O. Petrov, A. Samarin and A. Chernychev (1996). *Phys. Let.* **A 219**, 89.
8. V. Tsytovich (1994). *Comm Pl. Phys.Contr.Fus.* **15**, 349.
9. L. Landau and E.Lifshitz (1955). *Electrodynamics of Continuous Media* Pegramon press, London N.Y.
10. S. Hamaguichi (1997). *Comm Pl. Phys.Contr.Fus.* **18**, 95.
11. Ya. Khodataev, R. Bingham, V. Tarakanov, and V. Tsytovich (1996). *Fiz. Plazmy* (Russia), **22**, 1028.
12. A. Ignatov (1995). *Comments P.N.lebedev Inst.A* **58**, 1.
13. Ya. Khodataev, G. Morfill, and V. Tsytovich (2001). *J. Plasma Phys.* **65**, 257.
14. M. Lampe, V. Gavrishchaka, G. Ganguli, and G. Joyce (2001). *Phys. Rev. Lett.* **86**, 5278.
15. M. Lampe, G. Joyce, and G. Ganguli (2001). *Phys. Scr.* **T89**, 106.
16. V. Tsytovich, Ya. Khodataev, and R. Bingham (1996). *Comments on Plasma Phys. Contr. Fusion* **17**, 249.
17. Sh. Amiranashvili Sh., N. Dusein-zade and V. Tsytovich V.(1999), Phys,Rev.A, **8**, 3110.
18. Ya. Khodataev, G. Morfill, and VVV. Tsytovich (2001). *J. Plasma Phys.* **65**, 257.
19. V.Tsytovich, Ya. Khodataev, G. Morfill, R. Bingham, and J. Winter (1998). *Comments in Plasma Physics and Controlled Fusion* **18**, 281.
20. R. Bingham and V. Tsytovich (2001). *IEEE Trans. Plasma Sci.* **29**, 158.
21. S.V. Vladimirov, K. Ostrikov, and A.A. Samarian (2005). *Physics and Applications of Complex Plasmas*, Imperial College, London.
22. S.V. Vladimirov and K. Ostrikov (2004). *Phys. Rep.* **393**, 175.
23. L.Spitzer (1978). *Physical Processes in the Interstellar Medium*, John Wiley and Sons, New York.
24. S. Weidenschilling and J. Cuzzi (1993). *Protostars and Planets III*, edited by E. Levy and J. Lunine, Univ. Arizona Press, Tucson, p. 1031.
25. S. Kempf, S. Pfalzner, and T. Henning (1999). *Icarces* **141**, 388.
26. P. Meaking (1991). *Rev. Geophys. Res.* **29**, 317.
27. J. Blum, G. Wurm, S. Kempf *et al.* (2000). *Phys. Rev. Lett.* **85**, 2426.
28. L. Boufendi and A. Boushoule (1994). *Plasma Sources Sci. Technol.* **3**, 262.
29. A. Bouchoule (1999). *Technological Impacts of Dusty Plasmas*in: *Dusty Plasmas: Physics, Chemistry and Technological Impacts in Plasma Processing*. John Wiley and Sons.
30. J. Blum and G.Wurm.(2000). **143**, 138.
31. A. Gasgarden *et al.* (1994). *Plasma Sources Sci. Technol.* **3**, 329.
32. A. Boushoule *et al.* (1991). *J.Appl.Phys.* **70**, 1991.
33. V. Tsytovich and J. Winter (1998). *Phys. Uspekchi* **41**, 815.
34. J. Winter (1996). *Plasma Phys. Control. Fusion* **38**, 1503.
35. J. Winter, A. Nefedov, and V. Fortov (2001). *J. Nucl. Materials* **290–293**, 509.
36. A. Kukushkin and A. Rantzev-Kartinov (1999). *Long Lived Filaments in Fusion Plasmas: Review of Observations and status of Hypothesys of micro-product assembled skeletons* (Preprint INNN RFS "Kurchatov Institute").
37. S.V. Vladimirov, S.A. Maiorov, and N.F. Cramer (2003). *Phys. Rev. E* **67**, 016407.
38. S.V. Vladimirov, S.A. Maiorov, and O. Ishihara (2003). *Phys. Plasmas* **10**, 3867.

39. A.A. Samarian, S.V. Vladimirov, and B.W. James (2005). *JETP Lett.* **82**, 858.
40. V. Tsytovich and G. Morfill (2002). *Fiz. Plazmy* (Russia), **28** 195; *Plasma Physics Reports* **28**, 171.
41. V. Tsytovich. (2003). *JEPT Lett.* **78**, 763.
42. R. Kompaneetz, V. Tsytovich, and G.Morfill (2004). EEE Trans Sc special issue "Dusty Plasma", "Weak Dust ion -acoustic and Dust-acoustic solitons with absorption of ions, ionisation and ion drag"(April 2004).
43. U. Konopka, D. Samsonov, A. Ivlev, J. Goree, V. Steinberg, V., and G. Morfill, G. (2000). *Phys. Rev. E* **61**, 1890.
44. O. Ishihara and N. Sato (2001) *IEEE Trans. Plasma Sci.* **29**, 179.
45. V. Tsytovich (2004). Contr.to *Plasma Phys.* **44**, 26.
46. V. Tsytovich (2005). *JETP Lett.* **81**, 448.
47. V. Tsytovich (2005). Contr.to *Plasma Phys.* **45**, 230.
48. C. Castaldo, U. de Angelis, and V. Tsytovich (2006). *Phys.Rev.Lett.* **96**, 075004.
49. V. Tsytovich, R. Kompaneets, U. de Angelis and C. Castaldo (2005). Contr.to *Plasma Phys.* **45**, 288.
50. V. Tsytovich and R.Companeets (2005). Contr.to *Plasma Phys.* **45**, 265.
51. Y. Al'pert, A. Gurevich, and L. Pitaevsky (1965). *Space Physics with Artificial Sattelites*, p. 186 (Consultant Bureaut), London, NY.
52. J. Laframboise and L. Parker (1973). *Phys. Fluids* **16**, 629–36.
53. V. Tsytovich and G. Morfill (2004). *Plasma Physics and Contrelled Fusion*, **45**, Number 13A, Special issue: Invited papers from the 31th European Physical Society Conference on Controlled Fusion and Plasma Physics, London, 28 June 2 Jely 2004, Institite of Physics Publishing.
54. U. Konopka, L. Ratke, and H. Thomas (1997). *Phys. Rev. Lett.* **79**, 1269.
55. U. Konopka, G. Morfill, H. Thomas, and L. Ratke (1998). *AIP Conf. Proc.* **446**, 53.
56. U. Konopka, G. Morfill, and L. Ratke (2000). *Phys. Rev. Lett.* **84**, 891.
57. A.Ivlev, U. Konopka, G. Morfill (2000). *Phys. Rev. E* **62**, 2739.

6

Experiments on Plasma Crystals and Long-range Correlations

The first experiments on complex plasma condensation into dust plasma crystals are [1, 2, 3, 4, 5, 6]. The physical explanation of the condensation takes into account general physical conditions met in the experiments. One can also use general features of a complex plasma as a state of matter described in details above as well as the new types of the grain attraction, collective and non-collective. Except general concepts, the detailed theory of the complex-plasma phase transition does not exist and the detailed investigation of the grain–grain interaction is still required both experimentally and theoretically. There are many steps to be done after fixing the nature of the pair grain interaction in order to obtain a complete theory of phase transitions in a complex plasma. From a general point of view, it is even difficult to introduce the concept of free energy (which is widely used in the theory of phase transitions in the ordinary matter) to begin with theoretical description of phase transitions in complex plasmas.

On the other hand, the existing experiments are not so detailed to make definite conclusions needed for the theory to be compared with experimental data. Indeed, the experiments are often done close to a wall in the plasma sheath, and the distributions of the electron and ion densities as well as the ion's drift velocities in the sheath are not measured till the present time. There are many difficulties with the probe measurements close to the wall. The real ion distribution close to the wall is unknown. It is certain at present that this distribution is not thermal, with some ion drift velocity of the order of the sound velocity (the Mach number is of the order of 1 according to the Bohm criterion); the real distributions are much more complicated as several experiments indicate. One cannot rely also on some analytical sheath models since many of them predict different types of density and drift distributions. Even if the plasma crystals are created far from the wall, one does not know the real value of the electric field and the ion drift velocity. Thus the experiments can give only general features of the conditions in which they are made, such as the average dust and plasma densities, the total drop of the plasma potential (not its distribution in space), etc.

V. N. Tsytovich et al.: *Experiments on Plasma Crystals and Long-range Correlations*, Lect. Notes Phys. **731**, 247–287 (2008)
DOI 10.1007/978-3-540-29003-2_6

Therefore, when speaking on the physics of the plasma condensation we can rely only on general properties of a complex plasma and classify experimental observations on the basis of estimates done from the averaged measurements. The only component which can be measured with good precision is the dust components. But the conditions are such that all components of the complex plasma can behave self-consistently.

We start with statements which can be checked from experimental data:

- Most plasma crystals obtained experimentally correspond to the conditions where the collective grain interaction should operate.
- The range of gas densities where the experiments are performed correspond to small values of the ion-neutral collision mean-free path where the collision-dominated consideration of the binary collective interactions is the most appropriate.
- The observations are done in the plasma sheath where the ion drift velocity can be important. However, the value of the ion drift in the collision-dominated sheath cannot be large having also in mind that in the presence of many grain layers of the crystal only the first one or two layers are in the sheath while the others are in the pre-sheath and the ion flow velocity there is smaller rapidly decreasing with the distance from the wall. No effect of a substantial decrease of the distances between the crystal layers was observed, which indicates that the role of the ion drift is small.
- The presence of the ion drift can stimulate the grain alignment along the ion flow which is not seen always and suggests the sometimes minor role of the ion drift in formation of such crystals.
- Separation between the grains is much larger than the ion Debye length and can be smaller than the electron Debye length. It can be much closer to the non-linear screening length modified by the grain collective interactions.
- The critical value of the coupling constant Γ_{cr} is often very large, which suggests either a very strong screening (since for measured grain charges the screening should be non-linear). Such a big screening makes the collective grain interactions effective.
- The temperature of the crystal melting is rather low.

Then we present the experimental data. It is up to the reader to check the validity of the above given statements for every experiment. After discussing the experimental data, we formulate the paradigm for the plasma crystal formation based on the above statements and show that by fixing of one appropriate parameter of the experiment we are able to explain three other observation parameters: the critical value of the coupling constant Γ_{cr}, the dust temperature for the transition $T_{d,cr}$ and the inter-grain distance.

First, we should answer a few general questions:

1. Is the size of the observed condensed state (or disordered state of the complex plasma before the condensation) larger or lesser than the ion-grain

mean-free path? If it is larger, one can expect that it is favourable for the collective attraction to operate; if it is smaller, the grain interactions can be considered as a sum of pair interactions as it is in ordinary matter (but modified by the non-collective attraction). The answer on this question for a typical plasma crystal experiment corresponds to the first case, i.e., to the presence of the collective attraction.

2. Is the mentioned size larger or smaller than the ion-neutral mean-free path? If it is larger, this is the collision-dominated case while the opposite is the collisionless case. The answer for a typical plasma crystal experiment corresponds to the collision-dominated case.
3. If the plasma crystal is created near a wall, one should estimate whether in average the plasma crystal is in the sheath, in the pre-sheath or far from the pre-sheath? Then, whether the ion-collision mean-free path is less than the pre-sheath size and the pre-sheath is determined by the ion-neutral collisions or the opposite case takes place? The answer is that at present crystals with up to several dozens and even hundreds of layers were obtained experimentally and the distance between the layers indicates that all of them are in the region with moderate ion flow of the order of the ion thermal velocity.
4. Is the mean inter-grain distance of the order of the non-linear screening length and is this distance much larger than the grain size? If this is the case and the size of the system is large then the induced dipole interactions are negligible and the collective dust attraction is the most probable process for the plasma crystal formation. The answer is indeed positive and the distance between the layers does not give much possibility to the induced dipole interaction to operate.
5. Usually in most experiments an external potential is present. If the crystal is in the plasma sheath close to the wall, this potential can be created perpendicular to the sheath, leading to modification of the near-wall structures. If an experiment is in the micro-gravity condition, the external potential perpendicular to the plates can be due to the finite size effects. The general question to be answered is what is the ratio of this external confinement potential to the depth of the potential well estimated by the grain collective attraction? If it is less, we can say that the observed plasma crystal is in the self-confinement state. In the opposite case we can see clusters of grains confined by an external potential. This comparison can answer the general question of the physical nature of the phenomenon of plasma condensation. The answer is that in present investigations the external confinement plays a minor role: probably it is needed because at the crystal surface the collective interactions become weaker and are therefore converted to non-collective ones.

We have answered these questions in fact only for experiments with large number of grains where the plasma condensation is observed and we call these structures “plasma crystals”. Another type of structure with small

number of grains, which correspond to the pair grain interactions, we call "plasma clusters" and we discuss them later in Chap. 7. The regular distribution of grains in clusters is mainly determined by the external confining potential although boundary-free clusters can also exist. There also exists an intermediate case where the size of the system is much larger than the mean-free path in one direction and is much less than the mean-free path in another direction. In such systems as mono-layer or double-layer systems, the main role is played by the interaction of grains in the plane and we classify these systems as mono-layer or double-layer crystals although interactions of grains from different layers are often non-collective (in the plasma sheath it is the wake interactions). Thus the real situation is complicated. In any case, it is useful to have in mind the possible change of the character of grain interactions with increase of the size of the system. In the corresponding discussion, we should take into account such new features of a complex plasma that there exists the long-range non-screened interaction of dust grains (both repulsive and attractive), that a simple screened Coulomb interaction can operate in exclusive cases only, that the screening is non-linear at least for low ion to electron temperature ratio (met in present laboratory experiments), that the high plasma absorption on grains related with the charging process (continuously operating to support the large grain charges) requires the continuous presence of an ionization source which together with the absorption on grains changes the ground state of the complex-plasma system, that the collective dust–dust interactions are a general phenomenon in a complex plasma and that a complex plasma is actually an open system, to which the concept of free energy is strictly speaking not applicable.

We make simple theoretical estimates after presenting the observation data. Having in mind that the detailed theory is still in its initial stage of development, we hope that these theoretical estimates can provide a deeper understanding of the existing observations and can show the direction for the theory to be further developed. Thus we indirectly provide proposals for future theoretical work based on these estimates. In the conditions where some theoretical models are already available, we compare them with the existing experimental data and discuss what is necessary and possible to do in future theoretical and experimental studies.

We first use a simple estimate for the ion–grain collision mean-free path and compare it with the size of the system L. Often L is much larger than both the ion–neutral and the ion–dust mean-free paths. The latter inequality is expressed as $L \gg L_{cr} = \lambda_{Di}^2/aP_0$. This estimate suggests that the concept of the collective dust–dust attraction should be used.

Another important estimate is whether ions and electrons in the system can be considered as thermal. Usually the high rate of plasma absorption on dust in existing experiments is compensated by the local ionization. In this case, the thermal electron and ion distributions are not created since the conditions for reaching the thermal distributions via the pair ion/electron–ion/electron collisions $Z_dP_0 \ll 1$ are not fulfilled. We should note that the

ionization process always produces non-thermal distributions and the dust charging process makes electrons and ions non-thermal (creates depletions of the high energy tail of electrons and of the low energy part of ions). Strictly speaking, the proper theoretical estimate should use the kinetic description in this case. This is not only complicated but the full kinetic theory still is in the stage of development (only the first steps toward its development are done). Therefore we use here the estimates of elementary processes for the thermal electron and ion distributions, having in mind that expressions for the system parameters in these estimates contain integrals with respect to the whole distributions of electrons and ions and that the non-thermal part of the actual distributions can change the numerical results by a factor of order 1.

An important feature is that dust grains are usually distributed thermally according to current observations and to theoretical estimates of the existing kinetic theory. The theory predicts that the dust distribution becomes thermal in a rather short time interval even by taking into account all new type of dust–dust interactions related with the collective effects. The physical reason is the high rate of dust–dust collisions, taking into account collisions with all collective effects included. This is due to large grain charges which make their interaction strong and the frequency (associated with the interaction) high. Even for the non-thermal electron and ion distributions, the existing theory predicts that the dust grain distribution should be thermal (the dust–dust collision integral contains only the integral over the ion and the electron distributions as a common coefficient in front of expressions vanishing for dust thermal distributions in the dust–dust collision integral [7, 8, 9, 10]). The experiments on plasma crystal melting (which we discuss in detail below) also indicate that after the melting the dust component has a thermal distribution. The dust–neutral collisions also thermalize the dust distributions if the neutral component is thermal. Therefore there exists a basis to assume that the dust grains are distributed thermally. Thus to make general qualitative conclusions about properties of the phenomenon of plasma condensation we use estimates based on the thermal distributions for all complex-plasma components.

It is easy to realize that there are three topics of interest for the phenomenon of plasma condensation: (1) the physics of the complex plasma state before condensation; (2) the physics of the strongly correlated complex plasma state after condensation and (3) the transition processes to the state with strong correlations (the phase transitions). All these three issues are important for experiments and theory.

The most complex is the transition problem which should be understood and described theoretically in the manner different from that used in the usual matter. The condensed states – the plasma crystal and liquid states – are also different from crystals and liquids in the usual matter and new approaches should be used for their description. The complexity of the transition problem is related to the fact that (contrary to the usual matter) the concept of free energy is generally not applied to a complex plasma. Therefore the Landau theory of phase transitions which employs an expansion of the free energy in

the order parameter η and identifies the phase transition with the point where this parameter becomes finite is generally not applicable for complex plasmas.

This does not mean that the order parameter cannot be introduced in a complex plasma. Moreover, one can introduce it in a rather general way if the transition occurs from the gaseous state, which can be described in the simplest way. We can present one example of the possibility of such kind of consideration. The phase transition should correspond to an instability threshold, which can in principle be determined in the gaseous state. We have already demonstrated above that in the gaseous state there exists a universal instability and that in certain conditions almost one periodical mode can be excited at the instability threshold. The appearance of the periodicity in disturbances at the threshold can serve as an indication that the system starts to have a periodical distribution of grains, or, in other words, can be regarded as an appearance of a crystal state. Of course, the linear analysis for such a problem is not sufficient but at least one can start with this instability as a candidate for description of the phase transition. In the case this mode is found to be responsible for the phase transition; its amplitude (on the nonlinear stage of the instability) can serve as the order parameter for the system. Of course, the scheme presented here is only one of possible scenarios for future research and at present there does not exist a detailed approach based on it.

Thus in a complex plasma, having in mind many new features discussed above, the most important method for investigation of the transition to a strongly correlated state and formation of the condensate is the investigation of the pair correlations as functions of the order parameter. As we stated above, these correlation functions are deeply related with the pair grain interactions, either collective or non-collective. One can therefore simply concentrate on experimental observations of the changes of the pair correlation functions during the transition stage and in the condensed phase of a complex plasma. The value of the order parameter for which the long-range correlations appear should correspond to the condition of the phase transition. Such an approach is obviously more sophisticated than the Landau theory but it can be used also in the conditions where the concept of the free energy is not applicable. We do not go here into the details of this problem, but only outline the existing difficulties and determine the ways by which they could be resolved. It is desirable that the new theory includes the possibility for using the scale invariance approach to find the universal indexes for fluctuations at the critical point. But such theory is not developed yet.

In the usual matter the transition to the crystal or liquid state is related with the strong coupling where the electrostatic energy substantially exceeds the kinetic energy of the interacting particles. This strong coupling leads to strong correlations, namely, it leads to the appearance of long-range correlations, i.e. long-scale order in crystals and short-scale order in liquids. In a complex plasma, relation between the strong coupling and the long-range correlations is not obvious. As an example, the long-range correlations can be related with dust attraction when the kinetic energy of dust particle is not

larger but of the order of the attraction potential well. Then, in the conditions where the long-range correlations exist, we deal with the middle-range interaction. Thus, strictly speaking, for the condensation to appear it is only needed that the long-range correlations just start to appear.

In experiments on complex plasmas, the parameter Γ_{cr} is measured as well as its dependence on various system parameters which can be altered. Usually, the value Γ_{cr} should be large enough for the transition to occur. To obtain such large values, we need to have high charges (i.e. large electron and low ion temperatures, and large dust sizes) and small kinetic grain temperatures. In most cases the experimentally obtained Γ_{cr} does not correspond to the value given by the One Component Plasma (OCP) approach. The OCP model was obtained numerically by using a fixed number of grains in the computational volume. This is not the case of the free-boundary crystal since by fixing the number of grains in the volume one should have an external pressure to confine these grains in the volume and the OCP model predicts a wrong value of Γ_{cr}. The observed values of Γ_{cr} are unusually high (and this gives the first puzzle to explain), the temperatures of phase transitions are very low (and this gives the second puzzle) and the distance between the grains in the condensed state substantially exceeds the linear screening length (this is the third puzzle). After describing observations we are able to explain these puzzles using simple qualitative arguments based on general properties of a complex plasma described in previous chapters.

After these comments we start to describe the experimental results and perform some estimates by using our description of elementary processes in a complex plasma. These theoretical estimates can serve only as a first approach to the problem and a detail theory is still waiting to be developed. We discuss also the critical value Γ_{cr} determined in experiments and existing theoretical models using collective interactions. We start with presenting observations of the pair correlation functions and the measured values of Γ_{cr} showing the presence of the long-range correlations after the plasma condensation transition.

6.1 Plasma Crystals

6.1.1 Crystal Structures Observed

Plasma crystals and the long-range correlations in complex plasmas were observed in quite different experimental conditions – different temperatures, charge component densities, gas pressures, and dust sizes. In the dust-force balance and formation of the crystals, the DC floating potential electric fields of the walls and other type of forces can also be important. Therefore the main questions are: What is common for experiments performed in different conditions? Are the values of Γ of the same order of magnitude or are they different in different experiments? Are the values of P_0 determining the collective

dust interaction of the same order or different for different experiments? Are the ratios of the dust size to the screening length different? How important is the ionization power? And so on. Not all of these parameters are available from experimental data, but some estimates can be done by using the approximately estimated experimental parameters and the above-described estimates of elementary processes in a complex plasma.

Observation of plasma crystals in different experimental conditions gives us a certain advantage for deeper understanding of the physics related to the plasma condensation. We start with the list of various experimental conditions and then describe in more detail the particular case of a radio-frequency(RF) discharge plasma most often used in current experiments.

There are several types of plasma devices that provide conditions for observations of the long-range correlations in complex plasmas. There are the RF discharge plasmas [1, 2, 3, 4], the low-power direct current (DC) discharge plasmas [5], the high-pressure combustion plasmas [11], the inductively coupled plasmas [12], the radioactive plasmas [13], etc. All these plasmas have been used successfully to generate the strongly coupled or the long-range correlated complex-plasma states [5, 11, 12, 13]. The largest part of the existing experiments is related to RF plasmas as well as to DC plasmas; these experiments contain the largest amount of information and are therefore described in more detail.

Here we start with an illustration of how different are the conditions where the plasma crystals can be observed. In RF discharges, the grain sizes range from $3\,\mu$m up to $10\,\mu$m, the gas pressure is in the range of up to $1-2$ Torr of Krypton gas, the ionization is homogeneous and produced by RF field, the ion density is about $5\times10^8\mathrm{cm}^{-3}$. The observed dust average spacing is about $260\,\mu$m, the dust charge is about $Z_d\approx10^4$, and the dust density is about n_d $(1\text{–}2)\times10^4\mathrm{cm}^{-4}$. The electric field of the plasma sheath is about $50-100\mathrm{V/cm}$ and can support rather heavy dust grains against gravity. The parameter Γ is in this case about 10^4 (much larger than the OCP critical value). The high value of the parameter Γ_{cr} directly means that the potential interaction of "bare" (non-screened) grains at the inter-grain distance in transition is four orders of magnitude larger than the kinetic energy of the grains. How can it be established? Obviously the screening should play a role (but as we intend to demonstrate such large values of Γ_{cr} can be established only by "over-screening", i.e., by grain attraction). The distance between the grains during the transition gives another puzzle since it is much larger than the ion Debye screening length (about $7-8$ ion Debye length) but less than electron Debye length (which is approximately 10 times larger than the ion Debye length).

In DC glow discharge plasmas, see Fig. 6.1, the configuration of the electric field in striations is three-dimensional, and, apart from the field along the discharge, the floating potential field of the cylindrical wall is important. On average, the field in the striations is about $10\mathrm{V/cm}$ which is much lower than that for RF plasmas near electrodes. The ionization is supported by DC current about several μA; the pressure ranges from 0.1 Torr to 1 Torr. The

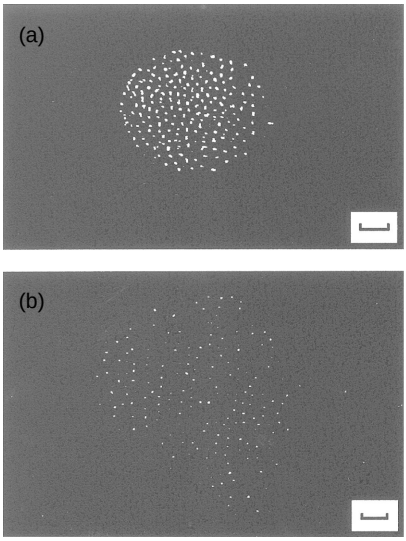

Fig. 6.1. Distribution of dust particles in the plasma crystal obtained in striations of a DC discharge plasma [5]. The images of dust grains in the horizontal (**a**) and the vertical (**b**) planes are presented for the current 1.2 mA, pressure 0.2 Torr; the bars correspond to 1mm

grain charges can be as high as $Z_d \approx 10^6$; the size of the grains ranges from $2\,\mu$m to $63\,\mu$m. Nevertheless, the inter-grain distance in the crystalline state is about $300 - 400\,\mu$m, which is similar to that in RF discharges; the grain density is about $10^4 \mathrm{cm}^{-3}$ and $\Gamma \approx 160-850$ as compared to $2 \times 10^4 - 10^5$ in RF discharges. Although the electric field inside the striation and the value of the ion drift velocity caused by the electric field are inhomogeneous, the inter-grain distance in the crystal state is almost constant. In both the type of experiments mentioned, the ion to electron temperature ratio is very small, $\tau \approx (10^{-2} - 2 \times 10^{-2})$.

Contrary to this data, in observations in the high density plasma at the atmospheric pressure the ion to electron temperature ratio is of the order of 1 [5]. The regular structure (see Fig. 6.2) is observed in the boundary region between the combustion plasmas and its condensation region with the dust density $10^6 - 10^7$, the temperature within the range $1900K-2000K$, without any external electric field and with $\Gamma \approx 0.5 - 18$; the electron density here is about $(0.3-3)\times 10^{10}$ and the dust charge is $Z_d \approx 500$–750. Another experiment with dust structures observed at the atmospheric pressure is performed in a nuclear excited plasma where the source of plasma ionization (due to the radioactive decay of nuclei) is localized in space, i.e. large fluctuations of numbers of the ionized electrons and ions take place as a function of the distance from the source. The grain sizes are $(1.8-4.8)\mu$m, the charge of the grains is about $Z_d \approx 10^3$, and the parameter $\Gamma \approx 30$. The spacing of the grains is again by the order of the magnitude close to that in all previously mentioned experiments and is about $200\,\mu$m. In glow discharges, structures with simultaneous presence of the crystal, liquid, and gaseous states were also observed (see Fig. 6.3).

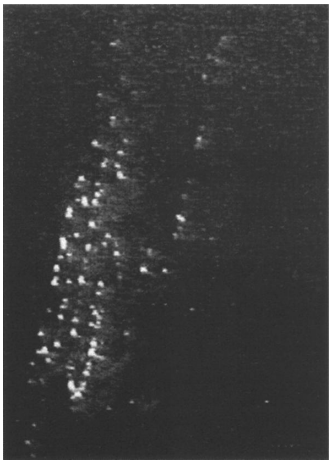

Fig. 6.2. Regular dust structure observed in the boundary region between the combustion plasmas and its condensation region [5]

Thus from different experimental conditions the measured values of the parameter Γ_{cr} differ substantially and significantly larger than 1. Nevertheless, the value of the parameter P_0 is in all experiments of the order of 1. This should be taken into account in theoretical models used for explanation of observations, in particular for estimates of the role of collective effects. Next, we describe in more detail experiments in RF discharge plasmas.

6.1.2 Observational Techniques

In high-frequency RF discharge plasmas, the physical situation is the simplest since the crystals are formed in the sheath region where the only important forces in the vertical direction are the gravity force, the sheath electric, and the drag force of plasma ions accelerated toward the wall by the sheath electric field. These are external forces in the absence of dust and they can be in principle measured. The presence of dust can substantially affect them, and the inter-dust interaction forces can be important; so these effects are of interest

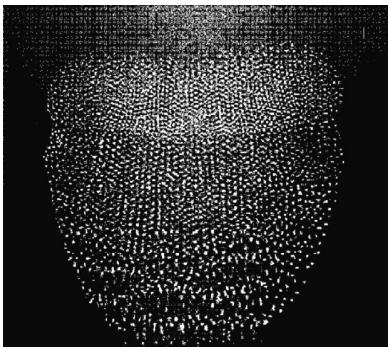

Fig. 6.3. Structures with simultaneous presence of the crystal, the liquid and the gaseous states observed in a glow discharge [5]

in investigation of the crystal formation in such plasmas. Note that the suspension of dust grains against gravity can be realized either electrostatically in the sheath, or by the neutral gas drag. The latter of course is much more difficult to control.

In RF plasmas, the electron temperature is often ≈ 2eV and the ion temperature is significantly (with a factor of order 100) smaller. The grain kinetic temperature is governed by collisions with neutral gas particles, which are often at room temperature; in the case of combustion plasmas the gas temperature can be substantially higher.

The optical detection system used to locate dust micro-particles is similar in all systems used so far. Its principle is straightforward. The micro-particles are illuminated by a narrow sheet of a laser (e.g., of a $He-Ne$ laser) of thickness about $100\,\mu$m, and are detected via their scattered light using a CCD camera. The optics used for producing the laser light sheet varies, but in principle a combination of cylindrical lenses and reflection mirrors completes the set-up. The thickness of the sheet is smaller than two lattice plane separations so that it is possible to detect a single lattice plane. This system works very well; the laser sheet can be arranged horizontally and viewed from the top, or vertically and viewed from the side, or both.

In general, the frame rate of CCD cameras of about 50Hz is sufficient for most processes investigated so far. The reason is the slow-down of the plasma processes due to the large mass and inertia of the micro-spheres (this does not include phenomena such as pure ion or electron modes, of course). The so-called "dust-plasma frequency"

$$\omega_{pd} = \sqrt{\frac{4\pi n_d Q_d^2}{m_d}} \tag{6.1}$$

is much lower than the ion plasma frequency ω_{pi}. This is because the micro-particle masses are usually 100 billion times larger than the ion mass

$$\frac{\omega_{pd}}{\omega_{pi}} = \left(\frac{n_d Z_d^2 m_i}{n_i m_d}\right)^{1/2} = \left(P Z_d \frac{m_i}{m_d}\right)^{1/2} , \tag{6.2}$$

which in the extreme limit, where the electron density is small ($n_i \gg n_e$ and for $P \approx 1$) and is given by

$$\frac{\omega_{pd}}{\omega_{pi}} \approx \left(Z_d \frac{m_i}{m_d}\right)^{1/2} . \tag{6.3}$$

This ratio is $\approx 10^{-4}$ or even less for typical values of current experiments. Since the ion plasma frequency in a typical RF plasma (under the conditions used for complex plasma investigations) is ≈ 1MHz we see that the processes up to the dust plasma frequency are readily observable using normal CCD cameras. For more detailed applications the cameras with much higher frame rate are available too.

By scanning through the system it is possible to detect the full 3D structure. This technique is reasonable and has been successfully employed for experiments on plasma crystals; however, it is currently too slow for 3D observations of phase transitions. Hence, one of the main research goals is the 3D investigation of critical processes (such as melting or sublimation) at the kinetic level and its comparison with macroscopic properties; this has not yet been reached. Two-dimensional investigations of melting transitions have already been done and will be discussed later.

6.1.3 Structure of Crystals

Most experiments report observations of particles arranged in a simple hexagonal structure where the particles in the horizontal direction are on a triangular lattice, with one particle above another in the vertical direction. The early investigation [1] reported simultaneous coexisting of the Body Centered Cubic (bcc) and Face Centered Cubic (fcc) crystal structures for certain experimental parameters. These results are based on the visual observation of various lattice planes coming into view while adjusting the microscope's focus. The first determination of the 3D structure of the plasma crystals [1, 14] (see Fig. 6.4) used separate horizontal and vertical laser sheets. The data contain a stack of the horizontal planar images resolved by selective illumination by 90 μm thick sheath of light from a focused, swept laser beam.

These results are obtained in 1.4 Torr Krypton plasmas formed by applying 13.56MHz RF voltage with a power 2.3 W with non–mono-dispersive

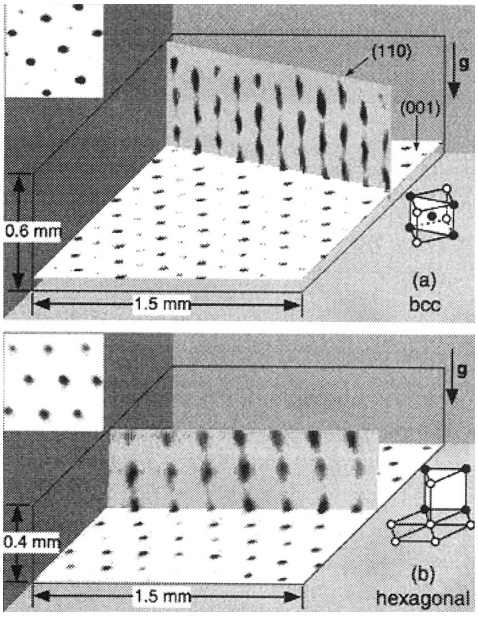

Fig. 6.4. Images within a 3D volume of the plasma crystal formed by 9.4 μm diameter polymer spheres in 1.4 Torr Kr discharge [2, 14]. In each image are shown cross sections; the inside shows the vertical plane viewed from above. The particle images appear longer in the vertical direction due to the infinite thickness of the laser sheath. (**a**) The (*bcc*) structure; (**b**) The simple hexagonal vertical stacked (*hvs*) structure [4, 14, 15]

$9.4 \pm 0.3\,\mu$m polymer dust spherical particle injected into the discharged volume. The measured electron temperature was $8eV$, the electron density from $3.2 \times 10^8 \text{cm}^{-3}$ up to $1.8 \times 10^9 \text{cm}^{-3}$. The (bcc) and Hexagonal Vertical Stacked (hvs) structures (no (fcc) structures) were observed. These structures can coexist in certain conditions or the whole volume is occupied by (bcc) or (hvs) structures. The free energy of different types of structures is different and the possibility of their coexistence apparently is related with the already mentioned non-applicability of the concept of free energy to a complex plasma. The latter conclusion is also supported by the observation of (hvs) structures. The parameter important to estimate physical reasons for the vertical stacking is the size of the dust cloud of $2\,\text{mm} = 2000\,\mu$m and the average particle spacing in the horizontal direction of $195 \pm 1\,\mu$m.

The investigations suggest that the plasma crystal structure can be often an (hvs) structure. This is an unexpected state for usual crystals since the minimum free energy levels arguments suggest (fcc) or (bcc) structures, as determined in molecular dynamic simulation studies [16]. The observations imply that an additional source of energy has to be available to keep the plasma crystal in such (hvs) state (which for thermal systems is an excited state). On the other hand, this is what can be expected for a complex plasma. We emphasized many times that complex plasmas are open systems and it is therefore not surprising that in such an open system the crystal structure in the ground state is different from that in usual matter.

The energy source always exists in a complex plasma and it can be identified as the flow energy of plasma ions in the sheath resulting in the anisotropic screening and the ion-wake formation [17, 18, 19, 20, 21, 22, 23, 24, 25, 26] or as an energy source due to plasma ionization; we have discussed that above for the homogeneous ground state of a complex plasma. In fact, the two energy sources have the same origin since the ion flow appears in the sheath due to the constant ionization in the volume supported by RF power.

Here, we estimate when each of the two possible anisotropy effects is important, namely, the anisotropy due to the single particle wake field effect and the anisotropy due to the collective wake field. The crystal is obviously formed by many grains. By the single grain effect we mean that interactions of many grains can be considered as a sum of pair interactions of each grain with all others. In this case, estimates can be done by considering a single grain or, more exactly, by considering interactions of a pair of isolated grains and then summing up the interactions. The ion flow produces a drag force in this case as well as an anisotropic screening distribution and an induced dipole component due to the ion charge concentration behind the grain in the direction of the ion flow. With two particles, the interaction becomes much more complicated.

In the collective case, even two-particle interactions depend on the average dust density in the system and the dust–dust interaction becomes collective (as demonstrated earlier). Both the collective and the non-collective wake field interactions lead to the anisotropy which is higher in the collective case.

If a particle is not isolated, its nearest neighbors interact with it in the six-fold way. By denoting particles with p and screening clouds with s, we have interactions p_1p_2, s_1s_2, p_1s_1, p_2s_2, p_1s_2, and p_2s_1. This is, as we noted before, the non-linearity in the interactions. Also, each neighboring particle partially shields another one from the collisions with ions and neutrals, with the net effect as a non-collective or collective force. All these forces can play a role in formation of the crystal structure for small size clusters.

For the non-collective case, numerical results for interaction of two grains in the presence of an ion flow [27, 28] confirm the presence of asymmetry and a formation of positive charge concentration of ions behind the grain which can serve as a potential well for another grain. This agrees with experimental observations [22, 29] for interactions of two grains. The main question for further interpretation of experiments is: when these type of interactions take place in formation of the crystal and when other interactions such as collective attraction are responsible for the crystal formation? The non-collective wake is present to produce the asymmetry but can be weaker than the collective interaction in other directions thus supporting the observed alignment of particles along the ion flow while the collective effects produce the main potential well forming the crystal. Attraction forces seem to be necessary for explanation of the observations, and these attraction forces should be collective.

For estimates, we use the described relations for the grain interaction assuming that the ion temperature is the room temperature $0.025eV$ and the ion Debye length is $\approx 35\,\mu$m. The criterion for the collective interaction to operate is that the size of the dust cloud L should be larger than $L_{cr} = \lambda_{Di}^2/aP_0$. From experimental data [2] we estimate $P_0 = n_d Z_d/n_i \approx 0.3$ and $\lambda_{Di} \approx 35\,\mu$m, thus obtain $L_{cr} \approx 0.43\,$mm. The size of the dust cloud is $\approx 2\,$mm which means that the collective interactions can dominate. In [14], estimates were done for the non-collective case. Thus for both cases the anisotropy needed for the (hvs) structure to exist is predicted. Note that the non-collective case gives the inter-grain distance in the plane perpendicular to the flow to be larger than the electron Debye length $\lambda_{De} \approx 450\,\mu$m while observations give $\approx 200\,\mu$m which is about twice less. For the collective case, the simplest is to estimate the value of Γ_{cr} (which is done below); it indicates that the collective interaction gives the best fit of observations.

Alignment of particles along the ion flow is not observed in some experiments [24] performed in a symmetrically driven directly coupled RF chamber, (see Fig. 6.5). The plasma crystal is very stable at these conditions. The 3D structure is determined by scanning a vertical laser beam horizontally across the system and recording the position of each particle with a CCD camera in x, y, and z directions. The scanning speed of the laser beam (and CCD camera) is 0.30 mm/sec; the total scan takes 18.3 sec. Due to the finite width of the laser beam, the micro-particles are seen typically as 15 consecutive video images. The actual particle position is located at the center of elongated light trace.

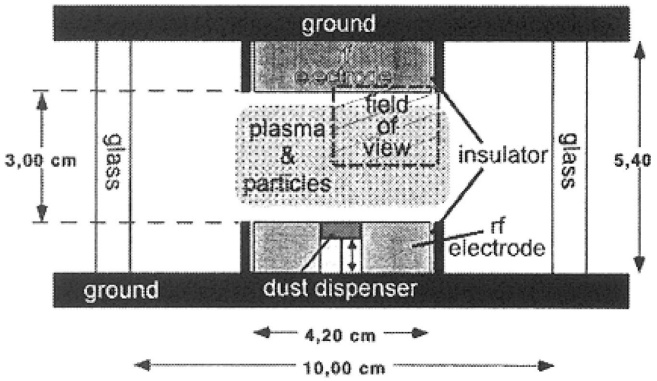

Fig. 6.5. Chamber employing a symmetrical parallel plane reactor installed in a glass cylinder. The electrode dimensions are given on the figure providing a cylindrical plasma regime of diameter 5 cm and height 3 cm. A piston operating dust dispenser, covered by a wire mesh of size 20 μm, is inserted in the center of the lower electrode. Mono-disperse polymer particles of diameter 14.9 μm can be injected in plasma by remote command. The gas in plasma chamber is Kr, the operating pressure 0.4 mbar. The particles are illuminated by a vertically arranged thin sheath of laser light (sheath thickness about 100 μm) and visualized using a CCD video camera. The field of view is indicated – it covers roughly 1/4 of the system, which is assumed to be cylindrically symmetric [24]

The size of the dust cloud is about 3cm. The total number of grain in the volume is 2×10^4 which corresponds to the average density 2×10^3 and $P_0 \approx 0.04{-}0.05$. The critical length is $L_{cr} \approx 0.7\,\mathrm{cm}$, which is significantly less than the size of the dust cloud. But due to small value of P_0, the collective parameter is also small $\eta_{coll} \approx 10^{-3}$ and thus in the perpendicular direction where the influence of the ion flow is small the inter-grain distance estimated from the collective attraction is given by $\approx \lambda_{Di} \ln(1/\eta_{coll} \approx 242\,\mu\mathrm{m}$; the observed inter-grain distances are presented in Fig. 6.6).

In [24], the non-collective interaction was estimated in the model of Debye shielded potential. One should have in mind that $\lambda_{Di} \approx 35\,\mu\mathrm{m}$ while $\lambda_{De} \approx$

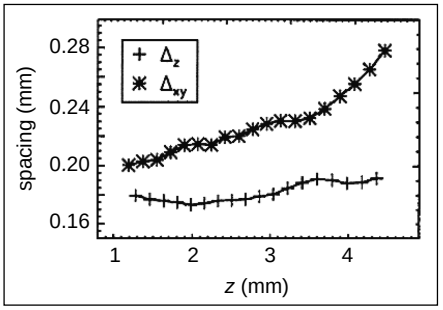

Fig. 6.6. Vertical distance (+) between the horizontal planes, Δ_t, and the mean inter-particle distance (*) in each plane, $\Delta_{x,y}$, as a function of the vertical position z [24]

350 μm. If one relies on the ion flow which makes the shielding to be equal or larger than electron Debye length, the value of the latter is somewhat too large than that observed. The gravity influences the structure since with an increase of the vertical distance z the spacing between the grains increases. In the model of the collective attraction, this can be related with a decrease of the ion density with height in the sheath region. In [24], estimates are performed to show that the gravity can operate as an additional pressure from the upper layers; this effect can explain the change of separation between the plains but not inside the plains. Note that the electron density has the opposite dependence in the sheath and therefore the presence of the ion flow in the non-collective model cannot be responsible for such a dependence of the inter-grain separation in the plane.

Besides that the ion flow seems to be not much influencing the crystal structure; it is not able to produce the alignment in the vertical direction as in other experiments [14]. This is illustrated in Fig. 6.7 [24]. The (fcc) and Hexagonal Close Packed (hcp) lattice coexist in this crystal, while the (bcc) structure and the vertically aligned structure are not detected. The absence of alignment in the observed lattice structure indicates that the effect of ion flow on the inter-particle interactions is weaker. This can be due to the fact that the vertical interaction is determined by the collective wake interaction in this case which is proportional to the square of the dust size a^2 (the dust

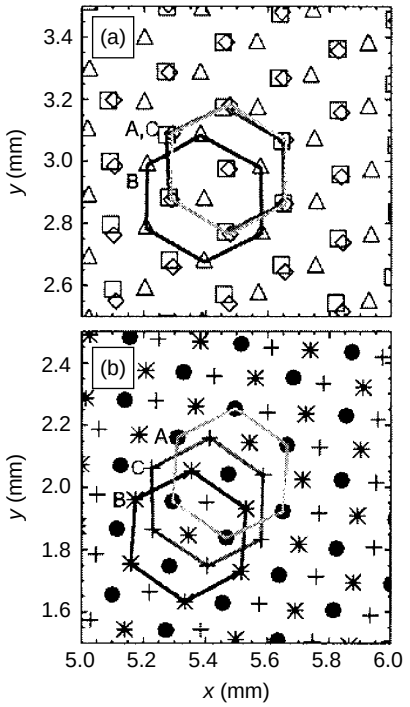

Fig. 6.7. Top view of three superimposed crystal layers near the bottom of the crystal. The fourth (*squares*), fifth (Δ), and sixth (*circles*) layers counting from the bottom are (hcp) in (**a**), the first ($\cdot$) second (*) and third (+) layers in (**b**) are either (fcc) or (bcc) with (111) plane parallel to electrodes [24]

surface) and to the square of the dust charge (another $\propto a^2$). In experiments [24], as compared to the other experiments [14], the dust size is 3.2 times less, which decreases the collective wake effect by two orders of magnitude.

An important characteristic of the plasma crystal state is the binary correlation function, defined by the relation

$$g(\mathbf{r}) = \langle \delta n_d(\mathbf{R}) \delta n_d(\mathbf{R}+\mathbf{r}) \rangle \; . \tag{6.4}$$

This correlation function gives in general the probability to find two grains at the distance $\mathbf{r}$. Another correlation function $g(r)$ can be introduced which describes the probability to find two grains at the absolute value of distance r independently on the angle between the grain (i.e., independent on the direction of the vector $\mathbf{r}$). This correlation function $g(r)$ describes the radial (pair) density distribution and measures the translational order in the structure. For an ideal crystal at zero temperature $g(r)$ is a series of δ-functions with positions determined by the particle separations in a perfect lattice. Another type of correlation function is the so-called bound orientational function g_6 defined in terms of the nearest-neighbor bound lattice angles. In a perfect hexagonal lattice all bounds have the same angle modulo $\pi/3$ with respect to an arbitrary axis. For a perfect hexagonal crystal at zero temperature the g_6 correlation function is constant equal to unity, while for other phases it decays with r. It is accepted for the usual matter that in the crystalline phase $g(r) \propto r^{-\eta(T)}$, $\eta(T) < 1/3$, and $g_6 = const$, while in the liquid state both correlation functions decay exponentially with distance, with factors characterizing the translational and orientational order.

From the early (basically 2D) measurements [30], it is possible to calculate the 2D pair correlation function $g(r)$, as applicable to a given horizontal plane. One such result, with the normalized pair correlation function versus the normalized distance, is shown in Fig. 6.8. To fit to the measurements it is assumed that the δ-functions are Gaussian attenuated by the overall envelope; so they decay exponentially as

$$g(r) = g_0 \exp(-r/\xi) \; . \tag{6.5}$$

Shown in Fig. 6.8, the envelope is the solid line, and locations of peaks expected for hexagonal lattice are indicated by the vertical lines. Experimental and least squares which fit the pair correlation function are shown, as well as the δ-functions for a perfect crystal (the latter are shown as peaks with correct positions and relative heights in an arbitrary vertical scale). Decay of the translational order can be expressed as an exponential decay factor $\exp(-\eta\Delta)$. Here, Δ is the mean grain separation and $1/\eta$ is the decay length of correlations. The transition between the ordered ($\eta\Delta \ll 1$) and the disordered ($\eta\Delta \gg 1$) states occurs at $\eta\Delta \approx 1$ [30]. In the example shown in Fig. 6.8, $\eta\Delta \approx 1.6 \times 10^{-3}$, which signifies a high degree of order. The mean inter-particle spacing is $\Delta = 270\,\mu\text{m}$, $\eta = 0.059$, and Debye–Waller factor (see below) $b = 0.013$. The measured g_6 correlation function is presented in

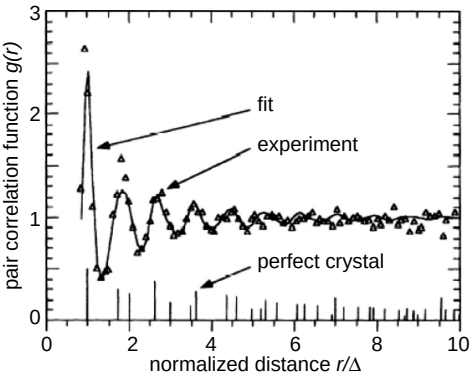

Fig. 6.8. Pair correlation function versus normalized distance [30]. Here, $g(r)$ is normalized by the average areal density of the particles, which as $1200\,\mathrm{cm}^{-2}$. Experimental and best-fit correlation functions are shown. The δ-functions for a perfect crystal are shown as with correct positions and relative heights. The fit yielded the mean inter-particle spacing $\Delta = 290\,\mu\mathrm{m}$ and the correlation length $\xi = 2\Delta$

Fig. 6.8. Fitting g_6 to an exponential decaying one $\propto \exp(-r/\xi_6)$ yields the scale length $\xi_6 = (1.4 \pm 0.1)\Delta$, while fitting to a power-law $\propto r^{-\eta}$ leads to a coefficient $\eta = 1.05 \pm 0.05$.

The pair correlation functions measured, see Fig. 6.9, indicate that the (bcc) structure is not present in these experiments [24]. Figure 6.9 clearly shows an agreement with the presence of both the (fcc) and (hcp) phases, but not the (bcc) phase. This observation is not surprising because of the openness of the system and is not applicable in this case for those MD simulations predicting the (bcc) lattice structure for suitably large values of Γ. The detailed investigation shows that the (fcc) and (hcp) crystal structures occur in different regions (domains) of the plasma crystal separated by an unidentified intermediate structure [31]. Figure 6.10 shows the first result of observation of the (bcc) lattice [4]. The 3D structure was measured by using

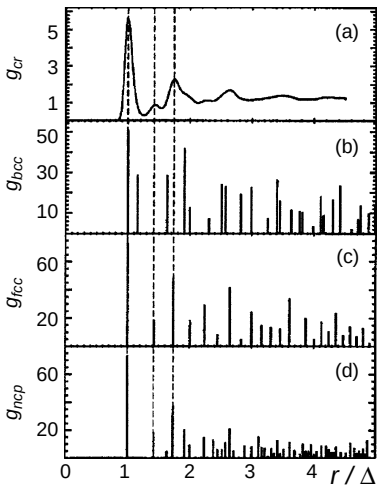

Fig. 6.9. 3D correlation function $g_{cr}(r)$ averaged over observed space (**a**), and the correlation functions for ideal lattice types: (*bcc*) (**b**), (*fcc*) (**c**), (*hcp*) (**d**) [24]

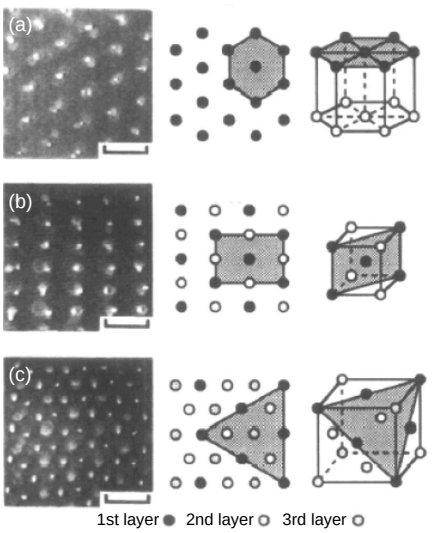

Fig. 6.10. Micrographs and sketches of different crystal structures: (**a**) hexagonal; (**b**) (*bcc*); and (**c**) (*fcc*). The center column corresponds to the structures in the micrographs. The graded area in the sketches are normal to the optical axis. The bars correspond to 200 µm [2]

a revolving mirror to "sweep" the sheet of laser light across the system and thus to consecutively illuminate different lattice planes.

The "most 3D-like" plasma crystal seen in the laboratory so far has 19 vertical planes and about 40 horizontal planes [30]. By the "normal" crystal standards this is still quite small; the system contains only about 3×10^4 particles. Nevertheless it marks a major progress in this field. At the end of this description, let us give for the general case the major observed characteristics of the plasma crystals (the (hvs) crystal type in terms of their lattice structure) through the following parameters.

Characterization parameters of plasma crystals

- Wigner-Seitz cell (2D): $A_S = \frac{\sqrt{3}}{2}\Delta^2 \approx 3.5 \times 10^{-4}\text{cm}^{-2}$;
- Wigner-Seitz radius (2D): $r_S = \left(\frac{\sqrt{3}}{2}\right)^{1/2}\Delta \approx 0.019\text{cm}$;
- Wigner-Seitz cell (3D): $V_S = \frac{\sqrt{3}}{2}\Delta^3 \approx 6.9 \times 10^{-6}\text{cm}^{-3}$;
- Wigner-Seitz radius (3D): $r_S = \left(\frac{9}{8\pi\sqrt{3}}\right)^{1/3}\Delta \approx 9 \times 10^{-3}$;
- Separation of lattice planes: $d = \frac{\sqrt{3}}{2}\Delta \approx 0.017\text{cm}$;
- Ion Debye length: $\lambda_{Di} \approx 0.0035\text{cm}$;
- Electron Debye length: $\lambda_{De} \approx 0.03\text{cm}$;
- Lattice wave speed: $v_L = \sqrt{\alpha\Delta/m_d} \approx 5\text{cm}/s$ (definition of α see below (7.12));
- Debye frequency: $\nu_D = v_L/\pi\Delta \approx 80s^{-1}$;
- Gruneisen constant: $\gamma = (\Delta/c_L)dc_L/d\Delta$;
- Compressibility: $\beta = \delta r_S^2/T$.

For other lattice structures, the geometry and hence the characteristic parameters can be different. More sophisticated experiments can be carried out as the understanding of these newly discovered plasma states grows and the technology advances for their investigation [11, 15, 30, 32, 33, 34].

Let us emphasize the main unusual aspects in the physics of complex-plasma condensation and the existing understanding of observations.

- Coupling of long-range correlations in usual matter can be achieved due to the presence of chemical binding. The latter for small particle kinetic energies can create long-range interactions and usual crystals. Without the presence of molecular attraction in usual matter, the boundary-free crystals are difficult (may be impossible) to create.
- In complex plasmas, the molecular binding is negligible and collective and non-collective attraction could serve as the mechanisms for formation of plasma crystals. The criterion that the kinetic grain energy is small as compared to the Coulomb interaction energy cannot provide the mechanism of the crystal formation. Numerical simulations using periodic boundary conditions seem to be inadequate for a complex plasma. The free-boundary Coulomb system without attraction is always unstable and cannot form the crystal state, but in a complex plasma the boundary free crystals can be created.
- Most of the experiments where the plasma crystal is observed correspond to the conditions for existence of the collective attraction.
- The values of observed Γ_{cr} are unusually large.
- The openness of the complex plasma systems introduces a principal new physics with major role of collective plasma fluxes providing attraction between each pair of grains as well as self-confinement of the system with the collective flux.
- The presence of external sources provides the energy which can explain coexistence of different crystal structures.
- The free energy concept used in ordinary crystal problems often does not operate in a complex plasma due to the openness of the system.

In connection with these statements we should make some remarks.

The first point is that, shortly, most of the processes discussed in p. 248 and related with the openness of the system can play a role. Here, we have given rough estimates only using the introduced elementary processes in a complex plasma. More experiments is necessary in future to vary such important parameters as, for instance, the size of micro-particles (making the crystal formation independent of the particle weight with particles which are hollow inside), the ion temperature, the parameter P_0, etc. The conclusion which is clear in general is that the ground state should be determined experimentally and can be different for different plasma sources. In this sense the observed structures correspond to the ground state for particular sources used in particular experiments.

Another point of the measurements worth noting is related to the already observed inhomogeneity of plasma crystal structures. The volume of the crystal actually scanned is shown schematically in Fig. 6.10. This shows that only about half of the cylindrical system is actually measured. The approximate location of the observed (fcc) and (hcp) zones is marked. There is a tendency for (fcc) structures to be located in the central portions of the system, whereas (hcp) structures are at the perimeter. This points toward a radial variation (albeit a subtle one) in the crystal ordering parameters. Presumably there are radial pressure gradients in addition to the observed vertical gradients so the crystal is inhomogeneous. This is not surprising since the complex plasma state preceding the crystal has a general property to form an inhomogeneous state. Also, the forces between dust particles could be different because of different relations between non-collective and collective attraction and possibly due to different values of the ion drift velocity at the center and at the periphery of the structure. The ratios of the inter-particle forces to the vertical bulk forces are also different at the center and at the periphery. The bulk forces are always needed to suspend the particles by electrostatic fields and the ion drag forces act at the lower plate sheath in the same direction as gravity. In the horizontal direction, the balance of the bulk field does not play a significant role or is much smaller if the drag and electric fields are not strictly vertical. This seems to be significant enough to influence rather subtle energy differences between (fcc), (hcp), and (bcc) lattices. In other words, the center and the periphery of the structure could be in different external source conditions. The question is whether this inhomogeneity increases with an increase of the crystal size and whether a very large plasma crystal cannot be created? This point is not investigated yet. If the size of the plasma crystal is universally limited, the situation is different from usual matter where there is no obvious limits for the crystal sizes (although an increase of crystal defects can give a limit on the possible maximum size). Obviously, this is not only an experimental question but could also be a general physical question, namely do there exist general physical processes restricting the existence of a large-size plasma crystal?

Let us discuss now the topics of interest for future research. They can be formulated here by using results of the experiments already performed:

- It is important to investigate the transition regions between different lattice structures on the microscopic level (namely on the kinetic level), geometry of the structural transition, its stability and/or dynamics, and its responses to several types of small vibrational perturbations (e.g., is the 3D annealing possible?).
- It is important to investigate how the change of the global energy supply can change the type of crystal structure (e.g., by adjusting the gas cooling or the RF power). Is it possible that by changing the energy supply the region of one lattice type will grow and finally only one type of the structure will be present? How this groth of crystals occurs?

- As it was stated, the observed lattice structure should be considered as a ground state of the crystal in an open system which strongly depends on the energy sources. The question is, how the crystal structure depends on the ground state of a complex plasma system?
- Is it possible to determine timescales for the propagation of, e.g., (fcc)/(hcp) transition fronts and how such propagation depends on the external experimental parameters determining the energy supply to the system?
- What is qualitatively changed for the so-called force-free crystals under micro-gravity conditions? The micro-gravity excludes the gravity field from the bulk force balance equation and the electric field does not need to support the particles against gravity in this case. Then there is no need of electric field, but the "force-free" condition requires also that the other two terms, namely the "ion drag force" and the "electric field force," are absent. This means that the grains should be far from the walls. But any experiment in the micro-gravity conditions includes chamber walls. Many micro-gravity experiments show the simultaneous presence of not only the plasma crystal discussed above, but also the void and convective structures.
- It is interesting to determine conditions where the grains forming the crystal are far from the walls and far from any other electric fields which can cause the ion drift and the ion drag. Then the complete force-free condition is reached. The main requirement is that the gravity, electric field, and ion drag forces have small influence on the inter-grain interactions. Somehow grains should be confined to this region by some forces and these forces should alter the interaction only at the periphery. The possibility for finding such a condition is supported by the presence of the collective flux created by all grains forming the crystal. This flux can create in principle a sufficient ram pressure to confine the system. This will be a natural self-confinement. The crystal of this kind is a boundary-free crystal. Note that at present it is not clear what role can be played by a weak confinement at the periphery of the crystals (the so-called confining rings); if it is weak enough, the corresponding crystals are already the crystals with free boundaries. This problem has not been addressed yet.

Note finally that experimental investigations of recently discovered new plasma states such as plasma crystals also benefit other related research, as it has often been in the past.

6.1.4 Dislocations and Defects

Crystalline plasma states exhibit crystal defects and dislocations in a way similar to that of their better-known "normal" crystalline counterparts in usual matter. We mentioned this in connection with the transition from (fcc) to (hpc) crystal structure (see also Fig. 6.11). However, true 3D analysis of the crystal defects is still outstanding: there are more research results and data

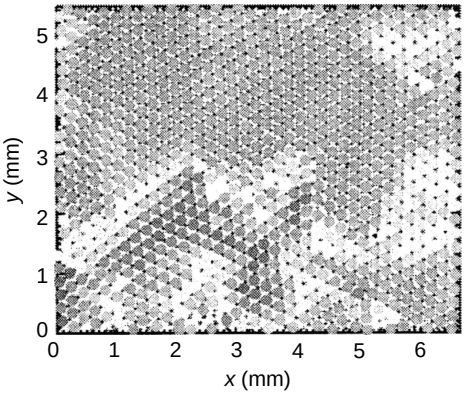

Fig. 6.11. Coexistence of (fcc) (*black*) and (hcp) (*white*) lattices in the middle of the crystal (from eighth to tenth horizontal layers)

available [15, 24, 31] on 2D investigations, involving 2- or 2.5-dimensional plasma crystals. In 2D measurements, for usually horizontally located lattice planes, the well-known hexagonal structures dominates. The lattice defects involve a local break-up of this hexagonal structure, the most common (and simplest) defect being the "7/5 defect," where two interlocking cells represent septagons and pentagons. Such lattice defects lead to the end (or beginning, respectively) of a lattice "line." Other lattice defects involving only two cells are possible in principle (e.g., 6/4 defects), but are probably energetically not favored (speaking about energetic favoring in open system, we have in mind all change of energy operating in the appearance of dislocation including the external energy, for instance the ionization source energy). It is more likely to have more complex defects such as 7/5/7 or 5/7/5 defects, involving three interlocking cells.

So far no systematic investigation of the energetics of defects has been performed. This should be a delicate investigation including measurements of vibrational energies of the micro-spheres in defect cells with measurements of changes in the defect cells and measurements of the external energy source supply as compared to the mean value without defects. It was noted that particles in defects tend to be more excited (in terms of their vibrational energy) than those in average in the crystal, which could be an indication that the external energy supply at the defect locations can be larger. Probably, local defects can be created by local change of external energy supply such as the local change of ionization. Such experiments were not performed so far. Also, the lattice energy states of defects have not yet been computed or measured.

A first and rather promising step in this direction is the investigation of the "deformation energy" of small systems involving small numbers of particles. The technique, employed for the first time in [35, 36], is to "push" individual particles through radiation pressure using a laser light beam and to determine the point when slippage occurs, i.e., when the system does not rotate as a solid body anymore. The measurements show that small systems

containing the "magic numbers" $(12, 19, \ldots)$ have a greater "binding energy" than others. The reason lies in the sixfold symmetry. This latter point is discussed in connection with the "ordering rules" [36]. The question as to how this ordering can be influenced by the change in the external source was not investigated, but it is clear that this problem can be more relevant for a set of several separated coexisting small systems not forming together a crystal, or small systems coexisting with a homogeneous background of a "sea" of other (smaller or larger) dust particles forming and not forming a strongly correlated state. It is clear, however, that this whole field, the microscopic study of defects on the kinetic level including the defect migration, annealing using changes in the energy source (e.g., via chopping laser sheet [37]), is a very rewarding field for future research, which might have significant spin-offs in applications once the knowledge is transferred (when it can be transferred) to other systems in ordinary matter. This may be of particular relevance for surface physics involving mono-layers (about mono-layer plasma crystal see Chap. 7). In addition, 3D nature of observed dislocations, i.e., the length of the "dislocation lines" and their (probably fractal) structure, has not been investigated so far. Here we have to await more micro-gravity experiments (low-stress or "force-free" experiments), whilst systems experiencing comparatively high gravitational stresses could be investigated sooner.

6.2 Melting and Phase Transitions

6.2.1 General Description of Phase Transitions

It is well known that usual matter can be in different states such as solid, liquid, and gaseous states, and there are phase transitions between the states. Analogous transitions are possible in a complex plasma but obviously the physics of them can be quite different. In usual matter the phase states are characterized by macroscopic state variables (e.g., pressure and temperature for gases) which themselves can be considered as appropriate integrals of kinetic particle properties. One of the most fascinating subjects is related to understanding phase transitions on the kinetic level, in particular the melting transitions. In usual matter, observations at the kinetic level, i.e., on the level of individual atoms or molecules, are not possible in general, so that in ordinary matter a direct comparison of the kinetic theory and experiments is ruled out.

This is not the case for complex plasma crystals, as we have remarked several times already. Here, one component (the most massive and energetically dominant grain component) can be observed at the kinetic level, at sufficiently high time and spatial resolutions, without over-damping so that the kinetic theory and experiments are, for the first time, on a roughly equal footing. Nevertheless, the accessible range of physically different systems is quite broad. We can investigate the homogeneous (glassy) systems with several different micro-particles, anisotropic systems consisting of the micro-rods

(with additional rotation degrees of freedom), we can in principle investigate a broad range of associated parameters ($\Gamma, K, P_0, a/\lambda_{Di}$, etc.), the stressed (in the presence of gravity) and the stress-free (in the micro-gravity) systems, etc. Of course, such experiments are quite demanding and the level of sophistication in the data analysis is quite high, too. It is not surprising therefore that so far only a few experiments have been performed [38, 39, 40]. Also, the cited experiments are "2 and 1/2 dimensional," with at most 10 horizontal lattice planes, and all are restricted to 2D diagnostics. This implies that particles could be observed leaving or entering a particular horizontal lattice plane, but the broader 3D picture is yet unknown.

6.2.2 Phenomenological Description

Whilst in [40] great emphasis is placed, in particular, on migration of lattice defects during preliminary stages of the melting transition, other studies [30, 41] concentrated more on phenomenology of the transition, changes in the 2D correlation function (the translational order), growth and dispersion in particle temperatures (velocity distribution), variation in the orientational order, self-diffusion and viscosity. The melting transition can be initiated and controlled by lowering gas pressure in the plasma chamber. It reduces the friction damping of the particles, increases the collisional mean-free path of ions and electrons, lowers the plasma ion and electron densities, and increases the sheath width. All these processes act in a complicated way to decrease the coupling constant Γ and to initiate the melting.

Transition from the crystalline to the liquid state is accompanied by an increase of vibrational excitations of particles at the lattice defects, followed by the defect migration (see Fig. 6.12). This behavior, expected from classical annealing studies, is confirmed on the microscopic level for complex plasma

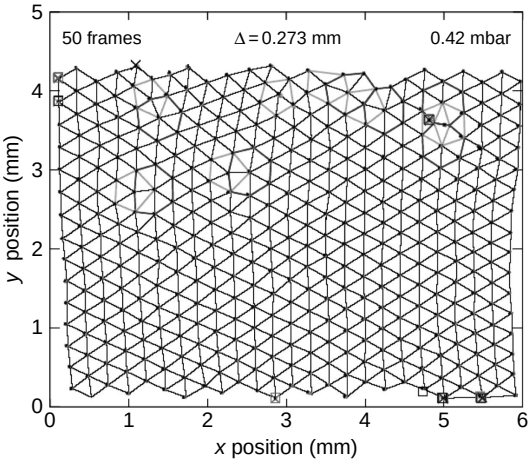

Fig. 6.12. Appearance of crystal defects [40]

systems. Next, particle migration across horizontal lattice planes becomes more frequent. Whether this is a response to a structural re-alignment in the vertical direction is not known. Of interest is the asymmetric response to the vertical particle migration. When a particle enters a horizontal lattice plane, it naturally leads to a displacement of the nearest neighbors. Observations show that almost only the particle adjacent cells are involved. This process of adjustment might be expected to proceed at the propagation speed of the "dust-lattice wave"; however, it is found to be about two orders of magnitude slower (see Fig. 6.13). When a particle leaves a horizontal lattice plane, again a readjustment of the nearest neighbors takes place. In contrast to the symmetric displacement of the nearest neighbors seen in the (above) case when a particle is added to the lattice, a disappearing particle produces a direct flow along a given lattice string, which may extend over many (up to 10) neighboring cells, (Fig. 6.13). Thus there is a fundamental asymmetry in the readjustment of particles in a given horizontal lattice to the addition or loss of a particle.

Next, parts of the system start to "flow." Although it was not possible to confirm this experimentally, the conception is that these flow regions could look like mini-convection cells, involving two or three horizontal lattices. At the same time, other regions retain quite stable crystalline domains of varying size, typically 10–50 Wigner–Seitz cells in one lattice plane. This structure is reminiscent of a classical first-order phase transition, e.g., as water and ice, where liquid and solid regimes coexist. It was named the "flow and floe" phase [40]. Its appearance is related to certain neutral gas pressure and is shown in Fig. 6.14 together with other phase states.

The expectation is, naturally, that this melting process would simply proceed – the "floes" should get smaller until the whole system becomes liquid. However, the expected development does not happen. Instead liquefying further, the complex plasma assumes a new (and unexpected) intermediate state.

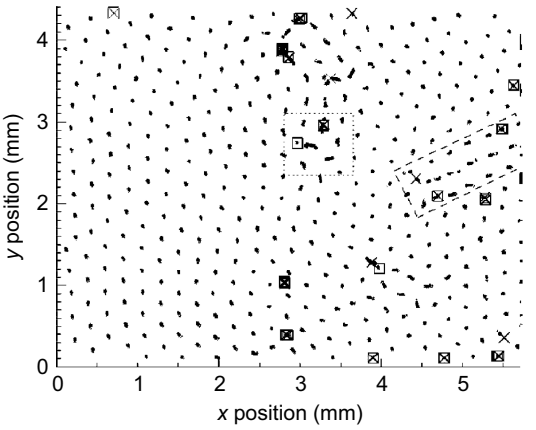

Fig. 6.13. Particle migration and appearance of the "flow and floe" stage, $\Delta = 0.265$ mm, pressure 0.36 mbar [40]

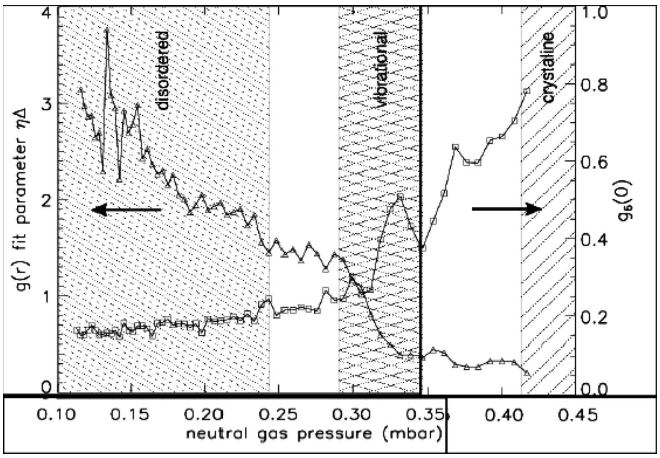

Fig. 6.14. Evolution of the transitional (Δ) and orientational (squares) order parameters during observed phase transitions as function of the neutral gas pressure. The following regions are shown: at ≈ 0.42 mbar the crystalline state, around 0.32 mbar the vibrational phase, and below ≈ 0.245 mbar the disordered state. The intermediate "flow and floe" phase occurs at special configuration at ≈ 0.36 mbar [40]

Starting in a few locations that are not obviously associated with lattice defects (this evidence is in part circumstantial, but not 100% certain, because only one lattice plane was observed and information about neighboring planes and their defects is not known), individual particles start to vibrate with substantial amplitudes up to about 10% of the lattice separation (see Figs. 6.14 and 6.15). The associated increase in the kinetic energy is about a factor of 10 or more. Subsequently, as the melting transition proceeds further, more particles start to vibrate and the vibration amplitudes increase. This stage of the phase transition has the appearance of the classical Lindemann picture, with particles vibrating in their lattice sites around equilibrium positions, increasing the vibration amplitudes – until finally making a transition to a disordered (fluid or gaseous) state (Figs. 6.14 and 6.15).

From the top view (Fig. 6.14) we see the basic crystal-like structure as well as substantial vibration amplitudes (some circular or oval), some line-shaped and some appear not to vibrate. This could be due to projection effect as shown in the side view in Fig. 6.15. A cursory "head count" of different vibration plane orientations shows that the vibrations are essentially isotropic, suggesting an energizing process (natural for open systems as we emphasized many times) that is either not directional or a process that rapidly randomizes the particles. Observations of individual particles suggest a coherence time in the vibrational orientation of a few vibration periods until the directional information is lost.

Note that in the vibrational state the orientational order is more pronounced than in the "flow and floe" state. In the disordered state the particles

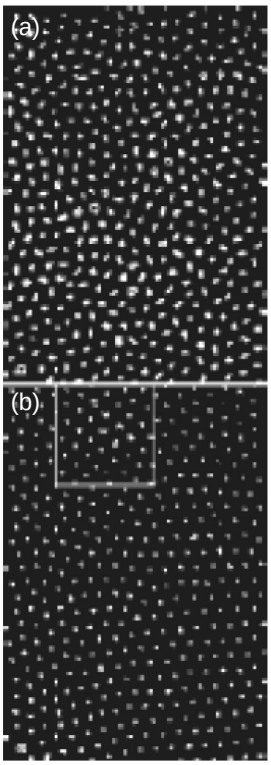

Fig. 6.15. The original images (the consecutive video frames overlayed) at the beginning (**b**) and the end (**a**) of the vibrational state at pressures of 0.32 mbar (**b**) and 0.29 mbar (**a**). In the marked window (**b**) the vibrations are first observed, then they spread through the crystal

move very fast, with kinetic energies far in excess of 1eV. Consequently, particle trajectories are visible as "lines" in individual video frames of Fig. 6.15. Also clearly visible are sudden "kinks" in the particle trajectories caused probably by Coulomb collisions. In principle, the statistics of such collisions could be used for diagnostic purposes, but this has not been attempted so far.

6.2.3 Translational and Orientational Order

Determination of translational and orientational order is a standard technique to quantify crystal structures [41]. For the translational order, one usually employs the radial pair correlation function $g(r)$, fitted to the appropriate lattice structure (e.g., hexagonal) normalized by the mean lattice separation Δ and broadened by the so-called Debye–Waller factor. This accounts, for instance, for the thermal broadening but one should expect that the broadening in the case of plasma crystal is not thermal. Since the correlations generally decrease with increasing distance r, an exponential decay constant, η, can be determined from the fit, which is usually written in the normalized dimensionless form $\exp(-\eta\Delta)$. Clearly, the smaller $\eta\Delta$ is, the longer the correlation holds (in terms of lattice planes) and the greater is the translational order. Thus $\eta\Delta$ can be used as the transitional order parameter.

For the orientational order, the bond orientational correlation function $g_6(r)$ is usually employed. This is defined in terms of the nearest neighbor bond angles and measures the six fold symmetry in the structure [42]. Only the nearest neighbors were used in [42] to evaluate the $g_6(0)$ by averaging over all particles. Hence in [42] one was looking at the very local orientational order. Clearly, in a crystal this parameter is most sensitive to dislocations, e.g., if there appears a pentagon or septagon structure instead of the usual hexagon structure. But it is also sensitive to statistical variations in the particle positions as a result of the charge (and other plasma parameters) fluctuations or other collective variations, since in [42] an average of particles, positions in time was not done. High orientational order then corresponds to large value of $g_6(0)$, the optimum being 1.

The translational and orientational order parameters are plotted in Fig. 6.14 as function of the gas pressure [42], which was used as a control parameter. The crystalline, vibrational, and disordered states are hatched; the "flow and floe" state occurs in the intermediate region between the former two. It develops more or less continuously from the "fully crystalline" to "mainly crystalline with migrating defects" to "crystalline island in viscous liquid" until the vibrational state is reached. It is interesting to note that the onset of the vibrational state is indicated, in both ordering parameters, by a return to a more ordered structure.

6.2.4 Dust Grain Temperatures

Since the micro-particle component of the complex plasma can be visualized with high time resolution at the kinetic level, it is possible to measure the velocity distribution function of dust grains directly. This distribution function can then be compared with, for instance, Maxwell distribution or one can take the distribution moments to identify flow velocities, etc. Since it was noted from the visual inspection that there were indeed stages during the phase transition when a directed flows occur, suitable analysis needs to be done to quantify them. In Fig. 6.16, we show the particle velocity distribution and compare it with a best-fit Maxwellian (solid line) at different neutral gas pressures indicated. The correlation function measured during the phase transition is shown in Fig. 6.17.

The results are as follows [30, 38, 39, 40, 41, 42, 43, 44]:

- In the crystalline state (the pressure is 0.42 mbar) the particles have a Maxwellian velocity distribution with a thermal temperature of 0.036 eV. The system is clearly in equilibrium (probably some kind of thermodynamics can be used although the concept of free energy is not appropriate). The temperature is slightly above the room temperature.
- In the "flow and floe" state (0.36 mbar) the velocity distribution of particles is still Maxwellian to a very good approximation, with a temperature of 0.037 eV, which is identical (within experimental errors) to that found in the crystalline state.

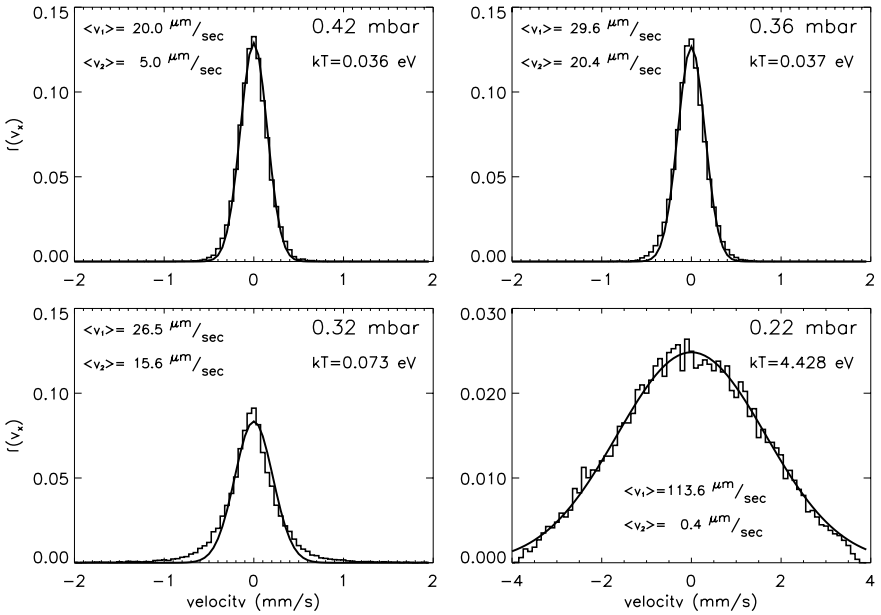

Fig. 6.16. Change of the dust particle distribution with pressure where the crystal melting occurs. T is the dust temperature, v_x shown on the vertical axis is the velocity in the x-direction (in the plane of crystal-parallel to electrode), the distribution is approximated by bi-Maxwellian distributions with the average velocities $\langle v_1 \rangle$ and $\langle v_2 \rangle$

- In the "vibrational" state (0.32 mbar) there is clear evidence for bi- or multi-Maxwellian distributions. The best fit with 0.073 eV is clearly not adequate. A bi-Maxwellian fit with 60% of the particles at 0.04 eV and 40% at 0.9 eV is much better. This indicates that at this stage many particles have made the transition to the vibrational dynamics.

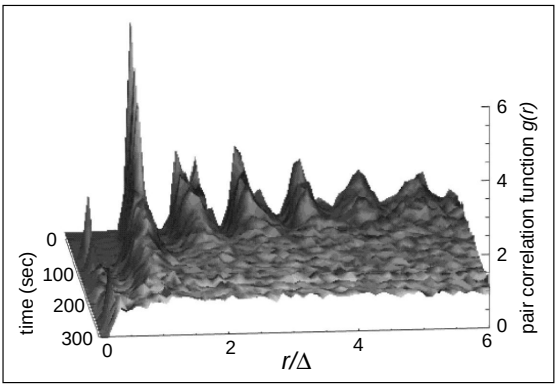

Fig. 6.17. Change of the correlation function during melting. The pair correlation function $g(r)$ for different gas pressures

- In the "disordered" state (0.22 mbar) the distribution function is again a near-perfect Maxwellian, with a temperature 4.43 eV. This is more than two orders of magnitude above the equilibrium value observed at the crystalline state. Considering only a neutral gas friction, this implies that in order to maintain the particle temperatures an amount of energy ≈ 3.0 eV/sec has to be provided per particle. This means that an external power of a few watts is required to maintain the plasma. Thus the external energy source plays important role in the transition. Also the kinetic theory predicts that in the gaseous state the complex plasma can rapidly reach a thermal equilibrium and that the grain distribution can be thermal (the thermal distribution satisfies the dust–dust collision integral for all attraction interactions included). Thus there is some theoretical basis for the grain distribution to reach quickly a thermal distribution at least in the "disordered" state.

As mentioned earlier, the ion and electron distribution are usually not thermal, which can cause direct micro-particle flows in the intermediate regimes of phase transitions. Such direct flows can occur, for instance, during annealing of lattice defects, but they also manifested themselves (in a much more dominant way) during the "flow and floe" phase. In order to characterize the directed flow characteristics qualitatively, two "drift" velocities were calculated [44].

6.3 Paradigms for Plasma Crystal Formation

6.3.1 Applicability of New Paradigms

As was already mentioned, we consider conditions where the collective and non-linear screening operate, i.e. when $\beta \gg 1$ and $L \gg L_{cr} = \frac{\lambda_{Di}^2}{aP_0}$. For existing observations [15, 24, 44] of plasma condensation, L is of the order of 1cm while $\lambda_{Di} \approx 30-50\,\mu$m, $a \approx 10\mu$m, and $P_0 \approx 0.3$–0.5. This corresponds to $L_{cr} \approx 0.1|!-0.01$cm, $\beta \approx 35$, and the theory should be based on the collective interactions of dust grains. For the reasons discussed in the introduction to this chapter, we neglect effects of the ion flow and consider creation of crystals in the plasma bulk.

A generalization of such a consideration for the presence of the ion flow can in principle be considered. But any self-consistent consideration of non-linear effects close to the wall where the ion flow takes place requires fully non-linear treatment of the sheath. This should take into account space variation of the ion flow with the distance from the wall, and the presence of the electric field which drives the flow, and also depends on the distance from the wall, as well as interactions of the non-linear field of the grain with the non-linear field of the sheath and the change of the sheath structure in the vicinity of the grain. All these problems are too complicated to treat them self-consistently and not necessary for the problem of crystal formation in the bulk plasma where the crystals are far from the wall.

Consider here the case of crystal formation in the bulk plasma where the ion flow is absent. We assume that the main mechanism of the positive charge between two interacting grains is the ion friction in neutral gas as it should be for the conditions where $\beta \gg 1$ and the drag friction of ions on grains becomes small. Because a complex plasma is actually an open system, the electrons and ions are not thermal as the time of ion–ion, ion–electron, and electron–electron collisions (which can only make their distribution thermal) is much larger than the ion–dust collision and ionization times (the processes which make the ion and electron distributions non-thermal). The condition that ion-dust collisions dominate over ion-ion collisions is

$$Z_d P_0 \gg 1 \,. \tag{6.6}$$

It is fulfilled in most experiments on a complex plasma performed so far. Thus electron and ion distributions become non-thermal due to the charging process which depletes the high-energy part of the electron distribution and the low-energy part of the ion distribution [9]; the plasma ionization also produces non-thermal distributions.

The natural question arises about the dust distribution, whether it is thermal or not. There exists the possibility that this distribution is thermal because of very high rate of dust–dust collisions due their large charges. The dust charge also depends strongly on the electron and ion distributions and therefore, strictly speaking, one also cannot apply the concepts of thermodynamics and free energy to the dust component to derive its equation of state. We are speaking here about the problem of finding the equation of state for the dust component exclusively. Nevertheless we can try to introduce the dust temperature since the dust distribution itself can be thermal; it was found theoretically [10] that dust–dust collisions indeed thermalize the dust distributions. Also, dust distributions measured in experiments are often close to the thermal distributions.

Another effect operating in the presence of many grains is the charge reduction of the individual grain by collective effects. The latter effect is small if the number of grains in the Debye sphere times the ratio of the dust size to the Debye length is small. In most experiments this factor is indeed not large and often small. So for simplicity we neglect this effect here.

First, we consider the case most applicable to the existing experiments, namely the case of collective dust–dust interactions, $\beta \gg 1$, and estimate the critical values of the coupling parameter Γ_{cr}. We then consider the Van der Waals approach [45] for $\beta \ll 1$ and for weak collective and non-collective interactions and point out that the parameter Γ_{cr} depends on the size of the system in this case. Finally, we show that for screened Coulomb (Debye) interaction, phase transitions are not possible neither for $\beta \gg 1$ nor for the Van der Vaals approach when $\beta \ll 1$.

6.3.2 Paradigms for Crystal Formation

Strong Non-linear Collective Attraction, $\beta \gg 1$. For the case of large β we use the approach described above with the plot of the potential shown in Fig. 6.18. The paradigms for the plasma crystal formation are formulated in the following way:

1. The grains can interact strongly only at short inter-grain distances and therefore spend only a small fraction of time at these distances.
2. Due to the strong non-linearity in screening, the derivative of the screening factor ψ with respect to r at distances where the non-linearity becomes weak is large enough for collective effects dominates at distances of the order of the non-linear screening length.
3. The next grain is located at the minimum of the first attraction well and the inter-grain distance is determined by the position of the first attraction well.
4. The Lindemann criterion for the phase transition is given by

$$\Gamma_{cr} = \frac{1}{\psi_m} \,, \tag{6.7}$$

   with ψ_m being the absolute value of the screening factor at the minimum of the potential well.
5. The temperature of the phase transition is determined by the depth of the first potential well.

These paradigms compromise strong and weak interactions: although the grain repulsion can be indeed strong, the grains cannot stay for long at closer positions because they are strongly repelled from each other. On the other hand, the parameter Γ_{cr} is not the measure of the strong grain interaction since it is given for the non-existing case of bare grains. The field of grains is not only screened but is over-screened in a way that the repulsion is changed to the

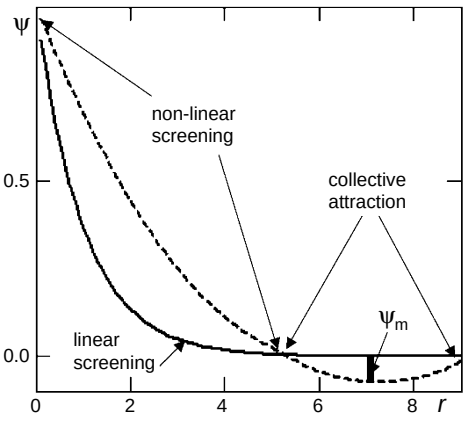

Fig. 6.18. The screening factor ψ in the grain interaction $V = \frac{Z_d^2 e^2}{r}\psi(r/\lambda_i)$ as a function of distance r in units of λ_{Di}, which serves as a basis for explanation of plasma crystal observations with the non-linear collective grain interaction

attraction and the attraction well is relatively weak as compared to fictitious case where the grains are located at the same distance but are not screened. Since experiments give for Γ_{cr} different values from about 2−6 in dense plasmas [5] up to very large value of about 10^4 in RF discharges [1, 2, 4] and glow discharges [46], one is able to check whether (6.7) indeed can explain all sets of existing experiments.

Figure 6.19 presents results of calculations of Γ_{cr} as a function of the non-linear parameters β and ν for the set of parameters corresponding to collisions dominated by the ion-neutral friction and non-linear collective attraction minimum given in Fig. 5.10 and the value of the potential well given in Fig. 5.11 [47, 48].

In all the cases one can recognize the possibility of rather large values of Γ_{cr} for large β – of the order of 10^3−10^4. These large values of Γ_{cr} for $\beta \gg 1$ were previously not predicted by any existing theoretical approaches but were observed in many experiments [1, 2, 4, 15, 44]. For low β, the values of Γ could be of the order of $2-10$, in accordance with observations in dense plasmas [5, 46]. Notice also that the ionization rate α_{ion} in Fig. 6.19 is related with the Havnes parameter $P = Z_d n_d/n_0$ by the condition of the global power balance:

$$P_0 = \frac{2\sqrt{\pi}\alpha_{ion}}{1 + 2\sqrt{\pi}\alpha_{ion}} \,. \tag{6.8}$$

The presented approach can give a reasonable explanation of the major features of observations of phase transitions to plasma crystals in a complex plasma. This includes both the low-pressure discharges such as discharges in RF fields [1, 2, 4] and glow discharges with striations [46], and the high-pressure discharges [5]. The depth of the potential well shown in Fig. 5.11 for β ranging from 5 to 30 is about 2−40eV, which corresponds to the measured melting temperature of plasma crystals. Also, the inter-grain distance as the position of the first attraction minimum shown in Fig. 5.10 corresponds to the

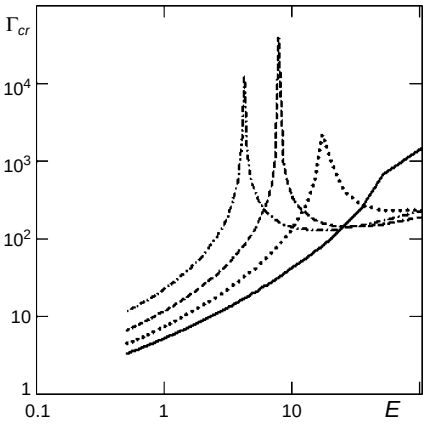

Fig. 6.19. Effective coupling constant $\Gamma_{cr}(\beta, \nu)$ for $\tau = 0.01$, $a/\lambda_{in} = 0.1$, $\alpha_{ion} = 0.1$; the solid line corresponds to $\nu = 0.1$, the dotted line corresponds to $\nu = 0.3$, the dashed line corresponds to $\nu = 0.5$, the dash-dotted line corresponds to $\nu = 0.7$

value observed for plasma crystals. This comparison serves as a first approach to explanation of observations by using simple elementary processes. It is still long way to go to create the full theory of phase transitions in a complex plasma.

Weak Linear Collective Attraction $\beta \gg 1$. This case can be met in experiments with τ close to 1 (thermal plasmas and small sizes of grains) where $\beta = za/\lambda_{Di}$. The Lindemann criterion gives

$$\Gamma_{cr} = \frac{1}{\eta_{col,in}^2 f_{scr}^2} = \frac{\sqrt{\pi}\lambda_{in}(1+z_0)}{2aP_0(1+P_0 z_0)} \,. \tag{6.9}$$

The last expression is written for the collision-dominated case, where the ion friction is determined by collisions with neutral atoms and λ_{in} being the ion-neutral mean-free path. This value of Γ_{cr} can be also large and is restricted by the condition $a \ll \lambda_{Di}$. The inter-grain distance is larger than the Debye length by the factor $1/\eta_{coll,in}\sqrt{P_0}$.

6.3.3 Van der Waals Equations and Collective Interactions

Collective Attraction for $\beta \ll 1$. When $\beta \ll 1$, analytical expression for the potential well can be used. Thus it is possible to write an approximate equation of state for the grain component which has a thermal distribution. Similar procedure in the case $\beta \gg 1$ demands numerical calculations using the structure of the first potential well; in principle, this can be performed in future. Here, we base our consideration on the analytical expressions for the attraction potential known in the limit $\beta \ll 1$. The Van der Waals approach [45] employs well-known methods of statistical physics [49]. Here, we use prescriptions of statistical physics for dust component only [45]. However, there exists a question on whether it is possible to define an equation of state in a complex plasma. This can be done obviously with some limitations and for grain component only.

First of all, it is desirable to write an equation for dust component and particularly for dust pressure p_d, which for the case where the dust is considered as an ideal gas is determined by the relation $p_d = n_d T_d$. It is emphasized already that

$$(p_d + p_0)(1 - n_d/n_0) = n_d T_d \,, \tag{6.10}$$

where the pressure correction term (containing the new quantity p_0) and the density correction term (containing the new quantity $1/n_0$ are defined in statistical mechanics through the partition function [49]

$$B(T_d) = 2\pi \int_0^\infty \left(1 - \exp\left(-\frac{V_{dd}(r)}{T_d}\right)\right) r^2 dr \approx \frac{1}{n_0} - \frac{p_0}{n_d^2 T_d} \,. \tag{6.11}$$

The last two terms in (6.11) are due to approximate division of integration with respect to r in the region of strong interaction, $V_{dd}(r)/T_d \gg 1$ (the first

term) and in the region of weak interaction, $V_{dd}(r)/T_d \ll 1$ (the second term). We simply rewrote here the known Van der Waals equation with subscript $_d$ in expressions for density and temperature.

In (6.10), V_{dd} is the dust–dust interaction energy depending on inter-dust distance r, and integration is performed with respect to inter-dust distances. The first part of the integral determines the density corrections and appears from integration in the range where the energies of interaction are much larger than the temperature and the exponent term can be neglected. The second term is determined by the integration in the range where the dust energy interaction is small as compared to the dust temperature and the exponent can be expanded. Thus

$$\frac{1}{n_0} \approx \frac{2\pi}{3}\bar{r}^3 \,, \tag{6.12}$$

where $\bar{r}$ is the distance at which the interaction energy is of the order of the dust temperature (it is assumed that $\bar{r} > a$, otherwise in the density correction term one should substitute the dust size a for $\bar{r}$). If $\bar{r} \ll \lambda_{scr}$, we can approximately use the dust Coulomb interaction and obtain $\bar{r} \approx \Gamma_d/n_d^{1/3}$. It is easy to estimate that with all non-linearities in the screening taken into account we have $\bar{r}$ larger than the screening length. For both cases $\eta_{coll} \ll 1$ and $\eta_{coll} \gg 1$ we have $\bar{r} \approx r_{lin} Z_d T_i/T_d \gg r_{lin}$ (r_{lin} is the distance where the linear approximation used before for the collective dust–dust interactions starts to be valid). Because of high collisions with neutrals the dust temperature cannot be very much different from the ion temperature and Z_d is very high. Even during the phase transitions where the dust temperature can increase by one or two orders of magnitude it cannot reach $Z_d T_i$ for usual values of $Z_d \approx 10^3 - 10^4$. Thus to estimate $\bar{r}$ we can use the collective interactions (already found) containing the linear dielectric permittivity. This gives for $\beta \ll 1$ and $\eta_{coll} \ll 1$ the density correction term

$$\bar{r} \approx \frac{Z_d e^2}{T_d}\eta_{coll}, \quad \frac{1}{n_0} = \frac{2\pi}{3}\left(\frac{Z_d^2 e^2}{T_d}\right)^3 \eta_{coll}^3 = \frac{\Gamma_d^3 \eta_{coll}^3}{2n_d} \,, \tag{6.13}$$

and the pressure correction term

$$p_0 = n_d^2 \frac{\pi Z_d^2 e^2 \lambda_{Di}^2}{P_0 \tau} \,. \tag{6.14}$$

The condition of applicability of (6.14), namely $\bar{r} > a$, can be written as $T_d < T_e \eta_{coll} z$. In existing experiments $3 < z\eta_{coll} < 10$ and the dust temperature at its highest value during the melting of the plasma crystal does not exceed the electron temperature by an order of magnitude, which means that the finite dust size correction in the density (volume) term can be of the order of the interaction correction only in the conditions close to melting point.

Expressions (6.13) and (6.14) were obtained by integration of the collective dust–dust interaction potential $(Z_d^2 e^2 \eta_{coll}/r) cos(r/\lambda_{coll})$ from $\mathbf{r}$ up to infinity assuming $\bar{r} \ll \lambda_{coll}$ (the distance of the first collective attraction minimum

is $\pi\lambda_{coll}$), and weak damping due to the ion-neutral collisions cancels the interaction at very large distances. The first assumption $\bar{r} \ll \lambda_{coll}$ means approximately that in the collisionless limit

$$Z_d \eta_{coll}^{3/2} (a/\lambda_{Di}\sqrt{\tau}) z_0 \sqrt{P_0} (T_i/T_d) \ll 1 \, .$$

Although the first factor Z_d is large, all other factors are rather small due to the assumption $\eta_{coll} \ll 1$ made in the derivation of this inequality. Therefore it can be easily satisfied. Usually one defines the volume occupied by dust V_d and the total number of particles in this volume N_d such that the dust density is $n_d = N_d/V_d$. The dependence of the volume correction and the pressure correction on V_d for a complex plasma is quite different from an ordinary gas. For example, in an ordinary gas n_0 is independent of V while in a complex plasma $n_0 \propto V_d^6$; furthermore, p_0/n_d^2 is in ordinary gas independent of V while in (6.13) it is inversely proportional to V_d. This makes the Van der Waals equation for the dust component in a complex plasma [45] quite different from the Van der Waals equation for an ordinary gas [49].

Most laboratory experiments are performed in the plasma sheath with the presence of the ion flow which changes the collective interactions. Unfortunately, for this case an analytical expression for the interactions is difficult to obtain because there exists an anisotropy, but the estimated above type of integrals, determining the density and pressure corrections in the Van der Waals equations, can be calculated numerically. Thus a large amount of future work remains – not only to calculate the set of interaction curves for different angles to the flow but also to make an interpolation between these curves to be able to calculate the corresponding integrals numerically. Similar situation appears in the presence of a strong magnetic field. Calculations performed here are given for illustration and to point out problems remaining for future theoretical efforts (along with experimental efforts to measure the potential of dust–dust interactions, distributions of ions in the ion flow in the velocity space).

As soon as one determines the dependence of the dust pressure on V_d from (6.14), the critical temperature for the phase transition can be found from two relations

$$\frac{\partial p_d}{\partial V_d} = 0, \quad \frac{\partial^2 p_d}{\partial V_d^2} = 0 \, . \tag{6.15}$$

Due to the dependence different from that in a usual gas, expression for the critical temperature has a different numerical coefficient which in the collisionless limit is 15/22 [45] instead of usual 8/27 [49]. This coefficient enters in the expression

$$T_{d,cr} = \frac{15}{22} \frac{p_0 n_0}{n_d^2} = 0 \, . \tag{6.16}$$

After substituting (6.13) and (6.14) in (6.16), the latter gives a threshold value for Γ for the phase transition

$$\Gamma_{cr} = \sqrt{\frac{15}{11}} \left(\frac{3}{4\pi}\right)^{1/6} \frac{n_d^{1/3}\lambda_{Di}}{\sqrt{P_0\tau}\eta_{coll}^3} \ . \tag{6.17}$$

When comparing this expression with (6.9), we should take into account that $4\pi n_d/3 = 1/r_{min} = \pi\eta_{coll}\sqrt{P_0\tau}$ (the grains are located in the first potential well); thus we obtain the difference in the numerical coefficient only, namely 0.211 in (6.17) and 0.25 in (6.9). We see that the Lindemann criterion and the Van der Vaals approach give almost the same results except small difference in the numerical coefficients. However, the factors η_{coll} are different as determined above.

For $\eta_{coll} \gg 1$, the potential well for the collective attraction is rather deep

$$U_{well} \approx Z_d T_i z_0 \frac{a}{\lambda_{Di}\sqrt{\tau}} \sqrt{P_0} \ . \tag{6.18}$$

This case can be reached in regions where the ion flow is absent and the coefficients α_{dr} and α_{ch} are of the order of 1. This means from $\eta_{coll} \gg 1$, $a/\lambda_{Di}\sqrt{\tau} \gg 1$ and therefore $U_{well} \gg Z_d T_i$, which is in most conditions much larger than T_d. Then the Van der Waals approach, which assumes the opposite inequality, cannot be apparently applied.

Van der Vaals Equations and Non-collective Interactions. The specific aspect of the non–collective dust-dust interaction is that they can be applied only for finite systems. On other hand, the non-collective interaction provides the existence of a single attraction well which is located at

$$r_{well} \approx \lambda_{Di}^2/a\eta_{st} \ . \tag{6.19}$$

In the case when only the ion shadow effect is important, the sticking coefficient η_{st} is equal to the ion sticking coefficient $\eta_{st,i} \approx 1$, which indicates that the applicability limit of using the non-collective interactions in the Van der Vaals equation is given by $P_0 \ll 1$. In the case where the neutral flux dominates, the effective sticking coefficient is expressed through the neutral sticking coefficient $\eta_{st,n}$ by the expression $\eta_{st} = \eta_{st,n} n_n T_n T_i / 4T_e^2 z^2$, which can be for high dust pressures much larger than 1, and in this case the condition can be less restrictive allowing $P_0 \approx 1$. In any case the size of the system cannot be larger L_{cr}. We assume that $L > r_{well}$. The parameters n_0 and p_0 are found by using the non-collective potential of interaction containing the long-range repulsion and attraction parts. Integration on small distances r gives

$$\bar{r} \approx \min\left\{ r_{well}, \frac{Z_d e^2}{T_d}\eta_{ncoll} \right\} \ , \tag{6.20}$$

where η_{ncoll} is the coefficient of the non-collective interaction. Integration on large distances r should be restricted by the size of the system L. This assumes that the inhomogeneity of the distributions inside the system is not large. Due to the accepted condition that the size of the system is larger than r_{well}, the

integral for large r is determined by the non-collective attraction term. We obtain

$$p_0 = \eta_{ncoll,attr} n_d^2 \frac{Q^2 L^2}{2T_d} \tag{6.21}$$

and find

$$\eta_{ncoll,attr} n_d \frac{Q^2 L^2}{T_d} = \frac{3^{7/5}}{27^{2/5}} \approx 1.07 \, . \tag{6.22}$$

This expression can be rewritten as an expression for the critical dust temperature containing L/L_{cr}:

$$T_{d,cr} = 0.074 Z_d T_i \frac{\eta_{st}}{P_0} \frac{L^2}{L_{cr}^2} \, . \tag{6.23}$$

Two factors entering this expression, $Z_d \gg 1$ and η_{st}/P_0, are large, while the numerical coefficient and the factor $(L \ll L_{cr})^2$ are small.

Absence of Phase Transitions for Screened Coulomb Potential. Physically, the absence of phase transitions follows from $B(T_d)$ being positive for all distances and the absence of attraction and as a result $p_0 < 0$. Similarly, the above-given calculations give all coefficients and the result is that the phase transition conditions can be satisfied only if $n_d < 0$, which is obviously impossible.

6.4 Inspiration from Experiments

It is certain that current experiments are ahead of theory in the general description of the new state of matter and in the kinetic description. Nevertheless, even within the frames of the existing simplified approaches many estimates can be done. These estimates can take into account various forces in the wave description, the theory of equilibrium stability and oscillations of clusters with arbitrary forces, the general description of modes in a complex plasma in an external magnetic field, MD numerical simulations with the real forces, etc. In general, breakthroughs in the mentioned areas already exist but the final complete description which can be used in experiments is not yet available. In the nearest future this will be the subject of intensive studies. The experiments already performed should be repeated as soon as better theoretical understanding of the processes is achieved. Future theoretical problems can be formulated at present although the full theoretical description will take a lot of time. It is clear that experiments will also be spread in different directions, especially those having industrial applications as well as those designed to resolve new general physical problems. Hopefully the future theory will be able to get more insights along with new forthcoming experiments and explain in detail the observations. Finally, better diagnostics of experimental parameters will help substantially in comparing theory and experiments.

References

1. H. Thomas, D. Morfill, V. Demmel, and J. Goree (1994). *Phys.Rev.Lett.* **73**, 652.
2. J.U. Chu and I. Lin (1994). *Physica* **A 205**, 183.
3. A. Melzer, T. Trottenberg, and A. Piel (1994). *Phys. Lett.* **A 191**, 301.
4. Y. Hayashi, K. Tachibana (1994). Jpn. Appl. Phys.**33**, L804.
5. V. Fortov, A. Nefedov O. Petrov, A. Samarin, and A. Chernychev (1996). *Phys. Let.* **A 219**, 89.
6. V. Fortov, V. Molotkov, A. Nefedov, and O. Petrov (1999). *Phys. Plasmas* **6**, 1759–68.
7. V.Tsystovich and U. de Angelis (1999). *Phys.Plasmas* **6**, 1093.
8. V. Tsytovich, U. de Angelis (2000). *Phys. Plasmas* **7**, 554.
9. V. Tsystovich and U. de Angelis (2001). Phys. Plasmas **8**, 1141.
10. V. Tsytovich and U. de Angelis (2002). *Phys. Plasmas* (USA), **9**, 2497–506.
11. V. Fortov, A. Molotkov, A. Nefedov, A., and O. Petrov (1999). *Phys. Plasmas*, **6**, 1759–68.
12. V. Fortov, A. Nefedov, V. Torchinsky, V. Molotkov, O. Petrov. A. Samarin, A. Lipaev. A. and A.Khrapak (1997). *Phys. Let.* **A 229**, 317.
13. V. Fortov, A. Nefedov, V. Shnel'schikov, A. Usachev, and A. Zobin,(2000). *Phys. Rev. Lett.* **267**, 179 , Morfill, G., Thomas, U., Konopka U. and Zuzic M., *Physics Plasmas* **6**, 1769 (1999).
14. J.Pieper, J. Goree, and R.Quinn (1996). *Phys.Rev.E* **54**, 5636.
15. G. Morfill, H. Thomas, U. Konopka, and M. Zusic M (1999). *Phys. Plasmas* **6**, 1769.
16. Ya. Khodataev, R. Bingham, V. Tarakanov, V. Tsytovich and G. Morfill. (2001), *Phys. Scr.* **T89**, 95.
17. S.V. Vladimirov and M. Nambu (1995). *Phys. Rev. E* **52**, R2172.
18. S.V. Vladimirov and O. Ishihara (1996). *Phys. Plasmas* **3**, 444.
19. G. Lapenta (1999). *Phys.Plasmas* **6**, 1442.
20. G. Lapenta (2000) *Phys. Rev. E* **62**, 1175.
21. M. Lampe, G. Joyce, and R. Ganguli (2001). *Phys. Scr.* **T89**, 106.
22. V. Schweigert, A. Melzer, and A. Piel. (2000). *J. Phys. IV, Proc.* (France), **10**, 421.
23. A. Melzer, V. Schweigert, and A. Piel. (1996). *Phys. Scr.* **61**, 494.
24. M. Zuzic A. Ivlev, G. Goree, G. Morfill, H. Thomas H. Rothermel U. Konopka, R. Sutterline, and D. Goldback (2000). *Phys.Rev.Let* **85**, 4064.
25. F. Melanso and J. Goree (1996). *Vac.Sci Techol. A* **14**,511.
26. R. Kompaneetz and V.Tsytovich (2005) *Contr. to Pl. Phys.*, **45**, 254.
27. S.V. Vladimirov, S.A. Maiorov, and N.F. Cramer (2003). *Phys. Rev. E* **67**, 016407.
28. S.V. Vladimirov, S.A. Maiorov, and O. Ishihara (2003). *Phys. Plasmas* **10**, 3867.
29. A.A. Samarian, S.V. Vladimirov, and B.W. James (2005). *JETP Lett.* **82**, 858.
30. R. Quinn, C. Cui, J. Goree, J., Ppieper H. Thomas, and G. Morfill (1996). *Phys.Rev. E* **53**, R2049.
31. U. Konopka, G. Morfill, and L. Ratke (2000). *Phys. Rev. Lett.* **84**, 891.
32. Ya. Khodataev, G. Morfill, and V. Tsytovich (2001). *J. Plasma Phys.* **65**, 257.
33. H. Schollmeyer, A. Melzer, A. Homann, and A. Piel. (1999). *Phys. Plasmas* **6**, 2693–8.

34. U. Konopka, G. Morfill, H. Thomas, and L. Ratke (1998). *AIP Conf. Proc.* **446**, 53.
35. S. Homann, A. Melzer, and A.Piel (1996). *Phys. Lett. A* **223**, 389.
36. S. Homann, A. Melzer, S. Peters, and A. Piel (1997). *Phys. Rev. E* **56**, 7138.
37. M. Klindworth, A. Melzer, A. Piel, V. Schweigert (2000) *Phys. Rev. B* **61**, 8404–10.
38. H. Thomas and G. Morfill (1996). *J. Vac. Sci. Technol. A, Vac. Surf. Films* (USA), **14**, 501.
39. H. Thomas and G. Morfill (1996), Nature (UK), **379**, 806–9.
40. G. Morfill and H. Thomas (1996). *J. Vac. Sci. Technol. A, Vac. Surf. Films* **14**, 490.
41. G. Morfill, H. Thomas, U. Konopka, H. Rothermel, and M. Zuzic (1998). *AIP Conf. Proc.* (USA), **446**, 184.
42. I. Schweigert V. Schweigert, A. Melzer, and A. Piel. (2000). *Phys. Rev. E* **62**, 1238–44.
43. G. Hoffmann and H. Lowen (2000). *J. Phys., Condens. Matter.* **12**, 7359.
44. A. Piel and A. Melzer (2002). *Plasma Phys. Control. Fusion* (UK), **44**, R1–R26.
45. V. Tsytovich, A. Ivlev, and G. Morfill. (2003). Contr.to *Pl.Phys.* **43**, 439.
46. V. Fortov, A. Nefedov, O. Petrov, A. Samarian, and A. Chernyschev (1996) *Phys. Rev. E* **54**, R2236.
47. V. Tsytovich (2005). *JETP Lett.* **81**, 448.
48. V. Tsytovich (2005). Contr.to *Plasma Phys.* **45**, 230.
49. L. Landau and E. Lifshits (1972). Statsctical Physics, Pergamon Press.

7

Mono-layer Plasma Crystals and Clusters

7.1 Mono-layer Plasma Crystals

7.1.1 Specific Properties of Mono-layers

There are two types of complex plasma mono-layers. First, there is an isolated monolayer, suspended electrostatically against the pull of gravity. Most current mono-layer experiments are of this type. They include studies of the wave propagation and dispersion analysis, some melting experiments as well as sublimation and crystal defect studies. Second, there is an attached monolayer (e.g., consisting of smaller micro-particles) located at the top of another mono-layer (of larger particles), or on the top of a system containing several lattice planes (of larger particles) or a system of larger particles in an uncorrelated state (in this case it is possible to crystallize the mono-layer and not the background complex plasma). Mono-layer crystals are determined by binary dust interactions if their in-plane size is less than L_{cr} or by collective dust interactions in the opposite case. Dust particles in the double-layer structure always interact in the direction perpendicular the plane by the binary particle interactions of each grain with other grains. Experiments of the second type (the attached mono-layer) have not been reported in the literature so far, but promise to be very interesting from a basic physics point if view.

Mono-layer crystal formation at present requires micro-particles within a very narrow mass range. This is due to the gravity force, i.e., the vertical force balance dictates that. In addition, the equipotential of the levitating electric field should have the horizontal planes of significant extent in order to be able to produce a large system. Radio-frequency and inductive discharges appear to be best suited for the latter requirement, and experiments reported on dust mono-layers utilize such plasma devices [1, 2, 3]. Figure 7.1 shows the structure of the mono-layer crystal observed in [1, 2]. [4, 5]. In principal physical point of view it is not clear if it is a mono-layer crystal with the mean-free path for plasma absorption parallel to the plane less than its size or if it is plasma cluster with the mean-free path larger the the size of the

V. N. Tsytovich et al.: *Mono-layer Plasma Crystals and Clusters*, Lect. Notes Phys. **731**, 289–331 (2008)
DOI 10.1007/978-3-540-29003-2_7

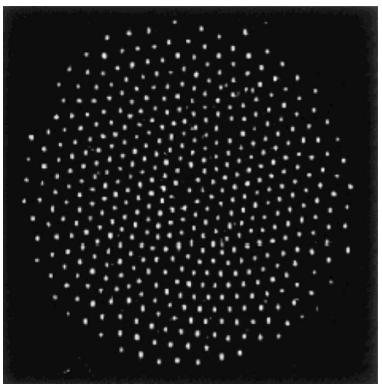

Fig. 7.1. An example of a 14mm diameter mono-layer plasma crystal containing 434 particles of the size $a = 0.5\,\mu$m levitating above the parabolic well of a lower electrode. Power into the plasma is 4W and the pressure is 100mTorr [1, 2]

cluster. In any case perpendicular to its plane the size is much less than the mentioned mean-free path and being in the sheath ion flow, the wake fields can be created below this mono-layer.

Mono-layers are special in many ways:

- The wake effects in the ion flow below the sheath can be insignificant for the grain interactions, especially if the ion flow is supersonic and an information on the ion focusing in the "wake" below the micro-spheres (or similar effects with a large damping involved) cannot propagate upstream or in the perpendicular plane.
- The wake field, however, can create a weak attraction between the grains in the plane of the sheath (which is an attraction of grains to the positive charge of the wake of the neighbor grain).
- Parasitic charge depletion is not important since the supply of plasma electrons and ions comes from the top (or from the bottom, or perpendicular to the plane of the mono-layer) of the system. This suggests that the particle charge should not vary systematically (e.g., in large 3D systems one might expect the reduced value of charge at the center). The reduction of the charges due to their mutual interaction in the plane can survive but this is the part of the dust–dust interactions which forms the layer.
- The non-collective shadow attraction of grains in the layer could be important for large grains.
- By having the mono-layer located on the same equipotential surface (or the same electric field ($E = mg/Q = const$) the relevant plasma parameters, e.g., the Debye length, the ion and electron temperatures, the ion flow velocity, etc., should be the same everywhere. This of course depends on the quality of the plasma chamber design.
- A mono-layer of micro-particles does not modify plasma electron and ion components as much as compared to a system containing many layers.
- Mono-layers are easy to manipulate in a controlled way, e.g., using lasers. This is in part due to lack of interactions with neighboring particle layers, and in part due to the smaller total mass of micro-particles involved.

These features make mono-layers particularly interesting for applications, e.g., for controlled deposition. In such a deposition experiment a mono-layer crystalline structure of micro-particles is first formed in a suspension and then it is deposited onto a substrate by simply turning the plasma off. From a basic physics point of view, active experiments (such as those involving waves, shocks, shear flows, etc.) are of particular interest, too, as to be expected from the above points.

Let us consider the micro-particle charge in a mono-layer. There is a simple experimental test. We have already referred several times to the equilibrium condition for the levitating charged micro-particles in the electrostatic field of the sheath and the drag force field of the ion flow in the sheath, in particular, in connection with the study of the form of the shielded potential around these particles using collision experiments. One of the earliest techniques to determine the particle charge was to excite vertical oscillations [3]. The method is as follows. Assuming [3] that the drag force is small we have for the equilibrium position z_0 of the grain

$$m_d g = QE(z_0) \; . \tag{7.1}$$

For small deviations from z_0 we can expand the electric field

$$E = E(z_0) + \frac{\partial E}{\partial z}(z - z_0) + \ldots \; , \tag{7.2}$$

where the higher-order terms are ignored and $\partial E/\partial z$ is assumed to be constant. Assuming a constant charge Q on the particle, the electric and gravitational forces then form a parabolic potential well

$$V = \frac{1}{2} Q \frac{\partial E}{\partial z}(z - z_0)^2 \tag{7.3}$$

which has a resonance frequency

$$\omega_0^2 = \frac{Q}{m_d} \frac{\partial E}{\partial z} \; . \tag{7.4}$$

By modulating the lower electrode with a variable frequency ω, the suspended micro-particles are subjected to forces, and reveal simple damped harmonic motion. The damping, as mentioned earlier, is due to the friction with the neutral gas. Having measured ω_0, one can then proceed in two ways. Either one can use the sheath model to determine $\partial E/\partial z$ at z_0, or one can measure the ion density and relate it to the field gradient via the Poisson equation. In either case, a reasonable determination of Q becomes possible.

In the sheath region, the drag force contributes comparably to the electric field force. Indeed, using the corresponding expression for the drag force and assuming as earlier that the charge of the dust grain is constant, we find that oscillations are determined by an effective potential in the way that $\partial E_{eff}/\partial z$ should be substituted instead of $\partial E/\partial z$, where

$$\frac{\partial E_{eff}}{\partial z} = \frac{\partial E}{\partial z} + \frac{2\tau n_i(z_0)}{n_e(z_0) z \lambda_{Di}^2} \left(\frac{1}{M(z_0)}\right)^2 \left(\ln \Lambda - \frac{M(z_0)^2}{4z^2}\right) \frac{\partial M}{\partial z} - \frac{\tau}{z\lambda_{Di}^2 M(z_0)^2} \left(\ln \Lambda + \frac{M(z_0)^2}{2z} + \frac{M(z_0)^4}{4z^2}\right) \frac{\partial}{\partial z} \frac{n_i(z_0)}{n_e(z_0)} \,. \quad (7.5)$$

Here, $M(z_0)$ is the local Mach number of the ion flow in the sheath known to be of the order of 1 (note that dust does not change much the structure of the sheath for mono-layers). We remind also that $z = Qe/T_e a$ is the dimensionless dust charge at the position z_0. We give this analytic expression with the drag force included in the equilibrium position of the charge to show that the assumption of neglecting the drag force (sometimes done as, e.g., in [6]) is strictly speaking not correct since by the order of magnitude the drag force contributes to the frequency an additional term of the order of 1. Indeed, roughly estimating the electric field in the sheath as the ratio of the wall potential to the sheath distance gives $E \approx eT_e/\lambda_{De}^2$, while the coefficient in the drag force is of the order of $eT_e n_i \tau / z n_e \lambda_{Di}^2$, which is the same order of magnitude in case the gradients of the Mach number and the ratio of ion to electron densities in the sheath are of the same order as the gradient of the electric field. Thus the changes introduced by the drag force in the estimate of the charge Q give a factor of the order of 1. Having in mind that it is necessary to use some sheath model (with uncertainties in it), the estimate of the absolute value of Q cannot be probably done more accurately [6]. In future, the role of the ion drag force should be investigated in more detail.

In experiments, it turns out that the vertical resonance frequency ω_0 is almost the same for a single particle, a particle chain, and a mono-layer [7]. All particles oscillate up and down with the same phase and hence the longitudinal coupling effects are small (if the amplitudes and phases are exactly the same, the horizontal coupling is not be affected at all). An example of the resonance curve obtained [7] is shown on Fig. 7.2. This observation supports

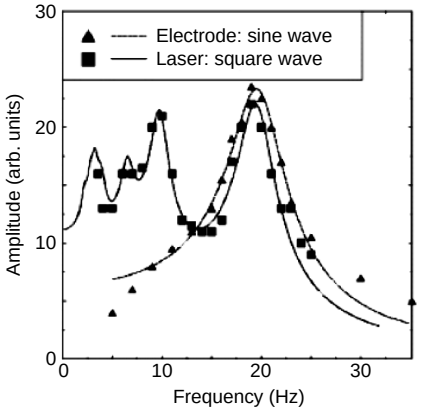

Fig. 7.2. Resonance curves of dust particle oscillations obtained by the electrode voltage modulation and laser excitation at 20Pa. The symbols denote the experimental data and lines are the least-square fits of the theoretical response functions. The electrode voltage was modulated by a sine wave while the laser excitation by the square wave form [7]

our statement about the special role that mono-layers play. It also implies that any systematic charge variations across a homogeneous mono-layer are small – otherwise the resonance frequency would be position-sensitive.

7.1.2 Theory of 2D Dust-lattice Waves

Waves and collective modes change substantially when only one layer of crystal exists. Waves analogous to DAW in 3D crystals exist also for 2D structures. Waves in 2D mono-layers are dust-lattice waves (DLW), dust shear waves, and dust bending waves. In the gaseous state of a complex plasma, many dissipation mechanisms operate which can disturb the transition of information from one dust grain to another creating damping or instabilities. If the momentum exchange between particles via the non-linearly screened Coulomb interaction (or via the collective interaction) becomes important and comparable with the grain inertia then the information about perturbations can propagate through the micro-particle component. When the micro-particles are packed into a 2D crystal lattice then their direct non-linearly screened Coulomb interaction and collective interactions dominate in the lattice plane.

The simplest derivation of dust-lattice waves employs the "linear chain" model [8, 9, 10, 11]. For simplicity, only nearest neighbor interactions and neutral gas friction are taken into account. Furthermore, although Debye screened potential is an over-simplification and the non-linear screening model should be used, it changes only some numerical coefficients at the position of the grain in the lattice and therefore for illustration the Debye screening can be used. We derive the force acting on the micro-particle number n (do not mix this notation with the notation used previously for the ion density), which is the integer number counting the grains in the chain with a distance between the grains equal to of the mean lattice spacing Δ. Define δ_n as the particle's deviations from the ideal lattice site and introduce $x_n \equiv \delta_n/\Delta$. Then in the limit $x_n \ll 1$ we find

$$m_d \Delta \frac{d^2}{dt^2} x_n = \alpha \left(x_{n-1} - 2x_n + x_{n+1} \right) - \nu_{nd} m_d \Delta \frac{d}{dt} x_n \ , \tag{7.6}$$

with the coupling constant defined by the potential of interaction of two grains. Particularly, for grains interacting with the Debye potential of a constant grain charge (which serves as the simplest example) the interaction energy is $V = (Q^2/r) \exp(-r/\lambda_D)$. Then we have

$$\alpha \equiv \frac{Q^2}{\Delta^2} \exp(-K) \left[(1+K)^2 + 1 \right] \ , \tag{7.7}$$

where $K \equiv \Delta/\lambda_D$. In the case of another type of interaction, we find a similar expression but with different coupling constant. Making use of the Bloch condition that in the zero order (a regularly spaced array of particles with the distance r_0) is described by the lattice vector $\mathbf{l} = \{n\Delta\}$, $r_n = r_0 + n\Delta$, we have

$x_m = \exp(i\mathbf{k}\cdot\mathbf{l})x_0$, where $\mathbf{k}$ is the given wave vector, $\mathbf{l}$ is the lattice vector, and the subscript 0 denotes our origin. In an infinite lattice, the origin position is arbitrary (so we pick the position n). Then we obtain $x_{n-1} = x_0 \exp(-ik\Delta)$, $x_n = x_0$, and $x_{n+1} = x_0 \exp(+ik\Delta)$. The force equation is given by

$$m_d \Delta \frac{d^2}{dt^2} x_0 = -2\alpha x_0 (1 - \cos(k\Delta)) - m_d \nu_{nd} \Delta \frac{d}{dt} x_0 \ . \tag{7.8}$$

The dispersion relation is then

$$\omega^2 - \beta^2 sin^2 \left(\frac{k\Delta}{2} \right) + i\omega\nu_{nd} = 0 \ , \tag{7.9}$$

where $\beta^2 \equiv \frac{4\alpha}{m_d \Delta}$. We mentioned earlier that for externally driven system ω is real and k has real and imaginary components. Hence, in order to be able to compare the "active manipulation" experiment (see below) with the theory we have to derive the decay of the amplitudes of the displacements of the micro-particles with distance, as the wave propagates through the crystal. Hence we derive the spatial damping coefficient. We have

$$k\Delta = 2 \sin^{-1} \left[\frac{\omega^2 + i\omega\nu_{nd}}{\beta}^2 \right]^{1/2} \ , \tag{7.10}$$

where $k = k_r + ik_i$ is split into real and imaginary components. The imaginary component k_i gives the spatial damping constant of the amplitudes, which evolves as $\exp(ikx)$ along the propagation axis, x, of the wave. For small values of k, the damping constant is given by

$$k_i^2 = \frac{2\omega^2}{\beta^2 \Delta^2} \left[-1 + \sqrt{1 + \left(\frac{\nu_{nd}}{\omega} \right)^2} \right] \ . \tag{7.11}$$

In the limit of small ν_{nd}/ω (or large ω) this reduces to $k_i\Delta = \nu_{nd}/\beta$, i.e., to a constant (frequency-independent) damping. In the limit of large ν_{nd}/ω (or small ω) we have $k_i\Delta = \sqrt{2\mu_{nd}\omega}/\beta$, i.e., the damping increases proportionally to the square root of frequency.

For low frequencies (small k), the waves are non-dissipative ($\omega \propto k$) and similar to acoustic waves. They are Dust Lattice Waves (DLW). The DLW velocity V_{DLW} is given by (see the list of crystal parameters on p. 274)

$$V_{DLW} = \sqrt{\frac{\alpha\Delta}{m_d}} \ . \tag{7.12}$$

Here, $\alpha\Delta$ plays a role of an effective temperature or an effective energy determining the wave velocity.

Generalizing this result to include more than just the nearest neighbors and extending the calculations to 2D lattice (mono-layer) yields for the equation of motion

$$m_d \Delta \frac{d^2}{dt^2} x_{jl} = \sum_{m=-\infty}^{\infty} \sum_{n=-\infty}^{\infty} \left\{ K_{mn}^{jl} (\delta x_{jl} - \delta x_{mn}) \right\} - m_d \nu_{nd} \frac{d}{dt} x_{jl} \ . \quad (7.13)$$

The wave propagates in the x-direction; Δx_{jl} are displacements of the micro-particles jl which are normally located in the lattice at the unperturbed positions $x_{jl,0}$ and $y_{jl,0}$. The coupling between particles at different sites mn with the particles under the consideration (jl) is described by K_{mn}^{jl}. For the case of the Coulomb shielded (Debye) potential we have

$$K_{mn}^{jl} \equiv \left[(x_{jl,0} - x_{mn,0})^2 \left(3 + 3\frac{r}{\lambda_D} + \frac{r^2}{\lambda_D^2} \right) - r^2 \left(1 + \frac{r}{\lambda_D} \right) \right] \times \frac{Q^2}{\Delta^4} \exp\left(-\frac{r}{\lambda_D} \right) \ , \quad (7.14)$$

where r is the distance between the particles mn and jl. Using the trial solution $\Delta x_{jl} \propto \exp[i(kx_{jl,0} - \omega t)]$, the dispersion relation is given by

$$\omega^2 - \frac{4}{m_d} \sum_{m=1}^{N_m} \sum_{m=-N_n}^{N_n} K_{mn}^{00} \sin^2 \left(\frac{k \Delta x_{mn,0}}{2} \right) - i\omega\nu_{nd} = 0 \ . \quad (7.15)$$

The result for the linear chain can be recovered by putting $N_n = 0$, and the expression can be solved for any given crystal structure.

7.1.3 Experiments on 2D Dust-lattice Waves

Measurements using periodically perturbed particle assemblies have been performed by using different techniques. Perturbations of the sinusoidal voltage applied to a wire located in the plasma near the plasma crystal are simple to produce experimentally [12]. They suffer from "side effects," however, as much as the perturbing potential modifies also the ion and electron flows and there can be coupling to the electrodes, which in turn can influence the dynamics of the plasma crystal; in short, this system is quite complicated. Perturbations by using the light pressure from a suitable laser beam [13] are experimentally more demanding; on the other hand, these interactions are better defined. The experimental set-up is shown schematically in Fig. 7.3 for a linear chain and for a mono-layer crystal [12]. These experiments are ones of the most thorough investigations to date. They were performed in a parallel plate RF discharge at 13.56MHz. The lower electrode has a diameter of 170 mm, the upper electrode, a grounded mesh grid, has a winilar wire. The two electrodes are separated by a gap of width 65 mm. The gas used is Helium at pressure in the range of 10–100Pa. A light inert gas was chosen in order to reduce the frictional damping as much as possible and to allow the dust- lattice waves to propagate. The discharge power is in the range of 5–10Watts. The micro-particles are mono-disperse melamine formaldehyde particles with 9.47 μm

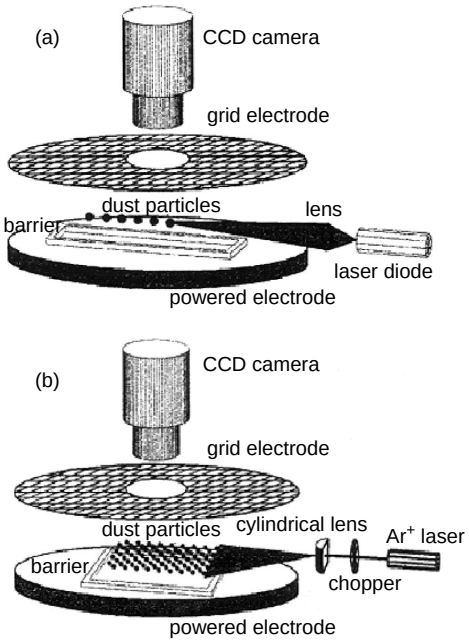

Fig. 7.3. Sketch of apparatus for excitation of longitudinal lattice waves by laser pulse (**a**) in a linear chain and (**b**) in a mono-layer plasma crystal [12]

diameter. The size variation is a few percent, too small to introduce measurable dispersion or scattering effect. As shown in the schematic Fig. 7.3, the particles are pushed periodically at a predetermined frequency (square wave current) using a laser trained on the end micro-particle. Since in this set-up the particles can only be pushed (not pulled), a confining box potential is set up using an elevated barrier on the lower electrode, its height chosen to be comparable to the scale size of the sheath. This set-up allows the micro-particles to be pushed up against the far-side potential barrier, and to relax back when the radiation force is off.

The corresponding measurements for the linear chain are shown in Fig. 7.4; they present a series of 15 snapshots taken at 100msec interval. Displacement of the micro-particles in the right part of the chain is clearly visible, as is the brightness of the end micro-particle during the illuminated phase, when the laser diode is "on." It is also clear from the measurements that the damping is quite substantial (due to dust friction with the neutral gas). From such data it is possible to derive the dispersion relation and obtain k_r (the real part of the wave number) and k_i (the damping term) as functions of the frequency ω. For the mono-layer plasma crystal, the results obtained [12] are shown in Fig. 7.5. In this case a good fit to the theoretically predicted 2D dispersion relation for linearly screened Coulomb interactions yields a shielding parameter $K = 0.8$, which is a little bit less than in the linear chain. The error is ± 0.4.

Dust-lattice waves with wavelengths much larger than the inter-grain distances can be described by the continuous differential non-linear equation

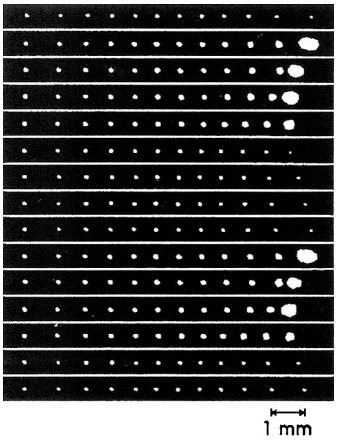

Fig. 7.4. Measurements for the linear chain by a series of 15 snapshots taken at 100 msec interval [13]

[14]. Here, the DLW velocity, the linear dispersion, and the nonlinear term are functions of the coupling constant which is related with the interaction potential of two neighboring grains. A solitary non-linear wave can be a solution of this equation [14]. An advantage of experimental investigations of DLW solutions is the possibility to determine the type of interaction between grains in a complex plasma. Up to present, only the screened Coulomb interaction was used in DLW studies and no attempt was done to fit the curves with other type of interactions although it is obvious that the screened Coulomb interaction can be an improper one due to collective, nonl-inear, and charging processes.

Theoretical efforts were not done so far in order to determine the lattice wave characteristics by including interactions other than the screened Coulomb interaction. This will have no principal difficulties since taking into

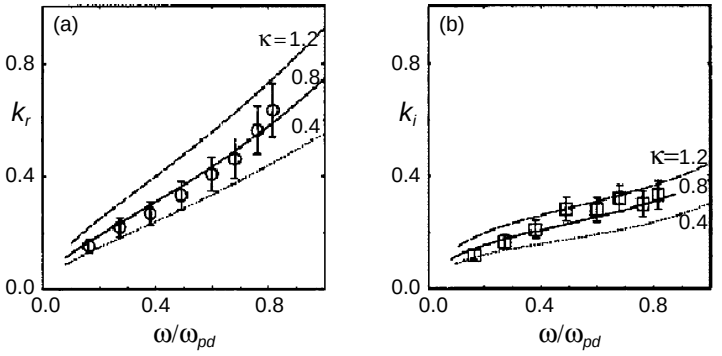

Fig. 7.5. Measured dispersion relations for dust-lattice waves. The comparison with the theory takes into account only the screened Coulomb potential and does not take into account other forces; this is why for different curves different adjusting parameters are used [12]

account other type of interactions in the dispersion relation and in the non-linearities changes the DLW speed in a way that only the value of the potential interaction and its derivatives enter. An important question is whether other interactions described above and the non-linearity in screening might have an important effect. Experimental results give the range of the shielding parameter as $0.7 \leq K \leq 1.2$. It seems also that K is in fact smaller for mono-layers. The physical arguments for that can be found both in the model of the screened Coulomb potential and in models of other interactions. They could be the following.

- In the plane perpendicular to the ion flow all particles should have the same charge. "Parasitic" removal of free charges (ions and electrons) is unlikely to play a role in the mono-layers: the supply from the main plasma is plentiful and each particle is directly accessible to the ion flow. This suggests that the charge modification by this effect is minor, hence Q could be the same for all particles, provided the plasma conditions (i.e., pressure, RF power, etc.) and the ion drift velocity are kept constant.
- Introducing a larger number of micro-particles into a fixed geometry potential well does change one important parameter, the particle pressure. This would suggest that in the equilibrium the system is more compressed since more particles are introduced. In fact the ram pressure of the collective flux produced by all particles is increased with an increase in the number of particles. This might be related with the effect of self-confinement we mentioned earlier several times. Bearing this in mind, it is quite reasonable to conclude that a more tightly packed 2D system should exhibit a systematically smaller K than a "looser" 1D chain. Some support is given by the fact that linear chain observations (in equilibrium without a lattice wave excited) are often seen to have a bigger spacing between particles at the end of the chain as compared to the (more compressed) central regions.
- However, such an effect could also be obtained if the plasma is inhomogeneous and the screening length varies in the appropriate way. This inhomogeneity should be then produced by the chain itself and is related with some self-contraction.
- At present we can only estimate the role of other forces between the micro-particles which might be responsible for changing the lattice waves. Note that in the corresponding analysis we cannot directly refer to the dust collision experiments where the ratio a/λ_D is 10^{-4} since in the discussed experiments $a/\lambda_{Di} \approx 0.3$. On the other hand, non-collective attraction effects depend on $(a/\lambda_{Di})^2 \approx 1/10$, and since in the grain collision experiments the screening length is close to the electron Debye length λ_{De}, which is approximately 7 times larger than λ_{Di}, we have an estimate $a^2/\lambda_{Di}^2 \approx 5{\cdot}10^{-3}$. This estimate shows us that the attraction forces are expected to be 20 times larger in these experiments [13] than in the dust collision experiments. The attraction forces should occur at the distance close to the electron Debye length and this is the length close to the inter-grain distance.

One cannot therefore exclude their possible role in the difference observed [15] between the values of K for 1D chain and in mono-layer. On other hand, one should have in mind that experiments on 1D chain and on 2D mono-layers as well as the collision experiment [16] are performed in the sheath region with the presence of the ion flow, and the anisotropy in screening discussed earlier can play an important role.

- From physical point of view we can expect that collective effects in grain attraction are larger in 2D case than in 1D case, i.e., the factor K should be less in 2D case than in 1D case. This is qualitatively what is observed but quantitative answers are not available at present.

We have mentioned that 3D experiments could be very important to perform. The "topological transition" from 1D to 2D and to 3D systems should be a function of the compressibility of the plasma crystal, i.e., it should depend on the strength of the inter-particle forces and the attraction forces (especially for the collective attraction forces) and should play much more important role. The self-confinement effects, related with the collective flux and collective effects of self-organization as well as structurization should be more pronounced in 3D systems. A systematic investigation of the dependency of the parameter K on the number of micro-particles in the confining well, including the above-mentioned topological transitions, will probably shed some light on the basic self-organization processes in equilibrium open systems. Such investigations could be of fundamental value.

7.1.4 Stimulated Plasma Crystal Sublimation

An improvement of the radiation pressure active manipulating technique is to "guide" micro-particles in a controlled way by using two lasers. This makes the active control independent of the potential field geometry and natural relaxation timescales. Such an improved control could be used, for instance, to extend the frequency range to explore the potentially existing regime of the crystal Debye frequency. Theoretically, at that frequency (corresponding to the dust acoustic wavelength equal to twice the particle separation, $\lambda = 2\Delta$) the propagation of information becomes impossible, at least for acoustic modes. This is wellknown in the crystal physics. However, there is a possibility that the energy can be converted to other wave modes or that parametric instabilities and non-linear effects can occur, perhaps leading to a crystal disruption. To observe this at the kinetic level for a model system is clearly one of the exciting topics for future research.

However, as mentioned above, the interactions are very complex and their interpretation is correspondingly difficult. For this reason we confine ourselves to the presentation of observations at this stage, which is only a heuristic attempt. The particle motion in the horizontal plane is initially quite small (almost thermal). When the frequency increases from 34 to 35 Hz, a single particle obtains a large horizontal momentum at some point. Its energy is in

excess of 3eV, which is three orders of magnitude higher than in the previous stage and 1/50 second earlier. This particle then plunges through the crystal and disrupts it, leading to complete sublimation at the timescale of 1/10 second. This disruption is not possible through dissipation of the initial energy of a single particle, of course. The sublimed (disordered) particles all have energies in excess of 10eV, so the single "trigger" particle merely liberates the energy stored in the system. There are two kinds of the stored energy, the vertical oscillations and the potential (electrostatic) energy. One clear fact to note is that the crystal is moving up and down as a solid body, with a large amplitude of about 500 μm, i.e., there is a large amount of stored energy present, about 20eV per particle. Thus a disruption of the crystal by a single particle liberates this energy and thermalizes it because of the horizontal adjustment that takes place in the response.

The questions therefore are as follows:

- What leads to the "break-out" of the trigger particle in the first place?
- Is it a purely statistical effect – and then is there always one particle that starts the process?
- Is there a systematic change in the crystal structure that facilitates the process, or even makes it possible in the first place?
- What process(es) is/are responsible for the collective crystal vibration and what is/are its/their stability criterium(a)?

To answer these questions (and many others), more research needs to be done. This seems to be well worthwhile since observations of sublimation processes on the kinetic level are currently not feasible in any other way.

Regarding possible systematic changes in the crystal structure just prior to the sublimation transition, there is an intriguing development. The particle separations are very similar initially (except for the edge particles, as remarked earlier). As the wave frequency slowly increases to the critical value where the sublimation sets in, it has been noted [17] that the structure of the crystal undergoes a systematic change, with neighboring lattice planes adopting a short–long–short–long separation. This is the signature expected for a compressional (sound) wave that has a wavelength $\lambda = 2\Delta$, twice the lattice separation. Whilst this could be, of course, a coincidence or an unfortunate geometrical effect, it is nevertheless sufficiently intriguing to follow up with a systematic investigation, possibly one where vertical oscillations of the crystal (the potential energy reservoir) are produced by modulating the potential of the lower electrode and where dust lattice waves are excited using two laser beams – in order to avoid the electrostatic coupling.

7.1.5 Theory of Dust Bending Waves

For special laboratory conditions in the presence of gravity, the electrostatic suspension of micro-particles leads to fundamental asymmetry which is important regarding the wave propagation. In particular, it makes possible

propagation of dust bending waves. In RF discharges, the particles are suspended in the horizontal layers and the supporting sheath electrostatic field is in the vertical direction. The ion flow is also in vertical direction, toward the lower electrode. Electrostatic focusing by the negatively charged microparticles leads to an enhanced ion density, which is a wake below the particle [18, 19, 20] (although dissipative processes, collisional or collisionless, can disperse the wake). The combined particle and wake system can be thought of (to some extent) as a vertically aligned asymmetric charge/dipole system. In the presence of many grains due to the change in dust interactions the picture can change substantially and does not correspond to the collection of charge/dipole components. For simplicity, we speak below about the dipole component which in reality is an asymmetric non-linear and a collective screening effect. The wake model is valid in the case where the vertical dimensions of the system are much less than the ion–dust mean-free path, but these conditions are the best for observation of the dust shear waves and therefore we concentrate here on this model.

For horizontally propagating waves (DLW) we ignored the dipole component (although we apply the argument that the presence of the ion flow changes the screening in the horizontal direction). If the waves are excited by using laser light pressure acting on the particles, the wake just follows the disturbed particle. If the waves are excited electrostatically using a wire, then whilst the negatively charged particles are accelerated in the positive, x-direction, the positively charged wake is accelerated in the negative x-direction, which in principle leads to additional complexity. In the case of shear waves, if these are excited in the horizontal plane with laser light pressure we may again assume that the wake interaction is marginal. However, if they are excited vertically, another type of waves, namely the "bending waves" [9, 10, 11] (as they bend the mono-layers out of its original plane) is generated where the interaction with the wakes can be important especially if the amplitudes are sufficiently large. DLW also become modified by the aligned dipole scenario and it is possible that suitable experiments can be described to explore and measure the influence of the wake quantitatively in future.

In DC discharges, it is possible to produce long vertical strings of microparticles suspended in the electrostatic field of striations as it was described already in detail. Here the ion wake is located again below the particles; however, the dipoles are now aligned with the particle strings. Waves associated with grain motions along the strings [21] are mostly affected by the wakes in this case. Only one type of shear waves exists in this case, which is different from the shear waves discussed earlier. There can, however, be an asymmetry for waves propagating downward and upward because the wake is only attached to "its" upstream particle.

The scenario with dipoles is a very rough picture for the strongly screened and strongly coupling systems. Full description of all modes including shear and bending waves can be obtained, as usual, by considering linear perturbations of initial non-linear stationary state and solving the corresponding

equations of motion [9, 10, 11]. We have in the simplest case [9]:

$$\omega(\omega + i\nu_{nd}) = \omega_s^2 - (1 + k\Delta)\,\frac{\omega_{pd}^2}{\pi}\exp(-K\Delta)\sin^2\left(\frac{k\Delta}{2}\right)\,. \tag{7.16}$$

The main difference with the compressional dust-lattice waves is in the ω_c^2 term, which merely reflects the normal mode oscillations in the vertical confining potential (e.g., a singly undamped particle would simply have $\omega = \omega_c$. Also,

$$\omega_{pd}^2 = \frac{4\pi Q^2 n_d}{m_d} = \frac{4\pi Q^2}{m_d \Delta^3} \tag{7.17}$$

is a formally introduced dust-plasma frequency here. In the case of two vertically arranged chains, the lower grains are in the wake of top-chain grains, and a new wave mode (mostly affected by the wake) associated with counterphase motions of grains can propagate [10].

7.1.6 2D Dust Shear Waves

A normal plasma does not support shear waves. However, in plasma crystals waves called "Dust Shear Waves" (DSW) associated with in-plane motions of grains can exist, and their observations have indeed been done [22, 23]. Figure 7.6 shows such DSW [22]. Due to small amplitude of the laser-excited shear, many data sets have to be superposed to extract the systematic particle motion from the random thermal noise, so great care has to be taken with both the measurements and the data analysis. The verification of the existence of these very slowly propagating DSW is quite exciting because the technique can in principle be improved to investigate the bending wave and aligned dipole case as well. Theoretical dispersion relation can again in the simplest case be

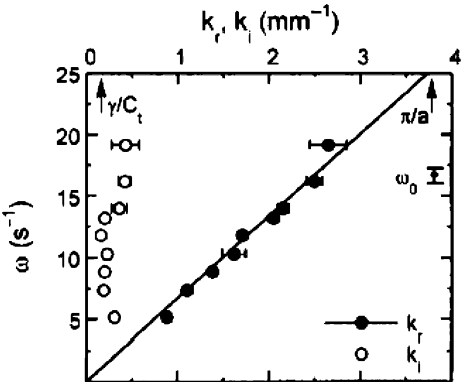

Fig. 7.6. Dispersion relation for shear lattice waves [22]: experimentally measured k_i and k_r are shown as filled and open circles respectively. The solid line indicates sound speed

obtained [22, 24] by considering only the "nearest neighbors" interactions in a linear chain. The transverse mode dispersion relation reads as follows:

$$\omega(\omega + i\nu_{nd}) = \omega_s^2 + \frac{\omega_{pd}^2}{\pi} \exp(-K\Delta) \sin^2\left(\frac{k\Delta}{2}\right) , \tag{7.18}$$

which looks similar to the dust lattice bending waves [9]. The difference is the ω_s^2 term, which reflects the normal mode oscillations in the horizontal confining potential.

7.1.7 2D Dust-lattice Wave Mach Cones

We already mentioned possible excitation of the Mach cones of volume DAW and DSW by a grain. Note that the Mach cones are well known to be excited in any material by objects moving faster than the phase velocity of the waves of the system. The Mach cones in 2D layer have specific properties related to 2D lattice waves; they were observed experimentally [17, 25] being excited in a mono-layer plasma crystal by a fast charged grain moving below the dust layer. The fast particle usually excites two cones, the first one associated with the density compression and the second cone (which follows the first one) associated with the density rarefication. In experiments [17, 25], the crystal is located in an RF discharge with particle sizes of 8.9 μm and 4.8 μm, the electron temperature $\approx 1eV$ and the ion density $n_i \approx (5-1) \times 10^9\,\mathrm{cm}^{-3}$. The gases used are Xe, Kr, and Ar, the dust separation in the crystal is about 400 μm and the fast dust particles move below the plane crystal at the distance 200 μm from its surface with the speed of 30–60 mm/s starting spontaneously to form the second dust layer below the first (existing) layer. The grain is supersonic as compared to the speed of DLW and DSW so it excites the DLW and DSW Mach cones. The crystal is located at a relatively large distance from the electrode (about 8 mm) which is much larger than the electron Debye length (the value of the ion drift velocity at the position of the crystal was not measured), the dust charges are about $Z_d \approx 10^4$. The Mach cones were identified on a particle speed map and on the particle density map, (see Fig. 7.7).

It was observed in experiments [25] that the Mach cones correspond to the shocks excited in the crystals. The Mach cone can serve as a diagnostic method to determine parameters of the crystal by adjusting experimental results to a theoretical model, which in [25] was the screened Coulomb model. This allows to determine two parameters, namely the charge and the ratio of inter-particle distance to the screening length. But usually one need to take into account other forces as we discussed above. In some experiments [26] the Mach cones were excited in a similar experimental device by the laser beam focus which moved with a supersonic velocity. The action of the laser beam on the particles in a mono-layer crystal is due to the radiation pressure of the focused beam. A multiple Mach cone structure is observed in this case, with

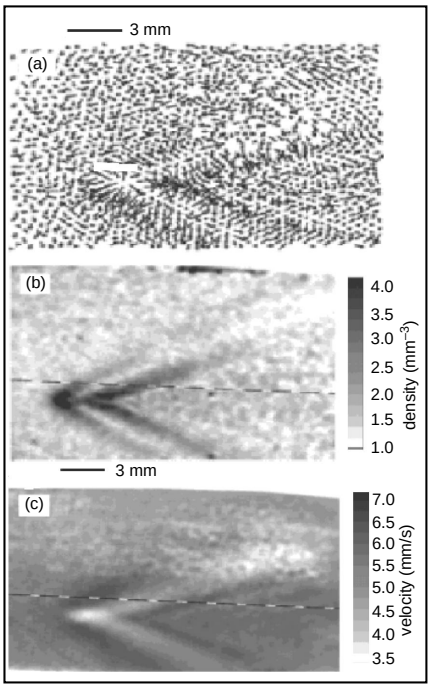

Fig. 7.7. The Mach cones in a layer of 8.8 µm particles in a Kr 100W discharge [17, 25]. The supersonic particle moves to the left: (**a**) The particle velocity vector map derived from the particle positions in two consecutive video fields; (**b**), (**c**) The grayscale number density maps averaged from data for 20 video frames. The dashed lines indicate the location of cross-sectional slices of the velocity and density profiles

at least three distinct Mach cones as shown in Fig. 7.8. The Mach cone angle relation can be verified over a wide range of Mach numbers for both the first and the second cones. The sound speed, measured from the first Mach angle, increases with the dust number density. The results were compared with the

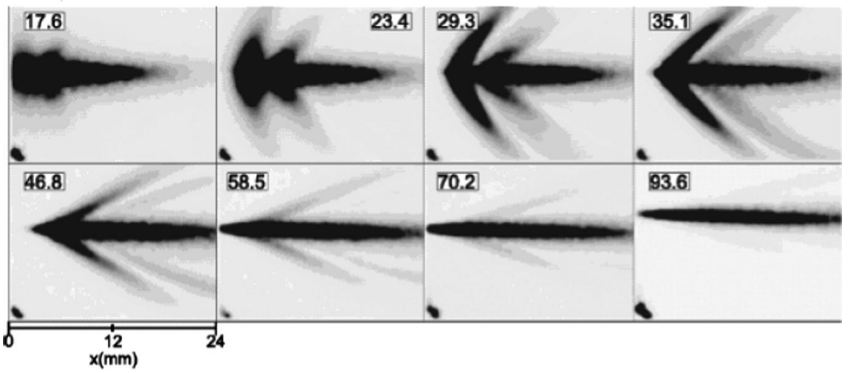

Fig. 7.8. Gray scale maps of the particle speed $v = |\mathbf{v}|$ for different speeds of the laser spot $\mathbf{V}$ [27]. Dark gray values correspond to high particle velocities (black correspond to $\approx$ 4mm/s). The numbers in the boxes indicate the laser speed in mm/s. The dark spot on the lower left corner is an artifact and it is unrelated to the Mach cones

theory of DLW, which uses the two-parameter dust interaction as the screened Coulomb model to determine the screening length and the dust charges.

Some concluding remarks are as follows:

- The Mach cones are effective diagnostic methods for dust crystals which can be applied to more refined theoretical investigations as well.
- Determination of the intensity distributions in the wave lengths is still an open experimental task for future investigations.

7.2 2D Plasma Clusters

7.2.1 Introductory remarks

Physical properties of dust structures with small numbers of grain are quite different from those with large numbers of grains. Different physical conditions correspond to the case where the size of the system is much larger or much smaller than the mean-free path for absorption of plasma particles (ion and electrons) on grains. The Grain Clusters (GC), observed experimentally [2, 28, 29, 30, 31], consist of small number of grains and their size is much less than the mean-free path for ion/electron absorption on grains. They can also form an ordered state of Cluster Crystals (CC) which seems to be similar to the crystal state but is different from it. They can be also melted and transformed to the gaseous and liquid states, and can also form the disordered dust cluster structures (DCS). One can expect at the first glance that the difference between plasma crystals (PC) and CC is that an increase of the inter-grain distance from the center to the periphery should be more pronounced for CC than for PC. Observations of CC were so far performed only in the presence of an external confining potential (which contributes substantially to the force balance), while for PC the presence of small confining potential is unimportant. Therefore CC can have more homogeneous distributions of the inter-grain separation. Physically, the main difference between these two types of structures is the type of grain–grain interaction which for PC as well as for large-size disordered states are of collective nature (where the pair grain interactions depend on the distributions of all other grains), while for CC and DCS the pair grain interactions are the same as for two isolated grains and the total energy of interaction can be described as the sum of all pair interactions.

As demonstrated above, in the disordered state there exist a universal instability and in certain conditions almost one periodical mode can be excited at the its threshold. Similar instability can occur for transitions to CC in cluster systems of small number of grains. The term “strong coupling” does not really express the meaning of the state to which the complex plasma can condensate. In a usual matter, the transition to the crystal or liquid state is indeed related with the strong coupling where the electrostatic energy substantially exceeds the kinetic energy of the interacting particles. However, as

shown above, a simple equalization of the dust temperature with the depth of the collective attraction well gives the value of $\Gamma_{cr} = 1/\psi_m$ and the term "strong coupling" cannot be used for the PC state. The same is true for crystallization of clusters. In experiments, the factor Γ_{cr}, as well as its dependence on other system parameters which can be altered is measured. For CC the grain attraction is not collective but the transition can occur also by an instability related with the coupling of longitudinal and transversal modes.

Investigation of CC can give a detailed information on the pair grain interaction, although this information cannot be applied to PC. Nevertheless, the clusters are themselves interesting objects of investigation. In the case of a few grains, the 2D clusters resemble classical atoms where the grain distribution is a shell-like. Those clusters were investigated [32] in external traps confining charged ions. A big effort was also done to investigate the screened Coulomb interaction in the cluster state [32]. But the grains interaction differs significantly from that. In the case of Coulomb and screened Coulomb interactions, it was observed that there exists only one shell for a few grains, then by increasing the number of grains the second shell, third shell, and so on appear. The question is, how the interactions typical for dust grain can affect this general picture? In certain conditions, the subsequent shell creation can also be observed but its appearance is different from that for Coulomb and/or screened Coulomb clusters. Additionally, dust clusters can in principle exist without an external confining potential due to the presence of non-collective dust attraction at large distances.

We discuss in the next sections not only interpretation of dust cluster observations [2, 28, 29, 30, 31] but also the ways how to proceed in experiments to obtain the pair grain interactions. In experiments on Earth, 2D clusters are usually located in the plasma sheath which affects their interaction by the sheath electric field and the ion flow to the electrode. Thus although in plasma clusters the grain interactions correspond to the binary interactions, the analysis of the sheath field needs to be performed. Another possibility opens with experiments on small grains levitating in the small electric field where the influence of the sheath field is reduced; however, the non-linear screening is also reduced in this case. We need a compromise between these effects; below in the section, we discuss what is the best way to find it. The easiest possibility is to make experiments in micro-gravity conditions which naturally lead to the problem of 3D clusters. We show in this chapter that in three dimensions the clusters can appear as helical clusters with constant separation between the plains and with constant angle of rotation between the plains. For double-winding helical structures, the systems reminds the DNA structure, so the possibility of modeling of biological molecules by grain clusters is also discussed. The helical clusters for ions in laser traps were already observed [33, 34, 35] and in future planned experiments on dust in long plasma tubes the 3D grain helical clusters can probably be observed. The best to obtain the pair grain interaction is related to experiments in

micro-gravity conditions using the 3D helical clusters. Of course of interest are intermediate conditions where (with an increase of the number of grains) CC are converted to collective complex plasma states. This problem has not been investigated so far. In principle, 2D and 3D clusters can be used for measuring non-collective as well as collective dust–dust interactions which should serve as basic interactions in complex plasmas. A kind of useful information can be obtained by investigation of hybrid clusters with grains of different sizes. For example, small grains can satisfy the condition that their inter-grain distance is small and the mean-free path for the ion-grain absorption is much less than the size of the systems while a few large grains satisfy the opposite condition. Then the large grains have additional interactions due to collective effects produced by the small grains. Experiments using the hybrid structures can be the simplest ones to measure the collective interactions directly. Therefore we also discuss here the hybrid helical grain clusters.

7.2.2 Experiments on Small and 2D Clusters

One of experimental priorities is to check the screening (predicted theoretically to be non-linear) and the non-collective attraction (predicted to depend on the dust size and the properties of the dust surface–sticking coefficients of neutrals and ions) of grains. Methods of measuring the binary non-collective interaction by using equilibrium, stability, and oscillations of small 2D dust clusters in an external parabolic confinement potential constitute a relatively simple experimental approach. First experiments on dust 2D clusters demonstrated their existence and the shell structure, having no aim to measure the grain–grain interaction. Therefore we analyze here the possibility of altering such experiments for direct measurements of the grain–grain interactions.

Two comments should be made concerning particle distributions in a complex plasma:

1. Usually in current experiments, the high rate of plasma absorption on dust is compensated by local ionization. In this case, thermal electron and ion distributions are not created since the conditions for reaching thermal distributions via pair ion/electron–ion/electron collisions, $Z_d P_0 \ll 1$, are not fulfilled. We note that the ionization process always produces non-thermal distributions and the dust-charging process makes plasma electrons and ions non-thermal (creates depletions of high-energy electrons and low-energy ions). Strictly speaking, proper theoretical estimate should use the kinetic description. This is not only overly complicated but the kinetic theory is not fully developed yet. Therefore we use estimates for thermal electron and ion distributions having in mind that expressions for the parameters in these estimates contain integrals with respect to the whole electron and ion distributions and that the non-thermal part of the distributions can change the result by a factor of the order of 1.
2. Dust grains are distributed thermally according to existing observations as well as theoretical estimates. The existing theory predicts that even by taking

into account all new type of dust–dust interactions related with collective effects, the dust distribution becomes thermal in a rather short time interval. This is due to the high rate of dust–dust collisions (with all collective effects included). Even for the non-thermal electron and ion distributions, the dust–dust collision integral contains only an integral over the ion and the electron distributions as a factor in front of expressions vanishing for dust thermal distributions in the dust–dust collision integral. The dust-neutral collisions also thermalize the dust distribution if the neutral component is thermal. Therefore there exists a good basis to assume that dust grains have a thermal distribution.

In clusters or dust molecules, binary interactions between a finite number of "components" dominate the physics since their size is $L < L_{cr}$. Such a physical criterion does not exist in ordinary matter, where in most cases interactions are of the binary type. Of course one cannot take a "small" volume of a complex plasmas as an analogue of a small volume in ordinary matter, since the physics of transition from CC to PC is different. But still even for $L < L_{cr}$ some features similar to the crystalline formation can be found in dust clusters.

Dust clusters are of interest as new dust structures. From experimentally obtained eigen-frequencies of cluster oscillation modes and from the cluster stability criteria and equilibrium conditions one can determine the binary plasma interactions. The clusters contain a finite number, of dust grains N. There exists a necessary condition for such kind of experimental technic. Usually, it is not difficult to measure the mode frequencies for 2D clusters if the number of grains is not large. By fitting these frequencies with some type of potential one can obtain the sets of parameters determining interactions for different N. There should be the same value of the ratio of screening length to the cluster size and the same ratio of the dust separation to the screening length for all values of N. If this requirement is not fulfilled (as it takes place for the screened Coulomb interaction), the interaction is different from that taken as a test interaction. This is not surprising since usually the screened Coulomb interaction does not operate for grains with large charges. One can also derive exactly the potential energy of the grain interactions from the cluster oscillation frequencies.

Dust clusters are of interest themselves with their transitions from ordered to disordered states; they give the rare possibility to observe these transitions at the kinetic level, to make measurements of the binary binding energy and its dependence on sources (for instance, the ionization power), the shear modules, the global modes of cluster oscillations, their compression and elasticity, etc.

In usual matter, numerous investigations were performed for 2D clusters confined by an external parabolic potential. In a complex plasma, such an external confinement is, generally speaking, not needed due to the presence of the long-range non-collective attraction at sufficiently large distances. Obviously, interactions in mono-layer small clusters are different from interactions in 3D volume crystals. Also, as we many times emphasized, in laboratory-

produced structures (levitated in the plasma sheath), the ion flow makes the interactions asymmetric by creating wakes where the interaction of particles along the ion flow is different from the interaction perpendicular to the flow. In mono-layer clusters in the plasma sheath, the formation is perpendicular to the ion flow. Nevertheless the ion flow can modify the attraction potential well even in the direction perpendicular to the flow. Finally, the continuous transformation from small dust clusters with small number of grains to clusters with large number of grains is of interest since it can include new phenomena; this is a separate field of research with its own problems [30, 31, 32, 36].

Even in the absence of all complications related with special dust behavior, investigation of clusters formed in ordinary matter is a wide field of research. These clusters are usually confined in some traps. In the case of ordinary particles their interaction is a simple Coulomb interactions and such clusters are called Coulomb clusters. 3D Coulomb clusters are found for ions in Paul and Penning traps [37, 38], and 2D clusters formed by electrons are found in liquid helium [39] and in colloidal suspensions [40]. Note that liquid colloidal suspensions are not suitable for investigation of dynamical processes because of the large over-damping due to interaction with viscous electrolyte.

In a complex plasma, not only the new type of grain interactions but also the dust–neutral collisions are important. The latter can alter properties of clusters in two aspects: (1) they can damp the dust motion thus allowing some stable cluster configurations (unstable in the absence of dust–neutral collisions) and (2) the damping can be much weaker than in colloids; therefore the cluster eigen-modes of oscillations can be a large field of investigations.

7.2.3 Observations and Ordering Rules

Ordered 2D clusters are usually obtained in experiments on Earth as mono-layer structures levitating against the gravity in the plasma sheath close to the electrode of the gas discharge chamber. The sheath electric field force acts on grains in the vertical direction to compensate the gravity and drag forces. The electric field also creates the ion flux to the wall. A complication in the interpretation of 2D cluster formation in the presence of Earth gravity is that the cluster formation occurs perpendicular to the ion flow. Nevertheless the ion flow can modify the grain interaction potential perpendicular to the flow, too.

The 2D clusters were experimentally observed in complex plasmas in a number of experiments [28, 29, 30, 31, 36]. The results were compared with the screened potential model. In [29], damped cluster modes were observed for small numbers of grains. The experimental set-up and distribution of grains for clusters containing $N = 3$, $N = 4$, and $N = 5$ grains are shown in Fig. 7.9. The experiments were performed in argon gas for grains with the size of $\approx 10\mu$m and mass of 6.73×10^{-10}g. The first two images for $N = 3$ and $N = 4$ clusters show the existence of one shell only, while for $N = 5$ cluster one particle is in the center corresponding to the appearance of the second shell. The

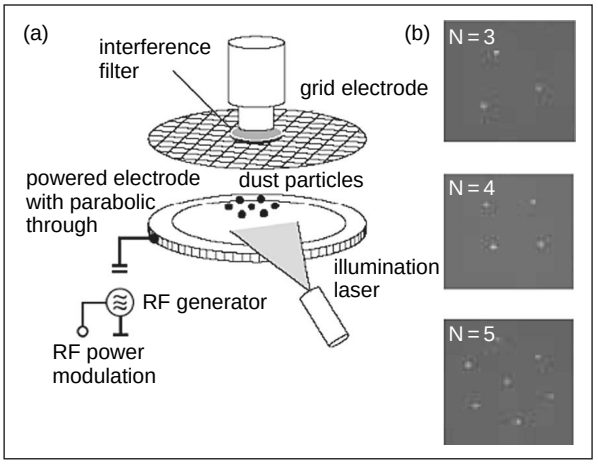

Fig. 7.9. (**a**) Scheme of experimental set-up, (**b**) Images of observed grain clusters with $N = 3$, $N = 4$, and $N = 5$ grains [29]

external perpendicular confining potential $V_{ext} = m_d\omega_0^2 r^2$, which determines the frequency ω_0, was chosen in a way that at the position of the grains the bare Coulomb electric field force is of the order of the external confining force. For pure Coulomb repulsion (as well as for the screened Coulomb interaction) it is expected that for the first shell the repulsion of grains positions them at the same distance from the center and with equal distances between the grains. This was indeed observed.

If grains attract each other at larger distances, the position of the shell is changed. This can be checked by changing the external potential (the ω_0). Such experiments were not performed so far. The type of screening (the Debye screening or non-linear screening) can be in principle checked but each of them also gives the grain distribution at equal distances from the center for the first shell. With an increase in the number of grains in the cluster, there appear new shells as demonstrated by Fig. 7.10 taken from experiments [30], where clusters with $N = 9, 15, 27, 71$ grains are shown.

For $N = 9$ and $N = 15$ clusters, one can see that the second shell contains 2 and 5 grains, respectively, while for $N = 27$ the third shell with 3 grains can be seen (with 9 grains in the second shell and 15 grains in the outer shell). All this reminds the periodic table of elements but the shell formation in dust clusters is not due to quantum effects of atom binding (as in usual matter) but mainly due to confining in the external potential. The main problem to be solved is whether the shell-like structure can be observed for small confining potentials where the cluster size is large and the attraction potential becomes important (or the shell-like structure can even be observed without the confining potential; these clusters related with dust–dust attraction will be a new type of structures specific to complex plasmas). However, such experiments need a special design with flexible value of the external confining potential; they have not been performed so far. An indication that the external confinement plays important role in present experiments is that the second shell appears

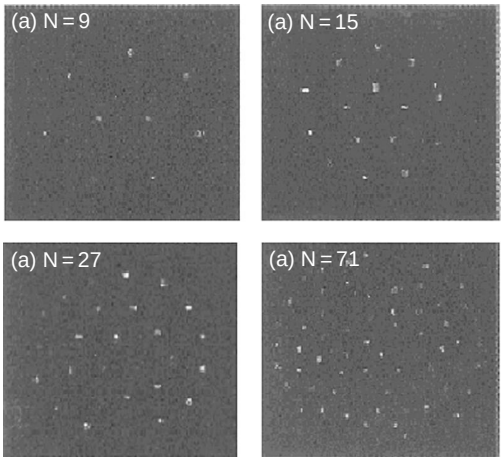

Fig. 7.10. Clusters observed in experiments [30]: (**a**) cluster of 9 grains, with 2 located in the central shell and 7 located in the outer shell; (**b**) cluster of 15 grains, with 5 in the central shell and 10 in the outer shell; (**c**) cluster of 27 grains with 3, 9, and 15 particles in the shells; and (**d**) cluster of 71 grains where the shell structure is not well pronounced

for different number of grains ($N > 6$ in [29] and $N > 7$ in [30]) in different experiments. The critical numbers for the next shell to appear can be named the "magic numbers of complex plasmas" (with analogy of the Mendeleev's periodic table of elements in usual matter) when they are independent of the external potential (which is not the case of current experiments). If the shells can be observed in the absence of an external confining potential, their appearance is universal and a new table of complex plasma elements (grain complexes) as basic elements of the new state of matter (complex plasma) can be obtained. Figure 7.10d showing the observed $N = 71$ cluster demonstrates that although the shell structure cannot be so well seen in this case but obviously for many grains in the central region, the role of external potential is small and the main role is played by grain interactions. Since grains in this region are close to each other, the attraction is probably not large, and the screening is not much pronounced as well. Weakly damped cluster global modes were measured in [29], where the low gas pressure of 1.6Pa was used (with the neutral density less than 10^{14}cm^{-3} compared to the neutral density larger than 10^{16}cm^{-3} in standard experiments). Some of these modes are shown in Fig. 7.11.

Figure 7.12 from [29] demonstrates that the screened Coulomb interaction, $V = (Z_d^2 e^2/r)\exp(-r/\lambda_D)$, with the phenomenological screening parameter λ_D used in [29] for estimates of grain-grain interactions, does not satisfy the requirement that the screening parameter is the same for different global modes. The frequency ω_0 (used for normalization of the frequencies of observed modes) and the distance r_0 (used in normalization in the horizontal axis) are fixed in the experiments, $(1/2)\omega_0^2 r_0^2 = Z_d^2 e^2/r_0^2$, and thus the screening factors λ_D are quite different, which proves that the screened Coulomb interaction is not applicable. This is not surprising since large grain charges ($Z_d \sim 10^4$) in these experiments make interactions non-linear. Thus different values of κ (see Fig. 7.12) fit the experimental results for different clusters.

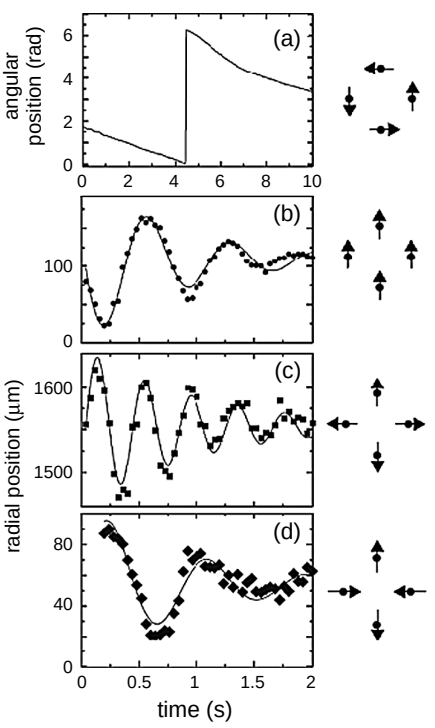

Fig. 7.11. Normal global modes of $N = 4$ cluster: (**a**) rotation around the center of the potential well; (**b**) center of mass motion; (**c**) breathing mode, (**d**) antisymmetric mode. The lines are the best fits of damped oscillations to the experimental data. At the right side of each part, grain motions in the corresponding global mode are demonstrated

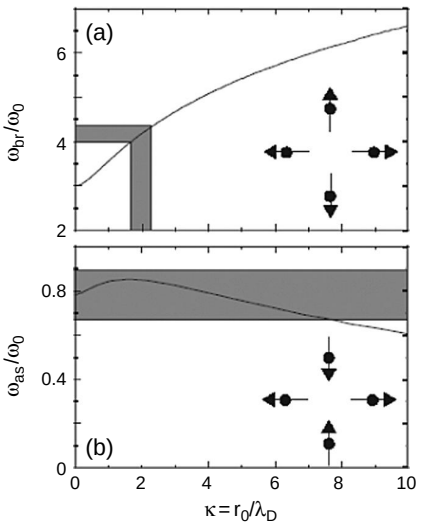

Fig. 7.12. Normalized global frequencies of (**a**) the breathing mode and (**b**) the antisymmetric mode for $N = 4$ clusters as a function of $\kappa = r_0/\lambda_D$. The shadowed area corresponds to the experimentally measured frequencies, the solid line corresponds to the frequencies obtained for screened Coulomb interactions theoretically

This becomes apparent for the observed antisymmetric cluster modes where the parameter κ is large. The conclusion drawn from this result is that *the screened Coulomb potential does not fit the observations.*

It was obtained in a pure Coulomb 2D systems that the cluster shells have "magic numbers" of particles in each subsequent shell [41] as in the usual Mendeleev's periodic table. These numbers are different for dusty 2D clusters as compared to those for Coulomb clusters. Figure 7.13 [36] illustrates different structures and sets of magic numbers observed for N-particle clusters with screened Coulomb interaction. Analogous study for non-linear screening has not been performed yet. However, it is clear from this figure that there exist differences in configurations of the grain clusters and the Coulomb clusters. This comparison was done for the same confining well (as mentioned, the cluster magic numbers can depend on the confining potential). Universal magic numbers can exist only for self-confined clusters in the presence of grain attraction. It is also possible that (for the same number of grains) the magic numbers are changed when an external force is applied to rotate one shell with respect to other. Such phenomena were found in experiments [36] demonstrating that the rotation can displace a grain from one shell to the closest shell. The magic numbers are determined by the stability of the shell structure: if the number of particles in one shell becomes too large, the new inner shell is created. This stability criterion depends of course on the strength of the external confining potential. The number of particles in the respective shells

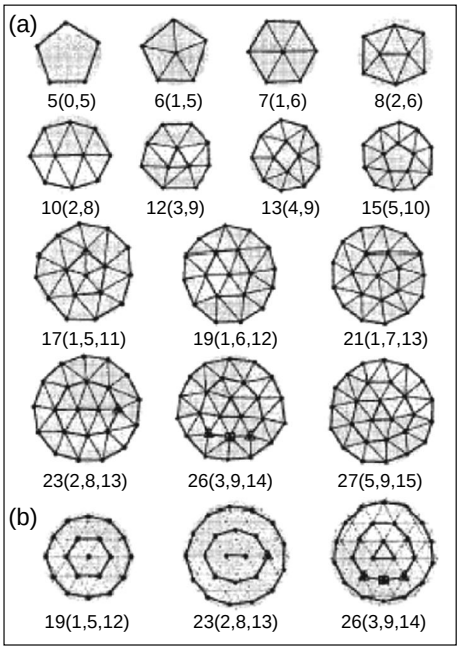

Fig. 7.13. (**a**) Grain clusters with screened Coulomb interaction and (**b**) unscreened Coulomb clusters. The confining potential is the same for both cases; below each figure we show (in brackets) the number of grains in subsequent shells

and the ordering into the "magic numbers" is related to the energetics (including external sources) of the structures produced. In [31], a comparison was made between the measured "plasma cluster" structures and the hard-sphere configurations (both are located in a quadratic external potential well). The obvious difference probably reflects the effects of the long-range non-screened potential and/or the presence of attraction forces.

Studies of dust clusters, of 2D as well as 3D types, promise to constitute a very interesting field of research which has just started. Apart from current investigations of homogeneous clusters, the work should proceed into investigation of grain clusters of one size in a homogeneous "sea" of grains of another size (probably, lower size) in order to measure the role of collective attraction produced in a complex plasma. Also, very promising are investigations of binary mixtures (clusters with grains of different sizes), of inhomogeneous clusters, and those of the influence of the confining potential (in plain 2D clusters) on the cluster structure. It is easy to see that certain configurations – in particular, those that conform to the preferred hexagonal structures minimizing energy – are more difficult to "dislodge" than those already in an elevated energy state. The "magic numbers" have a meaning similar to that they have in usual atomic physics although the details are completely different, of course. Moving on furthermore to larger systems, the point to note is that the geometry of the confining force (e.g., cylindrical) begins to assert itself more and more.

Future theoretical investigations taking into account the non-linear screening potential and non-collective attraction can provide universal magic numbers for self-confined structures in the absence of an external confinement. These "magic numbers" will then resemble the Mendeleev's periodic table rules in ordinary chemistry and we can say *that they are as much important in the super-chemistry of "plasma clusters" as the Mendeleev's rules are in ordinary matter.*

7.2.4 Theory of 2D Clusters

A general theory was recently developed for 2D clusters where interactions between components are described by arbitrary forces and the system is confined (in the plane) by an external parabolic potential well [42]. This allows us to analyze experimental data for any grain charges, any screening (including non-linear screening), any grain–grain interactions (including attraction and repulsion interactions). The theory is useful for experimental evaluation of actual forces by analyzing global cluster modes, their stability, and oscillation frequencies. This opens a unique possibility to investigate binary dust–dust interactions in a complex system.

General Expressions to Compare with Observations. The theory [42] considers equilibrium and normal global mode oscillations for 2D clusters of arbitrary numbers of grains N which form either a single shell (where the grains are distributed at equal radius at a certain distance) and many shells (where

the grains are distributed on shells on different radiuses). The confining potential is assumed to be parabolic, $V_{ext} = m_d\omega_0^2/2$, and inter-dust interaction is considered to be arbitrary. The conversion of one-shell structures to double-shell structures, three-shell structures, etc. occurs with an increase of the number of grains N in the subsequent shell because dispersion relation for the structure starts to have unstable solutions. Thus the "magic numbers" appear which can be compared with observations. The interactions and oscillation frequencies of normal modes are different for linear and non-linear screening and depend on the strength of the non-collective attraction. The number of parameters on which the normal modes depend is small. Thus by obtaining the value of an oscillation frequency (from experimental data) for one mode we can calculate the corresponding frequencies of other modes and compare them with observations. Our aim here is to illustrate the application of the theory for the experiments [29] (note that this procedure can be used in any other experiments of this type). We write the results [42] in dimensionless units equalizing $m_d r_0^2$ from the coefficient of the external potential with the Coulomb factor of interaction $Z_d^2 e^2/r_0$. Thus we use $r_0 = (Z_d^2 e^2/m_d\omega_0^2)^{1/3}$ for normalizing distances and $m_d\omega_0^2 r_0^2$ for normalizing the energy. Then the external energy is $V_{ext} = r^2/2$ (where r is the dimensionless distance from the center of the cluster) and the pair interaction energy is written as $V(r_{i,j}) = f(r_{i,j}^2)$, where $r_{i,j}$ is the dimensionless distance between the interacting particles i and j. The equilibrium condition and the frequency of oscillations can be expressed through the derivatives of f with respect to its argument $\xi = r^2$ (to obtain the results, used in the analysis given below, from [42] it is sufficient to put in the final result of [42], $m_d = 1, q = Z_d e = 1$, $\omega_0^2 = 1$).

We use two types of the grain interaction: the screened Coulomb interaction with non-collective attraction $f_Y(\xi)$, and the non-linear screening with non-collective attraction f_N, where

$$f_Y(\xi) = \frac{1}{\sqrt{\xi}}\left[\exp(-\kappa_Y\sqrt{\xi}) - \alpha_{ncoll}\right]; \kappa_Y = \frac{r_0}{\lambda_D}$$
$$f_N(\xi) = \frac{1}{\sqrt{\xi}}\left[(1-\kappa_N\sqrt{\xi})^4 - \alpha_{ncoll}\right]; \kappa_N = \frac{r_0}{\lambda_{nscr}}\,. \tag{7.19}$$

We do not fix here the value of the linear screening λ_D (although the linear theory provides an expression for it) as well as the value of the non-linear screening λ_{nscr} (although the non-linear theory also provides an expression for it). The reason is that the theory can be used to find the dimensionless values of κ_Y and of the cluster size $R_Y = r_{cl}/\lambda_D$ for the linear interaction as well as those of κ_N and $R_N = r_{cl}/\lambda_{nscr}$ for the non-linear screening interaction, with r_{cl} being the size of the cluster. The clusters with a single shell only exist up to $N \leq 6$, while for $N = 7$ there appears a new particle in the center. For first clusters up to 4 grains the possible grain motions in global modes are shown in Fig. 7.14. In [29], detailed data are given for modes (b),(e),(h) shown in Fig. 7.14. We start with the mode (e), i.e., with the breathing mode $N = 4$

(Fig.7.14(e)). According to [42], the equilibrium conditions and frequencies for these modes are

$$\omega_0^2|_{N=4} = -\frac{4}{m_d}(f'(2r_{cl}^2) + f'(4r_{cl}^2));\ \omega_0^2|_{N=3} = -\frac{6}{m_d}f'(3r_{cl}^2)$$
$$(\omega_{br}^2)_{|N=3} \equiv \omega_b^2 = \frac{36r_{cl}^2}{m_d}f''(3r_{cl}^2);\ \ (\omega_{ass}^2)|_{N=4} \equiv \omega_h^2 = \frac{32r_{cl}^2}{m_d}f''(4r_{cl}^2)$$
$$(\omega_{br}^2)|_{N=4} \equiv \omega_e^2 = 16r_{cl}^2(f''(2r_{cl}^2) + 2f''(4r_{cl}^2))/m_d \ .(7.20)$$

Using the dimensionless units, we should substitute $\omega_0^2 = 1$, $m_d = 1$, and the frequencies ω are in units of ω_0 as they are shown in Fig.7.12. To compare the theory with experiments, we use ω_e^2 given in Fig.7.12(a). The arrow bars are given in [29] for all three modes [(b), (e), and (h)] for the absolute value of this frequency: $\omega_b = 15.42 \pm 0.1 s^{-1}$; $\omega_e = (16.14 \pm 0.1) s^{-1}$; $\omega_h = 6.93 \pm 0.45$. The normalization of frequencies can be found from Fig. 7.12(a). This gives the normalized frequencies: $4.136 < \omega_e^2 < 4.245$ (which is inside the shadowed area in Fig. 7.12) $(4 < \omega_e^2 < 4.375)$; $3.773 < \omega_b^2 < 3.872$; and $0.675 < \omega_h^2 < 0.876$. We can analyze both the linearly screened interactions and the non-linearly screened interactions as well as the role of non-collective attraction. The point is that all relative frequencies and the equilibrium conditions contain only three parameters, $\kappa = r_0/\lambda_{scr}$, $R = r_{cl}/\lambda_{scr}$, and α_{ncoll}, where $\lambda_{scr} = \lambda_D$ for linear screening and $\lambda_{scr} = \lambda_{nscr}$ for non-linear screening, and only the cluster size R is different for $N = 4$ and $N = 3$ clusters. Thus the experimental data are sufficient to check the theory. We start with linearly screened interactions assuming absence of non-collective attraction as in [29].

Linear Screening, $\alpha_{ncoll} = 0$. We start with the breathing $N = 4$ clusters denoting their dimensionless size as $R_{4,Y}$ (and *kappa* as $kappa_Y$). We obtain

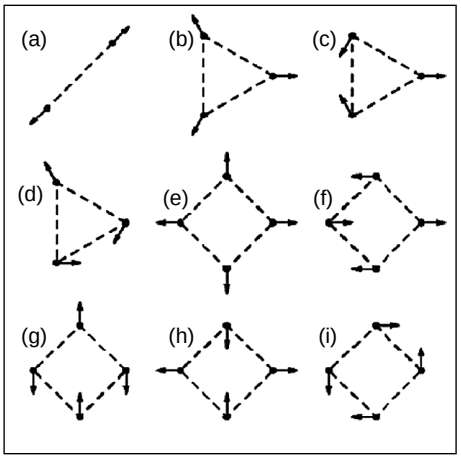

Fig. 7.14. Grain motions in global modes up to $N = 4$ clusters

$$1 = \frac{1}{\sqrt{2}}\frac{\kappa_Y^3}{R_{4,Y}^3}\left[\exp(-\sqrt{2}R_{4,Y})(1+\sqrt{2}R_{4,Y})+\right.$$
$$\left.\frac{1}{2\sqrt{2}}\exp(-2R_{4,Y})(1+2R_{4,Y}) - \alpha_{ncoll}\left(1+\frac{1}{2\sqrt{2}}\right)\right];$$
$$\omega_e^2 = \frac{1}{\sqrt{2}}\frac{\kappa_Y^3}{R_{4,Y}^3}\left[\exp(-\sqrt{2}R_{4,Y})(3+3\sqrt{2}R_{4,Y}+2R_{4,Y}^2)+\right.$$
$$\left.\frac{1}{2\sqrt{2}}\exp(-2R_{4,Y})(3+6R_{4,Y}+4R_{4,Y}^2) - \alpha_{ncoll}\left(1+\frac{1}{2\sqrt{2}}\right)\right] \quad (7.21)$$

The value of κ_Y should be considered as fixed for all clusters with screened Coulomb interactions since it is determined only by the system's properties (which do not change with grain's position) and by the external potential (which is also the same for different clusters). The equilibrium within the range of the frequency's uncertainty found above gives then the size $1.165 < R_{4,Y} < 1.25$, $1.53 < \kappa_Y < 1.688$. We then have a discrepancy with the results shown in Fig. 7.12; this is only due to different normalizations of κ in [29] (denoted as κ_{mkp}) and in our consideration here ($\kappa_{mkp} = 2^{1/3}\kappa_Y$). For our calculated range the latter gives $1.928 < \kappa_{mkp} < 2.127$, which is inside the interval shown in Fig. 7.12 from [29], where $1.6 < \kappa_{mkp} < 2.3$. Thus we gave the starting point of coincidence with the results of calculations [29]. The cluster equilibrium conditions and frequencies depend only on the above two parameters and the value obtained numerically can be compared with that observed for the frequencies of all global cluster modes (κ_Y is known to be the same for all other modes). For the breathing mode of $N = 3$ cluster (see Fig. 7.14(b)) we have for the screened Coulomb interaction

$$1 = \frac{1}{\sqrt{3}}\frac{\kappa_Y^3}{R_{3,Y}^3}\exp(-\sqrt{3}R_{3,Y})(1+\sqrt{3}R_{3,Y});$$
$$\omega_b^2 = \sqrt{3}\frac{\kappa_Y^3}{R_{3,Y}^3}\left[\exp(-\sqrt{3}R_{3,Y})(1+\sqrt{3}R_{3,Y}+R_{3,Y}^2) - \alpha_{ncoll}\right] \quad (7.22)$$

With the value of κ_Y obtained, the cluster size is $1.098 < R_{3,Y} < 1.178$ and $2.87 < \omega_b^2 < 2.93$ while according to the above estimates using data [29], this frequency should be $3.773 < \omega_b^2 < 3.872$. This shows a large disagreement between the observations and the calculations. The difference between the maximum calculated value of the square of the frequency 2.93 and the minimum observed value 3.773 is 0.843 (and is even less than the observed one) and this difference is 8.5 times larger than the possible frequency difference measured.

It should be nevertheless mentioned that the mode damping was not taken into account in the calculations performed. However, from all modes the one shown in Fig.7.14(h) is the most damped. In experiments, the damping is due to collisions with neutrals and is almost constant for all modes since the pressure and therefore the density of neutrals is fixed. The mode (h) has the

lowest real part of its frequency and therefore the mode frequency can be comparable with the damping rate which is indeed the case since according to Fig. 7.14(h) the amplitude of this mode decreases by 3 times (approximately by the factor e) on the period of the mode. Usually in this case the real part of the frequency is $\sqrt{\omega^2 - \gamma^2}$, where γ is the damping rate. For γ close to ω, the real frequency is lowered and therefore the damping only increases the disagreement. Namely, the frequency of the (b) mode which we consider by taking into account the damping calculated from (h) mode is in the range $2.225 < \omega_b^2 < 2.716$, and the difference between the maximum calculated square frequency and the minimum observed is 1.063. This is by factor 10.84 larger than the observed difference by a factor of 10.84. This demonstrates that the screened Coulomb interactions do not fit observations.

We should continue this comparison by adding the asymmetric mode for $N = 4$ cluster (see Fig. 7.14(h)) for which frequency is also measured [29]. The values of κ_Y and $R_{4,Y}$ are the same as for the breathing mode (Fig. 7.14(e)). The squared frequency $\omega_{ass,4}^2$ determined from [42]

$$\omega_h^2 = \frac{1}{4}\left[\exp(-2R_{4,Y})(3 + 6R_{4,Y} + 4R_{4,Y}^2) - \alpha_{ncoll}\right] \tag{7.23}$$

is $0.344 < \omega_h^2 < 0.375$ and is again outside the range measured [29] ($0.675 < \omega_h^2 < 0.876$). The minimum observed value 0.675 is by 0.299 less than its maximum calculated value. The damping (when taken into account in the calculations in accordance with the observed values for this mode) shifts down the calculated frequency and gives a very large disagreement between the theoretical model and observations. Experimental results indicate that the damping of this mode can be rather large. The discrepancy found (even without checking other modes) is sufficient to conclude that *screened Coulomb potential does not operate for grain interactions in the clusters observed*. The question is now whether the non-collective attraction can correct the calculated frequencies in a way that they fit the ranges of the frequencies observed.

Non-linear Screening, $\alpha_{ncoll} = 0$. To check the non-linear screening, we start again with the breathing mode of an $N = 4$ cluster. For κ_N and $R_{4,N}$ we obtain

$$\begin{aligned}
1 &= \frac{1}{\sqrt{2}}\frac{\kappa_N^3}{R_{4,N}^3}\left[(1-\sqrt{2}R_{4,N})^3(1+3\sqrt{2}R_{4,N})\right. \\
&\quad \left. + \frac{1}{2\sqrt{2}}(1-2R_{4,N})^3(1+6R_{4,N}) - \alpha_{ncoll}\left(1+\frac{1}{2\sqrt{2}}\right)\right]; \\
\omega_e^2 &= \frac{3}{\sqrt{2}}\frac{\kappa_N^3}{R_{4,N}^3}\left[(1-\sqrt{2}R_{4,N})^2(1+2\sqrt{2}R_{4,N}+2R_{4,N}^2)+\right. \\
&\quad \left. \frac{1}{2\sqrt{2}}(1-2R_{4,N})^2(1+4R_{4,N}+4R_{4,N}^2) - \alpha_{ncoll}\left(1+\frac{1}{2\sqrt{2}}\right)\right].
\end{aligned} \tag{7.24}$$

We find $0.2855 < \kappa_N = 0.305$ and $0.23 < R_{4,N} = 0.241$. We can use the value of κ_N in the equilibrium and frequency relations for the breathing $N = 3$ mode described by

$$1 = \frac{1}{\sqrt{2}} \frac{\kappa_N^3}{R_{3,N}^3} (1 - \sqrt{3} R_{3,N})^2 (1 + 3\sqrt{3} R_{3,N});$$

$$\omega_b^2 = \sqrt{3} \frac{\kappa_N^3}{R_{3,N}^3} \left[(1 - \sqrt{3} R_{3,N})^2 (1 + 2\sqrt{3} R_{3,N} + 3R_{3,N}^2) - \alpha_{ncoll} \right]. \quad (7.25)$$

This gives $0.198 < R_{3,N} < 0.208$ and $4.057 < \omega_b^2 = 4.165$, while observations give $3.773 < \omega_b^2 < 3.872$. We see that the non-linear screening approach predicts larger frequencies than those observed (while the linear screened Coulomb approximation predicts frequencies significantly lower than those observed for the same node). For the non-linear screening, the difference between the minimum predicted squared frequency, 4.057, and the maximum observed one, 3.872, is only 0.185, which is only 1.87 times larger than the difference of the measured squared frequencies (and much less than the corresponding difference, 8.5, for the linear screened Coulomb interaction).

For the asymmetric mode of an $N = 4$ cluster, we use

$$\omega(h)^2 = \frac{3}{4} \frac{\kappa_N^3}{R_{4,N}^3} \left[(1 - 2R_{4,N})^2 (1 + 4R_{4,N} + 4R_{4,N}^2) - \alpha_{ncoll} \right] \quad (7.26)$$

and find that $0.892 < \omega_h^2 < 0.894$, while the measured values are $0.675 < \omega_h^2 < 0.876$. We can see again that the theoretical values are larger than those given by observations and this is qualitatively different from the prediction for linear screening. We can fit this range with observations by taking into account the damping. The ratio γ/ω required to put the calculated range of square frequencies into the range of observed ones is $0.143 < \gamma/\omega < 0.567$, with the larger value being in full agreement with observations for this mode. So the complete fit of the (h)-mode is reached. For the (e)-mode with larger frequency this ratio is $0.064 < \gamma/\omega < 0.253$, i.e., the shift is up to $3.799 < \omega_b^2 < 3.855$, which is inside the whole range of the observable interval. Thus the non-linear screening can well fit the observations even in the absence of the non-collective attraction.

Role of Non-collective Attraction. General calculations show that the frequency interval for different modes can be sensitive for even a weak non-collective attraction. We performed similar calculations by increasing α_{ncoll} from 0.01 to 0.1. We obtained that for the screened Coulomb interaction the frequency intervals of global modes are shifted with the increase of α_{ncoll}. For the (b) mode, this shift is opposite to the direction of the observation interval reaching for $\alpha_{ncoll} = 0.033$ the range $2.759 < \omega_b^2 < 2.805$, which is out of the observational range $3.733 < \omega_b^2 < 3.872$. For the (h) mode the calculated interval is only slightly shifted in the direction of the observational interval and for the same value of α_{ncoll} reaches $0.434 < \omega_h^2 < 0.406$ (in

the absence of non-collective interactions it was $0.344 < \omega_h^2 < 0.375$). Contrary to the case of linearly screened Coulomb interaction, the non-collective attraction lowers the discrepancy between theory predictions and observations. For the non-linear screened interaction, an increase of α_{ncoll} leads to the ranges of calculated squared frequencies ω_b^2 and ω_h^2 moving toward the observed ranges. For $\alpha_{ncoll} = 0.033$, the calculated interval for the (b) mode is $3.823 < \omega_b^2 < 3.904$, which completely covers the observed interval $3.773 < \omega_b^2 < 3.872$ for small damping. The calculated interval for the (h) mode is shifted to $0.896 < \omega_h^2 < 0.899$, which is very close to the observed interval $0.675 < \omega_h^2 < 0.876$ (and coincides with observations by taking into account the damping). We find that the mentioned ranges of frequencies are very sensitive to the coefficient of non-collective attraction for both linear and non-linear screening which means that it can serve as a very effective tool to measure the non-collective attraction. The main conclusion that the non-linear screening fits observations while the linear screening cannot fit them survives when the non-collective attraction is taken into account.

Problems to Solve. We aimed in the above analysis to demonstrate effectiveness of the global cluster mode method to measure inter-grain interactions. The future investigations can extend this method and answer many questions. Let us list them:

1. It is necessary to extend the calculations for all modes measured, with strong requirement that the value of κ be same for all modes.
2. The relative size of different clusters measured does not contain the screening length and can be used as a tool for choosing the interaction type.
3. The ratio κ/R does not contain the screening length and can be calculated and compared with observations.
4. The value of κ can be calculated and compared with experiments.
5. It is not difficult to obtain grain properties with large non-collective attraction coefficient determined by the shadow effect of the neutral flux (the neutral attachment coefficient can be made large for specially prepared grains with special surfaces) and use an increase of the neutral gas pressure to vary the attraction coefficient. Then measurements of the mode frequencies directly give the dependence of the potential on the distance.
6. The presence of the sheath can substantially change the real potential of grain interactions and therefore experiments in plasma bulk are preferable (these can be done in micro-gravity conditions).
7. Grain clusters can be used to investigate sheath properties (and problems) in industrial applications.

7.2.5 Boundary-free 2D Clusters

General Remarks. Boundary-free clusters are of special interest since their parameters are universal depending only on the strength of the non-collective attraction. Therefore they can be the best objects to measure the non-collective attraction. In the absence of an external confinement potential

$\omega_0 = 0$, the dimensionless size of the cluster can be normalized with respect to the screening length ($R = r_{cl}/\lambda_{scr}$, where $\lambda_{scr} = \{\lambda_D, \lambda_{nscr}\}$) for linear and non-linear screening. One should have in mind that in the plasma bulk $\lambda_D = \lambda_{Di}$ and $\lambda_{nscr} = 3.6\lambda_{Di}/\mu^{1/5} \gg \lambda_{Di}$; in this case, the dimensionless cluster size for non-linear screening is smaller than that for linear screening.

The first question to ask is whether a boundary-free cluster can exist. In the absence of an external confining potential, the equilibrium needs an attraction. We consider the range $0.0001 < \alpha_{ncoll} < 1$ including a very weak attraction. For $\alpha_{ncoll} > 1$, the attraction is larger than the repulsion even if the grains contact each other (this case should be referred as the grain agglomeration). The criterion for agglomeration requires $R = a/\lambda_{scr}$ (remember that a is the grain size) and we can eventually answer the question as to which value of α_{ncoll} is sufficient for it. In the absence of an external potential there exists no center of the cluster, i.e., it has the translational freedom where the cluster center can move (although the friction on neutrals should stop this motion at some position). The simplest way to produce such clusters is to use a flat external potential with rigid walls, with distances between them larger than the cluster size. If the equilibrium relative positions for the boundary-free cluster are determined, next natural questions are on the cluster stability and the frequencies of global modes. The latter depends also only on α_{ncoll} and therefore can be quite useful for measurements of the non-collective attraction strength.

Equilibrium Size. The size of a single shell cluster is defined as the radius R at which N cluster grains are located. The radii R are different for non-linear screening and for linear screening since the screening constants are different. Without fixing the real value of the screening length one can deal with the dimensionless size R normalized differently for non-linear and linear screening. The value of R is a function of N and α only. In calculations, the values of R can be obtained directly from equilibrium conditions and their calculated ratios (independent of normalization) can be compared with the measured ones. This procedure can be used for different types of grain interaction without fixing the actual cluster radius, which for linear screening (where $\lambda_{scr} = \lambda_{Di}$) depends on the ion density (not precisely known in experiments) and for non-linear screening depends on $\lambda_{scr} = 3.6\lambda_{Di}(za/\tau\lambda_{Di})^{1/5}$, i.e., additionally on the temperature ratio τ and the grain size a.

The calculations show that with an increase of N (in the same shell) the size R increases and with an increase of the attraction coefficient α_{ncoll} it decreases. The calculations proceed up to $N = 7$ in order to find the first magic number where the second shell starts to form. In this case we need to consider also another configuration for the same grain number N where all grains are in one shell and where $N-1$ grains are in the shell and an additional one grain is in the cluster center. (The equilibrium dimensionless sizes differ for linear and non-linear screening). By putting $\omega_0 = 0$ we find that in the presence of attraction the equilibrium cluster size always exist starting with a very weak attraction $\alpha_{ncoll} = 0.0001$.

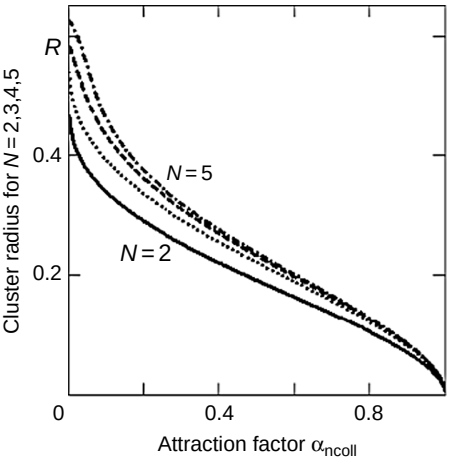

Fig. 7.15. Cluster equilibrium size for the non-linearly screened interaction. The solid line corresponds to $N = 2$, the dotted line corresponds to $N = 3$, the dashed line corresponds to $N = 4$, and the dash-dotted line corresponds to $N = 5$

The calculations performed up to $\alpha_{ncoll} \approx 0.998 \sim 1$ are shown in Fig. 7.15 for non-linear screening in $N = 2, 3, 4, 5$ clusters. The equilibrium size depends only on the number of cluster grains. There is nothing unusual for such dependencies also for $N = 6, 7$ clusters; these curves not shown in Fig. 7.15 are slightly above the shown curves and they do not change the shown tendency qualitatively. The range of sizes is $0 < R < 0.652$ for non-linear screening, where zero is not reached since for $R < a/\lambda_{nscr}$ the grains touch each other (i.e., agglomeration of grains occurs). It can be seen that the equilibrium size exists for all clusters in the whole range of α_{ncoll}. The curves can be used to estimate the value of α_{ncoll} necessary for agglomeration. For the linear screening we obtain qualitatively similar pictures, but the range of sizes R is different: $0 < R < 5$. The most important difference between the non-linear and the linear screening is in the ratio $r_N = R_N/R_{N-1}$. The results of calculations are shown in Fig. 7.16 for $N = 4, 5, 6, 7$ clusters.

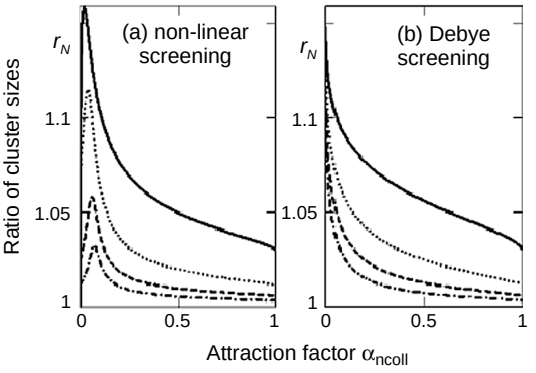

Fig. 7.16. Ratio of cluster sizes $r_N = R_N/R_{N-1}$ for $N = 4, 5, 6, 7$ clusters: (**a**) non-linear screening and (**b**) lienar screening. The solid line corresponds to $N = 4$, the dotted line corresponds to $N = 5$, the dashed line corresponds to $N = 6$, and the dash-dotted line corresponds to $N = 7$

Oscillation Frequency. A larger difference between linearly and non-linearly screened clusters occurs for frequencies of cluster modes. We demonstrate that for all modes shown in Fig. 7.14. Figure 7.17 gives the corresponding squared frequencies for non-linear screening, while Fig. 7.18 gives the squared frequencies for linear screening. The frequency branches for non-linear and linear screening are quite different. The frequencies of several modes increase substantially when α_{ncoll} is increased. This is accompanied by a decrease of the size of the cluster. For α_{ncoll} close to 1 the squared frequency ω^2 can reach large values of order $10^4 - 10^5$. If these oscillations are thermal then obviously their amplitudes are decreasing $\propto 1/\omega^2$. Note that $\omega^2 < 0$ means instability and for non-linear screening the (h) mode is unstable for small α_{ncoll}, while for linear screening the (b), (c), and (d) modes are unstable for large α_{ncoll}. If only one of the cluster modes is unstable the whole cluster becomes unstable and converts in another configuration for the same number of grains. For $N = 4$ cluster, it is dissociated into $N = 3$ cluster and a free grain, and the latter obtains the energy difference of two configurations and moves away but then it is stopped at some distance by the friction on neutrals. There is also another possibility to have $N = 3$ grains forming a triangle with the fourth grain at its center; we call this a "centered cluster." Which of these two possibilities is realized depends on the energy difference of a dissociated cluster and a centered cluster. For some values of α_{ncoll} $N = 4$ grains are unstable while for other values of α_{ncol} they are stable. The instability threshold can be used to estimate the value of α_{ncoll}.

It is interesting to note that for any fixed value of α_{ncoll}, a finite spectrum of frequencies is possible, as for atoms in usual matter. This analogy is of course remarkable. In experiments, the ratio of different frequencies can serve as a test determining the grain interactions. For known interactions the measured frequencies directly determine the value of the attraction coefficient.

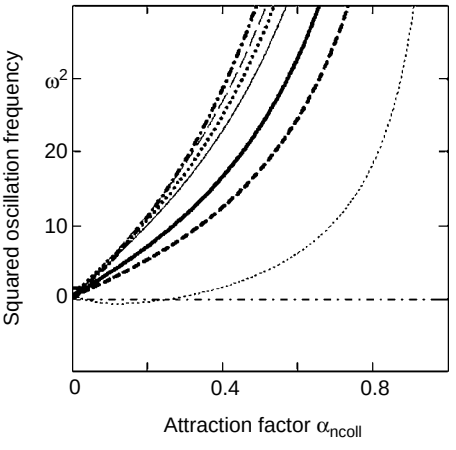

Fig. 7.17. Squared frequencies of cluster oscillations for non-linear screening. The solid thick line corresponds to the mode (**a**) ($N = 2$) in Fig. 7.14, the dotted thick line corresponds to (**b**) ($N = 3$), the dashed thick line corresponds to (**c**) and (**d**) ($N = 3$), the dash-dotted thick line corresponds to (**e**) ($N = 4$), the solid thin line corresponds to (**f**) and (**g**) ($N = 4$), the dotted thin line corresponds to (h) ($N = 4$), the dashed thin line corresponds to (**i**) ($N = 4$), and the dash-dotted thin line corresponds to $\omega^2 = 0$

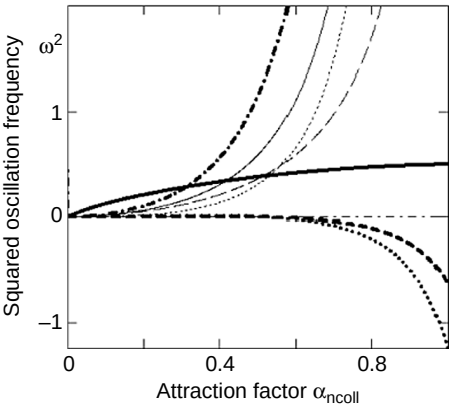

Fig. 7.18. Squared frequencies of cluster oscillations for linear screening. The solid thick line corresponds to the mode (**a**) ($N = 2$) in Fig. 7.14, etc. – the same as in Fig. 7.17

Cluster Energy. The energy depends on the number N of grains in the cluster and on the attraction coefficient. Figure 7.19 demonstrates that the larger is the number N of grains in the cluster the more energetically favorable is the cluster. This takes place for non-linear as well as linear screening. Figure 7.19(a) is calculated for single-shell clusters with non-linear screening. Similar figure can be obtained for linear screening. The difference is the normalized energy range: for non-linear screening it is $0 < V < -80$, while for linear

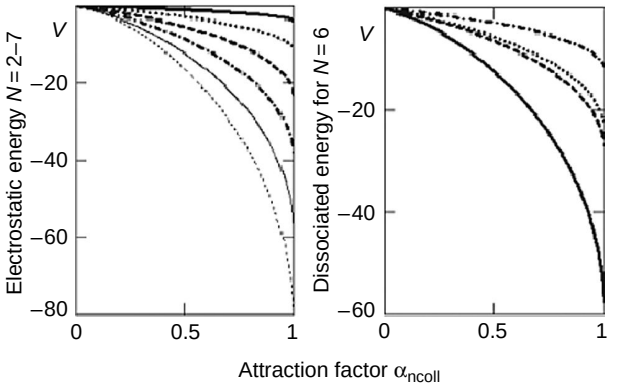

Fig. 7.19. (**a**) The electrostatic cluster energy in the units of $Z_d^2 e^2/\lambda_{nscr}$ for non-linear screening of grain interactions. The solid thick line corresponds to $N = 2$, the dotted thick line corresponds to $N = 3$, the dashed thick line corresponds to $N = 4$, the dash-dotted thick line corresponds to $N = 5$, the solid thin line corresponds to $N = 6$, the dotted thin line corresponds to $N = 7$. (**b**) The electrostatic $N = 6$ cluster energy for non-linear screened grain interactions in the units of $Z_d^2 e^2/\lambda_{nscr}$. The solid line corresponds to $N = 6$, the dotted line corresponds to two $N = 3$ clusters, and the dashed line corresponds to the sum of energies of $N = 4$ and $N = 2$ clusters, and the dash-dotted line corresponds to three $N = 2$ clusters

screening it is $0 < V < -20$, i.e., four times less. This is partially related with the ranges of cluster equilibrium sizes, which for linear screening are 10 times larger than those for non-linear screening.

One should have in mind that the actual non-linear screening length for non-linear screening is much larger than that for linear screening. The energy differences between the curves shown in Fig. 7.19(a) correspond to the binding energy for N cluster dissociation into $N-1$ cluster and a free grain. The curves for given N give the total binding energy for complete dissociation of the cluster. This energy is substantially larger for non-linear screening than that for linear screening, and increases with the number of cluster grains as well as with the attraction coefficient. For larger than $N = 4$ cluster, the dissociation can be possible to other clusters. For example, $N = 6$ cluster can dissociate not only into $N = 5$ cluster and a free grain but also into (1) two $N = 3$ clusters , (2) $N = 4$ and $N = 2$ clusters, and (3) three $N = 2$ clusters. However, energies of these combinations are higher than the energy of $N = 6$ cluster and such dissociations are not favorable energetically. These energies are given as an example for $N = 6$ cluster in Fig. 7.19(b).

The smallest energy difference ΔV_N is between the energy of N cluster and $N-1$ cluster with an additional grain in the center. If the energy changes from a positive to a negative value, it determines *the critical value for the second shell to appear, i.e., the magic number for a boundary-free cluster.* The value of $\Delta V_N = V_{N,c} - V_N$ is the energy of N grains forming a shell with an additional grain in the center; it is given in Fig. 7.20 for non-linear and

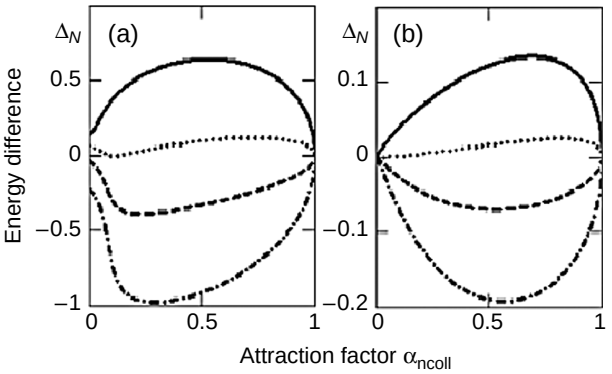

Fig. 7.20. (**a**) The difference of electrostatic energies Δ_N in clusters for non-linear screening of grain interactions in the units of $Z_d^2 e^2/\lambda_{nscr}$. The solid line corresponds to $N = 4$, the dotted line corresponds to $N = 5$, the dashed line corresponds to $N = 6$, and the dash-dotted thick line corresponds to $N = 7$. (**b**) The difference of electrostatic energies Δ_N in clusters for linear screening in the units of $Z_d^2 e^2/\lambda_D$. The solid line corresponds to $N = 4$, the dotted line corresponds to $N = 5$, the dashed line corresponds to $N = 6$, and the dash-dotted thick line corresponds to $N = 7$

linear screening ($N = 4, 5, 6, 7$). For example, for $N = 4$ the cluster $4c$ is a triangle with a grain in the center, for $N = 5$ the cluster $5c$ is a square with a grain in the center and so on. Although the curves for non-linear screening are different as compared to those for linear screening, both of them give the first magic number $N_{magic} = 5$. Note also that the scales of the energy difference for non-linear screening and linear screening are different and are larger (about 5 times) for non-linear screening.

Future Experiments. We can list a number of interesting problems for future experimental investigations of boundary-free 2D clusters (note that large 2D clusters were started to be investigated in [43]):

1. The simplest experimental device could have an external potential which is almost flat in wide central region, with rapid and large increase of the potential at the borders. Experiments of such type should be planned in the future.
2. It is possible to inject a few grains first to form a simple cluster, e.g., $N = 2$ or $N = 3$ cluster, far away from the walls (which are the regions of the rapid increase of the external potential) that can move freely inside the flat potential region being reflected from the walls. This implies a low pressure such that the damping on neutrals does not stop the translational motion of the cluster soon.
3. The space for motion should be sufficiently wide for another cluster to be formed by injecting 2 or 3 more grains in the places not coinciding with existing clusters.
4. An interesting case appears when separate clusters can be formed to investigate their interaction and possible merging.
5. An experimental question is, how different clusters interact with each other and whether they can merge into a larger cluster?
6. Collisions of clusters could be important showing the type of interactions of the self-organized structures.
7. By forming larger clusters one can investigate the universal ordering rules and magic numbers.
8. By increasing the number of cluster grains one can investigate how they convert into 2D crystal when the size of the system becomes large as compared to the ion–grain absorption mean-free path.

7.2.6 Numerical Simulations of Boundary-free Clusters

Molecular dynamic (MD) simulations are useful to investigate cluster formation from originally random distributions of grains. For comparison of the final equilibrium states by identifying the appearance of global cluster mode oscillations, we preferably use the general theory [42]. It is not likely, however, that simple MD simulations with fixed charge particles and a fixed screening

length without taking into account the grain charge variations and considering the actual interaction potential are sufficient to model and understand all cluster behavior in a complex plasma.

In a number of already performed numerical simulations of some problems of charging, attraction interaction, and cluster formation, the KARAT code [44, 45] was used. The advantage of this code is that it takes into account not only electrostatic phenomena but also electromagnetic processes and magnetic fields, the presence of charged particle beams, the possibility of non-thermal distributions, and works for MD as well as particle-in-cell (PIC) simulations. The latter were used in [44] to check the OML theory for kinetic effects in charging processes and to check the non-collective attraction forces. One should note that in the KARAT code the input and output can be made in physical units, for instance in μm for the dust size a. MD simulations of the transition from a random dust distribution to a plasma cluster were first performed in [44] where the dynamics of electrons and ions was not considered but it was assumed that they are responsible for the grain shielding, the long-range repulsion, and the non-collective attraction. The shielding was considered as a linear shielding (the linearly screened Coulomb potential) and the non-collective attraction was taken into account. The grain friction in the neutral gas was also taken into account. Only pair binary dust–dust interactions were taken into account in these simulations. This excludes the collective interactions although in principle MD calculations can be performed with large numbers of grains such that the size of the dust cloud exceeds L_{cr} where the collective interactions start to operate. But any extension to such sizes is inconsistent with the assumption that only the binary pair interactions are accounted for. The computations were performed together with a check that the limit of applicability of the pair dust interactions is not exceeded. This can be done by controlling the initial size of the dust cloud, the cloud evolution, and the final size of the dust cloud. The coefficients of the interactions were calculated in dimensional units using theoretical expressions and parameters typical for present experiments. These coefficients were used to look for the grain dynamics (initially distributed randomly in the calculation box).

The advantage of numerical simulations with a given interaction is that we can follow the dynamics of formation of an equilibrium cluster states and can consider clusters composed of large number of grains. Free-boundary 2D clusters were investigated numerically (for comparison, 3D clusters with larger number of grains assuming no symmetry in the initial state were also investigated). Results for final equilibrium cluster configurations were obtained with friction on neutrals taken into account being (which damps the grain motions). The frequency of friction of grains on neutrals is denoted as ν_{nd}. It was obtained that initially random distributions of grains form either 2D circular boundary-free structures (in 2D problems) or spherical 3D boundary-free structures (in 3D problems). These 2D and 3D MD simulations were made

Table 7.1. Table of parameters used in numerical MD simulations of 2D and 3D clusters; λ_D is the total Debye length; λ_M is the equilibrium size of a single dust molecule formed by two grains (i.e., the cluster with $N = 2$), which is estimated from balance of Yukawa screened potential and non-collective attractions

Parameter	2D simulation	3D simulation
T_i	0.03 eV	0.03 eV
T_i	3 eV	3 eV
n	3×10^9 cm^{-3}	3×10^9 cm^{-3}
a	2 μm	1 μm
N	50	200
Z_d	5200	2600
λ_D	23.4 μm	23.4 μm
λ_M	228 μm	228 μm
ν_{nd}	100 s^{-1}	280 s^{-1}
m_d	5×10^{-11} g	6.3×10^{-12} g

with about 50 grains (2D) and 200 grains (3D) in the computation box. The parameters for MD computations are shown in Table. 7.1.

The grains start to move from their initial random positions (Fig. 7.21(a)) due to forces acting between them including the screened Coulomb interaction, non-collective attraction, and friction on neutrals. They finally take new positions corresponding to a cluster structure shown for 2D case in Fig. 7.21(b). The inter-grain distance increase toward the periphery of the structure. For 3D case, we obtain similar type of cluster (but completely spherical), with an increase of the inter-grain distance toward the periphery of the structure. In this case, the structure is regular.

One can clearly see the hexagonal structure of the plasma cluster lattice obtained numerically. The binary correlation functions $g(r)$ obtained in the computations are shown for 2D and 3D simulations in Fig.7.22. The final size

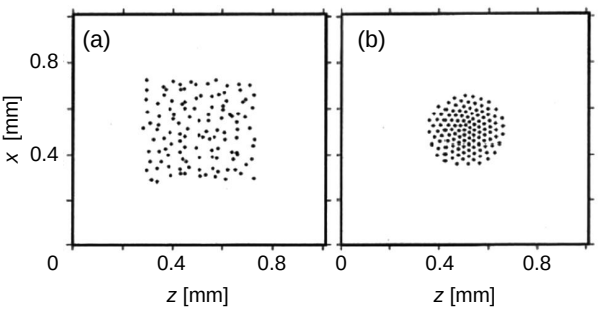

Fig. 7.21. (**a**) Random initial distribution of grains for numerical MD simulations of the dynamics of 2D cluster formation; the number of grains is 50. (**b**) The final equilibrium cluster structure in 2D case

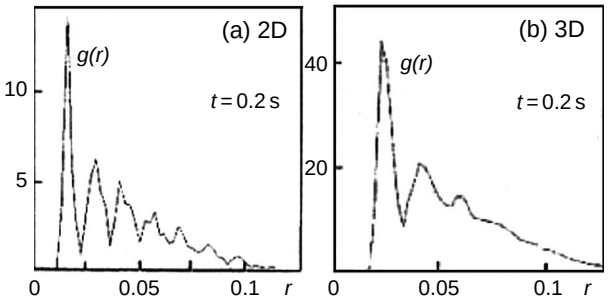

Fig. 7.22. (**a**) The pair correlation function $g(r)$ for the final cluster structure obtained in numerical MD simulations for 2D case. (**b**) The pair correlation function $g(r)$ for the final cluster structure obtained in numerical MD simulations for 3D case

of the dust cluster was 5000μm and 3000μm for 2D and 3D computations, respectively. It satisfies the condition $L < L_{cr}$.

The observed cloud self-organization into a cluster is due only to attraction forces, i.e., without presence of any external confining potential. Thus clusters obtained in these MD simulations are boundary-free clusters. It seems to be not appropriate to use larger total number of grains in these MD simulations since the size of the crystal structure obtained then exceeds the distance at which the collective effects are significant. For clusters with $L < L_{cr}$, the correlation length should be much smaller than L_{cr} in order to be used for description of the pair correlations.

Theory of dust correlations in the gaseous state was developed in [46, 47], where the correlation function was described in terms of the electrostatic plasma responses (see also [48]). In [48], the dielectric function for non-collective dust pair interactions found in [46] was used to describe the pair correlations theoretically for non-collective dust–dust attraction. The applicability of such approach is related to the smallness of the ratio of dust size to the Debye length $(a^2/\lambda_{Di}2 \ll \sqrt{\tau}$, as can be obtained from $L_{corr} \ll L_{cr}$ when one uses for the correlation length an estimate found from MD calculations [46] and theory [48]). The correlation function can have an oscillatory behavior even in the gaseous state. With the lowering of the dust temperature, the amplitude of the oscillations increases. It is a very surprising and interesting result for the theory of correlations in complex plasmas for the cases of non-collective interaction of dust grains. Indeed, the oscillations show that a complex plasma in its gaseous state becomes in some sense "prepared" to the phenomenon of plasma condensation. The latter can occur just if the dust temperature is lowered.

So far, no simulations studies have been reported in the literature that treat the charged grains and the plasma ions and electrons dynamics (i.e., all the complex plasma components) self-consistently. Some progress in this field can be noticed. An interesting development in this important field is the NRL

"dynamically shielded dust" (DSD) simulation code used also for the problem of particle shielding [49, 50]. This code utilizes MD techniques [51], PIC methods [52], the "particle–particle/particle–mesh" (P^3M) technique [53], and the "dressed particle repression" (DPR) [53].

References

1. H. Totsuji (2001). *Phys. Plasmas* **8**, 1865.
2. H. Schollmeyer, A. Melzer, A. Homann, and A. Piel(1999). *Phys. Plasmas* **6**, 2693–8.
3. G. Hebner, M. Riley, D. Johnson, P. Ho, and R. Buss (2001). *Phys.Rev.Lett.* **87**, 235001.
4. V.Tsytovich (2005). *JETP Lett.* **81**, 448.
5. V.Tsytovich (2005). Contr.to *Plasma Phys.* **45**, 230.
6. A. Ivlev, U. Konopka, and G. Morfill (2000). *Phys. Rev. E* **62**, 2739.
7. A. Holman A. Meltzer, and A. Piel (1999). *Phys.Rev. E* **59**, R3835.
8. F. Melanso (1996). *Phys. Plasmas* **3**, 3890.
9. S.V. Vladimirov, P.V. Shevchenko, and N.F Cramer (1997). *Phys. Rev. E* **56**, R74.
10. S.V. Vladimirov, P.V. Shevchenko, and N.F Cramer (1998). *Phys. Plasmas* **5**, 4.
11. S.V. Vladimirov, V.V. Yaroshenko, and G.E. Morfill (2006). *Phys. Plasmas* **13** 030703.
12. A. Piel, A. Homann, and A. Melzer (1999). *Plasma Phys. Control. Fusion* **41**, suppl.3A, A453–61.
13. S. Homann, A. Melzer, S. Peters, and A. Piel (1997). *Phys. Rev. E* **56**, 7138.
14. S.K. Zhdanov, D. Samsonov, and G.E. Morfill (2002). *Phys. Rev. E* **66**, 026411.
15. Y.Nakamura, H. Bailung, and P. Shukla (1999). *Phys.Rev.Let.* **83**, 1602.
16. U. Konopka, L. Ratke, and H. Thomas. (1997). *Phys. Rev. Lett.* **79**, 1269.
17. M. Zusic, H. Thomas, and G. Morfill (1996). *J. Vac. Technol.* **A14**, 496 (1996).
18. S.V. Vladimirov and M. Nambu (1995). *Phys. Rev. E* **52**, R2172.
19. S.V. Vladimirov and O. Ishihara (1996). *Phys. Plasmas* **3**, 444.
20. O. Ishihara and S.V. Vladimirov (1997). *Phys. Plasmas* **4**, 69.
21. S.V. Vladimirov and N.F. Cramer (1998). *Phys. Scr.* **58**, 80.
22. S. Nunomura, D. Samsonov and J. Goree (2000). *Phys.Rev.Lett.* **84**, 5141.
23. M. Zusic, H. Thomas, and G. Morfill (1996). *J. Vac. Technol.* **A14**, 496.
24. A. Ivlev and G. Morfill, G. (2000), Phys.Plasmas, **7**, 1094.
25. D. Samsonov, J. Goree, H. Thomas, and G. Morfill (2000). *Phys. Rev. E* **61**, 5557–72.
26. O. Havnes T. Aslaksen, T. Hartquiat, F. Meklanso, G. Morfill and G. Nitter (1995). *J.Geoph.Res.* **100**, 1731.
27. A. Melzer, S. Nunomura, D. Samsonov, Z. Ma, J. Goree (2000). *Phys. Rev. E* **2**, 4162–76 (2000).
28. A. Holman, A. Meltzer, and A. Piel, (1999). *Phys.Rev. E* **59**, R3835.
29. A. Melzer, M. Klindworth, and A. Piel (2001). *Phys. Rev. Lett.* **87**, 115002/1–4.
30. Wen-Tau Juan, Z.-H, Huang , J.-W Hsu , Y. Ju and I.,Li. (1998) *Phys. Rev. E* **58**, R6947–50.

31. J. Goree, D. Samsonov, Z. Ma, A. Ghatacharjie, H. Thomas, U. Konopka,U. and G. Morfill (2000). *Fronties in Dusty Plasmas*, Proceedings of the Second International Conference on the Physics of Dusty Plasmas -ICPDP-99, edited by Nakamura.Y., p. 92, Elsever.
32. V. Schweigert and F. Peeters (1995). *Phys. Rev. B* **51**, 7700–13.
33. J.J. Bolinger, D.J. Wineland, and D.H.E. Dubin (1994). *Phys.Plasmas***1**, 1403.
34. G. Birkl, S. Kassner, and H. Walther (1992). *Nature* **357**, 310.
35. J.D. Prestage, G.J. Dick, and L. Maleki (1989). *J.Appl.Phys.* **66**, 1013.
36. M. Klindworth, A. Melzer, A. Piel, V. Schweigert (2000). *Phys. Rev. B* **61**, 8404–10.
37. D. Wineland *et al.*(1987). *Phys Rev. Lett* **59**, 2935.
38. F. Diedrich, *et al.* (1987). *Phys.Rev.Let.* **59**, 2931.
39. P. Leiderer, W. Ebner, and S. Shikin (1982). *Surf. Sci.* **113**, 405.
40. S. Neser, T. Palberg, C. Blechinger, and P. Leiderer (1997). *Prog. Colloid Polim. Sci.* **104**, 194.
41. V. Fortov, A. Nefedov, V. Shnel'schikov, A. Usachev, and A. Zobin, A. (2000). *Phys. Rev. Lett.* **267**, 179.
42. Sh. Amiranashvili, N.Gusein-zade, and V. Tsytovich (2001). *Phys. Rev.E* **64**, 016407.
43. V. Fortov, A. Nefedov, V. Vladimirov, L. Deputatova, V. Molotkov, V. Rykov, and A. Khudyakov (1999). *Phys. Lett. A* **258**, 305.
44. Ya. Khodataev, R. Bingham, V. Tarakanov and V. Tsytovich (1996). *Fizika. Plazmy* (Russia), **22**, 1028.
45. Ya. Khodataev, R. Bingham, V. Tarakanov, V. Tsytovich, and G. Morfill. (2001). *Phys. Scr.* **T89**, 95.
46. V. Tsytovich, Ya. Khodataev, R. Bingham, and D. Resendes (1996). *Comments on Plasma Phys. and Contr.Fusion* **27**, 287.
47. V. Tsytovich and D. Resendes Fiz.Plasmy (1008) **24**,71.
48. V. Tsytovich, U. de Angelis, R. Bingham, and D. Resendes (1997). *Phys.Plasmas* **4**, 3882.
49. M. Lampe, G. Joyce, G. Ganguli, and S. Gavrishchaka (2000). *Phys. Plasmas* **7**, 3851–61.
50. G. Joyce, M. Lampe, and G. Ganguli (2001). *IEEE Trans. Plasma Sci.* **29**, 45.
51. H. Ohta, and S. Hamaguchi (2000). *Phys. Plasmas* **7**, 4506–14.
52. C. Bindsall and A. Langdon (1986). *Plasma Physics in Computer simulations*, Mc GrawHill Book Company, JOP, N.Y.
53. D. Hockeney and D. Eastwood (1988). *Computer simulations using particles*, JOP, N.Y.

8

Comments on Other Dust Structures: Concluding Remarks

Formation of structures is one of the most general phenomenon in complex plasmas and includes ordered as well as disordered grain distributions. The universal structurization instability operates also for both ordered and disordered states. Such an instability does not exist in an ordinary plasma without dust. Contrary to ordinary plasmas, dusty plasmas have a large rate of dissipation. Let us remind that ordinary plasmas is often unstable due to low rate of binary collisions. There was a long-term investigation on ordinary plasmas which led to conclusion that almost only binary particle collisions can thermalize their particle distribution (if contacts with thermal surfaces are not important). In ordinary plasmas, even small deviations in particle distribution from thermal distributions create instabilities. Complex plasmas, contrary to ordinary plasmas, are very dissipative systems that need a constant supply of energy and particles in order to exist. This opens a door for the universal instability related to the structure formation and to self-organization processes in ordered as well as in disordered states.

8.1 Dust Helical Clusters

8.1.1 General Remarks

We already demonstrated that the boundary-free clusters can be spherical. In the presence of cylindrical symmetry due to external confinement potential perpendicular to the cylindrical axis the helical dust structures appear to be the simplest 3D structures. The external cylindrical confinement can be experimentally produced by discharge in a long plasma tube where the floating potential of the wall can create the confinement potential.

There are indications that helical structures can be formed even in the absence of external cylindrical confinement. The simplest 3D structure observed in the laser-cooled ion traps was a helical structure and a proposal was made

V. N. Tsytovich et al.: *Comments on Other Dust Structures: Concluding Remarks*, Lect. Notes Phys. **731**, 333–363 (2008)
DOI 10.1007/978-3-540-29003-2_8

to use such structures in a new micro-computer technology [1]. The configuration of trap was not cylindrical since a quadruple storage ring was used. The equilibrium cylindrical 3D boundary-free clusters can also exist and the question of their stability can also be asked (and resolved). An example of stable 3D cluster in usual matter is the molecule of DNA.

The questions to be addressed for 3D grain clusters in complex plasmas are related to existence of an equilibrium state in the absence of external cylindrical confinement and its stability with respect to perturbations destroying the cylindrical symmetry. The first question was resolved positively by several examples given in [2]. The stabilities of such states for cylindrical disturbances were also considered in [2]. However, the full resolution of the stability problem of the boundary-free helical structures for non-cylindrical disturbances is not investigated so far. Apart of those problems specific to the boundary-free clusters there are many other problems for cylindrical clusters confined by external usually parabolic potential, such as the so-called bifurcations of the rotation angle which can be used as memory marks in new computer technologies.

Let us define the helical structure as that consisting of plane structures separated by a distance Δ along the axis of a cylinder. The number of grains in each plane, N, depends on the number of grains injected (in finite system) or on the number of grains per unit length (if the system is long and the edge effects do not affect the central part of the structure). N numbers the type of helical structure (such as $N = 1, 2, 3...$ corresponds to a single, double, triple,... structure, respectively). Grains in the neighboring planes can be relatively turned on some angle ϕ (e.g., for N=2 the line connecting two grains in one plane can be turned on the angle ϕ relatively to the line connecting two grains in the neighboring plane). Helical structures correspond to a constant separation between the planes Δ and to a constant rotational angle ϕ. Figure 8.1 demonstrates an example of the helical structure – the double-helical structure ($N = 2$) similar to that of DNA.

For this structure to be considered as a cluster, the radius R of the cylinder should be less than L_{cr}. Then interactions in the cluster can be considered as pair interactions with either linear or non-linear screening and with non-collective attraction between the grains. Here, we normalized the dust-dust

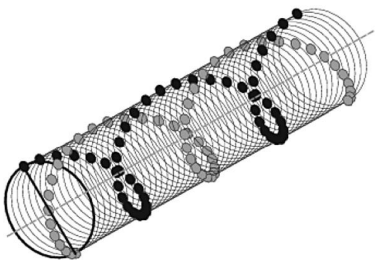

Fig. 8.1. Example of a dust double-helical structure. Positions of dust grains on every subsequent layer are rotated at the angle ϕ

interaction potential with respect to $Z_d e^2/\Delta$ and the distances – with respect to Δ. For non-linear screening, e.g., we have

$$V(r) = \frac{1}{r}\left[(1-Dr)^4\,\frac{1}{2}\left(1+\frac{1-Dr}{|1-Dr|}\right) - \alpha_{ncoll} + Ku^2\right] , \qquad (8.1)$$

where $u = \frac{2R}{\Delta}$ and R is the spiral radius (the distance in the direction perpendicular to the cylindrical axis), while r is determined by both the distances along the cylindrical axis and the distances perpendicular to the cylindrical axis. For linear screening, the first term in the square brackets of this expression should be changed to $\frac{1}{r}\exp(-D_Y r)$. Due to normalization different from that used for 2D clusters (Δ instead of λ_{scr}, the values α_{ncoll}, D, and D_Y are different than those used above; however, in applications the factor λ_{scr}/Δ can be easily taken into account.

8.1.2 MD Simulations and Analytical Results

MD simulations [2, 3, 4] demonstrate that in the cylindrically symmetric case the final equilibrium structure in the process of evolution of an initially random distribution is always a spiral structure with constant value of the rotational angle. For example, for $\alpha_{ncoll} = 0$ it was found that a decrease of the confining strength leads to a following chain of transformations for $N=1$ structures: linear ($\phi = 0$) chain–zigzag chain ($\phi = \pi$) and single-winding helical structure with rotational angle less than π (angle π divided by irrational number), (see Fig. 8.2).

Further transformation corresponds to formation of a double-winding ($N = 2$) helical structure (rotational angle equal to $\pi/2$), etc. Both the single-winding helical structures and the double-winding helical structures show bifurcations of the rotational angle. The bifurcation corresponds to the case where suddenly (for some radius larger than a critical one) two values of the rotational angle become possible. After the bifurcation, a new branch appears with the rotational angle π divided by an irrational number. These two

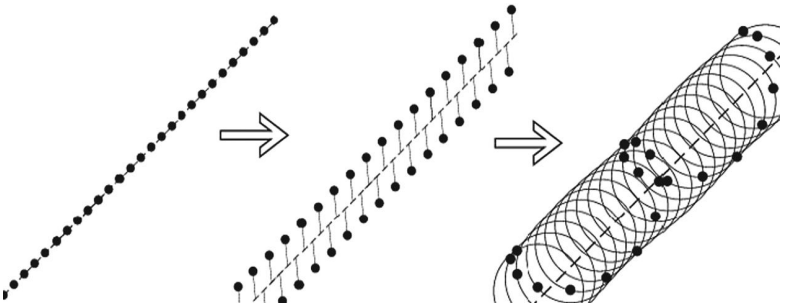

Fig. 8.2. Transformations correspond of $N = 1$ structures for linear screening when the confining strength is decreased, $\alpha_{ncoll} = 0$

branches exist with a further increase of the radius where the next bifurcation can appear. These structural bifurcations depend strongly on dust–dust interactions. The bifurcations mark the spiral structures. Different branches can be stable or unstable and have different energies. Not always the branch with the lowest possible rotational angle is stable. In MD simulations, one can reach different stable branches depending on the initial dust distribution. A general conclusion from all numerical simulations is that initially random distribution of grains is always reaching some stable helical cluster structure asymptotically in time. This is true for all interactions used so far. The interaction energy V can be written as a function of ϕ and u and depends on D (or D_Y) and α_{ncoll}. The equilibrium conditions are

$$\frac{\partial V}{\partial \phi} \equiv F(\phi, u) = 0; \quad \frac{\partial V}{\partial u^2} = 0 \, . \tag{8.2}$$

These equations give the phase diagram in the plane $\{\phi, u\}$. If for given u one finds different values of the equilibrium rotational angle ϕ, we speak about bifurcations since two new solutions appear usually in this case. The change of u means the change of the radius of the structure. The case $K = 0$ corresponds to the boundary-free structure and after bifurcation has both stable and unstable branches. The proof is that a stable boundary-free helical structure exists. Conditions for the stability are

$$\frac{\partial^2 V}{\partial \phi^2} \equiv F'(u, \phi) > 0 \;\; \frac{\partial^2 V}{\partial \phi^2}\frac{\partial^2 V}{\partial u^2} - \left(\frac{\partial^2 V}{\partial \phi \partial u}\right)^2 \equiv K'(u, \phi) > 0 \, . \tag{8.3}$$

Figure 8.3 [2] illustrates the appearance of bifurcations in the plane $\{\phi, u\}$ with an increase of u in the absence and presence of dust attraction.

The grain helical clusters and their global modes of oscillations, stability and energy differences of different branches are investigated intensively [2, 5, 6]. It is found [2] that the double-helical structure branch similar to DNA structures has the lowest energy. The whole spectrum of possible modes, stable branches, energy dependencies of branches on the attraction and screening coefficients, boundary-free helical structures and other problems are of large interest for future planning of micro-gravity experiments in long plasma tubes, (see Sect. 8.1.3).

8.1.3 Problems to Solve

1. Helical structures in 3D almost flat external potential with large potential increase at the edge can be used for investigation of the possibility of formation of boundary-free helical clusters. Since curved helical clusters were observed in quadruple ion traps, there exists a large probability that similar curved helical structures can be found in the mentioned configuration.
2. Interaction of different boundary-free helical clusters is an important problem to understand their role in nature, e.g., in space physics.

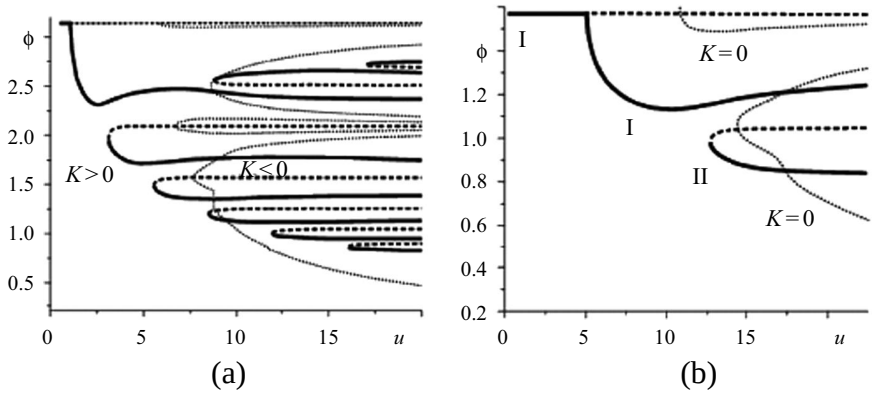

Fig. 8.3. (**a**) The phase plane $\{\phi, u\}$ for a helical cluster with linear screening $N = 1, D_Y = 1$, and weak non-collective screening $\alpha_{ncoll} = 0.01$. The set of bifurcations contains stable branches shown by thick solid lines and unstable branches shown by thick dashed lines. (**b**)The phase plane $\{\phi, u\}$ for helical cluster with non-linear screening $N = 2, D = 0.1$, and weak non-collective screening $\alpha_{ncoll} = 0.01$. The set of bifurcations contains stable branches shown by thick solid lines and unstable branches shown by thick dashed lines. The thin dotted line corresponds to boundary-free clusters when it intersects these branches in both the figures from the right side of this line, $K < 0$, and from left side of this line, $K > 0$. There exist stable and unstable boundary-free helical structures and in the presence of attraction there exist even stable branches with anti-confinement, $K < 0$. The number of bifurcations for $N = 1$ is always larger than for $N = 2$

3. Helical clusters could be used for modeling of biological molecules which have properties similar to those of grain clusters including attraction and shielding of large linear charge of DNA.
4. Bifurcations in helical structures can be used as memory marks for constructing new types of nano-computers. This problem has already been proposed for helical structures observed for ions in quadruple laser traps. The dust helical structures have many advantages, being more flexible in coefficients determining their structure. New nano-computer technology is therefore on the way to be created by using the helical grain clusters.

8.2 Disordered Grain Structures

8.2.1 Role of Plasma Fluxes

The material discussed so far was related to ordered dust structures with significant grain interactions. The most important point here is that *the major role in formation of the ordered states is played by plasma fluxes*; this role is especially important in the crystal formation. Many aspects of collective attraction discussed earlier are made on the level of estimates of possible role of

different effects based on understanding of the elementary processes in complex plasmas. We show that at present the only explanation able to predict all three major values observed (the coupling constant, the grain separation, and the melting temperature) by using a single parameter reasonably estimated from experiments invokes the pair-grain interaction modified by the presence of plasma fluxes leading to the grain attraction.

Further investigations require a construction of full theory of phase transitions based on these elementary estimates, and its detailed comparison with experiments. Such comparison needs also a better diagnostics of many experimental parameters. This is also a very important point since at present only the grain component is measured well even on the kinetic level. Until we obtain detailed distributions of other plasma parameters such as electron and ion densities and ion drift velocities, it is difficult to compare any theory with experiments. We then better stay with simple estimates based on elementary processes as we did in the previous chapters. Even this was not so simple since one should have in mind all the time the new physics introduced by the presence of plasma fluxes. We hope that our presentation helps to realize how important the new physics is and that even simple physical estimates cannot be made without general feeling of new possible effects introduced by the plasma flux effects.

As mentioned, the plasma flux can have two components, namely the regular averaged component and the random component. The random component introduces new pair-grain interactions as usual in current understanding of collective pair interactions in many-body systems. The regular component of plasma fluxes was not much discussed in previous chapters; this flux can be created by all grains and in this sense is collective. It produces different structures in disordered state; they were observed experimentally. These are not the subject of present consideration but it is worthwhile to mention briefly the physics of their creation because it is also the result of the collective flux, its regular averaged part.

8.2.2 Structures in Disordered States

One of puzzling observations in a complex plasma is not only that various disordered structures are formed but also that *the boundaries between the dust-containing and dust-free regions are very sharp.* Regions where dust is completely absent are called "*dust voids*". At the void's surface, all plasma parameters – electron and ion densities, temperatures, etc. – are continuous. Therefore the *virtual dust charge* is also continuous at this surface. The virtual dust charge at certain place in a dusty plasma corresponds to the value of the dust charge which appears on the grain if one puts this grain in this place in a plasma or at the surface dividing the dust-containing and dust-free regions. Surfaces dividing the dust and dust-void regions can exist for certain distributions of the electric field and the ionization degree; they actually are the **virtual surfaces** for dust grains. The force balance for a single grain

takes place on them independently on whether the grain exists at the surface or not. The balance depends on the virtual charge of the virtual grain [7, 8]. This means that if we put only one or a few grains on this surface, they stay there if the balance of forces is satisfied for a single grain, i.e., the balance of forces is such that any deviation of the particle from that surface returns it back to the surface. The existence of virtual void surfaces is a general phenomenon in complex plasmas which has an experimental verification; its possibility was obtained numerically for the first time in [11]. Contrary to the previously known physics where, e.g., the shock front is smoothed by dissipative processes in complex plasmas, the sharp boundaries are created by dissipative process [9, 8].

A collective regular plasma flux is usually present toward these surfaces. This is found both in the presence and in the absence of plasma ionization. In the first case, the flux is created by a kind of source in regions neighboring the structure. In the absence of ionization, the flux is the collective flux created by cloud of grains in the charging process. In the presence of ionization in the dust-free region, the flux is supported by the ionization. Thus to have a virtual void surface in the discharge one does not need to have many grains on each side of the surface.

Consider now the case where many grains are located on, say, right-hand side of the surface and no grains are on the left-hand side. The grain distribution from the right side of this surface is determined by equations of changes of plasma fluxes, dust charges, and dust and plasma densities. Stationary distributions are defined by the balance equations if the parameters at the surface are known. If there are no dust particles at one side of the surface and the size L of the dust-containing part satisfies $L \gg L_{cr}$, we call this structure as *the dust-void structure surface*. If there exist walls (as in many current experiments) then the ionization creates plasma fluxes in the dust-free region near the wall directed toward the dust-containing region as well as to the wall.

In the stationary case, the number of plasma particles created by the ionization source is equal to the number of particles absorbed by the wall and the dust region. In the absence of dust, the whole flux is directed to the wall; in the absence of a wall, the whole flux is directed to the dust-containing region. If there are dust-containing region and the wall, the flux is redistributed between them and the properties of the dust-void surface are changed as compared to the case where the wall is absent. We call these voids as the *dust wall voids*. In case the wall is far away from the dust-void surface, the electric field of the wall does not influence distributions of electric fields and plasma fluxes close to the dust-void surface, and the void corresponds to the *boundary-free void*. If there are two dust voids bounding the dust region, we call such a dust structure the *dust 3D layer*. The thickness of the layer should be larger than L_{cr}, otherwise this structure has to be regarded as a dust cluster or dust 2D layer discussed in detail before. The size of the dust 3D layer can be either less or more than the mean-free path for ion-neutral collisions. In the first case the layer is a **collisionless 3D layer** and in the second case

it is a **collision-dominated 3D layer**. We also speak about **collisionless voids** and **collision-dominated voids**. This terminology corresponds to the old terminology of **plasma sheaths** when no dust exists in a plasma. These are regions between the wall and the bulk plasma which were intensively investigated for more than 70 years starting with pioneering work of Langmuir and Tonks mainly because of many technological applications. The presence of dust can completely change properties of the near-wall region; this is very important for such technologies as etching, plasma deposition, etc. Thus, not only the properties of the dust surface are changed by the dust-wall voids, but the properties of the plasma sheath are changed by the presence of dust as well. This happens if the dust-void surface is not far away from the wall when the mutual influence of the wall and dust surfaces is important. In the case where another surface of the dust layer (from the side opposite to the wall) is a boundary-free void surface, we call such a structure the *dust sheath*. The dust sheaths can be collision-dominated and collision-less depending on the relation between the mean-free path of the ion-neutral collisions and the size of the dust sheath.

One can consider not only the plane geometry, where all parameters of dust plasma structures depend only on one coordinate perpendicular to the plain, but also the cylindrical and spherical geometries, where all parameters depend on the coordinate perpendicular to the cylindrical axis and on the radius (for cylindrical and spherical structures, respectively). It is fortunate that for these simplest cases of stationary structures can be considered numerically by solving balance equations. These balance equations include the force balance for grains, ions, and electrons together with continuity equations which take into account the ionization and absorption of plasma on grains and complemented by the grain-charging equation. All of them were given in previous chapters. The configurations investigated so far are of different types: boundary-free dust layers, dust sheath, dust layers surrounded from both sides by the wall voids and then by the walls, dust voids surrounded by two dust layers having on the outer side the free boundaries, the dust voids surrounded by two dust layers, which in turn are surrounded of two dust-wall voids and further with the walls (see Fig. 8.4).

In addition to the plane structures shown in Fig. 8.4, similar spherically and cylindrically symmetric structures for spherical and cylindrical geometry, respectively, were also investigated. In all cases discussed, the structures corresponded to the absence of external gravity (i.e., the structures in microgravity), the absence of external electric fields (with exception of some cases assuming that the latter can make the ionization inhomogeneous as in striations), and the absence of external temperature gradients (the externally created thermophoretic force is absent). The ionization was considered to be either homogeneous or at a remote region from the structure, the role of which is only to support plasma fluxes. Such a consideration can be easily generalized for the presence of external gravity and electric fields as well as the thermophoretic force.

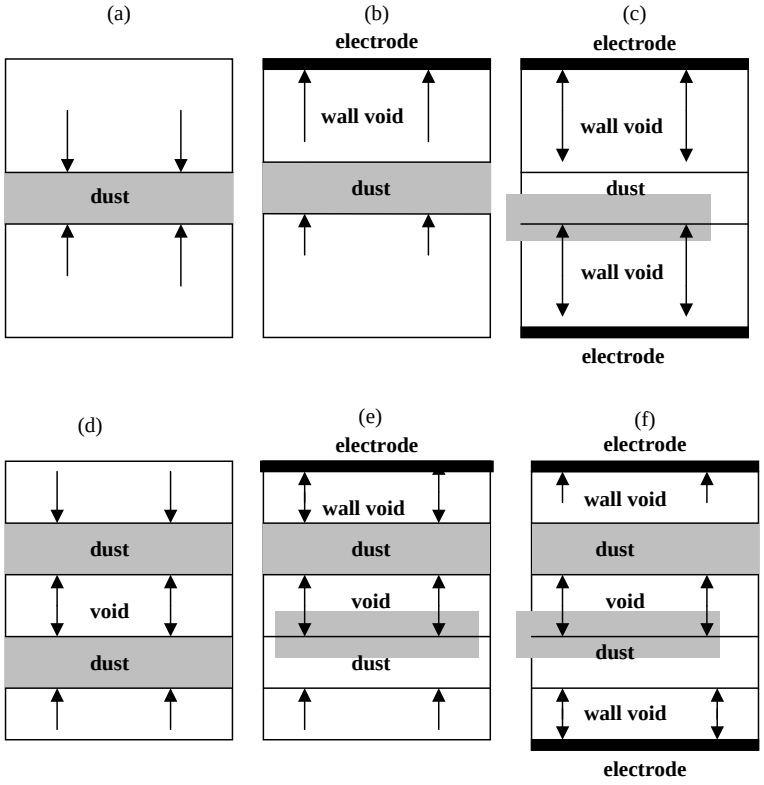

Fig. 8.4. Schematic drawing of flat equilibrium structures investigated numerically. The arrows show the direction of equilibrium plasma flux appearing in the stationary structure distributions. (**a**) the dust layer with two free boundaries, (**b**) the dust sheath close to the wall with one free boundary and the wall void at the side of the wall, (**c**) the dust layer between two electrodes surrounded by two wall voids, (**d**) the dust void with free boundaries, (**e**) the dust void close to the electrode surrounded by the wall void and the free boundary, (**f**) the dust void between two electrodes surrounded by two wall voids

8.2.3 General Features of Disordered Structures

General features of calculated and observed structures are somewhat unexpected. They are as follows:

- The equilibrium really exists for all considered configurations; this seems to be non-trivial since there are very few previously known examples of stationary equilibrium balance structures – and they include also the gravity. The most familiar example is a star with the balance between the pressure and gravity forces (Fig. 8.5(a)). Contrary to this case, all listed dust structures have equilibrium stationary solutions and the number of examples is

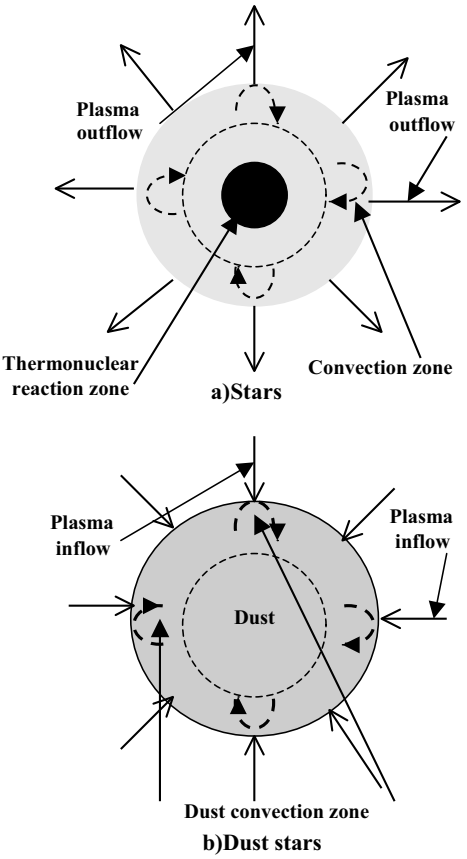

Fig. 8.5. (**a**) Schematic drawing of a star having the balance of gravity and pressure, (**b**) Schematic drawing of a dust star

quite big so that we need to restrict ourselves to the most typical examples. We note that dust structures investigated so far exclude the gravity. On the microscopic level used (hydrodynamical description), the role of gravity is played by the grain collective attraction and the contraction force is due to the collective flux ram pressure.

- For spherically symmetric geometry, such structures can be named as "dust stars" or "anti-stars" (see Fig. 8.5(b)) since their existence requires the plasma influx while in usual stars the plasma flux is directed outward creating the stellar wind (e.g., solar wind for the Sun).
- Spherical and flat dust structures have been already observed in several laboratory dusty plasma experiments, (see above the Figs. 1.21 and 1.22).
- The structures live because of the plasma influx absorbed by grains and in this sense they are typically self-organized structures.

- Due to the fast rate of dissipation in the structures, they are the objects of the fastest-known self-organization processes and can be used for investigation of the processes of self-organization and modeling of some biological systems.
- As all self-organized structures, properties of dust structures depend on a few parameters only; the simplest dust structures depend on just one parameter – the total number of grains in the structure. Therefore it is possible to investigate the balance of all possible structures which satisfy the conditions of equilibrium.
- The dust, plasma, and field distributions inside the structures are universal and described in dimensionless variables introduced in previous chapters.
- The range of universal parameters determining the structures is restricted (similarly to such known structures as stars) although many different forces are contributing to the equilibrium balance (such as the flux, drag, friction, and pressure forces).
- Information about theoretically found distributions of the structure parameters (such as the grain, charge, and density distributions, the ion and electron density distributions, and the ion direct velocity) are much more rich than that given by existing observations where the ion and electron distributions are not well known.
- Many qualitative features of numerical calculations coincide with observed features (see Fig. 1.21).
- In real experiments, the geometry is more complicated than that of the considered simplified models investigated numerically by imposing the flat, cylindrical, or spherical symmetry. Of special importance can be the structure edges, but one can sometimes use different configuration models for different parts of the structures observed. This is the largest disadvantage of the simplified geometrical conditions; some special experiments are however performed in the geometry close to that used in the balance calculation (Fig. 1.22).
- An important observation is that most of the structures have sharp boundaries which divide the dust-containing region from the region with complete absence of dust. The sharp surfaces appear when the stationarity structure is reached.
- To describe disordered structures, the use of hydrodynamic expressions has its disadvantages and advantages. There are two advantages: (1) these are the simplest expressions for the forces and (2) the continuity equation contains the average velocity's flux which from the conservation law does not contain the binary grain collisions (they are collective for $L \gg L_{cr}$ and include the collective dust attraction). But the averaged flux still contains all information on the collective influence of the flux on dust grains and therefore describes all effects which lead to the contraction of the dust cloud by the flux, i.e., to the collective attraction in the average form. A disadvantage is that the factors in these expressions for forces are determined by the electron and ion distributions which are in most cases the

non-thermal ones (caused both by the plasma ionization and by its absorption on the grains). Nevertheless, the hydrodynamic expressions for the forces are useful since they allow to investigate the full sequence of possible dust structures in a relatively simple manner. A future kinetic description should improve these factors and will allow more accurate description of the structures.

- In hydrodynamic description, the stationary force balance condition for dust particles differs from the single particle balance condition by a factor of n_d. The balance of the electric field force and the drag force $Z_d(\mathbf{E} - \alpha_{dr} n\mathbf{u}) = 0$ described in detail in previous chapters converts to $P(\mathbf{E} - \alpha_{dr} n\mathbf{u}) = 0$ and has two solutions, $P = 0$ and $\mathbf{E} - \alpha_{dr} n\mathbf{u} = 0$, which serve as two conditions at different sides of the boundary dividing the dust-containing region and the dust-void region.
- Calculations show [9] that none of dissipative processes can smooth the boundary, the only one is the dust pressure which gives an estimate of the sharpness of the boundary, and that the relative thickness of the boundary $\delta x/x_{str}$ (the ratio of the dimensionless boundary thickness δx to the dimensionless size of the structure x_{str}) is of the order as follows [10, 11]:

$$\frac{\delta x}{x_{str}} \approx \frac{T_d}{T_e Z_d} \,. \tag{8.4}$$

This ratio is independent of whether the size is dimensionless or not; we have written (8.4) for dimensionless sizes in notations used for x_{str}. In most existing experiments as well as in space the condition (8.4) is satisfied with a large safety factor. This gives an explanation why the sharp boundaries in complex plasma are met so often.

The real complicated structure with sharp boundary dust-void layers and dust vortices observed experimentally in PKE-Nefedov experiments on board the International Space Station [12] is presented in Fig. 8.6. In other PKE-Nefedov experiments, dust particles of two different sizes were injected: with the sizes 6.9 μm and 3.4 μm. More complicated structures appearing in this

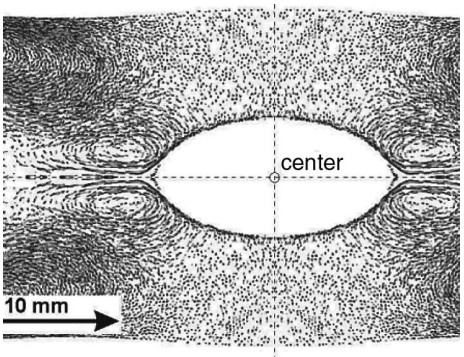

Fig. 8.6. Structures with sharp boundaries observed on board the International Space Station in micro-gravity conditions of PKE-Nefedov experiments [12]

case are shown in Fig. 1.24. From Fig. 8.6, we can clearly see the sharp boundary between the dust-containing region and dust-free region (central void); from Fig. 1.24, we see that the grains with different sizes are completely separated in space with a thin void (or thin interface sharp boundary) between small and large grains. In both examples, we can also clearly see the dust convection creating dust vortices on both sides of the complicated structure observed in the center. The central void is neither flat and nor spherical. The system is surrounded by flat electrodes of finite sizes and the edge effects can be important. However, some qualitative features such as the void size and separation of grains with different sizes with a thin interface are obtained in all simplified geometries used for numerical calculation of the force balance equations. The spherical structure shown in Fig. 1.22 was observed in parabolic flight micro-gravity experiments [7] by using a spherical camera.

8.2.4 Dust Void Problems

There is a difference between dust structures with and without ionization inside the structure. The simplest case is a homogeneous ionization which is present in most laboratory RF experiments in a complex plasma. In the presence of ionization, plasma fluxes can be excited at certain point and therefore move grains away from this point. An instability can appear when the removal of dust by fluctuations of plasma fluxes from some region decreases the absorption of electrons in this region and therefore increases ionization (which is proportional to the electron density) thus further increasing the flux and removing more grains from the region. Finally, a stationary void with total absence of dust can be created. First observations of voids in laboratory experiments were done in [13]; a theory of the void surface (which can be a virtual void surface) has been constructed [14] in the way similar to that described earlier for the boundary-free collisionless structures. The only difference is in accounting of the ionization and in the absence of conservation laws used to describe collisionless dust layer boundaries. This theory was first proposed in [14], then further developed and generalized for the collision-dominated case [15], took into account such dissipative processes as ion diffusion on neutral atoms [9], used the concept of virtual charges and boundaries [8], etc. (see also reviews [16, 17]). There exists a critical ionization rate for which the void can be developed; the void's surface is shown to be stable for large deviations from its equilibrium position. The size of the voids observed is in rough agreement with that calculated in the collision-dominated case. Dust voids were also found in most micro-gravity experiments on ballistic flights [18] and on board the International Space Station [12]. The appearance of voids becomes a general phenomenon in micro-gravity experiments and is considered as the main obstacle for plasma crystal formation in the micro-gravity condition since the crystals were found only at the periphery of the dust region surrounding the void region.

Thus the problem as to how to avoid the dust void became an important experimental issue. To solve this problem one should first understand the physics of the void formation and explain why its boundary is sharp. About the latter – there is a good understanding already explained. The creation of voids is obviously related to the presence of plasma ionization in the whole volume of the discharge. The homogeneous ionization seems to be inevitable for discharges caused by external radio-frequency fields with frequencies corresponding to wavelengths much larger than the size of the experimental chamber (as it is the case in most current experiments). Then there appear two conditions to close the void: the first is that the ionization should be sufficiently low for the central void not to form, and the second is that it should be sufficiently large to create a near-wall void which is necessary to have a plasma layer (with the closed void in the center of the chamber). We discuss the latter problem later when commenting on voids in the presence of walls.

First, discuss a virtual void boundary which does not depend on whether the particles are present on the other side of the surface or even whether some small number of grains exist on the void surface. We consider only the stationary condition and not the dynamics of the surface formation; we only mention that an important role is played by ionization processes in the creation of void. Assume that in some region, which we call as a "central region", the ionization is sufficiently high. It creates ion-electron pairs propagating from the central region and thus establishing an ion flux (ions are the most important for momentum transfer, and the ion drift velocity enters in the equation for the void surface). Assume that initially there exists a dust cloud which is approached by the ion flux. An important point in the evolution of dust distribution and creation of void is that the ion drag force in the vicinity of the void's surface is mainly acting on the first dust layer (which the ion flux meets) and that the drag moves this layer faster than the subsequent layers (where the force is depleted because of the ion flux absorption by the first layer). This creates large dust density gradients due to the steepening of the dust density in time and therefore rather sharp edges appear giving rise to a void formation in the final stationary stage. This final stationary void structure is observed in experiments.

The size of the observed voids is much larger than the size of thin voids surrounding boundary-free structures and this is an obvious consequence of ionization processes in regions with the absence of dust (which create intense plasma flux pushing dust from the regions). The drag force $F_{dr} = \alpha_{dr}(u, z)uzn$ depends much on the ion drift velocity and on the dust charge which is a virtual dust charge. This charge depends on possible mechanisms of dust charging. Also, the ion drift velocity and the electric field are created in the dust-free region by the ionization process; the ion drift depends much on the ion-neutral collisions which damp the ion flux. The surface of the void is adjusted to the position where the drag force is equal to the electric field force. For a finite size of the void, the self-consistent field and the drift velocity are increasing from its center and at certain point for large ionization rate this increase becomes

rapid enough to support a balance of the virtual drag force and the electric field force. At this point, as a rule, the drift velocity and the field are rapidly increasing in space and when the virtual balance is achieved, the virtual void surface is created in the region. This is the main result of numerical computations. The drag force depends on the grain size ($\propto a^2$), while the electric field force on grain is proportional to the the grain charge (or a), and in devices where the grain size is growing the virtual void surface appears easier.

A rapid increase of the ion drag force close to the void surface is the phenomenon which is not easy to detect experimentally but the drag force increase in this region is determined by the void size. Rough estimates of the (really existing) drag force at the void's surface by estimating the average drift velocity are meaningless. An important role is played also by the increase of the virtual grain charge and its growth with the grain size. Although the virtual void surface can exist with no grain on it, the actual position of this surface is determined by the region with the rapid increase of the ion drift velocity and with the increase of the dust virtual charge. Measurement of the drift velocity close to the void surface is not an easy experimental problem. Even in other regions far from the void surface the ion drift velocity is not measured properly and only its rough estimates can be obtained from experimental data. Thus the correct estimate of the drag force from experimental data is rather difficult. Therefore a self-consistent model of dust voids which is able to predict the void's sizes by using only global parameters of experiments (such as applied ionization power and gas pressure) is necessary. Apart from the value of the ion drift velocity and its increase close to the void's surface, proper models of the drag coefficient (for linear or non-linear shielding) are also important for the interpretation of existing experiments. An important statement is that *stationary dust voids are special dust structures* playing an important role in the physics of a complex plasma. Their presence can also be used for various technical applications such as plasma deposition and plasma etching.

First experiments where the voids were discovered [13] used rather small grains with the size of (0.1–0.3)μm in RF discharge with the gas (argon) pressure about 10^{-6} torr and electron temperature about 3eV. Small particles were used to exclude the gravity force. The dust grains were growing in size in time and after reaching a critical size of about 120nm, a sudden onset of instability rapidly creating a large void fast reaching its final non-linear stage (and filling a substantial part of the chamber) was detected (see Fig. 1.19).

The shape of the void was detected by an increase of emission due to enhanced electron density in the void since the electrons are no more absorbed on grains in the void region. The void boundary was very sharp. It was detected that during the first stage of the void growth the grains were rapidly expelled from the void region and filled the space outside the void region in the chamber. This indicated that the electric field force is substantially larger in the void region than the virtual drag force and the void phenomenon is

related with the electric field and ion drift distributions in the void region (and in this sense is a property of the discharge independent of the presence of grains). But the virtual grain charge and the virtual drag force depend on dust properties and therefore the void's surface depends on dust properties – the void formation is a collective phenomenon in a complex plasma.

Of course, the questions as to what kind of grain structure exists on the dust side of the void surface and what determines this structure depend completely on the number of grains and the size of the structure. The forces can be the binary grain forces and the size of the structure is small, or can be of collective nature depending on the number of particles and the size of the structure is large. The *important feature is that the creation of dust voids is due to the presence of plasma ionization and structures formed on the dust side of the void's surface are the ones for which the presence of ionization is rather important* – contrary to the structures discussed before where the source of ionization is a remote one and the ionization does not create fluxes inside the structure. Thus the *voids discussed here are the voids surrounding the grain structure, with internal ionization playing an important role.* The voids observed in [12] experiments are of the same kind. The difference from [13] is a larger grain size and higher gas pressures, which is possible for experiments in micro-gravity conditions.

8.2.5 Problems for Future Investigations

- For those laboratory applications where dust layer are observed, it is important to consider the layers with non-linear drag for $\tau/z \ll a$ where the structures can strongly depend on the grain size.
- Investigation of possible balance of structures with different sizes has applications for experiments as well as for astrophysics. With present understanding of the problem one can foresee a special separation of particles with different sizes.
- For astrophysical applications, an important problem is the detailed investigation of spherical structures with broad size distributions of grains which can provide an understanding of fragmentations of dust-molecular clouds.
- A big problem is the analysis of global modes and stability of grain structures – similar to the corresponding problem for grain clusters. An additional problem is the stability of the layer surfaces, which is currently only in the first step of investigation.
- Investigation of stability for 2D perturbations can clarify the question of excitation of dust vortices. According to [19], the threshold of convection instability is determined by the ion-neutral collisions and extended models [20, 21] which take into account the ion-neutral collisions in the collisionless limit [22] should be used.
- Up to present, the plasma layers were investigated only for large gas pressures not corresponding to the collisionless limit. Laboratory investigation

of collisionless layers is still the future experimental issue which has an advantage of available detailed numerical results to be compared with observations.

To conclude, we underline that *it is proved that the force balance conditions can indeed demonstrate possible existence of self-consistent structures of different shapes* – **without any gravity** present.

8.3 Dust Wall Sheaths

8.3.1 General Remarks

The usual plasma sheath without dust (which is the plasma layer close to the wall bounding the plasma) is known to be either collisionless or collision-dominated depending on the relation between the sheath depth and the ion-neutral mean-free path. A rapid decrease of plasma potential which is about $-3T_e$ at the wall is accompanied by the slow increase of the ion drift velocity in the pre-sheath up to the so-called Bohm velocity corresponding to the Mach number $M = \sqrt{2\tau}u$ of order 1.

The main question in the presence of dust close to the wall is whether the dust grains can form a stable equilibrium layer which we call as "plasma sheath". Both the cases – the collision-dominated dust sheath and the collisionless dust sheath – should be analyzed. The problem of possible existence of a stable equilibrium dust sheath close to the wall was solved in [10, 23]. The collision-dominated dust sheath was not yet analyzed although its investigation is not difficult in principle. Investigation of the dust sheath is of big importance for different industrial applications such as etching and plasma deposition.

The scheme of numerical computations is similar to that explained above. For the collisionless case, the difference for the starting calculations is another value of the drag coefficient for drift velocities for the case where the Mach number is of the order of 1. This expression is given by the model of multi-scattering at small angles, with the linear drag coefficient discussed in Chap. 3. These expressions are obtained by employing the same physical arguments, namely by averaging on the drifting thermal width distributions with $u \gg 1$ ($M = \sqrt{2\tau}u$ of the order of 1 and for $\tau \ll 1$ we obtain $u \gg 1$, $\beta \ll 1$). We have

$$\alpha_{ch} \approx \frac{1}{4u}\left(1 + \frac{M^2}{2z}\right) \quad \alpha_{dr}u \approx \frac{\tau}{M^2}\left[\ln \Lambda + \frac{M^2}{2z} + \frac{M^4}{4z^2}\right] . \tag{8.5}$$

We start with one important comment on applicability of this model for large drift velocities $z\sqrt{\tau}/M^3 \ll \lambda_{Di}/a$: it is different than that for the above-given $z/\tau \ll \lambda_{Di}/a$ and thus can be satisfied in most cases of interest. We mention two moments: (1) since the charging equation contains $\alpha_{ch}/\sqrt{\tau}$, the

charges on grains for this approximation *depend only on the Mach number*, and (2) by inserting τ in the normalization of the distance in the force balance and in the continuity equations, one can write all expressions containing only the Mach number M. This has physical consequences since the Mach number is expected to be of order 1 and the depth of the dust sheath is of the order of the scale at which the dimensionless size is of order 1. In dimensional units, this is of the order of $\lambda_{Di}^2/a\tau$, i.e., of order $1/\tau \gg 1$, larger than that for the case of the collisionless layer.

8.3.2 Collisionless Dust Wall Sheaths

The starting approach and the first steps in creating the theory of dust sheathe were done in [23]. It was investigated only in the case where the sheath was irradiated by the plasma flow created by a remote ionization source with the drift velocities corresponding to the Mach number $M_0 \sim 1$. This is the case where the drift velocities are between the earlier-found (for 1D calculations of a dust layer) limit $u_{max} = 1/\sqrt{2}$ and the values of u corresponding to Mach number of the order of 1. Only the collisionless case was analyzed. For $u > 1/\sqrt{2}$, the drift velocity inside the dust sheath increases with an increase of the distance from its outer surface. This increase can continue up to the wall if the boundary conditions for the floating potential can be satisfied at the wall. The main question is, *does such dust sheath exist as a stationary and force-balanced structure?* The study [23] proved that such possibility *can really exist*. We note that external gravity and thermophoretic forces were neglected in this study.

The outer layer of the sheath is a boundary-free surface irradiated by a supersonic flux with the Mach number $M_0 \sim 1$. The flux is created in a remote region from this surface, i.e., far from the sheath. The term "remote again" (as for 1D calculation of the boundary-free layer) depends on the thickness of the void surrounding the outer boundary of the dust sheath. The parameters of the first boundary of the dust sheath are found by applying the conservation laws as it was in detail described before; the difference is in the drag coefficient and in the distance normalization (the characteristic scales are $1/tau$ larger). Nevertheless, the relative thickness of this void appears to be small as compared to the thickness of the dust-containing sheath region.

From the data on the boundary-free fist surface of the dust sheath, the calculations continue to the second boundary and give the whole distribution of dust and plasma parameters in the dust region up to the boundary separating the dust region and the wall – the wall-void region. The data obtained at this second surface are used to describe the distributions of electron and ion densities and the ion drift velocity up to the wall where the floating potential boundary conditions are imposed (the ion and the electron currents are equal, and the ion current is related with ion drift). The results of calculations, as mentioned, are independent of τ (the parameter τ enters only in

the normalization of the distances). The main results of these calculations are as follows:

1. *The stationary dust sheath can indeed exist within a broad range of Mach numbers* M_0.

2. The size of the dust part (in the dimensionless units of length) is of order 1.

3. Both dust voids bordering the structure have the width (in the same units) of $x_v \ll 1$.

4. The main drop of the plasma potential between the first boundary and the wall occurs inside the dust region and the drop of the potential in both voids is relatively small as compared to that in the dust region.

5. The total drop of the potential can be larger than that in a usual plasma sheath without dust.

Let us emphasize that *all these properties occur only for the case where all described procedures indeed lead to the conclusion that for a particular* M_0 *all conditions can be satisfied and the stationary dust sheath exists.*

There were found three important restrictions:

1. Equations for the first virtual boundary should be satisfied. Investigations were done only for drift velocities such that their Mach number is of the order of 1, but it can be also less or larger than 1. If this restriction is violated, the computations show that the possible Mach numbers for which the sheath can exist are arranged in several bands (two or three), which looks as a kind of "quantization" of the Mach numbers. The lowest possible Mach number for the dust sheath to exist is less than 1 and the Bohm criterion (which states that in the absence of dust the ions entering the usual plasma sheath close to the wall should have the Mach number larger than 1) is violated in presence of dust. The bands of allowed Mach numbers are rather broad but depend on the sort of gas through the charging process which depends on the electron-to-ion-mass ratio.
2. It was found that not for all initial conditions (selected by the first restriction) the second void close to the wall can exist. The procedure of calculations gives the ion and electron densities and the ion drift velocities which allow to draw the virtual wall surface where the floating potential conditions are satisfied as a virtual ion density curve both inside the dust region and in the wall-void region. In case this virtual floating potential curve is located inside the wall void region, its intersection with the actual calculated ion density determines the size of the wall void. In case this curve for the virtual ion density is located in the dust region and intersects the real density curve, the wall-void region does not exist, the dust can contact the wall and fall on the wall. As a result, the dust sheath does not exist.

3. For some values of the allowed Mach numbers, one finds divergency in the dust-containing region where both dM/dx and dz/dx tend to infinity at some distance from the first surface of the sheath. This effect was first found [10] for dust sheaths but then also (for certain parameters in the presence of homogeneous ionization) for boundary-free layers, for layers between floating potential electrodes, for two-size dust layers and dust voids between electrodes [9]. The first discovery of this phenomenon was thought to be occasional but further investigation showed that for certain parameters it can also be found in other configurations. Mathematically, this effect appears due to zeros of Jakobian containing both dz/dx and dn/dx which lead to a large increase of the dust grain gradients. Understanding of this phenomenon is based on the disappearance of the divergency for circular dust motion requiring 2D treatment. A conclusion was made that these singular points correspond to excitation of dust convection and dust vortices [20]. Many types of vortices are indeed seen in micro-gravity experiments [12]. The 1D calculation should be stopped at the point where the 2D vortices start to be created.

The dust sheaths have many practical and industrial applications since the surface treatment creates dust injections into plasma volume from the wall. The main result for etching applications is that this dust layer can be much larger (of the order of $\lambda_{Di}^2/a\tau$) than the usual plasma sheath in the absence of dust (about $\lambda_{De} \approx \lambda_{Di}/\sqrt{\tau}$) and that the main potential drop close to the wall is of the order of a few T_e (being 2–3 times larger than in the usual sheath) and is redistributed over much larger distances while the potential gradients (the electric field strengths) are smaller.

The sheath problem has application for future fusion devices where close to the walls $\tau \approx 1$ and $n \approx 10^{11}\,\mathrm{cm}^{-3}$. The number of neutrals is small and this case corresponds to the collisionless sheath. One can for this purpose provide with practical formulas for the thickness of the dust sheath Δ_d and the total numbers of grains in the sheath N_d which can be used in future designs of controlled fusion devices such as ITER:

$$\Delta_d = 5.52 \left(\frac{T_e(\mathrm{eV})}{10(\mathrm{eV})}\right) \left(\frac{10^{10}\mathrm{cm}^{-3}}{n(\mathrm{cm}^{-3})}\right) \left(\frac{10^{-4}\mathrm{cm}}{a(\mathrm{cm})}\right)\ \mathrm{cm}\ , \tag{8.6}$$

$$N_d = 3.6 \times 10^{13} \left(\frac{10^{-4}\mathrm{cm}}{a(\mathrm{cm})}\right)\ . \tag{8.7}$$

8.3.3 Further Problems of Dust Wall Sheath Studies

We list here some of the problems:

- The role of ionization in the dust sheath is of importance, especially for homogeneous source of ionization often used in low-temperature complex plasma experiments.

- The collision-dominated sheaths are of future interest. Investigations have already been started for the collision-dominated case where two walls surround the dust layer in the presence and absence of ionization.
- Consideration of dust convection in the sheath should take into account both the possibility of the convective instability as well as excitation of the convection by edge effects and inhomogeneity of ionization.

8.4 Dust Structures between Walls

8.4.1 Collision-Dominated Single Flat Layer

The distributions are symmetric with respect to the plane $x = 0$ at the center between two electrodes and therefore only a half of distribution from the center up to the wall can be considered. The question is again whether the stationary balance can be achieved taking into account the boundary floating potential conditions at the wall. The size of the layer is assumed to be larger than the ion-neutral mean-free path as it is in experiments [12] where the parameters were adjusted to close the central void. The collision-dominated dust layer observed between the electrodes in this case is shown in Fig. 8.7.

For the existence of a grain layer, the most important feature is that the plasma flux changes its direction in the wall void. Thus there exists a surface in the wall-void region where the flux is changing its sign being for small distances from the dust layer directed to the dust region (which is necessary to compress the layer) and directed to the wall on the other side of this surface to satisfy the floating potential boundary conditions at the wall. The detailed scan of parameters d, τ, etc., performed [24] shows that the dust layer can occupy up to 90% of space between the electrodes.

The comparison of modeling with observations gives the following: the size of the void is about 2 cm, the ion-neutral mean-free path is about 0.1 cm, and

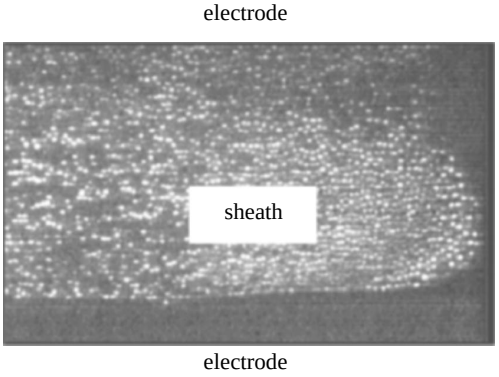

Fig. 8.7. The dust layer observed [12] after adjusting the ionization and gas pressure to close the central void. Shown is the half of the sheath, the scales are the same as in Fig. 8.6

for the dimensionless size 0.5 and $\tau = 0.05$ we obtain $0.5 \times 0.1\,(\mathrm{cm})/\tau \approx 2\,\mathrm{cm}$ for grain size used ($a \approx 3\mu\mathrm{m}$); the dimensionless density $n = 2$ corresponds to $4 \times 10^8\,\mathrm{cm}^{-3}$, which is of the order of the density value in the experiment.

8.4.2 Other Structures between Electrodes

We list here the equilibrium structures which can exist between electrodes:

- Numerical analysis of a dust layer with two-size grains shows that the larger-size particles are spatially separated and concentrated at the center part of the structure with a thin interface layer (this considered as very thin void) with the region of smaller size grains. The first dust layer (with larger particles) can be often without any point considered as starting point for vortex formation, but in the second layer no solutions were found with the absence of vortices. The full scan of the parameter range was not done yet and therefore possible existence of vortex-free double-size sheath is still an open question.
- Dust voids surrounded by two plasma sheaths and two electrodes at the floating potential were considered for the flat geometry for single-size grain and for two-size grains. The excitation of vortices can occur depending (for the same conditions) on the grain size – when it is doubled, for example. The case of two grain sizes shows that the smaller grains are spatially separated form the larger grains, with smaller grains located closer to the void with a thin interface (thin void) as observed in PKE-Nefedov experiments [12], (see Fig. 1.24). For this case, excitation of convective vortices is often found in calculations in accordance with observations of [12].
- The cylindrical and spherical walls with the floating potential were calculated similarly for the cases of a central spherical or a cylindrical structure surrounded by the wall void and electrodes. The main conclusion is that the total number of grains for, e.g., the spherical chamber cannot exceed certain number N, which corresponds for the usual pressure used in the existing experiment to about 3×10^7 grains – this seems to be an important limitation for experiments [25].
- The spherical structures obtained in calculations serve for explanation of the spherical structures observed in ballistic flight micro-gravity experiments (see Figs. 1.21 and 1.22).

8.4.3 Problems for Future Research

- The theoretical investigation should provide a complete set of equations for a possible equilibrium structure between electrodes taking into account various types of inhomogeneous ionization and various models of grain drag forces (linear and non-linear) complemented by different boundary conditions at walls.

- An interesting problem is whether several structures can simultaneously appear in the chamber and what is their interaction.
- Being self-organized, the structures can compete for plasma as a sort of food. This process can be observable for structures containing grains of different sizes.
- Experiments can answer the question as to whether structures can spontaneously divide themselves into smaller structures.

8.5 Dust Convection in Structures

8.5.1 General Remarks

As discussed above, in many cases stationary equilibrium structure distributions face the problem of excitation of stationary convective vortices. The convection can be excited by an instability of a stationary distribution as well as parametrically by modulation of such parameters as the ionization degree. The stability of plain, cylindrical, and spherical structures for creation of convection vortices was investigated (see, e.g., [20, 21, 26, 27]). The threshold of convection [26, 28] as well as the non-linear stage of convection was analyzed for plane structures [27] by the method of maximum unstable mode in the direction perpendicular to the plane of the structure. A set of two-line vortices rotating in opposite direction similar to that observed in micro-gravity experiments was obtained (see Fig. 8.8). The dust convection was often observed

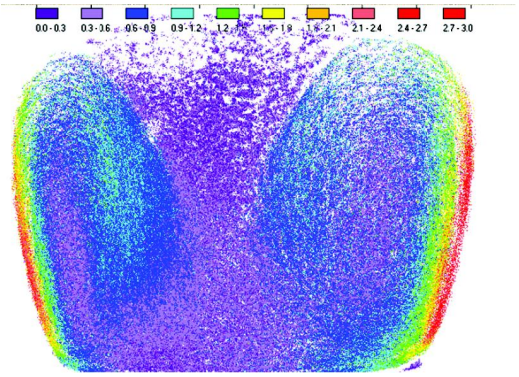

Fig. 8.8. Dust convection [28] observed in a cylindrical gas discharge with 2 μm grains. The size of the convection zone is about (1–2) mm in the radial direction and about 4mm in the axial direction. The structure observed corresponds to a toroidal vortex, and distributions in the plane crossing this toroid are shown. The convection velocity increases toward periphery of the structure from (0.3–0.6) mm/s (violet color) at the center up to (2.7–3)mm/s at the periphery; the diameter of the discharge chamber (50 mm) is much larger than the radial size of the structure

in the dust region neighboring dust voids. The dust convection seems to be a general phenomena for most combinations of dust voids and structures. The linear stage of dust convection is explained by a convective instability in which mainly the dust takes part while other plasma parameters are changed only slightly. The phenomenon of dust convection seems to be a new one since it differs from usual convection in gases: the dust-charging processes play an important role in the formation of convection cells and mainly only one component of a complex plasma, namely the dust component, is convected, while perturbations of other plasma components such as electron and ion densities, etc. are small [20, 21, 28]. Dust convection in cylindrical gas discharge was observed experimentally in [28]. In Fig. 8.8, experimental results show that convective velocities increase rapidly toward the periphery of the discharge.

The gas was neon or argon with the pressure of 1–10 torr, and the ion-neutral mean-free path is about 0.01 mm, i.e., much less than the size of the structure (which therefore should be considered as a collision-dominated one). The electron temperature is (3–5)eV and the ion temperature is about 0.025 eV; the ion density is of the order of $(3\times10^7$–$10^8)$cm/s, i.e., $z/\tau \gg \lambda_{Di}/a$ and the drag is non-linear. The vortices are stationary, which indicates that the difference between the electric field force and the drag force is compensated by the grain friction on neutral gas. The domain at the cylindrical axis was not occupied by the dust-convective structure and close to the axis often a *crystal state was observed*. Dust convection was also excited by an external probe introduced at the surface of the gas discharge [29, 30]. The convection of grain appears due to non-collinearity of the electric field force and the drag force. The electric force acting on grains is non-potential due to dust charge gradients $\nabla \times Z_d\mathbf{E} = (\nabla Z_d) \cdot \mathbf{E}$. Therefore the convection in a complex plasma is quite different from usual convection in gases which is determined by gradients of the gas pressure or Rayleigh–Benard convection, which is determined by temperature gradients.

Dust convection was investigated first for collisionless boundary-free layer assuming that the period in the plane of the layer corresponds to the maximum growth rate of convection instability. In this case the vortices are cylinders, both the vortex at one side of the layer rotates in the direction opposite to that on the other side of the layer and also opposite to the neighbor vortex at the same side of the layer. The system is a chain of two lines of vortices rotating oppositely. Dust convection in cylindrical structures corresponds to a set of toroidal vortices with periodically modulated ionization along the axis; rotation of the neighboring vortices is in the opposite directions. The convection observed in striations in a cylindrical tube [28] can be roughly modeled by considering a collision-dominated structure with modulation of the ionization rate along the cylindrical axis with the period corresponding to the size of the observed striation [20, 21]. The period of the modulation in this model is a free parameter which can be chosen to be of the order of the size of striation. This model does not go into details of the mechanism of appearing

of striation and therefore is in a sense more general than the detailed model using the striation description. But certainly the question of applicability of this model for the modulation of ionization in the striation is left for further studies. The aim of such simplified approach is to demonstrate that any modulation of plasma ionization along the axis of a cylindrical structure leads to phenomenon of grain convection with excitation of toroidal vortices and that the main qualitative property of this convection model coincide well with the observed features of the convection [28]. It was also checked that the dust convection leads to relatively small changes of other structural parameters such as the total flux, the ion drift velocity, and the ion and electron density, and creates a weakly modulated flux along the axis.

8.5.2 Problems to Solve

Let us give a list of problems to solve in the nearest future:

- The dust stationary convection is expected to be analyzed for most of the stationary self-organized structures discussed above.
- Dust convection in a system of different-size grains is of special importance; its investigation has just started [28].
- The case of spherical structures is of special interest for astrophysical applications where new objects – dust stars – might exist.
- Thresholds for the dust-convective instability has only started to be investigated; development of both experiments and theory is of big importance.
- One should answer the question as to whether the appearance of convection is a general problem for free boundaries of plasma crystals or those boundaries can exist without convection.
- The convection in the sheaths close to walls has several industrial applications as causing mixing of the deposited material and changing chemical reaction rates in the plasma chemistry.
- The dynamics of appearance of convection vortices can be analyzed on kinetic level, which is of practical interest for the physics of vortices when these are created by flows around obstacles.

8.6 Hybrid Dust Structures

We have discussed two classes of dust structures – dust clusters with sizes much less than the ion–dust absorption mean-free path, and larger dust structures such as plasma crystals and disordered structures (dust voids, dust layers, and dust sheaths) with sizes much larger than the ion–dust mean-free path. For both cases we found the possibility of *existence of a boundary free structures.*

In the presence of grains with different sizes and different concentrations, there exists another possibility for creation of hybrid dust structures. In these

structures, the condition that the size of the structure is much larger than the mean-free path for ion–dust absorption is fulfilled for smaller grains with large number density while for (a fewer number of) larger grains the opposite condition is valid – and the size of this partial structure is much less than the mean-free path for ion absorption on grains. It is natural to call these structures as *hybrid structures*.

The hybrid structures were investigated numerically [2] for cylindrical geometry where smaller grains form a self-consistent boundary-free structure with a difference of the electrostatic potential between the center and the boundary of the order of several T_e. For a few larger grains, the presence of small grains creates automatically a confining potential in the direction perpendicular to the cylindrical axis as well as creates a collective flux changing interactions of large grains. We should have in mind that for the structure formed by small grains there exists at each point a balance of the electric field force and the drag force acting on these dust grains. If in the field of these grains we then insert a grain (with the force balance for this grain) the following happens: the electric field force (being proportional to the dust size) is increased by the ratio of the dust sizes (e.g., doubled for the double-size grains) but the drag force (being proportional to the square of the dust size) is increased more (four times for double-size grains).

The drag force is due to the presence of the ion flux toward the center of the structure and therefore the larger grain will always feel a confining potential of the order of $V_s \approx Z_d T_e \rho^2 / \lambda_{str}^2$, where λ_{str} is the size of the structure formed by smaller grains. The large grains interact with the confinement potential created by small grains as well as with the collective attraction related to the collective flux of small grains. The structures of larger grains can therefore be classified as clusters.

According to the previous general result for equilibrium clusters in the case of cylindrical symmetry, these clusters should be helical clusters. The difference from previously considered helical clusters is that the grains forming the cluster in a hybrid structure can have both collective and non-collective attractions between them. Investigation of the role of collective attraction was made for both linear and non-linear screening by methods already described for non-collective interactions. The main conclusion is that the number of bifurcations and the number of branches for helical structures increases with an increase of the collective attraction. Also the regions where stable branches can be found with negative external confinement rapidly increase with an increase of the collective attraction.

The paper [2] contains detailed investigation of such hybrid structure with changes of the strength of collective and non-collective binary dust interactions and with different types of screening (linear or non-linear screening). The main conclusions are as follows.

1. The increase of bifurcations opens a new field of investigation of memory forms in nature with possible use in future mini-computers.

2. The ranges of equilibrium and stability for hybrid structures are much increased with an increase of attraction, and many boundary-free hybrid structures can in principle be created and perhaps already exist in space dusty plasmas.

3. The hybrid structures with more than two sizes of grains can form a complicated architecture of structures, with space separation of grains with different sizes and fast rate of interactions between the structures.

We do not go into further details of these studies since this very recent topic is still under investigation.

8.7 Micro-gravity Experiments

At present, two types of programs of micro-gravity experiments are done: the first one employs the parabolic flights, with typically 30 seconds available for the micro-gravity to exist, and the second one is related to space experiments such as those on board the International Space Station (e.g., the PKE-Nefedov and PK3–PK4 experiments). In all cases, complex dust structures were observed including the dust voids, the dust-convective cells, and the dust plasma crystals (the latter were recently observed in the PKE-Nefedov set of experiments). The observed crystals were embedded in various other complex liquid and gaseous parts of the dust plasma system including a big dust void and several dust vortices. On the basis of these observations, we can make some qualitative conclusions and list the expected new insights in the future micro-gravity experiments:

- The observation of the simultaneous presence of not only the standard (bcc) and the (fcc) structures but also the (hcp) structures which are thermodynamically not favorable having larger free energy looking surprising at the first glance. Recall that in the Earth-based experiments similar anomaly was also observed (and we discussed this point before in detail). For the experiments on Earth this anomaly can be still referred to the role of gravity that can give an additional stress energy. However, looking now at the micro-gravity system we have the impression that the appearance of these energetically not favorable crystal structures could be quite a *general phenomenon for a complex plasma*. This is indeed what can be expected in open systems prone to self-organization (note that all living creatures are also energetically not favorable). The flux of energy through the system is always existing in complex plasmas (that was emphasized many times in this book) and the concept of the free energy should not be applied to complex plasma systems. The micro-gravity observations give a further experimental evidence to the last statement. Thus the principles of self-organization in open dissipative systems should be used when considering structure formation and ordering in a complex plasma.

- The micro-gravity experiments also support our general statement that (initially) homogeneous complex plasmas are universally unstable with regard to the formation of various structures. Indeed, in experiments plasma crystal, dust void, and dust vortex structures were simultaneously observed.
- The PK3+ experiments are an order of magnitude more precise with less significant edge effects, connecting the grain distribution with some plasma parameters by optical measurement of the gas discharge in the dust region. There is a hope that the crystals can be larger in size, with many layers present, that the central void can be decreased and closed eventually, so that the crystal can be created in the center of the discharge camera. Then melting experiments can be performed when multi-layer crystals are obtained. The experiments with spherical camera and the ionization outside the plasma region (close to the walls) can help in confining and crystallization of grains in the center of the camera.
- The most probable candidate for observation of the helical dust structures is the future set of PK4 experiments with cylindrical gas discharge vessel, which was recently operating on parabolic flights with injection of high-velocity grains. The future experiment involves larger gas pressures to decrease the grain velocities and to stimulate formation of dust crystal structures. One of the simplest ones can be the helical structure; there also exists a possibility of injection of grains of two different sizes and formation of hybrid helical structures.

8.8 Future Research: Outlook for Complex Plasmas

What the self-organization means for future observations of the dust structures?

We certainly underestimated in the past the richness of nature in creating self-organized structures. It is desirable to demonstrate explicitly that the observed structures in complex plasmas are indeed the self-organized structures. This can be done by changing the number of grains in a structure. The characteristic feature of self-organized structures is that they depend only on a few global controlling parameters. In the example we have in mind one of those parameters is the total number of grains injected. If distribution of grains changes in a self-similar way as predicted by the concepts of self-organization, it can indicate that the considered structure is a self-organized one indeed. This is important in the sense that in the dust self-organized structures all other distributions such as the plasma electron and ion number densities, the ion drift velocities, and the grain charges are determined by the grain distributions. However, the problem is that most of the mentioned parameters can hardly be measured directly. Thus using the theory of self-organization

and knowing the experimental grain distribution one can make a reliable conclusion on the distributions of the electron and ion densities, the ion drift velocities, and the grain charges.

Is the collective attraction and grain pairing different from that leading to superconductivity?

The answer to this question is yes and no. It is similar in the sense that the attraction is caused by the exchange of virtual modes and it is different since the flux effects of classical nature determine the attraction in the case of a complex plasma. A special experiment should be designed in order to measure the grain collective attraction. The only method which seems to be obvious at present is the study of the pair interactions in the hybrid helical structures including those of the short length.

What is the structure of the boundaries in the boundary-free grain structures?

The organization of boundaries of the dust crystals should be complicated since in their vicinity the physics of the grain interactions is changed – it appears to be less collective since the flux at the boundary is collective only from one side, the dust side, of it. The collective attraction can be changed to a weaker non-collective attraction. Thus the separation between the grains changes forming some special surface structure. The sharpness of this surface as a function of the plasma flux is the topic of future investigation.

What is the interaction of spatially separated structures?

This topic has not started yet; however, it is of large interest since the dust structures separated by sharp boundaries can interact with each other in a rather complex manner. The questions are, can the interaction of separate structures be investigated, how this interaction will change the structures, and can the evolution of the hybrid grain structures lead to further complications of their structure by memorizing the changes occurring during their interactions?

Can complex plasmas be used to model biological systems?

The helical grain structures resemble many properties of DNA, the lowest energy seems to correspond to the dust double-helical structure. The interesting problem is whether the grain helical structures can have phase transitions to the toroidal helical structures with an increase of their length as was observed for DNA. The bifurcation of the radius of the dust helical cylindrical structure should be accompanied by the creation of vortices at the surface of the structure; this can be a mechanism of duplication of the dust helical structures. Such experiments could be important for understanding the possibility of the existence of different types of "life" in nature.

What is the outlook for space physics and astrophysics?

Can dust stars exist in space and what is their role in the dark matter and the star formation? The dust equilibrium configuration in the form of such a "dust star" is indeed possible, they are stable for global modes of oscillations such as the breathing mode where the type of structure is not changed. The study of other modes in such structures requires a long-term theoretical investigation similar to that already performed for usual stars. The question of how large can be the total mass accumulated in such "dust stars" is an important one not addressed presently. We can ask even a more fantastic question: Can a new type of intelligence exist in space based on interacting self-organized structures in complex plasmas? The observation of the regular modulation of infrared radiation observed with high resolution by the new Spitzer telescope requires a search in rather broad frequency interval which is not planned at present. The concept of the collective grain interaction has just started to be used in space and astrophysical plasmas where dust is widely present. It is important to understand the possibility of rapid grain agglomeration for planetary physics and physics of interplanetary clouds as well as the role of the dust "structurization" instability in the Universe structurized by the gravity.

8.9 Conclusion

This book deals with the physics of basic elementary processes in complex plasmas. The main accent here is on new physical problems which, we believe, will be the subject of intensive future studies. Estimates made here on the basis of the understood elementary processes serve as a first and necessary step toward detailed description that should be made on the kinetic level. We hope that this book can spread the new physical concepts among all interested in this new field of science as well as in general physics of self-organization in complex systems. We also believe that only deep understanding of such new physics can foster deep insights and breakthroughs in this and neighboring fields of research as well as opens wide doors for future applications and novel technologies.

References

1. G. Birkl, S. Kassner, and H. Walther (1992). *Nature* **357**, 310.
2. V. Tsytovich, N.Gusein-zade, and G. Morfill (2004). *IEEE Trans.Sci.* special issue Dusty plasmas, April.
3. Sh. Amiranashvili, N. Gusein-zade, and V. Tsytovich (2001). *Phys. Rev.E* **64**, 016407.
4. Sh. Amiranashvili, N. Gusein-zade, and A. Ignatov (1999). Stability of polygonal Coulomb crystals, *Phys. Rev.A* **59**, 3098–3100.

5. N. Guseim-zade N. and V. Tsytovich (2004). *Fiz.Plasmy* **31**, 107.
6. V. Tsytovich and N. Gusein-zade (2005). *Fiz.Plasmy*, **32**, 47.
7. G.E. Morfill, U. Konopka, M. Kretschmer *et al.* (2006). *New Journ. Phys.* **8**, 7.
8. S.V. Vladimirov, V.N. Tsytovich, and G.E. Morfill (2005). *Phys. Plasmas* **12**, 052117.
9. V.N. Tsytovich, S.V. Vladimirov, and G.E. Morfill (2004). *Phys. Rev. E* **70**, 066408.
10. V. Tsytovich (1997). *Theory of Dust Sheaths* CNRS Report p. 101.
11. V. Tsytovich (2000). *Comments on Plasma Phys. and Contr.Fusion Part C, Comments in Modern Physics* **1**, 1.
12. A. Nefedov, G. Morfill, V. Fortov *et al.* (2003). *New Journ. Phys.* **5**, 33/1.
13. D. Samsonov and J. Goree (1999). *Phys. Rev. E* **59**, 1047.
14. J. Goree, G. Morfill, V.N. Tsytovich, and S.V. Vladimirov (1999). *Phys. Rev. E* **59**, 7055.
15. V.N. Tsytovich, S.V. Vladimirov, G.E. Morfill, and J. Goree (2001). *Phys. Rev. E* **63**, 056609.
16. V. Tsytovich (2000). *Proceedings ICPCP-1999,Invited talks, Hakone, Japan, 1999*, Elsever Fronties of Pkysics, N.Y. p. 47.
17. V. Tsytovich, (2001). *Phys. Scr. Vol.* **T89**, 89.
18. G. Morfill H. Thomas, U. Konopka, H. Rothermel, M. Zuzic, A. Ivlev, and J. Goree (1999). *Phys.Rev.Lett* **83** 1598.
19. V.N. Tsytovich, S.V. Vladimirov, O.S. Vaulina *et al.* (2006). *Phys. Plasmas* **13**, 032305.
20. V.N. Tsytovich, S.V. Vladimirov, O.S. Vaulina, O.F. Petrov, and V.E. Fortov (2006). *Phys. Plasmas* **13**, 032305.
21. V. N. Tsytovich, S. V. Vladimirov, O. S. Vaulina, O. F. Petrov, and V. E. Fortov (2006). *Phys. Plasmas* **13**, 032306.
22. V. Tsytovich (2000). *Plasma Phys. Rep.* **26**, 688.
23. S. Benkadda, V. Tsytovich, and S.V. Vladimirov (1999). *Phys. Rev. E* **60**, 4708.
24. V. Tsytovich, U. Konopwa, G. Morfill, and H. Thomas (2003). *New Journ Phys.* **5**, 1.1–1.27.
25. F. Melanso and J. Goree (1996). *Vac.Sci Techol. A* **14**, 511.
26. M. Zuzic, A. Ivlev, G. Goree, G. Morfill, H. Thomas, H. Rothermel, U. Konopka, R. Sutterline, and D. Goldback (2000). *Phys.Rev.Let.* **85**, 4064.
27. U. Konopka, G. Morfill, and L. Ratke (2000). *Phys. Rev. Lett.* **84**, 891.
28. M. M. Vasiliev, S. N. Antipov, O. F Petrov *et al.*(2006). *Jporn of Phys.A.Math. and General* **39**, 4539.
29. D. Law, W. Steel, B. Annaratone, and J. Allen (1998). *Phys.Rev.Lett* **80**, 4189.
30. A. Samarin, O. Vaulina *et al.* (2002). *Phys. Scr.*, **98**, 123.